

DNA replication in the context of development: Tissue-specific remodeling of the DNA
replication fork and dynamic R-loop signatures across embryogenesis

By

Alexander Lucas Munden

Dissertation

Submitted to the Faculty of the
Graduate School of Vanderbilt University

In partial fulfillment of the requirements
for the degree of

DOCTOR OF PHILOSOPHY

In

BIOLOGICAL SCIENCES

June 30th, 2022

Nashville, Tennessee

Committee Members:

Katherine L. Friedman, PhD

Jared T. Nordman, PhD

Kendal Broadie, PhD

James G. Patton, PhD

David K. Cortez, PhD

Dedicated to Rachel, the light of my life, without whom this thesis would not exist.

ACKNOWLEDGEMENTS

I knew graduate school would be challenging, but I still underestimated how difficult it would be. Without the help of several people playing different but essential roles, I would not be here today. I thank Jared Nordman, my advisor. I wasn't an easy student to mentor, especially for a brand-new PI. He handled everything with aplomb and grace, and I think together we have laid the foundations for a great laboratory.

I thank my mom, Kathy, and sister, Amanda. They have given me emotional and psychological support over my entire life. Rachel's family, in particular her mom, Cathy, have also supported me and encouraged me to go back to graduate school and fulfill this dream.

I thank my committee members Kendal Broadie, Dave Cortez, Jim Patton, and my chair Kathy Friedman. They have given invaluable feedback and support on my science. Kathy especially supported the more emotionally taxing aspects of being a graduate student.

I have been lucky to have several people who encouraged me to go back to graduate school and believed in me even before I believed in myself. Some of the most important of these people are Laura Hover, Ty Abel, Michael Cooper, Hal Moses, Phil Owens, and Gerardo Valadez.

I've been lucky to work with a number of great people in my immediate lab. I thank Saumya Patel, Souradip Das, Dongsheng Han, Reyhaneh Tirgar, and Logan Richards, Jack Rong, and Amanda Sun. Mentoring Amanda was a wonderful experience, and I'm very proud of her own graduate career now. House parties at Logan's played a pivotal role in maintaining my mental health.

TABLE OF CONTENTS

DEDICATION.....	ii
ACKNOWLEDGEMENTS.....	iii
LIST OF FIGURES.....	vii
LIST OF TABLES.....	x
Chapter	
I: Introduction.....	1
Overview.....	1
The fundamental of DNA replication.....	3
The unique challenges of development.....	7
R-loops play multifaceted roles in the cell.....	10
II: Rif1 inhibits replication fork progression and controls DNA copy number in Drosophila.....	25
Abstract.....	25
Introduction.....	26
Results.....	30
Discussion.....	50
Materials and methods.....	56
Data access.....	68
Acknowledgements.....	68
Author contributions.....	68

III. Identification of replication fork-associated proteins in <i>Drosophila</i> embryos and cultured cells using iPOND coupled to quantitative mass spectrometry.....	88
Abstract.....	88
Introduction.....	89
Results.....	91
Discussion.....	102
Materials and methods.....	104
Acknowledgements.....	113
Author contributions.....	113
Data availability statement.....	114
Additional information.....	114
IV. R-loop mapping and characterization during <i>Drosophila</i> embryogenesis.....	154
Abstract.....	154
Introduction.....	155
Results.....	158
Discussion.....	176
Materials and Methods.....	181
Accession numbers.....	191
Funding.....	191
Conflict of interest.....	191
V: Summary and discussion.....	200
Rif1 at replication forks.....	200
Replication fork remodeling during embryogenesis.....	204

R-loop formation during embryogenesis is dynamic205
References.....215

List of Figures

Figure	Page
1-1. The replicative helicases of the replication fork are loaded at ORC binding sites....	4
1-2. Representation of a <i>cis</i> R-loop.....	10
1-3. Summary of the <i>in vivo</i> functions of R-loops.....	12
2-1. The SNF2 domain is essential for SUUR function and replication fork localization.....	31
2-2. SUUR associates with Rif1.....	36
2-3. Rif1 is required for underreplication.....	39
2-4. Rif1 regulates replication fork progression.....	42
2-5. Rif1 acts downstream of SUUR.....	45
2-6. SUUR is necessary to retain Rif1 at replication forks.....	46
2-7. The Rif1 PP1 interaction motif is necessary to promote underreplication.....	49
S2-1. Genome-wide copy number profile of the <i>SuUR^{SNF}</i> mutant.....	74
S2-2. Quantification of SUUR and <i>SUUR^{ΔSNF}</i> signal intensities at replication forks and heterochromatin.....	75
S2-3. Western blot analysis of heat-shock inducible SUUR constructs.....	76
S2-4. Verification of <i>Rif1</i> mutants and validation of anti-Rif1 antibody.....	77
S2-5. Genome-wide copy number profile of the <i>Rif1</i> mutant.....	78
S2-6. <i>Rif1</i> mutant salivary gland cells display a pattern of late replication.....	79
S2-7. <i>Rif1</i> mutant endo cycling cells have enlarged chromocenters.....	80
S2-8. The developmental window of gene amplification is not affected by loss of Rif1 function.....	81

S2-9. Quantification of SUUR signal intensity at replication forks in the presence and absence of Rif1	82
S2-10. Quantification of Rif1 signal intensity at replication forks in the presence and absence of SUUR.....	83
S2-11. Rif1 localizes to replication forks in cultured cells.....	84
S2-12. The Rif1 ^{PP1} protein expression level is similar to wild-type Rif1.....	86
S2-13. Genome-wide copy number profile of the <i>Rif1^{PP1}</i> mutant.....	87
3-1. Establishing iPOND in the developing embryo.....	93
3-2. iPOND coupled to quantitative mass spectrometry in the post-MZT embryos.....	95
3-3. iPOND coupled to quantitative mass spectrometry in S2 cells.....	98
3-4. BRWD3 affects genome stability and replication fork progression.....	101
S3-1. Analysis of iPOND and iPOND-TMT in S2 cultured cells.....	115
S3-2. Validation of RNAi-based depletion of targets.....	117
S3-3. Validation of BRWD3 combing and knockdown.....	118
4-1. R-loop abundance is developmentally regulated and R-loop homeostasis is necessary for development.....	159
4-2. The R-loop landscape changes as a function of development.....	163
4-3. R-loop signal as a function of transcription unit and sequence composition.....	166
4-4. Common chromatin features associated with R-loops.....	170
4-5. R-loop formation as a function of transcription.....	172
4-6. R-loops have the potential to trigger ATR activation at the MZT.....	176
S4-1. Expression of RNaseH1 constructs in early embryos.....	192
S4-2. Properties of R-loops in <i>Drosophila</i>	193

S4-3. Sequence properties of R-loops in Drosophila.....195

S4-3. Expanded chromatin associated factors associated with R-loops for every cell
type.....197

List of Tables

Table	Page
Table 2-S1. Underreplicated regions called by CNVnator	70
Table 2-S2. Half-Max called follicle widths.....	73
Table 3-S1. Unnormalized TMT Intensities for Embryo iPOND Replicates.....	119
Table 3-S2. Normalized TMT Intensities for Pulse-Enriched Embryo iPOND Replicates.....	134
Table 3-S3. Unnormalized TMT Intensities for iPOND S2 Cell Replicates.....	136
Table 3-S4. Normalized TMT Intensities for iPOND S2 Cell Replicates.....	151
Table 3-S5. Primers used in iPOND Study.....	153
Table 4-1. List of available CHIP-chip and CHIP-seq from modENCODE.....	187
Table 4-S1. Primers used in R-loop study.....	198
Table 4-S2. GO analysis of R-loop forming genes.....	199

CHAPTER I: INTRODUCTION

OVERVIEW

“But our manner of knowing is so weak that no philosopher could perfectly investigate the nature of even one little fly” - Thomas Aquinas.

DNA replication is a fundamental challenge of life. In order to proliferate, every organism must be able to replicate and divide its DNA into daughter cells. DNA is the unit of inheritance that underlies evolution and is the bedrock of the central dogma of biology: DNA is transcribed into RNA, which is in turn translated into proteins. Defects in DNA replication can cause mutations that can result in loss of function or defects in proteins and functional RNAs. These errors ultimately drive cellular dysfunction and disease. Since DNA is copied to daughter cells, every error that occurs is passed on to daughter cells and can propagate throughout the organism or tissue. Catastrophic DNA damage can even cause cellular death. DNA replication is meticulously regulated to ensure accurate transmission of genetic and epigenetic data. Therefore, the timely and accurate replication of DNA is of utmost importance to every life form. DNA replication must also overcome a multitude of challenges each and every time a genome is copied.

Challenges in DNA replication can range from conflicts between replication and transcription, limiting nucleotide pools, DNA secondary structures and many others (Zeman and Cimprich, 2014). In addition, epigenetic information must be accurately copied from one parent strand to the daughter strands to maintain chromatin organization and transcription programs (Alabert and Groth 2012). In multicellular organisms, DNA replication occurring in the context of development can pose unique challenges due to atypical cell cycles and unusual chromatin environments (Nordman

and Orr-Weaver, 2012). All these obstacles must be overcome to ensure the accurate and timely replication of the genome to maintain life.

In this introduction, I will review what has previously been discovered about DNA replication, focusing on the macromolecular machine that orchestrates DNA replication: the replication fork. DNA replication in the context of development will be detailed, focusing specifically on work in the fruit fly, *Drosophila melanogaster*, which has been an invaluable tool for studying DNA for over a century. Finally, I will detail R-loops, a nucleic acid structure that forms when nascent transcripts reanneals to the template DNA. R-loops have been shown to be a multifaceted factor in epigenetic regulation, a driver of genome instability and yet plays essential roles in DNA repair and replication (Skourti-Stathaki and Proudfoot, 2014). Understanding how R-loop dynamics change during development, influence establishment of the chromatin environment, and serve as triggers of the DNA damage response has been a focus of my thesis research. These ideas are essential to the research I conducted, which has focused on the central question of how DNA replication and the chromatin environment are regulated during the confines of development. More specifically, (1) if the replication fork itself can be remodeled during development to accommodate for cell-type specific replication programs and (2) how R-loop position and abundance changes during development. This work has furthered our understanding of DNA dynamics during development and moves us closer to fully understanding the nature of 'one little fly'.

The fundamentals of DNA replication

DNA replication occurs in multiple steps across the cell cycle, beginning in late mitosis and across G1. In eukaryotes, the six-member Origin Recognition Complex (ORC) binds to hundreds to thousands of sites across the genome, depending on the size of the organism's genome (Fig. 1-1) (Sun and Kong, 2010). These sites are termed origins of replication. In yeast, these sites are highly sequence specific, but in metazoans where ORC binds is not completely understood. While ORC binding is sequence independent in metazoans, origins of replications are enriched at open chromatin such as that found in promoters and enhancer regions of DNA (Hutchins et al. 2016). The local chromatin environment may also play a role in ORC binding, as histone acetylation and H4K20 methylation may contribute either directly or indirectly to ORC binding (MacAlpine et al. 2010).

The initial steps of helicase loading have been most well established in budding yeast. While highly conserved, the increasing complexity of metazoan helicase loading may be more intricately regulated. Helicase loading also requires Cdc6 and Cdt1 to act cooperatively and sequentially to load two heterohexameric MCM2-7 complexes head-to-head at a replication origin (Ticau et al. 2015). Single molecule studies have demonstrated that Cdc6 binds to ORC and recruits the first MCM complex that is bound to Cdt1 (Ticau et al. 2015). After loading of the initial MCM hexamer, ORC recruits a second MCM through similar interactions with Cdc6 and Cdt1. At this point, Cdt1, Cdc6, and ORC can all dissociate from the DNA leaving the two bound MCM complexes. Importantly, once loaded but before activation of the helicases, the two MCM molecules

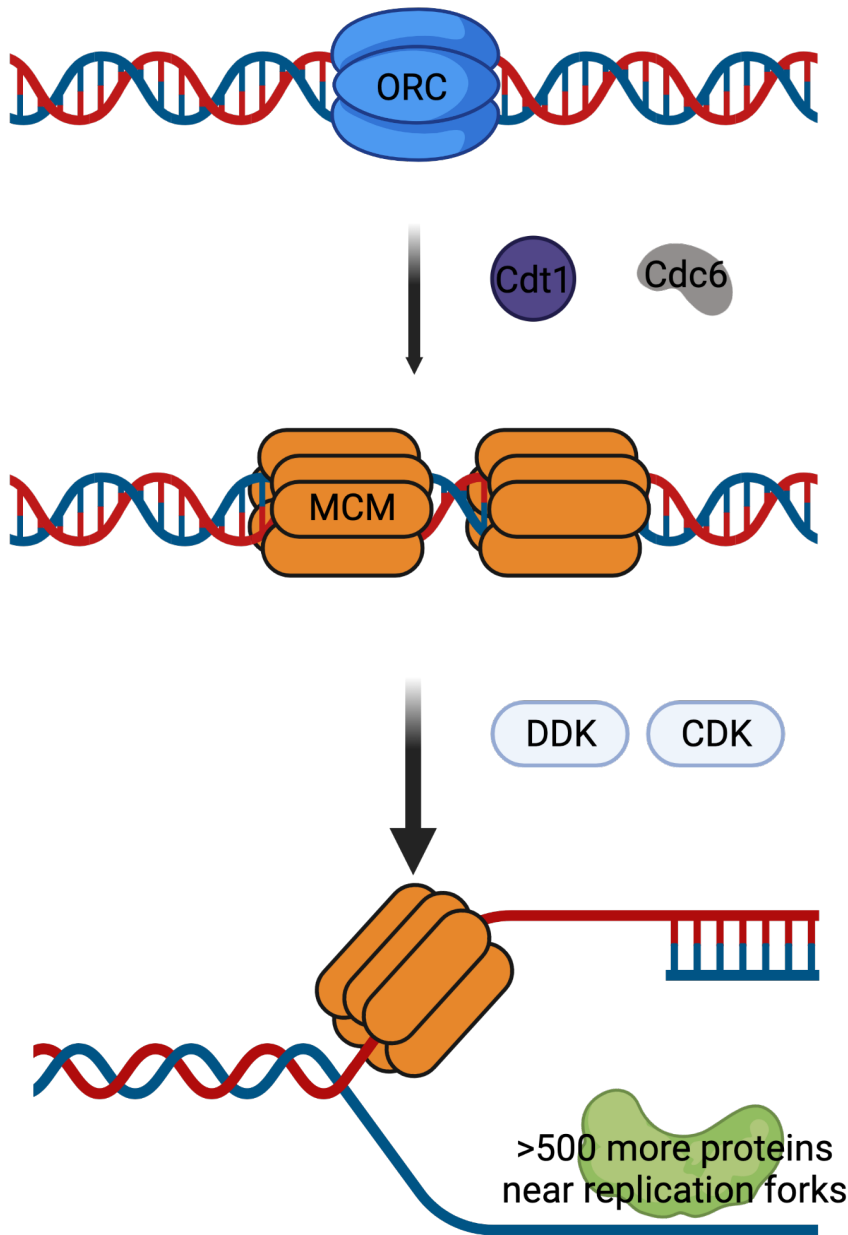


Figure 1-1: **The replicative helicases of the replication fork are loaded at ORC binding sites.** Orc binds to potential origins across the genome during late mitosis and G1. Through the activity of Cdt1 and Cdc6, 2 MCM helicases are loaded at these sites. During S Phase, the activity of the DDK and S-CDK kinases phosphorylate the helicases. Through the recruitment of hundreds more proteins, the replication forks form.

can 'slide' around the double-stranded DNA but are constrained by local chromatin (Remus et al. 2009). The two MCM complexes are the core helicases in the final

replication fork. Importantly, the activity and protein levels of ORC, Cdc6 and Cdt1 are regulated across the cell cycle to prevent reloading of MCM hexamers during S phase and the unintentional reduplication of the genome (Mimura et al. 2004; Pozo and Cook, 2017; DePamphilis, 2004).

At the beginning of S phase, the helicases are activated by Dbf4-Dependent Kinase or DDK. Both DDK and the S phase CDK (S-CDK) are required for the additional recruitment of the remaining essential firing factors (Sld2, Dpb11, GINS, Mcm10 and pol ϵ) and the initial unwinding of DNA (Douglas et al. 2018). Mcm10 promotes further unwinding of DNA and Replication Protein A (RPA) binds to the newly available single-strand DNA (ssDNA) (Douglas et al. 2018). Dozens of new proteins are ultimately recruited, including the remainder of the DNA polymerases (Sirbu et al. 2011). This final macromolecular machine is termed the replication fork or replisome and is capable of replicating both the genetic and epigenetic information.

In addition to simply unwinding and copying the DNA, the replication fork must also be able to unpack DNA from nucleosomes and repackage newly synthesized DNA after replication. To properly extricate and re-add nucleosomes, histone chaperones and chromatin remodeling complexes are required. FACT, Asf1, and Nhp6 are histone chaperones that work to disrupt the nucleosomes ahead of the replication fork (Alabert and Groth, 2012). FACT seems to be the most essential of these and associates with polymerase α and MCM2 (Zhang et al. 2020). Multiple chromatin remodeling complexes such as Acf1-Iswi and Ino80 seem to be required to replicate efficiently through chromatin, particularly in more tightly packaged heterochromatin (Alabert and Groth, 2012).

While the essential components of the replication fork have been defined *in vitro*, the composition of the replication fork *in vivo* is much more complex (Baris et al. 2022). In the past decade, new purification strategies coupled with mass spectrometry developed by the Cortez and Groth laboratories have vastly increased our understanding of the complex proteome associated with the replication fork. By purifying proteins associated with newly synthesized DNA, hundreds of additional proteins have been shown to associate with at least a subset of replication forks (Alabert et al. 2014; Sirbu et al. 2013). Combining purification strategies with replication stressors shows that the composition of replication forks is highly dynamic (Dungrawala et al. 2015).

The protein composition of the replisome can vary in response to a variety of replication stresses such as lack of nucleotides, DNA lesions, misincorporation of ribonucleotides, replication-transcription conflicts, repetitive DNA, or DNA secondary structure (Zeman and Cimprich, 2013). Eukaryotes have conserved DNA damage response proteins to resolve damage due to these sources. Ataxia telangiectasia and Rad3 related (ATR) is an essential protein in mammals that acts at stalled replication forks (Saldivar et al. 2017). After activation, ATR activates a cascade of signaling events to prevent the replication fork from collapsing and remodel the cell cycle. Origin firing is modulated, the replisome itself is stabilized, and recruitment of fork repair proteins occurs (Saldivar et al. 2017). Though replication stress can be caused by exogenous sources, many of these impediments arise naturally as part of the normal replication program. For example, TERF2 is recruited to heterochromatin topological barriers in response to ATM for the replication fork to proceed (Mendez-Bermudez et al.

2018). Understanding how cells deal with endogenous replication stress can guide the diagnosis and treatment of human diseases that result from defects in this process.

The unique challenges of development

Development from the single zygote to a developed organism is a monumental challenge. After zygotic genome formation, embryogenesis begins and altered cell cycles may occur. At the most extreme example, common in egg laying species such as *Drosophila*, an entire cell cycle can occur in less than ten minutes and happens without any gap phases (Farrell and O'Farrell, 2014). These early fast cycles are hypothesized to take advantage of maternally deposited resources and speed development to avoid predators (Yuan et al. 2016). In contrast, mammalian embryonic development proceeds much more slowly but still maintain cell cycle heterogeneity. The first cleavage cycle in mouse embryos occurs 36 hours post-fertilization, while the next four cell cycles take 12 hours each (Hogan et al. 1994). Later in development, the cell cycle can be completed within 2.5 hours (Mac Auley et al. 1993).

The altered cell cycle timing is not the only challenge the DNA replication program must overcome during embryogenesis. In *Drosophila*, the early embryo lacks most histone modifications found in mature tissue, and there are frequently developmental-specific histone variants (Hamm and Harrison, 2018; Loppin and Berger 2020). As the embryo develops and begins to form defined cell lineages, histone modifications that are critical for gene regulation and cell differentiation must be added. Initially, *Drosophila* embryos rely upon maternally deposited RNA and protein and do not make *de novo* transcripts (Tadros and Lipshitz, 2009). At some point, every embryo

undergoes a maternal-to-zygotic (MZT) transition whereupon the zygotic genome is activated, and maternally deposited RNA is degraded (Hamm and Harrison, 2018). In flies, there is a minor wave of zygotic genome activation (ZGA) at cell cycle 9, and the major wave at cell cycle 14 (Tadros and Lipshitz, 2009). Mammalian embryos undergo a similar stepwise activation, with the first wave of ZGA occurring at cell cycle 2, and the major wave at cell cycle 4 (Jukam et al. 2017). Finally, DNA replication itself may regulate cellular differentiation. Recent studies of mouse embryonic stem cells demonstrated that totipotent cells have much slower replication fork speeds and use many more origins to compensate (Nakatani et al. 2022). Artificially slowing replication fork speed and altering replication timing was sufficient to change the totipotency and differentiation of the tissue (Nakatani et al. 2022). This highlights the interplay between DNA replication and development.

Proteomic studies of replication forks in embryonic stem cells have identified proteins at replication forks that aren't present in fully differentiated cells (Aranda et al. 2014; Zhao et al. 2018). Many of these proteins are hypothesized to aid with the short cell cycle or are involved with epigenetic inheritance (Aranda et al. 2014). For example, the NuRD-HDAC was found to be at replication forks and had separately been shown to be required for early embryonic development in zebrafish (Aranda et al. 2014; Christov et al. 2018). Separate research identified a Filia-Floped protein complex at replication forks in mouse embryonic stem cells which seemed to aid activation of ATR signaling and provide more robust fork restarting (Zhao et al. 2018).

In addition to the challenges of rapid embryonic cycles, unique DNA replication programs exist across development. Polyploidy, wherein cells undergo repeated rounds

of DNA replication without mitosis and cytokinesis, is common in metazoans. Polyploidy is found within repairing kidney, bladder, and liver tissue in mammals (Bailey et al. 2021). Furthermore, many different tissues in *Drosophila* contain polyploid cells (Fox et al. 2020; Nandakumar et al. 2020; Unhavaithaya and Orr-Weaver, 2012). The function of polyploidy is not completely understood, but the increased genomic content may allow cells to increase transcriptional output, withstand environmental stresses, and allow specialized function by large cells (Calvi et al. 1998; Orr-Weaver 2015; Van de Peer et al. 2020). Polyploidy can also arise through wound healing due to cell fusions (Losick et al. 2013).

Programmed gene amplification and underreplication of specific genomic loci may also occur in polyploid cells (Spradling and Orr-Weaver, 1988). For example, in the follicle cells of the *Drosophila* ovary, specific regions of the genome go through repeated round of DNA replication to increase gene copy number (Spradling and Mahowald, 1980; Griffin-Shea et al. 1982). The increased gene copy number provides additional capacity to create transcripts associated with chorion (eggshell) production in a short developmental time (Calvi et al. 1998). Many polyploid cells in *Drosophila* also have regions of underreplication, where specific loci have fewer copies of the chromosome in comparison to the rest of the genome (Spradling and Orr-Weaver, 1987). Importantly for human health, both gene amplification and underreplication have also been observed in the giant trophoblast cells of the placenta (Hannibal and Baker, 2016).

R-loops play multifaceted roles in the cell

R-loops are a three-stranded nucleic acid structure canonically formed when nascent RNA from transcription reanneals to the template DNA strand, resulting in a displaced single strand of DNA (Fig. 1-2) (Aguilera and García-Muse 2012). Sequences that could form R-loops to their transcribed loci were identified at the highly transcribed 18S and 28S sequences within the rDNA locus of *Drosophila melanogaster* (White and Hogness 1977; Glover and Hogness 1977). In high heat and formamide-containing conditions, the abundant RNA could anneal back to the duplex DNA and cause the characteristic displacement of a single strand of DNA (Birnstiel et al. 1972). A decade later, R-loop formation *in vivo* was shown to occur in the context of *E. coli* plasmids (Dasgupta et al. 1987). Persistent R-loops were shown to form at the plasmid origin of replication as a result of nearby transcription (Dasgupta et al. 1987). R-loops

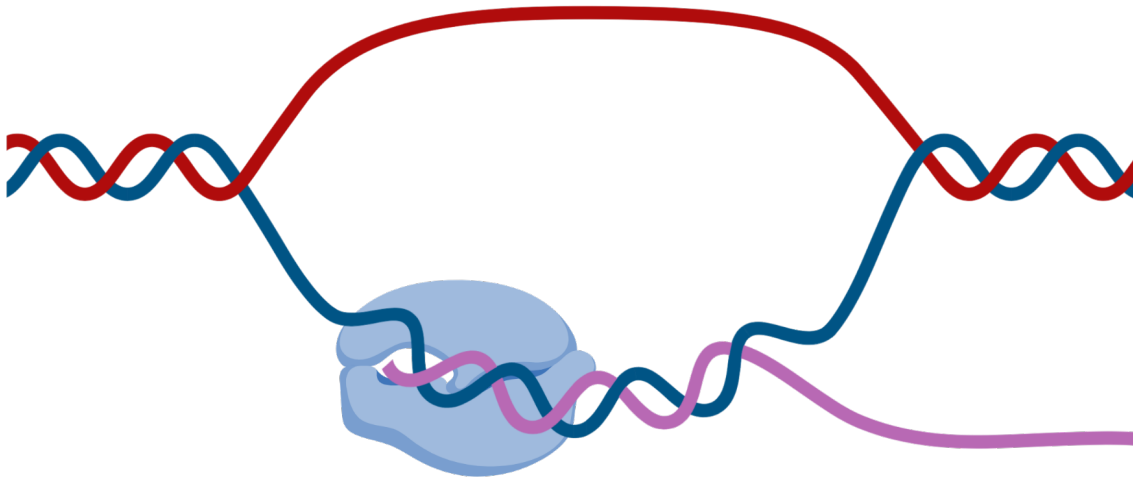


Figure 1-2: **Representation of a *cis* R-loop.** RNA is indicated by the purple strand. R-loops can also form in *trans*, in which case the polymerase would be absent.

spur initiation of DNA replication in this context through two methods (Fig. 1-3A). First, the RNA of the R-loop serves as the primer for DNA polymerase. The RNA moiety of the R-loop serves as the primer for normal DNA replication after cleavage by RNase H makes the 3' end accessible to DNA polymerase (Itoh and Tomizawa, 1980). Secondly, the displaced single-strand of DNA is available to the helicase and primase, where they can go on to initiate replication (Masukata et al. 1987). The formation of this R-loop is required for the plasmid to replicate. The most stable R-loop forms at a sequence of repeated deoxycytidine and guanine (Masakata and Tomizawa, 1990). Other research during this era highlighted the complexity of R-loop. Changes in the rate of transcription altered the efficiency of the RNA:DNA hybrid formation, giving the first hint as to the complexity of R-loop formation (Masakata and Tomizawa, 1990).

R-loop formation also occurs in the context of phage T4 infection and in the replication of mitochondrial DNA. At least two different origins of replication within the T4 genome form R-loops *in cis* and perform similar functions as they do in the plasmid (Carlies-Kinch and Kreuzer, 1997). Transcription initiates from the promoter upstream of the R-loop forming region (Carlies-Kinch and Kreuzer, 1997). Interestingly, the R-loop structure in T4 permits the transcription of RNA from the single-stranded, non-template strand that can also serve as the primer for DNA synthesis (Belanger and Kreuzer, 1998). In mitochondria from yeast to mammals, R-loops form *in cis* via transcription of the mtRNA polymerase near GC-rich cluster (Lee and Clayton, 1998). This R-loop likely acts as the primer for DNA replication, similar to plasmids in *E. coli* (Lee and Clayton, 1998). Surprisingly, *in vitro* studies suggest that widescale incorporation of mitochondrial transcripts can be incorporated *in trans* into the mitochondrial genome during replication

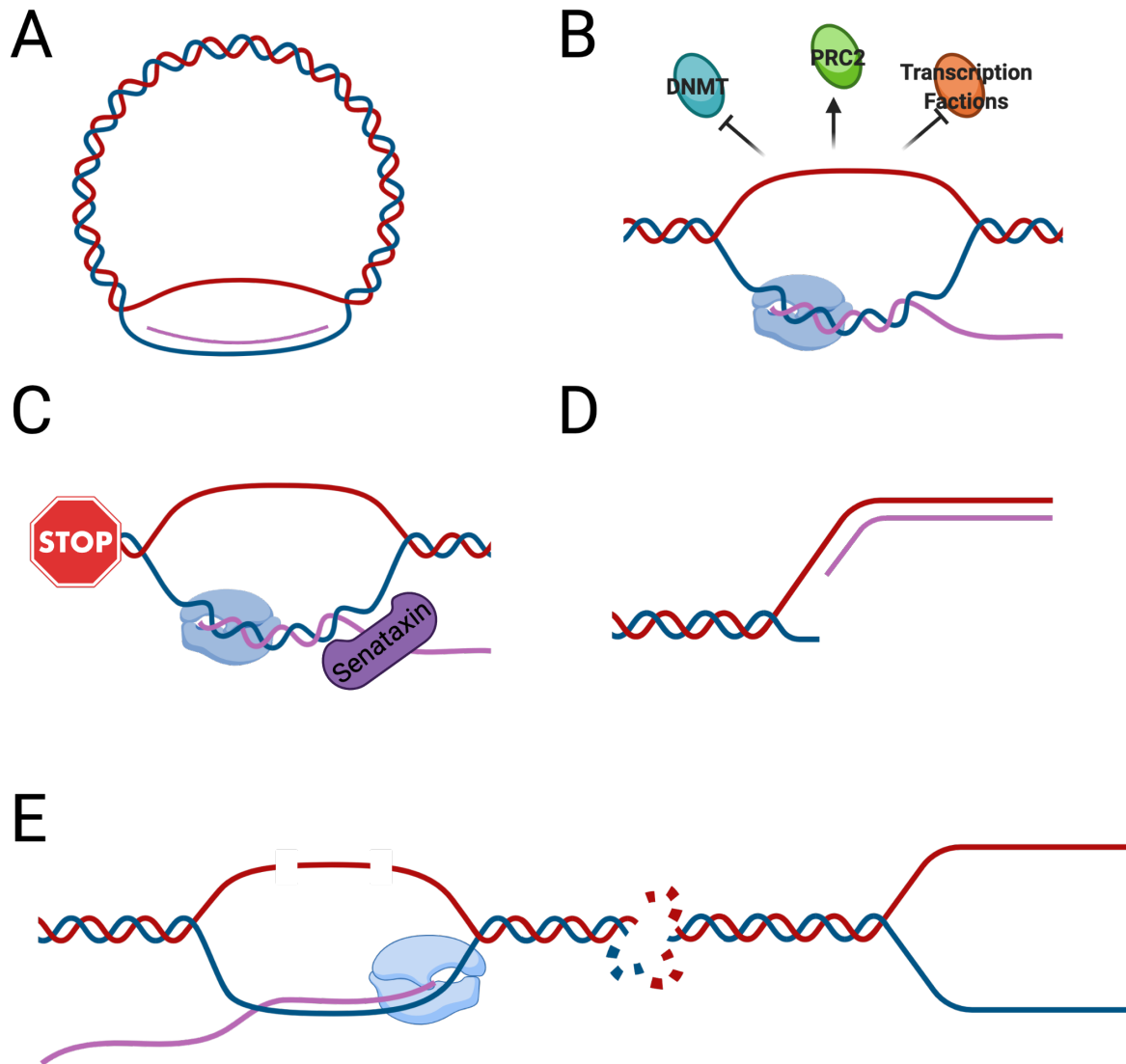


Figure 1-3: **Summary of the *in vivo* functions of R-loop.** (A) An R-loop in plasmids and mitochondria DNA to form initiation of replication. (B) R-loops recruit some chromatin modifying proteins, such as PRC2, and can block the recruitment of other factors such as DNMT and transcription factors. (C) R-loops at transcription termination sites work to halt the RNA polymerase and can recruit proteins such as Senataxin. (D) R-loops form at double-strand breaks to guide repair machinery and prevent excessive resection. (E) R-loops may also be a source of DNA damage. This can occur through damage at the displaced single-strand of DNA or when colliding with the replication fork machinery.

(Reyes et al. 2013). These early studies highlight two important aspects of R-loop biology.

Though R-loops primarily form co-transcriptionally, they can form in *trans*. Second, there is a throughline linking R-loop biology to initiation of DNA replication.

In eukaryotic nuclear genomes, the link between R-loops and initiation of DNA replication failed to be established. Instead, the first study demonstrating that R-loops can form in the eukaryotic genome and serve an important physiological function came from work in B cells. This research coupled bisulfite-treatment with PCR sequencing to demonstrate that R-loops form *in vivo* (Yu et al. 2003). Importantly, the formation of R-loops across the immunoglobulin class switch locus in cultured spleen cells was dependent upon activation with LPS, demonstrating that R-loops formed specifically as a response to transcription (Yu et al. 2003). In addition to demonstrating that R-loops form in cells and could serve a function at the immunoglobulin class switch region, this study highlights two additional aspects of R-loop biology. The bisulfite treatment to specifically mark the displaced strand of DNA has been repeatedly used to confirm, and more accurately map, the extent of R-loops. In addition, later research would show that the targeting of the class switch recombination machinery was due to extensive deamination along the exposed single-strand of DNA and subsequent formation of double-stranded breaks (Chaudhuri et al. 2003; Nambu et al. 2003). The link between R-loop formation and DNA damage would soon come to greater attention. Li and Manley published their seminal work demonstrating that loss of the spicing factor protein ASF/SF2 resulted in cell death and quiescence (Li and Manley, 2005). This phenotype was due to high levels of DNA damage that they linked to formation of R-loops (Li and Manley, 2005). Overexpression of RNase H1 was able to suppress this phenotype (Li and Manley, 2005). This work was bolstered by the previous observation that THO complex mutants in yeast resulted in DNA damage (Huertas and Aguilera, 2003).

These works demonstrated important biology behind R-loop formation. In *trans*, R-loop formation is thought to occur more easily in underwound DNA, where the RNA molecule can invade and displace the two strands of DNA (Toriumi et al. 2013). In *cis*, where cotranscriptional R-loops form, R-loop formation is slightly more complicated. Transient RNA:DNA hybrids form at the site of active transcription within the RNA polymerases (Nudler et al. 1997; Daube and von Hippel 1994). However, work in bacteria and T4 systems had previously demonstrated that extensive R-loop formation occurs after the nascent transcript has exited the polymerase where it reanneals back to still accessible single-stranded DNA (Roy and Lieber 2009). This is referred to as a *cis* R-loop. The propensity of RNA processing and splicing factors to suppress R-loop formation is thought to be a result of these factors ability to bind the nascent transcript and prevent it from reannealing to the DNA (Sollier and Cimprich, 2015). Separately, the nucleotide sequence of the displaced strand also impacts the propensity to form R-loops. For example, transcription from the sense but not the antisense direction of the class-switch region forms R-loops *in vitro* (Yu et al. 2003). The ability of the displaced single strand of DNA to form secondary structures strongly impacts R-loop formation (Belotserkovskii et al. 2010, 2017). If the non-template strand at the transcription bubble forms a G-quadruplex, a common DNA secondary structure formed by repetitive guanines, it can be stabilized and fail to quickly reform duplex DNA (de Magis et al. 2019). This exposes the template strand and allows the RNA to reanneal, forming an R-loop.

With the advent of next generation sequencing, it has become apparent that many diseases and cancers have recurrent mutations in RNA processing factors (Dvinge et al. 2016). The recent fascination with R-loops as a potential driver for oncogenesis and

genome instability arises partially from these findings. However, the question of how R-loops cause such dramatic DNA damage has not been completely defined, though recent research has provided valuable insight. There are thought to be two main types of DNA damage that result from R-loop formation (Fig. 1-3E). The major type has been found to be S phase dependent and seems to occur where a replication fork and R-loop meet (Gan et al. 2011). By combining estrogen-inducible transcription with flow cytometry to determine the cell cycle, widescale R-loop induced damage only occurred during S phase when replication forks would be active (Stork et al. 2016). Extensive work in bacteria and metazoan systems has linked how precisely the interplay between replication and transcription and how it can cause DNA damage.

The less severe class of genomic instability arises solely from the existence of the R-loop and potentially damage to the displaced single-strand of DNA (Beletskii and Bhagwat, 1996; Kim and Jinks-Robertson, 2012). This can be the result of deamination of the cytosine in cells that express cytosine deaminase or endogenous factors that react with single-strand DNA (Conticello 2008). This results in a specific mutational signature of cytosine to thymidine transitions and other point mutations (Beletskii and Bhagwat, 1996). However, there is compelling research to show that in some cases, this damage can be more extensive. In hyperactive R-loop forming mutants, the activity of transcription-coupled nucleotide excision repair (TC-NER) repair proteins such as XPF and XPG can cause double-strand breaks at R-loop forming sites (Sollier et al. 2014). The mechanism of this activity is thought to be from cleavage of the single-strand DNA at the edges of the R-loop (Sollier et al. 2014). Coupled with breaks in the displaced strand,

this can result in double-strand breaks. However, it is unclear if this phenomenon is coupled to replication or not (Crstini et al. 2019).

The orientation of both the replication fork and the transcription complex in R-loop driven DNA damage is important. Conflicts between replication and transcription can occur both co-directionally, in which the replication fork progresses in the same direction as the transcription complex, or head-on where the two complexes collide. Work in bacteria engineered to transcribe ribosomal RNA either codirectionally or in the head-on orientation with respect to the origin of replication demonstrated that only transcription in the head-on orientation resulted in a delay of the replication fork (French 1992). Bacterial genomes are generally arranged to minimize head-on conflicts between transcription and replication, though there are exceptions such as genes associated with stress survival (Rocha, 2008, Merrikh 2017). It is hypothesized that the head-on orientation for transcription associated with these loci is to encourage DNA damage and therefore increased mutagenesis to promote adaptation to stress (Merrikh and Merrikh, 2018). Additional work by the Merrikh lab linked the formation of R-loops specifically with head-on conflicts (Lang et al. 2017). Importantly, expression of RNase H III allowed for these conflicts to be resolved, as measured by lack of DNA damage and normal gene expression indicating that the R-loop, not the transcription machinery is responsible for the damage (Lang et al. 2017). One thing that is not clear is how R-loop formation occurs in these conflicts. Presumably, a stalled RNA polymerase allows for a permissive environment for R-loop formation. Active transcription is known to cause positive DNA supercoiling in front of the polymerase, and negative supercoiling behind it (Liu and Wang, 1987; Wu et al. 1988). The unwinding of DNA during replication also generates

positive supercoiling in front of the replication fork (Vos et al. 2011). This torsional stress could alter the dynamics at both the stalled replication fork and RNA polymerase machinery, allowing a more permissive environment for R-loops to form and change the stability of replication and transcription proteins on DNA. In this scenario, the resolution of R-loops would be required to allow the proper release of torsional stress. This model is supported by multiple lines of evidence demonstrating that topoisomerases are associated with R-loop formation and resolution (Lang and Merrikh, 2021; Manzo et al. 2018; Promonet et al. 2020).

The evidence for DNA damage due to replication-transcription conflicts in metazoans is also compelling. Common fragile sites are loci that frequently exhibit chromosomal instability (Debatisse et al. 2012). This damage is frequently transcription dependent (Debatisse et al. 2012). Common fragile sites are frequently found at long and/or highly transcribed genes, where transcription of a single gene may take an entire cell cycle (Helmrich et al. 2011). It has become apparent that directionality also plays an important role in metazoans. In yeast, plasmids undergo recombination when transcription occurs only in the head-on direction (Prado and Aguilera, 2005). Using an episomal system, Hamperl et al. demonstrated that head-on but not codirectional conflicts resulted in increased R-loop levels (Hamperl et al. 2017). By combining R-loop mapping data and Okazaki fragment sequencing data (OK-seq), which allows one to determine the directionality of the replication fork, R-loops were found to occur more frequently in head-on collisions. Importantly, greater R-loop-dependent DNA damage occurs by perturbing the normal replication program (Hamperl et al. 2017). Head-on collisions also activate the ATR DNA damage checkpoint, which often occurs at slowed or stalled replication forks.

It is important to note that not all codirectional conflicts are without damage. In bacteria with deficient transcript termination and translation, codirectional conflicts are also capable of forming double-strand breaks (Dutta et al. 2011). In eukaryotes, codirectional conflicts results in elevated activation of ATM, a DNA damage marker normally associated with double-strand breaks (Hamperl et al. 2017; Lee and Paull 2021). This activation may be due to very rare but damaging codirectional conflicts. It is not clear if this is the case or what factor(s) may precipitate these events if they do occur. Alternatively, it has been hypothesized that activation of ATM results in alternative splicing and transcription of DNA damage response genes and/or spliceosome components in order to help resolve R-loops (Tresini et al. 2016). In summary, conflicts between replication and transcription are an important source of genome instability. When they occur in the head-on orientation, they result in increased R-loop formation and DNA damage. Codirectional conflicts frequently, though not always, result in decreased R-loop levels and little to no DNA damage.

In addition to their roles in causing DNA damage, RNA:DNA hybrids also function to sense DNA damage and repair it. Work by the Zou group has demonstrated that RPA, a single-stranded DNA binding protein, is capable of binding the displaced DNA strand of an R-loop (Nguyen et al. 2017). This interaction is important for the recruitment of RNase H1 to resolve R-loops (Nguyen et al. 2017). The Zou group also showed that the ATR pathway can be activated during mitosis and this activation is dependent on R-loops (Kabeche et al. 2018). R-loop-dependent activation of ATR is dependent on Aurora A kinase, but how precisely ATR is activated by R-loops is still unknown. It appears to be via a separate mechanism than how ATR is normally activated, which normally occurs

via binding of RPA to single-stranded DNA and recruitment of the Rad9-Hus1-Rad1 complex to resected 3' DNA ends (Saldivar et al. 2017).

R-loops also serve important roles in the repair of double-stranded breaks (Fig. 1-3D) (DSB). The role of small non-coding RNAs generated by the DROSHA and DICER pathways had been previously linked to repair of DSB and activation of the DNA damage response (Francia et al. 2012). DRIP-ChIP and yeast genetics were combined with an inducible DSB system to probe whether R-loops form at DSBs. R-loops were shown to form at the induced site and manipulation of RNase H levels to stabilize or degrade R-loops resulted in repair defects (Ohle et al. 2016). Overexpression of RNase H led to excessive resection at DSBs, while loss of RNase H led to impaired RPA binding, slower repair, and increased chromosomal recombination (Keskin et al. 2014; Ohle et al. 2016). Later work suggested a role for R-loops in stimulating homologous recombination at DSBs in mitosis and meiosis (Ouyang et al. 2021; Yang et al. 2021). It has been hypothesized that, in addition to controlling recruitment of RPA and resection at DSBs, R-loops may play a role in guiding DSB repair factors to DSBs (D'Alessandro et al. 2018). R-loops that form at DSBs appear to form in *cis* via permissive transcription of the ssDNA, and RNA polymerase II is found at these sites (Ohle et al. 2016). However, both human and yeast Rad52, an important protein involved with DSB repair and homologous recombination, has been shown to catalyze formation of RNA:DNA hybrids *in vitro* (Keskin et al. 2014). It is therefore unclear if the R-loops at DSBs form in *cis*, *trans*, or some combination thereof. More research will be necessary to understand how, precisely, R-loops promote effective DSB repair, but it is clear they serve an important function.

R-loops have been linked to numerous human pathologies. The tumor suppressors BRCA1 and BRCA2 have been implicated in R-loop resolution (Racca et al. 2021; Bhatia et al. 2014). Components of the Fanconi-Anemia complex have also been linked to R-loop resolution (García-Rubio et al. 2015). Beyond tumorigenesis and genome stability, R-loops have been linked to a variety of neurodegenerative disorders. In cell lines derived from Friedreich's ataxia patients, R-loops have been shown to form at trinucleotide repeats and cause transcriptional silencing (Groh et al. 2014). Similarly, R-loops have been found at the promoter regions of FMR1 and may also cause gene silencing (Colak et al. 2014). Senataxin mutants have been an important tool to study R-loops as it was one of the first proteins found to unwind R-loops (Skourti-Stathaki et al. 2011). These mutations are also found in patients with oculomotor apraxia type 2 (AOA2) and amyotrophic lateral sclerosis type 4 (ALS4) (Groh et al. 2017). The recurrent findings of R-loops associated with human disease underscores the importance of understanding R-loops.

The advent of next-generation sequencing and the rediscovery of the S9.6 antibody, which specifically binds to the RNA:DNA moiety in an R-loop, recontextualized R-loop formation and abundance in the eukaryotic genome. Work done by the Chédin lab established DNA:RNA immunoprecipitation sequencing (DRIP-seq) and demonstrated that instead of being a rare byproduct of transcription, R-loops form at thousands of sites across the mammalian genome, occupying over 5% of the genome (Ginno et al. 2012). In the years since, R-loop mapping studies in bacteria, yeast, plants, insects and mammals demonstrated consistently high levels of R-loop formation, ranging from 5-10% of the mappable genome (Santos-Pereira and Aguilera, 2015; Dumelie and Jaffrey 2018;

Wahba and Koshland et al. 2016; Fang and Zhang et al. 2019; Xu and Sun et al. 2017; Yan and Liu et al. 2020; Zeller and Gasser et al. 2016; Chen and Fu et al. 2017; Chen and Fazzio et al. 2015; Crossley and Cimprich et al. 2020; Ginno and Chédin et al. 2012; Tan-Wong and Proudfoot et al. 2019; Chan and Hieter et al. 2014; Liu and Han et al. 2021). The presence of R-loops in all these species led to a new and deeper understanding of the regulatory functions of R-loops across the genome and where R-loops are prone to forming.

R-loops are most frequently found at the promoter, the 5'UTR, TSS, TTS and 3' UTR of genes (Sanz et al. 2016). Though they seem more likely to form in highly transcribed genes, especially the ribosomal DNA locus, high transcription is not a requirement (Sanz et al. 2016). R-loops are frequently found from the beginning of the 5' UTR and up to the first intron of genes (Sanz et al. 2016). They can also form across entire gene bodies in highly transcribed genes without introns (Sanz et al. 2016). In fact, insertion of introns into R-loop forming genes showed that recruitment of the splicing machinery reduced overall R-loop levels (Bonnet et al. 2017). R-loops also seem to form at sites of repetitive DNA such as centromeres and satellite DNA (Sanz et al. 2016; Zeng et al. 2021). This finding seemed surprising, as these sites are often thought of as transcriptionally repressed, and the function of R-loops at these sites is not well understood.

Though R-loops form throughout the genome, why they form and what their function is at each site varies. Since R-loops were first mapped in mammalian cells, their properties and genome-wide positions have been best characterized in mammals (Ginno et al. 2012). Perhaps the most well understood sites of R-loop formation is at promoters

and transcription start sites, where the CpG skew provides an ideal environment for stabilization of the displaced ssDNA due to secondary structures and reinvasion of the RNA to form R-loops (Fig. 1-3B) (Ginno et al. 2013). R-loops at these sites fall into two main types: TSS anchored that form across the promoter and through the TSS, and R-loop anchored that begin downstream of the transcription start site (TSS) in the exon and extend to the first intron (Chédin 2016). TSS anchored R-loops are characterized by chromatin that is highly accessible, histone modifications associated with active transcription such as H3K4me2/3, H3K9ac, and H3K27ac, and tend to have unmethylated promoters (Chédin 2016). At R-loop anchored regions, pausing of the RNA polymerase is more common and histone modifications are enriched for H3K36me and H3K4me1 (Chédin 2016). In contrast, R-loops at transcription termination sites (TTS) are enriched for repressive histone modifications such as H3K9me2 (Skourti-Stathaki et al. 2014). At TTS, R-loops seem to play a role in halting the RNA polymerase and causing transcript termination as well (Fig. 1-3C) (Skourti-Stathaki et al. 2011; Proudfoot 2016). Similarly, R-loops at repetitive elements are also associated with repressive histone modification (Nadel et al. 2015). The question of whether R-loops are more likely to form at sites of these chromatin markers and certain chromatin associated factors or whether they help establish the epigenetic environment around them is a question of vital importance to the field.

At promoters, R-loops prevent methylation of DNA. *In vitro* studies examining the binding of DNMT1 and DNMT3a/b, the maintenance and *de novo* DNA methyltransferases, respectively, demonstrated that they cannot efficiently bind to R-loops (Ross et al. 2010). Later work examining *Senataxin* hyperactive mutants that

decrease R-loops genome-wide had increased DNA methylation at hundreds of genes with concomitant gene silencing (Grunseich et al. 2018). Even in this seemingly clearcut case, however, there may be interplay between R-loop formation and the epigenetic landscape. Loss of the TET family of the enzymes, responsible for demethylating DNA, causes decreased R-loop formation without changes in transcription (Sabino et al. 2022). Conversely, tethering of a TET enzyme to a specific locus increases R-loop formation (Sabino et al. 2022). The authors hypothesize that 5hmC, an intermediate of the demethylation of cytosine (5mC), may promote R-loop formation and lend credence to this idea with *in vitro* assays (Sabino et al. 2022). This dynamic exchange between R-loop formation and DNA methylation, where a seemingly simple blockage of a protein by an R-loop becomes more complex with further investigation, highlights the difficulty in interpreting the causative role of R-loops in establishing the epigenetic landscape.

What is the evidence that R-loops modify the chromatin in their environment? Degradation of R-loops directly impacts the binding of PRC2 and Tip60-p400 and alters the histone markers at specifically at R-loop sites (Chen et al. 2015). Both proteins have biochemical evidence that they can interact with the nascent RNA of an R-loop (Guttman et al. 2011; Alecki et al. 2020). Additionally, a screen using histone mutants in yeast linked R-loop formation to H3S10P and chromatin compaction (Castellano-Pozo et al. 2013).

However, other evidence is much more corollary. H3K4me3 is enriched at promoters and the H3K4me3 methyltransferase SET1/COMPASS can theoretically bind to the single strand of an R-loop (Krajewski et al. 2005). Binding for PAF1 and LSD1, a histone methyltransferase and demethylase, respectively, are enriched at R-loops (Sanz et al. 2016; Pinter et al. 2021). A combination of mining of deposited ChIP-seq data and

new mass spectrometry screens for R-loop interacting proteins has revealed a plethora of potential candidates that could be recruited to R-loops and modify the chromatin (Sanz et al. 2016; Cristini et al. 2018; Wang et al. 2018; Mosler et al. 2021). While many of these interactions will be validated, there will undoubtedly be false positives. In addition, how the correct histone modifying proteins are recruited to R-loops at different regions despite their similar structure is entirely unknown.

It is also not fully understood which aspects of R-loop formation are universal or species specific. For example, yeast are much more likely to form R-loops over polyA tracts than other species (Wahba et al. 2016). In plants, antisense R-loops are more common and have been studied as important determinant of gene repression (Xu et al. 2017). For example, formation of R-loops at the promoter of COOLAIR causes transcriptional repression (Sun et al. 2013). In maize, extensive R-loop formation occurs at centromeres (Liu et al. 2021). R-loops formed from circular RNA help establish chromatin loops and cause deposition of CENH3, the centromeric H3 variant (Liu et al. 2020). While R-loops may serve similar functions in other species, as of now it is unknown.

In my thesis, I have conducted research examining how DNA replication is alternatively regulated during development. I identified a new function for the Rif1 protein controlling replication fork progression during underreplication and gene amplification. Quantitative mass spectrometry was performed of replication forks during *Drosophila* embryogenesis to identify their components. Finally, I adapted a technique to map R-loops during *Drosophila* embryogenesis. This work expanded our knowledge of the factors associated with R-loops formation and how they change during development.

Chapter II: Rif1 inhibits replication fork progression and controls DNA copy number in *Drosophila*

Abstract

Control of DNA copy number is essential to maintain genome stability and ensure proper cell and tissue function. In *Drosophila* polyploid cells, the SNF2-domain-containing SUUR protein inhibits replication fork progression within specific regions of the genome to promote DNA underreplication. While dissecting the function of SUUR's SNF2 domain, we identified an interaction between SUUR and Rif1. Rif1 has many roles in DNA metabolism and regulates the replication timing program. We demonstrate that repression of DNA replication is dependent on Rif1. Rif1 localizes to active replication forks in a partially SUUR-dependent manner and directly regulates replication fork progression. Importantly, SUUR associates with replication forks in the absence of Rif1, indicating that Rif1 acts downstream of SUUR to inhibit fork progression. Our findings uncover an unrecognized function of the Rif1 protein as a regulator of replication fork progression.

* This chapter has been published as Munden, A., Rong, Z., Sun, A., Gangula, R., Mallal, S. & Nordman, J. T. Rif1 inhibits replication fork progression and controls DNA copy number in *Drosophila*. *Elife* **7**, e39140 (2018).

Introduction

Accurate duplication of a cell's genetic information is essential to maintain genome stability. Proper regulation of DNA replication is necessary to prevent mutations and other chromosome aberrations that are associated with cancer and developmental abnormalities (Jackson et al., 2014). DNA replication begins at thousands of cis-acting sites termed origins of replication. The Origin Recognition Complex (ORC) binds to replication origins where, together with Cdt1 and Cdc6, it loads an inactive form of the MCM2-7 replicative helicase (Bell and Labib, 2016). Inactive helicases are phosphorylated by two key kinases, S-CDK and Dbf4-dependent kinase (DDK), which results in the activation of the helicase and recruitment of additional factors to form a pair of bi-directional replication forks emanating outward from the origin of replication (Siddiqui et al., 2013). Although many layers of regulation control the initiation of DNA replication, much less is known about how replication fork progression is regulated.

In metazoans, replication origins are not sequence specific and are likely specified by a combination of epigenetic and structural features (Aggarwal and Calvi, 2004; Cayrou et al., 2011; Eaton et al., 2011; Mesner et al., 2011; Miotto et al., 2016; Remus et al., 2004). Furthermore, replication origins are not uniformly distributed throughout the genome. The result of non-uniform origin distribution is that, in origin-poor regions of the genome, a single replication fork must travel great distances to complete replication. If a replication fork encounters an impediment within a large origin-less region of the genome, then replication will be incomplete, resulting in genome instability (Newman et al., 2013). In fact, origin-poor regions of the genome are known to be associated with chromosome fragility and genome instability (Debatisse et al., 2012; Durkin and Glover, 2007; Letessier

et al., 2011; Norio et al., 2005). This highlights the need to regulate both the initiation and elongation phases of DNA replication to maintain genome stability.

DNA replication is also regulated in a temporal manner where specific DNA sequences replicate at precise times during S phase, a process known as the DNA replication timing program. While euchromatin replicates in the early part of S phase, heterochromatin and other repressive chromatin types replicate in the latter portion of S phase (Gilbert, 2002; Rhind and Gilbert, 2013). Although the process of replication timing has been appreciated for many years, the underlying molecular mechanisms controlling timing have remained elusive. The discovery of factors that regulate the DNA replication timing program, however, demonstrate that replication timing is an actively regulated process.

One factor that regulates replication timing from yeast to humans is Rif1 (Rap1-interacting factor 1). Rif1 was initially identified as a regulator of telomere length in budding yeast (Hardy et al., 1992), but this function of Rif1 appears to be specific to yeast (Xu et al., 2004). Subsequently, Rif1 has been shown to regulate multiple aspects of DNA replication and repair. In mammalian cells, Rif1 has been shown to regulate DNA repair pathway choice by preventing resection of double-strand breaks and favoring non-homologous end joining (NHEJ) over homologous recombination (Chapman et al., 2013; Di Virgilio et al., 2013; Zimmermann et al., 2013). Rif1 from multiple organisms contains a Protein Phosphatase 1 (PP1) interaction motif and Rif1 is able to recruit PP1 to DDK-activated helicases to inactivate them and prevent initiation of replication (Davé et al., 2014; Hiraga et al., 2014; Hiraga et al., 2017).

In yeasts, flies and mammalian cells, Rif1 has been shown to regulate the replication timing program (Cornacchia et al., 2012; Hayano et al., 2012; Peace et al., 2014; Sreesankar et al., 2015; Yamazaki et al., 2012). The precise mechanism(s) through which Rif1 functions to control replication timing are not fully understood. For example, Rif1 has been shown to interact with Lamin and is thought to tether specific regions of the genome to the nuclear periphery (Foti et al., 2016). How this activity is related to Rif1's ability to inactivate helicases together with PP1 in controlling the timing program remains obscure.

Studying DNA replication in the context of development provides a powerful method to understand how DNA replication is regulated both spatially and temporally. Although DNA replication is a highly ordered process, it must be flexible enough to accommodate the changes in S phase length and cell cycle parameters that occur as cells differentiate (Matson et al., 2017). For example, during *Drosophila* development the length of S phase can vary from ~8 hr in a differentiated mitotic cell to 3 – 4 min during early embryonic cell cycles (Blumenthal et al., 1974; Spradling and Orr-Weaver, 1987). Additionally, many tissues and cell types in *Drosophila* are polyploid, having multiple copies of the genome in a single cell (Edgar and Orr-Weaver, 2001; Lilly and Duronio, 2005; Zielke et al., 2013).

In polyploid cells, copy number is not always uniform throughout the genome (Rudkin, 1969; Hua and Orr-Weaver, 2017; Spradling and Orr-Weaver, 1987). Both heterochromatin and several euchromatic regions of the genome have reduced DNA copy number relative to overall ploidy (Nordman et al., 2011). Underreplicated euchromatic regions of the genome share key features with common fragile sites in that they are

devoid of replication origins, late replicating, display DNA damage and are tissue-specific (Andreyeva et al., 2008; Nordman et al., 2014; Sher et al., 2012; Yarosh and Spradling, 2014). The presence of underreplication is conserved in mammalian cells, but the mechanism(s) mammalian cells use to promote underreplication is unknown (Hannibal et al., 2014). In *Drosophila*, underreplication is an active process that is largely dependent on the distribution of ORC and on the Suppressor of Underreplication protein, SUUR (Hua et al., 2018; Makunin et al., 2002; Nordman and Orr-Weaver, 2015).

Understanding how the SUUR protein functions will significantly increase our understanding of the developmental control of DNA replication. The SUUR protein has a recognizable SNF2-like chromatin remodeling domain at its N-terminus, but based on sequence analysis, this domain is predicted to be defective for ATP binding and hydrolysis (Makunin et al., 2002; Nordman and Orr-Weaver, 2015). Outside of the SNF2 domain, SUUR has no recognizable motifs or domains, which has hampered a mechanistic understanding of how SUUR promotes underreplication. Recently, however, SUUR was shown to control copy number by directly reducing replication fork progression (Nordman et al., 2014). SUUR associates with active replication forks and while loss of SUUR function results in increased replication fork progression, overexpression of SUUR drastically inhibits fork progression without affecting origin firing (Nordman et al., 2014; Sher et al., 2012). These findings, together with previous work showing that loss of SUUR function has no influence on ORC binding (Sher et al., 2012) and that SUUR associates with euchromatin in an S phase-dependent manner (Kolesnikova et al., 2013), further supports SUUR as a direct inhibitor of replication fork progression within specific regions

of the genome. The mechanism through which SUUR is recruited to replication forks and how it inhibits their progression remains poorly understood.

Here we investigate how SUUR is recruited to replication forks and how it inhibits fork progression. We show that localization of SUUR to replication forks, but not heterochromatin, is dependent on its SNF2 domain. We identify an interaction between SUUR and the conserved replication factor Rif1, indicating they are in the same protein complex. Importantly, we demonstrate that underreplication is dependent on *Rif1*. Critically, we have shown that Rif1 localizes to replication forks in an SUUR-dependent manner, where it acts downstream of SUUR to control replication fork progression. Our findings provide mechanistic insight into the process of underreplication and define a new function for Rif1 in replication control.

Results

The SNF2 domain is essential for SUUR function and replication fork localization

As a first step in understanding the mechanism of SUUR function, we wanted to define how it is localized to replication forks. SUUR has only one conserved domain: a SNF2-like domain in its N-terminal region that is predicted to be defective for ATP binding and hydrolysis (Makunin et al., 2002; Nordman and Orr-Weaver, 2015). To study the function of SUUR's SNF2 domain, we generated a mutant in which the SNF2 domain was deleted and the resulting mutant protein was expressed under the control of the endogenous *SuUR* promoter. This mutant, *SuUR*^{ΔSNF}, was then crossed to an *SuUR* null mutant so that it was the only form of the SUUR protein present (Figure 2-1A). We tested the function of the *SuUR*^{ΔSNF} mutant protein by assessing its ability to promote

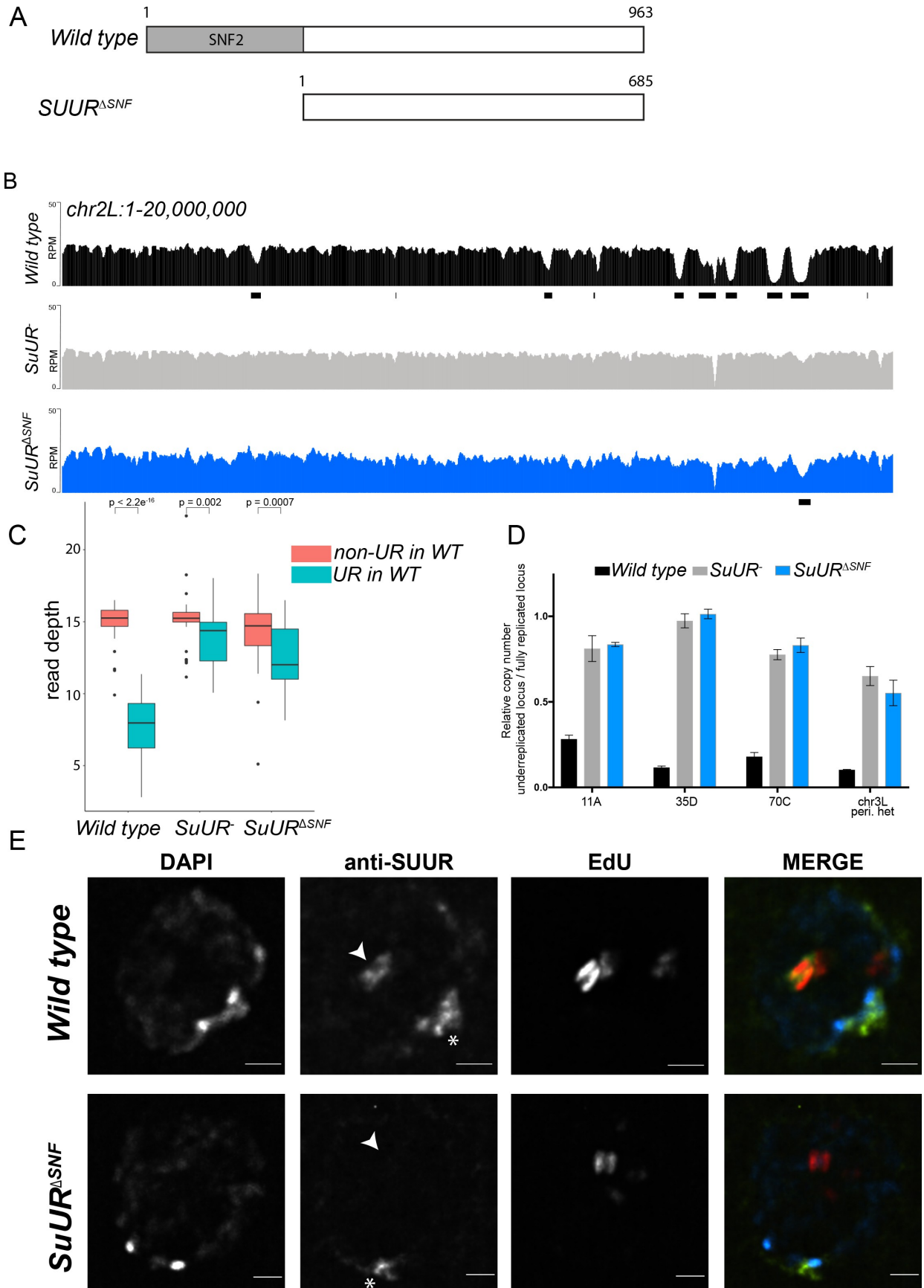


Figure 2-1: The SNF2 domain is essential for SUUR function and replication fork localization. (A) Schematic representation of the SUUR and SUUR^{ΔSNF} proteins. **(B)** Illumina-based copy number profiles (Reads Per Million; RPM) of *chr2L* 1 – 20,000,000 from larval salivary glands. Black bars below each profile represent underreplicated regions identified by CNVnator. **(C)** Average read depth in regions of euchromatic underreplication domains called in wild-type salivary glands vs. the fully replicated regions of the genome. A Welch Two Sample t-test was used to determine p values. **(D)** Quantitative droplet-digital PCR (ddPCR) copy number assay for multiple underreplicated regions. Each bar is the average enrichment relative to a fully replicated control region for three biological replicates. Error bars are the SEM. **(E)** Localization of SUUR in wild-type and *SuUR*^{ΔSNF} mutant follicle cells. A single representative stage 13 follicle cell nucleus is shown. Arrowheads indicate sites of amplification. Asterisk marks the chromocenter (heterochromatin). Scale bars are 2 μm. DAPI = blue, SUUR = green, EdU = red. Contributions: Analysis and visualization of data in B and C.

underreplication in the larval salivary gland. We purified genomic DNA from larval salivary glands isolated from wandering third instar larvae and generated genome-wide copy number profiles using Illumina-based sequencing. We compared the results we obtained from the *SuUR*^{ΔSNF} mutant to copy number profiles from wild-type (WT) and *SuUR* null mutant salivary glands. To identify underreplicated domains, we used CNVnator, which identifies copy number variants (CNVs) based on a statistical analysis of read depth (Abyzov et al., 2011). To be called as underreplicated, regions must not be called as underreplicated in 0 – 2 hr embryo samples that have uniform copy number and must be larger than 10 kb.

The effect of deleting the SNF2 domain was qualitatively and quantitatively similar to the *SuUR* null mutant. Qualitatively, underreplication was suppressed in the *SuUR*^{ΔSNF} mutant and the copy number profile was similar to the *SuUR* null mutant (Figure 2-1B, Supplemental Figure 2-1). Quantitatively, out of the 90 underreplicated sites identified in

WT salivary glands, 59 were not detected in the *SuUR*^{ΔSNF} mutant (Supplementary Table 2-1) and copy number was significantly increased in the euchromatic underreplicated domains similar to the *SuUR* null mutant (Figure 2-1C). We validated our deep-sequencing findings using quantitative droplet digital PCR (ddPCR) at four underreplicated domains (Figure 2-1D). Our findings show that the SNF2-like domain of SUUR is necessary to promote underreplication.

To determine if the *SuUR*^{ΔSNF} protein was still able to associate with chromatin, we localized *SuUR* and the *SuUR*^{ΔSNF} mutant proteins in ovarian follicle cells. During follicle cell development, these cells undergo programmed changes in their cell cycle and DNA replication programs (Claycomb and Orr-Weaver, 2005; Hua and Orr-Weaver, 2017). At a precise time in their differentiation program, follicle cells cease genomic replication and amplify six defined sites of their genome through a re-replication-based mechanism. Early in this gene amplification process, both initiation and elongation phases of replication are coupled. Later in the process, however, initiation no longer occurs and active replication forks can be visualized by pulsing amplifying follicle cells with 5-ethynyl-2'-deoxyuridine (EdU) (Claycomb et al., 2002). Active replication forks resolve into a double-bar structure, where each bar represents a series of active replication forks travelling away from the origin of replication (Claycomb and Orr-Weaver, 2005). By monitoring *SuUR* localization in amplifying follicle cells, we can unambiguously determine if *SuUR* associates with active replication forks.

SuUR has two distinct modes of chromatin association during the endo cycle. It constitutively localizes to heterochromatin and dynamically associates with replication forks (Kolesnikova et al., 2013; Nordman et al., 2014; Swenson et al., 2016). In agreement

with previous studies, SUUR localized to both replication forks and heterochromatin in amplifying follicle cells (Figure 2-1E) (Nordman et al., 2014). In contrast, the SuUR^{ΔSNF} mutant localized to heterochromatin, but its recruitment to active replication forks was severely reduced (Figure 2-1E; Supplemental Figure 2-2). Together, these results demonstrate that the SNF2 domain is important for SUUR recruitment to replication forks and is essential for SUUR-mediated underreplication.

SUUR associates with Rif1

Interestingly, overexpression of the SNF2 domain and C-terminal portion of SUUR have different underreplication phenotypes. Whereas overexpression of the C-terminal two-thirds of SUUR promotes underreplication (Kolesnikova et al., 2005), overexpression of the SNF2 domain suppresses underreplication in the presence of endogenous SUUR (Kolesnikova et al., 2005). The C-terminal region of SUUR, however, has no detectable homology or conserved domains (Makunin et al., 2002). These observations, together with our own results demonstrating that the SNF2 domain of SUUR is responsible for its localization to replication forks, led us to hypothesize that SUUR is recruited to replication forks through its SNF2 domain where it could recruit an additional factor(s) through its C-terminus to inhibit replication fork progression.

To test the hypothesis that a critical factor interacts with the C-terminal region of SUUR to promote underreplication, we used immunoprecipitation mass spectrometry studies to identify SUUR-interacting proteins. We generated flies that expressed FLAG-tagged full-length SUUR or the SNF2 domain of SUUR under control of the *hsp70* promoter, induced and immunoprecipitated these constructs and identified associated

proteins through mass spectrometry. We verified that both full-length SUUR and the SNF2 domain were expressed equally (Supplemental Figure 2-3B). If SUUR recruits a factor to replication forks outside of its SNF2 domain, then we would expect this factor to be present only in full-length purifications and not in the SNF2 domain purification. A single protein fulfilled this criteria: Rif1 (Figure 2-2A). This result raises the possibility Rif1 works together with SUUR to inhibit replication fork progression.

To ensure that the association between SUUR and Rif1 was not bridged by chromatin, we used NP40 to extract chromatin proteins and treated the extract with Benzonase to digest DNA. We then immunoprecipitated FLAG-SUUR and used Western blotting to determine if Rif1 could co-IP using a highly specific anti-Rif1 antibody (Supplemental Figure 2-4). Even in these conditions, SUUR was able to co-IP Rif1 (Figure 2-2B; Supplemental Figure 2-3A). We conclude that SUUR and Rif1 exist in the same protein complex and the interaction between SUUR and Rif1 is independent of chromatin bridging.

Underreplication is dependent on Rif1

If SUUR recruits Rif1 to replication forks to promote underreplication, then underreplication should be dependent on *Rif1*. To test this hypothesis, we used CRISPR-based mutagenesis to generate *Rif1* null mutants in *Drosophila* (Bassett et al., 2013; Gratz et al., 2013) (Figure 2-3A). Western blot analysis of ovary extracts from two deletion mutants, *Rif1*¹ and *Rif1*², show no detectable Rif1 protein (Supplemental Figure 2-4A). Also, no signal was detected in the *Rif1*¹/*Rif1*² mutant by immunofluorescence (Supplemental Figure 2-4B). The *Rif1*¹/*Rif1*² null mutant was viable and fertile showing

A

	Full length SUUR			SNF2 domain			negative control		
	Repl. #1	Repl. #2	Repl. #3	Repl. #1	Repl. #2	Repl. #3	Repl. #1	Repl. #2	Repl. #3
SUUR	36	48	26	21	18	10	1	1	2
Rif1(CG30085)	29	24	14	1	0	0	0	0	0

Comparison of Rif1 abundance*	
Full length vs. SNF2	p < 0.00010
Full length vs. neg. ctrl	p < 0.00010

*Fisher's Exact Test

B

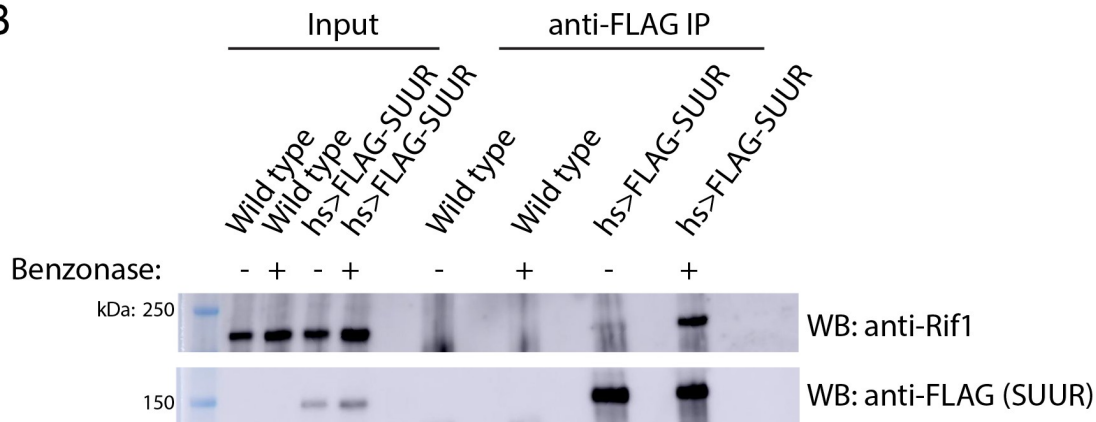


Figure 2-2: **SUUR associates with Rif1.** (A) Total spectrum counts of FLAG-SUUR, FLAG-SNF2 and Oregon R (no FLAG control) for three independent IP-mass spectrometry experiments (biological replicates). A Fisher's Exact test of spectrum counts was used to determine significance. (B) Immunoprecipitation of FLAG-SUUR and no FLAG control (wild-type) from 0 to 24 hr embryos extracted with NP40 lysis buffer with or without Benzonase treatment. Membranes were probed with anti-Rif1 and anti-FLAG antibodies to monitor Rif1 and SUUR, respectively. Contributions: None.

only a modest defect in embryonic hatch rate relative to wild-type flies with a 92% hatch rate for wild-type embryos vs. 88% for the *Rif1¹/Rif²* mutant embryos (Supplemental Figure 2-4C). This is in contrast to a previous study reporting *Rif1* is essential in *Drosophila* (Sreesankar et al., 2015) and consistent with a recent study that generated an independent *Rif1* null mutant using CRISPR-based mutagenesis (Seller and O'Farrell, 2018). *Rif1*'s essentiality, however, was based on RNAi and not a mutation of the *Rif1*

gene (Sreesankar et al., 2015). The most likely explanation for this discrepancy is that the lethality in the RNAi experiments was due to an off-target effect.

To determine if *Rif1* is necessary for underreplication, we dissected salivary glands from *Rif1¹/Rif1²* (herein referred to as *Rif1⁻*) heterozygous larvae and extracted genomic DNA for Illumina-based sequencing to measure changes in DNA copy number. Strikingly, underreplication is abolished upon loss of *Rif1* function (Figure 2-3B,C; Supplemental Figure 2-5). We validated our sequence-based copy number assays with quantitative PCR at a subset of underreplicated regions using ddPCR (Figure 2-3D). Furthermore, we determined the read density at all euchromatic sites of underreplication called in our wild-type samples, which quantitatively demonstrates that *Rif1* is essential for underreplication (Figure 2-3C). These results demonstrate that underreplication is dependent on *Rif1*.

It is possible that the *Rif1* mutant indirectly influences underreplication through changes in replication timing. Underreplicated domains, both euchromatic and heterochromatic, tend to be late replicating regions of the genome (Belyaeva et al., 2012; Makunin et al., 2002). Therefore, if these regions replicated earlier in S phase in a *Rif1* mutant, then this change could prevent their underreplication. In fact, SUUR associates with late replicating regions of the genome (Filion et al., 2010; Pindyurin et al., 2007). Due to their large polyploid nature, salivary gland cells cannot be sorted to perform genome-wide replication timing experiments. Because heterochromatin replicates exclusively in late S phase, however, late replication can be visualized when EdU is incorporated exclusively in regions of heterochromatin. To assess if *Rif1* mutants have a clear pattern of late replication in larval salivary glands, we isolated salivary glands from early 3rd instar larvae, which are actively undergoing endo cycles. We pulsed these salivary glands with

EdU to visualize sites of replication and co-stained with an anti-HP1 antibody to mark heterochromatin. In wild-type salivary glands, only rarely (1 of 238 EdU+ cells; 0.4%) did we detect EdU incorporation in regions of heterochromatin (Supplemental Figure 2-6). This is consistent with the lack of heterochromatin replication due to underreplication. In contrast, in both *SuUR* and *Rif1* mutants, we could readily detect cells that were solely incorporating EdU within regions of heterochromatin (32 of 327 EdU+ cells; 9.8% for *SuUR* and 70 of 385 EdU+ cells; 18.2% for *Rif1*) (Supplemental Figure 2-6). Therefore, we conclude that *Rif1* mutants still have a clear pattern of late replication. Given that heterochromatin underreplication is suppressed in a *Rif1* mutant, although it is still late replicating, indicates that replication timing cannot solely explain the lack of underreplication associated with loss of Rif1 function.

While characterizing Rif1's role in underreplication and patterns of DNA replication in endo cycling cells, we did observe differences in the heterochromatic regions of *SuUR* and *Rif1* mutants. First, although underreplication is suppressed in both mutants (Figure 2-3 and Supplemental Figure 2-5), the chromocenters were abnormally large in the *Rif1* mutant relative to an *SuUR* mutant as observed by DAPI staining consistent with the 'fluffy' enlarged chromocenters seen in *Rif1* mutant mouse cells (Supplemental Figure 2-7) (Cornacchia et al., 2012). Although, this phenotype was present in all endo cycling cells, it was especially dramatic in the ovarian nurse cells (Supplemental Figure 2-7). Second, Illumina-based copy number profiles revealed an increase in copy number in some pericentric heterochromatin regions in the *Rif1* mutant relative to the *SuUR* mutant (Supplemental Figure 2-5). Collectively, these results suggest that heterochromatin is partially, but not fully replicated in *SuUR* mutant endo cycling cells, consistent with

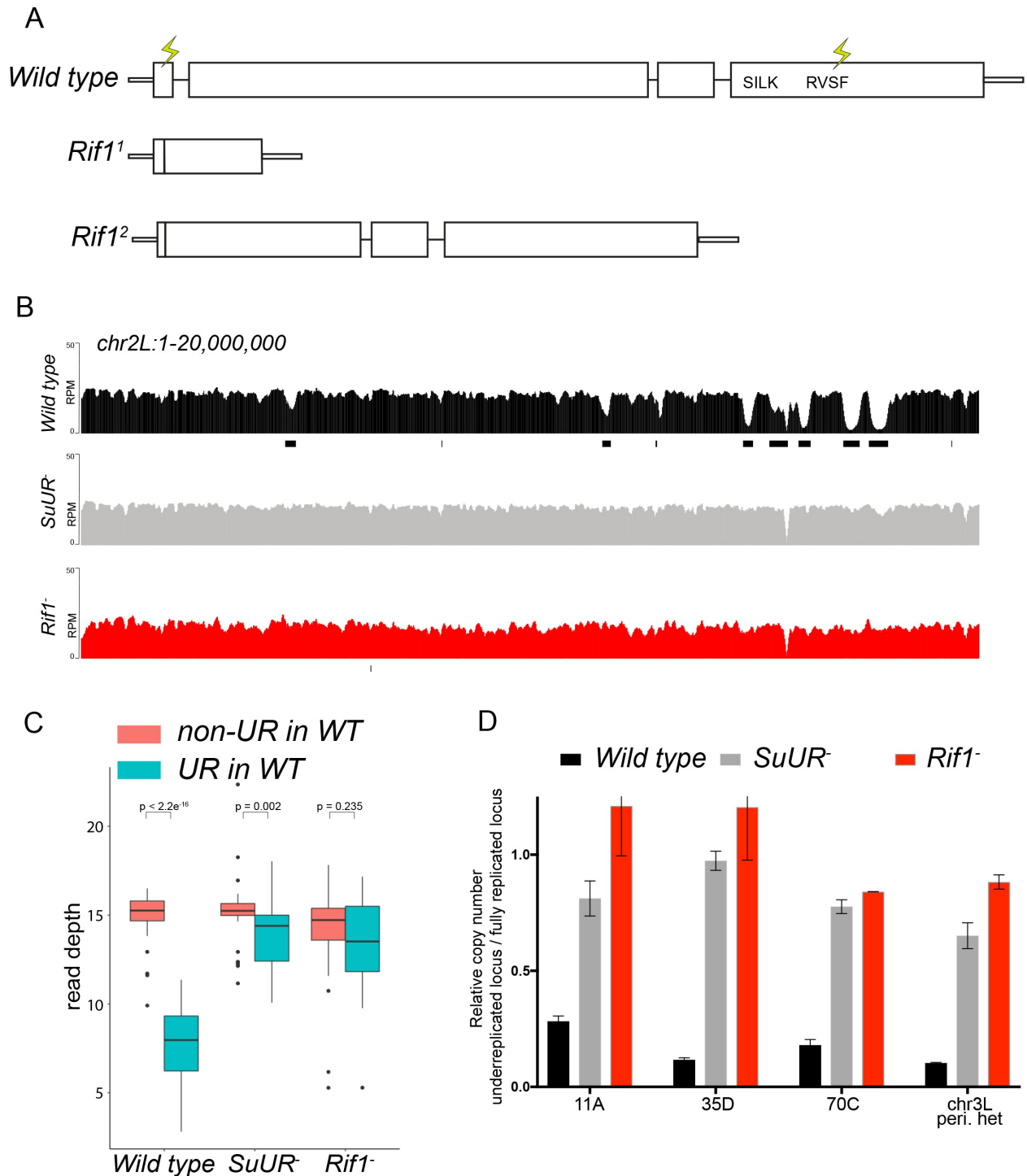


Figure 2-3: *Rif1* is required for underreplication. (A) Schematic representation of the *Rif1* gene and CRISPR-induced *Rif1* mutants. Lightning bolts represent the 5' and 3' gRNA positions. (B) Illumina-based copy number profiles of the *chr2L* from larval salivary glands. Black bars below each profile represent underreplicated regions identified by CNVnator. The wild-type and *SuUR* profiles are the same as in Figure 1b. (C) Average read depth in regions of euchromatic underreplication domains called in wild-type salivary glands vs. the fully replicated regions of the genome. A Welch Two Sample t-test was used to determine p values. (D) Quantitative droplet-digital PCR (ddPCR) copy number assay for multiple underreplicated regions. Each bar is the average enrichment relative to a fully replicated control region for

three biological replicates. Error bars are the SEM. Contributions: Data analysis and visualization for B and C.

previous cytological analysis (Demakova et al., 2007). In contrast, loss of Rif1 function appears to completely restore heterochromatic replication in endo cycling cells.

Rif1 affects replication fork progression

SUUR-mediated underreplication occurs through inhibition of replication fork progression (Nordman et al., 2014; Sher et al., 2012). If SUUR acts together with Rif1 to promote underreplication, then Rif1 is expected to control replication fork progression. DNA combing assays in human and mouse cells from multiple groups have come to different conclusions as to whether Rif1 affects replication fork progression (Alver et al., 2017; Cornacchia et al., 2012; Hiraga et al., 2017; Yamazaki et al., 2012). Rif1, however, has been shown to be associated with replication forks through nascent chromatin capture, an iPOND-like technique used to isolate proteins associated with active replication forks (Alabert et al., 2014). To determine directly if Rif1 controls replication fork progression, we performed copy number assays on amplifying follicle cells.

Gene amplification in ovarian follicle cells occurs at six discrete sites in the genome through a re-replication based mechanism. Copy number profiling of these amplified domains provides a quantitative assessment of the number of rounds of origin firing and the distance replication forks have travelled during the amplification process, allowing us to disentangle the initiation and elongation phases of DNA replication. To determine if Rif1 affects origin firing and/or replication fork progression, we isolated wild-type and *Rif1* mutant stage 13 egg chambers, which represent the end point of the amplification process, and made quantitative DNA copy number measurements. Loss of Rif1 function

resulted in an increase in replication fork progression without significantly affecting copy number at the origin of replication at all sites of amplification (Figure 2-4A). The increase in fork progression observed in the *Rif1* mutant was not due to a lengthening of the developmental time window for gene amplification, as there was no significant difference in egg chamber distribution between wild-type and *Rif1* mutant ovaries (Supplemental Figure 2-8).

To quantify the changes in fork progression we observed at sites of amplification, we computationally determined the peak of amplification and the region on each arm of the amplified domain that represents one half of the copy number at the highest point of the amplicon (Nordman et al., 2014). This quantitative analysis of origin firing and replication fork progression revealed that origin firing was not affected in the *Rif1* mutant, as no major change in copy number was detected at the origin of replication when comparing wild type and *Rif1* mutant stage 13 follicle cells (Supplementary Table 2-2). In contrast, the width of each replication gradient, which represents the rate of fork progression, was significantly increased at all sites of amplification (Figure 2-4A; Supplementary Table 2-2). Based on the observation that the *Rif1* mutant does not affect origin firing, but specifically affects the distance replication forks travel during the gene amplification process, and there was no change in the developmental window of gene amplification in the *Rif1* mutant, we conclude that *Rif1* regulates replication fork progression.

Given that the *Rif1* mutant phenocopies an *SuUR* mutant with respect to replication fork progression, we next wanted to determine the cause of increased replication fork progression at amplified loci upon loss of *Rif1* function. Previously, it was shown that a

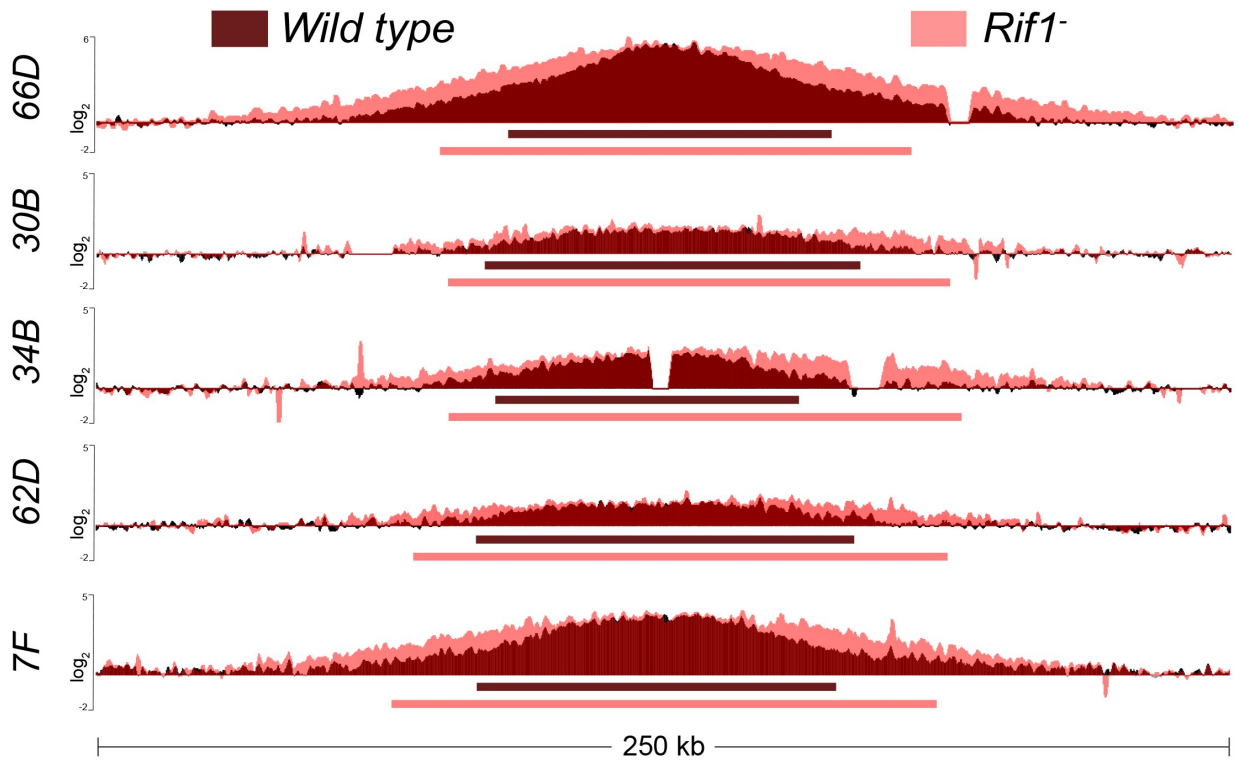
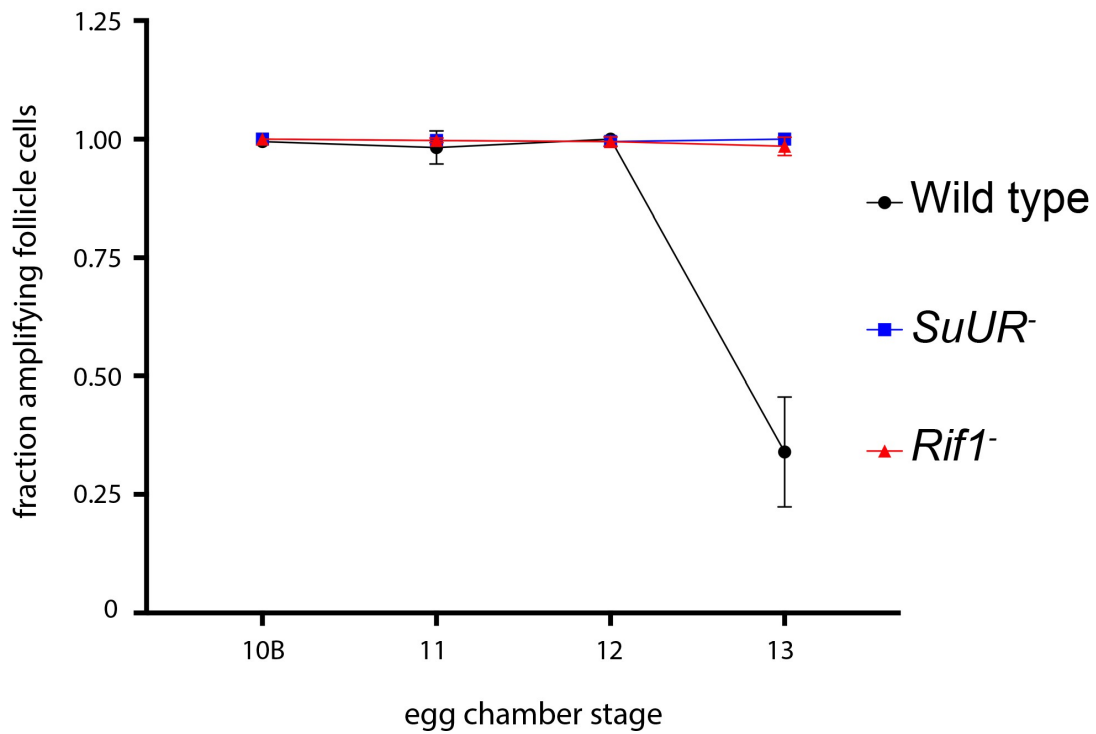
A**B**

Figure 2-4: **Rif1 regulates replication fork progression.** (A) Illumina-based copy number profile of sites of follicle cell gene amplification. DNA was extracted from wild type and *Rif1* mutant stage 13 egg chambers and compared to DNA extracted from 0 to 2 hr embryos. The resulting graphs are the \log_2 -transformed ratios of egg chamber relative to embryonic DNA. Bars below the graphs represent the distance between the half-maximum copy number on each side of the replication origin. (B) Fraction of cells that display visible amplification foci in each stage of gene amplification. Average of two biological replicates in which two egg chambers from each stage were used per biological replicate. 100 – 300 follicle cells were counted per genotype. Error bars are the SEM. Contributions: Analysis and visualization for A.

prolonged period of EdU incorporation in the *SuUR* mutant, within the 7.5 hr span of gene amplification, gives rise to the extended replication gradient at sites of amplification (Nordman et al., 2014). Gene amplification starts synchronously in all follicle cells at stage 10B of egg chamber development (Calvi et al., 1998). By the end of gene amplification, however, only a subset of follicle cells display visual amplification foci as judged by EdU incorporation, likely representing a stochastic end to the gene amplification process (Nordman et al., 2014). To determine if Rif1 controls replication fork progression by increasing the period of EdU incorporation within the 7.5 hr time window of gene amplification, comparable to an *SuUR* mutant, we quantified the fraction of stage 13 follicle cells that were EdU positive. Similar to an *SuUR* mutant, loss of Rif1 function also resulted in a prolonged period of EdU incorporation with 34% of follicle cells visibly incorporating EdU in wild-type follicle cells, 100% in an *SuUR* mutant and 98.5% in the *Rif1* mutant (Figure 2-4B). This result suggests that Rif1 has a destabilizing effect on replication forks, resulting in a premature cessation of replication fork progression.

Rif1 acts downstream of SUUR

Rif1 could control SUUR activity and underreplication by at least two different mechanisms. Rif1 could act upstream of SUUR and directly or indirectly regulate SUUR's ability to associate with chromatin. For example, Histone H1 and HP1 affect

underreplication by influencing SUUR's ability to associate with chromatin (Andreyeva et al., 2017; Pindyurin et al., 2008). Alternatively, Rif1 could act downstream of SUUR to control replication fork progression. We sought to distinguish between these possibilities by determining whether SUUR could still associate with replication forks in the absence of Rif1 function.

To monitor SUUR's association with heterochromatin and replication forks in the same cell type, we localized SUUR in amplifying follicle cells where replication forks (double bars) and heterochromatin (chromocenter) can be visualized unambiguously, in the presence and absence of Rif1. SUUR localized to both replication forks and heterochromatin in the absence of Rif1 function (Figure 2-5; Supplemental Figure 2-9). Therefore, we conclude that Rif1 acts downstream of SUUR to inhibit fork progression and that SUUR lacks the ability to inhibit replication fork progression in the absence of Rif1.

Rif1 localizes to active replication forks

Although our genetic data indicate that Rif1 affects replication fork progression, we wanted to determine if Rif1 controls replication fork progression through a direct or indirect mechanism. If Rif1 directly influences replication fork progression and/or stability, then it should localize to active replication forks. To assess this possibility, we visualized Rif1 localization during gene amplification in follicle cells using a Rif1-specific antibody (Supplemental Figure 2-3).

Rif1 localization pattern was strikingly similar to that of SUUR. First, Rif1 is localized to heterochromatin in all stages of amplifying follicle cells (Figure 2-6). Second,

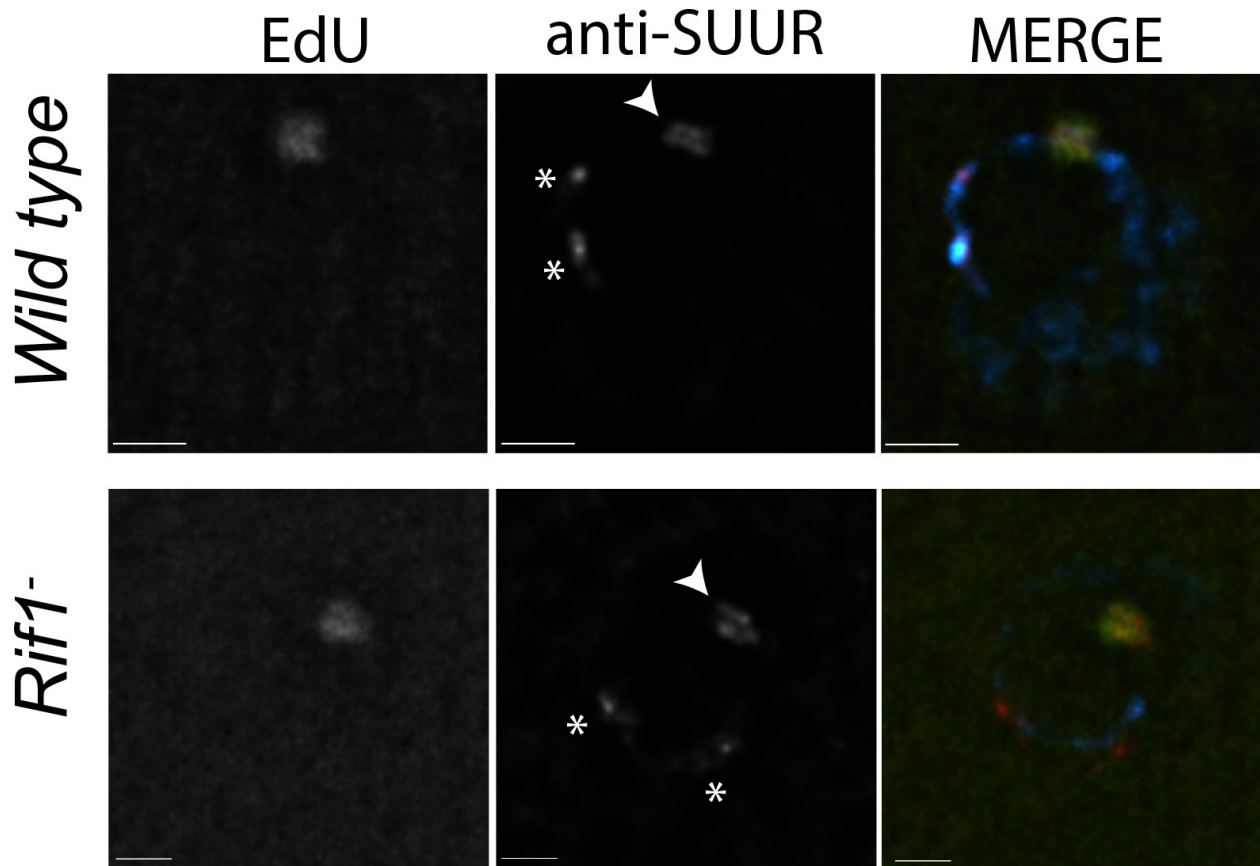
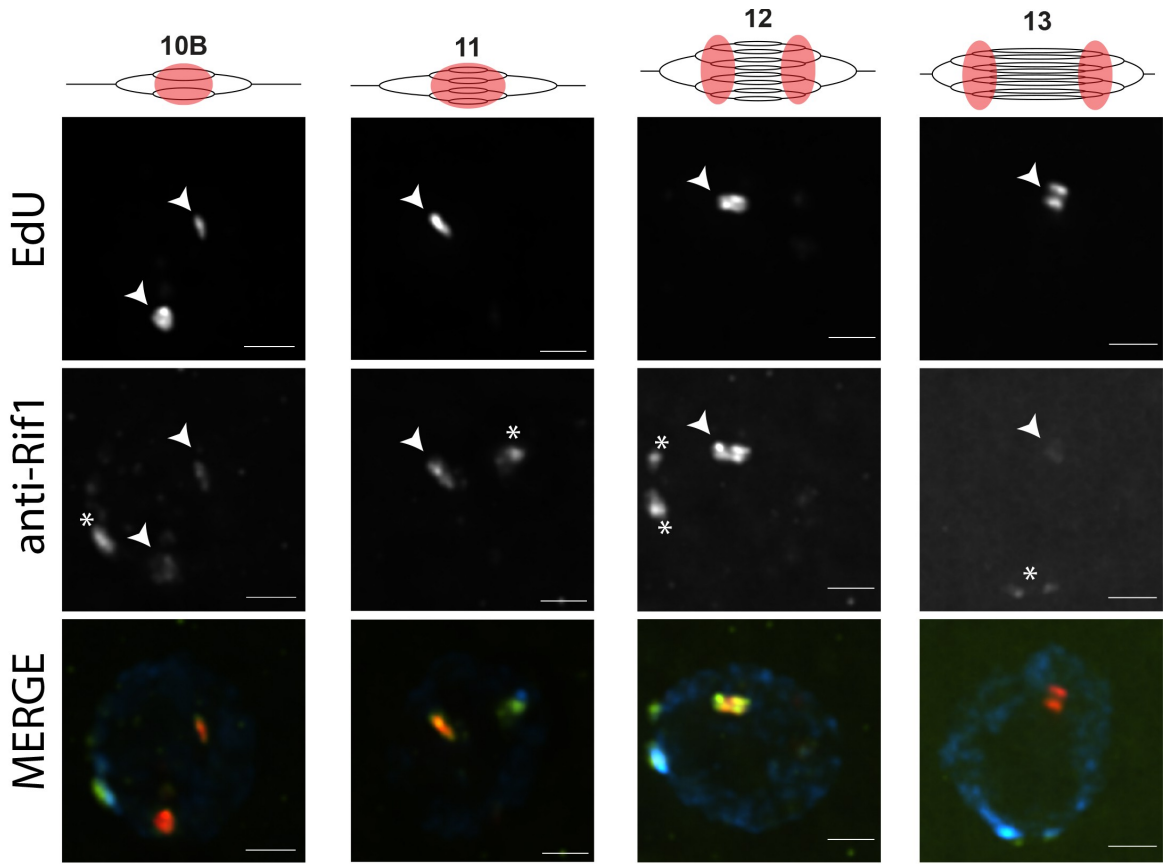


Figure 2-5: **Rif1 acts downstream of SUUR.** Localization of replication forks (EdU) and SUUR in a wild-type and *Rif1* mutant follicle cell nuclei. A single representative stage 13 follicle cell nucleus is shown. Scale bars are 2 μ m. Arrowheads indicate sites of amplification. Asterisks marks the chromocenter (heterochromatin). DAPI = blue, SUUR = green, EdU = red. Contributions: None.

Rif1 localized to sites of amplification even prior to the formation of double bar structures (Supplemental Figure 2-9). Third, in the later stages of gene amplification Rif1 was localized to active replication forks. Taken together, these results demonstrate that Rif1 dynamically associates with replication forks to regulate their progression.

To verify that Rif1 associates with replication forks in a context other than the gene amplification, we used iPOND to determine if Rif1 is associated with replication forks in cultured *Drosophila* S2 cells. Briefly, cells were pulsed with EdU and immediately fixed in formaldehyde or chased with thymidine prior to fixation. Proteins associated with newly synthesized DNA (replication forks) can be identified based on their enrichment in pulse

Wild type



SuUR⁻

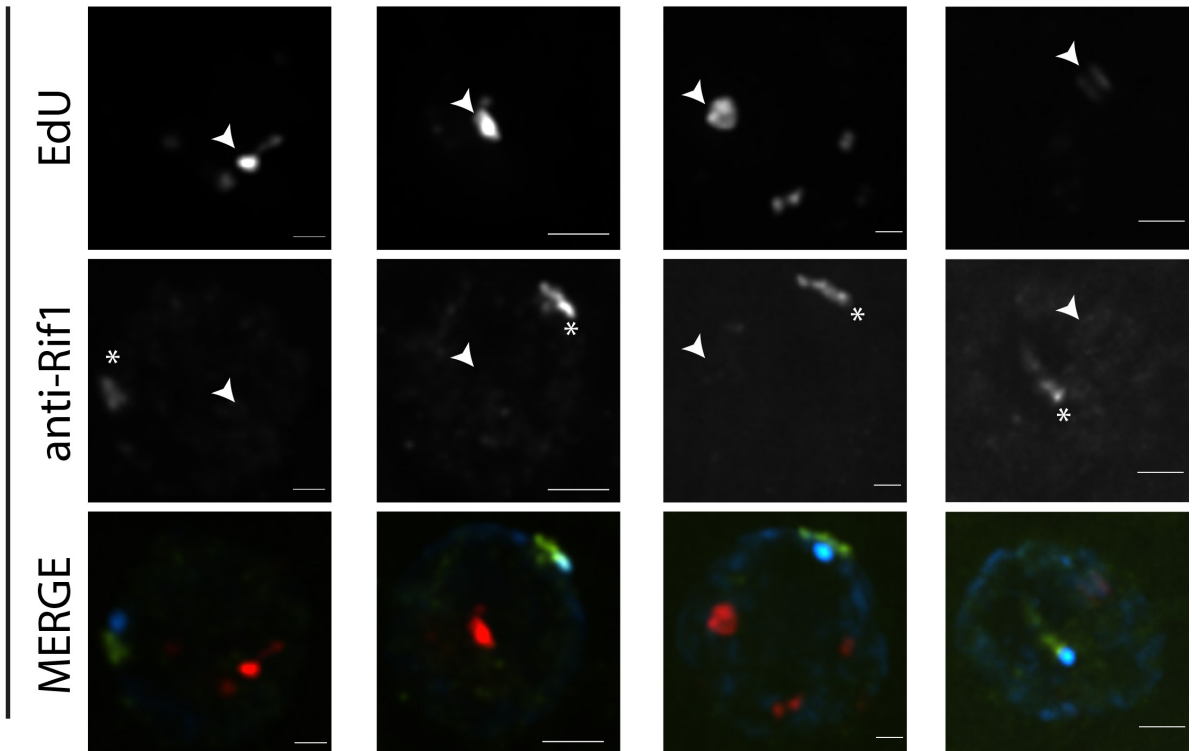


Figure 2-6: **SUUR is necessary to retain Rif1 at replication forks.** Localization of active replication forks (EdU) and Rif1 in a wild-type and *SuUR* mutant follicle cell nuclei. Single representative follicle cell nuclei are shown for each stage. Scale bars are 2 μ m. Arrowheads indicate sites of amplification. Asterisk marks the chromocenter (heterochromatin). Contributions: None.

samples relative to chase samples (Dungrawala and Cortez, 2014; Sirbu et al., 2011). We used mass spectrometry to quantify Rif1 protein abundance in EdU pulse and chase samples (Sirbu et al., 2013). Consistent with Rif1 association with replication forks in amplifying follicle cells, Rif1 was enriched in EdU pulse samples relative to chase samples in cultured cells (Supplemental Figure 2-11A). Although this enrichment was not as abundant as our PCNA-positive control, this is expected for a protein that associates with a subset of replication forks.

To independently verify that Rif1 is localized to replication forks in cultured cells, we performed a proximity ligation assay (PLA)-based approach with nascent DNA (Roy et al., 2018; Tagliatalata et al., 2017). *Drosophila* S2 cells were pulsed with EdU, fixed and EdU was subsequently biotinylated. A PLA assay was then performed using two different anti-biotin antibodies as a positive control, or an anti-biotin antibody together with an anti-Rif1 antibody. As a negative control, the same PLA assays were performed using cells that were not pulsed with EdU. Consistent with our iPOND mass-spec results, PLA foci were generated using anti-Rif1 and anti-biotin antibodies only when cells were pulsed with EdU (Supplemental Figure 2-11B). Together, these results indicate that Rif1 is associated with replication forks in amplifying follicle cells and cultured cells.

SUUR is required to retain Rif1 at replication forks

Based on our observations that SUUR and Rif1 are part of the same protein complex, and that a *Rif1* mutant phenocopies an *SuUR* mutant, we hypothesized that

SUUR recruits a Rif1/PP1 complex to replication forks. If true, then Rif1 association with replication forks should be at least partially dependent on SUUR. To test this hypothesis, we monitored the localization of Rif1 in *SuUR* mutant amplifying follicle cells. We found that Rif1's association with replication forks was largely dependent on SUUR, as the Rif1 signal was lost in late-stage amplifying follicle cells in an *SuUR* mutant (Supplemental Figure 2-10). Rif1's recruitment to replication foci, however, was not completely dependent on SUUR. In a subset of stage 10B and 11 egg chambers, when both initiation of replication and fork progression are still coupled, we observed Rif1 localization to amplification foci in a subset of follicle cells (Supplemental Figure 2-10). Rif1 staining was lost, however, in stage 12 and 13 egg chambers. We conclude that while the initial recruitment of Rif1 to sites of amplification is not completely dependent on SUUR, SUUR is necessary to retain Rif1 at replication forks.

The PP1-interacting motif of Rif1 is necessary for underreplication

Because Rif1 is known to recruit PP1 to replication origins to regulate initiation, this led us to ask if the same interaction between Rif1 and PP1 is important for Rif1's regulation of replication fork progression. Rif1 associates with Protein Phosphatase 1 (PP1) through a conserved interaction motif, thereby recruiting PP1 to MCM complexes and inactivating them (Davé et al., 2014; Hiraga et al., 2017; Hiraga et al., 2014). PP1 has also been shown to associate with Rif1 in *Drosophila* (Seller and O'Farrell, 2018; Sreesankar et al., 2015). Based on this model of Rif1 function, we wanted to determine if Rif1's PP1 interaction motif was necessary for Rif1-mediated underreplication. We used CRISPR-based mutagenesis to mutate the conserved SILK/RSVF PP1 interaction motif

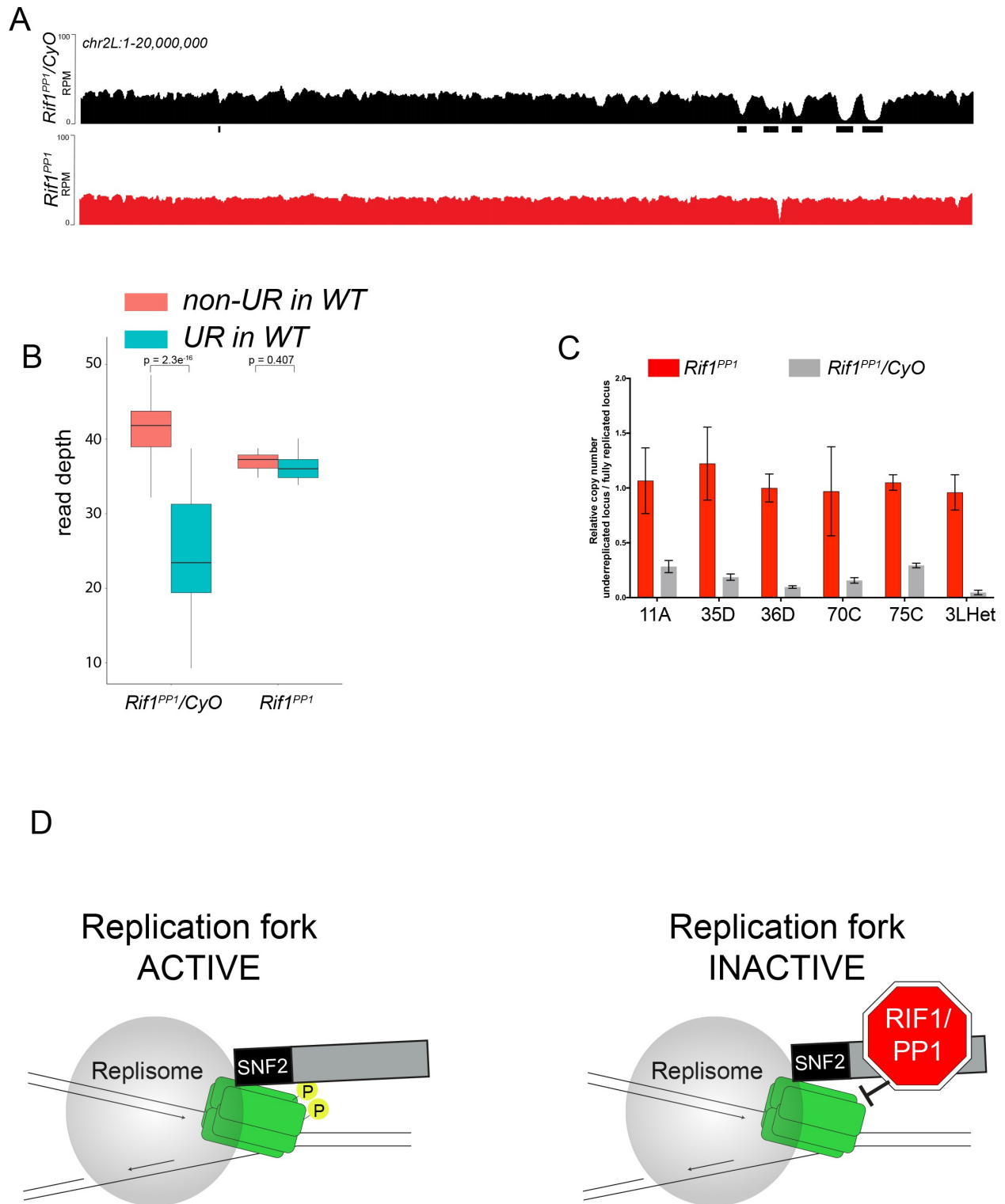


Figure 2-7: The Rif1 PP1 interaction motif is necessary to promote underreplication. (A) Illumina-based copy number profiles of *chr2L* 1 - 20,000,000 from larval salivary glands. Black bars below each profile represent underreplicated regions identified by CNVnator. *Rif1^{PP1}/CyO* was used as the wild-type control. (B) Average read depth in regions of euchromatic underreplication domains called in wild-type salivary glands vs. the fully replicated regions of the genome. A Welch two-sample t-test was used to

determine p values. (C) Quantitative droplet-digital PCR (ddPCR) copy number assay for multiple underreplicated regions. Each bar is the average enrichment relative to a fully replicated control region for three biological replicates. Error bars are the SEM. (D) A new model for SUUR-mediated underreplication. In this model, SUUR serves as a scaffold to recruit a Rif1/PP1 complex to replication forks where Rif1/PP1 inhibits replication fork progression through dephosphorylation of a component of the replisome. Contributions: Analysis and visualization of A and B.

to SAAK/RASA. Western blot analysis showed that mutation of the SILK/RSVF motif did not affect protein stability (Supplemental Figure 2-12). Mutation of this motif has been shown to disrupt the Rif1/PP1 interaction in organisms from yeast to humans (Alver et al., 2017; Davé et al., 2014; Hiraga et al., 2017; Hiraga et al., 2014; Mattarocci et al., 2014; Sreesankar et al., 2015; Sukackaite et al., 2017). We isolated salivary glands from wandering 3rd instar larvae of the *Rif1^{PP1}* mutant and *Rif1^{PP1/+}* heterozygous animals as a wild-type control. We then extracted DNA and generated genome-wide copy number profiles by Illumina sequencing. Similar to the Rif1 mutant, underreplication was largely abolished in the *Rif1^{PP1}* mutant (Figure 2-7A-C; Supplemental Table 2-1). Thus, Rif1's PP1-interaction motif is necessary to promote underreplication, suggesting that PP1 is a mediator of underreplication. It still remains possible, however, that an additional protein(s) could interact with this motif to promote underreplication.

Discussion

The SUUR protein is responsible for promoting underreplication of heterochromatin and many euchromatin regions of the genome. Although SUUR was recently shown to promote underreplication through inhibition of replication fork progression, the underlying molecular mechanism has remained unclear. Through biochemical, genetic, genomic and cytological approaches, we have found that SUUR recruits Rif1 to replication forks and that Rif1 is responsible for underreplication. This

model is supported by several independent lines of evidence. First, SUUR associates with Rif1, and SUUR and Rif1 co-localize at sites of replication. Second, underreplication is dependent on Rif1, although *Rif1* mutants have a clear pattern of late replication in endo cycling cells. Third, SUUR localizes to replication forks and heterochromatin in a *Rif1* mutant, however, it is unable to inhibit replication fork progression in the absence of Rif1. Fourth, Rif1 controls replication fork progression and phenocopies the effect loss of SUUR function has on replication fork progression. Fifth, SUUR is required for Rif1 localization to replication forks. Critically, using the gene amplification model to separate initiation and elongation of replication, we have shown that Rif1 can affect fork progression without altering the extent of initiation. Based on these observations, we have defined a new function of Rif1 as a regulator of replication fork progression.

SNF2 domain and fork localization

Our work suggests that the SNF2 domain of SUUR is critical for its ability to localize to replication forks. This is based on the observation that deletion of this domain results in a protein that is unable to localize to replication forks, but still localizes to heterochromatin. SUUR has previously been shown to dynamically localize to replication forks during S phase, but constitutively binds to heterochromatin (Kolesnikova et al., 2013; Nordman et al., 2014). SUUR associates with HP1 and this interaction occurs between the central region of SUUR and HP1 (Pindyurin et al., 2008). Therefore, we speculate that the interaction between SUUR and HP1 is responsible for constitutive SUUR localization to heterochromatin, while a different interaction between the SNF2

domain and a yet to be defined component of the replisome, or replication fork structure itself, recruits SUUR to active replication forks during S phase.

Uncoupling of SUUR's ability to associate with replication forks and heterochromatin also provides a new level of mechanistic understanding of underreplication. Overexpression of the C-terminal two-thirds of SUUR is capable of inducing ectopic sites of underreplication. In contrast, overexpression of the SUUR's SNF2 domain, in the presence of endogenous SUUR, suppresses SUUR-mediated underreplication (Kolesnikova et al., 2005). Together with the data presented here, we suggest that overexpression of the SNF2 domain interferes with recruitment of full-length SUUR to replication forks, by saturating potential SUUR binding sites at the replication fork. Although the C-terminal region of SUUR is necessary to induce underreplication (Kolesnikova et al., 2005), the C-terminal portion of SUUR remains associated with heterochromatin in the SuUR^{ΔSNF} construct, but this protein is not sufficient to induce underreplication. We suggest that at physiological levels, the affinity of SUUR for replication forks is substantially diminished in the absence of the SNF2 domain. Our work raises questions about the biological significance of SUUR binding to heterochromatin, since without the SNF2 domain SUUR is still constitutively bound to heterochromatin, yet unable to induce underreplication. Additionally, SUUR dynamically associates with heterochromatin in mitotic cells although heterochromatin is fully replicated (Swenson et al., 2016).

Rif1 controls underreplication

While trying to uncover the molecular mechanism through which SUUR is able to inhibit replication fork progression, we have uncovered an interaction between SUUR and Rif1. Through subsequent analysis, we demonstrated that Rif1 has a direct role in copy number control and that Rif1 acts downstream of SUUR in the underreplication process. Although underreplication is largely dependent on SUUR, there are several sites that display a modest degree of underreplication in the absence of SUUR (Demakova et al., 2007; Sher et al., 2012). In a *Rif1* mutant, however, these sites are fully replicated and there is no longer any detectable levels of underreplication within any regions of the genome. It is possible that Rif1 is capable of promoting underreplication through a mechanism independent of SUUR. Therefore, we conclude that Rif1 is a critical factor in driving underreplication.

Further emphasizing the critical role Rif1 plays in copy number control, we have shown that Rif1 acts downstream of SUUR in promoting underreplication. SUUR is still able to associate with chromatin in the absence of Rif1 but is unable to promote underreplication. Underreplicated regions of the genome, including heterochromatin, tend to be late replicating, raising the possibility that changes in replication timing in a *Rif1* mutant suppresses underreplication. *Rif1* mutant endo cycling cells of *Drosophila* display a cytological pattern of late replication, where heterochromatin is discretely replicated. While Rif1 controls replication timing in *Drosophila* and is necessary for the onset of late replication at the mid-blastula transition (Seller and O'Farrell, 2018), we argue that the changes in copy number associated with loss of Rif1 function are not solely due to a loss of late replication. This is supported by the clear pattern of late replication of heterochromatin in *Rif1* mutant endo cycling cells, although heterochromatin appears to

be fully replicated in these cells. Previous work in mammalian polyploid cells has shown that underreplication is dependent on Rif1, which was attributed to changes in replication timing (Hannibal and Baker, 2016). It is important to note that Rif1-dependent changes in replication timing were not measured in this system and that many genomic regions transition from early to late replication in a *Rif1* mutant (Foti et al., 2016). Our work raises the possibility that Rif1 has a direct role in mammalian underreplication through a mechanism similar to that of *Drosophila* and may not simply be due to indirect changes in replication timing. Future work will be necessary to define the role of mammalian Rif1 in underreplication.

Rif1 regulates replication fork progression

Our analysis of amplification loci demonstrates that Rif1 controls replication fork progression independently of initiation control, thus demonstrating that Rif1 has a specific effect on replication fork progression. Therefore, we have uncovered a new role for Rif1 in DNA metabolism as a regulator of replication fork progression and copy number control. Rif1 has been identified as part of the replisome in human cells by nascent chromatin capture, a technique that identifies proteins associated with newly synthesized chromatin (Alabert et al., 2014). Multiple studies have assessed whether loss of Rif1 function affects replication fork progression in yeast, mouse and human cells, but have come to different conclusions (Alver et al., 2017; Cornacchia et al., 2012; Hiraga et al., 2017; Yamazaki et al., 2012). DNA fiber assays have been used to measure fork progression in these studies and nearly all have shown that *Rif1* mutants have a slight increase in replication fork progression, although not always statistically significant. There

could be several reasons for these differing results; Rif1 may control replication fork progression in specific genomic regions that may be underrepresented in some assays, Rif1 function could vary among different cell types, or sample sizes may have been too small to reach significance. Our observations, taken together with these previous studies, leave open the possibility that Rif1-mediated control of replication fork progression could be an evolutionarily conserved function of Rif1. We do not suggest that Rif1 is constitutively associated with replication forks in all cell types. Rather, Rif1 could be recruited to replication forks at a specific time in S phase, or in specific developmental contexts, to modulate the progression of replication forks and provide an additional layer of regulation of the DNA replication program.

How could SUUR and Rif1 function in concert to inhibit replication fork progression? We have shown that Rif1 retention at replication forks is dependent on SUUR. Additionally, underreplication depends on Rif1's PP1-binding motif, raising the possibility that a Rif1/PP1 complex is necessary to inhibit replication fork progression. Rif1/PP1 dephosphorylates DDK-activated helicases to control replication initiation (Davé et al., 2014; Hiraga et al., 2017; Hiraga et al., 2014). More recently, however, DDK-phosphorylated MCM subunits were shown to be necessary to maintain CMG association and stability of the helicase (Alver et al., 2017). This result suggests that continued phosphorylation of the helicase is necessary for replication fork progression (Alver et al., 2017). We propose that SUUR recruits Rif1/PP1 to replication forks where it is able to dephosphorylate MCM subunits, ultimately inhibiting replication fork progression. Although this mechanism needs to be tested biochemically, it provides a framework to address the underlying molecular mechanism responsible for controlling DNA copy

number and could provide new insight into the mechanism(s) Rif1 employs to regulate replication timing.

Materials and Methods

Key Resources Table

Reagent (species) or resource	type	Designation	Source or reference	Identifiers	Additional information
Gene (<i>Drosophila melanogaster</i>)		<i>Suppressor of Underreplication (SuUR)</i>	NA	FBgn0025355	
Gene (<i>D. melanogaster</i>)		<i>Rap1 interacting factor 1 (Rif1)</i>	NA	FBgn0050085	
Strain, background (<i>D. melanogaster</i>)	strain	WT: Oregon R			
Strain, background (<i>D. melanogaster</i>)	strain	<i>SuUR</i>	(Makunin et al., 2002) PMID: 11901119		<i>w¹¹⁸; SuUR^{ES}</i>
Strain, background (<i>D. melanogaster</i>)	strain	<i>SuUR^{ΔSNF}</i>	This paper		<i>SuUR^{ES}, PBac{w⁺ SuUR^{ΔSNF}}</i>
Strain, background (<i>D. melanogaster</i>)	strain	<i>hs > FLAG-SUUR</i>	This paper		<i>w¹¹⁸; hs > FLAG-SUUR</i>
Strain, background (<i>D. melanogaster</i>)	strain	<i>hs > FLAG-SNF2</i>	This paper		<i>w¹¹⁸; hs > FLAG-SNF2</i>
Strain, background (<i>D. melanogaster</i>)	strain	<i>Rif1¹</i>	This paper		<i>w¹¹⁸; Rif1¹</i>
Strain, background (<i>D. melanogaster</i>)	strain	<i>Rif1²</i>	This paper		<i>w¹¹⁸; Rif1²</i>
Strain, background (<i>D. melanogaster</i>)	strain	<i>Rif1⁻</i>	This paper		<i>w¹¹⁸; Rif1¹/Rif1²</i>

Strain, background (D. melanogaster)	strain <i>Rif1^{PP1}</i>	This paper		<i>w¹¹⁸</i> ; <i>Rif1^{PP1}</i>
Cell line (D. melanogaster)	S2-DGRC	Drosophila Genomics Resource Center (DGRC)	embryo derived	isolate of S2 used for RNAi in the DRSC modENCODE line
Antibody	anti-SUUR (Guinea pig, polyclonal)	(Nordman et al., 2011) PMID: 25437540		
Antibody	anti-Rif1 (Guinea pig, polyclonal)	This paper		(1:200)
Antibody	anti-Rif1 (Rabbit, polyclonal)	This paper		(1:1000)
Antibody	HRP-anti-FLAG (Mouse, monoclonal)	Sigma-Aldrich	A8592	(1:1000)
Antibody	anti-HP1 (Mouse, monoclonal)	The Developmental Studies Hybridoma Bank (DSHB)	C1A9	(1:1000)
Antibody	anti-biotin (Mouse, monoclonal)	Sigma-Aldrich	SAB4200680	(1:20,000)
Antibody	anti-biotin (rabbit, polyclonal)	Bethyl	A150-109A	(1:3,000)
Antibody	HRP-secondaries	Jackson ImmunoResearch		(1:20,000)
Recombinant DNA reagent	pCaSpeR-hs	(Thummel and Pirrotta, V.) Drosophila Genomics Resource Center		
Recombinant DNA reagent	pStinger	(Barolo et al., 2000) PMID: 11056799		
Recombinant DNA reagent	CHORI-322 (CH322-163L18)	BACPAC Resources		
Recombinant DNA reagent	pET17b	Millipore-Sigma	69663	
Recombinant DNA reagent	pET17b-Rif1 (694–1094)	This paper		Progenitors:PCR, pET17b
Peptide, recombinant protein	Rif1(694–1094)	This paper		Ni-NTA purified
Commercial assay or kit	PLA probes	Duolink Sigma		
Commercial assay or kit	PLA probemaker	Duolink Sigma	DUO92010	
Commercial assay or kit	PLA Detection Reagents	Duolink Sigma	DUO92008	

Chemical compound, drug	Alexa Fluor Azide 555	Life Technologies	A20012	
Chemical compound, drug	Biotin-TEG Azide	Berry and Associates	BT 1085	
Chemical compound, drug	EdU (5-ethynyl-2-deoxyuridine)	Life Technologies	A10044	
Software, algorithm	Sequest	Thermo Scientific		
Software, algorithm	Scaffold 4.3.4	Proteome Software		
Software, algorithm	Skyline version 4.1	Schilling et al. (2012) (PMID:22454539)		
Software, algorithm	deepTool 2.5.0	Ramírez et al. (2016) (PMID:27079975)		
Software, algorithm	CNVnator 0.3.3	Abyzov et al., 2011 (PMID:21324876)		

Strain List

JTN110: WT – Oregon R

JTN109: $SuUR^-$ – w^{118} ; $SuUR^{ES}$

JTN038: $SuUR^{\Delta SNF}$ – $SuUR^{ES}$, $PBac\{w^+ SuUR^{\Delta SNF}\}$

JTN143: w^{118} ; $hs > FLAG-SUUR$

JTN146: w^{118} ; $hs > FLAG-SNF2$

JTN305: w^{118} ; $Rif1^1$

JTN307: w^{118} ; $Rif1^2/Rif1^-$ – w^{118} ; $Rif1^1/Rif1^2$

JTN292: $Rif1^{PP1}$ – w^{118} ; $Rif1^{PP1}$

BAC-mediated recombineering

BAC-mediated recombineering (Sharan et al., 2009) was used to delete the portion of the *SuUR* gene corresponding to the SNF2 domain. An *attB-P[acman]* clone with a 21

kb genomic region containing the *SuUR* and a *galk* insertion in the *SuUR* coding region (described in [Nordman et al., 2014]) was used as a starting vector. Next, a gene block (IDT) was used to replace the *galk* cassette and generate a precise deletion within the *SuUR* gene. The resulting vector was verified by fingerprinting, PCR and sequencing. The *SuUR*^{ΔSNF} BAC was injected into a strain harboring the 86 F8 landing site (Best Gene Inc.).

Generation of heat shock-inducible, FLAG-tagged SuUR transgenic lines

The portion of the *SuUR* gene encoding the SNF2 domain (amino acids 1 to 278) was fused to the SV40 NLS (Barolo et al., 2000) and a 3X-FLAG tag sequence was added to the 5' end of *SuUR* SNF2 sequence. The resulting construct was cloned into the pCaSpeR-hs vector, which contains a *hsp70* promoter (Thummel and Pirrotta, V.: Drosophila Genomics Resource Center), using the NotI and XbaI restriction sites. A 3X-FLAG tag sequence was added to the 5' end of the *SuUR* coding region and cloned into the pCaSpeR-hs vector also using the NotI and XbaI restriction sites. The resulting constructs were verified by sequencing and injected into a *w*¹¹¹⁸ strain (Best Gene Inc.).

CRISPR mutagenesis

To generate null alleles of *Rif1*, gRNAs targeting the 5' and 3' ends of the *Rif1* gene were cloned into the pU6-BbsI plasmid as described (Gratz et al., 2015) using the DRSC Find CRISPRs tool (<http://www.flyrnai.org/crispr2/index.html>). Both gRNAs were co-injected into a *nos-Cas9* expression stock (Best Gene Inc.). Surviving adults were individually crossed to *CyO/Tft* balancer stock and *CyO*-balanced progeny

were screened by PCR for a deletion of the *Rif1* locus. Stocks harboring a deletion were further characterized by sequencing. Both *Rif1*¹ and *Rif1*² mutants had substantial deletions of the *Rif1* gene and both had frame shift mutations early in the coding region. *Rif1*¹ has a frame shift mutation at amino acid 14, whereas *Rif1*² has a frame shift mutation at amino acid 11.

To generate a *Rif1* allele defective for PP1 binding, the pU6-BbsI vector expressing the gRNA targeting the 3' end of *Rif1* was co-injected with a recovery vector that contained the mutagenized SILK and RVSV (SAAK and RASA) sites with 1 kb of homology upstream and downstream of the mutagenized region. Surviving adults were crossed as above and screened by sequencing.

Cytological analysis and microscopy

Ovaries were dissected from females fattened for two days on wet yeast in Ephrussi Beadle Ringers (EBR) medium (Beadle and Ephrussi, 1935). Ovaries were pulsed with 5-ethynyl-2-deoxyuridine (EdU) for 30 min, fixed in 4% formaldehyde and prepared for immunofluorescence (IF) as described (Nordman et al., 2014).

For IF using both anti-Rif1 and anti-SUUR antibodies, ovaries were dissected, pulsed with 50 μ M EdU and fixed. Ovaries were then incubated in primary antibody (1:200) overnight at 4°C. Alexa Fluor secondary antibodies (ThermoFisher) were used at a dilution of 1:500 for 2 hr at room temperature. EdU detection was performed after incubation of the secondary antibody using Click-iT Alexa Fluor-555 or -488 (Invitrogen). All images were obtained using a Nikon Ti-E inverted microscope with a Zyla sCMOS

digital camera. Images were deconvolved and processed using NIS-Elements software (Nikon).

For salivary gland IF, third instar larvae were collected prior to the wandering stage. Salivary glands were dissected in EBR, pulsed with 50 μ M EdU for 30 min and fixed with 4% formaldehyde. Salivary glands were incubated in anti-HP1 antibody (Developmental Studies Hybridoma Bank; C1A9) overnight at 4°C. Alexa Fluor secondary antibodies staining and Click-iT EdU labeling were performed as described above.

Image quantification

All images were quantified using Nikon NIS- Elements AR v4.40. To determine Rif1 and SUUR signal intensities at sites of gene amplification, Regions Of Interest (ROIs) were identified based on the EdU intensity. SUUR or Rif1 mean signal intensity was then determined within each ROI. Ten randomly selected regions outside of the nucleus were selected and the mean signal intensity for these regions were averaged to determine the background signal for each image. The average background signal was subtracted from the signal at amplified regions to normalize each image for varying amounts of background. To quantify the SUUR signal intensity at heterochromatin, SUUR ROIs were manually defined due to their non-uniform shape. The sum intensity of the fluorescent signal within these regions were extracted. The sum signal intensity was then normalized to ROI area to account for the difference in shape of each ROI. To quantify PLA signals, ROIs were generated based on DAPI signal to mark all nuclei. PLA foci were then identified for each image and the number of foci in each DAPI ROI was determined.

Rif1 antibody production

Rif1 antiserum was produced in guinea pigs and rabbits (Cocalico Biologicals Inc.). Briefly, a Rif1 protein fragment from residues 694 – 1094 (Sreesankar et al., 2012) was C-terminally six-histidine tagged and expressed in *E. coli* Rossetta DE3 cells and purified using Ni-NTA Agarose beads (Qiagen). The purified protein was used for injection (Cocalico Biologicals Inc.) and serum was affinity purified as described (Moore and Orr-Weaver, 1998). Affinity purified guinea pig anti-Rif1 antibody was used for immunofluorescence.

IP-mass spec

Flies containing heat shock-inducible *SuUR* transgenes were expanded into population cages. 0 – 24 hr embryos were collected, incubated at 37°C for 1 hr, and allowed to recover for one hour following heat shock treatment. Wild-type embryos were used as a negative control. Embryos were dechorionated in bleach and fixed for 20 min in 2% formaldehyde. Approximately 0.5 g of fixed and dechorionated embryos were used for each replicate. Embryos were disrupted by douncing in Buffer 1 (Shao et al., 1999), followed by centrifugation at 3000 x g for 2 min at 4°C and resuspended in lysis buffer 3 (MacAlpine et al., 2010). Chromatin was prepared by sonicating nuclei for a total of 40 cycles of 30' ON and 30' OFF at max power using a Bioruptor 300 (Diagenode) with vortexing and pausing after every 10 cycles. Cleared lysates were incubated with anti-FLAG M2 affinity gel (Sigma) for 2 hr at 4°C. After extensive washing in LB3 and LB3 with 1M NaCl, proteins were eluted using 3X FLAG peptide (Sigma). Crosslinks were reversed by boiling purified material in Laemmli buffer with β -mercaptoethanol for 20 min.

Immunoprecipitated samples were separated on a 4 – 12% NuPAGE Bis-Tris gel (Invitrogen), proteins were stained with Novex colloidal Coomassie stain (Invitrogen), and destained in water. Coomassie stained gel regions were cut from the gel and diced into 1 mm³ cubes. Proteins were reduced and alkylated, destained with 50% MeCN in 25 mM ammonium bicarbonate, and in-gel digested with trypsin (10 ng/μL) in 25 mM ammonium bicarbonate overnight at 37°C. Peptides were extracted by gel dehydration with 60% MeCN, 0.1% TFA, the extracts were dried by speed vac centrifugation, and reconstituted in 0.1% formic acid. Peptides were analyzed by LC-coupled tandem mass spectrometry (LC-MS/MS). An analytical column was packed with 20 cm of C18 reverse phase material (Jupiter, 3 μm beads, 300 Å, Phenomenex) directly into a laser-pulled emitter tip. Peptides were loaded on the capillary reverse phase analytical column (360 μm O.D. x 100 μm I.D.) using a Dionex Ultimate 3000 nanoLC and autosampler. The mobile phase solvents consisted of 0.1% formic acid, 99.9% water (solvent A) and 0.1% formic acid, 99.9% acetonitrile (solvent B). Peptides were gradient-eluted at a flow rate of 350 nL/min, using a 120 min gradient. The gradient consisted of the following: 1 – 3 min, 2% B (sample loading from autosampler); 3 – 98 min, 2 – 45% B; 98 – 105 min, 45 – 90% B; 105 – 107 min, 90% B; 107 – 110 min, 90–2% B; 110 – 120 min (column re-equilibration), 2% B. A Q Exactive HF mass spectrometer (Thermo Scientific), equipped with a nanoelectrospray ionization source, was used to mass analyze the eluting peptides using a data-dependent method. The instrument method consisted of MS1 using an MS AGC target value of 3e6, followed by up to 15 MS/MS scans of the most abundant ions detected in the preceding MS scan. A maximum MS/MS ion time of 40 ms was used with a MS2 AGC target of 1e5. Dynamic exclusion was set to 20 s, HCD collision energy was set to 27 nce, and peptide

match and isotope exclusion were enabled. For identification of peptides, tandem mass spectra were searched with Sequest (Thermo Fisher Scientific) against a *Drosophila melanogaster* database created from the UniprotKB protein database (www.uniprot.org). Search results were assembled using Scaffold 4.3.4 (Proteome Software).

Genome-wide copy number profiling

Embryos were collected immediately after 2 hr of egg laying. Salivary glands were dissected in EBR from 50 wandering 3rd instar larvae per genotype and flash frozen. Ovaries were dissected from females fattened for 2 days on wet yeast in EBR and 50 stage 13 egg chambers were isolated for each genotype and flash frozen. Tissues were thawed on ice, resuspended in LB3 and dounced using a Kontes B-type pestle. Dounced homogenates were sonicated using a Bioruptor 300 (Diagenode) for 10 cycles of 30' on and 30" off at maximal power. Lysates were treated with Rnase and Proteinase K and genomic DNA was isolated by phenol-chloroform extraction. Illumina libraries were prepared using NEB DNA Ultra II (New England Biolabs) following the manufacturers protocol. Barcoded libraries were sequenced using Illumina NextSeq500 platform.

Bioinformatics

Reads were mapped to the *Drosophila* genome (BDGP Release 6) using BWA-MEM with default parameters (Li and Durbin, 2009). CNVnator 0.3.3 was used for the detection of underreplicated regions using a bin size of 1000 (Abyzov et al., 2011). Regions were identified as underreplicated if they were not identified as underreplicated in 0 – 2 hr embryonic DNA and were greater than 10 kb in length. The number of reads

for underreplicated regions was called by using bedtools multicov tool for the underreplicated and uncalled regions. Average read depth per region was determined by multiplying the number of reads in a region by the read length and dividing by the total region length. Read depth was normalized between samples by scaling the total reads obtained per sample. Statistical comparison between the regions was with a t-test. For read depth in pericentric heterochromatin regions, the chromatin arm was binned into 10 kb windows and the number of reads for each window was called using bedtools multicov using only uniquely mapped reads.

Half maximum analysis of amplicon copy number profiles was performed as described previously (Alexander et al., 2015; Nordman et al., 2014). Briefly, \log_2 ratios were generated using bamCompare from deepTools 2.5.0 (Ramírez et al., n.d.) by comparing stage 13 follicle cell profiles to a 0 – 2 hr embryo sample. Smoothed \log_2 -transformed data was used to determine the point of maximum copy number associated with each amplicon. The chromosome coordinate corresponding to half the maximum value for each arm of the amplicon was then determined.

Copy number analysis by droplet-digital PCR (ddPCR)

Genomic DNA was extracted from salivary glands isolated from wandering third instar larvae as described above. Primer sets annealing to the mid-point of the indicated UR regions were used (previously described in [Nordman et al., 2014; Sher et al., 2012]). ddPCR was performed according to manufacture's recommendations (BioRad). All ddPCR reactions were performed in triplicate from three independent biological replicates. The concentration value for each set of primers in an underreplicated domain

was divided by the concentration value of a fully replicated control to generate the bar graph. Error bars represent the SEM.

Western blotting

Ovaries were dissected from females fattened for 2 days on wet yeast and suspended in Laemmli buffer supplemented with DTT. Ovaries were homogenized and boiled and extracts were loaded on a 4–20% Mini-PROTEAN TGX Stain-Free gel (BioRad). After electrophoresis the gel was activated and imaged according to the manufacturers recommendations. Protein was transferred to a PDVF membrane using a Trans-Blot Turbo Transfer System (BioRad). After blocking and incubation with antibodies, blots were imaged using an Amersham 600 CCD imager.

iPOND mass spectrometry

We obtained *D. melanogaster* S2 cells directly from the Drosophila Genomics Resource Center (DGRC). Cells were checked for mycoplasma contamination by PCR. S2 cells propagated as recommended by the DGRC. *Drosophila* S2 cells were grown in Schneider's Drosophila Medium with 10% heat-inactivated FBS (Gemini Bio Products) and 100 units/mL Penicillin-Streptomycin (Life Technologies). For each biological replicate, 5×10^8 cells were pulsed with 10 μ M EdU and immediately fixed in 2% formaldehyde (pulse samples) or pulsed with 10 μ M EdU for 10 minutes and chased with 100 μ M Thymidine for 30 min prior to fixation (chase samples). iPOND purifications were done according to (Dungrawala and Cortez, 2014) with the exception that LB3 was used

in place of RIPA buffer. Purifications were processed for mass spectrometry as described above.

To quantify protein abundance in by mass spectrometry, raw mass spectrometry data were imported into Skyline version 4.1 (Schilling et al., 2012). Chromatographic traces were manually inspected for proper peak picking and where necessary adjusted manually in the chromatographic window. Only matching isotopic envelopes that had an error <5 ppm, an isotope dot product >0.9, and similar retention times between samples were used. MS1 peak areas from each peptide and observed charge state were summed to get the intensity for a given protein. To account for variation between samples, each sample was normalized to histone H3 summed areas.

Proximity Ligation Assay (PLA) with nascent DNA

S2 cells were grown in Schneider's Drosophila Medium with 10% heat-inactivated FBS (Gemini Bio Products) and 100 units/mL Penicillin Streptomycin (Life Technologies). For nascent DNA PLA, asynchronously growing S2 cells were seeded onto Concanavalin A-coated coverslips. After attaching to coverslips for 1 hr, cells were pulsed with 125 μ M EdU for 10 min. Cells were washed with PBS and fixed in 4% paraformaldehyde for 15 min, then permeabilized in PBS + 0.25% Triton X-100 for 60 min. The cells were biotinylated using standard click chemistry conditions for 30 min. After washing 3 times, blocking was performed for 1 hr with Duolink blocking solution. Cells were incubated with their primary antibody overnight at 4°C. The following day, cells were washed in Duolink Wash Buffer A, then incubated at 37°C with the appropriate Plus and Minus PLA probes at a 1:5 dilution. After an hour, the cells were washed in Wash Buffer A twice, ligation

buffer was made at 1:40 dilution and incubated for 30 min at 37°C. Cells were washed 2x in Wash Buffer A, then incubated in amplification buffer at 1:80 for 100 min at 37°C. Slides were washed in Wash Buffer B, then 1:100 dilution of Wash Buffer B before being mounted in Duolink In Situ Mounting Media with DAPI.

Data access

Data sets described in this manuscript can be found under the GEO accession number: GSE114370.

Acknowledgements

We thank Kristie Rose and Hayes McDonald at the Vanderbilt Proteomics core for mass spectrometry and Olivia Koues from the VANTAGE core at Vanderbilt for Illumina sequencing. We would like to thank Terry Orr-Weaver, Stephen Bell, Katherine Friedman, James Dewar, Dave Cortez and members of the Nordman lab for providing critical comments on the manuscript. We thank Brooke Hamilton for assistance in generating the Rif1 mutants. This work was supported by an NIH award P30 AI110527 to SM and an NIH R00 award 5R00GM104151 to JTN.

Author contributions

Alexander Munden, Zhan Rong, Formal analysis, Investigation, Visualization; Amanda Sun, Formal analysis, Investigation, Methodology; Rama Gangula, Formal analysis, Methodology; Simon Mallal, Supervision, Methodology; Jared T Nordman,

Conceptualization, Formal analysis, Supervision, Funding acquisition, Validation, Investigation, Visualization, Writing—original draft.

Supplementary Table 2-1: Underreplicated regions called by CNVnator

chr	start	end	OregonR	<i>SuUR</i>	<i>SuUR</i> ^{ΔSNF}	<i>Rif1</i> ⁻	<i>Rif1</i> ^{PP1}	<i>Rif1</i> ^{PP1/+}
chrX	9001	52000	+		+			
chrX	80001	108000	+					
chrX	2976001	3125000	+					+
chrX	12052001	12382000	+					+
chrX	14062001	14101000	+					
chrX	14292001	14563000	+					+
chrX	20686001	20957000	+					+
chrX	20962001	20998000	+					+
chrX	21525001	21544000	+	+		+		+
chrX	21667001	21807000	+	+	+			+
chrX	21814001	21829000	+					+
chrX	21843001	21895000	+	+	+			+
chrX	21904001	21965000	+	+	+			+
chrX	21972001	22433000	+	+	+		+	+
chrX	22611001	22787000	+	+				+
chrX	23053001	23064000	+	+				
chrX	23175001	23205000	+					+
chrX	23285001	23535000	+	+	+			+
chr2L	4538001	4777000	+					
chr2L	8013001	8024000	+					
chr2L	11587001	11777000	+					
chr2L	12781001	12799000	+					
chr2L	14722001	14946000	+					+
chr2L	15306001	15721000	+					+
chr2L	15960001	16154000	+					+
chr2L	16161001	16217000	+					+
chr2L	16948001	17199000	+					+
chr2L	17201001	17312000	+					+
chr2L	17520001	17951000	+		+			+
chr2L	19345001	19358000	+					
chr2L	20128001	20199000	+	+	+			+
chr2L	21833001	22085000	+					+
chr2L	22284001	22522000	+					+
chr2L	22614001	22752000	+					+
chr2L	23198001	23406000	+	+	+	+	+	+
chr2L	23415001	23513712	+		+	+		+

chr2R	1	699000	+	+	+	+	+	+
chr2R	1194001	1206000	+					
chr2R	1379001	1501000	+	+	+			+
chr2R	1557001	1589000	+					
chr2R	1609001	1700000	+					+
chr2R	1707001	1968000	+	+	+			+
chr2R	1975001	2163000	+	+	+	+		+
chr2R	2170001	2409000	+	+	+	+		+
chr2R	2421001	2500000	+	+	+			+
chr2R	2508001	2546000	+	+	+			+
chr2R	2551001	3506000	+	+		+	+	+
chr2R	3513001	3871000	+	+	+	+	+	+
chr2R	4414001	4425000	+	+				
chr2R	4871001	5057000	+					+
chr2R	6283001	6476000	+	+				+
chr2R	10623001	10637000	+			+		
chr2R	23133001	23313000	+					+
chr3L	4850001	5034000	+					+
chr3L	5043001	5075000	+					+
chr3L	13559001	13805000	+					+
chr3L	15196001	15475000	+					+
chr3L	18190001	18431000	+					+
chr3L	22577001	22627000	+					
chr3L	22803001	22820000	+					
chr3L	23157001	23173000	+		+			
chr3L	23355001	23538000	+					+
chr3L	23550001	23679000	+					
chr3L	23775001	24005000	+					+
chr3L	24056001	25075000	+	+	+			+
chr3L	25135001	25838000	+	+	+			+
chr3L	25844001	25965000	+		+			+
chr3L	26085001	26161000	+		+			+
chr3L	26166001	26311000	+	+				+
chr3L	26315001	26705000	+	+	+		+	+
chr3L	27391001	27815000	+			+	+	+
chr3L	28042001	28110227	+					
chr3R	1	1257000	+	+	+	+	+	+
chr3R	1266001	1655000	+	+			+	+
chr3R	1664001	2569000	+	+	+		+	+

chr3R	2572001	2824000	+	+	+	+	+	+
chr3R	2831001	3034000	+	+	+	+	+	+
chr3R	3040001	3129000	+	+		+	+	+
chr3R	3136001	3533000	+	+	+		+	+
chr3R	3674001	3692000	+	+				
chr3R	3827001	3842000	+	+				
chr3R	3890001	4175000	+		+			+
chr3R	6159001	6327000	+					
chr3R	6515001	6624000	+					
chr3R	7572001	7714000	+		+			+
chr3R	10919001	11142000	+		+			+
chr3R	16712001	16948000	+					+
chr3R	19704001	19715000	+					
chr3R	22142001	22303000	+			+		
chr3R	28020001	28252000	+					+

Supplementary Table 2-2: Half-Max called follicle widths

<i>Wild type</i>		max (log2)	left arm (bp)	right arm (bp)	half max total (bp)	fold change relative to wild type
7F	<i>chrX</i>	3.911	8439400	8518500	79100	1
22B*	<i>chr2L</i>	1.961	1888300	1937200	48900	1
30B	<i>chr2L</i>	1.798	9504800	9587600	82800	1
34B	<i>chr2L</i>	2.33	13371800	13438500	66700	1
62D	<i>chr3L</i>	1.678	2231600	2314900	83300	1
66D	<i>chr3L</i>	5.494	8694700	8765800	71100	1

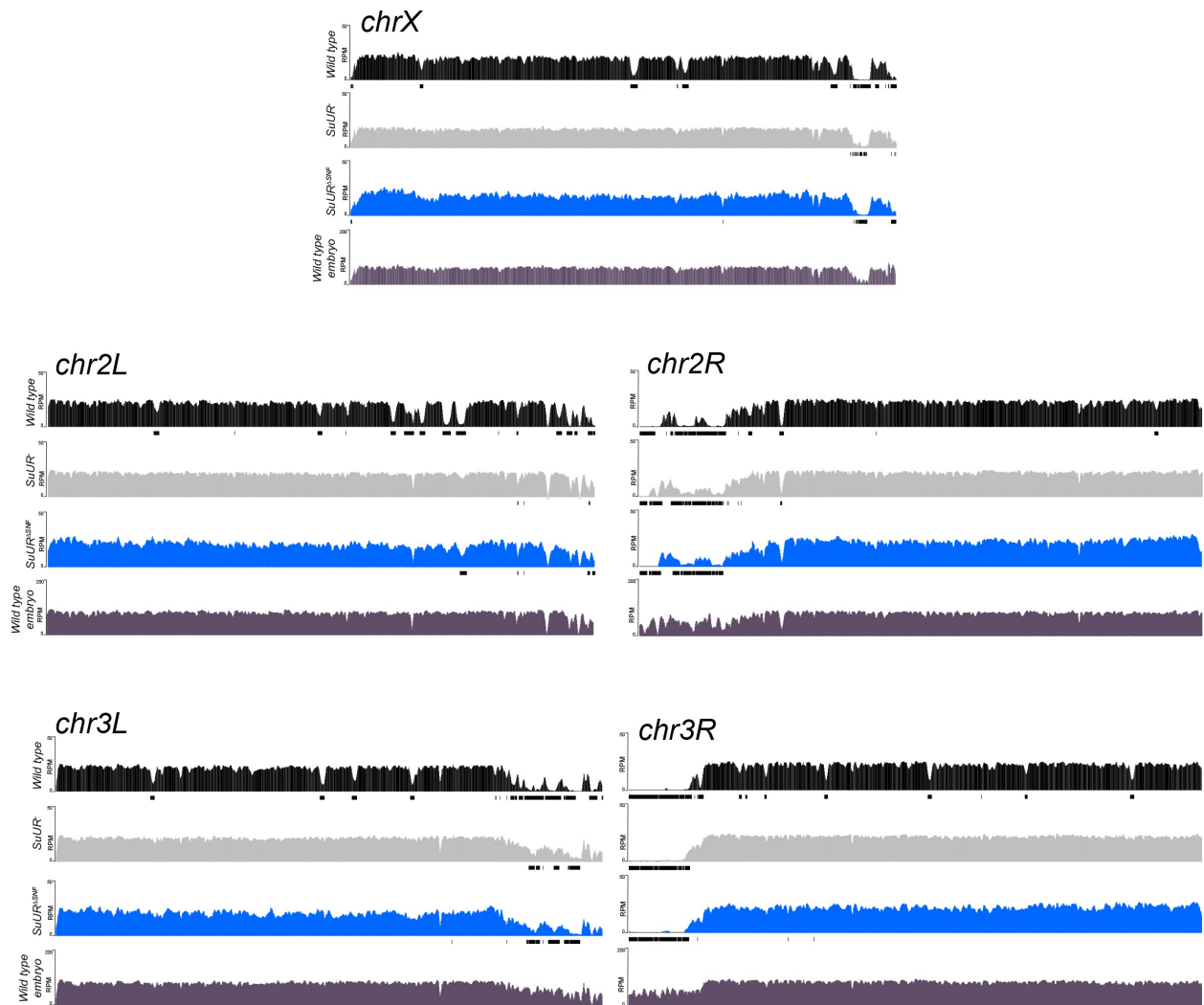
half max position

<i>SuUR-</i>		max (log2)	left arm (bp)	right arm (bp)	half max total (bp)	
7F	<i>chrX</i>	3.528	8425000	8528900	103900	1.313527181
22B*	<i>chr2L</i>	NA	NA	NA	NA	NA
30B	<i>chr2L</i>	1.682	9506100	9607700	101600	1.22705314
34B	<i>chr2L</i>	2.355	13364800	13473500	108700	1.629685157
62D	<i>chr3L</i>	1.745	2221200	2342400	121200	1.454981993
66D	<i>chr3L</i>	4.88	8685700	8778600	92900	1.306610408

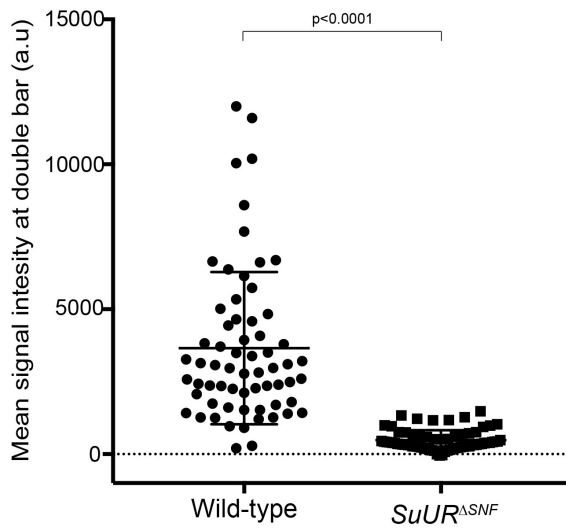
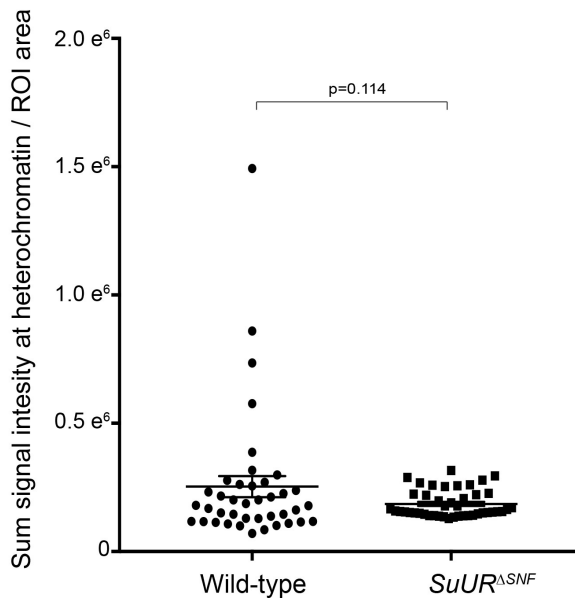
half max position

<i>Rif1-</i>		max (log2)	left arm (bp)	right arm (bp)	half max total (bp)	
7F	<i>chrX</i>	3.824	8420700	8540700	120000	1.517067004
22B*	<i>chr2L</i>	NA	NA	NA	NA	NA
30B	<i>chr2L</i>	1.807	9496800	9607300	110500	1.334541063
34B	<i>chr2L</i>	2.474	13361400	13474400	113000	1.694152924
62D	<i>chr3L</i>	1.719	2217900	2335500	117600	1.411764706
66D	<i>chr3L</i>	5.465	8679700	8783500	103800	1.459915612

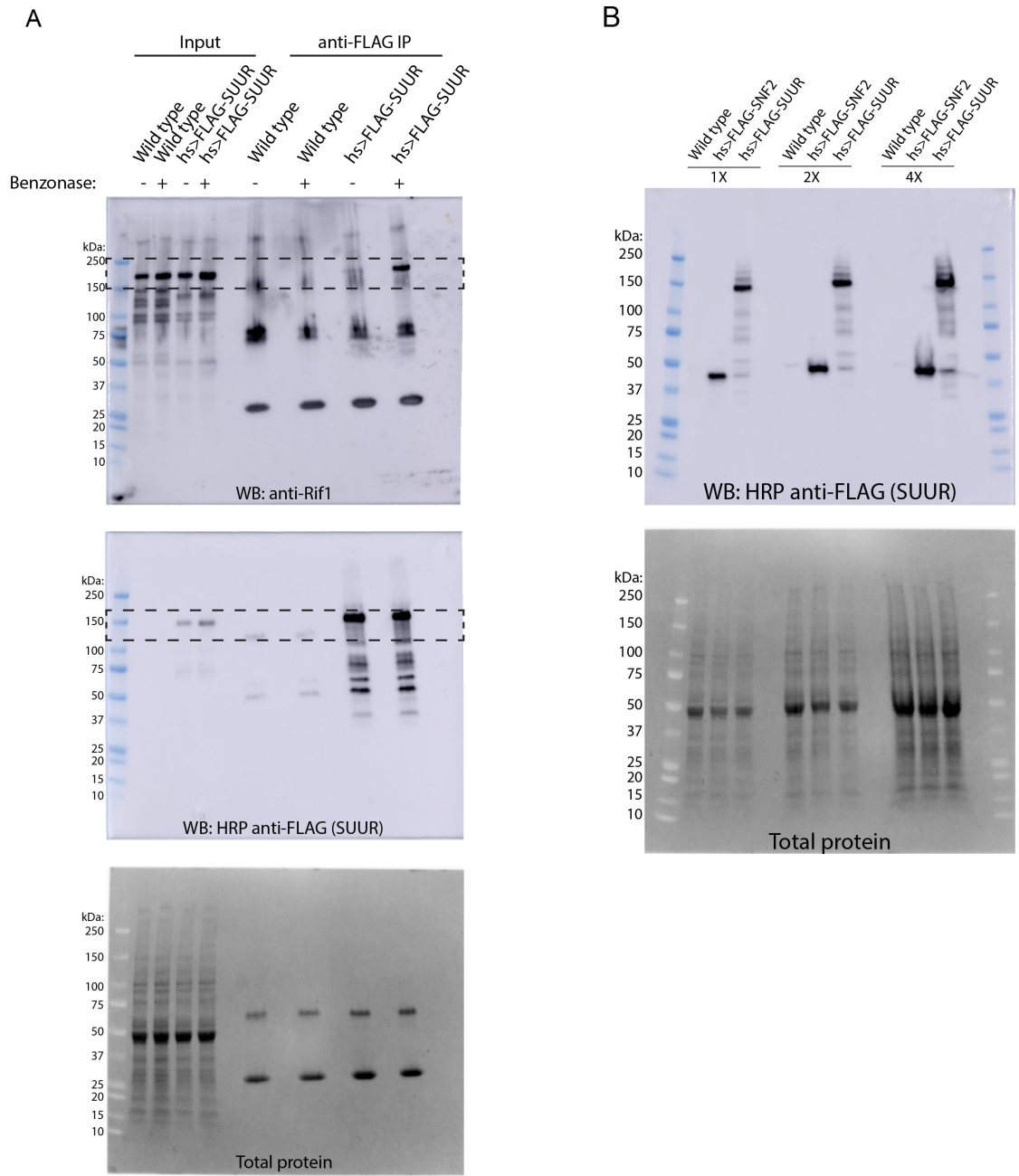
*22B is a strain specific amplicon present in Oregon R and not *SuUR* and *Rif1* mutants



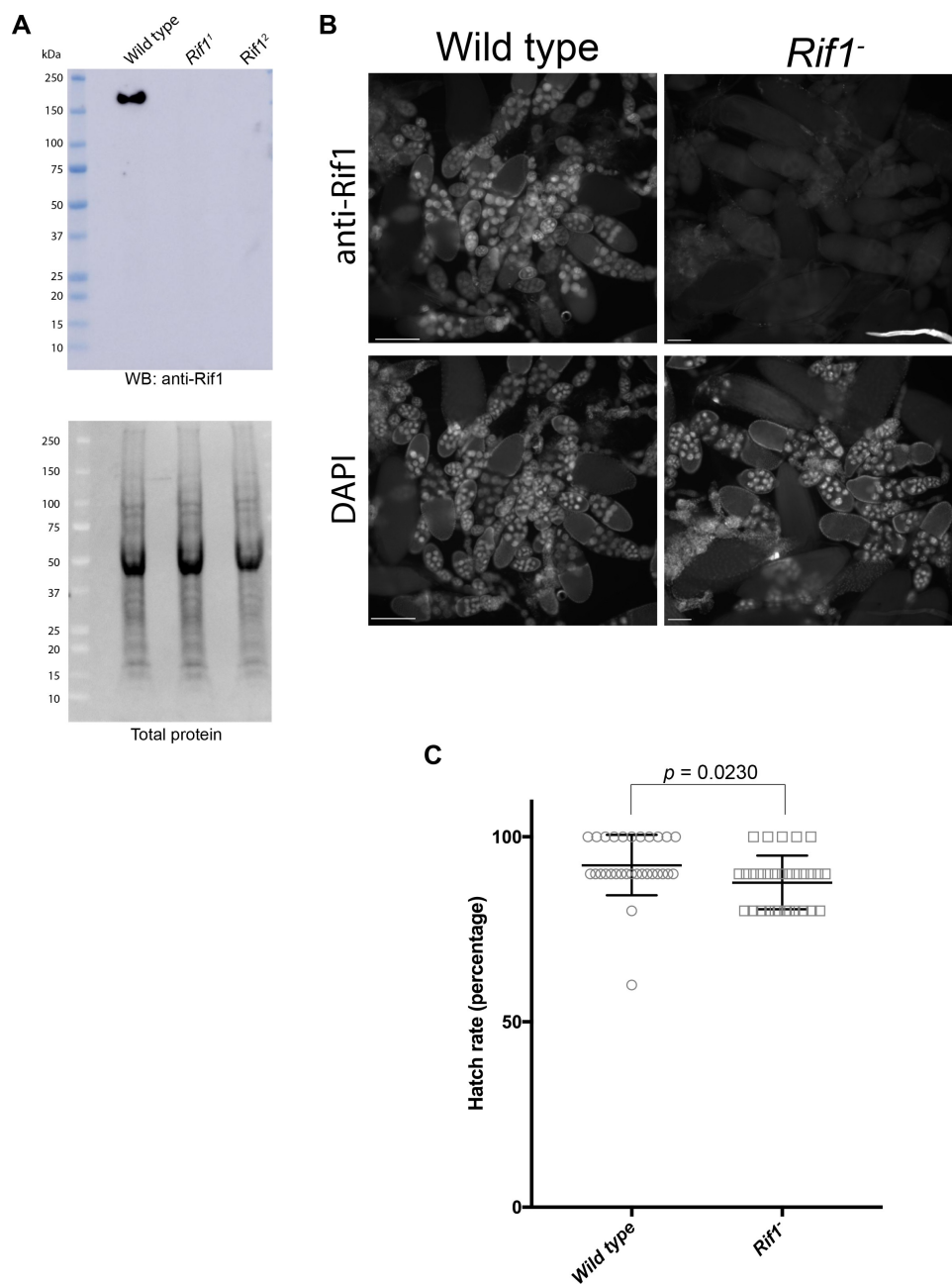
Supplemental Figure 2-1: **Genome-wide copy number profile of the *SuUR*^{ΔSNF} mutant.** Illumina-based copy number profiles of all chromosome arms except the fourth for larval salivary glands of the indicated genotypes and wild type 0 – 2 hr embryos in which DNA is fully replicated. Black bars below each profile represent called underrepresented regions. Contributions: Analysis and visualization.

A**B**

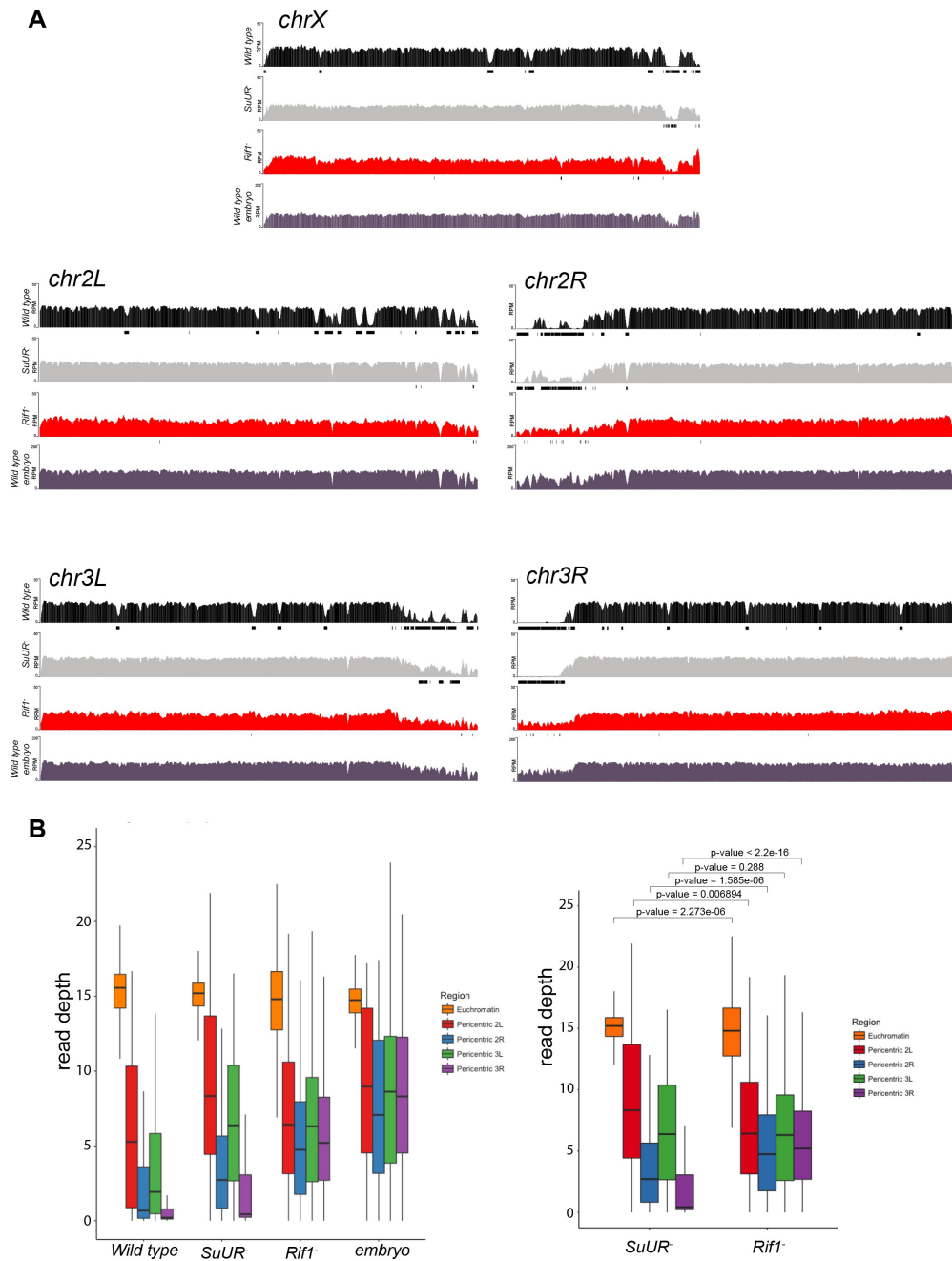
Supplemental Figure 2-2: **Quantification of SUUR and $SUUR^{\Delta SNF}$ signal intensities at replication forks and heterochromatin.** (A) SUUR and $SUUR^{\Delta SNF}$ mean signal intensities, normalized for background levels, at double bar structures from stage 12 egg chambers. Results are from two biological replicates. A two-tailed Welch's t test was used to determine significance. $n = 64$ for wild-type and $n = 69$ for the $SuUR^{\Delta SNF}$ mutant. (B) SUUR and $SUUR^{\Delta SNF}$ signal intensity, normalized to area, at heterochromatin in stage 12 egg chambers. Results are from two biological replicates. A two-tailed Welch's t test was used to determine significance. $n = 40$ for wild-type and $n = 44$ for the $SuUR^{\Delta SNF}$ mutant. No outliers were excluded. Contributions: None.



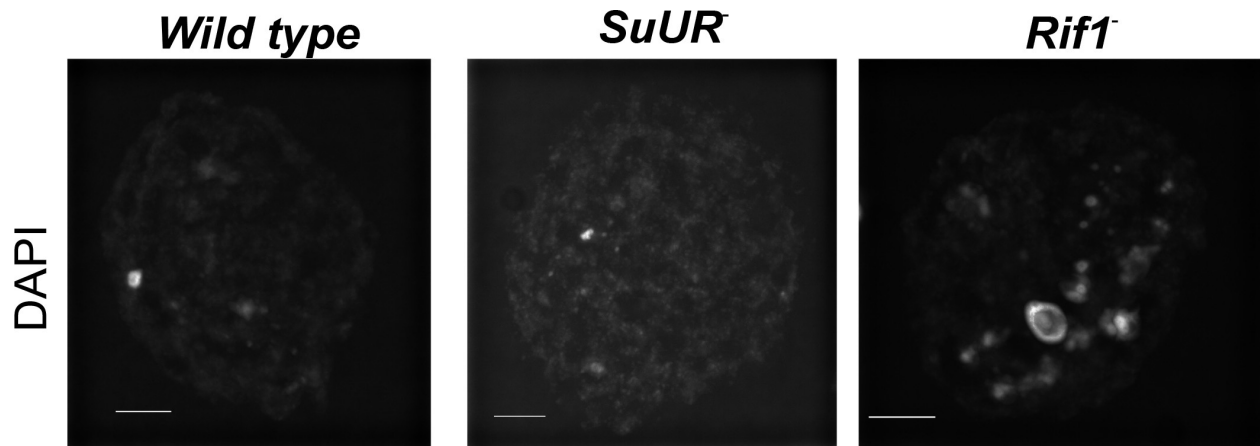
Supplemental Figure 2-3: **Western blot analysis of heat-shock inducible SUUR constructs.** (A) Full Western blots of images used in Figure 2B with total protein loading control. (B) Western blot analysis of FLAG-SUUR and FLAG-SNF2 heat-shocked 0–24 hr embryos with a total protein loading control. Contributions: None



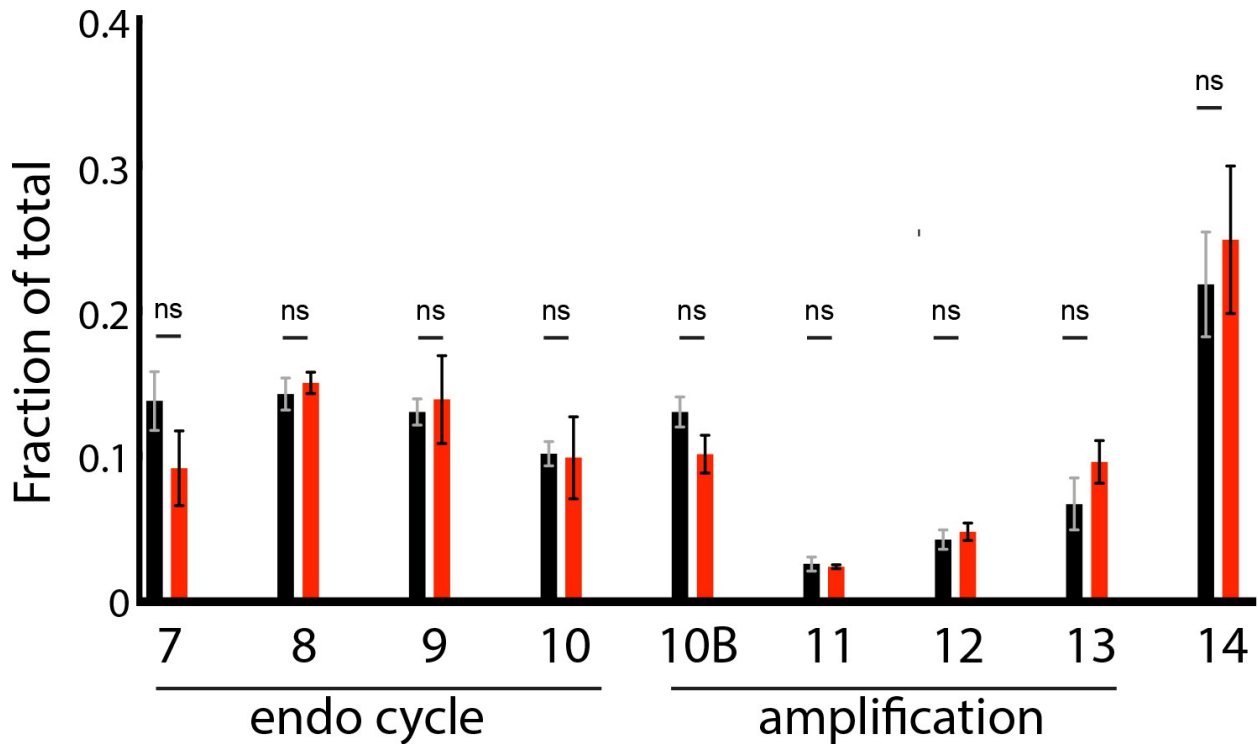
Supplemental Figure 2-4: **Verification of *Rif1* mutants and validation of anti-Rif1 antibody.** (A) Western blot analysis of ovary extracts prepared from the indicated genotypes. Serum produced in guinea pigs was used at 1:1000 dilution. (B) Immunofluorescence of ovaries using affinity purified anti-Rif1 antibody produced in guinea pigs. Exposure times were equal between the two genotypes. (C) Embryo hatch rate assay comparing embryos laid by wild-type or *Rif1¹/Rif1²* mutant mothers. $n = 300$ embryos per genotype. Each data point represents the hatch rate of a group of 10 embryos. An unpaired student t-test was used to generate the p value. Contributions: None.



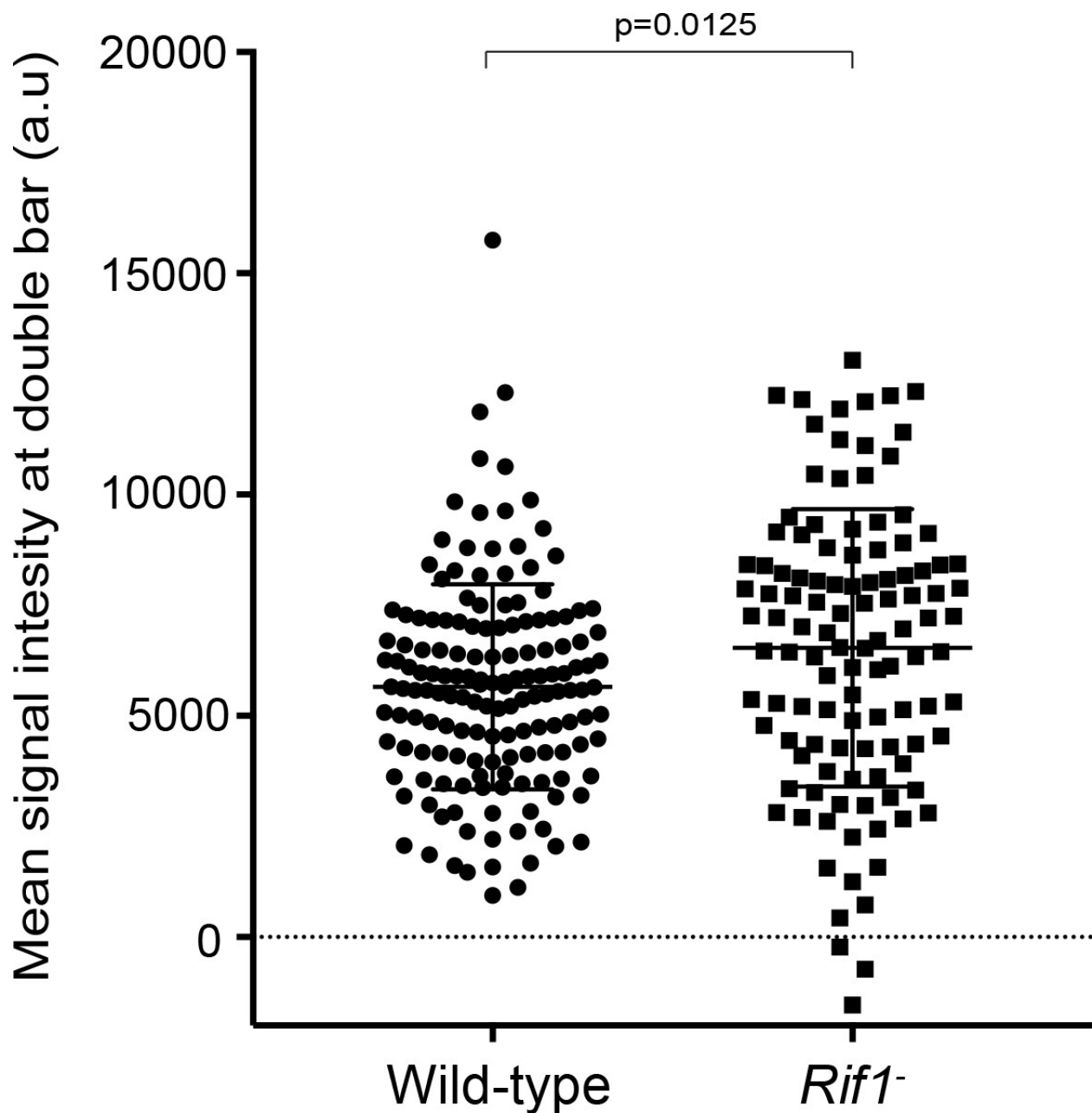
Supplemental Figure 2-5: **Genome-wide copy number profile of the *Rif1* mutant.** (A) Illumina-based copy number profiles of all chromosome arms except the fourth for larval salivary glands of the indicated genotypes. Black bars below each profile represent called underreplicated regions. (B) Box plot represents read depth in 10 kb bins in the pericentric chromatin regions for *chr 2L*, *2R*, *3L* and *3R*. A Welch Two Sample t-test was used to compare the same regions between *SuUR* and *Rif1* mutants. The same wild-type, *SuUR* and 0 – 2 hr embryo plots as in Supplemental 2-1. Contributions: Analysis and visualization.



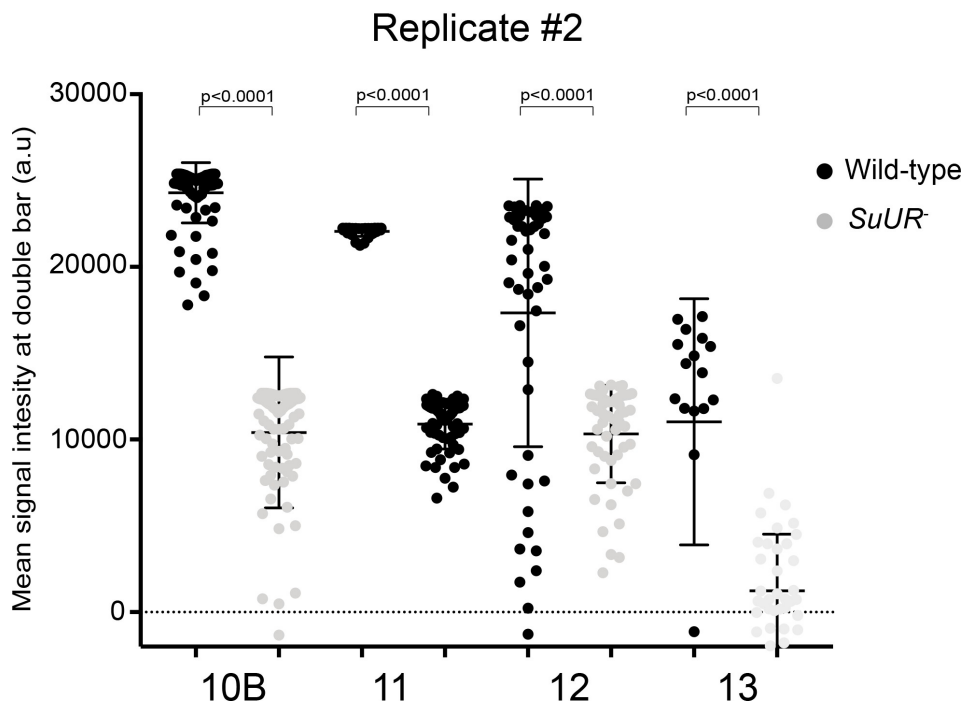
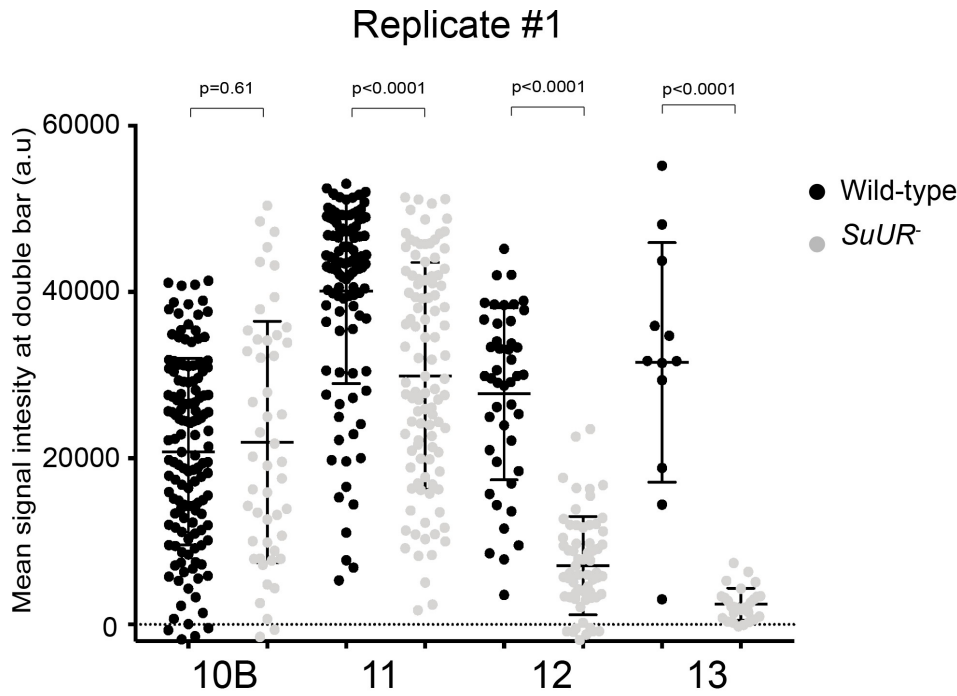
Supplemental Figure 2-7: ***Rif1* mutant endo cycling cells have enlarged chromocenters.** Representative images of single nurse cell nuclei from stage 10 egg chambers. Egg chambers were stained with DAPI. Scale bar is 10 μ m. Exposure times and scaling are equal in all images. Contributions: None.



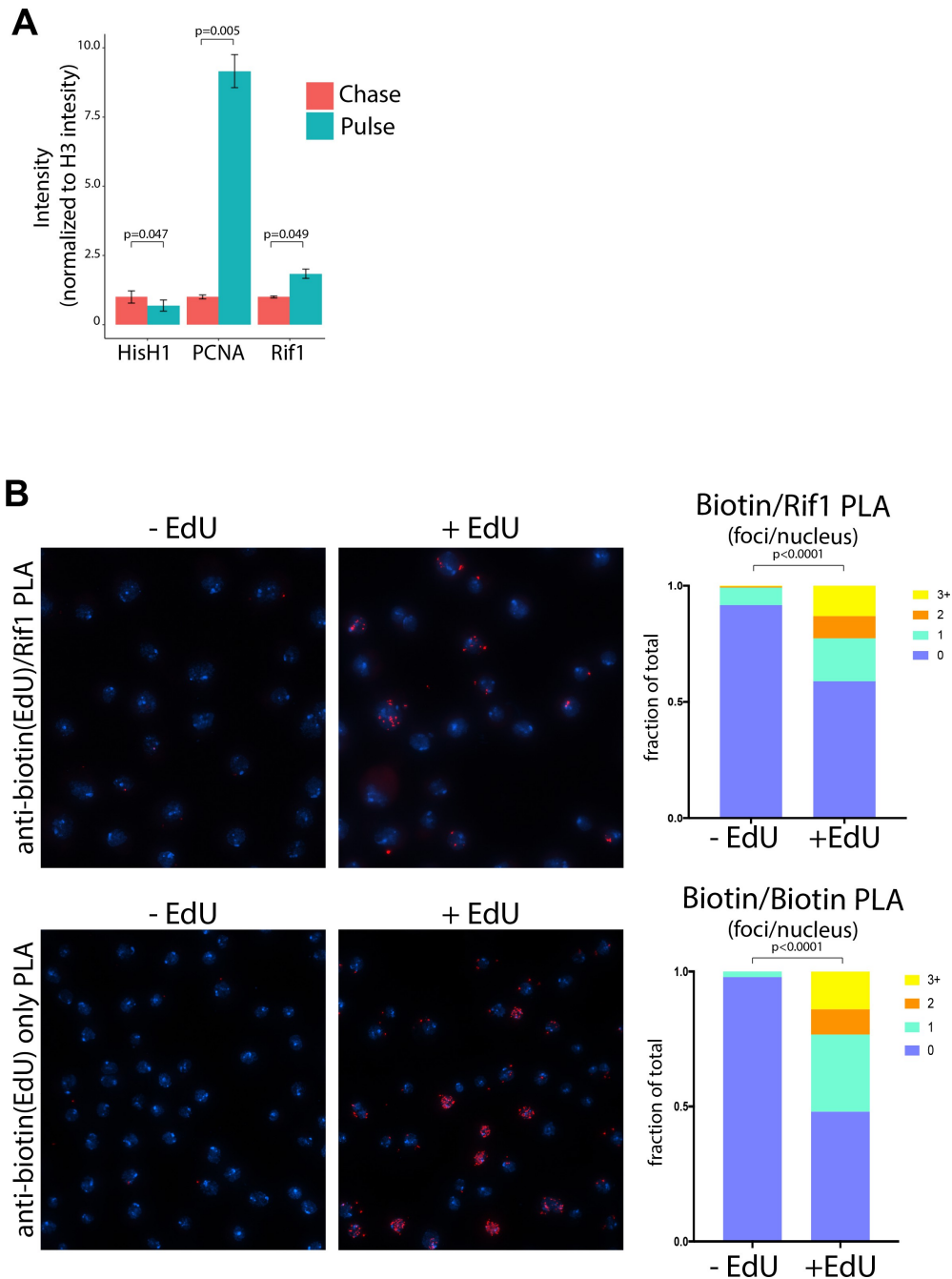
Supplemental Figure 2-8: **The developmental window of gene amplification is not affected by loss of *Rif1* function.** Egg chamber distribution from wild-type and *Rif1* mutant ovaries fattened for 2 days on wet yeast. Bars represent the fraction of a given egg chamber stage relative to the total population of counted egg chambers (stages 7 – 17) for five biological replicates. Error bars represent the SEM. A student t test was used to compare the fraction of staged egg chambers for each biological replicate between wild-type and the *Rif1* mutant ovaries ($p=0.12$ stage 7; $p=0.79$ stage 8; $p=0.77$ stage 9; $p=0.92$ stage 10; $p=0.33$ stage 10B; $p=0.94$ stage 11; $p=0.86$ stage 12; $p=0.33$ stage 13 and $p=0.30$ stage 14). Total number of egg chambers counted: 800 for wild-type and 800 for the *Rif1* mutant. No outliers were excluded. Contributions: None.



Supplemental Figure 2-9: **Quantification of SUUR signal intensity at replication forks in the presence and absence of Rif1.** SUUR mean signal intensity at double bar structures, normalized for background levels, from stage 12 egg chambers. Results are from two biological replicates. A two-tailed Welch's t test was used to determine significance. $n = 156$ for wild-type and $n = 113$ for the *Rif1*⁻ mutant. No outliers were excluded. Contributions: None.

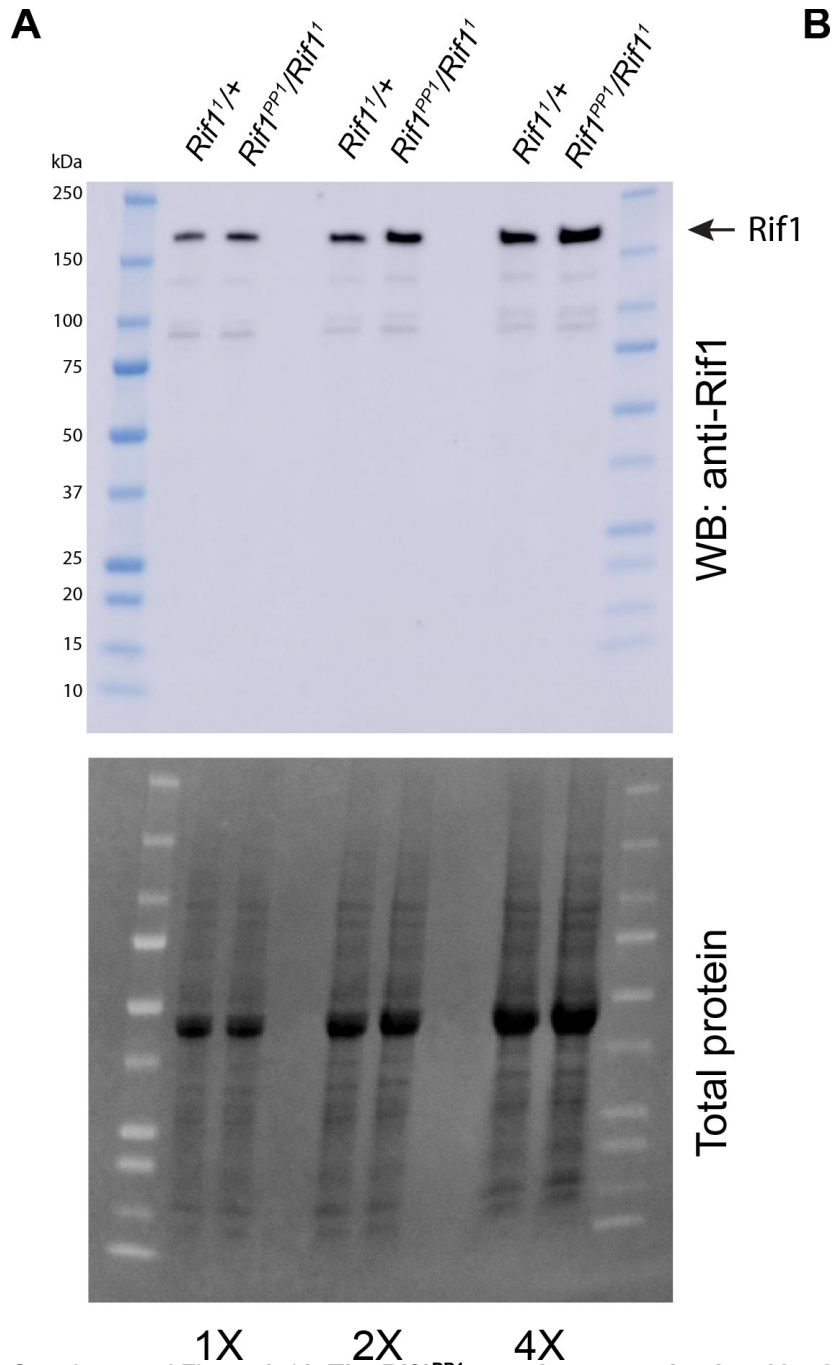


Supplemental Figure 2-10: **Quantification of Rif1 signal intensity at replication forks in the presence and absence of SUUR.** Rif1 mean signal intensity at double bar structures from stage 10B, 11, 12 and 13 egg chambers. Results from two biological replicates are shown independently. A two-tailed Welch's t test was used to determine significance between the same stage of different genotypes. No outliers were excluded. Contributions: None.

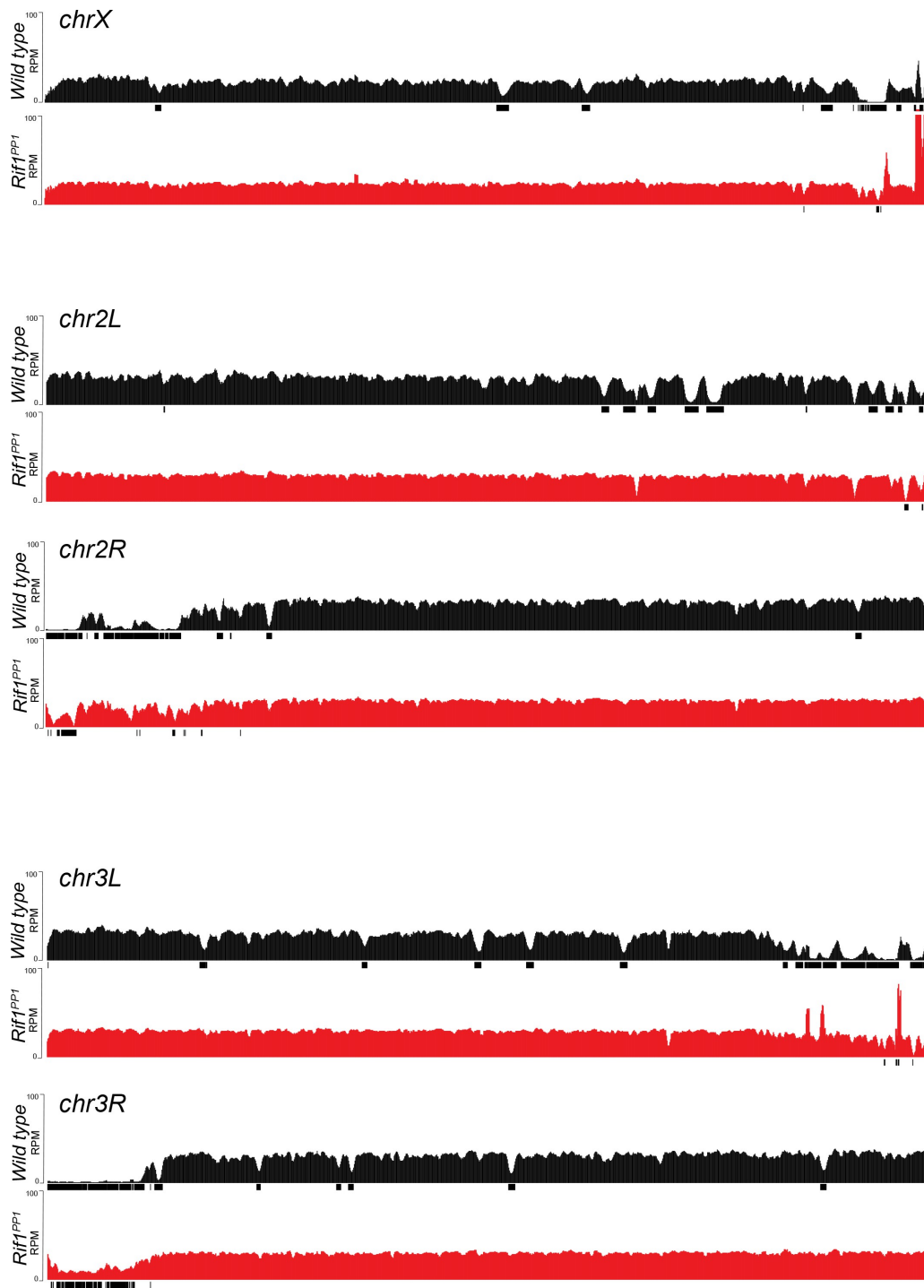


Supplemental Figure 2-11: **Rif1 localizes to replication forks in cultured cells.** (A) Quantification of protein intensity from iPOND mass spec data in cultured S2 cells. Intensities represent the summed MS1 spectrum for each peptide identified for Histone H1, PCNA or Rif1. Each sample was normalized to the protein intensity for Histone H3 to account for differences in protein abundance between each sample. Bars represent the average of three biological replicates and the error bars are the S.E.M. A paired t test was used to determine significance. (B) Proximity Ligation Assay (PLA) with nascent chromatin in cultured S2 cells reveals a signal between biotinylated EdU (nascent DNA) and Rif1. Representative images from anti-biotin and anti-Rif1 assay in the presence or absence of an EdU pulse. As a positive control, mouse and rabbit anti-biotin antibodies were used together in the presence or absence of an EdU pulse. Number of PLA foci per nucleus in quantified. Quantification of two biological replicates were used per condition. N (total number of nuclei counted)=775 for -EdU and 669 for + EdU (Biotin only). N = 773 for -EdU and 406

for + EdU (Rif1 and Biotin). A two-tailed Welch's t test was used to determine significance. Contributions: Experiment, Analysis, and visualization for A. Trained undergraduate who performed experiment in B.



Supplemental Figure 2-12: **The *Rif1^{PP1}* protein expression level is similar to wild-type *Rif1*.** (A) Western blot analysis of ovary extracts from *Rif1^{PP1}/*Rif1*¹* and *Rif1^{1/+}* adults. Serum was produced in guinea pigs and used at 1:1000 dilution. Contributions: None.



Supplemental Figure 2-13: **Genome-wide copy number profile of the *Rif1^{PP1}* mutant.** Illumina-based copy number profiles of all chromosome arms except the fourth for larval salivary glands of the indicated genotypes. Black bars below each profile represent called underreplicated regions. Contributions: Analysis and visualization.

Chapter III: Identification of replication fork-associated proteins in *Drosophila* embryos and cultured cells using iPOND coupled to quantitative mass spectrometry

Abstract

Replication of the eukaryotic genome requires the formation of thousands of replication forks that must work in concert to accurately replicate the genetic and epigenetic information. Defining replication fork-associated proteins is a key step in understanding how genomes are replicated and repaired in the context of chromatin to maintain genome stability. To identify replication fork-associated proteins, we performed iPOND (Isolation of Proteins on Nascent DNA) coupled to quantitative mass spectrometry in *Drosophila* embryos and cultured cells. We identified 76 and 278 fork-associated proteins in post-MZT embryos and *Drosophila* cultured S2 cells, respectively. By performing a targeted screen of a subset of these proteins, we demonstrate that BRWD3, a targeting specificity factor for the DDB1/Cul4 ubiquitin ligase complex (CRL4), functions at or in close proximity to replication forks to promote fork progression and maintain genome stability. Altogether, our work provides a valuable resource for those interested in the DNA replication, repair and chromatin assembly during development.

* This chapter has been published as Munden, A., Wright, M. T., Han, D., Tirgar, R., Plate, L. & Nordman, J. T. Identification of replication fork-associated proteins in *Drosophila* embryos and cultured cells using iPOND coupled to quantitative mass spectrometry. *Scientific Reports* **12**, 6903 (2022).

Introduction

Each and every time a cell divides it must accurately replicate both its genetic and epigenetic information. Core replication factors are known to assemble at replication forks to replicate the genome (e.g. helicase, polymerases). There are, however, likely hundreds of proteins that function at or in close proximity to the replication fork to facilitate replication of difficult-to-replicate sequences, propagate epigenetic information and coordinate replication with other chromatin-related processes such as transcription (Wessel et al. 2019; Dungrawala et al. 2015; Alabert et al. 2014). Replication of the eukaryotic genome requires thousands of replication forks functioning simultaneously to complete replication in a timely manner. Errors generated at a single replication fork during genome duplication can result in mutations or genomic alterations with the potential to cause cell lethality or drive tumor formation (Tomasetti et al. 2017). Further complicating DNA replication is the need to allow regulatory flexibility to accommodate cell-type specific changes in cell division and cell cycle rates that occur during cell differentiation and development (Shermoen et al. 2010; Matson et al. 2017). How replication fork composition and activity is remodeled in response to difficult-to-replicate regions of the genome and in response to changes in developmentally programmed changes in S phase regulation has yet to be defined.

Drosophila provides an ideal system to understand how developmentally-programmed changes in S phase impact replication fork composition. In contrast to the ~8hr S phases associated with mitotic cell division in differentiated cells, S phases during early embryonic development are extremely rapid. During early embryogenesis and prior to the maternal-to-zygotic transition (MZT) S phases are 3-4 minutes in length. S phase

gradually lengthens as development approaches the MZT and slows to ~75 minutes at the MZT (Yuan et al. 2016; Shermoen et al. 2010). While S phase length can drastically differ during development, the rate of replication fork progression is similar in these different contexts (Blumenthal et al. 1974). The chromatin context that replication forks must navigate also change with development. In pre-MZT embryos, chromatin is devoid of heterochromatin and transcription is largely inactive. Around the time of the MZT, condensed heterochromatin is formed and zygotic transcription is activated (Tadros and Lipshitz 2009; Shermoen et al. 2010). In fact, the extension of S phase at the MZT is largely driven by the onset of late replication and the bulk of S phase is dedicated to replication of heterochromatic sequences (Seller and O'Farrell 2018; Shermoen et al. 2010).

In recent years, several techniques have been established to isolate active replication forks to identify replication fork-associated proteins (Sirbu et al. 2011; Alabert et al. 2014; Gambus et al. 2006). One technique, isolation of proteins on nascent DNA (iPOND), has become widely employed due to its ease of use and the only technical requirement being a short pulse of the nucleotide analog 5-ethynyl-2'-deoxyuridine (EdU) (Sirbu et al. 2011). For iPOND, cells are incubated with a brief pulse of EdU and proteins are crosslinked to nascent DNA. EdU can be biotinylated using click chemistry and newly synthesized DNA and associated proteins are purified using streptavidin beads (Dungrawala and Cortez 2014). A key to identifying proteins at or in close proximity to active replication forks, rather than general chromatin-associated proteins, is a chase sample where a thymidine chase is introduced after the EdU pulse. Proteins enriched in pulse only samples relative to the chase samples are largely replication fork-associated

proteins (Sirbu et al. 2011, 2013; Dungrawala et al. 2015). Another advantage of iPOND is that it can be coupled to quantitative mass spectrometry to identify replication fork-associated proteins in an unbiased manner (Wessel et al. 2019; Dungrawala et al. 2015; Cortez 2017). While iPOND coupled to quantitative mass spectrometry has been used extensively in mammalian cultured cells, it has not been applied in *Drosophila* or in a developing organism.

To identify proteins at or in close proximity to active replication forks in *Drosophila*, and to determine if replication fork composition is influenced by development, we have performed iPOND in combination with tandem mass tag (TMT)-based quantitative mass spectrometry in *Drosophila* post-MZT embryos and cultured cells. Using an iPOND-TMT approach, together with a stringent statistical analysis, we identified 76 and 278 replication fork-associated proteins in post-MZT embryos and *Drosophila* cultured S2 cells, respectively. While we have confirmed many known replication fork components, we have identified many proteins that do not have known roles at the replication fork. By performing a targeted RNAi-based screen of select factors, we have identified the Cul4 E3 ubiquitin ligase specificity factor, BRWD3, as a replication fork-associated protein that affects replication fork progression.

Results

Establishing iPOND in the developing embryo

To define the landscape of proteins at or in close proximity to active replication forks during development, we turned to *Drosophila* due to its well-characterized S phase programs that are known to significantly change during development. To identify

replication fork-associated proteins, we chose to use iPOND because it does not require protein tags or extensive multi-step purifications (Sirbu et al. 2011). We chose post-MZT *Drosophila* embryos (3-5 hours after egg laying -AEL) for our embryonic sample. During this developmental time point, S phase is ~ 75 minutes with the bulk of that time devoted to replication of heterochromatin (Fig. 3-1A) (Shermoen et al. 2010).

Nucleotide analogs and other small molecules are unable to enter embryos without permeabilization or direct injection (Limbourg and Zalokar, 1973). To obtain sufficient EdU-labeled embryos for iPOND, we developed a large-scale permeabilization strategy. Starting with 3–5 h embryos collected from a population cage, embryos were permeabilized and pulse labeled with EdU for 10' using custom collection baskets (see “Experimental procedures”; Fig. 3-1B). Using this approach, we could routinely isolate 100–200 mg of EdU-labeled embryos from a single collection basket. To determine if EdU-labeled 3–5 h post-MZT embryos could be used for iPOND, we biotinylated embryos using Click chemistry as previously described and the EdU-labeling efficiency was determined by staining embryos with fluorescently labeled streptavidin (Fig. 3-1C) (Dungrawala and Cortez, 2017). Two key controls were also used; following the 10' pulse of EdU, embryos were immediately transferred into medium containing thymidine for 30' (chase sample). Second, age-matched embryos were mock treated and biotinylated exactly as the pulse and chase samples (no EdU control). To determine if iPOND could be used to isolate replication-dependent chromatin, we performed a single-step purification of biotinylated EdU-containing chromatin from our pulse, chase and no-EdU samples. We probed lysates for histone H3 as a mark of total chromatin (Fig. 3-1D) (Sirbu et al. 2011). We found that the recovery of chromatin was dependent on EdU

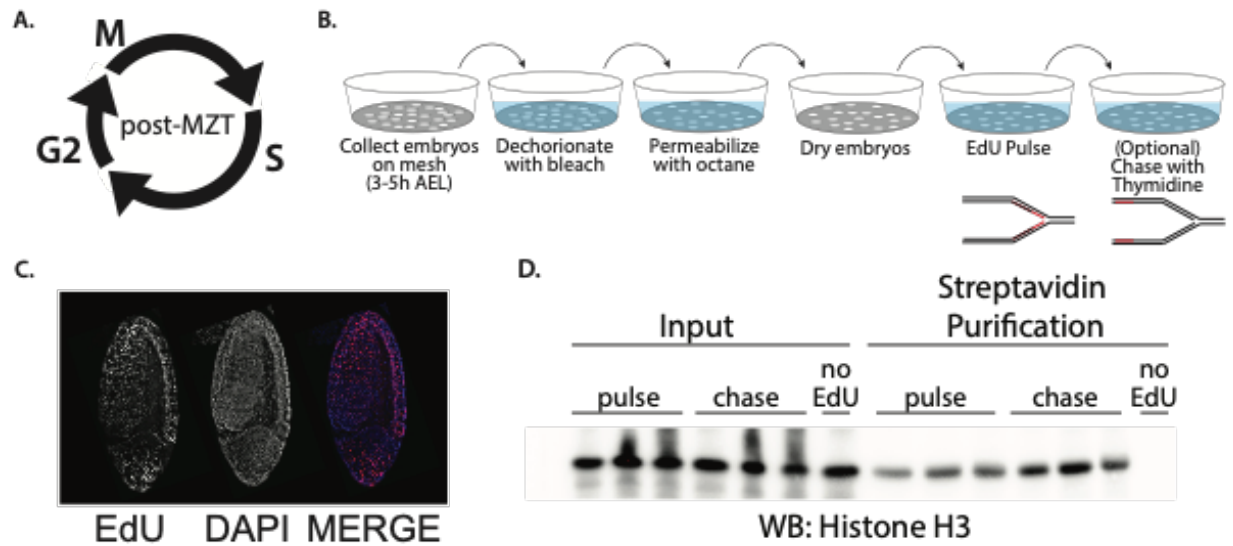


Figure 3-1: Establishing iPOND in the developing embryo. (A) A schematic of the rapid cell cycle in post-MZT embryos (3–5 h AEL). (B) Experimental design for large-scale EdU labeling of embryos for iPOND. (C) Representative image of an EdU-labeled post-MZT embryo used for iPOND purifications. Embryo labeling was deemed successful if > 50% of the embryos were uniformly labeled. (D) Western blot of three biological replicates for pulse and chase iPOND samples with a no EdU pulse control. Anti-H3 antibody is used as a marker of total chromatin recovery. Contributions: None.

incorporation. This indicates that iPOND can be applied to *Drosophila* embryos to isolate native chromatin.

iPOND mass spectrometry identifies proteins at or in close proximity to active replication forks in *Drosophila* embryos

Now that we established iPOND as a technique to identify proteins at or in close proximity to active replication forks in *Drosophila* embryos, we wanted to identify the repertoire of proteins associated with replication forks in early embryos in an unbiased manner using quantitative mass spectrometry. Therefore, we coupled our iPOND purifications to tandem mass tag (TMT) labeling, which allows us to multiplex and quantify the relative abundance of peptides across multiple biological replicates in a single mass spectrometry experiment (McAlister et al. 2012). We optimized the amount of labeled

embryos necessary for reproducible purification and mass spectrometry experiments. Ultimately, we found that 0.5g of EdU-labeled embryos routinely provided robust and reproducible mass spectrometry results. We collected EdU-pulsed embryos from four biological replicates of 3-5h embryos. EdU-pulsed embryos were either fixed immediately (pulse) or chased with thymidine for 30 minutes prior to fixation (chase). After EdU purification and verification via Western blot, peptides derived from pulse and chase samples were TMT labeled, separated using multidimensional protein identification technology (MudPIT) and quantified by mass spectrometry (Fig. 3-2A).

To identify proteins at or in close proximity to active replication forks, we focused on proteins that were enriched in the EdU pulse samples relative to the thymidine chase controls. To ensure that the differences were not due to differences in purification and/or labeling efficiencies, we normalized proteins to histone H4 (see Methods). Using this analysis, we identified 76 proteins that were significantly enriched in either the EdU pulse or thymidine chase samples (Supp. Table 3-1). Most of the proteins enriched in our experiments were derived from the EdU pulse samples (Fig. 3-2B; 74 of 76). This is likely due to the relatively short thymidine chase time we adopted to allow us to focus on replication fork-associated proteins. Several lines of evidence indicate that our iPOND strategy is effective in isolating replication fork-associated proteins from *Drosophila* embryos. First, out of the top 25 enriched proteins in our data set, 18 are known replication factors (Supp. Table 3-2). Second, a Gene Ontology (GO) analysis of the 76 proteins enriched in the EdU pulse samples was highly enriched for DNA replication and DNA replication-associated processes (Fig. 3-2C). Therefore, we conclude that iPOND is an

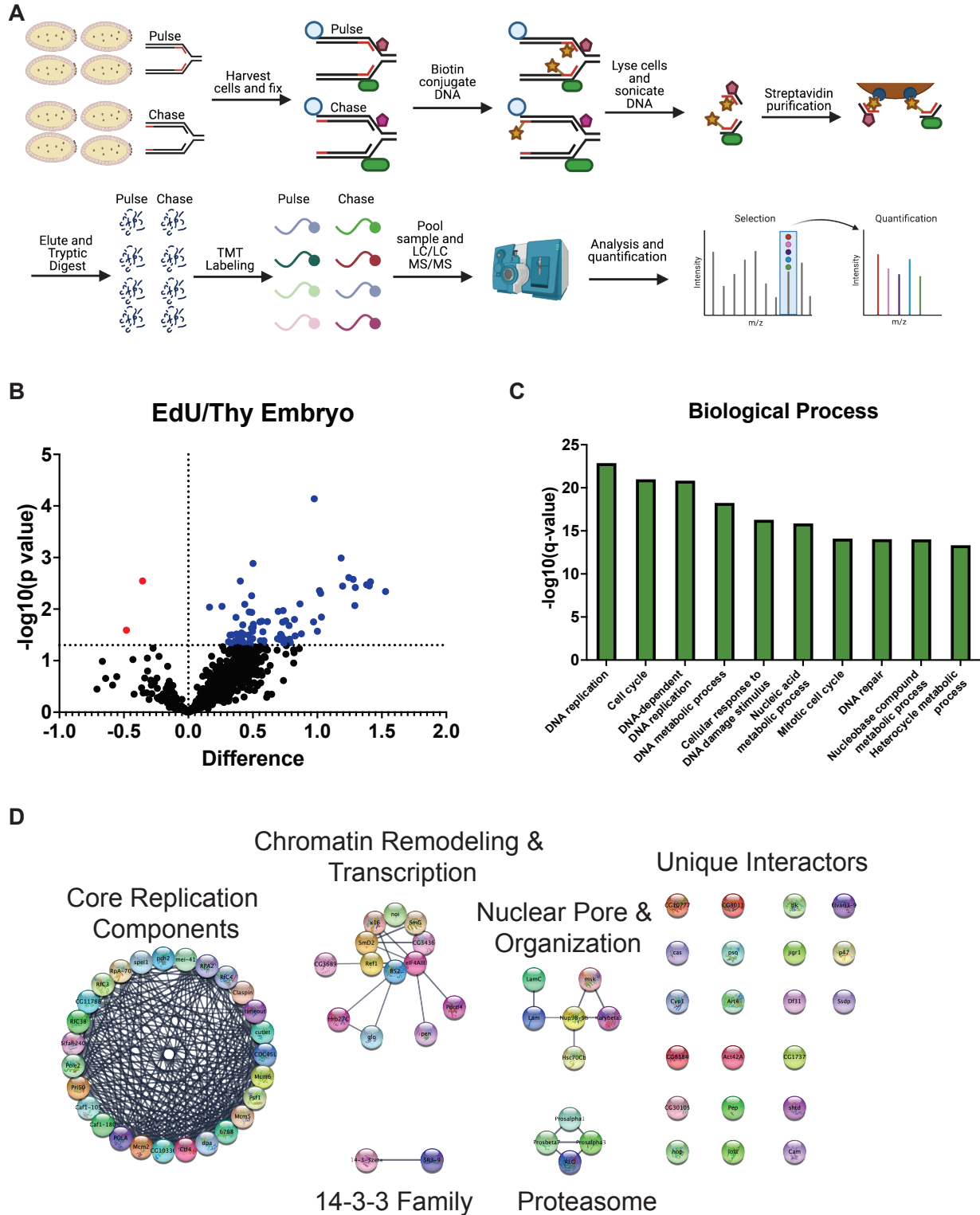


Figure 3-2: iPOND coupled to quantitative mass spectrometry in the post-MZT embryos. (A) A schematic of the labeling and mass spectrometry process for iPOND-TMT in *Drosophila* post-MZT

embryos. **(B)** Volcano plot visualizing proteins identified as enriched or depleted in the pulse versus the chase embryo samples. Enrichment on the X-axis ($\log_2[\text{pulse}] - \log_2[\text{chase}]$) and $-\log_{10}(\text{p-value})$ on the Y-axis. **(C)** The top 10 enriched biological processes of the proteins enriched in the pulse sample as determined by Gene Ontology (GO) analysis. **(D)** Network map of the proteins enriched in the pulse sample, clustered into groups of known interactors using the STRING database with no additional interactors added. Contributions: TMT labeling for the experiment, analysis, visualization.

effective strategy to proteins at or in close proximity to active replication forks during *Drosophila* embryogenesis.

We wanted to categorize the proteins in our data set in an unbiased manner to identify existing and potentially new protein networks centered around the replication machinery. To this end, we analyzed all enriched proteins using the STRING network in Cytoscape to identify proteins known to interact with one another. This analysis identified a network cluster of 27 known DNA replication and repair proteins (Fig. 3-2D). This cluster contains known helicase subunits, DNA polymerases, clamp loading factors and other factors (Fig. 3-2D). Additionally, it contains proteins involved in replication fork stability and response to DNA damage (Mei-41/ATR, Timeout/Timeless, CG10336/Tipin and Claspin) (Sibon et al. 1999; Benna et al. 2010; Lee et al. 2012; Gotter et al. 2007; Saldivar et al. 2017). Unexpected clusters were also identified. For example, we identified a cluster of proteins involved in RNA processing and a cluster involved in nuclear organization and the nuclear pore. We also identified several unique replication fork-associated proteins that did not readily form interaction networks. Together, we conclude that iPOND can be used in *Drosophila* embryos to identify existing and potentially new replication fork-associated proteins.

iPOND mass spectrometry identifies proteins at or in close proximity to active replication forks in *Drosophila* cultured cells

To extend the utility of iPOND in *Drosophila*, we performed iPOND in *Drosophila* S2 cultured cells. We previously performed iPOND in S2 cells, but did not couple iPOND to quantitative mass spectrometry (Munden et al. 2018). First, we validated that iPOND functions in S2 cells (Supp. Fig. 3-1A). Next, we performed iPOND coupled to quantitative mass spectrometry with TMT labeling using $\sim 10^9$ cells/ biological replicate (Fig. 3-3A). Similar to our results in embryos, all of the enriched proteins were found in the pulse sample rather than the chase (Fig. 3-3B). This is likely due to the short chase time we used in these experiments. One difference we noted, however, is that we identified 278 proteins at or in close proximity to active replication forks in S2 cells (compared to 76 in embryos) (Supp. Table 3-3). While significantly higher than embryos, this protein number is similar to other iPOND and iPOND-like data sets in mammalian cells.

Similar to our embryo data set, multiple lines of evidence indicate that our purifications successfully captured replication fork-associated proteins. Out of the top 25 enriched proteins in our data set, 22 are known replication factors (Supp. Table 3-4). Next, a Gene Ontology (GO) analysis of proteins enriched in the EdU pulse samples was highly enriched for DNA replication and DNA replication-associated processes (Fig. 3-3C). We attempted to generate an unbiased interaction network map using the STRING network in Cytoscape for the 278 enriched proteins, however, the networks were too dense to effectively visualize any meaningful interaction network hubs (Supp. Fig. 3-1B). For prioritization, we selected the proteins with an adjusted p value of < 0.05 and greater than 1.8-fold enrichment in the pulse relative to the chase. These stringent statistical cutoffs

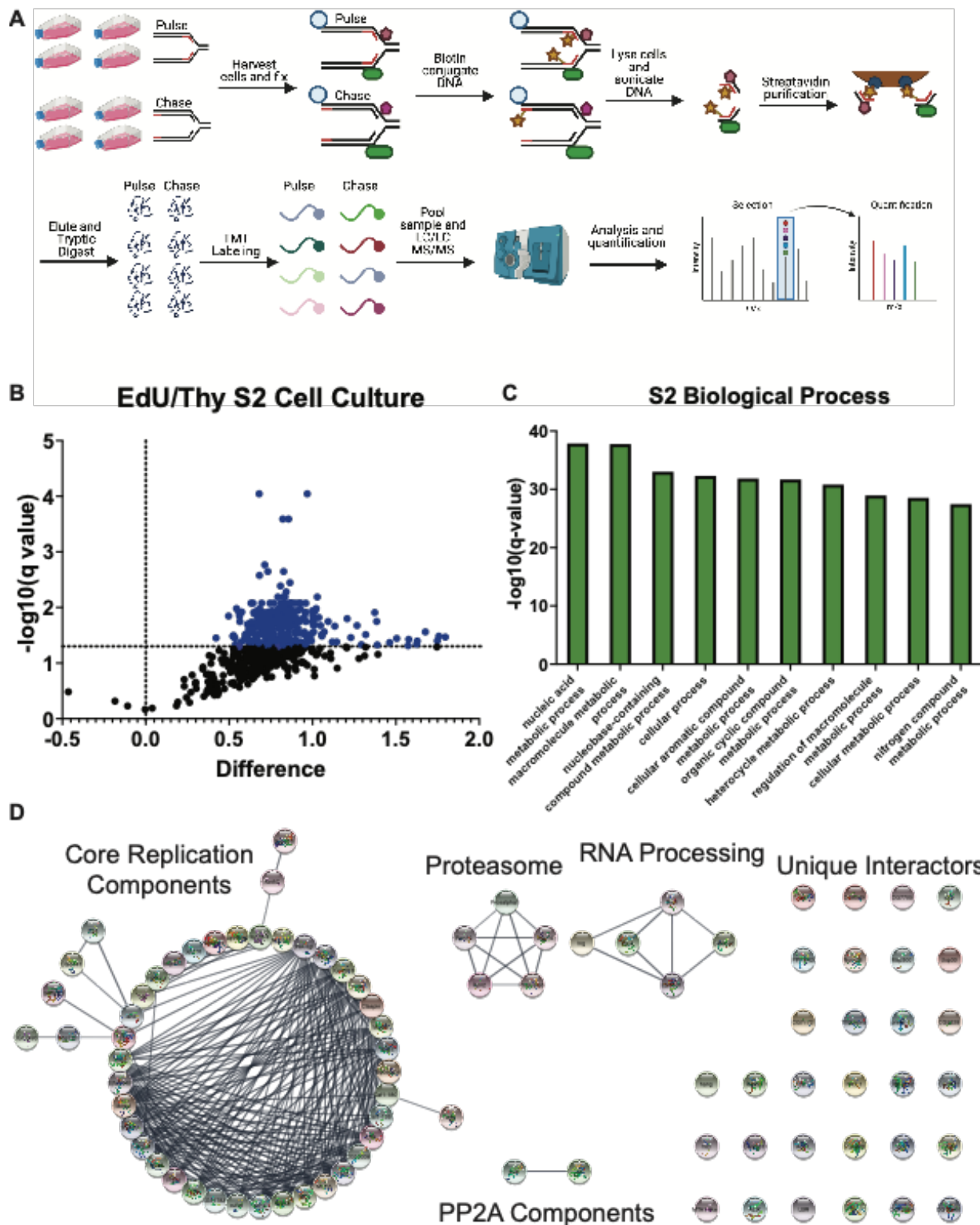


Figure 3-3: iPOND coupled to quantitative mass spectrometry in S2 cells. (A) A schematic of the labeling and mass spectrometry process for iPOND-TMT in *Drosophila* S2 cells. (B) Volcano plot visualizing

those proteins identified as enriched or depleted in the pulse versus the chase cell culture samples. Enrichment ($\log_2[\text{pulse}] - \log_2[\text{chase}]$) on the X-axis and $-\log_{10}(\text{p-value})$ on the Y-axis. (C) The top 10 enriched biological processes of the proteins enriched in the pulse sample as determined by Gene Ontology (GO) analysis. (D) Network map of the proteins enriched in the pulse sample, clustered into groups of known interactors using the STRING database with no additional interactors added. For visualization, we included proteins with a corrected p value of < 0.05 and a > 1.8 -fold fold enrichment (99 total proteins). The full list of enriched interactors can be found in Supplemental Table 4. Contributions: Experiment, analysis, and visualization.

revealed 99 high-confidence proteins that were ultimately used to generate interaction network clusters, which consisted of known replication fork factors, further validating this data set and statistical analysis (Fig. 3-3D). Also, we identified networks containing proteasome components, RNA processing factors, protein phosphatase 4 complex (PP4) and a number of proteins with no recognized network connections (Fig. 3-3D)

BRWD3 affects genome stability and replication fork progression

To determine if any of the replication fork-associated factors we identified affect genome stability, we used RNAi to deplete select factors and measured the global level of DNA damage. We chose to perform this targeted screen in S2 cells rather than post-MZT embryos due to the rapid and efficient depletion that can be obtained in S2 cells without the need to generate new reagents (Echeverri and Perrimon 2006). To quantify the global levels of DNA damage, we measured the level of phosphorylated H2Av (γ -H2Av), the *Drosophila* equivalent to mammalian γ -H2Ax, which is found at double strand breaks and stalled replication forks by immunofluorescence (Madigan et al. 2002; Mah et al. 2010). Of the 15 factors we chose, some but not all have known functions in DNA replication or DNA repair (Jin et al. 2006; Vannier et al. 2013; Townsend et al. 2021; Bell et al. 2011; Bandura et al. 2005; Mansfield et al. 1994; Kappes et al. 2011; Sousa-Nunes et al. 2009; Klymenko et al. 2006; Sibon et al. 1999). We validated knock down efficiency

and the effect on cell proliferation for all factors (Supp. Fig 3-2A and 2B). As our negative control, we used a non-targeting RNA to *GFP* that is not present in S2 cells. As a positive control we targeted DNA polymerase alpha (*DNA pol α*), which is necessary for continual priming of the lagging strand (Fig 3-4a) (Muzi-Falconi et al. 2003). Depletion of several factors resulted in increased H2Av phosphorylation (Fig. 3-4a). For example, depletion of *Cul4*, *RTEL*, *ELG1* and *BRWD3* all caused increased DNA damage consistent with mammalian studies (Jin et al. 2006; Vannier et al. 2013; Townsend et al. 2021; Bell et al. 2011). Interestingly, knockdown of *polybromo*, a component of the Brahma chromatin remodeling complex (Thompson 2009), also caused an increase in DNA damage (Fig. 3-4a). Depletion of several factors caused a decrease in γ -H2Ax signal intensity, suggesting these factors contribute to DNA damage detection or signaling (Fig. 3-4a). Consistent with this hypothesis, depletion of *mei41* (the *Drosophila* ATR ortholog) decreased γ -H2Av intensity.

BRWD3 is a targeting specificity factor for the DDB1/Cul4 ubiquitin ligase complex (CRL4) (Jackson and Xiong 2009). In mammalian cells, one of the BRWD3 orthologs DCAF14/PHIP associates with replication forks upon DNA replication stress (Townsend et al. 2021). Depletion of DCAF14 results in a modest increase in DNA damage, which is exacerbated upon replication stress (Townsend et al. 2021). Depletion of BRWD3 in *Drosophila* S2 cells causes an increase in γ -H2Ax levels in unstressed cells (Fig. 3-4a). This suggests that BRWD3/DCAF14 has an evolutionarily conserved role at the replication fork to maintain genome stability. Given these observations, we wanted to determine if BRWD3 affects replication fork progression in unchallenged *Drosophila* cells. To this end, we developed a DNA combing protocol for *Drosophila* S2 cells. While we

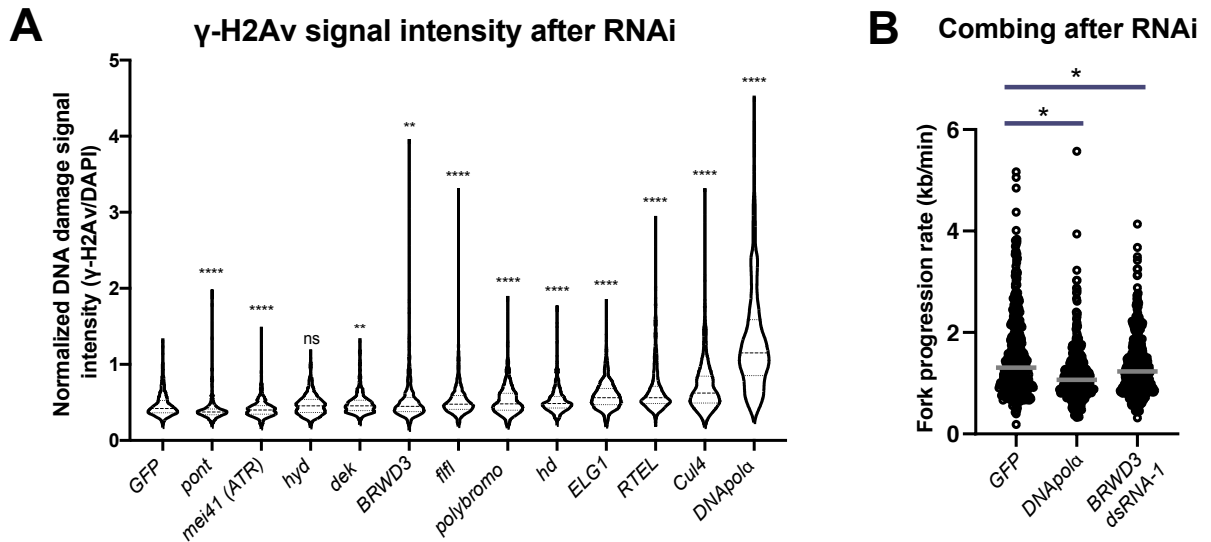


Figure 3-4: **BRWD3 affects genome stability and replication fork progression.** (A) RNAi-based depletion screen of candidate replication fork-associated proteins in S2 cells. Violin plots of the γ -H2Av intensity per nucleus normalized to total DNA content. Each distribution represents the signal intensities of 700 randomly selected cells from two biological replicates. **** $p < 0.0001$ and ** $p < 0.01$ using a Kruskal–Wallis one-way analysis of variance. (B) Rate of fork progression in control and BRWD3 depleted S2 cells. 400 fibers from two biological replicates were pooled. BRWD3 dsRNA-1 was used for this experiment. Bars represent the median fork speed. * $p < 0.05$ using a Kruskal–Wallis one-way analysis of variance followed by a Dunn’s multiple comparison post-test. Contributions: None.

initially attempted to perform DNA combing with both IdU and CldU nucleoside analogs, we were unable to successfully perform combing with IdU (data not shown). This would have allowed us to measure fork rate, fork asymmetry and inter-origin distance. To solely measure the rate of fork progression, we performed DNA combing analysis with CldU as the sole nucleotide analog. As positive and negative controls, we used interfering RNAs against *DNA pol α* and *GFP*, respectively. Depletion of *BRWD3* caused a decreased rate of fork progression in untreated cells (Fig. 3-4b). To rule out an off-target effect of the RNAi construct, we performed the DNA combing assay with an independent RNAi construct (Supp. Fig. 3-3A). We also validated the knock down efficiency of both RNAi constructs by Western blot (Supp. Fig. 3-3B). Thus, we conclude that BRWD3 functions

at or in close proximity to the replication fork to promote replication fork progression and genome stability in *Drosophila*.

Discussion

By developing a large-scale EdU labeling protocol in *Drosophila* embryos, we were able to perform iPOND in a developing organism. By coupling iPOND to quantitative mass spectrometry we identified 76 replication fork-associated proteins in *Drosophila* post-MZT embryos. Giving confidence to this method of identifying replication fork-associated proteins, 32 proteins we identified have known roles in DNA replication or repair. We note, however, that not all known replication fork-associated proteins were identified in our data set. Multiple reasons likely explain this observation. First, we used a stringent statistical cut off in our analysis to avoid false positives (see Methods). Second, either due to loss in purification or difficulty in mass spectrometry, some replication proteins are simply not detected by mass spectrometry, resulting in false negatives. Therefore, we suspect that 76 proteins are an underestimate of the total number of replication fork-associated proteins in post-MZT embryos.

While iPOND-TMT identified 76 proteins in post-MZT embryos, the same technique uncovered 278 proteins in *Drosophila* cultured cells. Although this number of proteins is higher than what we observed in embryos, it is similar to recent iPOND and iPOND-like experiments coupled to quantitative mass spectrometry performed in mammalian cells (Wessel et al. 2019; Alabert et al. 2014). The difference in protein number between post-MZT embryos and cultured cells could be due to cell-type-specific factors in S2 cells or technical differences when performing iPOND in embryos vs.

cultured cells. It should be noted, however, that the rate of replication fork progression is similar in *Drosophila* embryos and cultured cells (Blumenthal et al. 1974). Given that a single pulse of EdU is the only technical limitation with iPOND, it seems unlikely that differences in the amount of EdU labeling are responsible for the differences in protein number between the two developmental states. One complicating factor when trying to compare iPOND data sets for cell-type-specific factors is that lack of a protein in one sample could be due to a limitation in peptide detection in mass spectrometry. Therefore, we cannot use the lack of a protein in one developmental sample as direct evidence that a protein is cell-type specific. Nonetheless, our data reveal numerous replication fork-associated proteins in *Drosophila* embryos and cultured cells that can serve as a resource for anyone interested in replication fork composition and activity.

One factor that we identified as a replication fork-associated protein is BRWD3. Interestingly, one of the BRWD3 orthologs in mammalian cells also functions at the replication fork to maintain genome stability upon replication stress (Townsend et al. 2021). One key difference, however, is that in *Drosophila* BRWD3 functions at or in close proximity to active replication forks in the absence of exogenous replication stress. Therefore, while BRWD3 and DCAF14 are both substrate specificity factors for CRL4, they likely function differently in mammalian cells and *Drosophila*. While it is tempting to speculate that CRL4^{BRWD3} targets a critical factor for ubiquitylation at the replication fork, further work will be necessary to test this hypothesis. For example, BRWD3 could alter the activity of a factor that directly controls fork progression away from a replication fork. Therefore, although BRWD3 can be found at or in close proximity to active replication forks, its effect on replication fork progression could be indirect.

In summary, we have developed a protocol for the biochemical isolation of replication fork-associated proteins in *Drosophila* embryos and cultured cells. Our work suggests that replication fork composition can be modulated during development. Importantly, we have provided a resource of replication fork-associated factors in *Drosophila* for those interested in DNA replication, DNA repair and chromatin dynamics during replication.

Materials and Methods

EdU pulsing of embryos

Oregon R flies were expanded into population cages on grape juice plates supplemented with wet yeast. Cages were kept at 25°C in a humidified room and plates changed daily. Prior to embryo collections, flies were precleared for at least two hours. To acquire post-MZT embryos, flies were allowed to lay for two hours, and the plate was aged for three hours at 25°C to obtain 3-5 hours AEL embryos. Embryos were transferred to a container with a wire mesh bottom, washed in water and embryos were dechorionated in 50% bleach for two minutes. After washing, embryos were arranged in a monolayer on the mesh and bucket were dried with paper towels. Embryos were allowed to air dry 4-10 minutes, then submerged in octane for precisely 3.5 minutes with gentle shaking. Embryos were then air dried for one minute while shaking. Permeabilized embryos were pulsed with 10 M EdU in EBR for 10 minutes. For chase samples, EdU-pulsed embryos were transferred to a new solution containing 20M of thymidine for an additional 30 minutes. After pulse/chasing, embryos were transferred to a scintillating flask in 10mL of heptane. 10mL of 4% PFA was added (2% final) and embryos were

shaken vigorously at room temperature for 20 minutes. After fixation, the bottom layer of PFA was removed and an equal volume of methanol was added. Embryos were shaken by hand for one minute, settled and heptane was removed. Embryos were washed in methanol twice and transferred to PBS + 0.1% Triton X-100 and permeabilized overnight at 4°C. For each batch of embryos, a small fraction was taken and biotinylated and incubated with 568-Streptavidin to ensure that at least 50% of embryos were labeled. Successful collections were pooled to obtain 500 L of embryos per biological replicate.

EdU pulsing of S2 cells

S2 cells were obtained directly from the DGRC. Cells were confirmed negative for mycoplasma contamination via PCR. Cells were grown in Schneider's Drosophila Medium with 10% heat-inactivated FBS (Gemini Bio Products) and 100 U/mL of Penicillin/Streptomycin (Fisher Scientific) and kept at 25°C. Cells were pulsed as described in (Dungrawala and Cortez 2014). Briefly, three T225 flasks of 70% confluent cells were pulsed with 10 M of EdU for 9 minutes. Cells were scraped and spun down for three minutes at 300xg. 10mL of 2% paraformaldehyde (PFA) was added to each flask and samples were fixed at room temperature on a nutator for 20 minutes. Paraformaldehyde was neutralized with glycine and cells were centrifuged for five minutes at 900xg at 4°C and resuspended in PBS with 0.1% Triton X-100 at 4°C until processing. For the chase sample, after centrifuging the cells were resuspended in cell media with 20 M thymidine and incubated for 30 minutes in the cell culture incubator before fixation. Three T225 flasks were pooled for each replicate (~7.5e⁸ cells per replicate).

iPOND

Embryos and S2 cells were biotinylated as described in (Dungrawala and Cortez 2014). Briefly, PBS, CuSO₄, Biotin-Azide, and sodium ascorbate were mixed and added to labeled cells and embryos for 30 minutes. After biotinylation, cells or embryos were washed with PBS + 0.1% Triton X-100. A crude nuclear extract was generated by douncing embryos in Buffer 1 (15 mM HEPES pH 7.6, 10 mM KCl, 5 mM MgCl₂, 0.1 mM EDTA, 0.5 mM EGTA, 350 mM sucrose) (Shao et al. 1999) twelve times using a B-type homogenizer and centrifuged for 15 minutes at 8000xg. This pellet was resuspended in 1.2mL of LB3 (1 mM EDTA, 0.5 mM EGTA, 10 mM Tris pH 7.5, 100 mM NaCl, 0.1% Na-Deoxycholate, 0.5% N-Lauroyl sarcosine) (MacAlpine et al. 2010) with 2X protease inhibitors. Cells were resuspended in 1.2 mL LB3 lysis buffer with 2x protease inhibitors. Samples were sonicated in a Bioruptor Plus (Diagenode) at high power, 10 cycles at 30" seconds on/30" seconds off. After a short break, samples were vortexed and this was repeated until 40 total cycles were achieved. 100 L of Streptavidin C1 Dynabeads were extensively washed with LB3 and added to each sample. Samples were incubated at 4°C for two hours on a nutator. The unbound material was reserved to verify chromatin fragmentation. Beads were washed five times in LB3, with the 4th wash containing 500 mM NaCl. To elute, samples were incubated at 65°C overnight on thermoblock in 1:1 combination of LB3:SB (20% glycerol, 20% SDS, 120 mM Tris pH 6.8). The next day, the eluate was removed from the beads and added to 2x Laemmli buffer with DTT and boiled for 10 minutes. This lysate was used for western blot and mass spectrometry experiments.

Western blotting

Lysates from iPOND samples were loaded onto a 4-15% Mini-Protean Stain-free protein gel (BioRad). After running the gel, samples were transferred onto 0.2 M PVDF using the Transblot Turbo system (BioRad). Membranes were blocked in 5% milk, and incubated with the appropriate antibody for 1 hour at room temperature. Histone H3 (abcam 21054, 1:3000) was used to verify the success of iPOND. After washing in TBS + 0.1% Tween-20 (TBST), secondary antibodies (Jackson Labs) conjugated with HRP were added at 1:10,000 (mouse) or 1:20,000 (rabbit). After 30 minutes at room temperature, membranes were washed with TBST, incubated with Clarity ECL for 5 minutes (Bio-Rad) and visualized using a Bio-Rad ChemiDoc MP Imaging System.

TMT Labeling

After verifying iPOND was successful by Western blot (5% of total material), the remaining purified material was precipitated using methanol and chloroform and washed with methanol to remove excess detergent. Protein was resuspended in 5 L fresh 1% Rapigest. 32.5 L of mass spectrometry grade water with HEPES (pH 8.0 at a final concentration of 100mM). Disulfide bonds were reduced with freshly made 5mM TCEP and incubated for 30 minutes at room temperature. Fresh Iodoacetamide was added at a final concentration of 10mM to acetylate free sulfhydryl bonds. Protein was digested overnight with 0.5 g trypsin at 37°C with shaking and covered from light. The next day, samples were labeled using a TMT10plex kit (Thermo Scientific catalog #90110). TMT labels were resuspended in acetonitrile and each sample was incubated with the appropriate amount of TMT reagent for 1 hour at room temperature. Excess label was

neutralized with 0.4% final concentration of ammonium bicarbonate for 1 hour. Samples were mixed and acidified with formic acid to a pH 2. The mixed sample was reduced to 1/6 of the original volume using a SpeedVac, and brought back up to original volume with Buffer A (5% acetonitrile, 0.1% formic acid). Rapigest was cleaved by incubating for one hour at 42°C. The samples were centrifuged at 14,000 rpm for 30 minutes and the supernatant was transferred to a fresh tube and stored at -80°C until mass spectrometry analysis.

Liquid Chromatography – Tandem Mass Spectrometry

MudPIT microcolumns were prepared as previously described (Fonslow et al. 2012). Peptide samples were directly loaded onto the columns using a high-pressure chamber. Samples were then desalted for 30 minutes with buffer A (97% water, 2.9% acetonitrile, 0.1% formic acid v/v/v). LC-MS/MS analysis was performed using a Q-Exactive HF (Thermo Fisher) or Exploris480 (Thermo Fisher) mass spectrometer equipped with an Ultimate3000 RSLCnano system (Thermo Fisher). Embryo samples were analyzed on the Exploris480 while the S2 cell culture were analyzed on the Q-Exactive HF. MudPIT experiments were performed with 10µL sequential injections of 0, 10, 30, 60, and 100% buffer C (500mM ammonium acetate in buffer A), followed by a final injection of 90% buffer C with 10% buffer B (99.9% acetonitrile, 0.1% formic acid v/v) and each step followed by a 130 minute gradient from 5% to 80% B with a flow rate of 300nL/minute when using the Q-Exactive HF and 500nL/minute when using the Exploris480 on a 20cm fused silica microcapillary column (ID 100 µm) ending with a laser-pulled tip filled with Aqua C18, 3µm, 100 Å resin (Phenomenex). Electrospray ionization

(ESI) was performed directly from the analytical column by applying a voltage of 2.0kV when using the Q-Exactive HF and 2.2kV when using the Exploris480 with an inlet capillary temperature of 275°C. Using the Q-Exactive HF, data-dependent acquisition of mass spectra was carried out by performing a full scan from 300-1800 m/z with a resolution of 60,000. The top 15 peaks for each full scan were fragmented by HCD using normalized collision energy of 38, 0.7 m/z isolation window, 120 ms maximum injection time, at a resolution of 45,000 scanned from 100 to 1800 m/z and dynamic exclusion set to 60s. Using the Exploris480, data-dependent acquisition of mass spectra was carried out by performing a full scan from 400-1600m/z at a resolution of 120,000. Top-speed data acquisition was used for acquiring MS/MS spectra using a cycle time of 3 seconds, with a normalized collision energy of 36, 0.4m/z isolation window, 120ms maximum injection time, at a resolution of 45,000 with the first m/z starting at 110. Peptide identification and TMT-based protein quantification was carried out using Proteome Discoverer 2.4. MS/MS spectra were extracted from Thermo Xcalibur .raw file format and searched using SEQUEST against a Uniprot *Drosophila melanogaster* proteome database (downloaded February 6th, 2019 and containing 21114 entries). The database was curated to remove redundant protein and splice-isoforms, and supplemented with common biological MS contaminants. Searches were carried out using a decoy database of reversed peptide sequences and the following parameters: 10ppm peptide precursor tolerance, 0.02 Da fragment mass tolerance, minimum peptide length of 6 amino acids, trypsin cleavage with a maximum of two missed cleavages, dynamic methionine modification of 15.995 Da (oxidation), static cysteine modification of 57.0215 Da (carbamidomethylation), and static N-terminal and lysine modifications of 229.1629 Da.

iPOND-TMT data analysis

To determine enrichment or depletion of the proteins, the TMT intensities for each protein was \log_2 transformed and samples were normalized based on median TMT intensity per channel. Log₂-transformed, median normalized TMT intensities were further normalized to the level of Histone H4, as the resulting incorporation of this histone should be identical between each sample. Enrichment values were calculated based on this normalized data. Cellular localization data was determined for each protein using the Gene Ontology Cellular Compartment (FlyBase v2021_05). Proteins that lacked any nuclear or chromatin compartmental data were removed from the datasets. To determine if a protein was significantly enriched or depleted in the pulse or chase embryo samples, an unpaired t-test was performed for each protein. Our uncorrected p values were validated because our positive controls (known replication proteins) were identified. For S2 cell data, an unpaired t-test was performed for each protein with a Benjamini, Krieger and Yekutieli multiple test correction and false discovery rate of 5%.

For the pathway enrichment analysis of enriched proteins, PANTHER Gene Ontology was used (Ashburner et al. 2000; Carbon et al. 2020; Mi et al. 2019). Enriched proteins were inputted and the default background for *Drosophila melanogaster* was selected. The biological process pathway was used, and the results were exported to Excel and the top 10 pathways were chosen by q-value, and visualized in Graphpad Prism

For network clustering, all of the proteins enriched in the embryo and S2 pulse were loaded as separate networks in Cytoscape v3.9.0 (Shannon et al. 2003). The resulting interactions were visualized using the STRING network with the stringApp, using

the *Drosophila melanogaster* setting with 0 additional interactors and a confidence score cutoff of 0.8 (Szkarczyk et al. 2021; Doncheva et al. 2019).

RNAi and immunofluorescence in S2 cells

RNAi in S2 cells was performed as described (Rogers and Rogers 2008). Briefly, dsRNA against each candidate RNA was designed to be 200-500 bp. Primers used to generate dsRNA are listed in Supplemental Table 3-5. The dsRNAs were synthesized using the Invitrogen MEGAscript T7 Transcription Kit (Ambion). For each sample, 1.5 million S2 cells were seeded in 1 ml non-serum medium in a 6-well plate and 30 µg of dsRNA was added. After 45 minutes incubation at room temperature, 2ml of serum-containing medium was added and cells were incubated for an additional five days. Reverse transcription and quantitative PCR (RT-qPCR) and Western blotting was performed to determine the knock down efficiency using a rabbit anti-BRWD3 antibody at 1:500 (Morgan et al. 2017). For immunofluorescence, RNAi-treated cells were attached to Concanvan A-coated slides for 15 minutes, fixed for 15 minutes in 4% paraformaldehyde and permeabilized for 15 minutes in PBS supplemented with 0.3% Triton-X-100 (PBT). Cells were then blocked for 60 minutes in blocking buffer, containing 1% BSA and 0.2% goat serum in 0.1% PBT. After blocking, cells were incubated with rabbit anti-γ-H2Av (1:500, Rockland, # 600-401-914) antibody overnight at 4°C in blocking buffer. After washing with PBS, cells were incubated with goat anti-rabbit IgG secondary antibody (1:500, Life Technologies, # A11011) in blocking buffer for one hour at room temperature and stained with DAPI (0.1 µg/mL) in PBT for 10 minutes and mounted in Vectasheild (Vector Labs). All images were obtained using Nikon Ti-E inverted

microscope with a Zyla sCMOS digital camera with a 20X oil objective. For each biological replicate, all samples were captured at the same magnification and same exposure time. For quantitative analysis of γ -H2Av levels, regions of interest (ROIs) were defined based on the DAPI signal. The mean signal intensity of γ -H2Av was extracted for each ROI. The signal was normalized to the DAPI signal intensity to account for differences in the total amount of DNA. 350 randomly selected cells were used for each biological replicate. Two biological replicates were used for the data analysis. Kruskal-Wallis one-way analysis of variance was performed in GraphPad Prism for statistical significance.

DNA molecular combing

Drosophila S2 cells were pulsed with 20 μ M of CldU nucleoside (Sigma-Aldrich, C6891) for 20 minutes. Cells were washed with PBS then ~1.5-3.0 million cells were embedded in agarose plugs. The assay was performed as described in Genomic Vision's manufacturer instructions. The stretched and denatured DNA was stained with a CldU-specific antibody (Abcam Cat#ab6326) for 1 hour, washed in PBS, then probed with a secondary antibody (Thermo, A11007) for 30min. Coverslips were washed with PBS then mounted. Stained coverslips were imaged using a Nikon Ti-E inverted microscope with a Zyla sCMOS digital camera with a 40X oil objective. For each sample, 200 DNA fiber lengths were measured manually using Nikon NIS-Elements AR v4.40. Investigator was blinded to sample identity. Two biological replicates were performed per sample. The length of a given fiber is directly proportional to the rate of replication fork progression. Therefore, fiber lengths were converted to fork progression rates given the 20-minute pulse time (Fiber length *20min / 2kb•min⁻¹). Kruskal-Wallis one-way analysis of variance

followed by Dunn's multiple comparisons post-test was performed in GraphPad Prism for statistical significance.

Acknowledgments

We thank Martina Brienza-Ramos for assistance with EdU labeling of embryos used in this study. We thank David Cortez and Kavi Mehta for advice and guidance with DNA combing. We thank A. Shilatifard for providing the *Drosophila* anti-BRWD3 antibody. We thank Sarah Wessel and members of the Nordman lab for providing critical feedback on the manuscript. This work was supported by National Institutes of Health (NIH) General Medical Sciences awards R35GM133552 to L.P. and R35GM128650 to J.T.N.. M.T.W was supported by the Vanderbilt Chemistry-Biology Interface Training Program (T32GM065086) and the National Science Foundation Graduate Research Fellowship Program.

Author Contributions

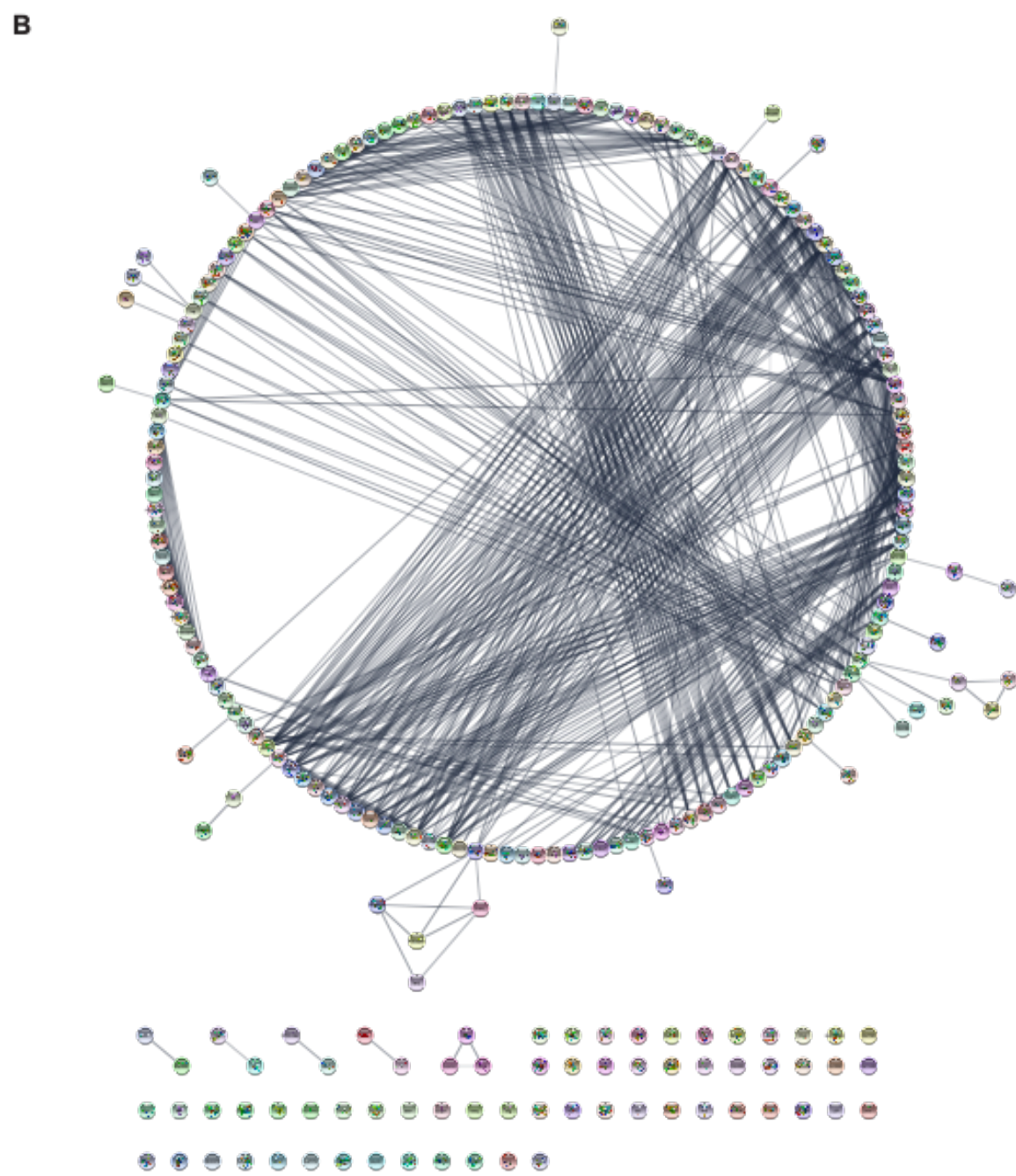
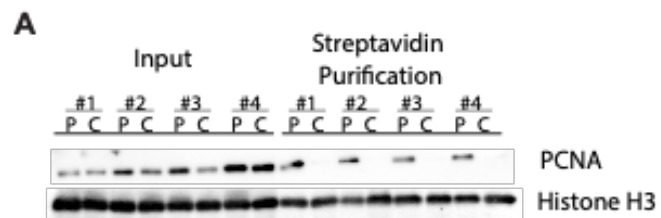
A.M. and J.T.N planned and designed the research; A.M., R.T, D.S performed experiments; A.M., M.W, D.H., and R.T. analyzed data with supervision from L.P and J.T.N; A.M. and J.T.N. wrote the manuscript with input from all of the authors. A.M., M.W., D.H., R.T., L.P. and J.T.N. edited the manuscript.

Data Availability Statement

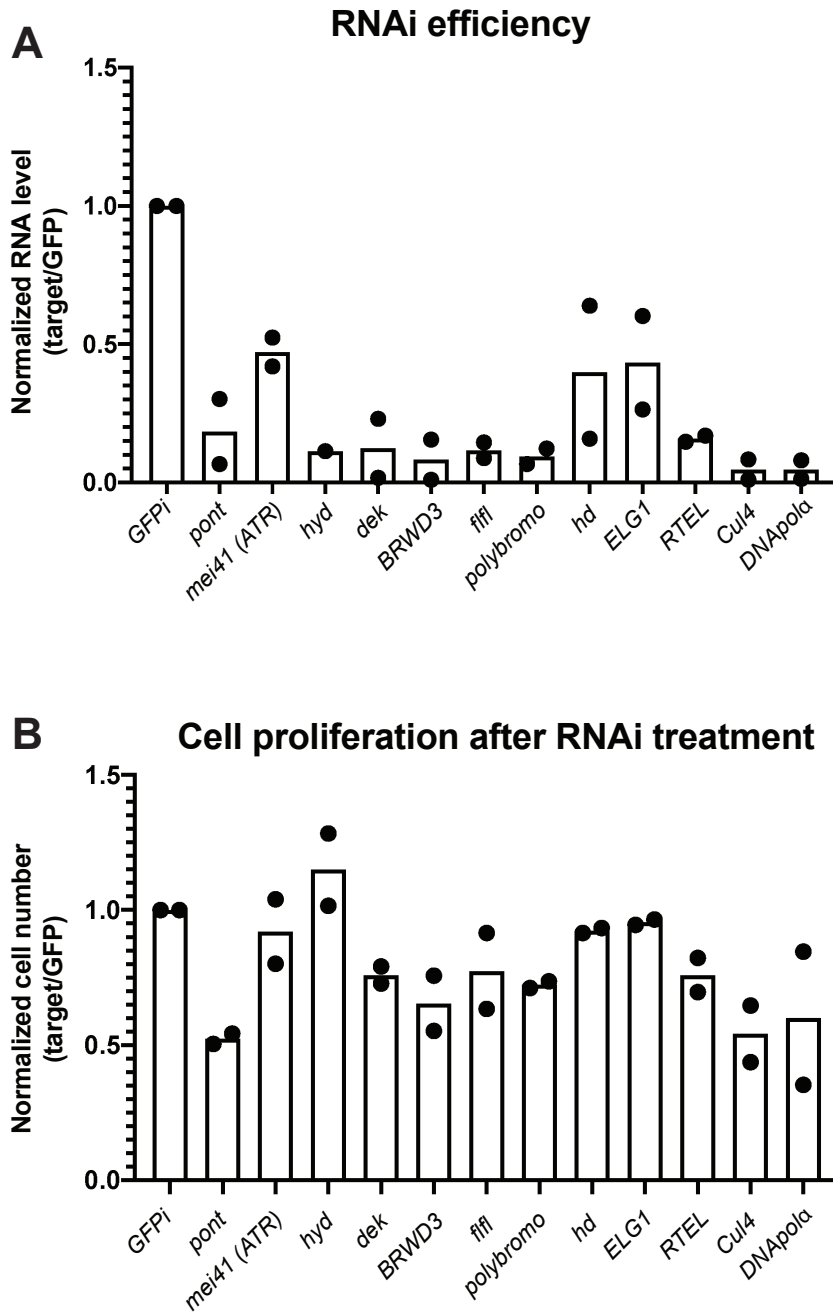
The mass spectrometry proteomics data have been deposited to the ProteomeXchange Consortium via the PRIDE partner repository with the dataset identifier PXD031165 <http://www.ebi.ac.uk/pride/archive/projects/PXD031165>

Additional Information

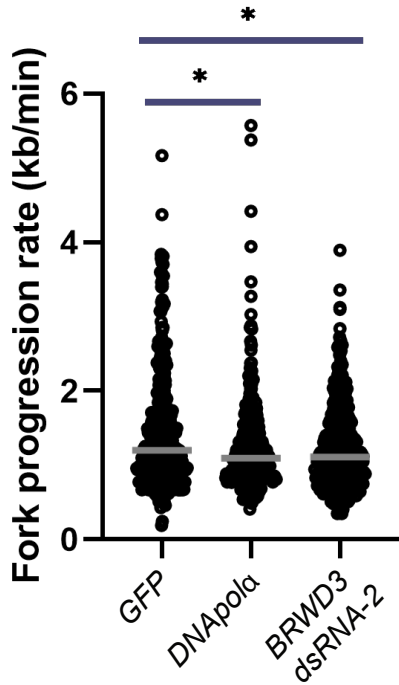
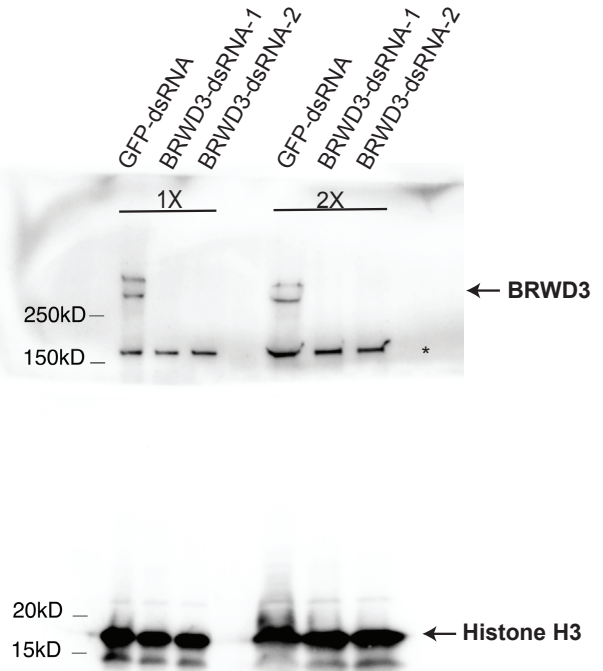
Supplementary information. Two supplemental figures and five supplemental tables. Competing interests: The authors declare no competing interests



Supplemental Figure 3-1. **Analysis of iPOND and iPOND-TMT in S2 cultured cells.** (A) Western blot confirmation of iPOND in S2 cells. The first eight lanes are from input and the last eight from the streptavidin purifications. PCNA is a marker for active replication forks and is enriched in the pulse sample purifications. Histone H3 is a general marker of chromatin and enriched in both the pulse and chase samples. P = Pulse, C = Chase, and #1-4 represent the replicate numbers. (B) Total network map of the 278 replisome-associated proteins in S2 cells. Contributions: Experiment, analysis, and visualization of A.



Supplemental Figure 3-2: **Validation of RNAi-based depletion of targets.** (A) Normalized depletion efficiency for two biological replicates. The normalized ratio is the target/*Tubulin* in the non-targeting *GFP* control divided by target/*Tubulin* in the RNAi-treated cells (B) Cell proliferation after five days of RNAi depletion relative to the *GFP* non-targeting control. Contributions: None.

A**B**

Supplemental Figure 3-3: **Validation of BRWD3 combing and knockdown.** **(A)** A second replicate of DNA fiber combing was performed for a second, independent BRWD3 RNAi. **(B)** Validation of the BRWD3 knockdown using western blot. Contributions: None.

Supplemental Table 3-1: Unnormalized TMT Intensities for Embryo POND Replicates

Accession	Description	Coverage [%]	# Peptides	# PSMs	# Unique Peptides	# AAs	MW [kDa]	calc. pl	Score	Sequest HT	# Peptides	# Razor Peptides	EdU Pulse R1	EdU Pulse R2	EdU Pulse R3	EdU Pulse R4	Thy Chase R1	Thy Chase R2	Thy Chase R3	Thy Chase R4
Q6AVN0	1,2-dihydroxy-3-keto-5-methylthiopentane dioxigenase OS=Drosophila melanogaster OX=	25	4	5	4	186	22.2	5.35	1.61	4	0	0	20.1	22.6	25.4	17.6	13.2	24.5	30.2	20.1
A1Z992	1,4-Alpha-Glucan branching enzyme OS=Drosophila melanogaster OX=7227 GN=AGBE F	11	7	18	7	685	79.1	6.25	19.43	7	0	353	409.5	386	325.7	256.5	414.4	443.8	332.3	
P48375	12 kDa FK506-binding protein OS=Drosophila melanogaster OX=7227 GN=FK506-bp2 PE	24	2	15	2	108	11.7	8.13	32.7	2	0	225.1	206.3	201.6	138	124.2	206.4	216.4	112.7	
P92177	14-3-3 protein zeta OS=Drosophila melanogaster OX=7227 GN=14-3-3zeta PE=1 SV=1	33	6	99	5	262	29.8	4.78	110.56	6	0	1963.2	2148.3	2132	1578.2	1421.9	1853.4	2301.7	1873.7	
P29110	14-3-3 protein epsilon OS=Drosophila melanogaster OX=7227 GN=14-3-3epsilon PE=1 SV=1	32	6	70	5	248	28.2	4.88	100.3	6	2	1361.5	1569.6	1513.9	1263.7	1112.6	1323.9	1697.7	1349.9	
Q9VFE9	2-[3-amino-3-carboxypropyl]histidine synthase subunit 2 OS=Drosophila melanogaster OX	8	2	2	2	469	52.1	5.25	0	2	0	0	0	0	0	0	0	0	0	0
Q9V3U6	26-29kD-proteinase OS=Drosophila melanogaster OX=7227 GN=26-29-p PE=1 SV=1	3	2	6	2	549	62.1	6.74	7.76	2	0	126.4	160.6	153.5	169	149.3	170.4	272.2	193.8	
AOA0B4K110	26S proteasome non-ATPase regulatory subunit 1 OS=Drosophila melanogaster OX=722	8	8	24	8	1029	114.4	5.19	34.34	8	0	571.5	702.4	759.1	610.8	544.5	701	1103	639.2	
Q9V3G7	26S proteasome non-ATPase regulatory subunit 6 OS=Drosophila melanogaster OX=722	22	7	27	7	389	45.4	6.48	50.09	7	0	775.3	846.5	923.3	742.8	658.8	942.6	1112.5	814	
Q9VFS8	26S proteasome non-ATPase regulatory subunit 9 OS=Drosophila melanogaster OX=722	10	2	5	2	220	23.9	5.66	2.65	2	0	69.4	72.4	73.7	52.4	56	80.7	103.8	62	
Q9V436	26S proteasome regulatory complex subunit p30 OS=Drosophila melanogaster OX=7227	16	4	25	4	264	30.2	6.06	43.78	4	0	290.6	347.7	374.1	330.2	254.2	365.3	500.5	336.1	
Q9V405	26S proteasome regulatory complex subunit p48A OS=Drosophila melanogaster OX=722	6	3	6	3	413	47	5.38	12.05	3	0	265.9	260.1	282.2	234.6	168.5	283.3	325.1	207	
Q7KMQ0	26S proteasome regulatory complex subunit p48B OS=Drosophila melanogaster OX=722	29	11	45	11	433	48.5	6.04	40.38	11	0	709.3	762.9	804.7	610.8	507.8	616.3	851.6	968.2	565
Q9V3V6	26S proteasome regulatory complex subunit p50 OS=Drosophila melanogaster OX=7227	23	6	41	6	428	47.8	5.34	69.08	6	0	485.3	622.5	580.7	361.5	509	592.8	712.7	388.6	
P48601	26S proteasome regulatory subunit 4 OS=Drosophila melanogaster OX=7227 GN=Rpt2 P	8	3	38	3	439	49.3	6.58	32.09	3	0	466.1	494.4	423.2	312.7	282.9	561.1	534.5	351.4	
O18413	26S proteasome regulatory subunit 8 OS=Drosophila melanogaster OX=7227 GN=Rpt6 P	8	3	14	3	405	45.8	8.41	18.33	3	0	453.5	528.2	552	500.9	371.9	532.9	715.4	557.6	
QE09B6	40S ribosomal protein S11 OS=Drosophila melanogaster OX=7227 GN=RpS11 PE=1 SV=1	12	2	13	2	155	18.1	10.93	18.18	2	0	362.3	440.1	446.4	360.4	588	597.4	713	533.3	
QO3334	40S ribosomal protein S13 OS=Drosophila melanogaster OX=7227 GN=RpS13 PE=1 SV=1	12	2	11	2	151	17.2	10.55	16.83	2	0	227.4	308.8	297.3	280	460.7	391	439.4	367	
QO2K11	40S ribosomal protein S14b OS=Drosophila melanogaster OX=7227 GN=RpS14b PE=2 SV=1	17	2	16	2	151	16.3	10.35	25.18	2	0	260.9	225.8	227	148.4	20.3	369.6	360.5	191	
P39018	40S ribosomal protein S19a OS=Drosophila melanogaster OX=7227 GN=RpS19a PE=1 SV=1	17	3	21	3	156	17.3	10.11	34.94	3	0	240.9	352.8	367.1	246.7	299.6	378.5	494.2	274.3	
P31009	40S ribosomal protein S2 OS=Drosophila melanogaster OX=7227 GN=RpS2 PE=1 SV=2	8	2	10	2	267	28.9	10.15	11.44	2	0	121.5	175.2	115.4	105	205.5	212.4	291.6	139.4	
P55828	40S ribosomal protein S20 OS=Drosophila melanogaster OX=7227 GN=RpS20 PE=1 SV=1	21	2	10	2	120	13.5	10.33	0	2	0	32.8	50.9	45.7	50.5	54.3	44.9	57.4	43.7	
QO6559	40S ribosomal protein S3 OS=Drosophila melanogaster OX=7227 GN=RpS3 PE=1 SV=1	19	2	21	2	246	27.5	9.39	47.42	2	0	380.5	538	608.7	488.7	852.1	675.3	872.4	565.1	
P55830	40S ribosomal protein S3a OS=Drosophila melanogaster OX=7227 GN=RpS3a PE=1 SV=1	19	4	28	4	268	30.3	9.61	50.59	4	0	704	748.4	716.5	544.9	741	1042.6	1015.5	681.9	
P41042	40S ribosomal protein S4 OS=Drosophila melanogaster OX=7227 GN=RpS4 PE=1 SV=2	8	2	6	2	261	29.1	10.18	8.19	2	0	164	213.4	209.7	211.1	251.9	299.8	333	218.5	
Q9VFE4	40S ribosomal protein S5b OS=Drosophila melanogaster OX=7227 GN=RpS5b PE=2 SV=1	7	2	16	2	230	25.7	8.54	34.46	2	0	484.1	652.8	679.5	608.7	851	867.8	1047.1	742.1	
P29327	40S ribosomal protein S6 OS=Drosophila melanogaster OX=7227 GN=RpS6 PE=1 SV=1	8	2	21	2	248	28.4	10.74	44.1	2	0	432.4	503	432.3	479.1	730.1	789.7	1047.1	742.1	
AOA0B4K6N1	40S ribosomal protein S8 OS=Drosophila melanogaster OX=7227 GN=RpS8 PE=3 SV=1	31	5	91	5	208	23.7	10.48	184.13	5	0	1030.7	1099	838.1	790.1	859.3	2367.4	2403.2	1780.1	
P38979	40S ribosomal protein SA OS=Drosophila melanogaster OX=7227 GN=Rsta PE=1 SV=3	17	2	7	2	270	30.2	8.77	10.21	2	0	173.8	491	256.4	119	174.5	572.3	296	145	
M8P2Y6	5'-3' exoribonuclease OS=Drosophila melanogaster OX=7227 GN=Rat1 PE=1 SV=1	5	4	9	4	968	103.9	7.05	13.21	4	0	352.1	236.9	273	236.1	160.6	318.7	331.2	268.7	
MP3F5	6-phosphogluconate dehydrogenase, decarboxylating OS=Drosophila melanogaster OX=	12	3	9	3	491	52.5	6.32	18	3	0	44.8	55.5	67	46.5	49	50.3	77.4	42.7	
P41128	60S ribosomal protein L13 OS=Drosophila melanogaster OX=7227 GN=RpL13 PE=1 SV=1	13	3	26	3	418	24.9	10.99	33.96	4	0	716.3	901.2	893.7	824.5	1133.5	1260.4	1569.1	1158.2	
Q9VNE9	60S ribosomal protein L13a OS=Drosophila melanogaster OX=7227 GN=RpL13a PE=1 SV=1	7	2	5	2	205	23.6	11.03	5.21	2	0	97	141.1	127.5	127.4	242.2	182.3	247.9	158.5	
P55841	60S ribosomal protein L14 OS=Drosophila melanogaster OX=7227 GN=RpL14 PE=1 SV=1	12	2	30	2	166	19.2	11.18	71.17	2	0	403.4	510.8	508	519.5	724	752.8	878	666.3	
O17445	60S ribosomal protein L15 OS=Drosophila melanogaster OX=7227 GN=RpL15 PE=1 SV=1	12	3	33	3	204	24.3	11.47	57.04	3	0	1481.4	1811.5	1378	1372.3	1183.8	1465.8	1705.3	1525.6	
Q9V534	60S ribosomal protein L18 OS=Drosophila melanogaster OX=7227 GN=RpL18 PE=1 SV=1	18	2	43	2	188	21.7	11.53	55.79	2	0	249.7	354.4	331	346.6	498.5	410.1	545.9	397.9	
P41093	60S ribosomal protein L18a OS=Drosophila melanogaster OX=7227 GN=RpL18a PE=1 SV=1	11	2	12	2	177	21	10.62	18.93	2	0	246.5	358.5	342.2	326.1	438.8	365.1	518.8	377.7	
P36241	60S ribosomal protein L19 OS=Drosophila melanogaster OX=7227 GN=RpL19 PE=1 SV=1	20	4	20	4	203	24	11	42.3	4	0	377.9	477.2	433.9	473.4	553.5	695.1	771.1	548	
P50887	60S ribosomal protein L22 OS=Drosophila melanogaster OX=7227 GN=RpL22 PE=1 SV=1	11	2	9	2	299	30.6	10.11	13.31	2	0	94.5	106.2	74.7	61.1	70.4	221.7	137.7	88.6	
O16797	60S ribosomal protein L3 OS=Drosophila melanogaster OX=7227 GN=RpL3 PE=1 SV=3	11	4	15	4	416	46.9	10.24	23.45	4	0	464.1	537.1	482.6	347.7	596.5	894.9	1055.8	587.4	
Q9V597	60S ribosomal protein L31 OS=Drosophila melanogaster OX=7227 GN=RpL31 PE=1 SV=1	21	3	17	3	124	14.5	10.2	26.93	3	0	578.1	641.4	541.9	738.7	589.5	787.1	907.8	608.6	
Q9W5R8	60S ribosomal protein L5 OS=Drosophila melanogaster OX=7227 GN=RpL5 PE=1 SV=2	13	4	11	4	299	34	9.77	11.09	4	0	252.7	232.6	229.7	132.1	219	393.2	424.9	150.3	
A1Z7K8	AArs-interacting multifunctional protein 1 OS=Drosophila melanogaster OX=7227 GN=AIM	15	3	10	3	323	34.4	8.91	7.58	3	0	7.9	11.9	8.3	9	10.5	8.8	17.5	12.1	
Q9VJ12	Acinus, isoform A OS=Drosophila melanogaster OX=7227 GN=Acn PE=1 SV=1	5	6	16	6	739	83.7	6.7	13.5	6	0	341.9	331.7	253.2	213.8	150.5	377.2	369.8	227.9	
Q9VIE8	Aconitase hydratase, mitochondrial OS=Drosophila melanogaster OX=7227 GN=mAcon1 F	3	2	3	2	787	85.3	8.24	1.97	2	0	11	9	22.4	8.1	23.4	16.6	11.3	5.6	
P02572	Actin-42A OS=Drosophila melanogaster OX=7227 GN=Act42A PE=1 SV=3	22	6	98	6	376	41.8	5.48	170.32	6	4	1949.8	2228.7	2426.6	2159.3	3133	2152.1	2746.8	1970.1	
P53501	Actin-57B OS=Drosophila melanogaster OX=7227 GN=Act57B PE=1 SV=1	16	5	78	5	1376	41.8	5.39	134.97	5	0	13.2	14.6	18.7	16	29.9	14.3	14.8	11.1	
Q9VU68	Actin-interacting protein 1 OS=Drosophila melanogaster OX=7227 GN=Ifr PE=2 SV=1	4	3	9	3	608	66.5	6.73	16.13	3	0	287.6	399	442.9	381.5	322.7	394.9	444.7	377.4	
P45889	Actin-related protein 1 OS=Drosophila melanogaster OX=7227 GN=Arp1 PE=2 SV=2	5	2	3	2	376	42.7	7.3	3.37	2	0	28	46.7	44.5	43.4	46.4	43.2	49.1	44.6	
Q9VMH2	Actin-related protein 2/3 complex subunit 4 OS=Drosophila melanogaster OX=7227 GN=Ar	11	2	3	2	168	19.6	8.46	3.6	2	0	31.8	37.4	38.9	32.9	38.9	31.8	47.5	30.4	
Q9VX09	Actin-related protein 8 OS=Drosophila melanogaster OX=7227 GN=Arp8 PE=1 SV=1	8	4	4	4	607	67.7	7.69	7.82	4	0	42.6	54.4	62.3	66.8	45.4	68.6	73	66.4	
P7KSM5	Activator of SUMO 1 OS=Drosophila melanogaster OX=7227 GN=Aos1 PE=1 SV=1	26	7	58	7	337	37.7	5.44	98.32	7	0	678.8	609.5	403.3	695.9	293.7	770.2	715.6	419.4	
M9NFF9	Ada2a-containing complex component 3, isoform D OS=Drosophila melanogaster OX=722	5	2	5	2	583	64	8.29	6.51	4	0	35.7	33.7	33.8	35.9	22.8	43.9	48.8	37.3	
Q9XYM0	Adapter molecule Crk OS=Drosophila melanogaster OX=7227 GN=Crk PE=1 SV=1	16	4	11	4	271	31.2	5.26	6.51	4	0	136.8	135.2	135.6	105.9	89.8	149	150.2	112.2	
Q9VHH7	Adenosine deaminase-like protein OS=Drosophila melanogaster OX=7227 GN=Ada PE=2	8	2	3	2	337	37.6	5.48	0	2	0	24.4	29.5	31.4	30.5	28.9	34.3	38.9	29.9	
X2JF40	Adenosylhomocysteinase OS=Drosophila melanogaster OX=7227 GN=Ahc PE=3 SV=1	5	2	3	2	432	47.3	6.2	15.74	2	0	133.7	102.2	109.4	76.1	70	179.2	145.6	83.8	
Q9Y0Y2	Adenylosuccinate synthetase OS=Drosophila melanogaster OX=7227 GN=AdSS PE=2 SV=1	11	4	14	4	447	48.9	6.84	19.64	4	0	62.7	75.5	78.9	61.7	60.9	68.2	87.1	69.3	
P25160	ADP-ribosylation factor-like protein 1 OS=Drosophila melanogaster OX=7227 GN=Arf1 PE=1	13	2	3	2	180	20.2	6.57	4.96	2	0	19.8	32.7	33.6	23.4	30.3	29.8	34.6	28.6	
Q26365	ADP-ATP carrier protein OS=Drosophila melanogaster OX=7227 GN=sesB PE=2 SV=4	12	4	17	4	312	34.2													

Q7JVG2	Aps, isoform A OS=Drosophila melanogaster OX=7227 GN=Aps PE=1 SV=1	16	2	2	2	177	19.9	6.05	2.47	2	0	15.4	17.6	14.1	16.2	11.6	16.1	15.9	17.5
Q9VGW7	Arginine methyltransferase 1 OS=Drosophila melanogaster OX=7227 GN=Art1 PE=1 SV=1	13	4	11	4	376	42.8	5.15	16.01	4	0	195.7	284.4	276.4	256.2	194.6	256.4	360.2	258.2
Q9VFB3	Arginine methyltransferase 3, isoform A OS=Drosophila melanogaster OX=7227 GN=Art3	6	2	3	2	516	58.9	4.73	6.93	2	0	16.3	17.3	22.5	14.4	16.8	16.8	25.5	13.8
F0JAJ1	Arginine methyltransferase 4, isoform B OS=Drosophila melanogaster OX=7227 GN=Art4	9	5	18	5	530	59.7	6.13	28.67	5	0	301.4	378.2	380.8	359.7	239	352.9	419.3	324.7
Q7K486	Arnadillo repeat-containing protein 6 homolog OS=Drosophila melanogaster OX=7227 GN	11	4	16	4	464	51.3	5.55	24.25	4	0	202.9	278.9	261.7	223.4	220.3	275.8	323.9	240.8
Q7KWT9	Asparagine synthetase OS=Drosophila melanogaster OX=7227 GN=AsnS PE=2 SV=1	8	4	7	4	558	63.2	6.49	5.17	4	0	54.9	71.4	67.7	63.1	49.6	77.7	78.6	61.2
Q9V434	Asparaginyl-RNA synthetase, isoform A OS=Drosophila melanogaster OX=7227 GN=AsnF	7	4	9	4	558	63.9	5.96	10.4	4	0	188.5	265.4	294.3	207.3	267	274.5	337.9	231.9
Q8IPY3	Aspartate aminotransferase OS=Drosophila melanogaster OX=7227 GN=Got2 PE=1 SV=1	6	2	4	2	431	48.1	8.5	10.38	2	0	30.2	52.7	84.5	79.4	192.3	70	63.8	42.7
Q7K0E6	Asparthyl-RNA synthetase, isoform A OS=Drosophila melanogaster OX=7227 GN=AspRS	4	2	6	2	531	59	6.81	4.64	2	0	61.7	85.6	105.7	105.7	118	92.1	117	86.2
Q9VJH2	Asparthyl-RNA synthetase, mitochondrial, isoform A OS=Drosophila melanogaster OX=722	8	7	18	7	1082	121.4	5.82	16.98	7	0	147.4	160.7	148.3	123.9	114	192.9	193.3	148.7
Q9VV75	AT02348p OS=Drosophila melanogaster OX=7227 GN=UQCR-C2 PE=1 SV=1	6	2	3	2	440	45.4	4.44	1.76	2	0	12.5	16.6	22.6	18.3	59.6	17.9	22	16.3
Q9VDV2	AT06125p OS=Drosophila melanogaster OX=7227 GN=BEST:GH15838 PE=1 SV=1	4	2	3	1	363	40.6	8.57	3.89	2	1	113.9	124.1	186.7	133.4	213.8	252.3	170.1	122.9
Q9VXF9	AT13091p OS=Drosophila melanogaster OX=7227 GN=mgo PE=1 SV=1	13	4	19	4	458	50.5	5.16	22.83	4	0	215.2	226.9	210.4	148.6	151.5	255.8	259.6	145.2
Q8IQF8	AT18092p OS=Drosophila melanogaster OX=7227 GN=ESTS_34F4T PE=1 SV=1	13	3	18	3	350	40.1	7.9	20.19	3	0	385.3	464.3	469.7	416.4	359.3	519.5	521	467.2
Q8TBW3	AT21416p OS=Drosophila melanogaster OX=7227 GN=Past1 PE=1 SV=1	8	5	9	5	540	61.5	6.42	11.49	5	0	127.5	129.4	145.8	100.2	117.9	146.9	159.8	106.9
Q9VM14	AT21758p OS=Drosophila melanogaster OX=7227 GN=muc PE=1 SV=1	3	2	3	2	512	54.2	9.57	7	2	0	23.4	24.1	36.1	26.7	28	33.3	41.3	20
Q7K2L1	AT22044p OS=Drosophila melanogaster OX=7227 GN=Orc3 PE=1 SV=1	6	3	16	3	721	82.2	7.37	21.54	3	0	55.2	62.3	57.5	63.8	52.6	163.5	77	86.7
Q9VGH5	AT27789p OS=Drosophila melanogaster OX=7227 GN=Hlo PE=1 SV=1	10	4	12	4	586	61.4	6.04	28.38	4	0	265.3	293.5	225.7	307.1	208.3	266.3	300.4	289.8
B9A0M7	AT31036p OS=Drosophila melanogaster OX=7227 GN=BODNA1.D21969 PE=1 SV=1	7	4	8	4	543	62.9	8.47	11.91	4	0	149.6	155.6	115.9	116.3	82	217.5	192.5	131.4
P35381	ATP synthase subunit alpha, mitochondrial OS=Drosophila melanogaster OX=7227 GN=b	15	7	36	7	552	59.4	9.01	75.51	7	0	371.5	474.3	608.6	548.2	1835.7	610	598.4	432.6
L0MQ04	ATP synthase subunit beta OS=Drosophila melanogaster OX=7227 GN=ATPsynbeta PE=1	13	5	23	5	511	54.6	5.27	37.42	5	0	64	69.8	84.2	107.9	392.9	81.4	100.3	77.6
Q01866	ATP synthase subunit gamma, mitochondrial OS=Drosophila melanogaster OX=7227 GN=	7	2	4	2	297	32.9	9.22	3.97	2	0	39.9	50.6	61.2	39.7	106.1	46	48.7	37.2
Q24439	ATP synthase subunit o, mitochondrial OS=Drosophila melanogaster OX=7227 GN=ATP	10	2	10	2	209	22.4	9.63	7.86	2	0	57.1	128.9	103.6	146.5	192.2	118.6	129.9	102.5
Q7KN85	ATP-citrate synthase OS=Drosophila melanogaster OX=7227 GN=ATPL PE=1 SV=1	10	8	39	8	1112	121.3	7.31	61.06	8	0	301.1	325.6	343.3	357.5	312.5	450.7	495.9	384.5
ADA0B4K7L1	ATP-dependent 6-phosphofruktokinase OS=Drosophila melanogaster OX=7227 GN=PKf	11	8	14	8	950	105.2	8.54	16.03	8	0	91.7	115.5	155.5	122.2	151.1	130.6	155.1	117.7
Q9VY14	ATP-dependent chromatin assembly factor large subunit OS=Drosophila melanogaster OX	10	12	80	12	1247	170.3	6.87	119.17	12	0	1480.9	1862.1	1719.6	1563.5	1052.4	2225.1	1884.5	1642.9
Q23976	ATP-dependent DNA helicase 2 subunit I OS=Drosophila melanogaster OX=7227 GN=Ht	3	3	5	3	631	72.5	6.68	3.45	3	0	44.9	64.7	54.4	59.5	44.7	70.3	84.9	57.4
Q9I7M8	ATP-dependent DNA helicase II subunit 2 OS=Drosophila melanogaster OX=7227 GN=Ht	5	2	3	2	699	79.8	5.38	6.82	2	0	33.9	52.4	41.4	42.8	34.9	59.1	65.3	50.4
Q9VNV3	ATP-dependent RNA helicase Ddx1 OS=Drosophila melanogaster OX=7227 GN=Ddx1 PE	3	2	3	2	727	80.8	6.87	2.01	2	0	51.3	63.5	54.3	51.7	48	60.4	74.2	51.9
AT29L3	ATP-dependent RNA helicase DHX8 OS=Drosophila melanogaster OX=7227 GN=pea PE=1	6	7	9	6	1242	141.8	8.76	12.28	7	1	93.3	124.7	98	103	76.6	144.2	140	115.5
Q8SY39	ATP-dependent RNA helicase OS=Drosophila melanogaster OX=7227 GN=CG6994 PE=1	4	3	3	3	827	93.3	9.72	5.23	3	0	27.3	31.6	30.4	24.2	18.6	44.4	40	37.6
P19109	ATP-dependent RNA helicase p62 OS=Drosophila melanogaster OX=7227 GN=Rm62 PE=1	20	14	77	14	719	78.5	9.6	156.95	14	0	1431.2	1527.8	1345	1325.2	875.9	1746.3	1763.4	1478.2
Q27268	ATP-dependent RNA helicase WMe OS=Drosophila melanogaster OX=7227 GN=He2E5 PE=1	15	5	42	5	424	48.6	5.66	55.51	5	0	773.4	874.3	843.6	727.4	527.1	1050.1	1003.7	815.3
Q9VEX6	ATPase family AAA domain-containing protein 3A homolog OS=Drosophila melanogaster	6	4	5	4	604	68.3	9.17	4.54	4	0	57.6	56.9	62.6	65.7	77.7	87.6	95.8	60.1
M9PER1	Autophagy-related 18a, isoform E OS=Drosophila melanogaster OX=7227 GN=Atg18a PE	4	2	3	2	447	47.9	6.74	1.95	2	0	59.6	72	80.4	55.7	54.7	83.8	97.1	74.4
A4V3G8	Balchen, isoform B OS=Drosophila melanogaster OX=7227 GN=bal PE=1 SV=1	6	4	24	4	599	66	8.86	39.25	4	0	726.8	629.8	699	738.8	711.8	1248.3	1075.1	926.8
Q7K204	Barricade, isoform A OS=Drosophila melanogaster OX=7227 GN=barc PE=1 SV=1	4	2	4	2	556	63.9	5.05	16.61	2	0	21.3	21.7	17.5	8.4	4.7	25.4	22.7	12.3
Q9Y162	BcDNA.GH02678 OS=Drosophila melanogaster OX=7227 GN=Vps4 PE=1 SV=1	7	4	8	4	442	49.6	6.96	14.29	4	0	240.2	276.8	271.2	246.5	193.9	289.6	362.5	268.1
Q7KMM4	BcDNA.GH04962 OS=Drosophila melanogaster OX=7227 GN=GCS2alpha PE=1 SV=1	3	3	7	3	924	105.7	6.51	12.83	3	0	123.6	195.7	185.2	192.5	211.3	164.4	342.6	167.3
Q9Y112	BcDNA.GH10614 OS=Drosophila melanogaster OX=7227 GN=AKR2E3 PE=1 SV=1	14	4	15	4	316	36.3	7.08	20.18	4	0	309.6	391.6	367.4	317.1	232.9	442.3	480.4	348.4
Q9V397	BcDNA.GH12558 OS=Drosophila melanogaster OX=7227 GN=Mpalpha PE=1 SV=1	7	5	6	5	783	84	9.17	5.35	5	0	18.7	34.6	44.1	26.6	83.6	43.9	39.3	22.1
Q7KLV9	BcDNA.LD02793 OS=Drosophila melanogaster OX=7227 GN=Pp19 PE=1 SV=1	7	3	9	3	505	55.2	6.9	10.07	3	0	262.2	285.2	264.9	249.1	152.1	328.6	347.6	293.5
Q9V311	BcDNA.LD08534 OS=Drosophila melanogaster OX=7227 GN=dUTPase PE=1 SV=1	30	5	53	5	188	19.9	5.47	103.65	5	0	1379.6	1346	1211.4	968.2	726.5	1388.6	1502.9	1020.4
Q8IO77	BcDNA.LD22910 OS=Drosophila melanogaster OX=7227 GN=Usp1 PE=1 SV=1	2	2	2	2	1078	116.3	7.23	1.67	2	0	12	14.6	12.7	11.7	9.1	17.5	19	12.5
Q7KMI3	BcDNA.LD23371 OS=Drosophila melanogaster OX=7227 GN=BcDNA.LD23371 PE=2 SV	6	5	13	5	1004	113.7	8.11	14.14	5	0	205.9	218.3	192.5	222	187.5	327	326.4	214.4
Q9V3Y5	BcDNA.LD23634 OS=Drosophila melanogaster OX=7227 GN=DmelCG4119 PE=1 SV=1	6	6	13	6	998	112.6	6.49	26.58	6	0	298.2	324.9	276.5	216.5	176.3	379.2	381.6	281.7
Q7KMH9	BcDNA.LD26050 OS=Drosophila melanogaster OX=7227 GN=wde PE=1 SV=1	5	7	16	7	1420	156.7	4.73	12.92	7	0	216.8	175.6	150.8	106	65.9	230.4	198.3	113.1
Q9V3H9	BcDNA.LD27873 OS=Drosophila melanogaster OX=7227 GN=Nab2 PE=1 SV=1	2	2	3	2	1004	112.9	9.58	1.85	2	0	15.7	18.5	13.7	17.2	12.2	18.4	22.2	17
Q9VHH8	Beag OS=Drosophila melanogaster OX=7227 GN=beag PE=1 SV=1	7	3	7	3	557	61.4	6.86	8.73	3	0	33.1	48	37.3	51.7	29.5	50.2	53.7	43.1
ADA0B4KGU4	Belle, isoform B OS=Drosophila melanogaster OX=7227 GN=bel PE=4 SV=1	7	5	7	4	801	85.4	7.77	9.73	5	1	136	181	199.3	156.3	211.8	167.7	217.1	148.9
Q9Y118	BG.DS07295.3 OS=Drosophila melanogaster OX=7227 GN=Pol32 PE=1 SV=1	12	3	8	3	431	47	9.28	17.23	3	0	95	138	87.4	65.8	47.7	104.9	109.5	70.7
P26668	Bifunctional glutamate/proline-4R-aminotransferase OS=Drosophila melanogaster OX=7227 GN=G	4	5	6	5	1714	189.3	8.63	1.63	5	0	35	46	52.7	41.8	67.9	51.6	68.6	44.8
Q7K4H4	Bifunctional lysine-specific demethylase and histidinohydroxylase NO66 OS=Drosophila me	6	4	12	4	653	73.1	7.84	18.47	4	0	242.1	253.4	207.9	204.1	134.3	465.8	372.5	272.4
Q9V4D9	Big2 OS=Drosophila melanogaster OX=7227 GN=big2 PE=1 SV=1	2	2	3	2	1406	154.4	9.23	0	2	0	32.5	27.9	22	24.8	27.5	47.8	27.9	27.9
Q9VRL8	blanks OS=Drosophila melanogaster OX=7227 GN=blanks PE=1 SV=1	8	2	2	2	324	35.6	8.27	2.24	2	0	20.2	23.7	16.4	18.1	17.9	25.6	27.6	16.3
Q9VGI8	Bloom syndrome protein homolog OS=Drosophila melanogaster OX=7227 GN=Bim PE=1	2	3	4	3	1487	166	8.5	3.97	3	0	87	118.3	115.1	91.7	54.3	120.4	123.9	83.3
ADA0B4KGE5	Bonus, isoform C OS=Drosophila melanogaster OX=7227 GN=bon PE=1 SV=1	3	3	4	3	1207	130.1	6.55	3.89	3	0	55.5	56	49.4	35.3	24.7	65.1	70.6	36.4
Q94513	Boundary element associated factor OS=Drosophila melanogaster OX=7227 GN=BEAF-3	12	4	5	4	282	31.8	6.54	5.81	4	0	168.1	164	126.3	141.7	118.5	210	215.9	166.9
P52172	Box A-binding factor OS=Drosophila melanogaster OX=7227 GN=isp PE=1 SV=2	2	2	3	2	1264	134.1	7.02	1.94	2	0	19.7	27.6	18.9	20	16.6	23.2	24.4	19
Q9W384	Brahma associated protein 1140kD OS=Drosophila melanogaster OX=7227 GN=Bap111 P	3	2	15	2	749	78.6	7.52	9.53	2	0	38.7	40.4	44.8	33.9	15.5	36.8	47.6	37.5
Q9VFO3	Brahma associated protein 155 kDa OS=Drosophila melanogaster OX=7227 GN=brm PE=1	9	10	25	10	1209	131.3	5.73	27.86	10	0	438.9	459.4	410.2	383.1	274.1	501.1	503.8	355.8
AT236M0	Brahma associated protein 170kD OS=Drosophila melanogaster OX=7227 GN=Bap170 P	3	4	9	4	1688	182.9	8.46	12.06	4	0	116.5	127.8	118.5	88.1	63.8			

AOA0B4JD46	CHC-type zinc finger nucleic acid binding protein, isoform B OS=Drosophila melanogaster	18	3	11	3	165	17.6	8.65	22.72	3	0	315.7	436.1	302	384.3	353.9	390.5	450.3	401.8
O96989	CDK45L OS=Drosophila melanogaster OX=7227 GN=CDK45L PE=1 SV=1	5	3	7	3	575	65.8	5.67	6.07	3	0	98	174.8	185.4	125.1	53.1	84.8	83.9	69.1
MPPEA2	CDK2-associated protein 1, isoform B OS=Drosophila melanogaster OX=7227 GN=CDK2A	8	2	5	2	295	30.7	8.44	5.73	2	0	13.3	11.7	11.5	14.3	14.4	17.9	19.7	12.5
Q7KPG8	CDK7/cyclin H assembly factor MAT1 OS=Drosophila melanogaster OX=7227 GN=Mat1 P	11	2	4	2	320	36.6	5.08	4.11	2	0	46.1	72.6	56.6	110	67.3	42.9	101.5	31.4
Q9VCN6	Cell division cycle 16 OS=Drosophila melanogaster OX=7227 GN=Cdc16 PE=1 SV=1	2	2	4	2	718	81.7	5.52	5.37	2	0	79.5	98.3	113.3	95.8	73	113.5	145	83.1
Q9I7L8	Cell division cycle 23, isoform A OS=Drosophila melanogaster OX=7227 GN=Cdc23 PE=2	4	2	10	2	678	77.5	6.51	12.56	2	0	63.4	95.5	82.6	84.6	323	81.8	140.1	80.3
Q9W0R0	Cell division cycle 5, isoform A OS=Drosophila melanogaster OX=7227 GN=Cdc5 PE=1 SV	9	7	17	7	814	93.8	8.19	28.94	7	0	376.8	461.4	416.4	424.5	305.3	660	569.6	503.1
Q9VHP9	Centromeric protein- α , isoform A OS=Drosophila melanogaster OX=7227 GN=Cenp-C PE=	1	2	4	2	1411	157.6	8.41	6.72	2	0	30	34.8	36.4	43.5	29.3	59.1	56.9	44
Q24478	Centrosome-associated zinc finger protein CP190 OS=Drosophila melanogaster OX=7227	12	10	32	10	1096	121.6	4.67	54.38	10	0	688.6	779.8	743.6	697.1	553.7	959	1022.6	784.8
Q9VXT3	Cervatins, isoform A OS=Drosophila melanogaster OX=7227 GN=Cerv PE=1 SV=2	12	2	4	2	230	26.1	5.53	3.89	2	0	49.2	56	38.6	39.9	26.9	59.4	56.9	40.4
Q9VM69	CG10206-PA OS=Drosophila melanogaster OX=7227 GN=CG10206 PE=1 SV=2	7	3	19	3	511	57.1	8.59	32.93	3	0	595.5	570.7	542.9	475.2	467.8	1020.2	852.5	832.1
O76752	CG12117-PA OS=Drosophila melanogaster OX=7227 GN=CG12117 PE=1 SV=1	16	4	9	4	261	29.2	7.03	10.78	4	0	125.7	147.5	142.3	143.2	86.6	131.7	186.2	141.1
Q7K0D3	CG12909 protein OS=Drosophila melanogaster OX=7227 GN=DmelCG12909 PE=1 SV=	12	3	4	3	281	32.1	8.95	9.36	3	0	66.8	75.8	57.8	79.9	56	92.4	93.6	77.6
F6J1D0	CG3595 OS=Drosophila melanogaster OX=7227 GN=CG3595 PE=1 SV=1	12	2	5	2	174	19.9	4.81	4.05	2	0	29.1	44.3	32.3	38.6	58.4	56.3	61	46
Q9W3T2	CG4593-PA OS=Drosophila melanogaster OX=7227 GN=DmelCG4593 PE=1 SV=1	7	2	5	2	209	24.8	6.57	8.4	2	0	180.9	201.9	169.2	154.1	171.3	188.8	220.8	159.9
A1ZB29	CG5757-PA OS=Drosophila melanogaster OX=7227 GN=DmelCG5757 PE=1 SV=1	11	2	2	2	211	23.8	7.44	2.68	2	0	12.7	18.3	20.5	18.1	18	31.5	24	15.4
Q9VIH1	CG9273 protein OS=Drosophila melanogaster OX=7227 GN=CPA2 PE=1 SV=2	9	2	15	2	246	26.4	5.08	27.41	2	0	390	491.8	570.3	348.3	132.6	258.6	275.3	204.5
A4V391	Chaperonin containing TCP1 subunit 1, isoform B OS=Drosophila melanogaster OX=7227	14	6	24	6	557	59.5	6.39	40.74	6	0	248.4	392	476.8	389.3	519.5	424.1	590.4	408
Q9W392	Chaperonin containing TCP1 subunit 2 OS=Drosophila melanogaster OX=7227 GN=CCT2	27	11	46	11	535	58	5.85	63.75	11	0	349.5	423.8	498.6	336.5	498.3	432.1	590.3	334.8
Q9VXQ5	Chaperonin containing TCP1 subunit 6 OS=Drosophila melanogaster OX=7227 GN=CCT6	4	3	8	3	533	58.2	6.62	12.09	3	0	252.6	283.4	341	197	252.5	340.8	351.4	211.2
Q7K3J0	Chaperonin containing TCP1 subunit 8 OS=Drosophila melanogaster OX=7227 GN=CCT8	21	9	39	9	546	59.4	5.31	54.15	9	0	541.3	774.5	877.1	702.6	868.9	710.8	1012.8	697.9
AOA0B4K7A3	Charlatan, isoform F OS=Drosophila melanogaster OX=7227 GN=Chn PE=4 SV=1	3	3	4	3	1286	137.2	3.95	15.31	3	0	15.6	24.1	20.6	15	12.6	21.3	23	19.1
Q9VEG6	Chorion peroxidase OS=Drosophila melanogaster OX=7227 GN=Cp PE=2 SV=3	4	2	4	2	809	90.5	6.9	7.76	2	0	19.9	32.2	25.1	28.7	21.1	19.9	29	22.3
A1Z988	Chromatin assembly factor 1, p105 subunit OS=Drosophila melanogaster OX=7227 GN=C	5	3	9	3	747	83.3	8.22	13.16	3	0	122.3	127.9	163.9	113.7	71	115.3	89.7	
Q9W3D1	Chromatin assembly factor 1, p180 subunit OS=Drosophila melanogaster OX=7227 GN=C	7	7	25	7	1183	133.4	7.03	31.57	7	0	602.4	734.5	806.5	611.1	266.8	574.2	587.6	495.8
E1J1L4	Chromatin assembly factor 1, p55 subunit, isoform B OS=Drosophila melanogaster OX=72	7	3	10	1	429	48.5	4.89	7.62	3	2	134.5	250.9	226.1	512.7	219	217.7	245.1	246.1
Q9VDY1	Chromatin remodeling ATPase Ino80 OS=Drosophila melanogaster OX=7227 GN=Ino80	1	2	2	2	1638	187	9.04	2.13	2	0	22.3	27.8	25.3	30.3	25.4	34.2	44.5	31.1
Q24368	Chromatin remodeling complex ATPase chain Isw1 OS=Drosophila melanogaster OX=7227	22	19	108	19	1027	118.8	8.29	150.51	19	0	2142.4	2324.4	2085.8	1810.9	1342.2	3164	2694.6	1991
Q96BS3	Chromator, isoform A OS=Drosophila melanogaster OX=7227 GN=Chro PE=1 SV=1	10	5	10	5	926	101	7.17	51.68	5	0	60.1	80	74.6	87.1	82.8	105.3	112.5	117.6
M9ND16	Chromodomain-helicase-DNA-binding protein 1, isoform B OS=Drosophila melanogaster O	1	3	5	3	1900	213.8	6.47	2.06	3	0	70.1	69.1	64.3	80.8	45.9	88.8	102	75.7
O16102	Chromodomain-helicase-DNA-binding protein 3 OS=Drosophila melanogaster OX=7227 G	5	4	7	4	892	103	8.48	10.12	4	0	109	131.5	115.6	126.1	90.8	195.3	177.9	148.6
Q9V3I5	Chromosomal serine/threonine-protein kinase JIL-1 OS=Drosophila melanogaster OX=722	1	2	5	2	1207	137	6.6	10.46	2	0	102	120.5	113.5	118.9	102.3	145	144.4	115.2
A1Z987	Chromosome associated protein G, isoform F OS=Drosophila melanogaster OX=7227 GN=	5	5	17	5	1351	153.8	7.55	17.57	5	0	122.3	138.2	141.3	139.9	122	212.4	179.7	149.2
Q494K2	Chromosome transmission fidelity 4 OS=Drosophila melanogaster OX=7227 GN=Ctfd	5	4	11	4	895	96.6	5.34	18.1	4	0	257.8	311.1	379.1	259.9	97.8	233	266	206.9
Q9VN58	Circadian trip, isoform A OS=Drosophila melanogaster OX=7227 GN=Ctrip PE=1 SV=4	1	3	3	3	3140	336.4	7.25	1.85	3	0	7.9	7.4	9.4	10.3	10.4	10.5	15.7	13.2
Q8IRB5	Claspin OS=Drosophila melanogaster OX=7227 GN=Claspin PE=1 SV=1	10	11	37	11	1465	165.2	4.79	56.77	11	0	575.5	609	648	445.4	311.6	497.9	570.2	477.6
X2JC31	Clathrin heavy chain OS=Drosophila melanogaster OX=7227 GN=Cnc PE=3 SV=1	5	6	8	6	1678	191.1	5.72	15.51	6	0	59.6	78.3	83.4	63.9	144	90.6	122.6	93.1
Q9VE14	Cleavage and polyadenylation specificity factor 73 OS=Drosophila melanogaster OX=722	4	3	6	3	684	76.8	5.67	6.3	3	0	43	52.9	50.4	46.9	27.8	56	62.8	49.4
Q9V726	Cleavage and polyadenylation specificity factor subunit 1 OS=Drosophila melanogaster O	4	5	8	5	1455	164.6	6.2	17.43	5	0	150.6	180.5	169.5	148.8	124.6	215.9	227.6	184.6
Q9V9V0	Cleavage stimulation factor 50 kD subunit OS=Drosophila melanogaster OX=7227 GN=C	4	2	5	2	424	46.9	5.95	8.64	2	0	61.8	77.1	70.5	59.2	43.7	83.4	91.3	79
Q9VE52	Cleavage stimulation factor 64 kD subunit OS=Drosophila melanogaster OX=7227 GN=C	7	3	8	3	419	46.2	5.78	7.25	3	0	78.9	87.6	82.3	71.1	43.7	93.4	111.1	79.1
PA5437	Coatamer subunit beta OS=Drosophila melanogaster OX=7227 GN=betaCOP PE=2 SV=2	3	3	3	3	964	107.3	6.32	3.81	3	0	6.7	8.9	13	10.6	22	8.8	14.4	11.1
PA5594	Cofilin/actin-depolymerizing factor homolog OS=Drosophila melanogaster OX=7227 GN=C	33	5	62	5	148	17.1	7.17	102.33	5	0	1459.4	1645.7	1380.4	1119.9	900.2	1804.2	1812.2	1275.3
Q9VAJ1	Condensin complex subunit 1 OS=Drosophila melanogaster OX=7227 GN=Cap-D2 PE=1	5	7	15	7	1380	157.4	5.86	30.24	7	0	239.6	292.1	291.5	245.7	231	393.9	380.9	271.4
Q9VIP9	Condensin complex subunit 2 OS=Drosophila melanogaster OX=7227 GN=barr PE=1 SV=	7	4	13	4	735	82.7	5.58	19.29	4	0	99.6	94.5	96.3	93.4	78.9	123.9	121.8	97.7
contaminant_KE contaminant_KE Keratin2		25	11	147	11	622	62	5.24	219.84	11	0	8850.8	3206.7	2719.7	2209.3	3992.8	2742.3	3607.2	3461.4
contaminant_KE contaminant_KE Keratin3		33	17	363	13	593	59.5	5.21	593.8	17	4	8627.2	7738.4	7305.7	4691.2	6675	8399.9	12993.7	9667.1
contaminant_KE contaminant_KE Keratin4		25	14	71	8	458	49.6	4.93	124.71	14	4	1644.5	1418.2	1096.5	449.1	1712.5	1314.8	1671.4	766.3
contaminant_KE contaminant_KE Keratin5		28	13	128	5	471	51.5	5.16	190.6	13	4	2407.8	1061.7	887.1	470.1	778.5	1241.4	2127.8	1029.4
contaminant_KE contaminant_KE Keratin8		23	11	82	5	469	50.5	5	127.18	11	0	1426.9	422.3	501.3	271.1	434.7	868.5	1183.2	524.9
contaminant_KE contaminant_KE Keratin10		16	7	44	1	400	44.1	5.14	86.38	7	0	86.8	35	43.3	17.9	27.6	40.2	62	52.7
contaminant_KE contaminant_KE Keratin12		29	13	53	7	431	47.9	5.02	98.85	13	1	423.5	359.5	398.2	279.6	480.7	628.8	937.7	583.8
contaminant_KE contaminant_KE Keratin13		23	12	672	10	643	65.5	6.62	1011.91	12	1	18646.1	10028.6	8399.5	6783.4	10780.1	9007.7	12966	11915.8
contaminant_KE contaminant_KE Keratin15		4	2	165	1	629	64.5	6.48	260.01	2	0								
contaminant_KE contaminant_KE Keratin16		3	5	456	3	534	57.2	6.61	613.34	5	0	306.2	347.3	217.4	93	290.5	333.2	204.5	63.4
contaminant_KE contaminant_KE Keratin17		16	10	210	7	590	62.4	8.06	353.32	10	0	1392.3	751.2	610	438.7	606.7	651.6	1268.9	718.3
contaminant_KE contaminant_KE Keratin18		19	11	223	7	562	59.8	7.94	392.25	11	1	2151.1	1048.5	1067.2	692.5	790.6	1477.8	2726.9	902.5
contaminant_KE contaminant_KE Keratin22		30	15	326	11	845	65.8	8	590.18	15	4	8746.8	5993.6	5958.1	4982.8	6331	6501.8	11523.1	7969.4
Q8SVY2	COP9 signalosome complex subunit 3 OS=Drosophila melanogaster OX=7227 GN=CSN3	9	5	20	5	445	50.7	6.25	50.79	5	0	377.8	453.1	475.5	434.3	327.7	496.9	589.3	428.7
Q9V345	COP9 signalosome complex subunit 4 OS=Drosophila melanogaster OX=7227 GN=CSN4	16	6	27	6	407	46.4	6.32	44.23	6	0	493.6	567.1	617.2	497.6	370.9	581.7	710.2	513.6
Q9XZ58	COP9 signalosome complex subunit 5 OS=Drosophila melanogaster OX=7227 GN=CSN5	9	2	5	2	327	37.1	5.58	12.42	2	0	62.1	85.7	82.6	68.8	52.1	83.3	93.3	66.3
Q9V4S8	COP9 signalosome complex subunit 7 OS=Drosophila melanogaster OX=7227 GN=CSN7	14	3	11	3	278	31	6.7	24.08	3	0	163.9	201.6	184.2	148.3	103.5	179.2	233.9	155.3
Q7KTH8	COP9 signalosome complex subunit 8 OS=Drosophila melanogaster OX=7227 GN=CSN8	14	3	7	3	182	21.4	4.87	9.95	3	0	169.9	194.4	183.3	173.2	138	183.6	225.7	183.1

L7EEU0	Dead box protein 80, isoform E OS=Drosophila melanogaster OX=7227 GN=Dpb80 PE=1	7	3	6	3	481	53.5	6.76	6.16	3	0	88.1	108.5	107.9	71	61.2	101.4	115.8	81.8
Q7K3M5	DEAH-box helicase 15, isoform A OS=Drosophila melanogaster OX=7227 GN=Dhx15 PE=1	10	7	14	6	729	82.6	7.06	21.26	7	0	319.2	344.8	347.4	354.2	302.5	448.6	524.4	395.4
M0NDR9	Defective in cullin neddylation protein OS=Drosophila melanogaster OX=7227 GN=SCCRD	11	2	7	2	297	34.7	5.57	4.08	2	0	7.2	8.4	10.7	9.3	5.3	13.5	16.2	12.2
Q8T0D3	Dek, isoform B OS=Drosophila melanogaster OX=7227 GN=Dek PE=1 SV=1	11	6	24	6	669	72.5	4.88	37.62	6	0	640.3	712.3	684	619.2	389.3	701.7	771.1	631.2
Q9VX98	Density-regulated protein homolog OS=Drosophila melanogaster OX=7227 GN=DENR PE=1	15	2	7	2	189	21.3	5.14	11.83	2	0	96.8	123.4	143.7	106	76.7	117.9	137.6	110
Q9V9U4	Deoxyhypusine hydroxylase OS=Drosophila melanogaster OX=7227 GN=nero PE=2 SV=2	7	2	6	2	302	33.5	4.73	5.73	2	0	72.4	81.8	83.2	57.6	48.1	81.3	123.3	68.3
Q9VSU6	Dihydropteridine reductase OS=Drosophila melanogaster OX=7227 GN=Dhpr PE=1 SV=1	18	3	2	3	235	24.5	6.34	9.48	3	0	155.3	181	161.5	127.5	91.4	170.7	204.5	139.7
M9PE16	Dikar, isoform F OS=Drosophila melanogaster OX=7227 GN=dikar PE=1 SV=1	1	2	8	2	3261	357.5	8.69	14.91	2	0	196	160.8	126.2	95	117.8	217.5	252.2	171.6
Q9VFC9	Dipeptidase B, isoform A OS=Drosophila melanogaster OX=7227 GN=Dip-B PE=1 SV=2	17	7	34	7	508	55.5	6.76	47.65	7	0	329.5	492.9	500.9	587.9	711.8	482.2	663.5	669.9
Q9VHR8	Dipeptidyl peptidase 3 OS=Drosophila melanogaster OX=7227 GN=DppIII PE=2 SV=2	12	9	28	9	786	89.1	6.43	34.83	9	0	685.2	809.9	753	706.1	548.6	836	1022.1	729.7
Q9VC93	Dia3, isoform A OS=Drosophila melanogaster OX=7227 GN=Dia3 PE=1 SV=1	13	9	24	9	982	112.1	6.68	21.73	9	0	257.8	217.6	263.8	277.9	212	326.9	332.5	282.3
Q9XY25	DNA damage-binding protein 1 OS=Drosophila melanogaster OX=7227 GN=pic PE=1 SV=1	12	10	61	10	1140	126	5.36	91.73	10	0	711.1	770.5	786.7	659.7	469.6	876.9	946.6	671.8
AOA084LEV2	DNA helicase OS=Drosophila melanogaster OX=7227 GN=dpa PE=1 SV=1	15	13	86	13	866	96.6	7.52	128.51	13	0	1506.2	1753.8	1920.5	1483.1	818.2	1797	1693	1287.9
Q9V433	DNA helicase RECQE OS=Drosophila melanogaster OX=7227 GN=RecQ5 PE=2 SV=1	2	2	2	2	1058	121.1	8.97	0	2	0	5.1	12.5	8.6	9.3	5.4	13.6	9.7	11.9
Q9W1H4	DNA ligase 1 OS=Drosophila melanogaster OX=7227 GN=DNAI1 PE=1 SV=2	11	7	39	7	747	84.7	6.62	63.02	7	0	484.6	655.3	650.9	498.7	335.2	662	709.8	488.6
P2619	DNA polymerase alpha catalytic subunit OS=Drosophila melanogaster OX=7227 GN=DNAp	11	13	38	13	1488	169.8	8.02	35.04	13	0	593.5	732.5	871.6	541.3	199.4	444.7	485.5	376.2
P54358	DNA polymerase delta catalytic subunit OS=Drosophila melanogaster OX=7227 GN=DNAp	10	10	32	10	1092	124.8	6.92	32.26	10	0	569	696.4	750.5	541.2	373.9	719.5	728.6	503
Q9V088	DNA polymerase delta small subunit OS=Drosophila melanogaster OX=7227 GN=DNAp	18	6	22	6	431	48	6.52	49.3	6	0	588.8	661.5	693.2	452.2	279	715.6	679	491.9
Q9V0N1	DNA polymerase epsilon catalytic subunit OS=Drosophila melanogaster OX=7227 GN=DN	8	17	64	17	2236	256.5	6.47	79.52	17	0	986.7	1384.3	1612.8	1032.8	434.7	795.7	900.8	643.5
Q9VRC7	DNA polymerase epsilon subunit OS=Drosophila melanogaster OX=7227 GN=DNApol-eps	8	7	14	7	525	58.7	6.48	24.56	7	0	94.8	126.9	84.2	84.2	44.6	66.7	86.3	61.5
Q9VPH2	DNA primase large subunit OS=Drosophila melanogaster OX=7227 GN=DNApol-alphaH0	12	7	23	7	533	61.4	6.96	46.25	7	0	663	913.3	1014.4	664	243.3	465.5	545.1	411
Q24317	DNA primase small subunit OS=Drosophila melanogaster OX=7227 GN=DNApol-alphaH0	12	7	26	7	438	50.2	7.5	29.05	7	0	325.5	469.6	502.4	389	136.9	263.2	283.7	216.6
Q9V3W9	DNA repair protein Rad23 OS=Drosophila melanogaster OX=7227 GN=Rad23 PE=1 SV=1	14	4	14	4	414	45.8	4.67	23.9	4	0	134.1	168.3	144.5	134.1	101.3	147	256.5	135.5
P49735	DNA replication licensing factor Mcm2 OS=Drosophila melanogaster OX=7227 GN=Mcm2	18	12	98	12	887	100.4	5.11	129.3	12	0	1799.3	2093.6	2236.3	1711.6	865.2	1938.7	1953	1471.7
Q9XYU1	DNA replication licensing factor Mcm3 OS=Drosophila melanogaster OX=7227 GN=Mcm3	24	15	69	15	819	90.9	6.4	142.14	15	0	2062.2	2237	2256.5	1607.4	851.7	2316.3	2052.9	1469.6
Q9V9W6	DNA replication licensing factor Mcm5 OS=Drosophila melanogaster OX=7227 GN=Mcm5	16	8	60	8	733	82.2	7.84	114.52	8	0	629.7	824	839.7	760	387.2	796.6	828.1	621.4
Q9V461	DNA replication licensing factor Mcm6 OS=Drosophila melanogaster OX=7227 GN=Mcm6	21	14	87	14	817	92.3	5.38	134.76	14	0	1653.9	1978.7	2121.8	1624.3	934.4	1926.9	1945.7	1596
Q9XYU0	DNA replication licensing factor Mcm7 OS=Drosophila melanogaster OX=7227 GN=Mcm7	19	11	54	11	720	81.2	6.99	103.24	11	0	936.6	1038	776.8	551.9	390.2	877.9	832.8	497.5
Q94883	DNA replication-related element factor, isoform A OS=Drosophila melanogaster OX=7227	10	7	31	7	709	80.7	5.86	44.03	7	0	702.4	704.8	674.3	583.6	507.3	946.6	846.8	651.7
P15348	DNA topoisomerase 2 OS=Drosophila melanogaster OX=7227 GN=Top2 PE=1 SV=1	16	20	260	20	1447	164.3	8.22	453.21	20	0	5532.2	5798	4743.8	5903.8	3797.4	9080.4	6208.6	4890.3
BY7Z29	DNA-(apurinic or apyrimidinic site) lyase OS=Drosophila melanogaster OX=7227 GN=Rrp1	13	8	61	8	706	77.3	8.91	87.75	8	0	1633.3	1724.5	1250.5	1237.3	1327.2	2938.9	2266.6	1811.7
P13469	DNA-binding protein modulo OS=Drosophila melanogaster OX=7227 GN=mod PE=1 SV=1	6	2	32	2	542	60.3	5.43	68.44	2	0	306.8	326	297.7	268.1	237.8	527.3	425.2	306.8
P91875	DNA-directed RNA polymerase I subunit RPA1 OS=Drosophila melanogaster OX=7227 GN	4	7	15	7	1642	185.3	7.64	11.56	7	0	208.2	230.2	213.3	256.4	220.3	366.2	356.1	283.1
P20028	DNA-directed RNA polymerase I subunit RPA2 OS=Drosophila melanogaster OX=7227 GN	4	3	5	3	1129	128.4	8.41	10.5	3	0	12.4	12.8	18.6	18.3	14.2	22.9	18.6	16.1
P04052	DNA-directed RNA polymerase II subunit RPB1 OS=Drosophila melanogaster OX=7227 G	6	9	22	9	1887	209	7.81	38.62	9	0	300.5	357.1	367.1	311.4	262.8	488.7	491	347
P08266	DNA-directed RNA polymerase II subunit RPB2 OS=Drosophila melanogaster OX=7227 G	6	8	16	8	1176	134	7.05	19.51	8	0	250.1	338.8	319.1	316.7	260.2	415.9	471.5	351.5
Q9VEA5	DNA-directed RNA polymerase II subunit Rpb4 OS=Drosophila melanogaster OX=7227 GF	12	2	3	2	139	16.2	4.82	5.63	2	0	69.1	48.3	46.9	29.2	28.4	65.9	51.8	38.9
Q53Z70	DNAJ-1 OS=Drosophila melanogaster OX=7227 GN=DnaJ-1 PE=1 SV=1	13	3	15	3	334	37	8.85	22.22	3	0	296.3	320.9	250.1	189.7	148	311.1	369.8	271.7
Q9VFX9	DnaJ-like-2, isoform A OS=Drosophila melanogaster OX=7227 GN=DroJ2 PE=1 SV=1	15	6	21	6	403	45.2	6.48	34.38	6	0	490.1	509.9	509.5	423.7	334.5	532.3	617.7	426.9
Q7KN75	Decora-satellite-binding protein 1, isoform A OS=Drosophila melanogaster OX=7227 GN	9	12	26	12	1301	144.2	6.2	26.12	12	0	302.2	396.5	452	386.2	258.3	412.1	516.7	417
Q24319	Dolichyl-diphosphooligosaccharide-protein glycosyltransferase 4B subunit OS=Drosop	6	2	6	2	449	50	5.59	8.05	2	0	60.2	85.4	92.4	71.8	140.6	78.6	135.4	89.5
AOA084LFX8	Domino, isoform G OS=Drosophila melanogaster OX=7227 GN=dom PE=1 SV=1	1	4	8	4	3233	353.5	8.98	8.85	4	0	172.3	184.8	193.7	144.4	130.8	269.7	358.2	166.4
P24785	Dosage compensation regulator OS=Drosophila melanogaster OX=7227 GN=mle PE=1 SV	5	4	4	4	1293	143.6	7.23	15.61	4	0	126.4	131.6	135.8	113.9	87.9	176.4	184.3	138.9
Q9XYZ4	Double-strand break repair protein OS=Drosophila melanogaster OX=7227 GN=mre11 PE	4	4	6	4	620	69.2	5.95	9.61	4	0	165.8	166.7	159.5	123	88.2	172.2	189.2	130.4
O18335	Drab11 OS=Drosophila melanogaster OX=7227 GN=Drab11 PE=1 SV=1	9	2	3	2	214	24.2	5.73	0	2	0	35	16.4	18.2	12.3	22.5	26.3	26.6	13.4
Q9V3I2	Drab5 OS=Drosophila melanogaster OX=7227 GN=Drab5 PE=1 SV=1	14	2	6	2	219	23.9	8.41	1.73	2	0	37.4	57	59.4	65.6	76	69.7	112.3	62.9
Q7KNF1	Drosha OS=Drosophila melanogaster OX=7227 GN=drosha PE=2 SV=1	2	2	3	2	1327	152.7	7.34	3.77	2	0	29.3	25.6	19.8	12.1	10.9	40.7	27.1	11.2
Q9V3V0	DroX protein OS=Drosophila melanogaster OX=7227 GN=drox PE=1 SV=1	14	3	9	3	258	27.9	11.56	13.26	3	0	203.6	210.6	142.9	188.6	112.3	181.7	196.1	155.7
P13496	Dynactin subunit 1 OS=Drosophila melanogaster OX=7227 GN=DCTN1-p150 PE=1 SV=2	3	3	3	3	1265	141.1	5.62	3.97	3	0	12	16.1	17.6	19.6	15.9	20.7	22.3	15
M9PBQ3	Dynein heavy chain 64C, isoform 1 OS=Drosophila melanogaster OX=7227 GN=Dhc64C P	1	3	3	3	4861	532.3	6.35	3.57	3	0	16.8	21.4	25.7	20.3	40.3	27.6	50.3	22.7
AOA084KJ7J	E3 SUMO-protein ligase RanBP2 OS=Drosophila melanogaster OX=7227 GN=Nup358 PE=1	2	5	8	5	2718	298.7	6.11	9.51	5	0	78.4	96.5	95.8	91.3	120.4	107.9	180.7	100.9
X2JGB3	E3 ubiquitin protein ligase OS=Drosophila melanogaster OX=7227 GN=Bre1 PE=3 SV=1	10	11	29	11	1044	119	6.21	45.34	11	0	578.2	564.1	545.3	503.8	397.3	811.5	770	538.7
Q9VB08	E3 ubiquitin-protein ligase RING1 OS=Drosophila melanogaster OX=7227 GN=Sce PE=1	5	2	2	2	435	47.2	7.12	1.73	2	0	22.8	28.8	24.8	18.1	16.2	25.5	34.8	23.4
J7JZD3	Eb1, isoform A OS=Drosophila melanogaster OX=7227 GN=Eb1 PE=1 SV=1	18	4	4	4	291	32.6	5.34	3.79	4	0	77.2	49.2	34.4	20.6	18.4	58.6	33.7	20.5
O76876	EG-132E8.1 protein OS=Drosophila melanogaster OX=7227 GN=sax PE=1 SV=1	8	4	8	4	485	53.4	7.01	15.8	4	0	143.9	155.1	128.8	128	95.6	149.8	172.3	160
O46048	EG-133E12.4 protein OS=Drosophila melanogaster OX=7227 GN=east PE=1 SV=1	1	3	6	3	2342	250	6.23	5.88	3	0	86	108.2	94.1	97.1	60.5	110.9	114.6	96
O18399	EG-152A3.5 protein (Fbn0003116.pn protein) OS=Drosophila melanogaster OX=7227 G	7	3	5	3	405	45.2	6.37	3.38	3	0	64.7	70.3	69.1	64.4	48.3	71.3	96.2	71.8
O46087	EG-25E8.1 protein OS=Drosophila melanogaster OX=7227 GN=EG-25E8.1 PE=1 SV=1	7	5	10	5	923	103.4	5.12	16.54	5	0	62.4	80	87.9	77.5	96.4	71.5	132.2	82.5
O46307	EG-30E.4 protein OS=Drosophila melanogaster OX=7227 GN=DnaI1411 PE=1 SV=1	6	4	5	4	771	88.5	4.98	5.99	4	0	69.4	72	72.6	63	43.7	122	84.1	67.4
Q9XZ29	EG-BA/CR25B3.9 protein OS=Drosophila melanogaster OX=7227 GN=kp3A PE=1 SV=1	8	9	29	9	1212	135.7	7.01	30.53	9	0	291.5	361.1	356.2	337.4	273	544	463.2	414.9
Q9N4H0	Elongation factor 1-gamma OS=Drosophila melanogaster OX=7227 GN=eEF1gamma PE=1	20	6	30	6	431	48.9	7.05	46.15	6	0	391.6	511.4	570.5	454.1	507.4	551.4	688.8	472.1
P13360	Elongation factor 2 OS=Drosophila melanogaster OX=7227 GN=EF2 PE=1 SV=4	12	7	77	7	844	94.4												

O02195	Eukaryotic translation initiation factor 3 subunit I OS=Drosophila melanogaster OX=7227 C	8	2	4	2	326	36.1	5.34	0	2	0	18.3	18.3	27.4	16.8	18.3	25.9	23.8	18.9
CQP42	Eukaryotic translation initiation factor 4A, isoform E OS=Drosophila melanogaster OX=722	23	8	105	8	403	45.8	5.66	142.05	8	0	1608.2	2046	2035.4	1921.8	1584.3	2055.7	2581.1	1925.6
ABDZ29	Eukaryotic translation initiation factor 4G1, isoform B OS=Drosophila melanogaster OX=72	3	5	8	5	1919	211	8.35	5.62	5	0	87.1	113.6	145.1	105.1	163	137.7	193.6	137.9
XJ2C79	Eukaryotic translation initiation factor 4H1, isoform D OS=Drosophila melanogaster OX=72	17	6	20	6	388	41.7	9.79	29.97	6	0	408.2	336.9	320.2	209.5	178.5	389	359.2	227.9
Q9VXK6	Eukaryotic translation initiation factor 5 OS=Drosophila melanogaster OX=7227 GN=elF5 f	6	3	6	3	464	51.7	5.26	7.44	3	0	92.1	101	111.3	95.2	114.6	108.6	125.3	89.6
Q9GU68	Eukaryotic translation initiation factor 5A OS=Drosophila melanogaster OX=7227 GN=elF5	22	2	21	2	159	17.6	5.15	36.92	2	0	196.2	195.8	205.3	140.5	107.5	212	238	174.3
Q9VZP5	Eukaryotic translation initiation factor 5B, isoform B OS=Drosophila melanogaster OX=722	6	6	25	6	1144	127.1	5.52	29.15	6	0	719.1	620	572.7	652	572.7	695.5	685	633
P56538	Eukaryotic translation initiation factor 6 OS=Drosophila melanogaster OX=7227 GN=elF6 f	13	2	2	2	245	26.5	4.73	2.16	2	0	17.3	18.9	17.1	15.5	17.7	14.9	26.4	18.1
M9PFR9	Eukaryotic translation release factor 1, isoform I OS=Drosophila melanogaster OX=7227 G	12	4	13	4	447	49.7	7.46	15.2	4	0	83.9	97.8	97.5	73.5	63.9	99.6	113.5	75.2
Q9VK85	Eukaryotic translation release factor 3, isoform A OS=Drosophila melanogaster OX=7227 G	4	2	2	2	619	66.4	5.35	0	2	0	17.4	21.4	22.3	15.3	23.6	18.6	30.9	19.4
Q9TYM2	Exportin-1 OS=Drosophila melanogaster OX=7227 GN=emb PE=1 SV=1	8	6	48	6	1063	122.7	5.87	69.41	6	0	442.7	517.2	502.9	395.9	434.3	648.1	769.1	445.4
Q9XZU1	Exportin-2 OS=Drosophila melanogaster OX=7227 GN=Cse1 PE=2 SV=2	7	5	20	5	975	110.1	5.82	33.75	5	0	309.4	424.4	425.3	398	303.9	405.4	517.2	338.2
P48603	F-actin-capping protein subunit beta OS=Drosophila melanogaster OX=7227 GN=cpb PE=1	12	4	7	4	276	31.3	5.44	10.68	4	0	119	140.4	129.4	81.3	86.3	149.8	181.7	83.4
Q8IRG6	FACT complex subunit sp116 OS=Drosophila melanogaster OX=7227 GN=dre4 PE=1 SV=1	12	13	69	13	1083	123.5	6.29	129.64	13	0	1243.1	1476.5	1346.9	1059	658.5	1899.1	1565.9	1130.4
Q05344	FACT complex subunit Ssr1 OS=Drosophila melanogaster OX=7227 GN=Ssrp PE=1 SV=1	7	5	61	5	723	81.5	5.63	95.32	5	0	649.6	819.9	808	632.7	389	962	902.4	737.3
Q95RI5	Failed axon connections OS=Drosophila melanogaster OX=7227 GN=fax PE=1 SV=1	2	3	4	3	418	47.1	5.25	4.99	3	0	32.8	37.8	44.4	46.5	125.9	43	60.5	38.7
Q8MYL1	Fancd2 OS=Drosophila melanogaster OX=7227 GN=Fancd2 PE=2 SV=1	2	3	4	3	1478	167.4	6.89	3.3	3	0	33	40.2	39.2	41.2	25.5	58	49.7	35.8
A1ZTL1	Fanconi anemia complementation group 1 OS=Drosophila melanogaster OX=7227 GN=FA	3	4	4	4	1481	169.9	6.89	0	4	0	47.9	46.2	45.8	46.9	35.6	51.8	59.9	45
Q9VFR1	Farnesyl transferase alpha, isoform A OS=Drosophila melanogaster OX=7227 GN=Frita P	8	3	6	3	331	38.9	5.17	6.02	3	0	138.6	133.9	126.3	102.4	72	126	170.6	98.1
Q9VZ62	Fasciottin OS=Drosophila melanogaster OX=7227 GN=fco PE=1 SV=1	4	3	11	3	871	78.1	8.98	15.59	3	0	198	263.2	245.8	229.7	219.6	336.2	358.9	281.1
Q8INK3	Fatty acid binding protein, isoform C OS=Drosophila melanogaster OX=7227 GN=fabp PE	20	3	23	3	157	17.1	6.01	32.01	3	0	757.5	959	860.3	607.6	481.8	791.6	1130.1	665.7
M9PJCT	Female sterile (1) homeotic, isoform G OS=Drosophila melanogaster OX=7227 GN=fs1(h	1	3	8	3	2046	205.9	9.23	9.86	3	0	110.6	128.3	98	113.2	68.5	134.7	155	128.9
ADA0B4K127	Feritin OS=Drosophila melanogaster OX=7227 GN=Fer1HCH PE=1 SV=1	11	2	5	2	245	27.9	6.05	4.49	2	0	62.8	63	63.2	91.3	92.8	70.6	111.3	82.5
ADA0B4KHFO	Feritin OS=Drosophila melanogaster OX=7227 GN=Fer2LCH PE=1 SV=1	7	2	11	2	236	26.2	6.52	24.25	2	0	484	587.9	526.6	621.7	550	554	758.1	560
Q9VUS0	Ft01202p OS=Drosophila melanogaster OX=7227 GN=DmelCG7372 PE=1 SV=2	3	3	6	3	971	109.3	7.15	6.69	3	0	106.8	130	119.9	93.5	67.5	140.5	139	123.1
Q9VW53	Ft01414p OS=Drosophila melanogaster OX=7227 GN=Mr3 PE=1 SV=1	9	3	5	3	326	36.6	5.21	3.77	3	0	76.6	95.6	95.9	78.4	63.2	96.4	106.7	89.2
Q9W2I4	Ft01566p OS=Drosophila melanogaster OX=7227 GN=Sgt29 PE=1 SV=2	8	2	3	2	289	32.1	8.63	0	2	0	9.8	9.6	12.2	9.8	5.8	11.2	15.8	9.8
Q9VVM8	Ft02004p OS=Drosophila melanogaster OX=7227 GN=DmelCG5290 PE=1 SV=1	4	3	3	3	798	92.1	6.06	3.92	3	0	44.4	41.7	56.3	43.4	44.1	62.2	103.4	41.7
Q9VDE8	Ft02071p OS=Drosophila melanogaster OX=7227 GN=DmelCG7044 PE=1 SV=1	2	2	2	2	974	112.9	6.14	1.67	2	0	25	23.5	26.3	29.2	23.3	27.5	38.1	22
Q9VWC7	Ft02109p OS=Drosophila melanogaster OX=7227 GN=DmelCG12702 PE=1 SV=1	4	3	6	3	870	97.1	6.71	3.11	3	0	5.7	10.7	13.5	6.7	9.9	10.8	11.3	8
Q9WR9	Ft03239p OS=Drosophila melanogaster OX=7227 GN=DmelCG1677 PE=1 SV=2	2	2	8	2	1000	109	5.76	12.89	2	0	164.1	194.5	165.9	170.1	104	224.4	230.9	181.9
Q9W247	Ft03324p OS=Drosophila melanogaster OX=7227 GN=DmelCG4752 PE=1 SV=2	2	2	2	2	1294	139.5	6.47	4.33	2	0	21.2	22.2	32.4	26.6	19.8	25.3	37.2	22
A4V1N8	Ft03688p OS=Drosophila melanogaster OX=7227 GN=Pm PE=1 SV=1	2	2	2	2	879	102.3	5.58	1.65	2	0	19.5	52.5	35.5	46.8	84.9	40.2	38.2	28.6
Q9W0G4	Ft03834p OS=Drosophila melanogaster OX=7227 GN=(J)02640 PE=1 SV=1	3	2	4	2	652	68.9	6.89	3.41	2	0	63.9	82	71.4	68.5	62.7	72.2	96.9	71.8
Q9Y095	Ft04011p OS=Drosophila melanogaster OX=7227 GN=XRCG1 PE=1 SV=1	6	3	4	3	614	68.7	9.22	4.8	3	0	73.1	86.8	82.4	77.1	58.3	112.8	109.4	84.2
Q95WY3	Ft04781p OS=Drosophila melanogaster OX=7227 GN=Nop56 PE=1 SV=1	8	3	12	3	496	54.8	9.22	21.48	3	0	291.4	265.5	235.1	190.4	180	527.4	378.4	335.8
Q9VKB0	Ft05224p OS=Drosophila melanogaster OX=7227 GN=ThRS PE=1 SV=2	8	6	6	6	747	85.9	7.78	8.28	6	0	98.7	117.6	122.6	64.7	88.1	122.3	143.2	88.3
Q9VYE9	Ft05227p OS=Drosophila melanogaster OX=7227 GN=DmelCG1622 PE=1 SV=1	10	2	4	2	398	45.4	9.39	0	2	0	5.9	7.5	10.2	10.4	5.6	13.1	16.9	9.4
Q9VGZ2	Ft06805p OS=Drosophila melanogaster OX=7227 GN=Rtp46 PE=1 SV=3	9	2	3	2	233	25.7	5.33	1.6	2	0	42.6	51.7	43.6	33.5	29.6	46.5	57.9	46.8
Q8IRL9	Ft06813p OS=Drosophila melanogaster OX=7227 GN=DmelCG2990 PE=1 SV=1	12	13	32	13	1100	124.5	6.74	45.97	13	0	469.9	617.1	475.8	282.7	609	625.1	487.8	
Q9W396	Ft06908p OS=Drosophila melanogaster OX=7227 GN=HP1b PE=1 SV=1	10	2	5	2	240	26	4.77	3.71	2	0	59.5	49.1	45	42.8	22.3	63.6	77.5	48.4
Q9VNN4	Ft07923p OS=Drosophila melanogaster OX=7227 GN=Karybeta3 PE=1 SV=1	7	7	26	7	1105	123.5	4.73	29.92	7	0	366.6	476	498.9	458.5	283.5	457.9	550.6	378.8
Q9VKI2	Ft09336p OS=Drosophila melanogaster OX=7227 GN=DmelCG4788 PE=1 SV=1	10	3	15	3	252	26.6	9.29	26.46	3	0	333.6	370.6	345.1	344.8	185.2	334	389.3	302.9
Q7KND8	Ft09619p OS=Drosophila melanogaster OX=7227 GN=Mad1 PE=1 SV=1	2	2	4	2	730	85	6.49	5.64	2	0	96.7	100.9	107.1	64.6	106.2	109.4	64.8	
Q9VIG1	Ft12406p OS=Drosophila melanogaster OX=7227 GN=(J)05287 PE=1 SV=2	3	2	3	2	1071	119.9	8.72	3.33	2	0	20.4	11.3	10.3	9.5	17.1	30.8	17.1	19
Q9VPL4	Ft17537p1 OS=Drosophila melanogaster OX=7227 GN=DmelCG4291 PE=1 SV=1	6	2	3	2	338	38.8	8.15	3.53	2	0	63.5	71.3	60.6	60.9	42.1	76.5	89.8	58.2
H0RN8	Ft17821p1 OS=Drosophila melanogaster OX=7227 GN=CG3760-RB PE=1 SV=1	15	3	3	3	265	29	5.31	10.62	3	0	99.9	95.9	100.5	91.1	83.5	87.2	115	95.8
A1Z9G2	Ft18620p1 OS=Drosophila melanogaster OX=7227 GN=fand PE=1 SV=1	5	4	12	4	883	103.3	5.64	3.95	4	0	77.4	82.5	84.8	86.2	53.9	103.2	118.4	76.7
Q9VUK8	Ft18749p1 OS=Drosophila melanogaster OX=7227 GN=GlyRS PE=1 SV=1	3	2	5	2	765	85.1	7.74	11.98	2	0	116.7	139.5	113.5	69.9	97.8	144.7	148.6	108.5
B7Z0E2	Ft18812p1 OS=Drosophila melanogaster OX=7227 GN=Unr PE=1 SV=1	3	2	2	2	1057	118.4	6.55	0	2	0	0	0	0	0	0	0	0	0
Q8IPT2	Ft18910p1 OS=Drosophila melanogaster OX=7227 GN=SMC5 PE=1 SV=3	4	4	9	4	1034	117.8	8.07	13.42	4	0	102.2	121.3	102.3	112.9	84.1	161.3	150.8	130.3
Q8IQZ7	Ft19014p1 OS=Drosophila melanogaster OX=7227 GN=Fim PE=1 SV=1	5	3	4	3	641	72	5.55	1.62	3	0	20.1	27.3	30.3	22.5	21.1	31.8	34.4	24.8
Q8IRH1	Ft19310p1 OS=Drosophila melanogaster OX=7227 GN=Psa PE=1 SV=1	9	9	27	9	1075	122.7	6.34	24.32	9	0	244	321.7	332.9	387.5	241.4	313.3	450.9	283.2
Q9V200	Ft19420p1 OS=Drosophila melanogaster OX=7227 GN=DmelCG1737 PE=1 SV=1	7	6	23	6	943	102.1	9.95	29.55	6	0	356.9	405.5	425.7	425.7	345.9	442.2	527.2	404.3
A1Z8D5	Ft20187p1 OS=Drosophila melanogaster OX=7227 GN=DmelCG18004 PE=2 SV=1	6	2	3	2	297	32.3	6.65	3.84	2	0	43.5	50.4	46.9	39.9	29.3	65.4	51.5	44.8
Q24113	Ft21126p1 OS=Drosophila melanogaster OX=7227 GN=nonA1 PE=1 SV=2	6	4	11	6	630	69.6	8.62	21.53	4	0	9	14.7	10.7	11.7	11.1	12.9	14.5	10.2
Q9VHC7	Ft21236p1 OS=Drosophila melanogaster OX=7227 GN=rump PE=1 SV=1	5	4	34	4	632	66.7	7.85	76.17	4	0	621.1	594.9	414.3	496.2	337	752	749.7	441.4
T2FFI3	Ft21265p1 OS=Drosophila melanogaster OX=7227 GN=mei-9 PE=2 SV=1	7	5	9	5	961	109.5	6.95	4.88	5	0	31.9	40.6	40.2	38.5	22.9	48.9	55.9	46
A1Z6L9	Ft21274p1 OS=Drosophila melanogaster OX=7227 GN=Tag1 PE=1 SV=1	7	4	18	3	891	77.9	7.59	35.28	4	0	8.9	5.3	7.4	3.9	11.7	20.6	8.7	4.9
Q9VJZ1	Ft21342p1 OS=Drosophila melanogaster OX=7227 GN=DmelCG59302 PE=1 SV=1	4	2	2	2	510	57.9	8.78	0	2	0	31.4	31.7	29.4	21.1	15.5	48.6	48.8	28.9
Q9W0D6	Ft22004p1 OS=Drosophila melanogaster OX=7227 GN=DmelCG7879 PE=1 SV=1	6	5	6	5	985	109.5	9.2	1.94	5	0	55.3	63.7	51.9	60.1	47.8	7.3	96.2	69.9
Q9VY73	Ft23714p1 OS=Drosophila melanogaster OX=7227 GN=Nd1 PE=1 SV=2	3	4	8	4	1147	132.7	5.15	10.33	4	0	65.4	71.4	85.1	71.1	50.5	83.5	80.7	62
Q9VPB0	Ft23914p1 OS=Drosophila melanogaster OX=7227 GN=HIPP1 PE=1 SV=2	2	2	3	2	926													

Q9VE98	GH01043p OS=Drosophila melanogaster OX=7227 GN=DmelCG8064 PE=1 SV=1	4	3	6	3	922	103.1	6.4	3.88	3	0	22	22.8	21.7	20.2	18.2	42.7	32.5	28.5
Q9VFF0	GH01077p OS=Drosophila melanogaster OX=7227 GN=UOCR-C1 PE=1 SV=2	5	3	3	3	470	51.8	6	6.95	3	0	74.5	83	108.5	89.1	191.7	102	122.8	60.2
Q7KRS9	GH01331p OS=Drosophila melanogaster OX=7227 GN=DmelCG1815 PE=1 SV=1	3	6	11	6	1664	181.8	8.35	11.7	6	0	145.3	160.4	158.9	104.7	192.4	192.4	220.8	154.5
Q7K3Z3	GH01724p OS=Drosophila melanogaster OX=7227 GN=p47 PE=1 SV=1	19	6	26	6	407	43.4	5.62	27.1	6	0	211.6	251.2	220.9	214.8	147	195	313	205.4
Q9VCW6	GH03051p OS=Drosophila melanogaster OX=7227 GN=Gclm PE=1 SV=1	6	2	2	2	285	31.5	5.74	1.72	2	0	33	33.3	34.7	32.7	24.4	32.7	42.9	35.5
Q9VKI8	GH03305p OS=Drosophila melanogaster OX=7227 GN=DmelCG6287 PE=1 SV=1	5	2	5	2	332	35.2	7.36	3.79	2	0	112.2	104.9	90.8	62.6	52.1	97	115.3	67.3
Q9VEP9	GH03554p OS=Drosophila melanogaster OX=7227 GN=Sl3a1 PE=1 SV=1	3	3	8	3	784	88	6.37	8.63	3	0	276.8	279.6	236.9	245.6	157	309.3	316.7	230.5
Q9V738	GH03795p OS=Drosophila melanogaster OX=7227 GN=DmelCG18178 PE=1 SV=1	8	2	2	2	374	42.5	9.16	3.02	2	0	53.8	33.8	24.4	17.9	20.1	91.2	49.5	23.9
Q9VNH5	GH04919p OS=Drosophila melanogaster OX=7227 GN=DmelCG2091 PE=1 SV=1	12	5	20	5	374	43	5.3	30.59	5	0	473.7	526.1	507.3	415.7	281.9	541.8	600.5	449.8
Q9W255	GH05812p OS=Drosophila melanogaster OX=7227 GN=qk58E-1 PE=1 SV=1	10	4	8	4	396	45.4	9.07	5.83	4	0	150.1	165.7	153.8	162.3	95.7	198.6	208.4	127.1
Q7K5M2	GH05839p OS=Drosophila melanogaster OX=7227 GN=DmelCG10139 PE=2 SV=1	18	4	19	4	224	25.5	7.33	27.4	4	0	406.9	444.3	366.4	432	324.9	474.2	511.7	440
Q9U5U4	GH06271p OS=Drosophila melanogaster OX=7227 GN=Mms19 PE=1 SV=1	4	2	2	2	959	107	5.91	5.72	2	0	27.8	32.5	37.9	30.7	34.9	30.4	34	39.7
Q9V7B3	GH06691p OS=Drosophila melanogaster OX=7227 GN=DmelCG11811 PE=1 SV=1	11	2	2	2	233	25.9	7.44	2.27	2	0	9.6	10.5	8.7	9.5	14.9	12.1	16.5	12.8
Q9VKU0	GH06740p OS=Drosophila melanogaster OX=7227 GN=Lm47 PE=2 SV=1	4	2	2	2	428	47.9	9.42	0	2	0	4.4	12.2	7.2	6	14.2	12.5	16.7	6.1
O97183	GH07456p OS=Drosophila melanogaster OX=7227 GN=Rpl133 PE=1 SV=1	13	2	12	2	275	31.2	4.82	25.6	2	0	153.4	179.6	168.6	164.3	127.9	212	211.6	178.8
Q9VEK8	GH07711p OS=Drosophila melanogaster OX=7227 GN=ads22 PE=1 SV=1	29	5	19	5	326	37.8	5.03	29.08	5	0	143.4	170.9	154.8	102.7	79.7	158.6	199.7	126.8
Q9VHX2	GH08043p OS=Drosophila melanogaster OX=7227 GN=DmelCG3223 PE=1 SV=1	8	3	7	3	415	45.1	5.25	9.22	3	0	100.5	100.9	109	99.2	73.7	120.7	140.5	106
Q24090	GH08712p OS=Drosophila melanogaster OX=7227 GN=Scrl PE=1 SV=2	8	3	10	3	370	41.9	5.27	14.8	3	0	223.2	278.5	272.5	260	173.5	298.1	300.2	266.9
Q7K1H0	GH09099p OS=Drosophila melanogaster OX=7227 GN=CG8491 PE=1 SV=1	6	2	3	2	324	36.5	6.65	2.16	2	0	96.7	75.5	88	88	106	111.2	122.5	89.4
8M2I3	GH10522p OS=Drosophila melanogaster OX=7227 GN=Rp90 PE=1 SV=1	4	2	7	2	818	88.2	9.36	9.73	2	0	86.8	115.3	112.1	114.4	118.8	166.2	191	139
Q96880	GH11150p OS=Drosophila melanogaster OX=7227 GN=TIIEalpha PE=1 SV=1	13	4	8	4	429	48.3	5	9.33	4	0	43	30.6	27.8	13	5.9	51.7	33.8	14.6
Q9V3Z4	GH11341p OS=Drosophila melanogaster OX=7227 GN=Rgn5 PE=1 SV=1	9	5	14	5	502	57.7	5.8	16.74	5	0	306.4	386.4	445.9	301.5	265.3	415.4	496.5	349.6
Q7KK90	GH14654p OS=Drosophila melanogaster OX=7227 GN=Gate1 PE=1 SV=1	10	2	11	2	224	24.9	5.91	8.16	2	0	89.1	134.5	130.4	141	97.9	110	209.8	88.2
Q9VA53	GH23275p OS=Drosophila melanogaster OX=7227 GN=DmelCG2246 PE=1 SV=2	8	3	8	3	406	44.8	8.21	10.48	3	0	91.5	110.4	123.8	88	91.5	111.3	134.9	95.4
Q8TOL3	GH24511p OS=Drosophila melanogaster OX=7227 GN=Luba1 PE=1 SV=1	16	12	84	12	1191	130.7	5.29	147.91	12	0	1091.1	1178.6	1165	829.8	642.1	1367	1386.7	888.7
Q9VSK9	GH24787p OS=Drosophila melanogaster OX=7227 GN=DmelCG6745 PE=1 SV=1	13	9	24	9	734	82.7	5.64	34.82	9	0	554.9	582.2	554.8	389.2	306.5	651.6	761	437.8
Q9VK60	GH25425p OS=Drosophila melanogaster OX=7227 GN=DmelCG6180 PE=1 SV=2	12	3	14	3	257	28.7	8.82	16.06	3	0	271.4	302.9	300.4	285.3	264.5	317.9	415.6	290.9
Q9VVA4	GH26789p OS=Drosophila melanogaster OX=7227 GN=DmelCG9674 PE=1 SV=2	3	8	20	8	2114	231.9	6.42	19.31	8	0	252.7	332.9	383	322.9	274.2	333.5	423.4	345.7
Q6NL44	GH28815p OS=Drosophila melanogaster OX=7227 GN=CG18238 PE=1 SV=1	4	2	3	2	478	53.6	7.05	3.72	2	0	33.5	41.4	44.7	38.4	30.9	51	53.9	41.4
Q9VJD1	Glucosidase 2 beta subunit, isoform A OS=Drosophila melanogaster OX=7227 GN=GC52	4	2	4	2	548	61.5	4.46	4.73	2	0	58.4	75	66.3	75	88.7	71.5	106	70.6
Q7JV16	Glutathione S transferase E13, isoform A OS=Drosophila melanogaster OX=7227 GN=Gs	10	2	4	2	226	25.8	6.61	4.31	2	0	22.5	29.9	31.5	30	23.1	24.1	32.1	28
A1ZB72	Glutathione S transferase E7 OS=Drosophila melanogaster OX=7227 GN=Gate7 PE=1 SV=1	11	2	3	2	223	25.5	6.57	0	2	0	22.9	29.4	29.8	28.8	20.2	31.7	36.9	25
Q9VSL6	Glutathione S transferase O1 OS=Drosophila melanogaster OX=7227 GN=GateO1 PE=1 SV=1	6	2	3	2	254	30	7.44	3.78	2	0	105.2	125.6	118.5	117.2	90.5	103.5	145.5	98.2
Q9VSL4	Glutathione S transferase O2, isoform B OS=Drosophila melanogaster OX=7227 GN=Gate	8	2	8	2	250	28.7	7.05	0	2	0	187.5	182.8	159.5	124.9	181.6	237.4	186.9	91.2
ADA084KFT5	Glutathione S transferase S1, isoform D OS=Drosophila melanogaster OX=7227 GN=Gate	12	3	3	3	250	27.8	4.59	3.89	3	0	97	109.9	110.5	109.6	84.2	98	138.3	94.1
M9PJN8	Glyceroldehyde-3-phosphate dehydrogenase OS=Drosophila melanogaster OX=7227 GN=	6	2	39	2	332	35.3	8.44	71.2	2	0	549.8	882.7	932.3	890.7	649.8	780.2	1096	771.6
Q9VFC8	Glycogen (starch) synthase OS=Drosophila melanogaster OX=7227 GN=GlyS PE=1 SV=2	3	3	4	3	709	81.7	6.65	1.7	3	0	53.4	63.6	67.1	64.5	60.6	77.6	83	58.9
A1Z6H7	Glycoprotein 210 kDa, isoform A OS=Drosophila melanogaster OX=7227 GN=Gp210 PE=	3	4	4	4	1876	209.7	6.47	9.92	4	0	17.2	29.3	25.2	42.4	34.6	23.8	35.5	30.1
Q9VAY2	Glycoprotein 93 OS=Drosophila melanogaster OX=7227 GN=Gp93 PE=1 SV=1	12	8	17	8	787	90.2	5.02	17.56	8	0	173.8	230.5	204.9	217.6	297	170.3	339.1	216.9
Q9VGO1	GM01350p OS=Drosophila melanogaster OX=7227 GN=alpha-KGDHC PE=1 SV=1	9	3	5	3	468	49.9	9.47	6.86	3	0	30.2	34.9	38.9	34.2	118	40.5	38.3	29.2
Q9VNH2	GM13341p OS=Drosophila melanogaster OX=7227 GN=DmelCG2100 PE=1 SV=1	4	2	4	2	477	55.3	9.01	3.85	2	0	70.4	94.4	92	84	58.9	104.4	106.7	80.5
Q9VPL0	GM13767p OS=Drosophila melanogaster OX=7227 GN=DmelCG3436 PE=1 SV=1	5	2	7	2	347	38.8	6.92	11.21	2	0	205.5	232.3	224	203.6	167.3	227.7	259.7	205.7
Q9V9T5	GM14617p OS=Drosophila melanogaster OX=7227 GN=Mccc1 PE=1 SV=2	9	6	10	6	698	76.5	6.2	21.64	6	0	99.9	131.6	186.7	156.3	192	260.1	176.5	124
Q7JKV6	GM27569p OS=Drosophila melanogaster OX=7227 GN=trsn PE=1 SV=1	9	2	4	2	235	27	5.5	5.62	2	0	42.8	42.3	39	28	34.4	45.4	46.9	33.3
Q9VN19	Golgi to ER traffic protein 4 homolog OS=Drosophila melanogaster OX=7227 GN=CG9855	5	2	7	2	339	38.5	6.54	7.83	2	0	118.2	137	129.8	142.3	125	155.8	168.6	155.9
M9PHT1	Grunge, isoform J OS=Drosophila melanogaster OX=7227 GN=Gug PE=1 SV=1	2	3	4	3	2007	213.7	7.46	4.69	3	0	75.4	75.3	72.6	63.5	42.5	77.7	110.7	76.2
Q6NP69	GST-containing FLYWCH zinc-finger protein OS=Drosophila melanogaster OX=7227 GN=	3	2	9	2	1045	119.2	5.99	12.02	2	0	7	6.5	9	5.1	4.6	9.6	14	3.4
P32234	GTP-binding protein 128up OS=Drosophila melanogaster OX=7227 GN=128up PE=2 SV=	6	2	3	1	368	41.1	8.6	1.65	2	0								
O18640	Guanine nucleotide-binding protein subunit beta-like protein OS=Drosophila melanogaster	10	3	25	3	318	35.6	7.47	43.87	3	0	468.9	590.9	648.3	555.5	790.4	751.5	865.8	581
Q8MT06	Guanine nucleotide-binding protein-like 3 homolog OS=Drosophila melanogaster OX=722	8	4	15	4	581	65.9	9.36	21.47	4	0	190.6	219	178.3	146.7	294.4	276	261.5	
AO4081	HAICA ribonucleoprotein complex subunit 4 OS=Drosophila melanogaster OX=7227 GN=H	9	4	22	4	508	56.8	9.28	29.95	4	0	681.7	568.8	506	320.3	331.3	1077.3	1175.4	555.2
B7Z0Z1	Hangover, isoform C OS=Drosophila melanogaster OX=7227 GN=hng PE=1 SV=1	2	3	3	3	2223	242.2	5.82	22.51	3	0	117.8	116.4	103.5	89.3	55.4	139.7	131.2	96.5
Q9VM75	HEAT repeat-containing protein 1 homolog OS=Drosophila melanogaster OX=7227 GN=H	2	3	4	3	2096	237.1	6.87	9.52	3	0	52.1	49.3	37.3	55.2	52.5	78.4	68.4	74.3
P11147	Heat shock 70 kDa protein cognate 4 OS=Drosophila melanogaster OX=7227 GN=Hsc70-	20	8	307	7	651	71.1	5.52	571.9	8	1	2538.7	2998.7	2901	2309	1832.7	3226.6	3666.5	2768.3
P29845	Heat shock 70 kDa protein cognate 5 OS=Drosophila melanogaster OX=7227 GN=Hsc70-	8	5	9	5	686	74	6.35	19.76	5	0	56.6	69.7	86.6	75.9	101.8	88	78.4	71.7
Q4H2F7	Heat shock factor, isoform D OS=Drosophila melanogaster OX=7227 GN=Hsf PE=1 SV=1	4	3	5	3	733	81.6	5.06	2.03	3	0	57.7	60.9	69.3	53.7	32.3	75.9	84.2	53.5
O2649	Heat shock protein 60A OS=Drosophila melanogaster OX=7227 GN=Hsp60A PE=1 SV=3	9	4	8	4	573	60.8	5.49	11.39	4	0	102.9	131.1	199.4	204.7	446.9	175	164.5	122.4
M9PBL3	Heat shock protein 83, isoform B OS=Drosophila melanogaster OX=7227 GN=Hsp83 PE=	26	14	97	13	717	81.8	5.02	136.26	14	1	2420.9	2764.5	2870.7	2056.6	2030.5	3061.7	3549.6	2151.6
E8N4A2	HECT and RLD domain containing E3 ubiquitin ligase 4, isoform C OS=Drosophila melano	2	2	2	2	1062	119.4	6.27	2.25	2	0	30.6	32.8	34.9	27.3	24.3	43.3	49.5	44.4
Q9VF02	Helicase 89B, isoform B OS=Drosophila melanogaster OX=7227 GN=Hel89B PE=1 SV=3	2	2	5	2	1923	212.9	7.01	7.89	2	0	18.4	24.4	17.9	17	16.1	27.4	32.1	27.1
P05205	Heterochromatin protein 1 OS=Drosophila melanogaster OX=7227 GN=Su(var)205 PE=1,	44	6	32	6	206	23.2	5.08	70.57	6	0	538.1	376.6	342.5	297.4	192.2	574.1	461.7	295.9
Q9VYY7	Heterochromatin protein 5, isoform B OS=Drosophila melanogaster OX=7227 GN=HP5 PE=	11	5	21	5	837	92.6	5.97	49.05	5	0	266.2	298.3	241.5	251.5	209.6	355.3	381.9	293.4
P48809	Heterogeneous nuclear																		

Q9VH11	Hyrax OS=Drosophila melanogaster OX=7227 GN=hyx PE=2 SV=1	8	5	10	5	538	61.3	9.63	7.95	5	0	146.5	197.7	193.3	166.6	134.6	227	260.6	209.4
M9NF14	IGF-II mRNA-binding protein, isoform L OS=Drosophila melanogaster OX=7227 GN=Imp P	2	2	3	2	638	69.9	8.15	1.73	2	0	59.5	73.5	63.3	64.5	89.2	62.9	106	68.1
XZJEB6	Imaginal disc growth factor 4, isoform C OS=Drosophila melanogaster OX=7227 GN=Idgf4	3	3	4	3	442	48.6	7.83	1.73	3	0	17.7	26.3	22.2	12	22.6	19.9	28	21.3
O76521	Importin subunit alpha OS=Drosophila melanogaster OX=7227 GN=Kap-alpha1 PE=2 SV1	5	2	4	2	543	60	5.34	3.8	2	0	20	19.2	27.5	20.7	14.1	20.1	26	18.9
Q9V455	Importin subunit alpha OS=Drosophila melanogaster OX=7227 GN=Kap-alpha3 PE=1 SV1	9	4	11	4	514	57	2.26	13.03	4	0	326.9	366.8	338.1	330.5	222.1	441.4	384	339.1
P52295	Importin subunit alpha OS=Drosophila melanogaster OX=7227 GN=Pen PE=1 SV=2	16	6	78	6	522	57.8	5.35	91.69	6	0	569.9	714.3	658.3	645	350.6	570.7	671.8	525.7
O18388	Importin subunit beta OS=Drosophila melanogaster OX=7227 GN=Fs2/Ket PE=1 SV=2	12	7	18	7	884	96.6	5.03	19.79	7	0	271	328.9	312	293.4	224.4	347.8	433	270.3
Q7JRJ9	Inner centromere protein, isoform A OS=Drosophila melanogaster OX=7227 GN=Inocent P	6	4	7	4	755	83.5	9.28	12.76	4	0	252	241.5	229.2	195.8	157.9	357.9	351.1	247.5
U77460	Inorganic pyrophosphatase OS=Drosophila melanogaster OX=7227 GN=Nurf-38 PE=1 SV1	12	3	23	3	338	37.9	7.01	41.99	3	0	443	432.7	438.5	259.3	296.5	407	449.1	278.3
O97477	Inositol-3-phosphate synthase OS=Drosophila melanogaster OX=7227 GN=Inos PE=1 SV1	6	3	8	3	565	62.2	6.23	11.64	3	0	75.9	90	96.3	87.8	82.4	96.5	117.5	97
Q9VHG5	Insulator binding factor 1, isoform A OS=Drosophila melanogaster OX=7227 GN=Ibf1 PE=1 SV1	23	5	10	5	242	27.7	6.44	13.83	5	0	302.8	211	266.8	235.4	204	365.9	373.1	332.3
Q9VHG6	Insulator binding factor 2 OS=Drosophila melanogaster OX=7227 GN=Ibf2 PE=1 SV1	18	2	6	2	195	21.9	8.03	15.82	2	0	153	156.2	131.4	83.8	68.8	226.6	188.8	115.1
Q9W1C5	Integrator complex subunit 1 OS=Drosophila melanogaster OX=7227 GN=IntS1 PE=1 SV1	3	5	9	5	2053	234.9	6.61	5.72	5	0	31.5	36.4	35.7	31.9	26.8	37.6	48.8	35.4
Q9VZM7	Integrator complex subunit 10 OS=Drosophila melanogaster OX=7227 GN=IntS10 PE=1 SV1	6	4	7	4	631	72.2	5.88	3.79	4	0	66.6	70.2	81.1	72.8	56.4	96.7	108.4	71.3
Q9VPY0	Integrator complex subunit 14 OS=Drosophila melanogaster OX=7227 GN=IntS14 PE=1 SV1	3	2	5	2	587	65	7.31	2.14	2	0	42.9	56.4	61.4	67.6	59.9	58.4	74.8	72.1
Q7PLS8	Integrator complex subunit 3 OS=Drosophila melanogaster OX=7227 GN=IntS3 PE=1 SV1	7	6	22	6	1068	123.9	7.11	40.4	6	0	169	231	232.1	210.7	151.6	278.3	297.8	262.6
Q9V741	Integrator complex subunit 7 OS=Drosophila melanogaster OX=7227 GN=IntS7 PE=1 SV1	3	3	4	3	1001	112.2	8.18	3.51	3	0	40.4	52.2	42.1	36.4	25	69.9	66.8	32.5
A1ZAK1	Integrator complex subunit 9 OS=Drosophila melanogaster OX=7227 GN=IntS9 PE=1 SV1	2	3	3	3	1007	113.4	6.49	5.89	3	0	68.4	78.7	67	77.8	49.9	90.7	100.1	81.1
Q9V400	Integrin linked kinase, isoform A OS=Drosophila melanogaster OX=7227 GN=Ilk PE=1 SV1	3	2	2	2	448	50.7	7.44	4.36	2	0	28.2	41	44.9	37.4	37.5	35.2	37.2	32.7
Q9W017	IP07275p OS=Drosophila melanogaster OX=7227 GN=Paft1 PE=1 SV2	24	4	10	2	202	23.3	7.77	13.82	4	2	288.7	370.1	429	272.2	93.3	429	180	170.8
Q9VEB1	IP09655p OS=Drosophila melanogaster OX=7227 GN=Mdh2 PE=1 SV1	5	2	4	2	336	35.3	9.11	1.67	2	0	17.4	37.7	37.2	36.2	45.4	43.4	41.9	51
Q9V4Z5	IP10727p OS=Drosophila melanogaster OX=7227 GN=DmelCG11788 PE=2 SV1	24	8	20	8	425	48.8	5.11	37.47	8	0	269.1	358.5	371.2	246.5	136.1	210.7	222.8	202.2
Q9VPM7	IP13529p OS=Drosophila melanogaster OX=7227 GN=DmelCG10708 PE=1 SV2	5	3	9	3	610	67.5	7.49	18.32	3	0	254.5	297.9	291.9	242.9	207	383.4	405.4	287.9
Q9VTE6	IP14658p OS=Drosophila melanogaster OX=7227 GN=anon-EST-f62H6 PE=1 SV3	5	4	5	4	1174	131.9	6.19	4.24	4	0	43.2	48.4	35	52.2	40.2	71.4	57.3	53.5
Q9VKC1	IP16805p OS=Drosophila melanogaster OX=7227 GN=Rpl7-like PE=1 SV2	9	3	6	3	257	29.1	10.1	10.1	3	0	126.1	153.7	115.1	160.9	100	182.2	178.8	161.1
Q9VCV4	Iron regulatory protein 1A OS=Drosophila melanogaster OX=7227 GN=irp-1A PE=1 SV1	7	6	11	2	902	98.7	5.78	16.34	6	4	295	324.7	330.9	285	212.4	302.4	406.5	293.7
Q9VZG3	Iron regulatory protein 1B OS=Drosophila melanogaster OX=7227 GN=irp-1B PE=1 SV1	7	6	13	2	899	98.5	5.95	15.42	6	0	11.9	10.2	10.3	12.9	8.6	8.7	13	10.4
B7Z0E0	Isocitrate dehydrogenase [NADP] OS=Drosophila melanogaster OX=7227 GN=Idh PE=1 SV1	10	4	27	4	479	53.6	7.3	25.85	4	0	528.6	634.3	744.3	580.8	517.5	684.3	860.8	607.6
Q8MSW0	Isoleucyl-tRNA synthetase, isoform A OS=Drosophila melanogaster OX=7227 GN=IleRS9	3	4	8	4	1229	141	7.52	10.63	4	0	100.5	162.2	188	145.8	270.2	172.8	264.2	191.9
Q9VGR7	J domain-containing protein CG6693 OS=Drosophila melanogaster OX=7227 GN=CG6693	18	4	16	4	299	34.9	8.59	26.64	4	0	598.2	629.9	485.8	427.8	357.6	762.8	713.3	488.6
B7YZK5	Jabba, isoform C OS=Drosophila melanogaster OX=7227 GN=Jabba PE=1 SV1	5	2	4	2	560	62.6	5	8.8	2	0	101.3	192.4	185.7	202.3	204.8	148.2	265.7	155.5
AOA0B4GX1	Jaguar, isoform L OS=Drosophila melanogaster OX=7227 GN=jar PE=1 SV1	3	4	4	4	1268	144.8	8.68	1.82	4	0	22.4	29.6	29.3	30.1	35	33.2	43.2	31.5
Q9VBP5	Jing interacting gene regulatory 1, isoform A OS=Drosophila melanogaster OX=7227 GN=J	10	3	18	3	336	38.8	6.18	35.56	3	0	405.4	513.6	542	442.1	282.8	437	471.4	368.7
Q9V700	Jumonj, AT rich interactive domain 2 OS=Drosophila melanogaster OX=7227 GN=Jand2 F	3	6	10	6	2351	252.4	9.11	10.86	6	0	114.6	328.2	131.7	122.7	142	169.1	202	158.5
Q9VPR6	Kinase OS=Drosophila melanogaster OX=7227 GN=Ipk2 PE=3 SV2	10	2	3	2	309	35.3	7.94	6.71	2	0								
P17210	Kinesin heavy chain OS=Drosophila melanogaster OX=7227 GN=Khc PE=1 SV2	4	4	6	4	975	110.3	5.77	8.27	4	0	80.6	105.5	121.8	99.2	112.8	123.5	150.2	98.8
M9PF24	Kinesin light chain, isoform B OS=Drosophila melanogaster OX=7227 GN=Klc PE=4 SV1	6	3	5	3	508	58	6.25	5.42	3	0	60.3	65.4	74.4	60.1	74	78.2	102	65.8
Q9VSW5	Kinesin-like protein at 67A, isoform A OS=Drosophila melanogaster OX=7227 GN=Klp67A	10	9	15	9	814	92.3	9.19	20.81	9	0	224.8	256.4	231.9	259.8	158.3	321.5	314.9	259.6
AV4A1	Kinesin-like protein OS=Drosophila melanogaster OX=7227 GN=Klp10A PE=1 SV1	4	3	6	3	805	88.6	7.21	7.53	3	0	64	82.6	68.1	56.7	43.7	98	102.9	74
AOA0B4L25	Kinesin-like protein OS=Drosophila melanogaster OX=7227 GN=ncd PE=1 SV1	8	6	20	6	700	77.4	9.17	29.76	6	0	426.1	397.3	367.3	296.6	208.7	590.8	550.4	363.4
Q9VZ55	Kinesin-like protein OS=Drosophila melanogaster OX=7227 GN=pav PE=1 SV1	4	4	3	6	887	100.6	9.23	8.41	3	0	37.2	43.1	37	33.6	29.3	71.4	59.8	35.1
AOA0B4LW1	Kinesin-like protein OS=Drosophila melanogaster OX=7227 GN=sub PE=3 SV1	15	9	26	9	628	71.3	5.48	43.75	9	0	391.3	471.3	391.9	416.8	271.3	585.9	607.3	473.8
B7Z0D2	Kismet, isoform C OS=Drosophila melanogaster OX=7227 GN=ks PE=1 SV1	2	9	14	9	5517	593.1	5.63	12.54	9	0	188.4	248.2	261.4	254.1	187.9	269.4	296	245.9
Q8SX89	Kugelkern, isoform A OS=Drosophila melanogaster OX=7227 GN=kuk PE=1 SV1	5	2	4	2	570	60	5.48	6.52	2	0	81.6	82.2	81.4	92.8	65.2	91.9	140.4	76.5
Q9Y134	L.2.35Df OS=Drosophila melanogaster OX=7227 GN=Mtr4 PE=1 SV1	8	8	15	8	1055	118.9	6.77	19.63	8	0	233	257.7	246.8	212.9	153.4	304.5	331.4	219.7
Q9VZ22	L(3)mbt interacting protein 1, isoform A OS=Drosophila melanogaster OX=7227 GN=Lint1	5	2	2	2	602	67.9	8.68	1.83	2	0	9.3	16.7	17.5	17.9	9.3	19.1	21.4	10.4
P40796	La protein homolog OS=Drosophila melanogaster OX=7227 GN=La PE=1 SV2	13	4	27	4	390	44.9	7.58	37.3	4	0	610.2	680.3	638.8	568.7	381.7	695.8	864.1	673.4
AOA0B4KFY9	Lamin C, isoform B OS=Drosophila melanogaster OX=7227 GN=LamC PE=3 SV1	11	6	8	6	640	72.1	6.67	12.25	6	0	86.4	100.5	94.9	89.3	99.5	88.5	121	79.6
Q8MLV1	Lamin-B receptor OS=Drosophila melanogaster OX=7227 GN=LBR PE=1 SV1	3	2	5	2	741	83.1	9.79	6.42	2	0	27.2	46.4	39.8	47.9	56.1	53.5	81.5	42.7
M9NE89	Lamin, isoform B OS=Drosophila melanogaster OX=7227 GN=Lam PE=3 SV1	33	20	93	20	622	71.3	6.47	151.13	20	0	2049.9	2394.1	2082.3	2408.4	2027.6	2028.9	3194.5	1989.3
Q95RY2	LD01461p OS=Drosophila melanogaster OX=7227 GN=CG17014 PE=1 SV1	10	3	14	3	262	29.3	5.62	15.72	3	0	222.7	254.4	260.8	217.8	201	275	347.2	260.6
Q9VL07	LD02225p OS=Drosophila melanogaster OX=7227 GN=Ulx PE=2 SV3	5	4	7	4	1136	129.3	7.81	8.4	4	0	88.8	108.4	116	117	83	143.2	164.1	141.6
Q7K180	LD02709p OS=Drosophila melanogaster OX=7227 GN=Map60 PE=1 SV1	9	4	38	4	440	47.6	6.77	20.26	4	0	353.9	575.6	352.4	431	308.9	461.6	533	423.5
Q9VXR5	LD02975p OS=Drosophila melanogaster OX=7227 GN=DmelCG9281 PE=1 SV1	9	4	12	4	611	69.5	7.53	18.47	4	0	128.1	175.7	170.7	170.7	204.7	171.5	232.1	174.9
Q9VFN5	LD03220p OS=Drosophila melanogaster OX=7227 GN=Slp1 PE=1 SV1	13	4	16	4	490	55.7	6.81	16.75	4	0	166.6	207.1	203	173.7	146.1	190	246.1	161.4
Q9VYW4	LD04461p OS=Drosophila melanogaster OX=7227 GN=DmelCG1703 PE=1 SV1	11	8	32	8	901	101.5	5.82	51.32	8	0	499.3	469.7	583.2	421	411.3	784.5	691.7	519.5
Q9VVU6	LD04472p OS=Drosophila melanogaster OX=7227 GN=DmelCG6841 PE=1 SV2	11	9	26	9	931	105.2	7.44	40.94	9	0	411.8	482.6	513	415.5	290.8	589.1	616.5	473.5
Q9VB52	LD05287p OS=Drosophila melanogaster OX=7227 GN=Jmi1 PE=1 SV1	2	3	7	3	1477	162.9	8.78	8.91	3	0	74.3	91.7	88	97.5	55.6	102.3	99.3	99.3
Q9VY75	LD06533p OS=Drosophila melanogaster OX=7227 GN=DmelCG10347 PE=1 SV1	7	5	8	5	580	65.3	5.78	10.81	5	0	131.2	141.7	141.4	125.5	123.5	174.1	189.3	142
Q9VQB4	LD06553p OS=Drosophila melanogaster OX=7227 GN=DmelCG3609 PE=1 SV1	10	3	15	3	335	37.3	7.52	30.24	3	0	217.3	292.3	272.3	248.1	212.3	275.8	336.5	247.7
Q9WS42	LD07342p OS=Drosophila melanogaster OX=7227 GN=mpj130 PE=1 SV3	4	4	7	4	986	110.4	5.27	8.1	4	0	84.9	91.9	93.4	93.4	80.6	115	137.6	106.9
Q9VSL0	LD07728p OS=Drosophila melanogaster OX=7227 GN=DmelCG6683 PE=1 SV1	13	2	4	2	197	22.1	6.86	7.14	2	0	33.4	32.2	29.7	27.4	19.4	32.2	35.8	39.1
Q9VCH9	LD07883p OS=Drosophila melan																		

Q9VTT2	LD20590p OS=Drosophila melanogaster OX=7227 GN=vers PE=1 SV=1	7	2	6	2	391	44.8	5.81	11.02	2	0	34.2	45	39.1	45.7	22.7	51.6	55.3	34
Q7K231	LD20635p OS=Drosophila melanogaster OX=7227 GN=CYC4 PE=1 SV=1	10	4	9	4	517	58.9	8.13	11.87	4	0	78.9	97.2	94.9	91.1	64.8	112.2	111.9	102.3
Q9VY91	LD21074p OS=Drosophila melanogaster OX=7227 GN=Pcdc4 PE=1 SV=2	10	4	14	4	509	56.3	5.97	30.72	4	0	278.4	390.5	359.1	332.7	284.3	317.9	432.5	351
Q59E33	LD21442p OS=Drosophila melanogaster OX=7227 GN=scat6 PE=1 SV=1	2	2	4	2	960	107.5	9.22	7.32	2	0	90.9	99.1	110.3	97.8	61.9	130.6	124.8	106.4
Q9VXW5	LD21606p OS=Drosophila melanogaster OX=7227 GN=DmelCG9114 PE=2 SV=1	3	2	3	2	619	71.3	5.25	2.11	2	0	41.9	39.2	36.3	36.6	38.6	49.2	118.6	34.8
Q9VW10	LD21924p OS=Drosophila melanogaster OX=7227 GN=DmelCG9300 PE=1 SV=1	4	2	3	2	673	76.3	5.63	1.77	2	0	10.6	10.3	9	9.6	6.5	20.9	14.5	14.3
Q9VD52	LD21931p OS=Drosophila melanogaster OX=7227 GN=DmelCG6015 PE=1 SV=1	3	2	4	2	576	65.4	7.34	3.78	2	0	62.4	85.1	75.5	71.8	55.5	101.4	100.9	86
Q9I728	LD21943p OS=Drosophila melanogaster OX=7227 GN=CG13372 PE=1 SV=3	3	4	5	4	1377	157.6	7.68	1.92	4	0	36.6	41.2	29.8	43.3	40.8	70.3	52.4	57.7
Q7KUA4	LD22577p OS=Drosophila melanogaster OX=7227 GN=Uba2 PE=1 SV=1	14	7	43	7	700	77.7	5.02	47.51	7	0	652.5	746	607.9	298.5	209.5	821.7	811.1	256.3
Q9VLX2	LD22651p OS=Drosophila melanogaster OX=7227 GN=DmelCG1754 PE=1 SV=1	3	2	4	2	861	95.9	6.1	9.19	2	0	44.2	47.8	47.1	53.6	36.9	58.7	85.5	41.5
Q9V9V7	LD23072p OS=Drosophila melanogaster OX=7227 GN=pasha PE=2 SV=1	5	3	3	3	642	72	5.81	2.18	3	0	47.6	35	36	29.1	20.7	48.9	47.1	30.5
Q9VL91	LD23102p OS=Drosophila melanogaster OX=7227 GN=z30C PE=1 SV=2	5	2	8	2	777	88.3	8.13	15.29	2	0	51.3	48.5	47.7	51.5	35.4	69.8	68	55.1
Q95TU2	LD23187p OS=Drosophila melanogaster OX=7227 GN=DmelCG6686 PE=1 SV=1	8	5	15	5	970	112.5	7.21	30.21	5	0	164.9	159.6	156.6	151.3	107.1	212.5	223.6	165.5
Q9VCF8	LD23561p OS=Drosophila melanogaster OX=7227 GN=anon-W00118547_306 PE=1 SV=1	8	2	4	2	371	41.8	5.62	8.45	2	0	21.1	24.9	27.8	26.4	25.2	30.2	35.7	30.1
Q9VK59	LD23647p OS=Drosophila melanogaster OX=7227 GN=DmelCG5787 PE=1 SV=2	14	13	50	13	950	100.2	9.74	68.81	13	0	1486	1457.9	1144.8	1281.1	985.6	1600	1666.2	1269.2
Q9VAA9	LD23804p OS=Drosophila melanogaster OX=7227 GN=DmelCG7946 PE=1 SV=1	18	8	50	8	475	52.8	8.18	35.36	8	0	571.7	550.8	500	479.2	386.5	812.8	701.1	562.4
Q9VNG2	LD24014p OS=Drosophila melanogaster OX=7227 GN=DmelCG3163 PE=1 SV=2	2	2	4	2	807	90.5	8.79	7.62	2	0	56.5	68.9	74.8	52.9	46.7	74.5	85.8	62.5
Q9WCF8	LD24355p OS=Drosophila melanogaster OX=7227 GN=DmelCG3163 PE=1 SV=2	6	2	2	2	368	41.5	8.34	1.85	2	0	22.3	32.2	34.1	15	16.5	36.6	30.1	22.4
Q8SX78	LD24469p OS=Drosophila melanogaster OX=7227 GN=Pch2 PE=1 SV=1	12	5	10	5	421	46.5	5.69	13.42	5	0	150.8	190.3	187.3	175.2	146.7	181.4	207.6	159.8
Q7JYH6	LD24669p OS=Drosophila melanogaster OX=7227 GN=DmelCG9436 PE=1 SV=1	10	3	7	3	311	35.4	6.78	11.39	3	0	205.4	187.9	143.5	143.5	96.9	33	221.6	126.5
Q9VQK5	LD24714p OS=Drosophila melanogaster OX=7227 GN=DmelCG3542 PE=1 SV=1	4	3	5	3	806	91.3	8.84	4.12	3	0	32.2	44.5	30.9	40.7	58.4	54.7	59.1	33
Q9V54	LD24737p OS=Drosophila melanogaster OX=7227 GN=I[Q]0007 PE=1 SV=2	5	5	5	5	1222	139.5	7.4	6.38	5	0	80.6	96.5	85.3	79.1	64.2	103.6	105.5	96.5
Q9VJ37	LD24793p OS=Drosophila melanogaster OX=7227 GN=Raf1 PE=1 SV=1	8	2	10	2	266	27.8	10.55	19.66	2	0	252.4	271.1	232	237.3	161.4	232.3	296.3	245.4
Q9VK44	LD24832p OS=Drosophila melanogaster OX=7227 GN=ufd2 PE=1 SV=1	5	7	15	5	7127	138.5	5.87	10.67	7	0	229.7	284.9	273.5	235.2	220.4	320.8	371.3	280.5
Q9VJE3	LD24839p OS=Drosophila melanogaster OX=7227 GN=DmelCG15141 PE=1 SV=1	14	5	11	5	404	45.9	4.93	18.03	5	0	323.1	331.3	319.6	271	180	356.7	378.3	326.8
Q9VG60	LD24919p OS=Drosophila melanogaster OX=7227 GN=DmelCG12267 PE=2 SV=2	3	2	3	2	522	59.8	6.81	2.4	2	0	63.3	68.5	73.4	68.5	59.1	90	100	83
Q9W003	LD24968p OS=Drosophila melanogaster OX=7227 GN=DmelCG3847 PE=2 SV=1	6	3	7	3	380	43.6	8.83	1.82	3	0	176.1	179	146.9	135.6	105.9	216.1	227.1	137.4
Q8MSW4	LD25448p OS=Drosophila melanogaster OX=7227 GN=CG42374-RA PE=2 SV=1	7	2	7	2	213	24	6.43	4.12	2	0	46.6	67	69.3	49.1	43.1	67.4	78.3	64.3
Q9VIZ3	LD25692p OS=Drosophila melanogaster OX=7227 GN=I[2]37Cb PE=1 SV=1	6	3	8	3	894	102.8	6.52	11.66	3	0	94.7	107.1	95.4	83.9	68.2	112.9	113.7	92.5
Q7K4R2	LD26477p OS=Drosophila melanogaster OX=7227 GN=DmelCG11504 PE=2 SV=1	6	2	9	2	410	46.4	6.6	7.62	2	0	123.7	133.8	122.5	118.9	96.1	204.3	158.2	159.2
Q9VT61	LD27033p OS=Drosophila melanogaster OX=7227 GN=DmelCG8108 PE=1 SV=1	6	5	15	5	919	102.9	6.21	19.52	5	0	524.8	509.1	342.8	240.1	202.7	608.1	559.4	275.1
Q95R17	LD28068p OS=Drosophila melanogaster OX=7227 GN=DmelCG17454 PE=1 SV=1	17	3	8	3	243	28.2	8.54	4.12	3	0	54.7	65.3	52.4	56	35.2	78.2	74.3	57.3
Q8T051	LD28458p OS=Drosophila melanogaster OX=7227 GN=CG4639 PE=2 SV=1	3	2	3	2	639	73.2	6.42	4.69	2	0	81.1	94.9	90.5	88.1	75	118.5	127.2	99.9
Q9VAX8	LD28793p OS=Drosophila melanogaster OX=7227 GN=Snu114 PE=1 SV=1	12	9	28	9	975	110.6	5.03	23.99	9	0	107.1	133.9	139.5	118.1	96.5	168.9	107	125.6
Q9VXR7	LD29573p OS=Drosophila melanogaster OX=7227 GN=Rex65 PE=1 SV=1	20	9	25	9	681	76.7	6.21	27.16	9	0	166.4	142.7	130.5	123.7	81	196.3	156.4	174.8
Q9VL71	LD29830p OS=Drosophila melanogaster OX=7227 GN=Srp54 PE=1 SV=1	4	2	4	2	513	58.3	11.33	1.77	2	0	126.1	134.7	75.6	124.2	63	136.4	136.7	129.5
Q9VN21	LD30155p OS=Drosophila melanogaster OX=7227 GN=lost PE=1 SV=1	11	5	9	5	545	59.7	9.06	15.62	5	0	190.7	192.2	195.1	135.3	222.5	187.1	240.3	160.2
Q9VHM3	LD30467p OS=Drosophila melanogaster OX=7227 GN=M1BP PE=1 SV=1	10	3	16	3	318	48.1	5.52	26.73	3	0	220.8	239.3	213.4	220.6	158	316.4	292.6	243.9
Q9VIE4	LD30995p OS=Drosophila melanogaster OX=7227 GN=DmelCG10098 PE=1 SV=1	5	2	2	2	353	37.5	4.79	2.19	2	0	26.7	36.3	32.9	28.8	30.4	34.8	46.9	27.3
Q9VUR2	LD31322p OS=Drosophila melanogaster OX=7227 GN=DmelCG12301 PE=1 SV=2	9	6	10	6	771	88.7	9.48	14.63	6	0	113.2	114.2	109.7	107.7	135.9	147.8	117.1	117.4
Q7JYH0	LD32459p OS=Drosophila melanogaster OX=7227 GN=DmelCG8435 PE=1 SV=1	6	2	5	2	333	37.7	6.86	13.64	2	0	95.9	115.2	104.8	120.2	90.7	116.6	126.8	125.8
Q9V3T8	LD32469p OS=Drosophila melanogaster OX=7227 GN=SC35 PE=1 SV=1	10	2	7	2	195	21.4	11.75	10.81	2	0	263.8	204	158.1	146.3	244.5	271.4	176.6	161.1
Q9VTC1	LD32732p OS=Drosophila melanogaster OX=7227 GN=DmrH27 PE=1 SV=1	12	8	25	8	791	87.2	6.99	36.89	8	0	397.5	468.5	442.2	405.3	289.1	554.5	585.4	458
Q9W3M7	LD32873p OS=Drosophila melanogaster OX=7227 GN=mahe PE=1 SV=1	6	4	8	4	945	100.4	9.14	10.43	4	0	15.9	16.9	17.1	18.6	19	16.4	18.4	16.2
Q9VP85	LD32951p OS=Drosophila melanogaster OX=7227 GN=Sin PE=2 SV=1	4	2	2	2	486	54.9	6.6	2.15	2	0	41.9	48.7	41.1	36.5	28.4	45.4	51.4	43.8
Q9VFB3	LD33178p OS=Drosophila melanogaster OX=7227 GN=CG12258 PE=1 SV=2	9	4	11	4	439	50	8.82	14.76	4	0	273.4	285.3	223.6	169.6	336.6	344.7	275.5	275.5
Q7K4L8	LD33749p OS=Drosophila melanogaster OX=7227 GN=DmelCG7878 PE=1 SV=1	5	2	3	2	703	78.5	6.7	0	2	0	0	0	0	0	0	0	0	0
Q9VM62	LD34181p OS=Drosophila melanogaster OX=7227 GN=SA PE=1 SV=2	5	6	10	5	1127	130	5.4	13.16	6	0	130.3	149.9	154.5	146.1	110.6	197.3	184.4	145.8
Q9VX15	LD35209p OS=Drosophila melanogaster OX=7227 GN=DmelCG8142 PE=1 SV=2	27	9	40	9	353	39.5	7.87	70.73	9	0	1013.8	1093	1088.7	666.6	364.6	1242.8	925	667.4
Q9VWQ3	LD35981p OS=Drosophila melanogaster OX=7227 GN=DmelCG6961 PE=2 SV=2	13	5	11	5	474	53	9.74	19.14	5	0	260	260.2	247.8	218.4	154.5	281.5	285.4	226.5
Q9VBX4	LD36051p OS=Drosophila melanogaster OX=7227 GN=CG10057 PE=1 SV=2	2	3	7	3	1150	129.2	9.57	3.95	3	0	27.6	37.8	31.5	42.7	26.1	45.3	42.5	44.1
Q9VBJ1	LD36095p OS=Drosophila melanogaster OX=7227 GN=SF1 PE=1 SV=3	2	2	2	2	787	87.3	9.61	4.85	2	0	148.8	117.9	92.9	70.8	56.2	158.1	143.1	109.6
Q9VX35	LD36501p OS=Drosophila melanogaster OX=7227 GN=CC4 PE=1 SV=1	13	5	13	5	336	37.4	9.73	2.14	5	0	169.9	118	103	80.7	101.1	267.1	145	87.8
Q9VK18	LD36945p OS=Drosophila melanogaster OX=7227 GN=DmelCG16812 PE=2 SV=1	7	3	5	3	455	49.8	9.99	3.91	3	0	56.4	69.8	60.5	65.3	50	77.8	76.1	69.5
Q9W379	LD37736p OS=Drosophila melanogaster OX=7227 GN=Zpr1 PE=1 SV=1	7	3	4	3	467	51.3	4.74	2.88	3	0	33.1	51.9	39.6	40.7	34.9	38.2	53.3	29.8
Q9VXL4	LD38104p OS=Drosophila melanogaster OX=7227 GN=Rp47 PE=1 SV=1	11	2	3	2	159	18.1	6.2	3.63	2	0	77.1	84.2	83.1	65.1	43	81	93	73.3
Q9VWD9	LD38919p OS=Drosophila melanogaster OX=7227 GN=Ubp6 PE=1 SV=1	5	2	7	2	547	58.8	5.11	17.8	2	0	40.9	43.4	43	53.1	44.8	40.5	60.4	44.9
Q96Q08	LD39850p OS=Drosophila melanogaster OX=7227 GN=DmelCG3511 PE=1 SV=1	8	4	8	4	637	71.7	7.14	8.31	4	0	115.9	130.3	141.1	125.2	91.3	173.2	196.7	133.8
Q9VJ26	LD40224p OS=Drosophila melanogaster OX=7227 GN=DmelCG4 PE=1 SV=1	20	2	8	2	216	23.6	6.86	21.35	2	0	0	0	0	0	0	0	0	0
Q7JYJ8	LD40262p OS=Drosophila melanogaster OX=7227 GN=Hsp190 PE=2 SV=1	3	4	12	4	1309	145.9	6.19	12.32	4	0	320.7	303.5	240.2	254.1	181.8	409.8	381.7	282.5
Q9V3W7	LD40489p OS=Drosophila melanogaster OX=7227 GN=SF2 PE=1 SV=1	12	3	11	3	255	28.3	9.91	18.94	3	0	536.5	534.8	447.4	463.1	307.4	491.7	585.2	493.6
Q7K4H1	LD40680p OS=Drosophila melanogaster OX=7227 GN=C8R185 PE=2 SV=1	4																	

Q9VQR8	Leucyl-tRNA synthetase, isoform A OS=Drosophila melanogaster OX=7227 GN=LeuRS PE=1 SV=1	2	2	6	2	1182	134.8	7.64	1.75	2	0	7.6	13.9	13.4	15.5	20.7	10	20.5	7.6	8.7
Q9VJ39	Leukotriene A(4) hydrolase OS=Drosophila melanogaster OX=7227 GN=DmelCG10602 F	7	4	10	4	684	76.8	6.55	7.11	4	0	61.2	35.8	28.9	13.7	7.6	42.4	43.8	12.6	
O62602	Licorice OS=Drosophila melanogaster OX=7227 GN=lic PE=1 SV=1	24	8	30	8	334	38.2	6.39	27.17	8	0	505.6	557.6	490.9	405.2	322.2	560.7	628	402.9	
Q7KNS3	Lissencephaly-1 homolog OS=Drosophila melanogaster OX=7227 GN=Lis-1 PE=1 SV=2	8	2	2	2	411	46.4	7.56	2.46	2	0	8	6.4	3.8	1.7		6.3	5.3		
MNEV0	Little imaginal discs, isoform C OS=Drosophila melanogaster OX=7227 GN=ld PE=4 SV=1	4	5	12	5	1838	203.9	6.62	14.51	5	0	140.7	182.3	158.1	144.5	112.6	218.1	243.9	161	
P42283	Longitudinalis lacking protein, isoform G OS=Drosophila melanogaster OX=7227 GN=loia F	10	8	22	8	891	96.2	6.46	35.01	8	0	367.5	769.8	422.4	403.1	270.4	451.9	461.7	339.3	
Q9VMX3	LP03982p OS=Drosophila melanogaster OX=7227 GN=DmelCG3756 PE=1 SV=1	9	2	2	2	333	38.1	6.74	0	2	0	10.9	12.5	12.7	12.5	9.5	13	13.1	10	
Q9VQI5	LP04564p OS=Drosophila melanogaster OX=7227 GN=CG3098 PE=1 SV=2	5	2	2	2	425	47.3	6.28	1.8	2	0	21.3	24.4	24.8	27.5	20.2	23.9	30.9	22.1	
Q9VEV3	LP07287p OS=Drosophila melanogaster OX=7227 GN=DmelCG14894 PE=1 SV=2	8	2	2	2	263	29.4	4.64	0	2	0									
Q9VKW5	LP07359p OS=Drosophila melanogaster OX=7227 GN=DmelCG5355 PE=1 SV=2	13	9	22	9	756	86.3	6.19	20.98	9	0	596.8	669.3	680.2	633	502.5	701.9	793.9	653.3	
Q9VHN7	LP07963p OS=Drosophila melanogaster OX=7227 GN=DmelCG8036 PE=1 SV=3	6	3	24	3	626	68.7	7.11	52.23	3	0	325.7	257.8	265.4	158.7	155.2	447.9	330.5	187	
Q9VGP4	LP08082p OS=Drosophila melanogaster OX=7227 GN=Ranbp9 PE=1 SV=1	10	7	28	7	1018	114.3	4.87	34.82	7	0	352.4	416.6	444	283.6	238.3	485.4	496.1	280	
Q9VKZ8	LP08774p OS=Drosophila melanogaster OX=7227 GN=Usp14 PE=1 SV=1	10	3	10	3	475	53.7	6.25	11.3	3	0	61.6	44.3	43.5	41	29.3	64.9	58.6	38	
Q9W0M4	LP10861p OS=Drosophila melanogaster OX=7227 GN=DmelCG13887 PE=1 SV=1	9	2	5	2	228	26.1	9.32	6.72	2	0	72	93.3	101.8	94.4	112.2	93.9	116.2	91.9	
Q9W2U7	LP18708p OS=Drosophila melanogaster OX=7227 GN=noct PE=1 SV=4	1	2	4	2	2309	235.4	9.22	1.64	2	0	48.7	76	69.9	63.8	57.4	64.3	86	68.8	
Q9VQL1	LP20978p OS=Drosophila melanogaster OX=7227 GN=SerRS PE=1 SV=1	4	2	3	2	501	56.4	6.49	3.45	2	0	70	66.1	79.7	46.2	56	54.7	79	60.5	
Q9W3Z7	Lysine-tRNA ligase OS=Drosophila melanogaster OX=7227 GN=LysRS PE=1 SV=2	8	5	8	5	607	68.5	7.08	5.39	5	0	106.2	177.2	197.1	175.1	227.7	185.4	253	170.1	
AOA0B4K8A5	Mahjong, isoform B OS=Drosophila melanogaster OX=7227 GN=mahj PE=4 SV=1	7	11	23	11	1544	172	5	29.4	11	0	424	490.2	499.1	480.5	333.5	566.9	512.8		
Q9VQX2	Maiette dehydrogenase OS=Drosophila melanogaster OX=7227 GN=Mdh1 PE=1 SV=2	11	4	29	4	337	36	7.39	49.21	4	0	863.2	987.2	900.5	847.8	569.1	843.7	1090.5	966.7	
E1JJK5	Mapmodulin, isoform D OS=Drosophila melanogaster OX=7227 GN=Mapmodulin PE=1 SV	9	2	33	2	363	40.7	4.26	21.37	2	0	237.2	246.4	218.1	195.5	152.3	329.9	329.7	256.8	
E1JH57	Mars, isoform B OS=Drosophila melanogaster OX=7227 GN=mars PE=1 SV=1	11	4	19	8	921	101.9	9.98	41.47	8	0	154.1	185.9	141.5	178.4	93.1	239.8	228.3	215.4	
Q9VGA4	MBD-R2 OS=Drosophila melanogaster OX=7227 GN=Mbd-R2 PE=1 SV=2	4	4	7	4	1169	130.1	8.03	10.4	4	0	39.2	45.7	48.7	48.7	33.5	68.4	57.1	48.9	
Q9VW47	Mediator of RNA polymerase II transcription subunit 12 OS=Drosophila melanogaster OX=	1	2	3	2	2531	279.3	7.58	3.97	2	0	58.9	46.6	61.8	43.2	46.1	71.8	63.3	53.7	
ABJNW4	Mediator of RNA polymerase II transcription subunit 13 OS=Drosophila melanogaster OX=	1	3	6	3	2768	295.5	6.83	7.6	3	0	66.9	71.1	82.4	70	65.1	83.9	94.3	75.6	
Q9VEC1	Mediator of RNA polymerase II transcription subunit 17 OS=Drosophila melanogaster OX=	7	4	7	4	642	71.5	7.37	7.28	4	0	54.7	72.5	65.1	57.1	54.7	77.7	116.9	46.4	
Q9W1X7	Mediator of RNA polymerase II transcription subunit 23 OS=Drosophila melanogaster OX=	2	2	7	2	1439	167	7.69	7.03	2	0	24.2	33.6	29.8	20.7	38.8	33.5	41.5	25.8	
Q9W0P3	Mediator of RNA polymerase II transcription subunit 30 OS=Drosophila melanogaster OX=	7	2	5	2	318	35.3	8.76	3.51	2	0	37.3	45.4	42.5	48.9	28.9	49.5	65.7	50.9	
AOA0B4KF9	Megator, isoform B OS=Drosophila melanogaster OX=7227 GN=Mtor PE=1 SV=1	9	19	42	19	2346	262.2	5.1	44.18	19	0	593.8	673.9	665	685.8	527.6	813.8	863.7	728	
Q9EBJ0	MERP-1, isoform A OS=Drosophila melanogaster OX=7227 GN=MERP-1 PE=1 SV=1	3	4	15	4	1152	124	5.03	16.2	4	0	208.2	257.9	239.4	205.4	116.2	270.3	303.3	207.6	
AOA0B4KG70	Metastasis associated 1-like, isoform D OS=Drosophila melanogaster OX=7227 GN=MTA1	12	8	24	8	922	100.9	9.29	33.17	8	0	264.8	314.2	330.5	259.3	183	346.7	426.6	304.7	
Q9VL89	Methionine aminopeptidase 2 OS=Drosophila melanogaster OX=7227 GN=und PE=1 SV=	11	5	21	5	448	49.8	6.68	32.45	5	0	473.9	505	507.7	464	478.4	711.8	683.3	544.5	
Q9VC48	Methionine aminopeptidase OS=Drosophila melanogaster OX=7227 GN=MAP1A PE=1 SV=	6	2	5	2	374	41.7	6.93	9	2	0	76.5	80.9	70.2	54.9	89.8	86	77.9		
Q9V9X4	Methylthioribose-1-phosphate isomerase OS=Drosophila melanogaster OX=7227 GN=CG	6	2	8	2	364	39.1	7.01	9.05	2	0	80.1	88	87.6	69	54.7	82.6	107.2	73.8	
Q9SE34	Mt-2, isoform B OS=Drosophila melanogaster OX=7227 GN=Mt-2 PE=1 SV=1	9	16	84	16	1983	224.2	5.64	161.67	16	0	1628.8	1930.2	1637.5	1449.7	985	2076.7	2195.8	1543.6	
E1JH39	Microcephalin, isoform D OS=Drosophila melanogaster OX=7227 GN=MCPH1 PE=1 SV=1	2	2	2	2	1028	115	9.7	3.63	2	0	11.9	13.3	11.3	7.6	5.9	15.7	16	12.1	
AOA0B4K700	Mini spindles, isoform D OS=Drosophila melanogaster OX=7227 GN=mssp PE=1 SV=1	1	3	6	3	2082	230.3	8.21	3.68	3	0	59.2	65	76.8	57.8	67.2	80	97.7	77.8	
Q9VM60	Mini-chromosome maintenance complex-binding protein OS=Drosophila melanogaster OX=	6	2	3	2	605	68	5.78	2.96	2	0	8.5	12.1	14.8	8.8	9.9	14.3	11.7	4.9	
Q9E8E8	MIP08013p1 OS=Drosophila melanogaster OX=7227 GN=Mcp2 PE=1 SV=1	6	2	5	2	356	38.8	8.88	8.18	2	0	53.7	62.7	62.9	71.7	199.2	77.2	85.7	48.1	
AVV0N4	MIP16230p OS=Drosophila melanogaster OX=7227 GN=Vha68-2 PE=1 SV=1	12	6	22	6	614	68.3	5.34	36.12	6	0	256.6	325.6	381.9	313.6	421.5	313.8	417.4	321	
H5V8B8	MIP33436p1 OS=Drosophila melanogaster OX=7227 GN=Pp2A-29B PE=1 SV=1	14	9	34	9	650	71.8	4.91	68.87	9	0	580.8	768.7	757.2	585.6	569.2	751.6	872.3	663.8	
X2JG23	Misato, isoform B OS=Drosophila melanogaster OX=7227 GN=mst PE=4 SV=1	4	2	2	2	574	64.7	5.03	6.75	2	0	33.1	44.4	48.9	52.4	48.4	43.9	43.1	39.1	
Q6BRB8	Mitochondrial transcription factor A, isoform B OS=Drosophila melanogaster OX=7227 GN=	8	2	4	2	284	33	9.96	4.24	2	0	26.5	28.8	20.2	27.8	33.9	26.9	33.3	30.3	
PA0417	Mitogen-activated protein kinase ERK-A OS=Drosophila melanogaster OX=7227 GN=rf PE=	10	3	5	3	376	43.1	6.07	13.14	3	0	71	75.9	79.6	76.6	66.2	87.3	95.5	82.9	
A1Z7C1	Mln1, isoform A OS=Drosophila melanogaster OX=7227 GN=Mln1 PE=4 SV=1	3	2	3	2	664	75.7	7.88	1.89	2	0	28.1	25.5	28.5	18.1	16.1	32.1	31	22.6	
Q9VAW1	Moca-cyp, isoform A OS=Drosophila melanogaster OX=7227 GN=Moca-cyp PE=1 SV=1	2	2	5	2	970	112.7	10.56	7.79	2	0	116.6	158.1	102.3	132.1	187	136.4	184.9	129.9	
Q86B87	Modifier of mdg4 OS=Drosophila melanogaster OX=7227 GN=mod(mdg4) PE=1 SV=1	4	2	8	2	610	67.1	5.07	9.14	2	0	267	265.9	267.4	145	133.2	309.1	324.8	241.8	
CTLAH9	Moesin, isoform K OS=Drosophila melanogaster OX=7227 GN=Moe PE=1 SV=1	14	7	46	7	646	75.8	6.16	74.73	7	0	328.9	357.8	327.6	268.3	273.6	395.4	510.1	306.7	
AOA0B4K56	Molting defective, isoform D OS=Drosophila melanogaster OX=7227 GN=mld PE=4 SV=1	1	2	3	2	1965	218.6	6.24	4.74	2	0	6.8	5.2	2.8	5.1	3	6.3	6.7	4.3	
P39205	Molybdenum cofactor synthesis protein cinnamon OS=Drosophila melanogaster OX=7227 GN=	3	2	2	2	601	65.7	6.24	4.17	2	0	37.6	57.2	62.5	56.8	60.2	62	76.3	60	
AOA0B4KHJ7	MORF-related gene 15, isoform B OS=Drosophila melanogaster OX=7227 GN=MRG15 PE	7	2	5	2	429	47.7	8.13	0	2	0	20.9	26.8	27.1	30.1	21.1	28.5	33.4	28.6	
Q9VY44	mRNA-capping enzyme OS=Drosophila melanogaster OX=7227 GN=mRNA-cap PE=2 SV=	10	8	23	8	649	74.7	6.95	28.83	8	0	459	636.4	484.8	494.5	457.8	769.4	752	558.8	
Q9I7S8	Multifunctional protein ADE2 OS=Drosophila melanogaster OX=7227 GN=ade5 PE=2 SV=	10	4	10	4	429	47.3	8.07	16.11	4	0	154.6	203.3	213.2	193.2	197.5	183	229.7	205.6	
M9PFR8	Multiprotein bridging factor 1, isoform E OS=Drosophila melanogaster OX=7227 GN=mbf1	11	2	7	2	188	20.4	10.23	13.94	2	0	215	210.2	152	160	136.9	205.7	221	211.2	
Q9VY97	Mutagen-sensitive 101 OS=Drosophila melanogaster OX=7227 GN=msu101 PE=1 SV=1	9	10	24	10	1425	158.3	6.51	23.46	10	0	151.3	156.8	151.3	136.2	91.5	210.9	242.6	176.8	
Q9W5E4	Myb-binding protein 1A OS=Drosophila melanogaster OX=7227 GN=Mybbp1A PE=1 SV=1	1	2	6	2	1133	127.8	7.55	9.74	2	0	191.5	200.2	157.3	149.3	122.7	282.6	246.2	238.1	
M9ND95	Myosin heavy chain, isoform U OS=Drosophila melanogaster OX=7227 GN=Mhc PE=1 SV	13	24	52	1	1949	222.8	6.25	87.99	24	0	9.5	14.1	17	7.6	37.9	17.5	9.7	6.9	
AOA0S0WH4	Myosin heavy chain, isoform V OS=Drosophila melanogaster OX=7227 GN=Mhc PE=1 SV	13	24	51	1	1962	224.4	6.32	83.84	24	22	836.2	1184.1	1319.7	816.5	2987.1	1167.2	857.1	565.6	
Q99323	Myosin heavy chain, non-muscle OS=Drosophila melanogaster OX=7227 GN=zfp PE=1 SV	12	19	50	19	2057	236.5	5.68	92.95	19	0	507.9	634.3	635.1	521.5	863.4	717.1	787.7	741.5	
Q9VW2	N(A)alpha-acetyltransferase 15/16, isoform A OS=Drosophila melanogaster OX=7227 GN=N	5	4	11	4	890	103	7.27	10.85	4	0	77.9	105.1	130.6	91.1	143.9	107.6	139.9	97.6	
Q9VCE6	N6-adenosine-methyltransferase MTA70-like protein OS=Drosophila melanogaster OX=72	3	2	2	2	608	68.1	5.55	1.76	2	0	41.1	42	45.9	43.2	35.3	52.4	54.3	40.4	
Q9VLP7	N6-adenosine-methyltransferase non-catalytic subunit OS=Drosophila melanogaster OX=7	7	2	3	2	397	44.8	8.68	2.45	2	0	24.4	30.2	30.1	32.6	30.3	28.2	39	30.7	
Q9VK34	NAD-dependent histone deacetylase siruin-1 OS=Drosophila melanogaster OX=7227 GN=	3	2	2																

Q9U1H9	Nuclear RNA export factor 1 OS=Drosophila melanogaster OX=7227 GN=sbr PE=1 SV=2	3	2	2	2	672	76.2	9	2.02	2	0	14.2	16.1	20.4	11.3	16	22.9	26.5	13.4	
Q9VV73	Nuclear RNA export factor 2 OS=Drosophila melanogaster OX=7227 GN=nt2 PE=2 SV=1	3	2	5	2	841	96.6	7.4	4.8	2	0	7.1	12	10.4	8.9	7.8	13.9	15.5	11.9	
Q9VIF0	Nucleolar complex protein 2 homolog OS=Drosophila melanogaster OX=7227 GN=CG924	3	2	4	2	766	86.6	7.3	7.4	2	0	55	60.8	46.1	42	49.6	95.4	76.2	49.5	
Q9VIB2	Nucleolar complex protein 3 homolog OS=Drosophila melanogaster OX=7227 GN=CG123	6	3	5	3	822	94.4	8.97	2.67	3	0	11	13.6	10	14	5.4	18.1	13.9	18	
AOA0B4LEY9	Nucleolar GTP-binding protein 1 OS=Drosophila melanogaster OX=7227 GN=Non1 PE=1	8	4	8	4	652	75.3	9.54	7.22	4	0	93.8	106	84.1	58.8	43.1	112.8	112.7	77.1	
Q7XJL4	Nucleolar GTP-binding protein 2 OS=Drosophila melanogaster OX=7227 GN=Ns2 PE=1 S	4	2	7	2	674	76.6	9.58	10.37	2	0	3.7	6.8	7.6	3.4	6.1	11.3	11.2	8.5	
Q8IH00	Nucleolar protein 6 OS=Drosophila melanogaster OX=7227 GN=Mat89Ba PE=1 SV=1	2	2	3	2	1193	136.3	9	1.65	2	0	12.2	19.7	12.9	10.8	13.1	19.3	16.1	6.7	
Q9VE85	Nucleoporin 43kD OS=Drosophila melanogaster OX=7227 GN=Nup43 PE=1 SV=1	8	2	3	2	358	40.1	5.22	0	2	0	18.9	20.3	15.3	21.1	22.8	27.5	32.2	25	
Q7K2X8	Nucleoporin at 44A, isoform A OS=Drosophila melanogaster OX=7227 GN=Nup44A PE=1	7	3	4	3	354	39.5	6.71	1.72	3	0	37.3	47.8	46.2	52.1	52.3	54.6	65.9	56.7	
Q9VDC9	O-GlcNAcase OS=Drosophila melanogaster OX=7227 GN=Oga PE=1 SV=1	4	3	6	3	1019	113.8	4.88	11.52	3	0	58.7	77.5	78.4	65.9	60.6	94.4	115	82.8	
EBPBV6	Obg-like ATPase 1 OS=Drosophila melanogaster OX=7227 GN=CG1354-RA PE=1 SV=1	7	2	9	2	397	44.9	7.71	12.94	2	0	171.8	205.9	205.7	188.6	165.6	210.2	227	176.9	
O16810	Origin recognition complex subunit 1 OS=Drosophila melanogaster OX=7227 GN=Orc1 PE	9	7	25	7	924	103.2	9.35	34.25	7	0	313.5	355.7	312.1	273	197.3	421.2	414.7	356.6	
Q24168	Origin recognition complex subunit 2 OS=Drosophila melanogaster OX=7227 GN=Orc2 PE	4	2	3	2	618	69	6.32	7.53	2	0	53.4	58.8	64.2	52.6	36.1	73.3	76.4	51.7	
Q9W102	Origin recognition complex subunit 4 OS=Drosophila melanogaster OX=7227 GN=Orc4 PE	8	3	7	3	459	51.9	8.22	7.44	3	0	80.7	80.9	84	81.7	47.8	118.9	110.7	80.4	
Q24169	Origin recognition complex subunit 5 OS=Drosophila melanogaster OX=7227 GN=Orc5 PE	10	4	10	4	460	52.1	6.55	14.73	4	0	146.7	165.8	154.4	116.2	93	224.7	199.9	147.9	
E1JIN6	Osa, isoform D OS=Drosophila melanogaster OX=7227 GN=osa PE=1 SV=1	2	2	5	8	5	2716	283.9	7.44	8.25	5	0	97.2	133.4	125.5	128.6	83.5	137.5	169.8	119.9
P20240	Olefin OS=Drosophila melanogaster OX=7227 GN=Ote PE=1 SV=2	14	3	6	3	424	46.6	9.55	8.34	3	0	926	1112.5	1005.6	865.6	711.9	1358	1454.4	1067.2	
X2J7U0	P-element induced wimpy testis, isoform 9 OS=Drosophila melanogaster OX=7227 GN=hp	16	13	57	13	843	97.1	9.57	69.05	13	0	547.3	569.8	516.2	447	321.1	685	772.6	561.7	
A1ZAK9	P-element somatic inhibitor, isoform C OS=Drosophila melanogaster OX=7227 GN=Psi PE=	10	8	29	8	797	81.7	8.13	37.7	8	0	1086.3	1264.8	1295.9	1295.9	1050.5	1188.8	1481.7	1175.9	
Q25007	Peptidyl-prolyl cis-trans isomerase OS=Drosophila melanogaster OX=7227 GN=Cyp1 PE=	13	3	83	3	227	24.7	9.22	84.15	3	0	4.8	8.7	10.5	9.4	5.8	9.7	17	6.3	
Q9W0Q2	Peptidyl-prolyl cis-trans isomerase OS=Drosophila melanogaster OX=7227 GN=Cyp1 PE=1	19	2	3	2	176	19.5	7.12	4.26	2	0	233.9	274.5	229.9	245.1	223.9	217.7	299.4	230.3	
Q9W227	Peptidyl-prolyl cis-trans isomerase OS=Drosophila melanogaster OX=7227 GN=DmelCG2	2	2	7	2	205	22.2	8.75	10.11	2	0	70.1	96.7	95.1	85.5	106.7	111.4	158.1	80.3	
Q7K3D4	Peptidyl-prolyl isomerase OS=Drosophila melanogaster OX=7227 GN=zda PE=1 SV=1	6	3	5	3	397	44.8	5.33	6.05	3	0	4.5	10.9	15.5	9.7	26.6	13.5	9.7	10.6	
Q9VEJ0	Peroxiredoxin 3 OS=Drosophila melanogaster OX=7227 GN=Pnx3 PE=1 SV=2	8	2	3	2	234	26.4	7.49	9.7	3	0	29.9	19.5	16.6	15	14.5	24.6	14.6	14.3	
Q9VQI7	Peroxiredoxin 8005 OS=Drosophila melanogaster OX=7227 GN=Pnx8005 PE=1 SV=1	12	2	2	2	222	24.8	5.36	5.82	2	0	61.3	87.9	107	81.8	91.7	90.3	95.4	82.9	
Q9VCA5	Phenylalanine-tRNA ligase beta subunit OS=Drosophila melanogaster OX=7227 GN=bat	7	3	6	3	589	65.7	6.04	5.9	3	0	30.9	46.5	41.4	37.4	20.9	51.4	50.7	39.1	
AOA0B4KHW1	Phosphatidylserine receptor, isoform B OS=Drosophila melanogaster OX=7227 GN=PSR1	6	2	5	2	441	51	9.58	6.05	2	0	99.4	121.8	105.4	94.6	82.8	123.5	153	102.8	
Q9V7Z4	Phosphoacetylglucosaminase OS=Drosophila melanogaster OX=7227 GN=st PE=1	6	3	6	3	549	60.5	6.29	6.04	3	0	353.4	430.5	425.4	398.7	338.2	391.1	489.3	380.3	
Q9VLU9	Phosphoglucomutase OS=Drosophila melanogaster OX=7227 GN=Pgm PE=1 SV=1	7	4	11	4	560	60.7	6.7	19.1	4	0	222.1	240.6	252.5	211.7	140.4	261	296.8	211	
Q9VY2	Phospholipase A2 activator protein, isoform A OS=Drosophila melanogaster OX=7227 GN	6	5	11	6	787	85.7	8.83	19.69	6	0	103.4	141.5	144.7	151	127.4	123.5	175.6	150.4	
A1Z7P1	Phosphomannomutase 45A OS=Drosophila melanogaster OX=7227 GN=Pgm2a PE=1 SV	3	2	2	2	623	69.9	5.45	8.26	2	0	32.2	31.8	20.9	23.7	20.6	34.4	40.7	23.5	
Q9VK58	Phl1D1, isoform D OS=Drosophila melanogaster OX=7227 GN=Phl1D1 PE=1 SV=5	2	2	5	2	1094	127.5	9.74	0	2	0	118.7	128.2	150.1	100	54.4	112.1	131	64.8	
A1Z8A6	Pipsqueak, isoform M OS=Drosophila melanogaster OX=7227 GN=psq PE=1 SV=2	3	2	3	3	1123	119.8	6.87	16.67	3	0	109.9	116.1	108.4	73.3	160.7	147.4	129.3	116	
P35875	Poly[ADP-ribose] polymerase OS=Drosophila melanogaster OX=7227 GN=Parp PE=1 SV	2	2	7	2	994	113.7	8.56	16.01	2	0	19.7	24.4	25.8	22.3	12.5	24.1	28.5	23.3	
O46043	Poly[ADP-ribose] glycohydrolase OS=Drosophila melanogaster OX=7227 GN=Parp PE=1	4	2	3	2	723	81.1	5.81	0	2	0	60.1	44	49.7	38	47.6	60.5	77.2	62.4	
Q8T6B9	Poly(U)-binding splicing factor half pnt OS=Drosophila melanogaster OX=7227 GN=hfp PE=1	7	2	3	3	637	67.9	5.96	0	3	0	88.5	90.5	79.2	66.1	63.1	280.5	671.3	74.3	
Q7KNF2	Polyadenylate-binding protein 2 OS=Drosophila melanogaster OX=7227 GN=Pabp2 PE=1	10	2	12	2	224	25.5	5.2	24.61	2	0	20.3	19.6	17	12.2	14.4	27	24.3	11	
P21187	Polyadenylate-binding protein OS=Drosophila melanogaster OX=7227 GN=Pabp PE=1 SV	4	2	3	2	634	69.9	9.31	1.9	2	0	497.9	645.3	640.8	577.1	369.9	703.2	781.4	551.4	
Q9VC36	Polybromo OS=Drosophila melanogaster OX=7227 GN=polybromo PE=1 SV=1	9	12	28	12	1654	189.6	6.71	40.08	12	0	10.4	10.8	13.6	9.7	5.6	15.2	18.3	11.6	
Q9NUG9	Polycomb protein Su(z)12 OS=Drosophila melanogaster OX=7227 GN=Su(z)12 PE=1 SV=	7	3	8	3	900	100	8.91	2.43	3	0	623.4	754	731.8	615.8	474	922	956.9	665.2	
Q9VK71	POU domain protein 2, isoform B OS=Drosophila melanogaster OX=7227 GN=ppm2 PE=2	4	2	2	2	893	98.4	6.9	0	2	0	235.3	263.3	257.3	247.7	170.2	280.5	336.3	248.1	
A1Z8U0	Pre-mRNA processing factor 8 OS=Drosophila melanogaster OX=7227 GN=Pp8 PE=1 SV	5	11	30	5	2396	279.8	8.88	54.46	11	0	18.4	21.3	20.5	22.3	27	36.8	18.6	18.6	
Q7KRW8	Pre-mRNA-processing factor 39 OS=Drosophila melanogaster OX=7227 GN=CG1646 PE=1	8	7	13	7	1066	120.5	5.24	20.69	7	0	44.8	58.8	50.6	47.1	37.5	56	51.9	44.2	
Q7JVL3	Pre-mRNA-splicing factor 38 OS=Drosophila melanogaster OX=7227 GN=Pp38 PE=1 SV=	8	2	4	2	330	40.1	8.98	3.51	2	0	114.3	127.2	113.8	109.2	93.6	150.5	171.1	131	
Q9VJ87	Pre-mRNA-splicing factor CWC22 homolog OS=Drosophila melanogaster OX=7227 GN=nc	4	4	8	4	1330	151.5	9.38	9.41	4	0	44.8	58.8	50.6	47.1	37.5	56	51.9	44.2	
Q9VAQ7	Pre-mRNA-splicing factor Slu7 OS=Drosophila melanogaster OX=7227 GN=Slu7 PE=1 SV	8	4	15	4	574	65.9	7.06	19.79	4	0	44.8	58.8	50.6	47.1	37.5	56	51.9	44.2	
Q9V5Q4	Pre-mRNA-splicing factor Syf2 OS=Drosophila melanogaster OX=7227 GN=Syf2 PE=2 SV	16	3	5	3	226	26.5	9.57	4.85	3	0	45.9	58.8	50.6	47.1	37.5	56	51.9	44.2	
Q9VP47	Pre-mRNA-splicing protein TSR1 homolog OS=Drosophila melanogaster OX=7227 GN=	4	3	5	3	814	93.7	6.87	5.9	3	0	156.8	192.6	186	182.4	132.1	262.2	244.8	198.2	
A1Z8S6	Precoccious dissociation of sisters 5, isoform A OS=Drosophila melanogaster OX=7227 GN=	6	6	20	6	1218	138.8	7.64	29.71	6	0	114.9	133	118.4	129.4	102	192.9	177.8	143.3	
Q9VW52	Precurator RNA processing 3, isoform A OS=Drosophila melanogaster OX=7227 GN=Pp3	7	4	6	4	598	67.3	9.73	10.16	4	0	97.4	118.1	129.5	116	109	97.2	146.5	110.2	
Q9VGP6	Prefoldin subunit 3 OS=Drosophila melanogaster OX=7227 GN=pmr PE=1 SV=3	9	2	4	2	194	22.3	5.11	4.92	2	0	67.1	64.1	54.9	19.8	31.4	101.8	70.5	28.5	
Q9VZ64	Probable 6-phosphogluconolactonase OS=Drosophila melanogaster OX=7227 GN=CG17	12	2	4	2	243	26.7	8.21	3.84	2	0	27.8	49.6	47	37.5	59.2	43.1	60.2	44.8	
Q9VXN4	Probable arginine-tRNA ligase, cytoplasmic OS=Drosophila melanogaster OX=7227 GN=	3	2	3	2	665	75.5	7.44	4.38	2	0	53.5	55.7	44.8	59	35.3	86.5	66.7	50.5	
Q86B47	Probable ATP-dependent RNA helicase CG8611 OS=Drosophila melanogaster OX=7227	2	2	7	2	975	107.9	9.5	5.36	2	0	71.1	60.4	52.5	50.9	50.5	86.9	72.6	68.5	
P26802	Probable ATP-dependent RNA helicase Dbp73D OS=Drosophila melanogaster OX=7227	7	4	8	3	687	77.5	8.19	9.48	4	0	133.8	133	118.4	129.4	102	192.9	177.8	143.3	
Q9VD51	Probable ATP-dependent RNA helicase pitchose OS=Drosophila melanogaster OX=722	6	3	6	3	680	76.9	7.97	8.27	3	0	13.6	17.3	25.9	20.7	38.2	26.1	14.6	15.9	
Q9W401	Probable citrate synthase, mitochondrial OS=Drosophila melanogaster OX=7227 GN=cdn	8	3	4	3	464	51.5	8.81	3.72	3	0	159.7	234.3	192.5	158.4	114.3	222.1	261.7	178.3	
Q9V3D6	Probable cleavage and polyadenylation specificity factor subunit 2 OS=Drosophila melano	9	7	15	7	756	85.4	5.47	17.99	7	0	422.5	501.9	534.7	354.4	206.9	466.5	469.1	316	
Q9VLM0	Probable DNA mismatch repair protein Msh6 OS=Drosophila melanogaster OX=7227 GN=	6	8	19	6	1190	133.1	7.28	29.21	8	0	376.8	206.2	179.5	103.6	88.2	403.9	290.3	139.4	
Q7K7V0	Probable H2A ribonucleoprotein complex subunit 1 OS=Drosophila melanogaster OX=7	8	2	12	2	237	22.7	11.19	14.95	2	0	206.3	110.2	92.8	29.2	31.5	212.5	110.7	35.1	
Q24572	Probable histone-binding protein Caf1 OS=Drosophila melanogaster OX=7227 GN=Caf1 f	7	3	17	1	430	48.6	4.89	19.09	3	0	136.5	198.1	135.6	159.8	117.2	180.8	197.7	152.3	
Q8MT36	Probable histone-lysine N-methyltransferase Mes-4 OS=Drosophila melanogaster OX=722	5	7	9	7	1427	158.9	7.65	1.67	7	0	92	116.3	90.1	104	66.7	132	119.5	101.7	
Q9V333	Probable lysine-specific demethylase 4A OS=Drosophila melanogaster OX=7227 GN=Kdn	3	2	6	2	495	57	7.24	0	2	0	76.3	94.3	118.1	92.8	168.8	104			

P22769	Proteasome subunit alpha type-7-1 OS=Drosophila melanogaster OX=7227 GN=Prosalph	12	3	18	3	249	28	8.12	31.87	3	0	550.2	708.5	698.4	485.3	374.2	618.5	847.2	580.4	
AOAQH0	Proteasome subunit beta OS=Drosophila melanogaster OX=7227 GN=Prosbeta1 PE=1 SV=1	35	5	70	5	224	24.2	5.25	135.23	5	0	679.2	1030.1	919.6	777.6	605.5	817.1	1157.1	851	
Q9VUJ1	Proteasome subunit beta OS=Drosophila melanogaster OX=7227 GN=Prosbeta2 PE=1 SV=1	21	5	33	5	272	29.8	8.66	52.58	5	0	636.4	838.9	849.6	663.1	491.5	679.6	1011.4	770.9	
Q9VJJ0	Proteasome subunit beta OS=Drosophila melanogaster OX=7227 GN=Prosbeta4 PE=1 SV=1	9	2	23	2	201	22.5	6.39	29.51	2	0	425.5	464.5	383.7	314.3	211.5	339.7	515.4	399.2	
Q7K148	Proteasome subunit beta OS=Drosophila melanogaster OX=7227 GN=Prosbeta5 PE=1 SV=1	14	4	29	4	282	31.1	6.93	50.63	4	0	906.2	1196.7	1270.6	946.8	803.5	1168.9	1506.4	1084.5	
Q9VNA5	Proteasome subunit beta type-4 OS=Drosophila melanogaster OX=7227 GN=Prosbeta7 F	18	4	24	4	268	30	6.58	58.35	4	0	214.8	236	212	217.2	194.5	207.4	260.7	198.2	
Q9V677	Proteasome-associated protein ECM29 homolog OS=Drosophila melanogaster OX=7227 G	2	3	4	3	1890	212	6.86	3.39	3	0	30.8	31.1	34.4	29.5	27.9	38.9	46.2	31.7	
Q9VEX5	Protein asunder OS=Drosophila melanogaster OX=7227 GN=Asun PE=1 SV=1	6	2	4	2	689	75.7	8.46	9.59	2	0	82.3	88.7	83	84.9	53.6	113.1	122	103.4	
O76922	Protein aubergine OS=Drosophila melanogaster OX=7227 GN=aub PE=1 SV=1	4	3	3	3	866	98.5	9.28	3.86	3	0	26.8	41.1	39.8	40.4	39	32.9	50.5	33.6	
Q9VFR0	Protein BCPIP homolog OS=Drosophila melanogaster OX=7227 GN=CG9286 PE=2 SV=2	7	2	4	2	297	33.4	4.65	9.67	2	0	135.5	153.9	137	131.9	93.5	160.4	174.2	142.5	
Q9NK54	Protein chiflon OS=Drosophila melanogaster OX=7227 GN=chf PE=1 SV=2	1	2	3	2	1711	189.1	8.53	1.87	2	0	17.1	20.3	15.1	19.2	14.2	19.6	20.8	20.8	
Q7K284	Protein CLP1 homolog OS=Drosophila melanogaster OX=7227 GN=cbc PE=2 SV=1	1	2	6	2	423	46.8	6.89	8.61	2	0	97.1	124.6	117.3	96.1	92.9	130	152.3	109.5	
A1ZAB5	Protein clueless OS=Drosophila melanogaster OX=7227 GN=clu PE=1 SV=1	4	2	3	2	1448	160.8	6.6	1.95	2	0	8.4	11.3	12.4	6.4	13.8	13.1	17.5	14.9	
P17886	Protein crooked neck OS=Drosophila melanogaster OX=7227 GN=cm PE=2 SV=2	16	8	26	8	702	84.2	5.94	31.02	8	0	261.8	322.2	300.6	276.4	194.5	349.6	374.9	276	
Q9VH89	Protein dalmatian OS=Drosophila melanogaster OX=7227 GN=dmt PE=1 SV=1	4	3	5	3	857	96.5	9.39	6.64	3	0	92.5	98.5	94.9	74.7	67.5	130.1	148.8	102.9	
Q24573	Protein dead ringer OS=Drosophila melanogaster OX=7227 GN=retn PE=1 SV=2	5	3	16	3	911	97.3	6.23	23.92	3	0	70.3	127.1	111.4	141.1	89.9	110.8	127.1	89	
Q3YMU0	Protein disulfide-isomerase (Fragment) OS=Drosophila melanogaster OX=7227 GN=ERp6	11	4	16	4	489	55.3	5.87	9.39	4	0	242.3	296.2	297.1	145.9	206.5	283.8	478.9	230.4	
Q9V438	Protein disulfide-isomerase A6 homolog OS=Drosophila melanogaster OX=7227 GN=CAB1	6	3	9	3	433	46.7	5.69	4.21	3	0	130.7	137.4	144.1	132.1	177.7	161	231.9	135.6	
PS4399	Protein disulfide-isomerase OS=Drosophila melanogaster OX=7227 GN=Pli PE=2 SV=1	8	4	8	4	496	55.7	4.82	19.13	4	0	201.7	241.9	215.9	192.4	268.5	221.7	359.1	213	
Q9W032	Protein ecdysoneless OS=Drosophila melanogaster OX=7227 GN=ecd PE=1 SV=1	2	2	2	2	684	77.9	4.87	2.12	2	0	23.3	26.6	31.3	27.8	23.5	27.9	36.1	26	
Q9VWE6	Protein ELYS homolog OS=Drosophila melanogaster OX=7227 GN=CG14215 PE=1 SV=1	1	2	3	2	2111	235	5.33	0	2	0	0	0	0	0	0	0	0	0	
Q9VAY7	Protein FAM50 homolog OS=Drosophila melanogaster OX=7227 GN=CG12259 PE=2 SV=1	6	2	3	2	359	42.8	6.83	4.34	2	0	16.9	14.9	15.4	13.8	11.9	19.9	17	17	
P16371	Protein grouch OS=Drosophila melanogaster OX=7227 GN=gro PE=1 SV=3	6	5	28	5	730	80.2	7.17	23.47	5	0	411.7	559.3	524.7	546.4	312.8	560.5	671.2	454.5	
O1367	Protein held out wings OS=Drosophila melanogaster OX=7227 GN=how PE=1 SV=1	4	2	6	2	405	44.3	7.93	9.62	2	0	167.6	153.2	131.8	74.2	64.9	187.2	151.2	89.4	
Q9VBG6	Protein HGH1 homolog OS=Drosophila melanogaster OX=7227 GN=CG6073 PE=2 SV=2	8	2	3	2	369	41.8	4.97	0	2	0	17.3	28.5	24.1	20.3	28.3	19.3	22.5	23.1	
O17468	Protein HIRA homolog OS=Drosophila melanogaster OX=7227 GN=Hira PE=1 SV=2	5	4	8	4	1047	113.3	6.65	8.85	4	0	66.5	79.2	83.2	61.6	47	102.1	90.4	73.3	
Q8SYK5	Protein insensitive OS=Drosophila melanogaster OX=7227 GN=insv PE=1 SV=2	11	3	6	3	376	42.2	8.57	8.69	3	0	61.1	59.4	67.6	60.2	42.4	96.9	89.7	68	
Q9VNE2	Protein krasvazietz OS=Drosophila melanogaster OX=7227 GN=kra PE=1 SV=1	9	4	13	4	422	49.2	5.74	25.09	4	0	454.1	543.7	540.1	403	359.2	587.8	623.6	449.5	
Q24371	Protein lethal(2)denticleless OS=Drosophila melanogaster OX=7227 GN=(2)dl PE=1 SV=1	7	5	7	5	769	84.1	8.76	2.27	5	0	47	45.6	53.2	44	33.4	58.9	56.7	41.7	
P91891	Protein Mo25 OS=Drosophila melanogaster OX=7227 GN=Mo25 PE=2 SV=2	12	4	12	4	339	39.4	7.25	9.75	4	0	424	228.7	229.7	186.8	256.2	256.1	219.9	288.6	
Q9I7K6	Protein NASP homolog OS=Drosophila melanogaster OX=7227 GN=CG8223 PE=1 SV=1	15	4	28	4	492	51.9	4.39	43.71	4	0	523.5	598.9	540.3	495.3	292.6	535.4	642.1	495.7	
Q9W2H9	Protein panorax OS=Drosophila melanogaster OX=7227 GN=Panx PE=1 SV=1	3	2	3	2	541	61.1	6.46	2.31	2	0	53	64.3	66.2	63.7	34.9	64.9	295.1	54.6	
AOA0B4K6G3	Protein partner of snf, isoform B OS=Drosophila melanogaster OX=7227 GN=pns PE=1 SV=1	3	6	12	6	2018	222.1	8.79	4.03	6	0	109	112	109.2	104.3	78.6	128.5	131.8	109.4	
P36872	Protein phosphatase PP2A 55 kDa regulatory subunit OS=Drosophila melanogaster OX=7227 GN=PP2A PE=1 SV=1	17	7	20	7	499	56.9	7.09	26.1	7	0	388.4	481.8	445.2	337	505.4	552.4	435	435	
Q9V3J4	Protein SEC13 homolog OS=Drosophila melanogaster OX=7227 GN=Sec13 PE=1 SV=1	5	2	5	2	356	39.5	6.25	3.63	2	0	68.2	83.5	84.5	80.9	97.1	86	102.4	89.2	
Q8INM3	Protein slender lobes OS=Drosophila melanogaster OX=7227 GN=sle PE=1 SV=1	8	9	30	9	1420	158.6	5.24	44.2	9	0	627.2	660.9	527	619.5	320.7	746	796	642.7	
Q8SX83	Protein split ends OS=Drosophila melanogaster OX=7227 GN=spen PE=1 SV=2	0	2	5	2	5560	599.6	8.63	3.25	2	0	25.5	53	24.9	40.3	21.7	33.9	45.2	32	
A8JUV0	Protein strawberry notch OS=Drosophila melanogaster OX=7227 GN=sno PE=1 SV=2	6	7	8	7	1653	180.3	8.41	PE=1 SV=2	7	0	62.1	66.3	65.8	46.9	55.7	106.6	94.8	57.6	
P25991	Protein suppressor of forked OS=Drosophila melanogaster OX=7227 GN=su(f) PE=1 SV=1	8	6	11	6	765	88.2	8.25	10.86	6	0	279.8	245.9	244.9	191.8	165.9	339	306.3	219.7	
Q9VTE2	Protein suppressor of underreplication OS=Drosophila melanogaster OX=7227 GN=SuUR	6	4	13	4	962	107.6	9.77	19.47	4	0	63.6	75.8	63.7	65.7	68.6	81.7	98.1	87	
P20193	Protein suppressor of variegation 3-7 OS=Drosophila melanogaster OX=7227 GN=Su(var)	7	8	27	8	1250	139.9	6.43	57.59	8	0	578	630.5	590.3	654	394.7	712.8	790.9	630.8	
Q8INX3	Protein TIPIN homolog OS=Drosophila melanogaster OX=7227 GN=CG10336 PE=2 SV=2	11	3	4	3	307	34.1	5.11	4.89	3	0	77.3	103.9	51.5	81.4	39	49.8	52.1	28.2	
P42282	Protein tramtrack, alpha isoform OS=Drosophila melanogaster OX=7227 GN=ttk PE=1 SV=1	2	2	4	2	813	88.3	6.25	0	2	0	36.1	47.6	29.4	29.9	51.2	40.5	38.6	31.4	
AOA0B4K5Z8	Protein transport protein SEC23 OS=Drosophila melanogaster OX=7227 GN=Sec23 PE=1 SV=1	4	2	4	2	781	87.5	6.79	7.3	2	0	51.5	56.7	73.2	65.4	67.1	53.8	71.5	42.1	
Q9W517	Protein wings apart-like OS=Drosophila melanogaster OX=7227 GN=wapl PE=1 SV=1	5	5	7	5	1741	185	6.54	9.93	5	0	37.9	38.6	40.3	40.6	35.6	57.1	52.6	36.6	
AOA0B4K106	Puffeye, isoform H OS=Drosophila melanogaster OX=7227 GN=puf PE=1 SV=1	1	3	4	3	3930	442.1	6.2	0	3	0	9.6	9.3	9.5	5.1	7	16.3	15.1	11.4	
P23128	Putative ATP-dependent RNA helicase me31b OS=Drosophila melanogaster OX=7227 GN=me31b	4	2	6	2	459	51.9	7.64	5.41	2	0	95.2	74.9	63	37.8	50.2	101.6	86.4	49.5	
Q9VHM7	Putative elongator complex protein 4 OS=Drosophila melanogaster OX=7227 GN=CG690	8	2	6	2	437	48.7	5.88	12.07	2	0	0	0	0	0	0	0	0	0	
P36951	Putative hydroxyprolylase isomerase OS=Drosophila melanogaster OX=7227 GN=Gp PE=1 SV=1	7	2	6	2	264	29.1	6.54	10.18	2	0	227.3	262.6	253.1	244.1	225.6	229.5	319.8	240.1	
PS4353	Putative peptidyl-prolyl cis-trans isomerase dodo OS=Drosophila melanogaster OX=7227 GN=dodo	14	2	6	2	166	18.4	7.44	20.64	2	0	183.2	201	175.8	140.5	104.8	194.2	224.3	168.4	
Q9VXK5	Putative rRNA methyltransferase OS=Drosophila melanogaster OX=7227 GN=DmelCG89	8	5	12	5	817	93.3	9.04	15.3	5	0	173	199.2	113.9	168.1	113.9	257.4	207.1	211.7	
Q9VPK7	Putative rRNA pseudouridine synthase Pus10 OS=Drosophila melanogaster OX=7227 GN=Pus10	3	2	2	2	500	56.7	8.35	1.84	2	0	30.4	33.4	40.7	27.6	25.3	49.5	48.3	34.7	
Q9VUV9	Putative US small nuclear ribonucleoprotein 200 kDa helicase OS=Drosophila melanogaster OX=7227 GN=US200 PE=1 SV=1	9	15	60	9	15	2142	244.4	6.04	90.07	15	0	603	812.1	766.9	777.4	521.6	906.1	1019.8	777.3
Q9E9E2	Pyruvate carboxylase OS=Drosophila melanogaster OX=7227 GN=PCB PE=1 SV=1	10	9	45	9	1197	132.6	6.84	66.75	9	0	319.9	418.5	540.7	517.2	654.2	551.1	825	292.5	
Q7K5K3	Pyruvate dehydrogenase E1 component subunit beta OS=Drosophila melanogaster OX=7227 GN=PDH E1 beta	9	3	6	3	365	39.3	7.8	10.89	3	0	39.6	51.1	58.8	66.3	87.2	58.1	67.4	52	
O62619	Pyruvate kinase OS=Drosophila melanogaster OX=7227 GN=Pyk PE=2 SV=2	14	5	47	5	533	57.4	7.44	82.69	5	0	589.8	812	874.1	746.5	620	756	1047.9	792.9	
Q9W212	Quercosine salvage protein OS=Drosophila melanogaster OX=7227 GN=DmelCG9752 PE=1 SV=1	8	3	6	3	343	39.5	5.73	5.55	3	0	125.3	146.4	159.8	137.1	109	158.2	161.9	142.2	
Q9V1B7	Rab GDP dissociation inhibitor OS=Drosophila melanogaster OX=7227 GN=RabGDI PE=1 SV=1	11	4	23	4	443	49.9	5.72	49.6	4	0	384.7	435.1	454.2	314.9	269.1	439.6	517.8	353.7	
AOA0B4K7L0	Rad50, isoform E OS=Drosophila melanogaster OX=7227 GN=rad50 PE=1 SV=1	8	10	20	10	1318	152	7.65	18.33	10	0	193.3	184.3	192.1	147.2	139.4	281.2	312.1	176	
ADA126GUM4	Ran-binding protein M, isoform G OS=Drosophila melanogaster OX=7227 GN=RanBPM P	3	3	5	3	1127	123.7	5.19	6.78	3	0	36.4	41.5	44	46	42.6	43.6	69.4	47.8	
M9MSD3	Ranbp16, isoform F OS=Drosophila melanogaster OX=7227 GN=Ranbp16 PE=4 SV=1	2	2	2	2	1110	128.9	6.35	1.68	2	0	27.8	26.5	31.1	35.7	31.4	45.9	43.8	39.2	
M8MRT6	Rap1 GTPase, isoform B OS=Drosophila melanogaster OX=7227 GN=Rap1 PE=4 SV=1	12	2	5	2	184	20.9	6.68	7.94	2	0	68.7	109	112.1	98.7	133.1	119.6	164	110.2	
P48148	Ras-like GTP-binding protein Rho1 OS=Drosophila melanogaster OX=7227 GN=R																			

P54622	Single-stranded DNA-binding protein, mitochondrial	OS=Drosophila melanogaster OX=722	22	3	13	3	146	16.4	9.85	29.86	3	0	223.6	353.2	330	402.1	187.9	307.1	292.5	226
M9PC89	Small ribonucleoprotein particle U1 subunit 70K, isoform C	OS=Drosophila melanogaster OX=722	5	3	6	3	448	52.9	10.04	9.49	3	0	264.6	287.7	219.7	221.7	151.5	290.7	319.5	261.2
Q9V562	Smallminded, isoform A	OS=Drosophila melanogaster OX=722 GN=smid PE=1 SV=1	14	9	36	9	944	104.3	5.44	54.89	9	0	249.2	306.9	326.7	254.8	156.5	340.1	366.4	249.4
M9PGZ8	Smrter, isoform G	OS=Drosophila melanogaster OX=722 GN=Smr PE=1 SV=1	1	3	4	3	3607	379.6	9.44	3.46	3	0	44.8	61.8	56.8	59.4	40.6	60.1	80.8	65.5
Q9XZ21	Something that sticks like glue, isoform A	OS=Drosophila melanogaster OX=722 GN=smg	3	3	5	3	1231	139.9	9.73	3.78	3	0	62.8	65.7	49.9	64	44.1	86.7	86.5	73.4
M9ND86	Spellchecker1, isoform D	OS=Drosophila melanogaster OX=722 GN=spell1 PE=1 SV=1	11	10	46	10	917	103.2	5.92	73.13	10	0	1026.5	1248.6	1329.6	1086.6	642.4	1094.2	1227.7	934.4
Q9VHA1	Spermidine synthase, isoform A	OS=Drosophila melanogaster OX=722 GN=SpdS PE=1 SV=1	13	3	15	3	287	32.3	5.78	17.85	3	0	228.5	261.2	280.2	262	179.3	288.5	305.9	254.3
O46106	Splicing factor 3A subunit 3	OS=Drosophila melanogaster OX=722 GN=noi PE=1 SV=1	12	5	11	5	503	58.4	5.62	16.23	5	0	187.9	255.3	221.2	211.3	173.9	229.1	282	168.2
Q9VPR5	Splicing factor 3b subunit 1, isoform A	OS=Drosophila melanogaster OX=722 GN=Sp3b1	3	5	11	5	1340	149.5	6.67	20.57	5	0	287.7	340.3	314.2	302.7	221.4	404.2	442.3	359
Q9W0M7	Splicing factor 3b subunit 3	OS=Drosophila melanogaster OX=722 GN=Sp3b3 PE=1 SV=1	15	12	42	12	1227	136.5	5.47	39.46	12	0	724.7	945.6	892.3	821.3	666.7	1118.6	1200.6	956.5
Q9W0S7	Staphylococcal nuclease domain-containing protein 1	OS=Drosophila melanogaster OX=722	11	12	54	12	926	103.8	8.05	109.57	12	0	993.9	1318.8	1501.5	1236.3	1059.7	1367.1	1759.6	1204.7
Q9VCB8	Structural maintenance of chromosomes protein 6	OS=Drosophila melanogaster OX=722	4	5	6	5	1122	129.3	8.32	2.31	5	0	82	93.5	93.9	109.1	84.6	137.1	124.9	119
Q9V3A7	Structural maintenance of chromosomes protein OS=Drosophila melanogaster OX=722	14	13	27	13	1409	159.8	6.15	30.06	13	0	261.6	274.9	287.5	249.5	240.5	406	363.7	304	
Q9VCD8	Structural maintenance of chromosomes protein OS=Drosophila melanogaster OX=722	9	11	16	11	1238	142.8	6.73	18.47	11	0	296.8	370.4	338.8	346	288.4	463.2	435.5	492.7	
Q7KK96	Structural maintenance of chromosomes protein OS=Drosophila melanogaster OX=722	5	6	18	6	1179	134.3	8.18	18.84	6	0	298.2	308	326	276.2	241.2	452	427	310.4	
Q9VXE9	Structural maintenance of chromosomes protein OS=Drosophila melanogaster OX=722	13	13	18	13	1200	139.9	8.1	11.68	13	0	217.5	200.5	209.9	160.4	123.7	252	238.9	150.2	
A12958	Su(Va)2-HP2, isoform A	OS=Drosophila melanogaster OX=722 GN=Suv(Var)2-HP2 PE=1	14	23	27	14	3257	355.8	6.14	45.32	14	0	732.6	784.8	718.2	681.8	427	803.3	873.7	723
AOA0B4K6W1	Suppressor of hairy wing, isoform C	OS=Drosophila melanogaster OX=722 GN=Su(Hw) PE=1	2	2	3	2	941	105.7	6.71	2.29	2	0	43.7	42	42.3	35.4	33.6	61.8	52.4	40.9
Q9VDS6	Surfeit locus protein 6 homolog	OS=Drosophila melanogaster OX=722 GN=Surf6 PE=1	6	2	5	2	324	38.1	9.85	4.11	2	0	111.5	103.2	61.3	79.3	55.6	256.2	190.6	175.2
Q9V172	SWI5NF-related matrix-associated actin-dependent regulator of chromatin subfamily A co	OS=Drosophila melanogaster OX=722 GN=SWI5NF PE=1 SV=1	5	4	9	4	844	95.4	8.16	16.37	4	0	167.6	160.3	159.2	105.3	74.6	275.3	194.9	128.1
Q8MSU4	Symplekin	OS=Drosophila melanogaster OX=722 GN=Sym PE=1 SV=1	4	5	11	4	1165	132	6.49	14.4	5	0	165.9	251.4	278.8	267.3	189.3	282.2	357.5	217
Q9VK69	T-complex protein 1 subunit delta	OS=Drosophila melanogaster OX=722 GN=CCT4 PE=1	11	5	19	5	533	57.1	7.56	27.28	5	0	286.6	387.1	454.3	312.7	519.6	519.2	532.4	357
Q7KK10	T-complex protein 1 subunit epsilon	OS=Drosophila melanogaster OX=722 GN=CCT5 PE=1	4	2	8	2	542	59.2	6.25	19.46	2	0	171.5	205.6	234.7	91	134	252.8	253.5	106.1
Q9VHL2	T-complex protein 1 subunit eta	OS=Drosophila melanogaster OX=722 GN=CCT7 PE=1	9	5	17	5	544	59.3	6.34	30.81	5	0	356.3	486.4	580.6	435	602.6	437	635.8	438
AAV303	T-complex protein 1 subunit gamma	OS=Drosophila melanogaster OX=722 GN=CCT3 PE=1	15	9	33	9	544	59.4	6.8	62.35	9	0	602.2	803.1	934.9	748.4	1019.5	786.3	1077.8	729.9
Q9VH72	TAO1656p1	OS=Drosophila melanogaster OX=722 GN=DmelCG9471 PE=1 SV=1	21	4	20	4	204	22.7	7.49	45.32	4	0	208.2	241.3	206.2	186.7	159	247.5	280.5	224
Q07DP5	TATA box binding protein-related factor 2, isoform E	OS=Drosophila melanogaster OX=722	3	5	9	5	1715	194.6	5.02	14.01	5	0	197.8	215.7	200.4	177	115.9	238.7	262.4	180.3
AOA0B4K26	TATA box-binding protein-associated factor RNA polymerase 1 subunit B, isoform C	OS=Drosophila melanogaster OX=722	2	2	2	2	872	101.7	7.3	1.98	2	0	24.8	29.1	26.8	26.4	19.5	37	24.9	30.4
AOA0B4K602	TBP-associated factor 4, isoform E	OS=Drosophila melanogaster OX=722 GN=TaF4 PE=1	2	5	7	5	2172	244	5.31	11.52	5	0	111.3	143.2	143.6	135.7	114.1	178.8	194.8	153.8
BZ060	TBP-associated factor 4, isoform E	OS=Drosophila melanogaster OX=722 GN=TaF4 PE=1	3	3	5	3	1088	117.1	10.14	1.61	3	0	45.1	65.9	58.4	73.3	53.9	73.4	81.2	76.5
Q9XZ34	Telomere-associated protein RIF1	OS=Drosophila melanogaster OX=722 GN=Rif1 PE=1	13	17	46	17	1416	156.7	6.65	58.48	17	0	904.4	1018.3	1025.7	763.9	518.1	1211.6	1158.1	818.3
Q8IPU3	Tenzing nogay, isoform C	OS=Drosophila melanogaster OX=722 GN=tzn PE=1 SV=1	7	2	4	2	348	38.8	7.58	8.28	2	0	53.9	72.9	61	37.8	51.8	80.9	93.8	46.2
AOA0B4L724	TER94, isoform E	OS=Drosophila melanogaster OX=722 GN=TER94 PE=1 SV=1	17	13	26	13	825	91.9	5.38	120.97	13	0	1646	1884.5	1997.4	1462.4	1039.7	1879.2	2203.6	1517.9
Q9VGU5	Tetrapeptide repeat protein 14 homolog	OS=Drosophila melanogaster OX=722 GN=	2	2	6	2	872	99.8	10.39	0	2	0	32.2	26.7	24.8	26.3	22	32.1	29.5	22.2
Q9V3W1	Tetrapeptide repeat protein 2	OS=Drosophila melanogaster OX=722 GN=Trp2 PE=1	9	4	4	4	508	58	6.49	6.46	4	0	120.4	112	119.6	98	70.2	135	145.8	103
Q9W147	TFIIIF-interacting CTD phosphatase, isoform A	OS=Drosophila melanogaster OX=722 GN=	3	2	3	2	880	97.3	4.87	4.65	2	0	81.1	86.3	89.6	84.8	55.4	88.9	94.6	81.6
X2JF59	Thioredoxin peroxidase 1, isoform C	OS=Drosophila melanogaster OX=722 GN=Jafracl1	16	3	33	3	194	21.7	5.71	78.23	3	0	692.1	817.1	850.4	697.3	740.4	837.2	1013.2	742.3
P91938	Thioredoxin reductase 1, mitochondrial	OS=Drosophila melanogaster OX=722 GN=Trx1	10	5	34	5	596	64.3	7.91	72.93	5	0	726.1	908.6	916.7	820.3	696.9	803.6	1055.2	795.1
Q9W1F4	THO complex subunit 5	OS=Drosophila melanogaster OX=722 GN=thoc5 PE=1 SV=2	2	2	2	2	616	70.8	8.44	2.02	2	0	30.3	42.1	37.9	44.9	29	40.4	49.5	32.2
EQZCS8	Tho2, isoform B	OS=Drosophila melanogaster OX=722 GN=tho2 PE=1 SV=1	6	9	21	9	1642	188.5	8.82	35.08	9	0	321.7	375.9	301.7	188.2	188.2	452.5	463.5	301.4
Q8INH7	Timeout	OS=Drosophila melanogaster OX=722 GN=timeout PE=1 SV=2	11	13	44	13	1384	159.3	5.16	80.81	13	0	850.7	1137.1	1289.9	881.8	407.2	728.1	745.4	566
O72777	Torsin-like protein OS=Drosophila melanogaster OX=722 GN=Torsin PE=2 SV=2	9	3	4	3	340	38.1	8.62	3.49	3	0	18.9	13.6	14	18.1	13.8	22.9	26.9	13.7	
BZ126	Tousled-like kinase, isoform G	OS=Drosophila melanogaster OX=722 GN=TK PE=1 SV=3	3	5	10	3	1489	162.1	9.17	17.61	5	0	212.6	314.4	356.5	240.7	135.2	270.5	278.2	190.1
M9PF20	Trailer hitch, isoform H	OS=Drosophila melanogaster OX=722 GN=trh PE=1 SV=1	5	3	4	3	657	69.8	9.48	1.95	3	0	85.3	79.1	65.2	62.4	66.2	77.9	104.6	61.5
Q9V460	Transcription elongation factor SPT5	OS=Drosophila melanogaster OX=722 GN=Sp5 PE=1	7	7	14	7	1078	119.4	6.25	24.78	7	0	289.4	315.1	318.3	291.6	208.4	384.2	369.2	311.9
N9DB13	Transcription elongation factor spT6	OS=Drosophila melanogaster OX=722 GN=Sp6 PE=1	8	12	33	12	1831	208.5	5.31	49.95	12	0	394.4	432.6	372.9	285.8	564.2	592.2	424.1	
Q24318	Transcription factor Dp	OS=Drosophila melanogaster OX=722 GN=Dp PE=1 SV=2	7	2	2	2	445	49.7	6.76	2.36	2	0	24.5	23.6	24.6	26.1	23.3	31.2	36.7	27.7
O77051	Transcription factor E2F2	OS=Drosophila melanogaster OX=722 GN=E2f2 PE=1 SV=1	5	2	2	2	370	41.4	5.21	3.96	2	0	50.5	66.8	64	51.4	39.7	60.5	76.9	60.6
P29052	Transcription initiation factor IIB	OS=Drosophila melanogaster OX=722 GN=TFIIB PE=2 SV=2	15	4	4	4	315	34.3	8.29	19.61	4	0	242.1	258.8	211.2	208.2	160.6	275.7	301.4	199.5
Q24325	Transcription initiation factor TFIID subunit 2	OS=Drosophila melanogaster OX=722 GN=	7	7	13	7	1221	139.4	7.23	11.44	7	0	111.1	141.2	127.3	151.2	105.1	183.7	193.7	160.6
P49846	Transcription initiation factor TFIID subunit 5	OS=Drosophila melanogaster OX=722 GN=	4	3	6	3	704	79.3	6.38	6.04	3	0	81.4	79.6	90.6	70	53.4	112.8	117.4	85.8
P49847	Transcription initiation factor TFIID subunit 6	OS=Drosophila melanogaster OX=722 GN=	3	2	2	2	606	65.6	8.94	1.61	2	0	31.8	37.1	43.2	33.8	20.6	43.8	56.8	33.8
Q9VHY5	Transcription initiation factor TFIID subunit 7	OS=Drosophila melanogaster OX=722 GN=	8	4	6	4	479	55	5.1	3.16	4	0	121.4	134	112.4	93	78.7	184.2	146.9	98.9
Q27272	Transcription initiation factor TFIID subunit 9	OS=Drosophila melanogaster OX=722 GN=	11	3	7	3	278	29.3	9.32	6.27	3	0	171.4	151.7	137.2	92	78.2	194.9	162.5	91.6
Q8IBU7	Transcription-associated protein 1	OS=Drosophila melanogaster OX=722 GN=Nipped-A	1	4	5	4	3790	435.1	7.75	5.63	4	0	108	134.7	147.1	139.2	141.5	156.6	170.4	137.1
Q9G0N5	Transcriptional regulator ATRX homolog	OS=Drosophila melanogaster OX=722 GN=XNP	2	3	9	2	3131	148.1	8.44	6.2	3	0	135.1	143.7	141	104.3	79.5	211.4	168.5	133
Q9VWV6	Transferin	OS=Drosophila melanogaster OX=722 GN=Tsf1 PE=1 SV=1	2	2	2	2	641	71.8	7.06	3.72	2	0	73.5	61.7	52.5	49.5	42.4	62.7	72.4	48.9
AOA0B4J97	Transforming acidic coiled-coil protein, isoform K	OS=Drosophila melanogaster OX=722 GN=	2	2	2	2	1322	147.1	4.98	0	2	0	5.6	8.1	6	7.9	8.3	11.7	11.9	11.3
Q9VZ11	Transgenin	OS=Drosophila melanogaster OX=722 GN=Dncf64 PE=1 SV=2	16	3	5	3	188	20.6	8.43	0	3	0	47.5	62.4	44.9	36.4	36.4	59.3	77	50.2
Q9VGS2	Translationally-controlled tumor protein homolog	OS=Drosophila melanogaster OX=722 GN=	26	2	31	2	172	19.6	4.81	28.66	2	0	530.2	582.5	568.6	474.8	455.5	536.5	696.5	557.2
P00967	Trifunctional purine biosynthetic protein adenosine-3	OS=Drosophila melanogaster OX=72	4	5	8	5	1353	144.4	7.37	4.11	5	0	88.3							

Q9XZ61	Ubiquitin carboxyl-terminal hydrolase OS=Drosophila melanogaster OX=7227 GN=Uch-L5	16	4	25	4	324	37.6	5.21	35.71	4	0	465.1	537.9	520.2	455.3	355.9	579.1	664.7	527.8
Q9ZU70	Ubiquitin carboxyl-terminal hydrolase OS=Drosophila melanogaster OX=7227 GN=Usp5 PE	9	6	29	6	827	92.7	5.49	44.34	6	0	568.8	617.7	673.6	608.5	503.9	739.3	802.5	643.2
M9PB20	Ubiquitin conjugating enzyme E2M, isoform B OS=Drosophila melanogaster OX=7227 GN	12	2	11	2	181	20.7	7.15	23.92	2	0	240.2	251.1	227.5	217.2	177.5	280.9	323.4	252.5
Q7K4I5	UBX domain-containing protein 7 OS=Drosophila melanogaster OX=7227 GN=DmelCG88	13	5	18	5	496	55.1	5.01	30.73	5	0	287.9	330.8	317.9	289.4	191.9	360.3	398.2	310
Q90332	UDP-glucose:glycoprotein glucosyltransferase OS=Drosophila melanogaster OX=7227 GN	4	4	5	4	1548	174.2	6.15	2.37	4	0	16.9	29	32.2	22	37.1	26.3	44.1	36
Q9VB12	UMP-CMP kinase OS=Drosophila melanogaster OX=7227 GN=Dak1 PE=1 SV=1	15	3	13	3	253	27.8	8	20.44	3	0	298.8	267.1	249.4	172.9	154	322.8	300	193.9
Q9VCP1	Uncharacterized protein CG4449 OS=Drosophila melanogaster OX=7227 GN=CG4449 PE	13	5	10	5	424	47.7	6.57	12.44	5	0	100.4	112.1	101	90.7	99.4	133.7	144.5	113.5
A1A708	Uncharacterized protein CG4951 OS=Drosophila melanogaster OX=7227 GN=CG4951 PE	11	4	10	4	446	50.7	9.45	18.32	4	0	221.6	240.1	165.5	187.5	159.4	344.5	320.7	270.7
Q7YZA2	Uncharacterized protein CG7065 OS=Drosophila melanogaster OX=7227 GN=CG7065 PE	5	6	11	6	1231	136.7	9.23	6.74	6	0	100	112.1	86	103.6	80.9	122.2	140	116.1
Q9W0H6	Uncharacterized protein OS=Drosophila melanogaster OX=7227 GN=ACAT PE=1 SV=2	7	2	6	2	392	41.1	7.05	10.69	2	0	41.1	39.9	37.3	31.4	25.4	48.4	46.6	28.1
Q9VJG2	Uncharacterized protein OS=Drosophila melanogaster OX=7227 GN=cg12288 PE=1 SV=	5	2	3	2	435	47.9	10.04	2.34	2	0	36.1	46.5	27.4	37.7	28.2	57.6	41.2	38
BZ70I8	Uncharacterized protein OS=Drosophila melanogaster OX=7227 GN=CG14896 PE=1 SV=	6	16	25	16	3441	378.4	4.93	25.72	16	0	506.5	483.1	458.3	352.3	309.5	598.2	583.5	378.6
Q9VVV7	Uncharacterized protein OS=Drosophila melanogaster OX=7227 GN=cg3808 PE=1 SV=3	3	2	7	2	615	68.6	6.23	10.61	2	0	125.2	169.3	177.1	159.7	132.1	166.5	196.7	159.5
Q9VD07	Uncharacterized protein OS=Drosophila melanogaster OX=7227 GN=DmelCG12499 PE=	2	3	3	3	2059	237	6.76	6.43	3	0	51.8	41.8	31.2	29.5	34.3	91.2	56.2	47
Q9V9Z8	Uncharacterized protein OS=Drosophila melanogaster OX=7227 GN=DmelCG15561 PE=	15	4	4	4	357	39.9	9.17	2.48	4	0	60.6	39.9	34.5	24.2	20.2	68.7	53.7	32.9
A1ZAW6	Uncharacterized protein OS=Drosophila melanogaster OX=7227 GN=DmelCG30105 PE=	15	2	6	2	155	17.4	5.1	6.81	2	0	86.8	108.4	100.5	111.3	63.3	85.6	115.5	94.6
Q9VEP0	Uncharacterized protein OS=Drosophila melanogaster OX=7227 GN=DmelCG3995 PE=1	6	2	2	2	322	37.4	6.55	1.88	2	0	71.5	59.1	51.5	55.9	46.1	61.1	75.3	54.6
Q9V9K9	Uncharacterized protein OS=Drosophila melanogaster OX=7227 GN=DmelCG5913 PE=1	7	3	4	3	454	49.9	9.7	1.84	3	0	48.6	47.4	37.1	24.9	34.8	75.1	78.1	33.5
Q9WZN6	Uncharacterized protein OS=Drosophila melanogaster OX=7227 GN=DmelCG9346 PE=1	6	6	8	6	957	108.4	8.53	2.01	6	0	106	126.2	124	113.1	63.3	157.7	165.3	129.3
Q9W246	Uncharacterized protein OS=Drosophila melanogaster OX=7227 GN=CGM1751p PE=1 SV	1	3	5	3	233	311.7	7.74	1.84	3	0	14.9	17.1	17.8	14.8	13.6	24.6	21.2	15.3
A1Z6Z7	Uncharacterized protein, isoform A OS=Drosophila melanogaster OX=7227 GN=146745_	5	3	6	3	586	63.9	5.55	5.21	3	0	156.7	159.8	153.6	147.9	92.1	198.5	194.5	167.3
Q9VEA6	Uncharacterized protein, isoform A OS=Drosophila melanogaster OX=7227 GN=Aar2_	4	2	2	2	379	42.4	4.44	3.73	2	0	43.8	44.3	39.5	45	30.1	47.2	60.4	40.4
Q9V7Y2	Uncharacterized protein, isoform A OS=Drosophila melanogaster OX=7227 GN=anon-W0	13	3	10	3	317	35.8	6.11	12.03	3	0	162.5	149.6	117.9	86.3	66.4	157.3	171.7	99.6
Q8B8M0	Uncharacterized protein, isoform A OS=Drosophila melanogaster OX=7227 GN=CG3085	7	2	3	2	209	22.9	5.44	1.75	2	0	24.6	27.4	29.2	27.5	24.8	29.9	31.4	26.4
Q9VRP2	Uncharacterized protein, isoform A OS=Drosophila melanogaster OX=7227 GN=DmelCG1	15	4	8	4	391	42.7	7.11	4.36	4	0	100.2	94.3	100.1	56.7	65	129.2	119.1	80
Q9VYA4	Uncharacterized protein, isoform A OS=Drosophila melanogaster OX=7227 GN=DmelCG1	18	5	17	5	340	37.6	9.95	17.84	5	0	239.4	288.5	285.7	244.2	139.2	359	321.1	257.7
A1ZBW6	Uncharacterized protein, isoform A OS=Drosophila melanogaster OX=7227 GN=DmelCG1	17	9	28	9	726	82.6	7.24	35.81	9	0	666.9	573.2	374.4	386.2	349.2	859.8	638.9	744.5
A1Z830	Uncharacterized protein, isoform A OS=Drosophila melanogaster OX=7227 GN=DmelCG1	5	3	4	3	485	53.8	7.27	4.19	3	0	93.7	80.6	72.4	73.9	59.9	125.3	103.6	114.7
Q9W3W6	Uncharacterized protein, isoform A OS=Drosophila melanogaster OX=7227 GN=DmelCG1	2	8	18	8	3313	371.1	7.77	27.44	8	0	321.3	347.7	301.7	371.7	257.1	381.9	403.1	346.4
Q9VRD4	Uncharacterized protein, isoform A OS=Drosophila melanogaster OX=7227 GN=DmelCG1	11	2	6	2	288	31.6	5.39	8.11	2	0	70.7	80.7	76.1	93.7	63.3	76.1	95	81.3
Q7PL61	Uncharacterized protein, isoform A OS=Drosophila melanogaster OX=7227 GN=DmelCG1	1	4	4	4	2630	293.7	7.03	3.54	4	0	17.2	26.6	27.8	18.4	32.4	25.3	33.7	26.3
Q9VCD4	Uncharacterized protein, isoform A OS=Drosophila melanogaster OX=7227 GN=DmelCG1	20	3	5	3	144	16.9	8.83	6.91	3	0	134.8	114.1	108.8	85.9	76.4	244.2	390.5	294.2
Q9VZ60	Uncharacterized protein, isoform A OS=Drosophila melanogaster OX=7227 GN=DmelCG2	2	2	2	2	1128	122.6	9.6	2.17	2	0	34.5	42.8	42.2	45.4	26.8	35	41	39.6
Q9VB64	Uncharacterized protein, isoform A OS=Drosophila melanogaster OX=7227 GN=DmelCG4	18	2	3	2	212	23.6	5	2.79	2	0	8.8	12	6.6	6	5.5	7.8	9.4	8
Q9VXW9	Uncharacterized protein, isoform A OS=Drosophila melanogaster OX=7227 GN=DmelCG6	2	2	3	2	984	114.2	9.29	0	2	0	8.2	9.5	8.2	6.3	7.5	11.6	10.4	13.7
Q9VCR2	Uncharacterized protein, isoform A OS=Drosophila melanogaster OX=7227 GN=DmelCG6	4	2	5	2	401	45	5.62	4.53	2	0	105.3	113.9	129.8	107.9	84.4	107.7	142.3	95.4
Q9VEC4	Uncharacterized protein, isoform A OS=Drosophila melanogaster OX=7227 GN=DmelCG7	8	4	16	4	450	50.7	5.33	13.95	4	0	217.5	249.7	225	242.3	159.3	309.8	306.9	279.1
Q8IQM5	Uncharacterized protein, isoform A OS=Drosophila melanogaster OX=7227 GN=DmelCG7	7	2	3	2	317	34.7	4.4	0	2	0	31.8	34.1	34.2	34.7	24.4	36.7	45.5	34.6
Q8KHZ6	Uncharacterized protein, isoform A OS=Drosophila melanogaster OX=7227 GN=DmelCG7	12	3	7	3	253	27.2	8.05	7.78	3	0	62.1	71.9	82.9	68.3	93.2	103.9	113.9	80.2
Q9W039	Uncharacterized protein, isoform A OS=Drosophila melanogaster OX=7227 GN=DmelCG1	14	4	11	4	375	41.9	7.46	16.88	4	0	70.8	66.8	67.1	61.1	59.4	79.5	80.8	75.9
M9PFR8	Uncharacterized protein, isoform B OS=Drosophila melanogaster OX=7227 GN=Arts_APE	4	3	7	3	1080	120.8	4.86	7.25	3	0	27.6	23	27.2	12.8	11.5	25.5	28.9	11.9
Q9VID9	Uncharacterized protein, isoform B OS=Drosophila melanogaster OX=7227 GN=BEST_L	2	5	9	5	2663	292.4	5.27	14.08	5	0	89.6	100.3	105.6	91.4	77.1	122.2	139.6	95.2
X2JKF2	Uncharacterized protein, isoform B OS=Drosophila melanogaster OX=7227 GN=CG32585	4	2	4	2	687	78.1	9.35	5.79	2	0	53	50.8	56.3	46.1	36.1	64	73	60.8
M9PGG8	Uncharacterized protein, isoform B OS=Drosophila melanogaster OX=7227 GN=CG40016	21	3	12	3	182	20.7	5.05	13.21	3	0	320.9	366.6	257.6	311.5	184	343.9	359.8	250.7
A1ZBJ2	Uncharacterized protein, isoform B OS=Drosophila melanogaster OX=7227 GN=cg7461 P	3	2	2	2	627	68.3	7.77	4.31	2	0	19.4	22.9	31.4	26.2	59.2	31.1	27.9	18
AOA0B4KFV4	Uncharacterized protein, isoform B OS=Drosophila melanogaster OX=7227 GN=DmelCG1	9	2	3	2	243	28.5	4.92	1.75	2	0	11.7	7	10.8	6.5	5.2	10.1	8.2	4.6
AOA0B4K616	Uncharacterized protein, isoform B OS=Drosophila melanogaster OX=7227 GN=DmelCG3	4	2	5	2	508	55.4	6.99	5.88	2	0	104.1	118.3	119.2	100.6	75.9	96.4	147	92.7
BZ70N0	Uncharacterized protein, isoform B OS=Drosophila melanogaster OX=7227 GN=DmelCG3	10	3	9	3	355	39.8	6.4	14.94	3	0	247.8	225.5	186.1	158.9	144	300.8	241.2	197.5
Q9VT33	Uncharacterized protein, isoform B OS=Drosophila melanogaster OX=7227 GN=DmelCG6	7	2	2	2	388	42.7	7.4	2.15	2	0	52	71.8	75.8	52.9	58.2	66.4	88.2	62.1
BZ70D7	Uncharacterized protein, isoform B OS=Drosophila melanogaster OX=7227 GN=DmelCG7	1	2	2	2	1676	190.9	8.84	2.25	2	0	40.1	43.5	42.8	38.2	28.5	61.2	53.9	45.2
M9MRG2	Uncharacterized protein, isoform B OS=Drosophila melanogaster OX=7227 GN=Ndf PE=1	9	4	35	4	603	65.3	5.97	64.31	4	0	599	612.2	518.6	433.3	445.5	874.6	655.2	553.4
AOA0B4KFB8	Uncharacterized protein, isoform C OS=Drosophila melanogaster OX=7227 GN=CG33097	7	8	26	8	1123	129.7	8.27	28.25	8	0	431.2	505.2	403.4	379.3	278.6	563.7	644.8	429.2
Q8E8G6	Uncharacterized protein, isoform C OS=Drosophila melanogaster OX=7227 GN=Cpsf5 PE	8	2	10	2	237	26.9	8.85	17.71	2	0	283.1	326.9	261.1	256	220.6	242.3	319.4	260.3
X2JAQ5	Uncharacterized protein, isoform C OS=Drosophila melanogaster OX=7227 GN=DmelCG1	19	3	8	3	214	24.4	7.37	11.58	3	0	68.2	78.4	70.3	46.7	58.1	60.3	79	50.5
E1JGL8	Uncharacterized protein, isoform C OS=Drosophila melanogaster OX=7227 GN=DmelCG3	8	9	30	9	1272	140.5	5.01	32.2	9	0	531.1	600.4	540	520.9	381.3	620	759.2	554.7
E1JIV0	Uncharacterized protein, isoform C OS=Drosophila melanogaster OX=7227 GN=DmelCG5	6	2	5	2	243	28.2	8.03	7.21	2	0	130.5	156.1	125.2	142	121.4	162.5	170	168.3
Q7KSN8	Uncharacterized protein, isoform D OS=Drosophila melanogaster OX=7227 GN=CG14730	9	14	28	14	1486	172.2	6.1	14.89	14	0	315.9	388.7	354.9	274.8	243.5	458.9	457.1	303.6
AOA023GRW3	Uncharacterized protein, isoform D OS=Drosophila melanogaster OX=7227 GN=cg4896 P	4	2	2	2	949	107.6	8.22	0	2	0	0	0	0	0	0	0	0	0
X2JEJ0	Uncharacterized protein, isoform D OS=Drosophila melanogaster OX=7227 GN=DmelCG1	3	2	8	2	551	62.5	7.11	9.5	2	0	142.9	202.4	199.5	144.4	176.3	193.4	223.7	147.4
M9ND57	Uncharacterized protein, isoform E OS=Drosophila melanogaster OX=7227 GN=DmelCG7	2	2	2	2	1298	138	5.31	2.02	2	0	23.5	25.9	25.4	23.3	23.4	31.4	38.4	32
ABJN12	Uncharacterized protein, isoform F OS=Drosophila melanogaster OX=7227 GN=anon-EST	1	2	4	2	1655	185.8	10.8	5.8	2	0	113.5	110.1	86.9	114.4	82.7	145.8	167.3	136.6
X2JF73	Uncharacterized protein, isoform H OS=Drosophila melanogaster OX=7227 GN=URE-B1 F	1	4	5	4	5151	557.3	5.45	7.23	4	0	129.5	143.4	136	126.5	88.5	128.9	142.3	119.1
M9PGK3	Uncharacterized protein, isoform I OS=Drosophila melanogaster OX=7227 GN=CG4564 P	3	4	10	4	1367	143.2	9.2	6.81	4	0	170.7	172.6	176.2	156.4	87.2	197	222	132.6
AOA0B4K897	Uncharacter																		

E1JIP3	WRN exonuclease, isoform B OS=Drosophila melanogaster OX=7227 GN=WRNexo PE=4	9	2	15	2	354	40.4	9.14	12.6	2	0	104.9	126.2	119.5	108	92.6	227.8	161.6	153.6
Q9VJG0	Xaa-Pro aminopeptidase ApepP OS=Drosophila melanogaster OX=7227 GN=ApepP PE=	9	4	6	4	613	68.5	5.95	12.78	4	0	224.3	249.8	261.6	193.9	161.8	229.7	299.2	217.7
Q7KVP9	Xeroderma pigmentosum D OS=Drosophila melanogaster OX=7227 GN=Xpd PE=1 SV=1	5	4	6	4	769	88	6.77	6.07	4	0	103.7	121.5	121.7	100.7	80	146.4	151	98.5
A0A0B4KHA1	Yemanudein, isoform B OS=Drosophila melanogaster OX=7227 GN=yem PE=1 SV=1	2	2	2	2	1101	119.2	8.54	2.33	2	0	6.9	10	8.8	6	6.9	9.4	10.5	9.5
X2JB25	Yolk protein 2, isoform B OS=Drosophila melanogaster OX=7227 GN=Yp2 PE=1 SV=1	20	6	27	6	442	49.6	7.96	30.48	6	0	775.8	775	674.2	607.1	574	435.5	853.5	579.5
X2JEX8	Yolk protein 3, isoform B OS=Drosophila melanogaster OX=7227 GN=Yp3 PE=1 SV=1	14	3	59	3	420	46.1	8.5	98.79	3	0	761	893.3	759.8	872.6	753.6	546.6	921.5	712.8
M9NGY4	ZAP3, isoform E OS=Drosophila melanogaster OX=7227 GN=ZAP3 PE=1 SV=1	2	3	3	3	1885	205.1	5.69	0	3	0	16.8	15.7	14.5	13.5	12.4	20.9	19.4	12.9
Q9V468	Zinc finger matrin-type protein CG9776 OS=Drosophila melanogaster OX=7227 GN=CG97	2	2	2	2	1260	140.2	9.35	2.08	2	0	28.8	28.6	22.7	23.6	17.7	28.4	39.3	20.7
Q9W3Y0	Zinc finger protein 593 homolog OS=Drosophila melanogaster OX=7227 GN=CG3224 PE	16	2	2	2	162	18.9	9.67	1.85	2	0	13.9	21.4	20.6	15.9	14.2	19	21.5	14.9
Q8IRH5	Zinc finger protein CG2199 OS=Drosophila melanogaster OX=7227 GN=CG2199 PE=1 S	14	7	16	7	733	81.9	8.56	19.89	7	0	120.1	114	90.9	88	92.7	201.2	117.5	154.7
P41073	Zinc finger protein on ecdysone puffs OS=Drosophila melanogaster OX=7227 GN=Pep PE	14	9	58	9	716	78	5.58	107.08	9	0	1770.7	1897.7	1809.5	1765.4	1140.8	1887.4	2258.6	1759.9
Q86BI3	Zinc-finger protein at 72D, isoform B OS=Drosophila melanogaster OX=7227 GN=Zn72D F	7	5	10	5	884	96	8.44	20.01	5	0	169.8	188.5	172.9	184.3	121.6	225	235.7	180.2

Supplemental Table 3-2: Normalized TMT Intensities for Pulse-Enriched Embryo iPOND Replicates

Accession	Description	Edu Pulse R1	Edu Pulse R2	Edu Pulse R3	Edu Pulse R4	Thy Chase R1	Thy Chase R2	Thy Chase R3	Thy Chase R4	Pulse Average	Thy Aver	Pulse - Chase	Fold Change	p-value
P92177	14-3-3 protein epsilon OS=Drosophila melanogaster OX=7227 GN=14-3-3epsilon I	10.93899144	10.64259698	10.89815458	10.20515716	9.681451497	10.23578733	10.04783018	10.37368281	10.67121822	10.08536296	0.585855261	1.500928508	0.041109
P29310	14-3-3 protein zeta OS=Drosophila melanogaster OX=7227 GN=14-3-3zeta PE=1	10.41098127	10.2072143	10.41135665	9.897173421	9.354331976	10.77135648	9.652773367	9.921832432	10.23168141	9.676768356	0.554913054	1.469080095	0.017666
P02572	Actin-42A OS=Drosophila melanogaster OX=7227 GN=Act42A PE=1 SV=3	10.92911043	10.69353468	11.08218439	10.63967026	10.73497517	10.4390342	10.07229013	10.45446426	10.83610918	10.47419319	0.361915996	1.285131006	0.042803
O16043	Anon1A4 OS=Drosophila melanogaster OX=7227 GN=Df31 PE=1 SV=1	8.721782768	8.016865067	8.044408496	7.730349416	7.088862243	7.072902438	7.513794616	7.548388815	8.128350314	7.305980728	0.822363286	1.768315068	0.015279
F0JA11	Arginine methyltransferase 4, isoform B OS=Drosophila melanogaster OX=7227 G	8.235535607	8.23313307	8.448973299	8.155863757	7.303298526	7.979640966	7.837686683	7.962875056	8.268376433	7.770875308	0.497501125	1.41176614	0.027038
Q9VGH5	ATD27789p OS=Drosophila melanogaster OX=7227 GN=glb PE=1 SV=1	8.051480865	7.881435487	7.705253955	7.936771533	7.119952436	7.596639459	7.404862395	7.802699042	7.89373546	7.481938333	0.411797127	1.330341954	0.044642
AOA0B4LF57	Calmodulin, isoform C OS=Drosophila melanogaster OX=7227 GN=Cam PE=1 SV:	8.057450272	7.774889365	7.839222811	7.787800526	6.902052581	6.710296791	6.856590515	7.086337119	7.864480743	6.888819252	0.976021492	1.967033451	0.000703
Q96989	CDC45L OS=Drosophila melanogaster OX=7227 GN=CDC45L PE=1 SV=1	6.614709844	7.162582078	7.425590449	6.69223141	5.297212997	6.040035532	5.74936151	5.83222662	6.973778445	5.727909165	1.24406928	2.66865968	0.002447
Q9VIH1	CG9273 protein OS=Drosophila melanogaster OX=7227 GN=RPA2 PE=1 SV=2	8.607330314	8.597258233	9.023238428	8.111232135	5.617651645	5.566727512	7.291613104	7.1756255981	8.584814775	7.175620661	1.411757214	2.366602001	0.002954
A1Z898	Chromatin assembly factor 1, p105 subunit OS=Drosophila melanogaster OX=722	6.934280594	6.729255037	7.250335427	6.559817286	5.684621722	6.512318822	6.161990049	6.191499858	6.868422086	6.137607613	0.730814473	1.659575741	0.017886
Q9W3D1	Chromatin assembly factor 1, p180 subunit OS=Drosophila melanogaster OX=722	9.234577796	9.153856087	9.515965377	8.890329313	7.450039943	8.641814736	8.275687205	8.545705925	9.198682184	8.228311952	0.970370232	1.959343348	0.017765
Q494K2	Chromosome transmission fidelity 4 OS=Drosophila melanogaster OX=7227 GN=C	8.010108453	7.962216759	8.442611581	7.703911958	6.11169343	7.414926694	7.247009947	7.342321915	8.029712188	7.028987877	1.000724311	2.00100436	0.026927
Q81RB5	Claspin OS=Drosophila melanogaster OX=7227 GN=Claspin PE=1 SV=1	9.168672118	8.893493636	9.204847647	8.452014586	7.657039458	8.447868346	8.236672228	8.494208591	8.929870929	8.20894716	0.720923765	1.648237072	0.031932
Q81Q05	Cutlet OS=Drosophila melanogaster OX=7227 GN=cutlet PE=1 SV=2	7.99830835	7.988714568	8.423733958	7.528287091	6.246460674	7.28909634	7.053745385	7.24263411	7.984760992	6.953369776	1.031391216	2.043994361	0.0143
Q9VSD6	D-Importin 7/RanBP7 OS=Drosophila melanogaster OX=7227 GN=msk PE=1 SV=	9.429615964	9.280299206	9.486574556	9.219422183	8.244808699	9.048688479	8.983086975	9.092304513	9.535977977	8.887190209	0.466877768	1.382028884	0.031959
A0A0B4LEV2	DNA helicase OS=Drosophila melanogaster OX=7227 GN=dpa PE=1 SV=1	10.55669763	10.36113455	10.74960776	10.11902845	8.944458917	10.1937504	9.649175117	9.860154323	10.4466171	9.661884694	0.784732406	1.74272747	0.038241
P26019	DNA polymerase alpha catalytic subunit OS=Drosophila melanogaster OX=7227 G	9.21310422	9.150073899	9.626338263	8.72224869	7.061719707	8.294157828	8.02795424	8.16559135	9.177941267	7.867355781	1.290585486	2.462273119	0.008553
Q9VCN1	DNA polymerase epsilon catalytic subunit OS=Drosophila melanogaster OX=7227	9.946467699	10.03295591	10.50133462	9.617558126	8.101035787	9.085597842	8.830212373	9.904749718	10.02457909	7.30339893	1.294180158	2.452375945	0.003805
Q9VR07	DNA polymerase epsilon subunit OS=Drosophila melanogaster OX=7227 GN=DNA	6.563768278	6.718367084	6.875298315	6.143563784	5.064579328	5.713445629	5.758968414	6.1671785583	6.575249365	5.55894474	1.026304625	2.022731217	0.004389
Q9VPH2	DNA primase large subunit OS=Drosophila melanogaster OX=7227 GN=DNAPoal	9.37286506	9.456073642	9.842062899	9.005381351	7.32707851	8.356339119	8.178241983	8.287414941	9.419095738	7.032768638	1.3818271	2.605981966	0.003365
Q24317	DNA primase small subunit OS=Drosophila melanogaster OX=7227 GN=DNAPoal	8.346513733	8.533386042	8.842997354	8.264385106	5.660211035	5.80711567	7.330262371	7.405410149	8.496820559	8.21939117	1.277581442	2.42432186	0.002662
P49735	DNA replication licensing factor Mcm2 OS=Drosophila melanogaster OX=7227 GN:	10.81322003	10.60015208	10.96606488	10.3176068	9.018944507	10.2969942	9.834603866	10.04384913	10.67426095	9.798597926	0.875663022	1.834851139	0.030247
Q9V4V6	DNA replication licensing factor Mcm5 OS=Drosophila melanogaster OX=7227 GN:	9.298520857	9.32347671	9.573323591	9.19251921	7.946720946	9.087135555	8.720992029	8.856628749	9.34442701	8.652869335	0.691557675	1.150263818	0.037593
Q9VGH1	DNA replication licensing factor Mcm6 OS=Drosophila melanogaster OX=7227 GN:	10.68193525	10.518913525	10.89133625	9.125155327	8.258868949	9.829743308	10.15549693	10.58913677	10.58913677	9.848871265	0.704265503	1.670483234	0.005788
Q9V3J0	DX16 protein OS=Drosophila melanogaster OX=7227 GN=x16 PE=1 SV=1	7.669593751	7.421027343	7.055384722	7.261168945	6.296509817	7.076650792	6.950130628	6.950843487	7.35178319	6.793715099	0.558068091	1.472296349	0.041271
Q9VHU3	Enhancer of variegation 3-9 OS=Drosophila melanogaster OX=7227 GN=E(var)3-9	6.708739041	6.661468858	6.720671236	6.480821684	5.640706051	6.398429925	6.340500934	6.321175562	6.644412705	6.165203117	0.939790588	1.393979734	0.040158
Q9CP42	Eukaryotic translation initiation factor 4A, isoform E OS=Drosophila melanogaster C	10.65123112	10.57489196	10.83222642	10.47813017	9.825676318	10.37670481	10.19653147	10.41400507	10.63411992	10.20322942	0.430890499	1.348065409	0.031226
Q9XZU1	Exportin-2 OS=Drosophila melanogaster OX=7227 GN=Cse1 PE=2 SV=2	8.273329387	8.393002943	8.606115952	8.296082258	7.623671151	8.168297221	8.11004908	8.018966922	8.392132635	7.980246081	0.411886554	1.330424419	0.029120
Q9VY44	FI07923p OS=Drosophila melanogaster OX=7227 GN=Karybeta3 PE=1 SV=1	8.518062976	8.552162885	8.833057344	8.49218579	7.947753955	8.333947209	8.192172368	8.175075146	8.598867249	8.162012129	0.458855119	1.353650334	0.008088
Q9VZ00	FI19420p1 OS=Drosophila melanogaster OX=7227 GN=DmelCG1737 PE=1 SV=	8.477937609	8.329469919	8.527772894	8.893234957	7.963304349	8.286489086	8.134904901	8.26478303	8.4314856	8.102602342	0.330865259	1.24054144	0.04311
Q7K323	GH01724p OS=Drosophila melanogaster OX=7227 GN=p47 PE=1 SV=1	7.725195117	7.665569812	7.674689231	7.441391653	6.655137684	7.172744334	7.458192257	7.323026295	7.626709371	7.154594242	0.472151529	1.387411466	0.045324
Q9VBT3	GH06691p OS=Drosophila melanogaster OX=7227 GN=DmelCG11811 PE=1 SV:	3.263034406	3.26163525	3.075902853	3.119861636	3.602479443	3.391452073	3.638576638	3.510506401	3.180108536	3.535753639	-0.35654102	0.781520108	0.002849
Q9VPL0	GM13767p OS=Drosophila melanogaster OX=7227 GN=DmelCG3436 PE=1 SV=	7.682994584	7.55706687	7.694503933	7.367181444	6.827644198	7.383627408	7.215899044	7.334312379	7.57545162	7.190370757	0.385064405	1.305918005	0.03973
P48809	Heterogeneous nuclear ribonucleoprotein 27C OS=Drosophila melanogaster OX=7	6.968090752	7.095930687	7.255530956	6.961896226	6.41160866	6.884812764	6.821174933	6.845188874	7.077865879	6.755696308	0.322195752	1.205029241	0.03194
M9MSL3	HO70Cb, isoform G OS=Drosophila melanogaster OX=7227 GN=HO70Cb PE=1 S	9.930885147	9.828053464	10.06512006	9.838862304	8.881892906	9.591668119	9.466120168	9.531450285	9.865730244	9.36778037	0.497949874	1.412205337	0.037371
P52295	Import subunit alpha OS=Drosophila melanogaster OX=7227 GN=Hcn PE=1 SV=	9.154564982	9.115173588	9.227270173	9.965148761	7.814302677	8.633497875	8.449499035	8.626338585	9.115539376	8.380909543	0.734629833	1.663970473	0.010721
Q9WV07	IP07275p OS=Drosophila melanogaster OX=7227 GN=Psf1 PE=1 SV=2	8.173427297	8.203102078	8.618432111	7.769592547	6.048875884	7.063864014	6.962251778	7.07829875	8.191138508	6.788323207	1.402815301	2.444170673	0.003548
Q4V3Z5	IP10727p OS=Drosophila melanogaster OX=7227 GN=DmelCG11788 PE=2 SV=	8.071998581	8.15892868	8.396872002	7.632154753	6.558370012	7.278078484	7.016987276	7.108818543	8.064990055	7.025935616	1.025454448	2.035600483	0.004956
Q9VBP5	Jing interacting gene regulatory 1, isoform A OS=Drosophila melanogaster OX=72:	8.663202279	8.657621174	8.95087161	8.4417088	7.527708429	8.27039826	7.989701145	8.137862487	8.678350966	7.981417581	0.696933385	1.621055387	0.0111
AOA0B4KFY9	Lamin C, isoform B OS=Drosophila melanogaster OX=7227 GN=LamC PE=3 SV=1	6.432959407	6.394833366	6.473396423	6.225058484	6.134675092	6.09812893	6.2246194	6.027011745	6.381561445	6.121108794	0.260452651	1.197854477	0.008845
M9NE89	Lamin, isoform B OS=Drosophila melanogaster OX=7227 GN=Lam PE=3 SV=1	11.00133782	10.79283695	10.86481695	10.7909709	10.15468388	10.35885437	10.427327035	10.45881881	10.86242489	10.361140685	1.015018054	1.41521187	0.001306
Q9VPN5	LD03220p OS=Drosophila melanogaster OX=7227 GN=Stip1 PE=1 SV=1	7.38024459	7.397780864	7.554537734	7.147076626	6.649478116	7.137410456	7.146082462	7.000351955	7.369909954	6.982698623	0.387211331	1.307862915	0.035963
Q9VY19	LD21074p OS=Drosophila melanogaster OX=7227 GN=Pcd4 PE=1 SV=2	8.121015401	8.277527528	8.365549011	8.047730192	7.534763177	7.837562855	7.877917269	8.070119642	8.202955533	7.382090673	0.72826486	1.294921695	0.030406
Q8SX76	LD24646p OS=Drosophila melanogaster OX=7227 GN=pch2 PE=1 SV=1	7.236492618	7.280430679	7.440087484	7.158992517	6.652413312	7.074403021	6.925273502	6.986633597	7.279000825	6.909680858	0.369319967	1.291743807	0.014508
Q9V3E7	LD24793p OS=Drosophila melanogaster OX=7227 GN=Ref1 PE=1 SV=1	7.9795681	7.771312341	7.744398235	7.579442951	6.779764897	7.410833871	7.387025583	7.577307072	7.768680407	7.288732656	0.479947551	1.3	

Q8INH7	Timeout OS=Drosophila melanogaster OX=7227 GN=timeout PE=1 SV=2	9.732506644	9.760091135	10.18368509	9.398512128	8.013884148	8.964827169	8.584432652	8.728046139	9.76869875	8.572797527	1.195901223	2.29087894	0.003582
B7Z126	Tousled-like kinase, isoform G OS=Drosophila melanogaster OX=7227 GN=Tk PE	7.731997787	7.976853153	8.355216969	7.599157729	6.543547203	7.61792591	7.305213982	7.225712852	7.915806409	7.173099987	0.742706422	1.673311944	0.038221
A0A0B4JD97	Transforming acidic coiled-coil protein, isoform K OS=Drosophila melanogaster OX-	2.485426827	2.901662566	2.5475983	2.864278116	2.822194585	3.345724143	3.21438329	3.338877645	2.699741452	3.180294916	-0.480553464	0.716702621	0.025675
A1ZAW6	Uncharacterized protein OS=Drosophila melanogaster OX=7227 GN=DmeICG301	6.439623138	6.499797097	6.554914425	6.530252228	5.531534087	6.052808188	6.164239502	6.264736293	6.506146722	6.003329517	0.502817204	1.416977848	0.022586
Q0E8G6	Uncharacterized protein, isoform C OS=Drosophila melanogaster OX=7227 GN=Cc	8.145167939	8.030934466	7.912411727	7.684559765	7.196462227	7.468165484	7.484463797	7.658472882	7.943268474	7.451891097	0.491377377	1.405786374	0.011588
X2JF73	Uncharacterized protein, isoform H OS=Drosophila melanogaster OX=7227 GN=UF	7.016808288	6.887926398	6.985017494	6.707653933	5.978439484	6.588368733	6.435075455	6.581860465	6.899351528	6.395936034	0.503415494	1.417565594	0.01968
P41073	Zinc finger protein on ecdysone puffs OS=Drosophila melanogaster OX=7227 GN=	10.79010409	10.47051959	10.66495841	10.36049579	9.387711669	10.26051505	10.02329556	10.29010457	10.57151947	9.990406711	0.581112758	1.496002678	0.045314

Q9VAF1	Anilin OS=Drosophila melanogaster OX=7227 GN=nsca PE=1 SV=3	9.2	3	3	3	1239	135.9	6.24	6.92	3	0	248.6	88.6	178.1	161.3	93.4	91.7	104.6	106.5		
P22445	Anxin B10 OS=Drosophila melanogaster OX=7227 GN=Anx10 PE=2 SV=3	9.2	3	3	3	321	35.3	4.74	21.78	3	0	347.1	151.79	229.2	116.1	116.1	153.9	179.9	179.9		
AOA0B4KH34	Anxin OS=Drosophila melanogaster OX=7227 GN=Anx9 PE=1 SV=1	35.701	31	10	18	10	324	35.9	5.06	44.12	10	0	1329.2	443.9	1490.1	1133.7	475	394.5	654.7	2034.4	
O16043	Anon1A4 OS=Drosophila melanogaster OX=7227 GN=D31 PE=1 SV=1	21.714	22	4	4	4	183	18.8	42.77	14.8	4	0	1507.6	605.8	392.2	366.1	432.9	425	231.3	338.2	
Q9VNS5	Anonimeros, isoform A OS=Drosophila melanogaster OX=7227 GN=Anm PE=1 SV=1	12.054	9	4	4	4	538	60.8	9.29	10.59	4	0	1218.8	574.1	626.2	799.7	497.6	608.5	392.6	538	
Q24253	AP complex subunit beta OS=Drosophila melanogaster OX=7227 GN=AP-2beta PE=1 SV=1	7.621	11	7	7	7	621	101.2	11.1	38.91	7	0	389.1	206.3	296.2	206.3	206.3	99.6	106.8	246.2	
Q7KVR8	AP-1 complex subunit gamma OS=Drosophila melanogaster OX=7227 GN=AP-1gamma PE=1 SV=1	8.851	5	4	4	4	4	106.9	5.68	7.26	4	0	177.9	88.6	25.2	33.5	81.1	104.8	128.1	213.7	
P91286	AP-2 complex subunit alpha OS=Drosophila melanogaster OX=7227 GN=AP-2alpha PE=1 SV=1	12.556	4	3	4	4	3	940	105.6	7.18	12.16	3	0	536.8	223.8	840.8	528.7	214.4	226.4	337.4	516
MBR004	Apoptosis-inducing factor OS=Drosophila melanogaster OX=7227 GN=AIF1 PE=1 SV=1	10.177	11	7	7	7	7	178	11.1	17.77	10.177	11	0	111.1	17.77	10.177	10.177	10.177	10.177	10.177	10.177
Q9V431	Apoptosis inhibitor 5 homolog OS=Drosophila melanogaster OX=7227 GN=AI5 PE=2 SV=1	20.988	11	4	4	4	4	536	59.6	7.18	18.41	4	0	550.5	294.2	80.2	591.8	334.2	287.7	270.2	681.6
Q9VD11	Arac2 OS=Drosophila melanogaster OX=7227 GN=Arac2 PE=1 SV=1	53.806	21	6	28	6	0	405	43.6	7.88	78.74	6	0	2809.5	1433.2	5479.3	4879.1	979.4	1110.6	2275.1	2792
Q9VQV7	Arginine methyltransferase 1 OS=Drosophila melanogaster OX=7227 GN=ArMT1 PE=1 SV=1	11.153	9	7	7	7	7	176	17.6	18.46	11.153	9	0	1125.8	403.6	1125.8	403.6	413.4	391.2	591.2	403.6
Q9SXC2	Arginine N-transferase, mitochondrial, isoform A OS=Drosophila melanogaster OX=7227 GN=ArNTr-m PE=1 SV=1	11.031	7	4	4	4	4	594	68.3	8.28	9.96	4	0	229.1	127.4	485.2	420.6	81.5	99.3	204.4	310.9
Q9VPU7	Arouser, isoform C OS=Drosophila melanogaster OX=7227 GN=aru PE=1 SV=1	7.416	3	2	2	2	2	778	85.1	5.18	5.18	2	0	219.3	41.9	129.1	123.3	31.7	37.2	134.5	101.2
X2AJA2	Arp2/3 complex 3 kDa subunit OS=Drosophila melanogaster OX=7227 GN=Arp2 PE=3 SV=1	6.231	6	2	2	2	2	301	35.1	7.91	4.98	2	0	79.9	70.5	170.1	237.1	67.2	83.1	91.5	163.4
AOA0B4KE5	Arsenic resistance protein 2, isoform E OS=Drosophila melanogaster OX=7227 GN=ArSP2 PE=1 SV=1	28.236	7	8	8	8	8	935	102.2	5.69	19.81	8	0	1073.1	606.3	766.1	921.8	679.4	626.4	466.8	846.3
Q9V434	Asparaginyl-tRNA synthetase, isoform A OS=Drosophila melanogaster OX=7227 GN=AsnRS PE=1 SV=1	58.443	25	8	15	8	8	558	63.9	5.96	52.7	8	0	654.2	324.1	980.5	1062.5	356.6	325.9	529.2	611.1
Q9V061	Aspartate aminotransferase OS=Drosophila melanogaster OX=7227 GN=AspT PE=1 SV=1	100.195	22	8	52	8	8	424	47.2	8.78	174.75	8	0	1450.2	798.1	2718.8	2169.7	585.7	649.9	1100.7	1489.9
Q7K0E5	Asparityl-tRNA synthetase, isoform A OS=Drosophila melanogaster OX=7227 GN=AspRS PE=1 SV=1	62.193	16	5	14	16	5	531	59	6.81	57.24	5	0	689.3	312.1	908.9	868.6	302.6	359.3	434.4	643
Q9VJH2	Asparityl-tRNA synthetase, mitochondrial, isoform A OS=Drosophila melanogaster OX=7227 GN=AspRS-m PE=1 SV=1	88.17	15	13	24	13	102	121.4	5.82	93.62	13	0	3806.6	1665.1	4222.3	3639	1314.1	2012.4	2044	2410.5	
AOA0B4KF31	Asr1, isoform B OS=Drosophila melanogaster OX=7227 GN=asr1 PE=4 SV=1	42.467	24	4	11	4	4	258	28.7	6.43	41.33	4	0	279.7	151.2	603.9	514.2	68.8	116.9	299.4	307.1
Q7K3V6	AT1345p OS=Drosophila melanogaster OX=7227 GN=EF1T2 PE=1 SV=1	58.296	20	7	17	7	456	49.6	7.69	55.3	7	0	595.5	286	910.2	838.8	272.1	381.4	428.9	753.9	
Q9AWD5	AT2057p OS=Drosophila melanogaster OX=7227 GN=FCF6 PE=1 SV=1	17.132	5	3	3	3	1220	129.8	8.32	10.09	3	0	284.4	133.5	270.2	278.5	106.3	139.5	155.1	206.8	
Q9V775	AT0234p OS=Drosophila melanogaster OX=7227 GN=JQOR-C2 PE=1 SV=1	145.833	45	15	56	15	45	454	45.4	44.4	234.26	15	0	3148.8	1763.4	9698.3	7571.7	1241.6	1510.9	3785.1	7966.5
Q9VVD9	AT0467p OS=Drosophila melanogaster OX=7227 GN=AL PE=1 SV=3	51.066	16	8	21	8	575	84	9.1	62.04	8	0	1408.2	628	2160.6	1702.8	585.6	634.7	893.8	2379.8	
ASV22	AT0649p OS=Drosophila melanogaster OX=7227 GN=OmEG31460 PE=1 SV=1	17.232	9	4	4	4	511	57.7	6.24	12.47	4	0	588.8	222.2	656.2	683.9	171.2	189.9	251.6	329.3	
Q9VL10	AT10584p OS=Drosophila melanogaster OX=7227 GN=Muk PE=1 SV=2	9.017	11	2	2	2	2	408	45.7	8.37	3.66	2	0	25.9	15.7	38	19	13.8	23.1	14.8	18.7
Q9VZ24	AT12494p OS=Drosophila melanogaster OX=7227 GN=HD-822 PE=1 SV=1	18.643	25	5	10	5	144	17.4	9.5	30.13	5	0	866.8	476.3	1652.9	1426.5	368.5	462.1	775	1423.3	
Q9VXF9	AT12691p OS=Drosophila melanogaster OX=7227 GN=ATPysmB PE=2 SV=2	6.36	7	10	10	7	458	30.5	6.58	10.5	7	0	654.1	321	298.1	421.4	356.1	312.4	356.1	404	
Q9VQH5	AT13736p OS=Drosophila melanogaster OX=7227 GN=JQOR-Q3 PE=1 SV=1	6.36	19	3	7	3	8	189	10.1	10.08	5.88	3	0	687.7	388.8	1844.7	1031.3	188.3	288	834.7	519.2
Q9VMX4	AT19154p OS=Drosophila melanogaster OX=7227 GN=Scx PE=1 SV=1	23.352	18	3	7	3	251	28.2	8.28	26.26	3	0	504.7	303.7	1375.4	1173.1	173	253.2	569.4	697	
Q789V5	AT2157p OS=Drosophila melanogaster OX=7227 GN=Hsp70 PE=1 SV=1	28.903	12	12	12	12	12	640	61.5	15.32	34.73	12	0	1047.9	378.5	1422.7	1422.7	388.2	427.2	512.5	697.5
Q9VFT4	AT21757p OS=Drosophila melanogaster OX=7227 GN=Hn PE=1 SV=1	22.624	7	5	9	5	690	74.9	7.37	24.64	5	0	1046.8	505.7	1397.3	1273.3	473.3	551.6	727.3	540.9	
Q9VGH5	AT27789p OS=Drosophila melanogaster OX=7227 GN=olo PE=1 SV=1	41.163	14	7	14	7	586	61.4	6.04	51.76	7	0	3412.4	1213.5	1626.7	1629.5	1339.6	1151.5	911	1124.3	
AT313V6	AT29239p OS=Drosophila melanogaster OX=7227 GN=HrL47 PE=1 SV=1	14.529	9	4	4	4	4	271	31.7	9.89	11.67	4	0	322.6	139.7	539.9	546.1	121.3	158.1	262.6	411.4
AOA0B4H64	AT29239p OS=Drosophila melanogaster OX=7227 GN=HrL47 PE=1 SV=1	14.529	9	4	4	4	4	271	31.7	9.89	11.67	4	0	322.6	139.7	539.9	546.1	121.3	158.1	262.6	411.4
Q7K81	ATP binding cassette subfamily B member 7, isoform B OS=Drosophila melanogaster OX=7227 GN=ABCB7 PE=1 SV=1	53.928	16	7	15	7	7	709	76.7	9.26	52.48	7	0	636.7	335.4	1504.9	1113.4	227.6	311.2	653.2	779.9
P53381	ATP synthase subunit alpha, mitochondrial OS=Drosophila melanogaster OX=7227 GN=atp PE=1 SV=2	215.294	43	23	193	23	52	552	59.4	90.1	541.98	23	0	9041.2	4970.8	22908.5	19806.7	4150.8	4113	11014.3	14600.4
Q9V455	ATP synthase subunit beta, mitochondrial OS=Drosophila melanogaster OX=7227 GN=atpB PE=1 SV=2	151.541	37	17	143	37	17	443	51.9	102.2	251.8	37	0	4947.3	2603.8	12418.2	10314.2	2209.1	2544.9	5164.3	9514.4
AOA0B4LH17	ATP synthase subunit b, mitochondrial OS=Drosophila melanogaster OX=7227 GN=atpD PE=3 SV=1	39.711	37	6	26	6	178	20.2	5.57	76.44	6	0	2679.9	1468.3	7315.6	4438.7	1039.6	1311.1	3493.6	2906.4	
AT01666	ATP synthase subunit gamma, mitochondrial OS=Drosophila melanogaster OX=7227 GN=atpE PE=1 SV=1	60.263	10	20	116	20	10	207	32.8	6.26	18.26	10	0	2819.6	1639.4	7870.2	1899.4	272.1	589.4	401.7	589.4
Q24448	ATP synthase subunit c, mitochondrial OS=Drosophila melanogaster OX=7227 GN=atpF PE=2 SV=2	6.835	18	4	6	4	6	209	22.4	9.63	26.74	4	0	311.8	172.2	671.3	668.7	186.5	227.9	455.7	2227.6
D1Z3A2	ATP synthase-coupling factor 6, mitochondrial OS=Drosophila melanogaster OX=7227 GN=atpCF6 PE=1 SV=1	8.155	18	2	4	2	106	11.9	9.04	10.3	2	0	108	71.8	348.4	374.4	410.6	38.6	33.1	155.9	354.7
Q9WZ6	ATP synthase, delta subunit, isoform A OS=Drosophila melanogaster OX=7227 GN=atpDdelta PE=1 SV=1	68.838	5	4	4	4	5	157	16.7	5.99	190.09	5	0	1163.8	833.9	3208.2	1991.8	495.7	575	1243.1	1605.9
Q9VND9	ATP synthase subunit e, isoform A OS=Drosophila melanogaster OX=7227 GN=atpE2 PE=2 SV=1	1.706	22	2	2	2	2	138	14.4	7.98	7.34	2	0	93.3	630.5	307.9	307.9	47.7	50.7	22.6	54.4
Q9VKM3	ATP synthase, delta subunit, isoform B OS=Drosophila melanogaster OX=7227 GN=atpE2 PE=2 SV=1	2.22	4	5	4	4	5	109	10.9	7.67	7.34	2	0	22.4	14.7	65.4	65.4	40.7	22.6	54.4	54.4
Q7KMS5	ATP-citrate synthase OS=Drosophila melanogaster OX=7227 GN=ATPCL PE=1 SV=1	43.813	6	14	6	14	6	1112	121.3	7.31	55.29	6	0	1186.3	555.1	964.3	962.4	282.9	581.9	584.4	756.5
Q9V914	ATP-dependent dehydratase OS=Drosophila melanogaster OX=7227 GN=AD PE=1 SV=1	15.945	3	5	7	3	5	1476	170.3	6.87	14.44	3	0	215.8	99.3	338.2	280.1	83.9	39.7	239.2	394.9
Q9V914	ATP-dependent chromatin assembly factor large subunit OS=Drosophila melanogaster OX=7227 GN=ACF PE=1 SV=1	15.945	3	5	7	3	5	1476	170.3	6.87	14.44	3	0	215.8	99.3	338.2	280.1	83.9	39.7	239.2	394.9
Q9VKY3	ATP-dependent Cp protease protoyub subunit OS=Drosophila melanogaster OX=7227 GN=OmEG05045 PE=1 SV=1	8.455	10	4	10	4	10	253	27.6	7.8	25.28	4	0	1162.2	473.8	2298.4	2050.1	419.5	362.9	846	1999.5
Q9V914	ATP-dependent halita binding melanogaster OX=7227 GN=pea PE=1 SV=1	10.638	23	16	53	16	53	16	53	16	53	16	0	1063.8	153.25	604.8	516.6	598.6	516.6	598.6	516.6
Q9VHP0	ATP-dependent RNA helicase beta OS=Drosophila melanogaster OX=7227 GN=bel PE=1 SV=1	87.495	18	10	26	18	10	26	87	7.53	97.5	10	0	1620.9	815.5	1837.5	1694.4	652	815.5	1172.4	900.3
Q9VNV3	ATP-dependent RNA helicase Ddx1 OS=Drosophila melanogaster OX=7227 GN=Ddx1 PE=2 SV=1	11.128	4	3	3	3	3	727	80.8	8.76	9.29	3	0	792.6	340.6	560.9	651.8	297.6	377.8	307	477.3
AT12913	ATP-dependent RNA helicase DHX8 OS=Drosophila melanogaster OX=7227 GN=pea PE=1 SV=1	5.36	2	2	2	2	2	1242	141.8	8.77	3.89	2	0	226.9	101.6	195.8	222.3	119.4	108	117.4	163
P19108	ATP-dependent RNA helicase OS=Drosophila melanogaster OX=7227 GN=Rb2 PE=1 SV=3	102.958	23	16	53	16	53	16	53	16	53	16	0	601.5	2722.2	5395.5	5919.5	2611.2	2816.9	4046	4046
Q9VNV3	ATP-dependent RNA helicase VIM3 homolog, mitochondrial OS=Drosophila melanogaster OX=7227 GN=Su PE=1 SV=1	30.113	10	6	11																

Q9XZ53	Catalytic subunit 3B of the oligosaccharyltransferase complex OS=Drosophila melanogaster OX=7227 GN=St	6,101	4	2	3	2	774	87.6	9.0	5.02	2	0	319.2	143.3	510.6	442.7	91.4	164.8	292.9	201.2	
Q95029	Cathepsin L OS=Drosophila melanogaster OX=7227 GN=Cp	21,107	10	5	6	3	371	43.7	7.21	1.64	3	0	371	476.3	1678.2	279.34	1383.3	174.3	693.7	358.2	382.5
Q9VKJ6	Chaperone-transferring A1Fase OS=Drosophila melanogaster OX=7227 GN=COO1 PE=1 SV=1	26,988	6	4	5	4	1225	136.3	7.74	20.78	4	0	229	112.9	376.2	340.3	112.7	136.6	201.8	210.9	
AA0A84J4D6	CCH-type zinc finger nucleic acid binding protein, isoform B OS=Drosophila melanogaster OX=7227 GN=CN	15,274	22	2	2	5	2	165	17.6	8.65	11.54	2	0	336.2	131.9	195	270.2	138.2	76.7	121.4	137.2
Q9KVV5	CD2 antigen cytoplasmic tail-binding protein 2 homolog OS=Drosophila melanogaster OX=7227 GN=hoin1 PE	7,932	8	2	2	2	2	319	36.8	4.91	3.78	2	0	56.4	25.4	30.2	29.4	21.7	20.2	17.2	32.2
MANF8	CD22, isoform B OS=Drosophila melanogaster OX=7227 GN=Cd22 PE=1 SV=1	13,936	14	4	4	2	191	21.4	7.45	6.49	3	0	165.4	99.5	162.4	99.5	162.4	99.5	162.4	99.5	162.4
Q9VZ27	CDK2-associated protein 1, isoform A OS=Drosophila melanogaster OX=7227 GN=CDK2AP1 PE=1 SV=2	23,623	14	4	4	4	4	281	29.2	9.47	10.24	0	0	1567.4	740.8	852.7	769.5	555.4	521.6	499.2	377.6
Q9W0R0	Cell division cycle 5, isoform A OS=Drosophila melanogaster OX=7227 GN=Cdc5 PE=1 SV=2	42,002	13	6	6	6	6	1014	93.9	8.19	22.41	6	0	363.6	142.1	198.5	278.8	119.4	124.4	114.5	144.9
Q9VW99	Centromere-associated protein 1, isoform B OS=Drosophila melanogaster OX=7227 GN=CenpG PE=1 SV=4	34,346	10	5	5	5	5	157.6	16.21	11.66	11.66	0	0	105.1	57.3	62.4	57.3	62.4	57.3	62.4	57.3
Q24478	Centrosome-associated zinc finger protein CP190 OS=Drosophila melanogaster OX=7227 GN=CP190 PE=1	35,954	8	7	10	7	7	896	121.6	4.67	36.55	7	0	3591.6	1088.6	1395.2	1344.5	1222	1456.6	1054.1	970.1
Q9VX73	Cervantes, isoform A OS=Drosophila melanogaster OX=7227 GN=Cv PE=1 SV=2	8,384	13	3	3	3	3	230	26.1	5.53	8.41	3	0	1296.9	612.2	625.2	739.1	459.6	757.7	444.2	502.5
Q9VW69	CG1206-PA OS=Drosophila melanogaster OX=7227 GN=CG1206 PE=1 SV=1	30,686	21	10	10	10	10	571.7	110.8	34.40	34.40	0	0	1960.0	540.0	675.0	745.5	670.0	654.0	670.0	654.0
Q9K0D3	CG12900 protein OS=Drosophila melanogaster OX=7227 GN=DmelCG12900 PE=1 SV=1	6,225	8	2	2	2	8	231	32.1	8.95	6.25	2	0	785.5	294.4	319.4	418.8	293.4	229.7	211.1	475.3
Q9VYG8	CG1571-PA OS=Drosophila melanogaster OX=7227 GN=DmelCG1571 PE=1 SV=1	8,676	11	3	5	3	3	252	27.7	6.29	10.25	0	0	669.9	340.6	496.3	488.8	271.3	356.3	325.4	292.3
COMMA0	CG17950-PA OS=Drosophila melanogaster OX=7227 GN=Hmgp PE=1 SV=1	9,321	21	2	6	2	1	112	12.4	9.2	19.34	2	0	1005.2	245	358.7	379.5	396	325.8	211.8	265
Q9W124	CG18124 OS=Drosophila melanogaster OX=7227 GN=DmelCG18124 PE=2 SV=1	8,244	4	2	3	2	3	629	62.3	8.16	6.64	2	0	47.1	36.7	46.2	70.9	34.7	31.7	41.9	46.3
F6J1D0	CG3595 OS=Drosophila melanogaster OX=7227 GN=sgh PE=1 SV=1	9,473	13	2	3	2	2	174	19.9	4.81	8.32	2	0	684.8	232	252.5	479.7	206.7	273	304.8	475.8
Q9K511	CG3835-RA OS=Drosophila melanogaster OX=7227 GN=D2zghn PE=1 SV=1	28,391	18	6	16	6	6	533	58.3	6.93	41.76	6	0	851	490.8	1861.2	1354.6	322.6	394	745.1	860.8
Q9742	CG5915 protein OS=Drosophila melanogaster OX=7227 GN=Rab7 PE=1 SV=1	11,927	19	4	5	4	207	17.3	5.47	13.64	4	0	349.4	215.7	761.7	586.7	103.5	210.6	385.8	336.5	
Q9VDC2	CG5919 protein OS=Drosophila melanogaster OX=7227 GN=Idi PE=2 SV=1	16,427	13	3	5	3	256	29.8	7.12	17.59	3	0	152.2	101.1	266.9	302.9	67.8	117.3	106.5	220.8	
Q7JX4	CG6459 protein OS=Drosophila melanogaster OX=7227 GN=P32 PE=1 SV=1	61,103	26	5	33	5	263	29	5.08	105.58	5	0	753.1	423.4	1613.8	1186.1	302.5	348.6	793.5	2405.4	
Q9VJ17	CG1484 protein OS=Drosophila melanogaster OX=7227 GN=BcdNA-SD16138 PE=1 SV=2	8,406	18	2	2	2	178	19.9	5.66	6.76	2	0	103.2	61.7	182.4	175	51.8	61.3	85.9	101.8	
Q9V0R2	CG8844 protein OS=Drosophila melanogaster OX=7227 GN=ND-PDSV PE=1 SV=1	50,993	37	8	36	8	159	18.9	7.01	122.27	8	0	2278.2	1422.1	5693.5	4683.2	908.9	1304.3	2769.6	3437.5	
Q9VMJ5	CG9135 protein OS=Drosophila melanogaster OX=7227 GN=DmelCG9135 PE=1 SV=1	3,088	3	2	2	2	487	53.4	7.18	2.17	2	0	175.7	68	85.8	127	59.9	65.1	47.1	109.3	
Q9VH1	CG9273 protein OS=Drosophila melanogaster OX=7227 GN=HPA2 PE=1 SV=2	10,782	11	3	7	3	246	26.4	5.08	20.9	3	0	2074.3	1047	1007.4	897	727.5	387.6	260.1	364	
A4V391	Chaperonin containing TCP1 subunit 1, isoform B OS=Drosophila melanogaster OX=7227 GN=CCT1 PE=1 S	34,586	17	7	11	7	557	50.5	6.39	34.95	7	0	1010.7	382	965.4	1052	348.2	415.3	510.8	926	
Q9W92	Chaperonin containing TCP1 subunit 2 OS=Drosophila melanogaster OX=7227 GN=CCT2 PE=1 SV=2	46,424	23	9	22	9	535	58	5.85	65.98	9	0	1227.3	616.2	1389.7	1853.8	484.2	593.5	688	1357.8	
Q9VXQ5	Chaperonin containing TCP1 subunit 6 OS=Drosophila melanogaster OX=7227 GN=CCT6 PE=1 SV=1	26,668	12	6	10	6	533	58.2	6.62	27.2	6	0	1125.9	493	1037.8	1194.7	390.6	458.5	577.2	733.5	
Q7K3J0	Chaperonin containing TCP1 subunit 8 OS=Drosophila melanogaster OX=7227 GN=CCT8 PE=1 SV=1	18,946	28	1	1	1	846	84.6	8.46	22.11	11	0	3435.5	1525.2	2211	2360	1525.2	2211	2360	1525.2	2211
AA0A84KHN1	Cherio, isoform N OS=Drosophila melanogaster OX=7227 GN=cher PE=1 SV=1	159,355	17	28	56	28	2404	259.5	6.16	179.03	28	0	2086.8	2036	5186.5	5405.8	1920.3	2259.8	3114.7	3520.6	
Q9VY78	Ch24 intracellular channel, isoform A OS=Drosophila melanogaster OX=7227 GN=Cic PE=1 SV=1	11,258	13	3	6	3	260	30.2	6.29	16.81	3	0	670.1	257.5	430.4	485.5	259.4	193.3	217.2	578.6	
Q9W4K0	Ch24, isoform A OS=Drosophila melanogaster OX=7227 GN=Cic24 PE=1 SV=1	22,464	12	3	3	3	208	19.3	8.22	10.34	3	0	103.2	61.7	182.4	175	51.8	61.3	85.9	101.8	
A1Z898	Chromatin assembly factor 1, p105 subunit OS=Drosophila melanogaster OX=7227 GN=Caf1-105 PE=1 SV=2	22,188	17	5	5	5	477	83.3	8.22	14.48	5	0	1073.1	667.7	683.1	890.7	520.8	172.5	159.8	209.9	
Q9W3D1	Chromatin assembly factor 1, p180 subunit OS=Drosophila melanogaster OX=7227 GN=Caf1-180 PE=1 SV=1	24,116	6	7	12	7	1183	133.4	7.03	37.77	7	0	2827.4	1893.7	1917.7	2549	1291.5	528.7	453.7	693.4	
Q24358	Chromatin-nucleosome complex ATPase chain Iaw OS=Drosophila melanogaster OX=7227 GN=ChlI PE=1 SV	39,888	11	11	14	11	1027	118.8	8.29	45.3	11	0	4630.5	1842.7	1939.4	2316.6	1711.9	1622.7	1054	1281.2	
Q9B853	Chromatin-nucleosome complex ATPase chain II OS=Drosophila melanogaster OX=7227 GN=ChII PE=1 SV	39,888	11	11	14	11	1027	118.8	8.29	45.3	11	0	4630.5	1842.7	1939.4	2316.6	1711.9	1622.7	1054	1281.2	
Q7KJ24	Chromodomain-helicase-DNA-binding protein 1 OS=Drosophila melanogaster OX=7227 GN=Chd1 PE=1 SV=1	12,363	2	3	3	3	1883	211.7	6.38	8.74	3	0	971.3	392.8	444.8	468.3	369.1	393.9	309.6	242.6	
1016102	Chromodomain-helicase-DNA-binding protein 3 OS=Drosophila melanogaster OX=7227 GN=Chd3 PE=2 SV=1	10,256	5	4	4	4	827	103	8.48	12.4	4	0	74.8	28.5	99.4	113.2	31.9	45.1	41.5	76.3	
Q9V316	Chromodomain-helicase-DNA-binding protein 4 OS=Drosophila melanogaster OX=7227 GN=Chd4 PE=1 SV=1	12,363	2	3	3	3	1883	211.7	6.38	8.74	3	0	971.3	392.8	444.8	468.3	369.1	393.9	309.6	242.6	
Q94K2	Chromosome transmission fidelity 4 OS=Drosophila melanogaster OX=7227 GN=CtIF4 PE=1 SV=1	31,373	6	4	5	4	895	96.6	5.34	18.71	4	0	323.5	164.8	239.7	267.4	136.4	117.5	79.9	138.9	
AA0A84K32	CIN85 and CD2AP related, isoform E OS=Drosophila melanogaster OX=7227 GN=cindr PE=1 SV=1	24,979	6	3	5	3	848	88.4	9.26	21.8	3	0	466.8	238.5	555.8	586.2	193.9	249.6	339.1	183.5	
Q9VW99	CIRBP OS=Drosophila melanogaster OX=7227 GN=Cirp PE=1 SV=1	26,988	17	2	3	2	659	65.9	6.59	34.95	2	0	1010.7	382	965.4	1052	348.2	415.3	510.8	926	
XJ2C31	Clathrin heavy chain OS=Drosophila melanogaster OX=7227 GN=Cnc PE=3 SV=1	69,177	7	10	21	10	1678	191.1	5.72	71.22	10	0	900.5	415.8	1167.5	1192.9	376.5	472.7	663.3	786.2	
Q9V726	Cleavage and polyadenylation specificity factor subunit 1 OS=Drosophila melanogaster OX=7227 GN=Cof1F	9,117	2	3	3	3	1455	164.6	6.2	8.78	3	0	667.2	339.3	435.9	462	288.1	340.0	289.9	349.6	
Q9V9V0	Cleavage stimulation factor 50 kD subunit OS=Drosophila melanogaster OX=7227 GN=Csf50 PE=1 SV=1	6,837	6	3	3	3	424	46.9	5.95	7.25	3	0	432.1	159.1	255.4	255.5	151.7	167.3	132.1	173.1	
Q9V852	Cleavage stimulation factor 50 kD subunit OS=Drosophila melanogaster OX=7227 GN=Csf50 PE=2 SV=2	5,401	5	6	5	5	419	82.2	8.19	6.21	5	0	634.1	275.2	394.3	399.3	300.5	321.5	352	468.1	
Q9W0B8	Coatomer subunit alpha OS=Drosophila melanogaster OX=7227 GN=alphaCOP PE=1 SV=1	21,918	5	6	8	5	6	1234	139.2	7.65	17.75	6	0	602.2	300.5	656.1	656.1	251	321.5	352	468.1
P45427	Coatomer subunit beta OS=Drosophila melanogaster OX=7227 GN=betaCOP PE=2 SV=2	38,735	6	4	5	4	964	107.3	6.32	23.11	4	0	1011.1	155.1	509.9	531.8	138.3	156.6	247.5	551.3	
Q9W261	Coatomer subunit gamma OS=Drosophila melanogaster OX=7227 GN=gammaCOP PE=1 SV=1	18,026	11	4	5	4	1114	102.6	8.36	36.62	5	0	1102.2	470.2	508.6	508.6	180.2	202.2	202.2	202.2	
Q9W555	Coatomer subunit delta OS=Drosophila melanogaster OX=7227 GN=deltaCOP PE=1 SV=1	12,639	8	3	3	3	3	532	57.9	6.2	10.65	3	0	184.1	87	207.8	225.2	88.5	86.2	102.9	145.7
Q9V0Y5	Coatomer subunit epsilon OS=Drosophila melanogaster OX=7227 GN=epsilonCOP PE=1 SV=1	9,396	7	2	2	2	306	34.6	4.87	5.23	2	0	272.5	116.2	297.7	275.7	103.6	167.3	287.6	287.6	
Q9W055	Coatomer subunit gamma OS=Drosophila melanogaster OX=7227 GN=gammaCOP PE=2 SV=2	18,026	11	4	5	4	1114	102.6	8.36	36.62	5	0	1102.2	470.2	508.6	508.6	180.2	202.2	202.2	202.2	
A45594	Coffin-like polymerizing factor homolog OS=Drosophila melanogaster OX=7227 GN=Cif PE=1 SV=1	31,593	33	6	18	6	3159	315.9	7.17	82.29	6	0	3370.4	1442.7	2148.4	2365.0	1285	1223.3	1613.4	2192.1	
Q9VJ19	Collet-coiled-coil domain-containing protein 1-like OS=Drosophila melanogaster OX=7227 GN=Col1p1 PE=1	8,484	4	3	3	3	816	89	5.39	4.84	3	0	223.8	80.1	168.9	181.1	75.3	107.2	92.3	140.2	
Q9VW88	Collet-coiled-coil helix-coiled-helix domain containing 3 OS=Drosophila melanogaster OX=7227 GN=Chcd3 PE=1 SV=1	16,737	13	2	4	2	2	223	24.2	8.97	15.11	2	0	417.1	251.8	751.8	505.1	140.1	245.4	413.4	380.4
Q9VJ20	Collagen type I(V) chain OS=Drosophila melanogaster OX=7227 GN=Col1A1 PE=1 SV=3	78,844	8	11	36	8	1179	174.2	8.16	115.91	11	0	2074.4	870.2	1089.2	863.4	600.5	808.6	4020.6		

QBV5U6	Dihydropyridine reductase OS=Drasophila melanogaster OX=7227 GN=Dnr PE=1 SV=1	27.738	26	4	10	4	2355	24.5	6.34	28.74	4	937.6	555.3	1304.4	1104	332	408.1	496.8	465.7	
QBV674	Dihydropyridine dehydrogenase [NAD(P)] OS=Drasophila melanogaster OX=7227 GN=(su) PE=1 SV=2	26.34	5	7	10	1	1031	11.2	6.1	21.95	6	230.7	193.7	246.9	316	87	125.3	122.6	122.6	
QVH38	Dihydroxyacetone phosphatase 2, mitochondrial OS=Drasophila melanogaster OX=7227 GN=MtFB2 PE=2 S	17.237	8	3	4	3	452	52.1	7.46	13.68	3	130.5	70.4	287	154.5	43.3	64.4	128	88	
QVYFQ	Dipeptidase B, isoform A OS=Drasophila melanogaster OX=7227 GN=Dp-B PE=1 SV=2	84.579	24	10	32	10	505.5	55.5	7.66	17.55	10	1553.9	747.5	2547	2355.7	709.8	844.9	1132.3	1648.3	
QVHR8	Dipeptidyl peptidase 3 OS=Drasophila melanogaster OX=7227 GN=DppIII PE=2 SV=2	52.636	17	11	14	11	786	89.1	6.43	14.96	11	2886.2	1324.9	2807	2431.5	994.7	986.6	1160.6	2294.6	
QWV17	DNA polymerase delta 3, isoform A OS=Drasophila melanogaster OX=7227 GN=Dp3 PE=1 SV=2	8.157	2	10	2	2	1032	6.8	6.03	6.03	2	8.157	6.8	6.03	6.03	2	8.157	6.8	6.03	
QVVC3	DNA polymerase delta 1, isoform A OS=Drasophila melanogaster OX=7227 GN=Dp1 PE=1 SV=1	22.518	8	6	7	6	982	11.21	6.68	14.96	6	766.4	350.7	526.8	594.6	304.9	292.6	260.4	326.8	
MN022	Discs large 1, isoform O OS=Drasophila melanogaster OX=7227 GN=Dlg1 PE=1 SV=1	12.313	6	3	3	3	975	10.4	7.14	10.53	3	156.2	73.1	148.1	173.6	80.7	81.4	69.3	92.2	
QVYVZ5	DNA dependent protein kinase OS=Drasophila melanogaster OX=7227 GN=Dpk1 PE=1 SV=1	98.166	17	20	26	16	1140	126	10.66	126.06	16	1260	140.3	1483.7	1663.7	1159.5	1169.5	1423.6	1823.6	
AAO4B4LEV2	DNA helicase OS=Drasophila melanogaster OX=7227 GN=Dpa PE=1 SV=1	55.693	17	12	20	12	866	96.6	7.52	14.61	12	4329.2	1635.5	2094.2	2834.9	1633.9	1330.5	943.4	2443.7	
ZXJAA1	DNA helicase OS=Drasophila melanogaster OX=7227 GN=Mdm3 PE=1 SV=1	74.868	20	14	23	14	818	90.7	6.33	78.25	14	3294.2	1373.3	1850.6	2299.7	1258.6	1050.5	807.8	1599.1	
QVWH4	DNA ligase I OS=Drasophila melanogaster OX=7227 GN=DNAI1 PE=1 SV=1	21.747	7	7	7	7	217	21.7	6.52	18.03	7	217	21.7	6.52	18.03	7	217	21.7	6.52	
MNNEV8	DNA N-methyl adenine demethylase OS=Drasophila melanogaster OX=7227 GN=Ten1 PE=1 SV=1	1	3	3	3	3	2860	306.5	7.74	11.54	3	3	2860	306.5	7.74	11.54	3	3	3	
P2619	DNA polymerase alpha catalytic subunit OS=Drasophila melanogaster OX=7227 GN=DNApol-alpha180 PE=1 S	26.406	6	6	7	6	1488	169.8	8.02	20.15	6	837.3	384.8	520.3	566.6	326.5	217.3	196.3	391.2	
PA3358	DNA polymerase delta catalytic subunit OS=Drasophila melanogaster OX=7227 GN=DNApol-delta PE=2 SV=1	38.435	8	8	11	8	1092	124.8	8.92	30.19	8	1433.2	804.9	850	726.2	590.5	293.3	184	259	
QVW88	DNA polymerase delta small subunit OS=Drasophila melanogaster OX=7227 GN=DpS1 PE=2 SV=1	26.447	16	5	10	5	431	48	6.52	43.02	5	1214.8	612.3	894.6	780.1	485.3	267.1	170.4	284.6	
QVVC1	DNA polymerase epsilon catalytic subunit OS=Drasophila melanogaster OX=7227 GN=DNApol-epsilon255 PE=1 S	20.44	3	6	7	6	2236	256.5	6.47	19.06	6	1293.1	700.6	778.8	1199.3	570.9	334.4	270.6	606.1	
QVVR7	DNA polymerase epsilon subunit OS=Drasophila melanogaster OX=7227 GN=DNApol-epsilon55 PE=3 SV=1	5.456	4	2	2	2	526	58.7	6.48	5.11	2	228	118.1	159.8	165.3	87.8	74.9	55.8	69.2	
QVYV8	DNA polymerase gamma 33d OS=Drasophila melanogaster OX=7227 GN=DNApol-gamma35 PE=2 SV=2	19.994	16	4	4	4	361	41	7.39	13.55	4	193.9	103.1	298.3	266.6	96.5	103.5	159.9	205.7	
QZ7607	DNA polymerase subunit gamma-1, mitochondrial OS=Drasophila melanogaster OX=7227 GN=tm PE=1 SV=1	15.498	3	4	4	4	1145	129.7	7.46	11.58	4	315.9	170.9	606.5	517.9	130.9	141.9	273.1	470.5	
QVYPH2	DNA primase large subunit OS=Drasophila melanogaster OX=7227 GN=DNApol-alpha60 PE=1 SV=2	27.053	13	6	8	6	533	61.4	6.96	25.12	6	1548.7	777.4	905.1	981.3	683.1	404.4	275.5	424	
QZ4317	DNA primase small subunit OS=Drasophila melanogaster OX=7227 GN=DNApol-alpha50 PE=2 SV=2	4.399	3	2	2	2	438	50.2	7.5	4.68	2	410.9	207.5	305.2	389.5	147.5	83.1	75.6	304.5	
QZ4595	DNA repair protein complementing XP-C cells homolog OS=Drasophila melanogaster OX=7227 GN=Xpc PE=1 SV=1	8.087	1	2	2	2	1293	144.1	9.29	4.43	2	401.6	190.5	427.4	530.2	180.3	198.2	212.3	224.1	
PA9735	DNA replication licensing factor Mcm2 OS=Drasophila melanogaster OX=7227 GN=Mcm2 PE=1 SV=1	34.315	11	9	14	9	887	100.4	5.11	29.53	9	1201.1	580.5	973.5	1081.4	519.9	484.1	421	728.9	
QVYCW6	DNA replication licensing factor Mcm5 OS=Drasophila melanogaster OX=7227 GN=Mcm5 PE=1 SV=1	71.753	24	13	27	13	733	82.2	7.84	93.79	13	3123.1	1425.5	1906.3	2325.9	1288.2	1102.6	869.5	1463.5	
QVY41	DNA replication licensing factor Mcm6 OS=Drasophila melanogaster OX=7227 GN=Mcm6 PE=1 SV=1	52.743	15	10	16	10	617	92.3	5.38	53.72	10	2463.1	1041	1376.2	1640	900.4	886.6	583.4	1121.4	
QVYUO	DNA replication licensing factor Mm7 OS=Drasophila melanogaster OX=7227 GN=Mm7 PE=1 SV=1	41.596	14	8	13	8	720	81.2	6.99	38	8	1672.5	708	1006.6	1351	629.9	528.6	441.2	1323	
QV4883	DNA replication-related element factor, isoform A OS=Drasophila melanogaster OX=7227 GN=Drf1 PE=1 SV=1	25.947	7	5	7	5	1059	80.7	5.86	21.85	5	3796.2	1082	1339.8	1620.4	1307.3	1325.2	947.1	2092.8	
P15348	DNA topoisomerase 2, isoform A OS=Drasophila melanogaster OX=7227 GN=Top2A PE=1 SV=1	21.594	3	2	4	2	720	81.2	6.99	38	2	2024.5	1518.9	2045.4	2458.4	1509.9	1464.2	598.9	819.6	
QVNG98	DNA topoisomerase 3-alpha OS=Drasophila melanogaster OX=7227 GN=Top3alpha PE=2 SV=2	15.104	5	6	8	6	8	1250	136.1	8.31	6	1067.2	432.1	1550.7	1184	287.4	232.4	636.6	982.7	
QV9651	DNA topoisomerase 3-beta OS=Drasophila melanogaster OX=7227 GN=Top3beta PE=2 SV=2	8.816	2	2	2	2	875	96.9	8.19	6.37	2	482.6	205.6	544.7	578.1	170.9	229.1	299.7	312.6	
P13460	DNA-binding protein homolog 1 OS=Drasophila melanogaster OX=7227 GN=Dbp1 PE=1 SV=1	44.328	17	11	17	11	1442	163.3	6.83	48.08	11	2538.7	871.1	1077.4	1145.8	641.0	1019	64	1019	
PI9175	DNA-directed RNA polymerase I subunit RPA1 OS=Drasophila melanogaster OX=7227 GN=Rpl1 PE=1 SV=2	2	2	2	2	2	1642	183.5	7.44	6.37	2	657	52.3	30.3	42.3	17.7	33.4	22.2	57.3	
P20028	DNA-directed RNA polymerase I subunit RPA2 OS=Drasophila melanogaster OX=7227 GN=Rpl2 PE=1 SV=2	21.151	6	6	6	6	1428	128.4	8.41	20.38	6	359.4	142	205.3	225.4	136.9	132.6	115	212.9	
PA04052	DNA-directed RNA polymerase II subunit RPB1 OS=Drasophila melanogaster OX=7227 GN=Rpl215 PE=3 S	14.514	7	14	16	14	1187	209	7.81	21.89	14	1764.5	957.7	1238	1539.8	981.3	1121.7	849.4	1268.1	
QV9206	DNA-directed RNA polymerase II subunit RPB2 OS=Drasophila melanogaster OX=7227 GN=Rpl22 PE=2 SV=1	12.847	4	4	4	4	134	176	13.4	12.847	4	128.47	134	176	13.4	12.847	134	176	13.4	
QV9EA5	DNA-directed RNA polymerase II subunit RPB4 OS=Drasophila melanogaster OX=7227 GN=Rpl4 PE=2 SV=2	6.338	12	2	2	2	139	16.2	4.82	5.3	2	649.7	128.4	171.7	265.5	106	136.6	115.4	263.1	
AAJYJ3	DNA-directed RNA polymerase subunit OS=Drasophila melanogaster OX=7227 GN=RplIIIc PE=1 SV=1	4.032	1	2	2	2	1383	154.5	8.57	2.55	2	402.7	176.1	325.6	341.5	206	247.2	194.6	492.4	
QV9V2	DNA-dependent histone H4 acetyltransferase OS=Drasophila melanogaster OX=7227 GN=H4Ac PE=1 SV=1	22.594	12	2	2	2	104	102.2	3.24	104.22	2	453.2	206.6	412.3	296.6	142.3	142.3	206.6	296.6	
QV9V9	DNA-dependent histone H4 acetyltransferase OS=Drasophila melanogaster OX=7227 GN=H4Ac PE=1 SV=1	67.101	30	8	13	8	103	45.2	6.48	56.1	8	2754.7	1232.7	2037.7	1791.8	1004.6	1152.6	1194.7	980.3	
QVKN75	Dodeca-satellite-binding protein 1, isoform A OS=Drasophila melanogaster OX=7227 GN=Dp1 PE=1 SV=1	64.064	11	11	19	11	1301	144.2	6.2	59.43	11	11	1301	144.2	6.2	59.43	11	11	1301	
QZ4319	Dolichyl-diphosphoglycosyltransferase 4B kDa OS=Drasophila melanogaster OX=7227 GN=Dp4B PE=1 SV=1	9.589	5	4	5	4	449	50	4.49	27.12	5	449	50	4.49	27.12	5	449	50	4.49	
QV76N0	Dolichyl-diphosphoglycosyltransferase subunit 1 OS=Drasophila melanogaster OX=7227 GN=Dp1 PE=1 SV=1	15.85	10	4	4	4	458	51.7	8.05	9.99	4	232.8	92.4	344	365.5	487.3	86.6	86.6	173.8	
QV1012	Dolichyl-phosphate beta-glucosyltransferase OS=Drasophila melanogaster OX=7227 GN=wp1 PE=1 SV=1	5.084	2	2	2	2	326	37.1	8.04	4.36	2	85.5	38.2	130.7	157.1	41.8	27.2	62.5	108.6	
Q8MLW2	Dommo, isoform D OS=Drasophila melanogaster OX=7227 GN=Dom PE=1 SV=1	20.401	4	4	4	4	1193	348.2	8.87	20.66	4	353.2	170.2	374.9	319.7	165.2	181.1	204.7	166.9	
P17020	Dorsal protein 1, isoform A OS=Drasophila melanogaster OX=7227 GN=Dp1 PE=1 SV=1	28.386	6	6	7	6	6	623	143.6	7.23	6	1983	165.3	197.2	262.4	107	102	102	102	
PZ4785	Dorsal protein complementing regulator OS=Drasophila melanogaster OX=7227 GN=Dmr PE=1 SV=2	17.422	24	6	7	6	1293	143.6	7.23	10.63	6	1181.3	359.2	412.7	417.3	439.1	381.2	304.3	317	
Q18355	DREAM 1 OS=Drasophila melanogaster OX=7227 GN=Rab11 PE=1 SV=1	6.742	24	6	7	6	214	24.2	5.73	19.61	6	1085.7	548.1	1800.8	1596.7	309.8	512.6	917.5	1108.4	
QVYV2	DREAM OS=Drasophila melanogaster OX=7227 GN=Drm1 PE=1 SV=1	18.456	3	3	3	3	6	519	15.3	11.2	3	150.3	110.2	122.5	145.1	102.2	102.2	102.2	102.2	
QVYKH9	DREAM OS=Drasophila melanogaster OX=7227 GN=Stca PE=1 SV=1	5.475	3	2	2	2	2	227	57.4	9.8	4.9	2	153.7	81.1	195.6	123.3	65.1	105.6	99.6	59.5
Q8STQ9	DESeq1 alpha OS=Drasophila melanogaster OX=7227 GN=Sec1 alpha1 PE=1 SV=1	13.299	6	3	5	3	476	52.2	8.24	16.69	3	288.1	109.2	296.4	353.8	118.3	105.3	152.2	289.2	
QV3V0	DESeq1 beta OS=Drasophila melanogaster OX=7227 GN=Sec1 beta1 PE=1 SV=1	16.427	17	7	11	7	258	27.9	5.68	31.7	7	97.4	162.3	215.8	336.5	217.2	275.5	217.2	275.5	
QVYKAA	Dynactin OS=Drasophila melanogaster OX=7227 GN=Dct1 PE=1 SV=1	7.36	3	2	2	2	699	79.1	6.01	10.4	2	44.1	31.7	64.1	71.2	24.7	19.1	31.2	34.1	
QV7K10	Dynactin 4, p62 subunit OS=Drasophila melanogaster OX=7227 GN=DCTN4-p62 PE=1 SV=1	11.964	7	3	3	3	514	57.9	8.2	10.23	3	294.8	171.2	386.9	434.6	116	155.2	237.1	178.1	
P13496	Dynactin subunit 1 OS=Drasophila melanogaster OX=7227 GN=DCTN1-p150 PE=1 SV=2	12.302	3	3	3	3	3	1265	141.1	5.62	8.23	3	218.2	120.7	275.4	297.7	93.2	119.9	152.7	144
QV9P85	Dynamin associated protein 1, isoform A OS=Drasophila melanogaster OX=7227 GN=Dap160 PE=1 SV=1	8.566	6	6	6	6	1098	119.8	5.16	24.23	6	896	109.8	283.9	309.4	106.4	125.9	155.6	133.8	
QV9VE0	Dynamin related protein 1, isoform A OS=Drasophila melanogaster OX=7227 GN=Drc1 PE=1 SV=1	47.301	6	5	6	5	735	82.5	6.98	19.5	5	452.8	231.6	550.8	453.9	151.4	260	296.5	283.4	
MPE28	Dynamin heavy chain 64c, isoform C OS=Drasophila melanogaster OX=7227 GN=Dm64c PE=1 SV=1	23.376	3	11	11	11	4648	530.8	6.33	35.46	11	722.8	350.3	962.3	945.4	314.1	391	445.7	479.5	
QV2V20	Dynamin light chain 1, isoform A OS=Drasophila melanogaster OX=7227 GN=Dm64l PE=1 SV=2	13.254	3	3	3	3	1053													

PA8603	F-actin-capping protein subunit beta OS=Drosophila melanogaster OX:7227 GN=cpb PE=2 SV=1	3,223	8	2	3	2	2,676	31.3	5.44	3.87	2	0	277.8	106.4	256.1	354.7	101.2	129.1	122.6	203.2	
Q9VRE6	F-actin complex subunit alpha OS=Drosophila melanogaster OX:7227 GN=afa1 PE=1 SV=2	5,078	7	17	9	10,683	128.6	6.69	6.87	9	0	674.7	261.2	291.1	305.6	404	257.7	155.6	130.7	139.2	
Q05344	FACT complex subunit Sarp1 OS=Drosophila melanogaster OX:7227 GN=Sarp PE=1 SV=2	50,088	16	10	21	10	723	81.5	6.83	59.35	10	0	4801.7	1938.6	2279.1	2963.1	1796.2	1100	797	1654.3	
Q8MYL1	Fancd2 OS=Drosophila melanogaster OX:7227 GN=Fancd2 PE=2 SV=1	5,744	1	2	2	2	1478	167.4	5.69	5.02	2	0	482.9	197	347.7	629.4	160.1	213	173.2	530.1	
Q7KM61	Fam5ey1 phosphatase synthase OS=Drosophila melanogaster OX:7227 GN=Fpps PE=1 SV=1	26,664	12	5	10	5	419	47.9	6.92	29.38	5	0	684.9	313.7	1152.3	877.2	289.4	331.1	512.2	1415	
Q9VJ58	Fas-associated protein 2, isoform A OS=Drosophila melanogaster OX:7227 GN=Fat2 PE=1 SV=1	10,527	5	3	3	3	464	52.9	5.98	9.22	3	0	231.9	130.2	314.8	308.9	108.9	137.7	154.9	131.3	
Q9VKU1	Fatty acid (Long chain) transport protein, isoform B OS=Drosophila melanogaster OX:7227 GN=Fatlp1 PE=1 SV=1	12,809	6	3	3	3	626	70.1	8.84	6.74	3	0	117.1	99.5	333.9	355.7	86.8	116	169.7	133	
Q9VJ62	Fatty acid synthase 1, isoform A OS=Drosophila melanogaster OX:7227 GN=Fat1a PE=1 SV=1	12,809	6	3	3	3	626	70.1	8.84	6.74	3	0	117.1	99.5	333.9	355.7	86.8	116	169.7	133	
Q9VJ67	Fatty acid synthase 1, isoform B OS=Drosophila melanogaster OX:7227 GN=Fat1b PE=1 SV=1	169,513	18	28	48	28	2438	266.3	6.37	162.44	28	0	4666.4	1941.2	3873.5	4421.6	1544.8	2046.1	2195.5	3666.1	
MIMXJ2	Ferredoxin 1, isoform B OS=Drosophila melanogaster OX:7227 GN=Fdx1 PE=4 SV=1	12,106	11	2	3	2	172	19.7	7.03	10.51	2	0	46.6	26.4	78	63	20.3	33.5	40.5	40.1	
Q8S248	Ferredoxin 2 OS=Drosophila melanogaster OX:7227 GN=Fdx2 PE=4 SV=1	18,157	18	2	3	2	164	18.4	6.45	19.52	3	0	41.5	26.4	150.1	102.5	41.2	54.1	35.2	147.8	
H1JLJ2	Feritin OS=Drosophila melanogaster OX:7227 GN=Fer1 PE=1 SV=1	11,227	14	2	2	2	179	19.2	6.11	9.28	2	0	18.9	15.1	92	70.7	83.3	10.7	40.4	34.2	
Q9V958	Ferredoxin, mitochondrial OS=Drosophila melanogaster OX:7227 GN=FdCh PE=2 SV=1	25,394	13	5	13	5	384	43.6	8.4	3.9	5	0	333.8	208	870.2	652.6	159.2	162	367.8	388.8	
Q0E8X8	FI01416e OS=Drosophila melanogaster OX:7227 GN=FK[8] PE=1 SV=1	10,971	19	3	9	9	107	11.9	9	18.33	3	0	57.4	315.6	1090.1	634.3	227.7	237.2	630.5	481.8	
O18332	FI01544d OS=Drosophila melanogaster OX:7227 GN=FI1 PE=1 SV=1	21,410	10	3	7	7	205	22.7	5.47	41.46	4	0	439.1	243.9	953	938.8	214.8	282.3	408.6	616.9	
Q9W0A8	FI01588p OS=Drosophila melanogaster OX:7227 GN=Rpl23A PE=1 SV=1	21,410	10	3	7	7	207	29.4	10.95	22.64	3	0	756.4	333.1	764.8	466.5	264.5	406.2	648.2	242.5	
Q9VW43	FI01736p OS=Drosophila melanogaster OX:7227 GN=Rpl30 PE=1 SV=1	28,424	37	8	13	8	180	21.1	9.73	38.78	8	0	116.1	594.9	1986.4	1456.5	384.3	596	920.8	1019.9	
Q9VW6	FI02004e OS=Drosophila melanogaster OX:7227 GN=DmelCG5290 PE=1 SV=1	6,86	4	3	3	3	798	92.1	6.06	6.13	3	0	681.2	359.8	579.8	690.8	320.7	344.6	432.6	484.3	
Q9VWC7	FI02109e OS=Drosophila melanogaster OX:7227 GN=DmelCG12702 PE=1 SV=1	10,436	3	2	3	2	870	97.1	6.71	11.36	2	0	38.7	19.6	44	43.1	19.6	24.9	25	26.6	
Q9VBH8	FI02850d OS=Drosophila melanogaster OX:7227 GN=Rpl34a PE=1 SV=2	4,194	9	2	2	2	162	18.1	11.44	4.26	2	0	212.3	79	161.8	201.8	81.2	111.1	125	109.4	
A12803	FI02892e OS=Drosophila melanogaster OX:7227 GN=Manr PE=1 SV=1	25,146	20	5	5	5	340	38.1	8.54	20.15	5	0	371.6	291.7	1055.7	555.5	80.7	199.3	492.5	312.3	
Q9W9R9	FI03239e OS=Drosophila melanogaster OX:7227 GN=DmelCG1677 PE=1 SV=2	9,394	3	3	3	3	1000	109	5.76	9.32	3	0	757.9	281.1	447.9	462	299.2	338.1	277.7	362	
Q9N6D7	FI03258e OS=Drosophila melanogaster OX:7227 GN=hmg PE=1 SV=1	20,598	12	5	6	5	659	74.5	9.09	18.89	5	0	1171.3	532.2	707.5	772.8	473.2	477.8	330.4	413.4	
Q9VKC8	FI03495e OS=Drosophila melanogaster OX:7227 GN=Tom70 PE=1 SV=2	43,904	13	8	15	8	589	66.3	6.21	50.3	8	0	1162.1	751.7	1687.7	1345.3	410.8	791.2	848.7	981.7	
Q9VXR0	FI03659e OS=Drosophila melanogaster OX:7227 GN=CG18R164 PE=1 SV=1	11,968	8	2	2	2	492	54.8	5.81	8.7	2	0	117.8	70	167.4	220.6	69	85.9	92	232.6	
Q9VXR8	FI03680e OS=Drosophila melanogaster OX:7227 GN=DmelCG8128 PE=2 SV=1	10,550	10	5	5	5	330	38.1	8.92	15.41	5	0	289.9	168.4	515.6	430	139.8	148.8	221.3	227.6	
Q9VVL8	FI03887e OS=Drosophila melanogaster OX:7227 GN=TrpR-m PE=1 SV=1	22,189	8	4	7	4	665	72.8	9.22	22.91	4	0	103.2	68.2	219.4	187.1	50.2	54.5	88.3	131.1	
Q9VY05	FI04011e OS=Drosophila melanogaster OX:7227 GN=Hxcr1 PE=1 SV=1	39,111	10	6	7	7	214	48.7	5.47	5.47	7	0	574.7	262.4	729.9	574.7	228.4	239.4	404	473.1	
Q9VQ90	FI04424e OS=Drosophila melanogaster OX:7227 GN=DmelCG17593 PE=1 SV=1	14,923	7	2	3	2	476	54.1	5.33	10.06	2	0	74.8	41.9	89.7	74.6	38.7	38.7	40.4	73.1	
Q9W149	FI04483e OS=Drosophila melanogaster OX:7227 GN=DmelCG11414 PE=1 SV=1	11,865	4	2	2	2	867	95.9	8.82	7.8	2	0	524.5	238.7	657.4	678.8	208.9	296.2	382.9	287.4	
Q8SX2C	FI04503e OS=Drosophila melanogaster OX:7227 GN=CG16692 PE=1 SV=1	20,501	12	4	2	2	117	45.0	5.72	27.38	2	0	53.2	31.2	38	153.8	240.2	530.7	429.6	45.6	
Q9V8Q7	FI04601e OS=Drosophila melanogaster OX:7227 GN=DmelCG5116 PE=1 SV=1	6,385	6	3	9	3	526	59.2	8.78	33.53	3	0	147.8	104.1	195.6	216.6	103.3	109.9	102.8	119.2	
Q9W074	FI04779e OS=Drosophila melanogaster OX:7227 GN=HBS1 PE=1 SV=1	7,836	4	2	3	2	470	74.1	6.7	9.54	2	0	130.2	71.5	148.9	166.8	53.6	75.7	85.8	68	
Q95WY3	FI04781e OS=Drosophila melanogaster OX:7227 GN=Np5d PE=1 SV=1	5,89	5	2	2	2	696	54.8	9.28	5.29	2	0	292.2	100.5	154.1	207.8	113.1	94	75.9	207.4	
Q9VJ58	FI05024e OS=Drosophila melanogaster OX:7227 GN=CHK2 PE=1 SV=1	12,245	12	5	11	11	492	54.8	5.81	8.7	2	0	105.7	60.1	162.3	166.7	70	80.8	101.5	232.6	
Q9VVE9	FI05277e OS=Drosophila melanogaster OX:7227 GN=DmelCG1622 PE=1 SV=1	37,235	18	5	6	5	398	45.4	9.39	26.72	5	0	1151.6	456.8	517.1	590.7	443.5	490.6	352.9	397	
Q9VAZ0	FI05230e OS=Drosophila melanogaster OX:7227 GN=DmelCG5003 PE=1 SV=1	5,306	4	2	2	2	713	80.4	5.71	6.01	2	0	116.1	82.2	177.7	172.6	91.2	93.4	80.5	186.3	
Q9W9X6	FI06234e OS=Drosophila melanogaster OX:7227 GN=Hsp70 PE=1 SV=1	48,553	15	8	14	14	495	53.5	44.4	54.44	14	0	1083.2	329.2	1480	1283.2	518.5	645.6	737.2	812.2	
Q9V5W4	FI06490e OS=Drosophila melanogaster OX:7227 GN=RRF1 PE=1 SV=1	7,484	7	2	2	2	254	28.5	9.79	6.03	2	0	88.1	45.3	214.2	191.5	23.2	26.4	87.4	136.5	
Q9VW40	FI06578e OS=Drosophila melanogaster OX:7227 GN=Amar PE=2 SV=1	11,884	7	2	3	2	373	41.6	6.55	7.22	2	0	343	132.8	514.9	450.3	112.8	154.3	247.4	240.1	
Q9VJF6	FI06581e OS=Drosophila melanogaster OX:7227 GN=Hsp90 PE=1 SV=1	9,491	16	2	3	3	206	32.6	8.77	16.36	3	0	146.6	58	158.3	158.3	94.9	85	113	232.6	
Q9VGZ2	FI06805e OS=Drosophila melanogaster OX:7227 GN=Rp46 PE=1 SV=3	6,844	9	2	2	2	233	25.7	5.33	5.96	2	0	586.5	267.9	544.9	740	241.3	232.5	262.8	556.5	
Q9W936	FI06808e OS=Drosophila melanogaster OX:7227 GN=HP1b PE=1 SV=1	7,433	8	2	4	2	240	26	4.77	11.99	2	0	1098.1	554.3	647.9	698.1	450.7	567.3	422.4	319.6	
Q9VDU0	FI07686e OS=Drosophila melanogaster OX:7227 GN=DmelCG5377 PE=1 SV=1	46,254	13	5	15	5	278	31.7	8.27	50.14	5	0	1571.3	836.1	2948	2418.6	505.5	643.6	1263.5	1447	
Q9VJ61	FI07923e OS=Drosophila melanogaster OX:7227 GN=CG15713 PE=1 SV=1	6,374	5	2	2	2	953	103.3	6.64	8.13	2	0	147.5	75.2	127.4	156.2	39.2	41.6	47.5	148.2	
Q9VL66	FI09311e OS=Drosophila melanogaster OX:7227 GN=DmelCG4562 PE=1 SV=2	9,291	10	2	3	2	287	31.9	8.22	9.16	2	0	135.4	87.8	308.8	222.9	30.5	51.8	124.7	99.6	
Q9VK12	FI09336e OS=Drosophila melanogaster OX:7227 GN=DmelCG4788 PE=1 SV=1	6,442	7	2	3	2	252	26.6	9.29	9.45	2	0	1303.8	548.7	559.3	848.1	569.2	556.6	294.8	398.8	
Q9VJ62	FI09392e OS=Drosophila melanogaster OX:7227 GN=Hsp87 PE=1 SV=1	48,984	16	7	11	11	453	53.3	44.4	54.44	11	0	1158.8	675.8	2432.2	2432.2	617.2	617.2	371.2	461.2	
Q9INW7	FI11475e OS=Drosophila melanogaster OX:7227 GN=DmelCG178 PE=1 SV=1	8,076	6	2	2	2	557	62.1	5.51	4.06	2	0	101.1	58.4	214.9	348	54.7	72.7	91.1	149.3	
Q9E689	FI11703e OS=Drosophila melanogaster OX:7227 GN=Vid PE=1 SV=1	8,51	4	3	3	3	715	79.9	5	7.8	3	0	547.3	182.2	251.8	395.7	212.4	267.3	136	360.3	
Q9VW41	FI11742e1 OS=Drosophila melanogaster OX:7227 GN=CG58 PE=1 SV=2	24,871	24	2	3	3	158	73.6	11.87	21.03	3	0	101.1	176.1	202.1	176.1	202.1	176.1	202.1	176.1	
Q9V3E9	FI11738e1 OS=Drosophila melanogaster OX:7227 GN=Spag PE=1 SV=1	8,982	4	2	2	2	354	59.6	8.34	6.06	2	0	254.1	131.5	116.9	314.9	103.4	129.2	153.7	199.6	
HRN8	FI17821e1 OS=Drosophila melanogaster OX:7227 GN=CG3760-RB PE=1 SV=1	31,517	31	6	9	6	265	29	5.31	32.81	6	0	409.9	243.6	417.2	445.5	183.4	210.9	206	253.9	
HBV8D0	FI18307e1 OS=Drosophila melanogaster OX:7227 GN=SCAR PE=1 SV=1	19,227	8	4	5	4	641	70.1	6.92	17.3	4	0	65.1	328.9	935.2	966.6	223	348.8	517.8	431.4	
A12922	FI18620e1 OS=Drosophila melanogaster OX:7227 GN=Hsp90 PE=1 SV=1	13,013	5	2	2	2	953	103.3	6.64	8.13	2	0	147.5	75.2	127.4	156.2	39.2	41.6	47.5	148.2	
A12936	FI18626e1 OS=Drosophila melanogaster OX:7227 GN=Zn149B PE=1 SV=1	10,575	6	5	7	5	655	72.3	8.56	14.3	5	0	443.3	356.6	834.8	682.8	208.6	257.7	459.9	359.8	
Q9VB46	FI18644e1 OS=Drosophila melanogaster OX:7227 GN=Hmu PE=1 SV=1	18,133	8	4	8	4	579	63.4	9.35	26.21	4	0	789.9	420.6	1474.5	1474.5	722.2	331.1	433.7	783.9	667.3
Q9VJ62	FI1748e1 OS=Drosophila melanogaster OX:7227 GN=Hsp90 PE=1 SV=1	13,013	5	2	2	2															

Q7KR59	GH01331p OS-Drosophila melanogaster OX-7227 GN=DmelCG1815 PE=1 SV=1	6.517	1	2	2	2	1664	181.8	8.35	54.32	2	0	351.3	148.2	213.9	233	140.7	161.8	125.1	155.4
Q7KX33	GH01257p OS-Drosophila melanogaster OX-7227 GN=DmelCG2044 PE=1 SV=1	6.527	3	6	3	213	23.5	3.2	1.99	14.32	3	0	187.2	234.7	204.8	0	0	117.8	43.3	151.7
Q9VB10	GH01709p OS-Drosophila melanogaster OX-7227 GN=DmelCG5590 PE=1 SV=1	58.887	25	7	22	7	412	44.3	8.02	82.01	7	0	1460.9	617.9	258.2	1616	582.6	617.9	1000.4	1303.9
Q7K323	GH01724p OS-Drosophila melanogaster OX-7227 GN=pf4 PE=1 SV=1	58.219	25	6	11	6	407	43.4	5.62	43.94	6	0	894	442.4	586.8	589.8	365	412.9	308.6	332.1
Q9V233	GH01794p OS-Drosophila melanogaster OX-7227 GN=Rcd5 PE=1 SV=1	12.317	9	4	4	4	578	63.5	9.44	11.82	4	0	438.6	162.5	280.5	382.5	190.3	212	175	261.5
Q9V039	GH01801p OS-Drosophila melanogaster OX-7227 GN=CG15224 PE=1 SV=1	4.958	2	1	1	1	285	31.5	2.24	2.24	1	0	107.4	700.7	1866.8	1915.5	606.7	1017.2	1707.8	0
Q9VPE9	GH03554p OS-Drosophila melanogaster OX-7227 GN=SF3a1 PE=1 SV=1	10.957	7	6	8	6	874	88	6.37	21.91	6	0	2001.9	766.2	1070.1	1139.3	721.3	837.5	680.8	653
Q9VNH5	GH04919p OS-Drosophila melanogaster OX-7227 GN=DmelCG2091 PE=1 SV=1	6.608	9	2	2	2	374	43	5.3	4.39	2	0	16.4	11	9.9	14.7	9.3	9.9	6.2	7.9
Q9VNV5	GH05193p OS-Drosophila melanogaster OX-7227 GN=DmelCG1192-2 SV=1	16.244	16	2	4	3	351	40.3	5.82	5.58	2	0	149.3	277.2	58.6	494.6	487.1	486.4	281.6	464.8
Q8SQX1	GH05219p OS-Drosophila melanogaster OX-7227 GN=DmelCG9629 PE=1 SV=1	89.085	36	14	69	14	540	58.3	7.44	168.95	14	0	3089.6	1707.8	6275.1	4426.1	1047.6	1431.1	2723.8	3523.8
Q9VXP3	GH05406p OS-Drosophila melanogaster OX-7227 GN=mrpS3 PE=1 SV=1	16.402	9	18	9	9	557	65.1	8.47	10.8	9	0	537.2	319.6	1325.2	1034.6	246	360.8	598.4	1015
Q7K5K2	GH05459p OS-Drosophila melanogaster OX-7227 GN=DmelCG10120 PE=2 SV=1	53.678	20	6	12	6	224	25.5	7.07	6.33	6	0	170.7	286.7	61.2	812.2	333.7	412.3	403	326
Q9VLM6	GH05949p OS-Drosophila melanogaster OX-7227 GN=DmelCG17294 PE=1 SV=1	15.978	17	3	4	3	255	28.5	5.95	15.58	3	0	167.2	81.1	254.9	271.2	69.5	50.7	107.3	172.5
Q9U5U4	GH06271p OS-Drosophila melanogaster OX-7227 GN=Mma19 PE=1 SV=1	8.133	4	2	2	2	955	107	5.91	3.64	2	0	75.8	44	80.2	76.5	37.4	38.3	39.2	51
Q9VT83	GH06891p OS-Drosophila melanogaster OX-7227 GN=DmelCG11811 PE=1 SV=1	13.077	8	3	4	3	233	25.9	7.44	13.01	3	0	92.2	401.7	1039.9	826.6	233.8	362.3	479.5	580.3
Q9VWC5	GH06959p OS-Drosophila melanogaster OX-7227 GN=DmelCG9574 PE=1 SV=1	54.976	28	9	38	9	419	47.6	8.61	92.76	9	0	1074.4	720.7	1866.8	1915.5	606.7	1017.2	1707.8	0
Q9ZV55	GH07148p OS-Drosophila melanogaster OX-7227 GN=DmelCG1582 PE=1 SV=2	4.446	1	2	2	2	1288	146	7.4	4.7	2	0	204.9	119.3	220.8	276.2	159.4	149	125.5	178.2
Q9VD14	GH07286p OS-Drosophila melanogaster OX-7227 GN=DmelCG13850 PE=1 SV=3	5.775	20	9	17	9	546	61.8	9.13	58.47	9	0	1925.6	811.6	2891.1	1914.2	635.3	830.6	1212.3	2243.9
Q9VH4	GH07340p OS-Drosophila melanogaster OX-7227 GN=DmelCG1556 PE=1 SV=1	8.866	4	2	4	2	522	60	7.33	12.37	2	0	904.8	357.1	1085.8	763.8	313.6	371.6	532.2	343.1
Q9Y183	GH07456p OS-Drosophila melanogaster OX-7227 GN=RplI33 PE=1 SV=1	19.337	13	4	7	4	275	31.2	4.82	20.19	4	0	162.5	683.2	916.5	1197.7	675.4	833.2	675.3	732.3
Q9VFK8	GH07711p OS-Drosophila melanogaster OX-7227 GN=eds22 PE=1 SV=1	11.86	8	2	2	2	326	37.8	5.03	9.27	2	0	208.5	75.9	123.3	136.5	77	81.2	60.9	159.1
Q9VAY9	GH07821p OS-Drosophila melanogaster OX-7227 GN=mrpS2 PE=1 SV=1	24.778	14	5	12	5	393	45.8	7.74	37.63	5	0	1053.3	634.2	2475.4	1631.6	323.4	531.6	1143	1241.7
Q9VL02	GH08677p OS-Drosophila melanogaster OX-7227 GN=nmf PE=2 SV=1	15.943	5	3	3	3	369	41.5	8.22	9.32	3	0	150.6	82	172.6	184.1	66.4	87.1	92.3	83.1
Q24090	GH08712p OS-Drosophila melanogaster OX-7227 GN=Snr1 PE=1 SV=2	19.766	10	3	5	3	370	41.9	5.27	17.17	3	0	745.4	368.6	489.7	548.5	340.9	346	275.1	323.5
Q7K1H0	GH09096p OS-Drosophila melanogaster OX-7227 GN=CG491 PE=1 SV=1	13.177	10	3	3	3	324	36.5	6.65	8.83	3	0	302.2	104.6	209.7	250.8	119.4	113.4	121.7	321.7
Q8STA3	GH09289p OS-Drosophila melanogaster OX-7227 GN=Trf1 PE=1 SV=1	25.976	10	4	5	4	441	48	4.46	19.95	4	0	144.7	8.2	16.3	18.9	4.9	7	11.7	0
Q7K3W2	GH09295p OS-Drosophila melanogaster OX-7227 GN=CG8728-RA PE=1 SV=1	103.979	29	13	59	13	556	61	7.12	159.5	13	0	2886.6	1547	5644.4	4705.9	1751.7	1517.6	2615.7	4240.7
Q9VE08	GH10002p OS-Drosophila melanogaster OX-7227 GN=DmelCG6013 PE=1 SV=1	9.625	10	2	2	2	213	24.8	9.55	7.03	2	0	294.2	148.1	334.7	370.3	181.1	156.4	207.8	265.4
Q9VY45	GH10022p OS-Drosophila melanogaster OX-7227 GN=DmelCG134 PE=1 SV=2	12.213	10	2	2	2	173	22.7	4.33	4.33	2	0	171.7	72.2	215.7	248.8	66.9	79	93.2	213.9
Q8MZ13	GH10652p OS-Drosophila melanogaster OX-7227 GN=pp0 PE=1 SV=1	21.347	6	4	12	6	818	88.2	9.36	25.22	4	0	113.2	28.2	31.8	31.8	23.5	15	21.7	70.3
Q9VGV9	GH11067p OS-Drosophila melanogaster OX-7227 GN=DmelCG6567 PE=1 SV=1	4.685	9	2	2	2	235	26.2	8.15	4.51	2	0	34.3	18	44.6	53.7	13.3	15	21.2	70.3
Q9V690	GH11660p OS-Drosophila melanogaster OX-7227 GN=TH8ap3 PE=1 SV=1	13.664	11	3	3	3	429	46.3	7.14	10.28	3	0	1029.8	150.2	70.9	150.2	71.2	75.2	75.2	75.2
Q9VJM9	GH11285p OS-Drosophila melanogaster OX-7227 GN=Nmda1 PE=2 SV=1	7.107	3	2	2	2	324	35.5	7.88	1.64	2	0	41.3	61	126.4	176.8	19.5	51	73.7	70
Q9V3Z4	GH13411p OS-Drosophila melanogaster OX-7227 GN=Rpn6 PE=1 SV=1	6.123	4	3	5	4	502	57.7	5.8	10.66	3	0	674.1	279.4	448.2	587.5	253.2	253.7	218	503.6
Q9VNC0	GH1824p OS-Drosophila melanogaster OX-7227 GN=POLD12 PE=1 SV=1	72.336	35	9	23	9	410	46.3	7.14	92.92	9	0	1889.4	969.8	3372.5	2076.2	743.5	884	1366.9	2309.1
Q9VH8	GH1915p OS-Drosophila melanogaster OX-7227 GN=Thesau PE=1 SV=1	50.919	10	3	12	10	449	48.6	8.44	102.77	10	0	2037.7	1022.7	509.3	1022.7	509.3	1022.7	509.3	1022.7
Q8TQ04	GH13922p OS-Drosophila melanogaster OX-7227 GN=shb PE=1 SV=1	23.151	33	5	13	5	226	25.4	4.81	20.27	5	0	1335.3	449.8	881.5	1014	456.2	415.4	414.3	899
Q9VNH4	GH14121p OS-Drosophila melanogaster OX-7227 GN=DmelCG8043 PE=1 SV=1	42.82	21	5	13	5	348	39.5	8.68	46.86	5	0	1359.1	339.1	1352	1085.3	255.9	277.7	551.9	1130.2
E1Z9C3	GH11826p OS-Drosophila melanogaster OX-7227 GN=CG15224 PE=1 SV=1	25.976	2	2	2	2	35	26	1.52	1.52	2	0	124.9	493.7	326.4	493.7	326.4	493.7	326.4	493.7
Q8MRM6	GH15213p OS-Drosophila melanogaster OX-7227 GN=DmelCG12055 PE=1 SV=1	20.268	9	4	4	4	641	71.1	7.39	12.85	4	0	236.7	83.5	202.5	229	95.5	83.6	79.8	273.3
Q9VMU1	GH16729p OS-Drosophila melanogaster OX-7227 GN=DmelCG4230 PE=1 SV=1	16.688	15	3	4	4	323	36.6	5.55	11.4	3	0	356.8	157.6	425.3	391.7	111.9	148.4	203.1	289.9
Q8MRM8	GH16730p OS-Drosophila melanogaster OX-7227 GN=DmelCG4230 PE=1 SV=1	21.917	15	3	4	4	323	36.6	5.55	11.4	3	0	356.8	157.6	425.3	391.7	111.9	148.4	203.1	289.9
Q7K332	GH17625p OS-Drosophila melanogaster OX-7227 GN=CG3364 PE=2 SV=1	13.12	10	3	6	3	239	27.6	8.99	15.49	3	0	346.4	185.1	821.1	591.4	88.9	145.6	376	897.9
Q9VQ34	GH17801p OS-Drosophila melanogaster OX-7227 GN=DmelCG17660 PE=1 SV=3	8.888	8	2	2	2	536	60.1	5.99	3.88	2	0	52.7	54.4	131.9	113.5	20	31.9	55.6	60.3
Q9W127	GH17932p OS-Drosophila melanogaster OX-7227 GN=DmelCG3663 PE=1 SV=1	21.982	20	3	5	3	208	23.3	7.89	16.04	3	0	243.7	131.2	382.9	419.7	138.7	132.3	195.2	269.1
Q9W8W	GH18409p OS-Drosophila melanogaster OX-7227 GN=DmelCG8914 PE=1 SV=1	38.402	20	3	5	3	263	28.5	6.29	11.32	2	0	629.4	394.7	91.9	132.2	629.4	394.7	91.9	132.2
Q9VY15	GH19726p OS-Drosophila melanogaster OX-7227 GN=DmelCG1824 PE=1 SV=1	11.788	7	4	5	4	761	83.5	7.81	11.35	4	0	113.4	56.3	316.8	254	37.3	50.3	133.7	147.6
Q9VNA3	GH22173p OS-Drosophila melanogaster OX-7227 GN=DmelCG11999 PE=1 SV=1	20.44	22	4	5	4	216	23.6	6.8	14.08	4	0	246.7	108	175.3	368	64.5	79.9	366.7	478
Q9VBE6	GH2316p OS-Drosophila melanogaster OX-7227 GN=CG15224 PE=1 SV=1	13.944	12	2	3	3	509	44.9	2.84	11.84	2	0	91.6	47.8	121.6	138.4	42.9	49.9	52.2	111
Q9VIM6	GH22016p OS-Drosophila melanogaster OX-7227 GN=FBg0032858 PE=2 SV=1	6.216	5	2	3	3	459	53.1	5.45	7.67	2	0	124.7	60.3	84.5	60.3	44.5	25.2	41	101
Q9Y149	GH22139p OS-Drosophila melanogaster OX-7227 GN=Dmel_CG8026_FBR088611_mORF PE=2 SV=1	5.139	5	2	2	2	304	34.1	9.57	4.91	2	0	97.5	51.1	32.7	25.7	31.5	40.8	133.4	140
Q9S517	GH2309p OS-Drosophila melanogaster OX-7227 GN=DmelCG6129 PE=1 SV=1	15.29	14	3	4	4	253	24.3	6.07	11.64	4	0	150.9	142.6	142.6	142.6	142.6	142.6	142.6	142.6
Q9VEQ2	GH23451p OS-Drosophila melanogaster OX-7227 GN=DmelCG3878 PE=1 SV=1	16.586	16	3	4	3	322	32.7	7.05	11.16	3	0	157.7	74.8	190.4	247.5	65.1	72.7	100.5	143.8
Q7K1C0	GH23780p OS-Drosophila melanogaster OX-7227 GN=ND-15 PE=1 SV=1	7.916	22	3	3	3	101	12	7.72	7.72	3	0	260.7	135.3	528.2	396.3	96	103.2	235	274.5
Q9W245	GH24245p OS-Drosophila melanogaster OX-7227 GN=DmelCG4610 PE=2 SV=1	48.071	19	10	13	10	681	73.6	8.5	46.72	10	0	988.1	498.4	1171.2	944.3	355.3	406.8	533.4	512.3
Q8T0L3	GH24511p OS-Drosophila melanogaster OX-7227 GN=Hsp1 PE=1 SV=1	38.402	9	12	7	11	191	130.7	5.29	35.67	9	0	1963.9	1572.6	1945.7	1358.9	1349.5	1028	1105.1	0
Q9VQ30	GH25379p OS-Drosophila melanogaster OX-7227 GN=Jafra2 PE=1 SV=1	16.908	12	3	7	3	247	26.7	8.8	20.07	3	0	63.7	137.6	1524.5	1784.3	92.5	103.2	582.6	630.6
Q9VK60	GH25425p OS-Drosophila melanogaster OX-7227 GN=DmelCG618																			

A1V3J6	Heterogeneous nuclear ribonucleoprotein at 98Dc, isoform F OS-Drosophila melanogaster OX=7227 GN-Hrt	41.857	26	6	19	5	361	38.5	9.16	61.98	6	1	4217.3	1480.8	2491.2	2486.6	1597.4	1477.8	1307.7	2054	
F1J3N7	Heterogeneous nuclear ribonucleoprotein K, isoform E OS-Drosophila melanogaster OX=7227 GN-HrNP-K	55.992	19	9	15	3	493	49.8	4.65	48.3	9	1	1526	707.2	1252.1	1308	616.6	745.1	734.6	1741	
Q8IQX8	Histone RNA synthetase, isoform D OS-Drosophila melanogaster OX=7227 GN-HRS PE=1 SV=2	10.577	21	10	16	10	564	62.3	7.47	53.85	10	0	1535.5	716.4	2771.2	2506.8	1387.2	604.6	1179.5	1663.3	
Q9W1A9	Histone acetyltransferase OS-Drosophila melanogaster OX=7227 GN-enok PE=1 SV=2	10.574	1	2	2	2	2291	254.5	8.43	7.44	2	0	320	115.1	202	240.3	137.5	118.9	109.3	164.6	
Q0K183	Histone acetyltransferase type B catalytic subunit OS-Drosophila melanogaster OX=7227 GN-Hat1 PE=1 SV	14.108	12	4	4	4	405	47.9	6.73	10.87	4	0	1062.7	403	517.5	558.2	411.7	342.1	275.6	489	
Q9VYF3	Histone acetyltransferase OS-Drosophila melanogaster OX=7227 GN-Hat2 PE=1 SV=3	15.252	11	1	1	1	1252	124.1	10.16	10.16	1	0	369.3	136.1	246	193.5	146.3	195.7	195.7	363	
Q94517	Histone deacetylase Rpd3 OS-Drosophila melanogaster OX=7227 GN-Rpd3 PE=1 SV=2	19.588	8	3	4	3	521	58.3	5.76	16.81	3	0	392.6	107	146.6	189.6	128.4	96.1	79.3	119.8	
Q4ABD8	Histone H1 OS-Drosophila melanogaster OX=7227 GN-Ht1 CG33807 PE=3 SV=1	3.834	5	2	3	2	256	26.3	10.49	7.94	2	0	1404	357.6	347.5	403.4	532	686.6	340.4	635	
4R4B27	Histone H2A OS-Drosophila melanogaster OX=7227 GN-H2A PE=3 SV=1	13.413	41	4	4	4	124	13.4	13.4	1840.2	41	0	124	13.4	1840.2	41	13.4	1840.2	41	13.4	
ADA04KH25	Histone H2A OS-Drosophila melanogaster OX=7227 GN-H2aV PE=3 SV=1	16.494	27	5	10	4	216	15	10.24	21.03	5	0	1404	696.1	696.1	700.7	1136	927.2	630.5	1203.1	
P02283	Histone H2B OS-Drosophila melanogaster OX=7227 GN-H2B PE=1 SV=2	54.666	42	7	116	7	123	137	10.35	280.04	7	0	3671.7	908.4	1303.6	1894.1	1397.3	1976.1	1179.9	5885.2	
Q4HL66	Histone H3 OS-Drosophila melanogaster OX=7227 GN-H3a3 PE=1 SV=1	11.127	3	1	1	1	11	11.27	11.27	11.27	1	0	11.27	11.27	11.27	11.27	11.27	11.27	11.27	11.27	
P84240	Histone H4 OS-Drosophila melanogaster OX=7227 GN-H4 PE=1 SV=1	15.205	37	5	28	5	103	11.4	11.36	47.73	5	0	3271.2	1132.2	1132.2	1132.2	1332.1	1956.1	1170.6	7408.9	
Q9VNM3	Histone PARylation factor OS-Drosophila melanogaster OX=7227 GN-CG1218 PE=1 SV=2	14.896	11	4	5	4	449	51.7	10.33	10.44	4	0	591.1	276.7	686.8	575.1	224.3	232	316.6	982.9	
Q32KD2	Histone-lysine N-methyltransferase eggless OS-Drosophila melanogaster OX=7227 GN-egg PE=1 SV=1	13.934	3	2	2	2	1262	141.9	5.49	10.03	2	0	591.1	296	39.9	57.9	23.4	25.8	29	20.6	
Q1VW1	HL07669 OS-Drosophila melanogaster OX=7227 GN-RpL18 PE=2 SV=1	7.341	10	2	2	2	186	21.2	9.29	5.56	2	0	1484	71.8	311.5	260.4	42	60.5	124.2	246.7	
Q9LV70	HL08109 OS-Drosophila melanogaster OX=7227 GN-yfp2 PE=1 SV=1	54.393	22	5	33	5	398	41.6	8.51	97.37	5	0	738.9	403.8	1116.7	947.6	328.4	395.5	555.7	699.7	
ADA04LGS6	HMG protein Z, isoform C OS-Drosophila melanogaster OX=7227 GN-HmgZ PE=4 SV=1	12.533	18	2	5	1	111	12.6	29.9	17.47	2	0	1359.4	391.3	417	417.4	492.9	453.3	296.2	428.6	
D2NJK9	Hov60L, isoform B OS-Drosophila melanogaster OX=7227 GN-hov6 PE=1 SV=1	14.773	16	2	3	2	127	7.99	10.81	10.81	2	0	618.5	297.4	314.9	350.1	301.6	252.4	179.1	194.1	
ADA04LGS6	Holoacetyltransferase, isoform D OS-Drosophila melanogaster OX=7227 GN-Hcs PE=1 SV=1	8.873	4	2	2	2	999	110.9	7.2	6.77	2	0	23.9	13.2	39.2	13.1	20	15.2	35.5	5	
P13709	Homoecy protein female sterile OS-Drosophila melanogaster OX=7227 GN-Hfs1 PE=1 SV=2	26.626	7	7	9	7	2038	205.2	9.16	18.76	7	0	621.7	202.8	334.1	368.6	223.1	226.8	202.4	385.1	
Q96807	Homer OS-Drosophila melanogaster OX=7227 GN-Homer PE=1 SV=1	4.901	4	2	2	2	394	42.7	7.49	4.91	2	0	118.8	46.4	109.8	113.8	44.9	75.8	60.2	80.2	
Q9V4C8	Host cell factor OS-Drosophila melanogaster OX=7227 GN-Hcf PE=1 SV=2	29.953	4	5	5	5	1500	160.1	7.68	30.02	5	0	1165.1	490.4	644.1	781.9	469.7	544.2	405.9	490.6	
MPG82	HP1 and insulator partner protein 1, isoform B OS-Drosophila melanogaster OX=7227 GN-HIPPI1 PE=1 SV=2	29.784	10	6	7	6	924	99.7	6.89	24.32	6	0	1269.3	508.4	610.1	546.1	475	579	403.7	387.5	
EQD63	Hsc70p70-interacting protein related, isoform B OS-Drosophila melanogaster OX=7227 GN-HIPR PE=4 SV	22.268	10	4	4	4	377	41	5.35	14.46	4	0	202.5	85.9	113.2	88.8	69.1	62.1	62.5	38.8	
Q9V1C1	Hsc70C, isoform B OS-Drosophila melanogaster OX=7227 GN-Hsc70C PE=1 SV=1	46.493	13	10	16	10	604	88.4	5.43	47.21	10	0	2442.5	1005.7	1584.9	2039.2	837.2	897.9	869.8	1613.3	
Q24Z76	Hsp90 co-chaperone Cdc37 OS-Drosophila melanogaster OX=7227 GN-Cdc37 PE=1 SV=1	28.858	18	5	7	5	389	45.1	5.06	24	5	0	928.8	411.2	759.3	735.7	351.4	416.6	404.5	457.7	
ADA04K7A5	Hsp70, isoform B OS-Drosophila melanogaster OX=7227 GN-Hsp70 PE=1 SV=1	41.211	14	6	10	6	789	81.5	7.24	40.36	6	0	247.6	142	291.1	350.9	148.5	155	207.7	299.1	
ADA1	Hsp90 domain OS-Drosophila melanogaster OX=7227 GN-Hsp90 PE=1 SV=1	9.086	1	2	2	2	688	52.4	5.77	196.1	2	0	629.6	236.2	414.7	421.3	221.5	221.5	221.5	221.5	
ADA04LJ26	Huerialactin disc, isoform B OS-Drosophila melanogaster OX=7227 GN-Hyd PE=1 SV=1	13.161	1	3	3	3	2387	318.9	5.96	8.73	3	0	425.6	197.8	227.3	229.1	147.1	150.7	105.9	128.3	
Q9VH11	Hyalurase OS-Drosophila melanogaster OX=7227 GN-hy PE=2 SV=1	6.622	4	2	2	2	538	61.3	9.63	3.28	2	0	212	107.4	171.5	166	88.5	112.7	105.5	78.3	
Q9V455	Importin subunit alpha OS-Drosophila melanogaster OX=7227 GN-Importin-alpha3 PE=1 SV=1	6.627	1	1	1	1	614	57	10.66	10.66	1	0	409.7	142	109.8	174	109.8	174	109.8	174	
PS2295	Importin subunit alpha OS-Drosophila melanogaster OX=7227 GN-PE=1 SV=2	40.775	19	5	8	5	522	57.8	35.5	35.66	5	0	3719	128.6	281.2	337.7	145.6	140.5	127.5	259.8	
Q77460	Inorganic pyrophosphatase OS-Drosophila melanogaster OX=7227 GN-Nuf38 PE=1 SV=1	22.749	12	3	8	3	338	37.9	7.01	27.91	3	0	1395.1	674.8	1373.3	1428.8	527.1	583.3	587.4	802.4	
Q9VW77	Inosine triphosphatase phosphatase OS-Drosophila melanogaster OX=7227 GN-CG8891 PE=2 SV=1	14.684	14	2	4	2	191	21.4	6.92	12.98	2	0	1814.1	98.3	280.5	275.5	102.6	105.4	115.7	208.3	
Q9V477	Inositol 3-phosphatase OS-Drosophila melanogaster OX=7227 GN-InsP3 PE=1 SV=1	34.941	11	4	11	4	428	42.7	11.47	41.57	4	0	1343.9	577	1039.3	1039.3	471.3	685	460	685	
Q9VH65	Insulator binding factor 1, isoform A OS-Drosophila melanogaster OX=7227 GN-Ibf1 PE=1 SV=1	32.856	26	7	8	7	242	27.7	6.44	25.83	7	0	2428.7	725.2	721.1	1004	915.4	1186.6	620.8	924	
Q9VW77	Insulator binding factor 2 OS-Drosophila melanogaster OX=7227 GN-Ibf2 PE=1 SV=1	19.414	23	3	4	3	195	21.9	8.03	18.24	3	0	798.3	292.6	247.5	277.1	286.6	321.4	202.5	215.6	
Q2Z817	Insulin-like growth factor receptor OS-Drosophila melanogaster OX=7227 GN-IGF1R PE=1 SV=1	16.133	11	3	3	3	990	112.6	7.68	7.68	3	0	187.1	90.6	126.78	126.78	126.78	126.78	126.78	126.78	
ADA04U	IP06021p OS-Drosophila melanogaster OX=7227 GN=DmelCG10375 PE=2 SV=1	7.625	12	2	2	2	200	19.4	9.64	5.27	2	0	374.2	169.7	294.8	263.7	159.2	159.2	145.9	197.1	
Q95944	IP07454p OS-Drosophila melanogaster OX=7227 GN=DmelCG462 PE=2 SV=1	11.854	15	2	5	2	164	22.8	9.52	13.14	2	0	95.4	68.7	180.3	172	64.8	75.4	105.8	119	
Q9V4V9	IP07550 OS-Drosophila melanogaster OX=7227 GN=DmelCG10375 PE=2 SV=1	16.474	20	2	2	2	262	25.8	10.42	15.52	2	0	165.2	101.9	293.3	289.1	90.9	107.4	117.6	170.8	
Q9V5V0	IP06855 OS-Drosophila melanogaster OX=7227 GN=DmelCG14695 PE=1 SV=1	7.132	12	2	2	2	289	33.5	6.93	4.9	2	0	107.9	293.3	289.1	90.9	107.4	117.6	170.8	170.8	
Q9VEB1	IP06555 OS-Drosophila melanogaster OX=7227 GN=MhzA PE=1 SV=1	56.314	30	9	38	3	936	35.3	9.11	114.21	9	0	3455.3	1779	6953	5338.1	1100.1	1400.2	2559	6506.8	
Q9W19	IP09724p OS-Drosophila melanogaster OX=7227 GN=DmelCG15877 PE=1 SV=1	13.633	14	4	5	4	277	32	9.35	12.82	4	0	929.8	411.6	453	607	354.8	493.2	287.3	320.3	
Q9CQ70	IP09619 OS-Drosophila melanogaster OX=7227 GN=DmelCG15602 PE=1 SV=1	10.942	1	1	1	1	196	19.6	19.6	19.6	1	0	27.1	27.1	27.1	27.1	27.1	27.1	27.1	27.1	
Q4V3Z5	IP10727p OS-Drosophila melanogaster OX=7227 GN=DmelCG11788 PE=2 SV=1	22.773	13	3	3	3	425	48.8	5.11	12.99	3	0	691.8	361.9	350.5	350.5	139.5	108.2	69.8	69.8	
Q9VB17	IP11341p OS-Drosophila melanogaster OX=7227 GN=DmelCG561 PE=2 SV=1	21.929	21	7	8	7	326	35.6	7.01	17.79	7	0	788.7	397	1484.1	1073.2	238.1	284.1	613.3	670.5	
Q9VWC1	IP13211 OS-Drosophila melanogaster OX=7227 GN=IP13211 PE=1 SV=1	10.942	1	1	1	1	196	19.6	19.6	19.6	1	0	40.9	40.9	40.9	40.9	40.9	40.9	40.9	40.9	
IP4836p	IP14836p OS-Drosophila melanogaster OX=7227 GN=PfbA PE=1 SV=1	51.487	15	5	13	13	1	273	31.2	10.29	45.5	5	0	249.5	84.2	212.9	188	83.2	110.7	155.4	120.2
Q9VWF7	IP15825 OS-Drosophila melanogaster OX=7227 GN=Stom2 PE=1 SV=2	62.39	25	10	25	10	366	40.5	8.84	85.6	10	0	1517.3	727	2787.3	1984.1	569.7	748.2	1231.1	2175.5	
Q9VW98	IP16409 OS-Drosophila melanogaster OX=7227 GN=Stom2 PE=1 SV=2	22.416	13	3	3	3	439	43.9	38	38	3	0	100	130	130	130	130	130	130	130	
Q9VW1F	IP16805 OS-Drosophila melanogaster OX=7227 GN=RPL7A PE=1 SV=2	5.916	10	2	3	2	257	29.1	10.1	9.9	2	0	1242.8	457.5	491.6	436.9	501.6	559.1	328.5	281.9	
Q9LV77	IP17315 OS-Drosophila melanogaster OX=7227 GN=RPL36A PE=1 SV=2	3.561	12	2	2	2	104	12.5	10.8	2.29	2	0	325.4	139.5	250.2	223.2	90.2	173.4	252.2	109.5	
Q9W958	IP18235 OS-Drosophila melanogaster OX=7227 GN=RPL17 PE=1 SV=1	33.101	43	8	16	8	176	20.9	9.95	40.94	8	0	1008.2	509.7	2047.5	1683.3	368.3	500.1	772.2	1738.8	
Q9V5C6	IP18305 OS-Drosophila melanogaster OX=7227 GN=CG3849B PE=1 SV=1	11.918	16	5	2	2	49	32	8.24	12.07	2	0	1092	564.9	926.5	1101.3	438.4	532.2	222.8	716.2	
Q9VCV4	Iron regulatory protein 1A OS-Drosophila melanogaster OX=7227 GN-Irp-1A PE=1 SV=1	12.343	4	3	4	3	102	98.7	5.74	7.74	3	0	602.6	328.7	346	356.7	223.6	291	212.7	256	
Q9VZ23	Iron regulatory protein 1B OS-Drosophila melanogaster OX=7227 GN-Irp-1B PE=1 SV=1	13.248	4																		

Q9VP57	LD1904p OS=	Drosophila melanogaster OX7227	GN-pzg PE=1 SV=1	76.639	14	7	17	4	7	996	105	489	74.52	7	0	2535.6	850.5	1010.6	935.5	839.5	1148	837.3	622	
Q9VW69	LD1545p OS=	Drosophila melanogaster OX7227	GN-GDI PE=1 SV=1	12.863	23	1	1	1	1	201	23	44	9.72	4	0	5374	216.8	246.9	213.6	218.4	190.7	236	238.4	
QKZ64	LD1826p OS=	Drosophila melanogaster OX7227	GN-DmCG08569 PE=2 SV=1	5.786	3	2	2	2	2	608	68.8	8.51	4.1	2	0	12042	375.9	491.4	589.8	442.5	503.9	305.8	437.8	
Q9VUE5	LD1796z OS=	Drosophila melanogaster OX7227	GN-tsw1 PE=1 SV=1	39.302	12	9	10	9	10	1037	112.8	39.9	35.18	9	0	10787	467.1	688.4	717.5	417.7	558.1	397.1	647.6	
Q8SWM9	LD18126p OS=	Drosophila melanogaster OX7227	GN-EG-170111.2 PE=1 SV=1	23.427	7	2	4	2	4	632	75.7	9.38	17.71	2	0	12.9	4.9	27.5	16.8	4.5	3.4	11.6	7.5	
Q9VK20	LD18447p OS=	Drosophila melanogaster OX7227	GN-CO181 PE=1 SV=1	23.982	10	6	10	6	10	2392	146.1	6.3	28.3	2	0	142.6	110.6	29.2	6.2	110.6	81.9	291.2	302.8	
QYK110	LD18744p OS=	Drosophila melanogaster OX7227	GN-Delta PE=1 SV=1	18.977	10	5	6	5	6	694	69.2	9.17	17.47	5	0	758.2	317.4	479.9	961	247.2	289	459.6		
Q9VIL2	LD19544p OS=	Drosophila melanogaster OX7227	GN-DmCG02608 PE=1 SV=1	8.703	9	2	3	2	3	255	29.1	5.99	9.93	2	0	2187	82.6	122.8	183.5	81.4	84.5	81.9	118.6	
Q9VIT5	LD19813p OS=	Drosophila melanogaster OX7227	GN-P1 PE=1 SV=1	24.112	16	9	12	9	12	196	16.3	2.9	12.3	2	0	183.1	96.2	129.2	145.8	105.2	113.8	106.8	138.8	
QYVT2	LD20590p OS=	Drosophila melanogaster OX7227	GN-vtvs PE=1 SV=1	24.441	16	5	9	5	9	591	44.8	5.81	30.9	5	0	9142	342.2	589.3	458.4	364.6	450	437.5	283.8	
QKZ31	LD20635p OS=	Drosophila melanogaster OX7227	GN-CYC1 PE=1 SV=1	8.186	4	2	3	2	3	517	58.9	8.13	6.07	2	0	288.5	150.7	171.6	190.3	135.5	13.3	93.3	86	
QYVY1	LD1074p OS=	Drosophila melanogaster OX7227	GN-DmCG44 PE=1 SV=1	18.074	4	4	4	4	4	609	56.3	5.07	23.4	1	0	142.6	110.6	29.2	6.2	110.6	81.9	291.2	302.8	
Q8T02	LD21412p OS=	Drosophila melanogaster OX7227	GN-DmCG4282 PE=1 SV=1	13.556	3	2	2	2	2	652	75.2	7.34	9.36	2	0	10.98	45.8	90.4	91.7	45.8	42	53.3	58.4	
Q9W17	LD21876p OS=	Drosophila melanogaster OX7227	GN-Nap1 PE=1 SV=1	10.965	9	2	4	2	4	270	42.7	4.79	18.15	2	0	522	245.1	630.4	624.1	238.9	268.5	255	344.5	
Q9W5X0	LD21953p OS=	Drosophila melanogaster OX7227	GN-Rab35 PE=1 SV=1	10.095	10	2	5	2	5	31	20.1	2.8	8.54	10	0	103.8	63.9	188.6	62.6	57.7	58.8	89.6	85.1	
Q8MOJ5	LD22033p OS=	Drosophila melanogaster OX7227	GN-CO181 PE=1 SV=1	5.112	2	2	2	2	2	524	4.2	5.72	5.2	2	0	33.3	15.1	4	379.8	152.9	121.3	135.2	302.8	
QYKUA4	LD22577p OS=	Drosophila melanogaster OX7227	GN-Uba2 PE=1 SV=1	12.37	6	4	5	4	5	400	77.6	5.02	12.91	4	0	1086.9	572	493.3	494.6	471	436.2	300.9	261.4	
Q9VLX2	LD22651p OS=	Drosophila melanogaster OX7227	GN-DmCG1154 PE=1 SV=1	16.054	6	3	3	3	3	861	95.9	6.1	8.35	3	0	55.6	26.1	57.7	55.6	23.3	29.6	29.2	55.7	
Q9VL91	LD23102z OS=	Drosophila melanogaster OX7227	GN-F50C PE=1 SV=2	10.708	3	2	3	2	3	777	78.3	8.13	10.43	2	0	680.8	286.6	334.2	401.3	259.3	307.1	293.6	232.2	
Q9WZM0	LD23155p OS=	Drosophila melanogaster OX7227	GN-Rpn-5 PE=1 SV=2	20.985	6	2	3	2	3	647	74.9	5.38	12.27	2	0	26.6	94.2	193.5	187.3	99.8	191.1	186.4	406.4	
Q9VCF8	LD233561p OS=	Drosophila melanogaster OX7227	GN-anon-W00118547_306 PE=1 SV=1	10.557	7	2	5	2	5	271	41.8	5.62	17.96	2	0	6439.9	2462.5	3255.3	2943.2	2325.8	2526.2	2033.4	1734.9	
Q9V69	LD23647p OS=	Drosophila melanogaster OX7227	GN-DmCG05787 PE=1 SV=2	16.079	16	10	22	10	22	10	950	100.2	9.74	87.44	10	0	469.6	173	283.6	331.4	210.9	207.3	163.6	351.8
Q9VAA9	LD23804p OS=	Drosophila melanogaster OX7227	GN-DmCG07946 PE=1 SV=1	35.254	18	6	11	6	11	6	475	52.8	8.18	29.03	6	0	469.6	173	283.6	331.4	210.9	207.3	163.6	351.8
QYKAT8	LD23858p OS=	Drosophila melanogaster OX7227	GN-FBn 33734 PE=1 SV=1	18.209	6	2	7	2	7	458	52.4	8.06	28.75	2	0	344.8	168.8	641.4	638.1	209	431.8	468.3	408	
Q9VFW7	LD23875p OS=	Drosophila melanogaster OX7227	GN-DmCG10565 PE=1 SV=1	14.73	7	4	5	4	5	4	646	73.6	8.97	17.19	4	0	387.7	216.8	421.3	459.6	151.2	238.5	235.3	241.4
Q9VY6	LD23884p OS=	Drosophila melanogaster OX7227	GN-Coop PE=1 SV=2	98.6	31	17	26	17	26	14	681	74.4	8.18	78.43	17	0	149.1	80.9	284.3	269.17	599.1	766.8	1372.5	1745.8
Q9W9N9	LD24105p OS=	Drosophila melanogaster OX7227	GN-DmCG1032 PE=1 SV=1	46.733	17	4	13	4	13	4	410	43.4	8.68	52.98	4	0	1037.2	549.4	2002.1	1654.2	1654.2	473.3	895.1	1714
QYJR8	LD24265p OS=	Drosophila melanogaster OX7227	GN-Ech1 PE=1 SV=1	7.993	39	9	23	9	23	9	295	31.6	8.63	70.83	9	0	1168.5	669.6	2665.5	1996.5	584	616.6	1228	1961.2
QY747	LD24311p OS=	Drosophila melanogaster OX7227	GN-DmCG4313 PE=1 SV=1	10.364	12	2	9	2	9	106	45.7	6.86	27.82	2	0	60.3	1740	499.6	499.6	499.6	499.6	499.6	499.6	499.6
Q9W0X3	LD24657p OS=	Drosophila melanogaster OX7227	GN-Jhbp29 PE=1 SV=1	3.194	9	2	2	2	2	2	303	30.3	6.81	40.66	2	0	168.5	76	248.6	265.7	55.2	65.2	107.5	176.7
Q9VYQ9	LD24662p OS=	Drosophila melanogaster OX7227	GN-Tangp4 PE=1 SV=1	13.145	8	2	2	2	2	482	52.7	9.31	7.79	2	0	378.4	131.9	231.8	238.1	139.9	124.3	134.1	133	
LDV9V9	LD24663p OS=	Drosophila melanogaster OX7227	GN-DmCG02718 PE=1 SV=1	25.029	10	4	4	4	4	229	16.8	1.99	80.19	4	0	1576	608.7	1107	688.7	1107	688.7	823.8	816.8	
QYJH6	LD24669p OS=	Drosophila melanogaster OX7227	GN-DmCG09436 PE=1 SV=1	6.024	5	2	2	2	2	311	35.4	6.76	4.88	2	0	1103.3	496.6	605.2	638.4	404	400	450.5	339	
Q9VOK5	LD24714p OS=	Drosophila melanogaster OX7227	GN-DmCG03542 PE=1 SV=1	6.028	3	2	2	2	2	806	91.3	8.84	3.81	2	0	348.8	120.9	167.5	197.2	124.3	150.2	104.8	207.4	
Q9VJD4	LD24719p OS=	Drosophila melanogaster OX7227	GN-Sgt PE=1 SV=1	20.333	8	3	3	3	3	331	36.2	4.64	11.79	3	0	300.2	392.7	741.5	589.7	294.7	372.1	451.5	243.2	
Q9VYV3	LD24737p OS=	Drosophila melanogaster OX7227	GN-Ub190 PE=1 SV=2	9.198	9	3	3	3	3	1222	150.0	1.84	2.84	3	0	865.2	395.1	586.9	586.9	351.8	392.7	392.7	392.7	
Q9V3E7	LD24793p OS=	Drosophila melanogaster OX7227	GN-Ref1 PE=1 SV=1	21.688	11	3	6	3	6	266	27.8	10.55	23.98	3	0	984.4	383.1	494.3	709.2	373	408.7	278	413.6	
Q9VK44	LD24832p OS=	Drosophila melanogaster OX7227	GN-Hfd2 PE=1 SV=1	7.85	2	2	2	2	2	1217	138.5	5.87	8.2	2	0	286.6	142.7	254.5	287.6	105.8	124.9	133.8	191.6	
Q9VW53	LD24833p OS=	Drosophila melanogaster OX7227	GN-DmCG038 PE=2 SV=1	245.063	10	6	10	6	10	480	43.6	8.63	27.82	6	0	405.3	135.1	255.1	255.1	151.2	151.2	151.2	151.2	
Q9VW90	LD25118p OS=	Drosophila melanogaster OX7227	GN-HmRpl37 PE=1 SV=1	30.274	21	8	28	8	28	8	408	45.7	9.52	41.74	8	0	836.3	370.8	1439.6	1201.3	274.3	303.5	595.9	1793.3
Q9VZL4	LD25661p OS=	Drosophila melanogaster OX7227	GN-ND30 PE=1 SV=1	57.676	35	9	22	9	22	9	265	30	7.84	67.17	9	0	1042.8	604.2	2480.2	1890.7	375.1	533.3	1021	1429.5
LDV9H8	LD25662p OS=	Drosophila melanogaster OX7227	GN-DmCG126 PE=1 SV=1	24.128	24	11	28	11	28	24	268	52.8	6.2	24.28	11	0	1062.8	362.4	2999.3	2999.3	1062.8	1062.8	1062.8	1062.8
Q9VZ3	LD25692p OS=	Drosophila melanogaster OX7227	GN-Q2370C PE=1 SV=1	13.085	4	4	4	4	4	894	102.8	6.52	11.29	4	0	1161.6	498	775.7	1022.8	496.5	493.5	417.6	671.6	
Q9VBP3	LD26447p OS=	Drosophila melanogaster OX7227	GN-tzn PE=1 SV=2	12.883	12	3	3	3	3	305	34.2	6.64	11.43	3	0	385.5	181.9	530.5	496.5	157.8	160.5	241.5	322.3	
Q9W35	LD26546p OS=	Drosophila melanogaster OX7227	GN-H1J0320 PE=1 SV=1	18.274	8	2	4	2	4	2	302	33	4.84	17.32	2	0	90.1	42.8	131.1	121.1	39.8	52.5	77.7	53.6
Q9VW33	LD26547p OS=	Drosophila melanogaster OX7227	GN-C40 PE=2 SV=1	17.176	12	2	9	2	9	322	37	7.08	48.6	4	0	136.6	110	111	111	48.6	48.6	48.6	48.6	
QYVT61	LD27033p OS=	Drosophila melanogaster OX7227	GN-DmCG08108 PE=1 SV=1	15.545	7	6	8	6	8	919	102.9	6.21	20.93	6	0	940	388.8	468.6	440.9	338.2	411.5	319.8	308.8	
QYK0W1	LD27406p OS=	Drosophila melanogaster OX7227	GN-DmCG08531 PE=1 SV=1	20.824	10	6	6	6	6	545	60.9	8.16	17.64	6	0	431.2	261.8	835.5	816.2	129.5	228.9	406.9	649.9	
LDVZ51	LD27421p OS=	Drosophila melanogaster OX7227	GN-DmCG1746 PE=1 SV=1	11.711	4	1	1	1	1	41	11.711	4.1	11.711	1	0	111.5	111.5	111.5	111.5	111.5	111.5	111.5	111.5	
Q9VAX8	LD27939p OS=	Drosophila melanogaster OX7227	GN-Snu114 PE=1 SV=1	37.158	7	7	10	7	10	7	975	110.6	5.03	29.6	7	0	1475.1	678.7	1158.6	1132.6	624.4	668.4	664.7	735.9
Q9VH74	LD29322p OS=	Drosophila melanogaster OX7227	GN-DmCG08507 PE=1 SV=1	20.008	9	4	7	4	7	4	379	44.6	8.15	21.08	4	0	417.1	157	1655.8	1538	81.3	81.3	27.2	693.3
LDV9L5	LD29323p OS=	Drosophila melanogaster OX7227	GN-DmCG08507 PE=1 SV=1	8.44	6	4	7	4	7	6	505	56.9	6.12	12.12	4	0	417.1	157	1655.8	1538	81.3	81.3	27.2	693.3
Q9VLE1	LD29835p OS=	Drosophila melanogaster OX7227	GN-Srp54 PE=1 SV=1	21.428	8	3	6	3	6	3	513	58.3	11.33	22.71	3	0	4328	201	314.9	344.3	183.5	223.6	174.8	255.4
Q9VQ1																								

MBP2J	Lethal (2) giant larvae, isoform K OS=Drosophila melanogaster OX=7227 GN=2jlg PE=4 SV=1	15,974	3	3	3	3	1093	119.7	6.11	10.96	3	0	364.3	189.8	464.6	573.3	167.1	187.4	238.7	310.1	
QSM4.S7	Lethal (2) giant larvae, isoform D OS=Drosophila melanogaster OX=7227 GN=2jlg PE=1 SV=1	15,974	3	3	3	3	1161	36.7	10.96	19.93	3	0	257.0	165.4	200.7	643.6	161.4	327.1	144.3	927.1	
QV10D	Lethal (2) giant larvae, isoform A OS=Drosophila melanogaster OX=7227 GN=2jlg4505 PE=1 SV=1	42,297	25	5	19	5	279	31.8	7.2	78.96	5	0	1622.7	883.6	2790.3	1674.3	663.6	818.4	1286.9	1602.3	
AA0A84K7M9	Lethal (2) tumorous imaginal discs, isoform D OS=Drosophila melanogaster OX=7227 GN=H2k PE=1 SV=1	148,039	33	14	37	1	514	55.6	9.1	152.27	14	15	3691.8	1840.3	6107.6	4653.2	1349.7	1708.7	2665	3769.5	
QZ6202	Ligierine OS=Drosophila melanogaster OX=7227 GN=hc PE=1 SV=1	10,851	12	4	5	4	334	38.2	6.39	9.75	4	0	292.7	125.2	237.2	258.8	134.1	136.8	115.6	222.2	
QV17C3	Red SH2 domain protein OS=Drosophila melanogaster OX=7227 GN=Lasp PE=1 SV=2	23,373	13	10	13	10	427	35.7	7.6	10.56	10	0	485.6	249.6	485.6	249.6	485.6	249.6	485.6	249.6	
AA0A84K7U5	Ligierine, isoform H OS=Drosophila melanogaster OX=7227 GN=lig PE=1 SV=2	84,429	13	10	13	10	1330	134.3	6.92	58.22	10	0	1321.1	601.9	1436.6	1329.6	614.1	855.9	691.4	926.0	
QJ1QW6	Lipoyl synthase, mitochondrial OS=Drosophila melanogaster OX=7227 GN=Lsp PE=2 SV=2	11,17	10	2	2	2	377	42.7	7.65	6.36	2	0	68.6	45.5	169.2	177.5	22.5	36.6	59.5	72.6	
MBP2R7	Lipoyl synthase, mitochondrial OS=Drosophila melanogaster OX=7227 GN=Lsp PE=1 SV=1	11,17	10	2	2	2	377	42.7	7.65	6.36	2	0	68.6	45.5	169.2	177.5	22.5	36.6	59.5	72.6	
MN9EVO	Little imaginal discs, isoform C OS=Drosophila melanogaster OX=7227 GN=Hk4 PE=1 SV=1	71,123	7	8	11	8	1838	203.9	6.62	43.88	8	0	606.5	260.9	472.2	509.5	274.3	311.7	262.3	367.6	
QV7K17	Lon protease homolog, mitochondrial OS=Drosophila melanogaster OX=7227 GN=Lon PE=1 SV=1	112,962	13	32	13	32	1024	115	7.59	109.4	13	0	1238	574.8	2091	1522.6	458.8	483	981.1	1484	
PE2800	Lon protease weight phosphotyrosine protein OS=Drosophila melanogaster OX=7227 GN=lp	115,115	11	4	15	4	155	44.9	10.7	15.42	11	0	449.0	600.4	246.2	170.4	180.4	190.4	140.4	180.4	
QV7K7L	LP1207p OS=Drosophila melanogaster OX=7227 GN=Tpct1 PE=1 SV=1	15,115	1	3	5	3	332	36.7	9.71	20.58	3	0	293.5	175.3	355.4	385.5	154.6	175.3	225	225	
QV9V69	LP03457p OS=Drosophila melanogaster OX=7227 GN=DmelCG5844 PE=1 SV=1	34,168	20	4	6	4	378	41.6	5.68	27	4	0	262.7	128.3	466	359.4	113.9	117.2	217.3	331	
QV9V05	LP04564p OS=Drosophila melanogaster OX=7227 GN=DmelCG5988 PE=1 SV=2	11,683	7	3	5	3	425	47.3	6.28	7.44	3	0	285.7	116.8	200.5	301	118.1	140.5	142.2	141	
QV9V56	LP04955p OS=Drosophila melanogaster OX=7227 GN=RpL20 PE=1 SV=1	16,541	4	2	9	4	150	24.1	10.56	17.62	4	0	574.8	279.9	933.8	837.5	223.9	270.2	414.8	833.1	
QV9EV3	LP07287p OS=Drosophila melanogaster OX=7227 GN=DmelCG14894 PE=1 SV=2	5,397	11	3	3	3	263	29.4	4.64	7.52	3	0	343.7	169.5	419.8	426.6	155.3	187.7	192.5	305.8	
QV9VW5	LP07359p OS=Drosophila melanogaster OX=7227 GN=DmelCG5355 PE=1 SV=2	47,376	20	10	17	10	796	86.3	6.19	57.16	10	0	1408.6	663.5	1353.8	1103.3	515.7	576.7	626.4	702.5	
QV9V74	LP0802p OS=Drosophila melanogaster OX=7227 GN=Rpnp1 PE=1 SV=1	9,359	4	2	2	2	1018	114.3	4.87	4.29	2	0	12.2	9.2	14.6	20.3	5.1	7.8	12	15.8	
QV9KZ8	LP08774p OS=Drosophila melanogaster OX=7227 GN=Up14 PE=1 SV=1	17,769	6	2	3	2	475	53.7	6.25	11.12	2	0	174.2	70.4	151.4	211.6	57.4	68.7	73.7	121.9	
QV9V79	LP09089p OS=Drosophila melanogaster OX=7227 GN=DmelCG11095 PE=1 SV=1	18,637	14	3	7	3	283	32	9.35	23.29	3	0	278.5	152.1	512.5	520.4	205.9	196.9	249.3	303.5	
QV9V80	LP10523p OS=Drosophila melanogaster OX=7227 GN=RpS105 PE=1 SV=1	14,945	26	5	9	5	204	23.2	8.68	21.54	3	0	802.5	468.2	1613.7	1152.2	362.2	484.2	861.7	687.5	
QV9W01	LP10861p OS=Drosophila melanogaster OX=7227 GN=DmelCG13887 PE=1 SV=1	31,196	17	5	9	5	228	26.1	9.32	34.33	5	0	713.8	441.3	1088.1	968.8	241.8	493.4	591.4	453.1	
QV9V01	LP20978p OS=Drosophila melanogaster OX=7227 GN=SeRS PE=1 SV=1	15,986	7	3	6	3	501	56.4	6.49	16.22	3	0	808.2	466.3	903.6	963.6	372	324	464.8	372.1	
QV9R90	LP21249p OS=Drosophila melanogaster OX=7227 GN=Pas PE=1 SV=1	54,134	12	14	18	14	1053	120.2	6.47	53.38	14	0	1801.3	927.1	1928.7	1912.3	684.4	815.8	913	1570.4	
E2QC23	LP20359p OS=Drosophila melanogaster OX=7227 GN=DmelCG7705 PE=2 SV=1	12,055	4	2	2	2	592	68.1	5.54	7.44	2	0	232.9	175.7	362.1	362.1	77.4	108.5	196.1	145.6	
E1JH52	Lysine (K)-specific demethylase 4B, isoform B OS=Drosophila melanogaster OX=7227 GN=Kdm8 PE=1 SV=1	10,109	5	2	2	2	590	66.4	7.46	7.13	2	0	771.5	371.1	441.9	531.6	322.4	366.1	238.6	260.5	
QV9VX0	Lysine ketoglutarate reductase/saccharopine dehydrogenase, isoform A OS=Drosophila melanogaster OX=7227 GN=Kds1 PE=1 SV=1	201,694	24	21	137	21	1928	103.1	6.79	397.33	21	0	5242.1	3569.6	11581.8	8995.8	1974.3	3064	4981	6302.1	
QV9V55	Lysine-specific prolyl 4-hydroxylase, isoform 1 OS=Drosophila melanogaster OX=7227 GN=LysP4 PE=1 SV=1	22,937	6	2	6	2	637	68.5	7.07	119.74	6	0	1138.7	615.9	1138.7	615.9	1138.7	615.9	1138.7	615.9	
AA0A84K8A5	Majungin, isoform B OS=Drosophila melanogaster OX=7227 GN=Mahj PE=4 SV=1	6,544	1	2	2	2	1544	172	5	6.09	2	0	419.5	196.1	372.5	438.9	175	183	190.5	197	
P02825	Major heat shock 70 kDa protein Aa OS=Drosophila melanogaster OX=7227 GN=Hsp70a PE=2 SV=3	43,771	10	5	12	10	642	70.1	5.77	28.76	10	0	554	25.5	96.7	106.8	18	23	46.1	75	
Q21183	Major heat shock 70 kDa protein Ab OS=Drosophila melanogaster OX=7227 GN=Hsp70a PE=2 SV=3	43,771	10	5	12	10	642	70.1	5.77	28.76	10	0	554	25.5	96.7	106.8	18	23	46.1	75	
QV9G32	Malic enzyme OS=Drosophila melanogaster OX=7227 GN=Me PE=1 SV=1	29,979	13	9	19	9	975	84.3	7.21	57.89	9	0	1111.5	539.8	1611.8	1449.4	439	460.7	739.9	864.6	
QV9B69	Malic enzyme OS=Drosophila melanogaster OX=7227 GN=Me-b PE=1 SV=1	85,937	13	39	13	39	13	617	68.6	6.71	126.21	13	0	2693.1	1336.8	4581.2	4037.4	1008.7	1044.3	1824.2	4253.6
QV9CA4	MED-Ric OS=Drosophila melanogaster OX=7227 GN=MBD-R2 PE=1 SV=2	28,004	4	4	7	4	1169	130.1	8.03	23.52	4	0	788.8	300.2	408.6	530.3	317.7	339.1	258.9	473.6	
QV9VJ0	MED-Ric OS=Drosophila melanogaster OX=7227 GN=MBD-R2 PE=1 SV=2	28,004	4	4	7	4	1169	130.1	8.03	23.52	4	0	788.8	300.2	408.6	530.3	317.7	339.1	258.9	473.6	
QV9V05	Mediator of RNA polymerase II transcription subunit 1 OS=Drosophila melanogaster OX=7227 GN=MD1 PE=1 SV=1	46,324	3	2	2	2	1475	149.4	9.33	10.49	2	0	759.7	398.2	1028.4	438.8	269.6	313.7	233.8	186.8	
AA0A84KF9E	Mediator of RNA polymerase II transcription subunit 1 OS=Drosophila melanogaster OX=7227 GN=MD1 PE=1 SV=1	46,324	3	2	2	2	1475	149.4	9.33	10.49	2	0	759.7	398.2	1028.4	438.8	269.6	313.7	233.8	186.8	
PE5152	Methionine aminopeptidase OS=Drosophila melanogaster OX=7227 GN=Met-2 PE=2 SV=1	12,932	5	10	10	10	2346	262.2	5.1	28.6	10	0	1241	484.2	847.2	1067.3	418.3	474.3	430.1	695.7	
QV9EJ0	Methionine aminopeptidase OS=Drosophila melanogaster OX=7227 GN=Met-2 PE=2 SV=1	12,932	5	10	10	10	2346	262.2	5.1	28.6	10	0	1241	484.2	847.2	1067.3	418.3	474.3	430.1	695.7	
QV9EJ0	Methionine aminopeptidase OS=Drosophila melanogaster OX=7227 GN=Met-2 PE=2 SV=1	12,932	5	10	10	10	2346	262.2	5.1	28.6	10	0	1241	484.2	847.2	1067.3	418.3	474.3	430.1	695.7	
QV9V77	Methionine aminopeptidase OS=Drosophila melanogaster OX=7227 GN=Met-2 PE=2 SV=1	12,932	5	10	10	10	2346	262.2	5.1	28.6	10	0	1241	484.2	847.2	1067.3	418.3	474.3	430.1	695.7	
QV9V77	Methionine aminopeptidase OS=Drosophila melanogaster OX=7227 GN=Met-2 PE=2 SV=1	12,932	5	10	10	10	2346	262.2	5.1	28.6	10	0	1241	484.2	847.2	1067.3	418.3	474.3	430.1	695.7	
QV9V77	Methionine aminopeptidase OS=Drosophila melanogaster OX=7227 GN=Met-2 PE=2 SV=1	12,932	5	10	10	10	2346	262.2	5.1	28.6	10	0	1241	484.2	847.2	1067.3	418.3	474.3	430.1	695.7	
QV9V77	Methionine aminopeptidase OS=Drosophila melanogaster OX=7227 GN=Met-2 PE=2 SV=1	12,932	5	10	10	10	2346	262.2	5.1	28.6	10	0	1241	484.2	847.2	1067.3	418.3	474.3	430.1	695.7	
QV9V77	Methionine aminopeptidase OS=Drosophila melanogaster OX=7227 GN=Met-2 PE=2 SV=1	12,932	5	10	10	10	2346	262.2	5.1	28.6	10	0	1241	484.2	847.2	1067.3	418.3	474.3	430.1	695.7	
QV9V77	Methionine aminopeptidase OS=Drosophila melanogaster OX=7227 GN=Met-2 PE=2 SV=1	12,932	5	10	10	10	2346	262.2	5.1	28.6	10	0	1241	484.2	847.2	1067.3	418.3	474.3	430.1	695.7	
QV9V77	Methionine aminopeptidase OS=Drosophila melanogaster OX=7227 GN=Met-2 PE=2 SV=1	12,932	5	10	10	10	2346	262.2	5.1	28.6	10	0	1241	484.2	847.2	1067.3	418.3	474.3	430.1	695.7	
QV9V77	Methionine aminopeptidase OS=Drosophila melanogaster OX=7227 GN=Met-2 PE=2 SV=1	12,932	5	10	10	10	2346	262.2	5.1	28.6	10	0	1241	484.2	847.2	1067.3	418.3	474.3	430.1	695.7	
QV9V77	Methionine aminopeptidase OS=Drosophila melanogaster OX=7227 GN=Met-2 PE=2 SV=1	12,932	5	10	10	10	2346	262.2	5.1	28.6	10	0	1241	484.2	847.2	1067.3	418.3	474.3	430.1	695.7	
QV9V77	Methionine aminopeptidase OS=Drosophila melanogaster OX=7227 GN=Met-2 PE=2 SV=1	12,932	5	10	10	10	2346	262.2	5.1	28.6	10	0	1241	484.2	847.2	1067.3	418.3	474.3	430.1	695.7	
QV9V77	Methionine aminopeptidase OS=Drosophila melanogaster OX=7227 GN=Met-2 PE=2 SV=1	12,932	5	10	10	10	2346	262.2	5.1	28.6	10	0	1241	484.2	847.2	1067.3	418.3	474.3	430.1	695.7	
QV9V77	Methionine aminopeptidase OS=Drosophila melanogaster OX=7227 GN=Met-2 PE=2 SV=1	12,932	5	10	10	10	2346	262.2	5.1	28.6	10	0	1241	484.2	847.2	1067.3	418.3	474.3	430.1	695.7	
QV9V77	Methionine aminopeptidase OS=Drosophila melanogaster OX=7227 GN=Met-2 PE=2 SV=1	12,932	5	10	10	10	2346	262.2	5.1	28.6	10	0	1241	484.2	847.2	1067.3	418.3	474.3	430.1	695.7	
QV9V77	Methionine aminopeptidase OS=Drosophila melanogaster OX=7227 GN=Met-2 PE=2 SV=1	12,932	5	10	10	10	2346	262.2	5.1	28.6	10	0	1241	484.2	847.2	1067.3	418.3	474.3	430.1	695.7	
QV9V77	Methionine aminopeptidase OS=Drosophila melanogaster OX=7227 GN=Met-2 PE=2 SV=1	12,932	5	10	10	10	2346	262.2	5.1	28.6	10	0	1241	484.2	847.2	1067.3	418.3	474.3	430.1	695.7	
QV9V77	M																				

Q8W125	NADH dehydrogenase [ubiquinone] 1 alpha subcomplex subunit 8 OS=Drosophila melanogaster OX=7227 GN=NDH12 PE=1 SV=1	17,365	25	2	9	2	175	19.8	6.87	42.63	2	0	208.2	110.5	409.1	333.6	81.4	104.2	177.9	365.1
Q8W127	NADH dehydrogenase [ubiquinone] 1 beta subcomplex subunit 6, mitochondrial OS=Drosophila melanogaster OX=7227 GN=NDH12 PE=1 SV=1	17,463	14	2	11	2	175	21.3	6.99	36.96	3	0	208.2	110.5	409.1	333.6	81.4	104.2	177.9	365.1
Q9VM3	NADH dehydrogenase [ubiquinone] 1, mitochondrial OS=Drosophila melanogaster OX=7227 GN=NDH12 PE=1 SV=1	51,848	15	6	12	6	474	51.8	8.47	39.31	6	0	1028.4	574.8	2395.5	1731.4	331.6	509.7	1144	1301.9
MPQC1	NADPH-cytochrome P450 reductase OS=Drosophila melanogaster OX=7227 GN=Cpr PE=1 SV=1	12,391	7	4	5	4	679	76.3	5.9	10.23	4	0	514.3	257.6	828	848	190.5	248.8	450.1	385.4
Q9V379	NADPH-dependent oxidoreductase, mitochondrial OS=Drosophila melanogaster OX=7227 GN=dae PE=2 SV=1	54,296	20	6	13	6	486	51.3	8.38	61.2	6	0	589.9	345	1344	1160.2	242.8	274.5	572.3	529.7
AD0484L61	Nucleic acid binding protein 2 OS=Drosophila melanogaster OX=7227 GN=Nup153 PE=1 SV=1	28,617	23	8	17	4	1917	231	6.51	14.74	4	0	392.9	173.7	292.7	315	146.1	196	205.6	130.8
I1Z988	NAT1, isoform D OS=Drosophila melanogaster OX=7227 GN=NAT1 PE=1 SV=1	55,115	6	7	10	7	1488	162.8	8.53	40.56	7	0	448.5	220.7	508.9	565.6	177.5	229.3	287.8	444.5
Q9VXB0	NECAP1 nuclear protein CG9133 OS=Drosophila melanogaster OX=7227 GN=CG9133 PE=2 SV=1	9,624	10	3	3	2	246	26.6	8.81	8.7	3	0	1166.7	407.6	556.7	703	366.1	371.9	311.8	613.6
AD0484L1F3	Negative elongation factor C OS=Drosophila melanogaster OX=7227 GN=NelfE PE=4 SV=1	30,850	6	4	6	3	280	31.8	4.77	6.36	2	0	1166.7	407.6	556.7	703	366.1	371.9	311.8	613.6
P92204	Negative elongation factor E OS=Drosophila melanogaster OX=7227 GN=NelfE PE=1 SV=1	9,263	9	2	2	2	280	31.8	4.77	6.36	2	0	163.7	71.5	103.6	110.5	68.9	103.5	61.6	81.9
Q9W201	Nejre, isoform B OS=Drosophila melanogaster OX=7227 GN=nej PE=1 SV=2	4,909	1	2	2	2	3276	340.5	8.69	4.67	2	0	433.1	207.2	243.2	286.2	162.3	180.3	166.1	124.8
Q9W176	Neuramin homologue OS=Drosophila melanogaster OX=7227 GN=Nup153 PE=2 SV=1	20,842	4	2	4	2	1570	169.7	6.81	12.79	2	0	142.8	60.8	66.2	67.2	21.9	35.1	34.1	41.4
Q9W320	Neurat conserved at 73EF, isoform F OS=Drosophila melanogaster OX=7227 GN=Nc73EF PE=1 SV=1	110,451	23	23	120	4	1017	113.6	9.99	317.05	23	21	5318.9	3046.6	9615.2	8510.6	2939.4	2535.9	4185.2	6421.9
ABJN16	Neural conserved at 73EF, isoform I OS=Drosophila melanogaster OX=7227 GN=Nc73EF PE=1 SV=1	102,544	20	21	112	2	1105	122.8	6.93	294.87	21	0	139.3	98.3	325.2	268.9	7	79.7	138.4	170.7
Q95Y196	Neu11, isoform I OS=Drosophila melanogaster OX=7227 GN=Nup153 PE=2 SV=1	26,131	12	2	5	2	283	31.3	5.4	14.74	2	0	139.3	98.3	325.2	268.9	7	79.7	138.4	170.7
AD0484F23	Nep16B protein OS=Drosophila melanogaster OX=7227 GN=Nep16B PE=1 SV=1	18,577	3	4	4	4	1987	232	6.51	14.74	4	0	392.9	173.7	292.7	315	146.1	196	205.6	130.8
Q76484	Nlrkase and fragile histidine triad fusion protein NlrHt OS=Drosophila melanogaster OX=7227 GN=NlrHt PE=1 SV=1	10,558	15	6	12	6	460	52.2	7.61	26.95	6	0	513.9	325.8	1073.8	978.2	81.6	282.3	471.7	605.3
Q9VFK4	NlrK1, isoform A OS=Drosophila melanogaster OX=7227 GN=NK1 PE=4 SV=2	30,454	3	2	3	2	721	78.9	7.59	9.92	2	0	216.6	108.1	129.7	158.9	81.4	83.6	76.4	93.6
MPF74	No catalytic temperature entrainment, isoform D OS=Drosophila melanogaster OX=7227 GN=ncote PE=1 SV=1	52,367	4	7	10	7	2305	9.25	36.49	7	0	967.4	504.7	1255	1319.9	348.3	512.4	755.1	521.2	
X2JFR1	No on or off transient A, isoform D OS=Drosophila melanogaster OX=7227 GN=nonA PE=1 SV=1	87,004	24	13	19	12	700	76.9	9.35	70.73	13	1	2312	935.9	1368.6	1530	920.6	1064.6	802.1	1077
QJNE1	Non-histone chromosomal protein Prod OS=Drosophila melanogaster OX=7227 GN=prod PE=1 SV=1	25,054	18	4	7	4	346	39.4	5.3	27.54	4	0	1867.7	717.7	752.3	657.6	779.1	1352.3	559.9	563.5
EZQD16	Non-specific lethal 1, isoform M OS=Drosophila melanogaster OX=7227 GN=nl1 PE=1 SV=1	17,978	4	4	4	4	1570	169.7	6.81	12.79	2	0	1529.9	537.1	649.2	827.2	612.2	543.4	435.1	558.3
MPFZ1	Nopp140, isoform E OS=Drosophila melanogaster OX=7227 GN=Nopp140 PE=1 SV=1	4,337	2	2	2	2	773	78.1	9.16	4.37	2	0	417.2	141.8	155.3	182.6	186.8	154.6	96	101.4
Q9VVK7	NUC81 OS=Drosophila melanogaster OX=7227 GN=NUC81 PE=1 SV=3	8,383	4	2	2	2	569	67.3	5.3	6.34	2	0	174	100.8	57.2	510.9	24	45.1	248.2	223
Q7K4N3	Nuclear cap-binding protein subunit 1 OS=Drosophila melanogaster OX=7227 GN=Cpb80 PE=1 SV=1	14,011	4	2	2	2	800	93.2	6.55	9.1	2	0	216.6	108.1	129.7	158.9	81.4	83.6	76.4	93.6
Q9V316	Nuclear cap-binding protein subunit 2 OS=Drosophila melanogaster OX=7227 GN=Cpb20 PE=1 SV=1	9,982	2	2	2	2	154	17.7	7.78	7.1	2	0	967.4	504.7	1255	1319.9	348.3	512.4	755.1	521.2
Q9VVA6	Nuclear migration protein NudC OS=Drosophila melanogaster OX=7227 GN=NudC PE=1 SV=2	12,845	9	3	4	3	332	37.8	5.64	14.39	3	0	559	272.1	514.5	483	200.4	146.9	319.9	240.2
Q9V466	Nuclear pore complex protein Nup107 OS=Drosophila melanogaster OX=7227 GN=Nup107 PE=1 SV=1	22,763	7	4	5	4	885	97.3	5.94	16.91	4	0	411.2	210.7	413	451.1	148.3	209	218.2	224.9
Q9V3C9	Nuclear pore complex protein Nup133 OS=Drosophila melanogaster OX=7227 GN=Nup133 PE=2 SV=1	9,982	2	3	3	3	183	19.5	8.99	8.2	2	0	101.4	54.6	61.6	67.2	21.9	35.1	34.1	41.4
Q9VXE6	Nuclear pore complex protein Nup153 OS=Drosophila melanogaster OX=7227 GN=Nup153 PE=1 SV=4	9,582	2	3	3	3	183	19.5	8.93	8.64	3	0	568.1	185.2	448.9	495.3	177	172	225.6	248.6
Q9V463	Nuclear pore complex protein Nup154 OS=Drosophila melanogaster OX=7227 GN=Nup154 PE=1 SV=1	3,241	1	2	3	2	1365	153.8	6.58	4.38	2	0	123.5	63.6	185.4	299.4	117.4	117.4	122	178
Q9V1V9	Nuclear pore complex protein Nup205 OS=Drosophila melanogaster OX=7227 GN=Nup205 PE=1 SV=1	19,058	2	2	2	2	2026	205.8	20.27	35.2	2	0	1423.3	65.9	148.4	161.3	59	84.4	14.3	19.6
Q7KQD8	Nuclear pore complex protein Nup50 OS=Drosophila melanogaster OX=7227 GN=Nup50 PE=1 SV=1	9,992	12	5	5	5	564	59.4	8.43	17.7	5	0	275.4	146.1	71.1	928.2	430.4	447.9	447.6	524.4
I1YK02	Nuclear pore complex protein Nup75 OS=Drosophila melanogaster OX=7227 GN=Nup75 PE=2 SV=1	11,583	4	2	4	2	688	76.8	6.05	13.26	2	0	115.9	37.1	83.2	92.5	37.3	48.9	59.5	65.9
Q9XZ06	Nuclear pore complex protein Nup93 OS=Drosophila melanogaster OX=7227 GN=Nup93 PE=1 SV=1	21,786	5	5	5	5	823	93.8	6.27	17.37	5	0	718.3	259.4	437.2	618.4	235.8	251.4	238.6	340
Q9VCH5	Nucleolar cap protein Ncap80 OS=Drosophila melanogaster OX=7227 GN=Ncap80 PE=1 SV=1	25,453	3	3	3	3	1052	110.7	5.10	19.17	3	0	92.5	47.1	51.0	52.1	19.6	22.4	19.6	20.6
Q9VBP9	Nuclear protein localization protein 4 homolog OS=Drosophila melanogaster OX=7227 GN=Npl4 PE=1 SV=3	13,889	8	4	4	4	652	73.3	7.24	10.16	4	0	805.2	457.1	1020.5	1040.3	359.1	423.7	518	563.6
Q9V819	Nuclear RNA export factor 1 OS=Drosophila melanogaster OX=7227 GN=Nra1 PE=1 SV=2	5,179	3	2	2	2	672	76.2	9	5.5	2	0	452.6	221	350.7	377.6	188.4	214.2	189.6	203.3
AD0484L9Y	Nucleolar protein 1 OS=Drosophila melanogaster OX=7227 GN=Npl1 PE=1 SV=1	14,491	1	1	1	1	952	75.3	7.22	11.88	1	0	1188.8	401.1	526.6	595.2	149.1	149.1	149.1	149.1
AD0484K24	Nucleosplasin, isoform B OS=Drosophila melanogaster OX=7227 GN=Nlp PE=4 SV=1	26,333	22	3	8	3	152	17	4.61	28.14	3	0	4148.6	1337.5	1372.6	1365.9	1401.7	1211.8	689.4	848.1
AD0484L12	Nucleoside diphosphate kinase OS=Drosophila melanogaster OX=7227 GN=Nwd PE=1 SV=1	19,783	17	2	4	2	153	17.2	8.12	13.48	2	0	744.1	391.8	626.6	968.8	259.5	320.7	312.2	548.2
Q9V1V2	Nucleoside diphosphate kinase 2, mitochondrial OS=Drosophila melanogaster OX=7227 GN=Nwd2 PE=2 SV=1	22,546	23	2	4	2	153	17.2	8.12	13.48	2	0	744.1	391.8	626.6	968.8	259.5	320.7	312.2	548.2
Q9VBV5	Nucleoside exchange factor Sll1 OS=Drosophila melanogaster OX=7227 GN=CG10420 PE=2 SV=1	6,136	6	2	2	2	429	47.9	5.33	9.72	2	0	151.2	97.1	176.1	841	38.1	67.7	276.5	256
E6PBV6	Obg-like ATPase 8 OS=Drosophila melanogaster OX=7227 GN=CG1354-RA PE=1 SV=1	7,993	3	4	4	3	397	44.9	6.71	9.96	3	0	202.6	88.4	180.9	222.1	72.3	82.7	89.4	129.4
AD0484L8F5	Optic ataxia 1, isoform C OS=Drosophila melanogaster OX=7227 GN=Opt1 PE=1 SV=1	97,19	21	19	34	19	499	111.5	8.59	105.07	19	4	1761.9	948.8	3929.6	3098.8	577.2	875.3	1726.1	3285.4
AD0484K4H	Optic ataxia 1, isoform D OS=Drosophila melanogaster OX=7227 GN=Opt1 PE=1 SV=1	5,912	13	9	9	9	331	33.1	6.46	6.81	9	0	80.2	35.8	80.2	163.3	20.1	20.1	20.1	20.1
Q24189	Origin recognition complex subunit 5 OS=Drosophila melanogaster OX=7227 GN=Orc5 PE=1 SV=1	9,042	5	2	2	2	460	52.1	6.55	5.88	2	0	17.9	10.1	18.4	20.1	9.9	11.1	9.9	11.1
Q9VW26	Ominthine aminotransferase, mitochondrial OS=Drosophila melanogaster OX=7227 GN=Oat PE=2 SV=1	31,576	20	7	15	7	431	47.3	7.05	38.53	7	0	670.3	486	1051.4	733.2	304.8	438.6	454.3	745.2
P23240	Omp-like protein OS=Drosophila melanogaster OX=7227 GN=Omp PE=1 SV=1	6,547	20	2	4	2	44	4.6	4.24	4.6	2	0	1077.4	458	1255	1058	167.8	167.8	167.8	167.8
I1ZAW9	Omp-like protein OS=Drosophila melanogaster OX=7227 GN=Omp PE=1 SV=1	6,547	20	2	4	2	44	4.6	4.24	4.6	2	0	1077.4	458	1255	1058	167.8	167.8	167.8	167.8
Q9V3D2	Oxygen-dependent coproporphyrinogen-III oxidase OS=Drosophila melanogaster OX=7227 GN=Coprox PE=1 SV=1	45,857	23	8	17	8	390	44.4	8.72	67.85	8	0	988	450.5	2185.5	1493.6	250.3	369.5	859.9	1074.7
AD0484L2D2	Oxylanthranilate 3-oxo-5-oxopropyltransferase OS=Drosophila melanogaster OX=7227 GN=Oxyl PE=1 SV=1	20,765	10	10	10	10	1066	107.6	10.27	103.69	10	0	1034.9	1028.9	1034.9	1034.9	1034.9	1034.9	1034.9	1034.9
I1ZAK8	Palmitoyl transferase OS=Drosophila melanogaster OX=7227 GN=Pap1 PE=1 SV=1	23,495	5	3	5	3	797	81.7	13.1	19.82	3	0	1332	492.4	694.9	728	533.3	499.6	424.5	430.4
Q7KZV5	Palmitoyl transferase OS=Drosophila melanogaster OX=7227 GN=DmelCG1407 PE=2 SV=1	3,339	4	2	2	2	338	37.9	7.59	4.66	2	0	204.5	142.4	423.6	421.8	61.7	119.7	121.1	173.8
Q9E3E5	Par1-1 OS=Drosophila melanogaster OX=7227 GN=Par1 PE=1 SV=1	13,491	3	2	3	2	1058	114.8	9.88	8.73	2	0	174.3	91.3	193.1	187.9	67.4	81.8	203.3	119.8
Q9K04	Par6, isoform A OS=Drosophila melanogaster OX=7227 GN=Par6 PE=1 SV=1	11,499	3	2	3	2	544	51.9	6.74	9.08	3	0	204.5	142.4	423.6	421.8	61.7	119.7	121.1	173.8
AD0484L06	Par6, isoform B OS=Drosophila melanogaster OX=7227 GN=Par6 PE=1 SV=1	11,499	3	2	3	2	544	51.9	6.74	9.08	3	0	204.5	142.4	423.6	421.8	61.7	119.7	121.1	173.8
Q7																				

QV6G9	RE35509p OS-Drosophila melanogaster OX=7227 GN=CG14730 PE=1 SV=4	23.346	5	6	6	6	1483	171.9	6.1	17.17	6	0	588.9	237.3	389.2	427.2	264.9	234.3	263.9	283.3
QV6H2	RE35510p OS-Drosophila melanogaster OX=7227 GN=HrPE=1 SV=1	23.346	11	3	3	3	241	27.7	6.44	7.59	3	0	24.6	14.4	25.8	37	25.3	29.5	29.5	14.4
QV5R7	RE41059p OS-Drosophila melanogaster OX=7227 GN=VaRS-n PE=2 SV=1	9.134	3	3	3	3	994	113	6.71	6.03	3	0	86.9	58.4	170.8	160.6	86.8	74.9	152.1	
Q81P7	RE44908p OS-Drosophila melanogaster OX=7227 GN=Rrp40 PE=1 SV=1	8.824	8	2	2	2	232	25	8.31	5.91	2	0	300.8	110.2	183	211	111.2	88.2	76.1	453.2
QV9V7	RE45108p OS-Drosophila melanogaster OX=7227 GN=DmelCG4611 PE=1 SV=1	16.623	5	2	2	2	703	79.9	8.98	8.4	2	0	73.3	41.5	110.4	125.4	38.5	54.3	62	105.2
QV9L6	RE45308p OS-Drosophila melanogaster OX=7227 GN=DmelCG3676 PE=2 SV=1	3.156	3	1	1	1	173	31.7	6.74	6.74	1	0	287.9	100.4	346.6	287.9	100.4	346.6	287.9	100.4
QV9V8	RE47309p OS-Drosophila melanogaster OX=7227 GN=Rrp1-ike PE=2 SV=1	9.097	14	2	3	3	2158	18.24	10.39	2	0	450.5	150.3	263.2	282.2	182.4	190.1	143.8	438.2	
ESN69	RE48478p OS-Drosophila melanogaster OX=7227 GN=WRNexo PE=2 SV=1	14.348	12	3	6	3	353	40.3	9.2	16.73	3	0	190.9	657	583.4	724.6	702.9	795.9	419.8	533.3
QV9V2	RE50071p OS-Drosophila melanogaster OX=7227 GN=DmelCG14362 PE=1 SV=1	2.198	9	2	2	2	251	29	6.18	6.18	2	0	207.7	79.6	157.3	207.7	79.6	157.3	207.7	79.6
QV9V7	RE50072p OS-Drosophila melanogaster OX=7227 GN=CG2931 PE=1 SV=1	6.857	9	2	2	2	302	33.6	10.2	4.92	2	0	270.1	79.6	157.3	207.7	79.6	157.3	207.7	79.6
QV9CC2	RE50040p OS-Drosophila melanogaster OX=7227 GN=DmelCG5510 PE=1 SV=1	5.339	9	2	2	2	329	37.6	8.97	6.75	2	0	968.3	541.4	1113.6	1153.9	439.7	473.5	493.9	1010.9
QV9N9	RE50167p OS-Drosophila melanogaster OX=7227 GN=DmelCG11989 PE=1 SV=1	24.788	17	10	10	10	259	60	10.59	6.0	2	0	319.1	218.6	91.3	688.6	121.2	188.2	398.3	320
QV9F5	RE54691p OS-Drosophila melanogaster OX=7227 GN=DmelCG3803 PE=2 SV=1	14.51	9	3	4	3	393	44.3	10.08	14.9	3	0	135.1	79	203.9	216.2	60.1	68.6	90.7	150.8
Q85J9	RE55868p OS-Drosophila melanogaster OX=7227 GN=CG10438 PE=2 SV=1	13.076	16	3	3	3	248	27.6	8.37	9.88	3	0	200.6	109.5	338.7	324.1	95.1	80.6	139.9	476.8
RE64P3	RE56416p OS-Drosophila melanogaster OX=7227 GN=CG30022,CG30023 PE=1 SV=1	10.167	8	2	2	2	279	31.4	6.93	6.2	2	0	79.9	416.6	1510.3	306.9	403.9	403.9	403.9	1166
QV9C7	RE57078p OS-Drosophila melanogaster OX=7227 GN=DmelCG1948 PE=1 SV=3	53.121	13	5	9	4	493	49.9	6.74	31.81	5	0	683.2	235.5	337.7	386.8	253.7	259.9	196.9	311.1
Q494M1	RE58921p OS-Drosophila melanogaster OX=7227 GN=Top1 PE=1 SV=1	10.249	4	4	4	4	974	111.8	9.01	9.78	4	0	58.4	22.7	37.9	52.9	25.6	29.9	35.8	45.9
Q7JWH6	RE61424p OS-Drosophila melanogaster OX=7227 GN=DmelCG1888 PE=1 SV=1	7.645	8	2	3	2	372	42.2	6.05	9.9	2	0	682.9	227.7	37.9	52.9	25.6	29.9	35.8	45.9
Q7JZ7	RE62785p OS-Drosophila melanogaster OX=7227 GN=DmelCG12134 PE=1 SV=1	6.693	9	2	2	2	411	5.7	5.06	6.65	2	0	71	54.5	106.3	140	97.4	39.5	52.5	107.2
QV9L9	RE62833p OS-Drosophila melanogaster OX=7227 GN=DmelCG6638 PE=1 SV=1	32.183	15	6	9	6	420	46.2	8.18	28.5	6	0	461	256.4	896.5	877.4	187	188.3	374.8	1070.8
QV9E4	RE63269p OS-Drosophila melanogaster OX=7227 GN=DmelCG14291 PE=1 SV=1	6.161	4	2	2	2	524	59.9	7.08	4.91	2	0	120.8	65.3	394.4	509.9	32.1	28.7	172	147.5
QV9NR9	RE67659p OS-Drosophila melanogaster OX=7227 GN=DmelCG14450 PE=2 SV=1	16.892	16	5	6	6	372	41.8	9.33	16.86	5	0	383.6	200.4	589.4	145.7	187.1	285.3	291.7	
QV9Z7	RE68537p OS-Drosophila melanogaster OX=7227 GN=DmelCG10075 PE=2 SV=1	13.285	15	2	2	2	259	29.4	8.44	9.13	2	0	7	7.5	35.1	72.3	9.7	12.6	12.2	
QV9Z2	RE68649p OS-Drosophila melanogaster OX=7227 GN=DmelCG14966 PE=2 SV=1	11.411	16	2	3	2	140	14.7	9.85	6.21	2	0	194.6	101.1	238.1	195.2	75.9	86.9	115.2	149.8
QV9E4	RE70333p OS-Drosophila melanogaster OX=7227 GN=DmelCG1316 PE=1 SV=2	40.29	16	6	13	6	470	52.4	6.71	40.48	6	0	1103.3	504.8	662.7	666.4	448.2	459.5	380.9	424
Q7KVV1	RE70769p OS-Drosophila melanogaster OX=7227 GN=Spoon PE=1 SV=1	21.99	12	5	8	5	607	67.3	6.79	22.78	5	0	868.8	307.7	645.5	428.3	294.3	397.6	340	486.5
QV9D9	RE74312p OS-Drosophila melanogaster OX=7227 GN=Sart1 PE=1 SV=1	6.917	11	2	2	2	193	21.8	6.93	6.43	2	0	134.4	50.2	168.3	168.3	49.1	87.2	89	113
QV9B9	RE74858p OS-Drosophila melanogaster OX=7227 GN=DmelCG9775 PE=1 SV=1	26.767	16	5	8	5	421	46.1	12.48	25.22	5	0	189.13	777.4	876.7	844.4	707.4	829	545.5	514.5
P7786n	Regucanin homologue OS-Drosophila melanogaster OX=7227 GN=Rrp1 PE=1 SV=2	6.978	26	8	16	8	379	18.6	8.79	18.19	8	0	574.6	194.8	329	2182.3	259.8	293	293	114
QV9V1	Regucanin homologue OS-Drosophila melanogaster OX=7227 GN=Regucanin PE=1 SV=1	84.491	41	9	36	9	303	33.6	6.4	13.39	9	0	10093.2	5272	5241.9	5017.4	3401.2	5223.6	2783.2	2705.8
P25171	Regulator of chromosome condensation OS-Drosophila melanogaster OX=7227 GN=Roc1 PE=1 SV=2	53.192	20	5	13	5	547	58.8	7.94	49.28	5	0	765	265.5	340.2	447.9	305.8	351	250.4	321.8
QV9V3	Regulator of nonseamless T homolog OS-Drosophila melanogaster OX=7227 GN=Rgt1 PE=1 SV=2	11.161	16	2	3	3	1180	120.8	9.7	9.7	3	0	64.5	31.4	65.3	62.3	38.5	65	65	105.2
MP6I8	Regulatory particle non-ATPase 10, isoform B OS-Drosophila melanogaster OX=7227 GN=Rpo10 PE=4 SV=1	13.543	14	2	3	3	396	42.6	8.43	9.39	2	0	943.3	396.2	809.3	362.6	375.2	363.7	363.7	363.7
MP6E6	Regulatory particle non-ATPase 3, isoform B OS-Drosophila melanogaster OX=7227 GN=Rpo3 PE=1 SV=1	32.135	19	10	10	10	444	56	9	28.09	10	0	1258.6	592.8	1133.8	1258.6	592.8	575.9	615.8	909.6
AOA84K7Z5	Regulatory particle non-ATPase 6, isoform C OS-Drosophila melanogaster OX=7227 GN=Rpo6 PE=1 SV=1	20.636	11	5	5	5	422	47.2	5.88	16.07	5	0	629.8	320.6	477.9	591.8	238	293.8	245.5	401.6
QV9L4	RNA polymerase II, isoform 4 OS-Drosophila melanogaster OX=7227 GN=Rpo2 PE=1 SV=3	18.391	12	5	5	5	630	42.7	6.28	19.34	5	0	323.8	129	296.4	176.9	196.7	196.7	196.7	196.7
AOA84KER0	Relative of woc, isoform C OS-Drosophila melanogaster OX=7227 GN=rwo PE=1 SV=1	16.353	4	4	4	4	1301	146.1	8.06	10.98	4	0	496.4	166.4	276.5	286.4	223.5	169.1	141.3	503.1
QV9UQ1	Replication factor C 38kD subunit, isoform A OS-Drosophila melanogaster OX=7227 GN=RFC38 PE=1 SV=1	19.131	18	5	6	5	366	40.8	8.4	14.86	5	0	625.4	303.3	411.4	454.9	320.8	211.3	167.1	241
P3566f	Replication factor C subunit 1 OS-Drosophila melanogaster OX=7227 GN=RFC1 PE=1 SV=1	12.675	15	4	4	4	186	105.5	11.08	10.11	4	0	285.6	111	1389.11	1389.11	1275.4	1275.4	1275.4	1275.4
P5304	Replication factor C subunit 2 OS-Drosophila melanogaster OX=7227 GN=RFC2 PE=1 SV=1	18.707	11	5	8	5	331	37.2	7.72	20.16	5	0	2780.5	1584.6	1546.9	2066.6	1137.3	673.8	613.8	861
QV9KV3	Replication factor C subunit 3 OS-Drosophila melanogaster OX=7227 GN=RFC3 PE=1 SV=2	10.614	9	3	3	3	332	37.4	7.2	9.44	3	0	664.1	294.3	540	646.8	299.4	211.4	210.3	497
Q24492	Replication factor A 70 kD subunit, isoform B OS-Drosophila melanogaster OX=7227 GN=Rpa70 PE=1 SV=1	6.603	66	6	27	27	603	66.6	10.26	17.84	27	0	4362.0	2586.2	2586.2	1735.4	1067.1	1067.1	1067.1	1067.1
QV9G9	Rh2009p OS-Drosophila melanogaster OX=7227 GN=stai PE=1 SV=1	13.674	12	2	2	2	257	29.6	8.25	8.22	2	0	147.3	67.3	121.6	118.7	54.7	74.4	70.7	56
QV9UJ2	Rh9070p OS-Drosophila melanogaster OX=7227 GN=DmelCG3603 PE=1 SV=2	13.73	13	3	3	3	249	26.2	7.8	9.91	3	0	447.2	243.4	738.8	756.4	177	217.1	294.6	360.8
QV9L5	Rh34413p OS-Drosophila melanogaster OX=7227 GN=DmelCG11267 PE=1 SV=1	20.49	43	6	20	6	103	11	9.09	47.45	6	0	1494.3	754.4	2354.7	1655.4	546.9	561.2	1009	1541.1
QV9G3	Rh4171p OS-Drosophila melanogaster OX=7227 GN=DmelCG11752 PE=1 SV=1	11.436	19	2	4	4	1621	18.51	10.41	10.14	4	0	703.1	282.1	114	149.2	60.9	192.2	60.9	192.2
QV9Z1	Rh44935p OS-Drosophila melanogaster OX=7227 GN=DmelCG11752 PE=1 SV=1	11.648	19	2	4	4	109	10.9	9.61	10.96	2	0	164.2	74.4	248	251.4	64.9	71	133	274.7
A129W2	Rh47216p OS-Drosophila melanogaster OX=7227 GN=CG10220 PE=2 SV=1	14.082	12	3	6	3	320	36.4	9.38	18.93	3	0	232.8	146.6	1044.7	783.1	74.7	96.8	421.9	586.5
QV9V4	Rh54564p OS-Drosophila melanogaster OX=7227 GN=DmelCG11752 PE=1 SV=1	22.662	12	3	6	3	431	47.2	7.2	11.21	3	0	381.4	270.3	341.4	229.2	163.2	163.2	163.2	163.2
QV9J74	Rh55640p OS-Drosophila melanogaster OX=7227 GN=DmRH10 PE=1 SV=1	5.012	2	2	2	2	822	94.5	9.47	4.87	2	0	115.1	62.6	134.6	132.3	44.6	66.4	74.9	84
QV9D1	Rh59310p OS-Drosophila melanogaster OX=7227 GN=spidey PE=1 SV=1	12.885	9	2	3	2	321	35.1	9.47	10.47	2	0	165.1	63.8	197.7	212.9	69.4	87	97.6	159.5
QV9L2	Rh6195p OS-Drosophila melanogaster OX=7227 GN=spidey PE=2 SV=1	9.379	11	4	4	4	431	48.5	10.89	10.89	4	0	106.8	36.4	109.9	106.8	36.4	43.7	70.8	82.9
QV9B3	Rh7235p OS-Drosophila melanogaster OX=7227 GN=Vps2 PE=1 SV=1	4.109	6	2	2	2	226	27.3	5.66	6.56	2	0	107.6	46.5	96.4	90.9	43.9	46.8	82.3	
QV9Z4	Rh72958p OS-Drosophila melanogaster OX=7227 GN=DmelCG2076 PE=1 SV=1	8.519	9	3	3	3	341	35.8	9.96	8.63	3	0	64.5	65.2	327.3	318.6	17.5	38.2	118.6	173
QV9L8	Rh7327p OS-Drosophila melanogaster OX=7227 GN=DmelCG4598 PE=1 SV=2	24.602	21	6	10	6	281	31	9.23	27.69	6	0	858.2	422	1436.1	1184.2	330.5	358.8	615.5	1057.9
MP9V3	Rho GTPase-activating protein p10, isoform F OS-Drosophila melanogaster OX=7227 GN=RhoGAP29 PE=1 SV=1	10.919	4	4	5	4	1621	18.51	5.5	11.08	4	0	523.6	259.8	727.9	803.3	272.8	350.2	316	515.6
QV9D5	Rho GTPase-activating protein 92B OS-Drosophila melanogaster OX=7227 GN=RhoGAP29 PE=1 SV=1	11.352	3	4	4	4	740	83	8.46	11.352	3	0	358.7	171.1	418.4	439.9	123.4	169.1	234.4	275.2
Q494F5	Rhythmically expressed gene 2, protein OS-Drosophila melanogaster OX=7227 GN=Reg-2 PE=2 SV=1	13.318	16	4	5	4														

XZJD01	Serine/threonine-protein phosphatase OS=Drosophila melanogaster OX=7227 GN=mts PE=3 SV=1	15,872	17	3	6	3	309	364	5,34	17,29	3	0	706.6	277.7	459.1	406.2	200.7	257.3	294.1	418.8	
XZJG06	Serine/threonine-protein phosphatase OS=Drosophila melanogaster OX=7227 GN=Pp2c PE=3 SV=1	43,719	9	2	3	2	307	307	5,43	2,27	6	0	92.5	315.4	235.8	546	295.6	214.9	271.6	271.6	
OQ6044	Serine/threonine-protein phosphatase Pgam3, mitochondrial OS=Drosophila melanogaster OX=7227 GN=Pg	38,597	20	6	14	6	289	33.1	8.85	39.69	6	0	1107.8	630.2	253.7	1616.2	590.5	530.8	1176.6	1016.4	
AOA0484	Set1(Ash2) histone methyltransferase complex subunit ASH2 OS=Drosophila melanogaster OX=7227 GN=sp	4,774	4	2	2	2	556	63.2	6.92	4.52	2	0	325	144.4	220.6	292.5	122.8	113.8	127.6	177.5	
AAV3W1	Shaggy, isoform J OS=Drosophila melanogaster OX=7227 GN=sgg PE=1 SV=1	18,488	8	3	6	3	575	58.7	8.09	22.39	3	0	315.4	131.3	269.4	215.6	114.3	119.9	140.8	130.7	
AAV4R	Shaggy, isoform G OS=Drosophila melanogaster OX=7227 GN=sgg PE=1 SV=1	18,488	8	3	6	3	575	58.7	8.09	22.39	3	0	315.4	131.3	269.4	215.6	114.3	119.9	140.8	130.7	
A129J3	Shot protein, isoform H OS=Drosophila melanogaster OX=7227 GN=shot PE=1 SV=1	40,012	1	11	12	11	8705	988.9	5.71	30.11	11	0	979.7	480.7	1004.2	987.8	500.5	567.2	461.4	461.4	
QV9V13	Sideroflexin OS=Drosophila melanogaster OX=7227 GN=Sfn1-3 PE=1 SV=1	17,178	16	5	9	5	321	35.7	9.41	23.25	5	0	575.9	259.9	1188.9	974.8	119.1	241.2	530.4	695.5	
QV9U11	Sideroflexin OS=Drosophila melanogaster OX=7227 GN=Sfn1-3 PE=1 SV=1	17,178	16	5	9	5	321	35.7	9.41	23.25	5	0	575.9	259.9	1188.9	974.8	119.1	241.2	530.4	695.5	
QV9DK7	Signal recognition particle subunit SRP72 OS=Drosophila melanogaster OX=7227 GN=Spr72 PE=1 SV=1	13,888	7	3	4	4	650	72.8	9.06	10.08	3	0	253.6	108	282.2	287.3	112.3	161.1	161.6	162.1	
AOA044HS6	Signal transducer and activator of transcription OS=Drosophila melanogaster OX=7227 GN=Stat2E PE=3 SV	16,58	5	3	4	3	635	71.9	6.07	12.29	3	0	319.4	141.5	232.4	212.3	118.8	136	123.3	156.3	
QV9F72	Smg1, isoform G OS=Drosophila melanogaster OX=7227 GN=smg1 PE=1 SV=1	13,178	4	3	4	4	416	8.9	10.77	6.87	4	0	978.8	115.4	918.8	780.9	22.2	308.2	271.4	271.4	
AOA0484.F93	Smc4, isoform 1 OS=Drosophila melanogaster OX=7227 GN=Smc4 PE=1 SV=1	11,054	1	3	3	3	1747	186.3	7.23	9.66	3	0	1800.5	484.6	593.7	582.1	408	488.7	429.4	433.1	
P54622	Single-stranded DNA-binding protein, mitochondrial OS=Drosophila melanogaster OX=7227 GN=smS8 PE=1 SV	47,085	6	73	6	73	6	146	16.4	9.85	186.56	6	0	3181.3	1670.8	6322.5	4351.1	1081.8	3877	2594.6	2256.5
OQ5856	Small nuclear ribonucleoprotein-associated protein B OS=Drosophila melanogaster OX=7227 GN=SmB PE=1 SV	19,178	14	2	7	2	199	21	11.22	32.18	2	0	726.6	222.6	433.2	569.9	265.4	226.5	200.2	506.6	
M9PC99	Small ribonucleoprotein particle U1 subunit 70k, isoform C OS=Drosophila melanogaster OX=7227 GN=smR	17,86	13	6	6	6	448	52.9	10.04	20.28	6	0	278.4	1038.2	1479.9	876.7	1064.6	796.3	997.5	997.5	
O97102	Small ubiquitin-related modifier OS=Drosophila melanogaster OX=7227 GN=smr3 PE=1 SV=1	6,706	19	2	3	2	90	10.1	5.45	5.75	2	0	175.8	82.3	94	169.4	76.7	77.4	49	197.8	
QV9562	Smallmtded, isoform A OS=Drosophila melanogaster OX=7227 GN=smtd PE=1 SV=1	18,397	7	4	4	4	944	104.3	5.44	13.33	4	0	443.3	206.7	223.8	281.9	209.3	213.2	184	189.5	
P13607	Sodium/potassium-transporting ATPase subunit alpha OS=Drosophila melanogaster OX=7227 GN=Alphaha	52,283	8	10	8	10	1041	115.5	5.69	34.87	8	0	110	306.9	694.5	682.2	27.3	278	394.5	479.1	
QXZ21	Something that sticks like glue, isoform A OS=Drosophila melanogaster OX=7227 GN=snama PE=1 SV=1	5,953	2	2	2	2	1231	139	9.73	2.98	2	0	93.8	49	100.4	94.2	42.4	46.1	44.6	80.2	
MPF16	Spectrin beta chain OS=Drosophila melanogaster OX=7227 GN=beta-Spec PE=3 SV=1	29,912	3	7	7	7	2308	267.5	5.33	24.6	7	0	1291.1	577.9	1252.5	1371.2	480.9	582	744.8	749.8	
M9ND96	Splekhecker1, isoform D OS=Drosophila melanogaster OX=7227 GN=Spe1 PE=1 SV=1	16,222	6	6	6	6	917	103.2	5.92	12.45	6	0	1338.7	624.8	552.8	687.7	633.6	356.6	178.4	240.9	
QV97Y2	Sphingoglyco-1-phosphate lyase OS=Drosophila melanogaster OX=7227 GN=SpLy PE=1 SV=1	33,523	12	5	7	7	545	60.3	8.46	24.16	5	0	1084.6	555.3	2628.7	1548.8	387	568.4	1216.3	821.7	
AOA04BKU8	Splicing factor 1, isoform C OS=Drosophila melanogaster OX=7227 GN=SF1 PE=1 SV=1	8,949	3	3	3	3	323	37.6	11.14	8.49	3	0	723.3	340	391.3	469.2	290.6	274.4	231.4	282.3	
OA6106	Splicing factor 3A subunit 3 OS=Drosophila melanogaster OX=7227 GN=Sf3 PE=1 SV=1	12,683	8	2	3	2	503	58.4	5.62	10.79	2	0	125.2	68.1	117.2	109	62	65.7	47.8	59.3	
QV9W07	Splicing factor 3B subunit 3 OS=Drosophila melanogaster OX=7227 GN=SF3B3 PE=1 SV=2	6,85	2	2	2	2	1340	149.5	6.67	5.56	2	0	352.5	165.7	233.6	262.3	151	138.6	240.4	240.4	
QV9W07	Splicing factor 3B subunit 3 OS=Drosophila melanogaster OX=7227 GN=SF3B3 PE=1 SV=2	62,792	15	15	15	15	1227	136.5	5.47	54.78	15	0	1996.5	922.9	1386.7	1692.1	788.4	85.3	831.1	1067.7	
QV9V77	Splicing factor 3B subunit 5 OS=Drosophila melanogaster OX=7227 GN=SF3B5 PE=1 SV=1	4,914	18	2	2	2	121	14.2	9.32	4.83	2	0	126.8	41.2	124.1	125.1	57.3	64.9	77.6	79.9	
AOA04BKU6	Splicing factor 3B subunit 5 OS=Drosophila melanogaster OX=7227 GN=SF3B5 PE=1 SV=1	4,914	18	2	2	2	121	14.2	9.32	4.83	2	0	126.8	41.2	124.1	125.1	57.3	64.9	77.6	79.9	
QV9VH7	Splicing factor 3B subunit 5 OS=Drosophila melanogaster OX=7227 GN=SF3B5 PE=1 SV=1	4,914	18	2	2	2	121	14.2	9.32	4.83	2	0	126.8	41.2	124.1	125.1	57.3	64.9	77.6	79.9	
QV9VH7	Splicing factor 3B subunit 5 OS=Drosophila melanogaster OX=7227 GN=SF3B5 PE=1 SV=1	4,914	18	2	2	2	121	14.2	9.32	4.83	2	0	126.8	41.2	124.1	125.1	57.3	64.9	77.6	79.9	
MPH23	Ssu72 CTD phosphatase, isoform B OS=Drosophila melanogaster OX=7227 GN=Ssu72 PE=1 SV=1	13,846	2	2	2	2	194	22.6	5.26	14.9	2	0	670.8	37.6	37.6	37.6	40	25.1	30.3	20	34
MPH23	Staphylococcal nuclease, isoform B OS=Drosophila melanogaster OX=7227 GN=Stuor-SN	19,189	15	15	15	15	1103	132.6	6.87	63.26	15	0	1553.7	699.3	1068.7	1000.8	615.3	1033.8	1303.8	1303.8	
QV9W19	Stearoyl-CoA ligase, isoform B OS=Drosophila melanogaster OX=7227 GN=Stk PE=1 SV=2	21,940	4	5	5	5	1703	192	6.62	16.35	5	0	573.8	322.6	832.4	876.6	232.6	218.6	242	403.4	
P83094	Stromal interaction molecule homolog OS=Drosophila melanogaster OX=7227 GN=Stm PE=1 SV=1	9,634	6	3	4	4	570	64.8	6.43	8.96	3	0	244.8	113.7	294.8	236.3	120.2	115.1	150.6	150.8	
QV9C8	Structural maintenance of chromosomes protein 5 OS=Drosophila melanogaster OX=7227 GN=SMC2 PE=1 SV	9,378	2	2	2	2	1122	129.3	8.32	7.31	2	0	514	53.7	89.6	119.9	73.1	65.3	51.6	82.8	
QV9V27	Structural maintenance of chromosomes protein OS=Drosophila melanogaster OX=7227 GN=SMC3 PE=1 SV=1	73,749	9	9	9	9	409	81.8	4.57	11.57	9	0	2020.5	824	1421.1	1322.5	591.2	591.2	591.2	591.2	
QV9C8	Structural maintenance of chromosomes protein OS=Drosophila melanogaster OX=7227 GN=SMC1 PE=1 SV	40,625	9	9	9	9	1238	142.8	6.73	31.35	9	0	1719.7	687.2	718.1	959.9	661.7	934.8	515.5	530.5	
QV9K96	Structural maintenance of chromosomes protein OS=Drosophila melanogaster OX=7227 GN=SMC2 PE=1 SV	36,858	9	9	9	9	9	1238	142.8	6.73	31.35	9	0	3827	1460.1	1643.7	1583.8	1408.4	1480.9	1146.9	986.7
QV9V27	Structural maintenance of chromosomes protein OS=Drosophila melanogaster OX=7227 GN=SMC3 PE=1 SV=1	73,749	9	9	9	9	409	81.8	4.57	11.57	9	0	2020.5	824	1421.1	1322.5	591.2	591.2	591.2	591.2	
A12936	Substrate-2, isoform A OS=Drosophila melanogaster OX=7227 GN=Sub2 PE=1 SV=1	43,416	4	10	12	12	3257	355.8	6.14	39.41	10	0	3017.6	1347.0	1644.4	2262.5	1257.5	1311.7	828	1224	1224
QA4523	Succinate dehydrogenase [ubiquinol] flavoprotein subunit, mitochondrial OS=Drosophila melanogaster OX=7227 GN=SDH	208,574	36	16	84	36	166	661	72.3	7.12	318.18	16	0	2994.2	1670.6	5937.8	5507.5	1454.7	1566.8	2613.8	4958.2
P91914	Succinate dehydrogenase [ubiquinol] iron-sulfur subunit, mitochondrial OS=Drosophila melanogaster OX=7227 GN=SDH	19,378	3	3	3	3	287	34.7	10.66	25.76	3	0	326.3	290.3	370.2	1433.6	372.4	372.4	372.4	372.4	
Q8S216	Succinate dehydrogenase, mitochondrial OS=Drosophila melanogaster OX=7227 GN=SDH	16,612	25	3	6	3	120	13.9	9.07	21.57	3	0	451.2	260.5	55.74	526	218	205.5	521.6	521.6	
AOA04BJC4	Succinate-CoA ligase [ADP-forming] subunit beta, mitochondrial OS=Drosophila melanogaster OX=7227 GN=SLC	111,217	34	12	63	34	12	451	49	6.83	43.44	12	0	4373.4	2179.6	3338	5990.9	1746.5	1858.1	3214.6	4806.9
QA4522	Succinate-CoA ligase [ADP-forming] subunit alpha, mitochondrial OS=Drosophila melanogaster OX=7227 GN=SLC	9,569	7	2	7	7	2	328	34.4	8.98	13.26	2	0	424.5	204.1	753.2	880.9	109.3	106.6	299.6	505.2
QV9V74	Succinyl-CoA ligase [ADP-forming] subunit beta, mitochondrial OS=Drosophila melanogaster OX=7227 GN=SLC	77,486	10	25	10	25	10	516	54.9	8.37	82.74	10	0	1148.5	178.6	2142.9	2910.3	1950.6	565.5	601.7	1887.7
QV9V33	Sulfurtransferase OS=Drosophila melanogaster OX=7227 GN=DmelG12279 PE=1 SV=2	14,128	35	3	3	3	3	110	12.1	5.21	10.66	3	0	380	158.1	31.5	353.5	149.2	158.4	156.2	179.5
A12950	Superoxide dismutase [Cu-Zn], isoform 2 OS=Drosophila melanogaster OX=7227 GN=SuD2 PE=1 SV=2	18,962	11	2	3	3	580	87.2	6.26	9.91	3	0	35	95	41	95	41	95	41	95	
MPF91	Superoxide dismutase [Cu-Zn], isoform 1 OS=Drosophila melanogaster OX=7227 GN=SuD1 PE=3 SV=1	14,283	11	2	3	3	2	167	17.4	6.26	9.91	2	0	764.8	354.8	499.7	481.6	304.7	317	263.6	323
AOA04BLG01	Superoxide dismutase OS=Drosophila melanogaster OX=7227 GN=SuD2 PE=3 SV=1	10,225	14	2	4	2	217	24.6	7.93	14.41	2	0	212.1	91.3	304	247.7	82.6	64.3	43.1	63.8	
AOA04BLG02	Suppressor of hairy wing, isoform C OS=Drosophila melanogaster OX=7227 GN=SuHw3 PE=1 SV=1	15,452	4	4	4	4	441	105.7	10.17	12.45	4	0	573.3	1017	378	425.7	378	201.7	201.7	201.7	
AOA04DJ33	Suppressor of variegation-2-10, isoform L OS=Drosophila melanogaster OX=7227 GN=SuVar2-10 PE=1 SV=1	12,995	7	2	2	2	584	64.6	7.99	11.62	2	0	697	49.6	95.3	101.6	48.6	49.3	49.3	49.3	
QJ4JF3	SURF1-like protein OS=Drosophila melanogaster OX=7227 GN=Surf1 PE=2 SV=1	19,371	16	2	2	2	2	300	34	9.99	9.7	2	0	108.8	68.9	285	195.7	53.5	61.3	111.3	95.6
I818405	Surfact locus protein 4 homolog OS=Drosophila melanogaster OX=7227 GN=Surf4 PE=2 SV=1	10,532	4	2	3	3	710	30.5	8.97	10.37	2	0	470.5	293.8	591.9	505.5	162.9	329.7	349.2	371.1	
QV9L72	Synaptoblastic protein OS=Drosophila melanogaster OX=7227 GN=Synb1 PE=1 SV=1	13,941	13	3	3	3	644	85.4	8.16	10.23	3	0	1101	407.5	492.3	514.1	392.4	268.8	287.9	287.9	
QV9V76	Synaptonemal-associated protein OS=Drosophila melanogaster OX=7227 GN=Snap24 PE=1 SV=1	14,534	13	2	2	2	2	232	23.5	4.79											

QBVV7A	Tumor suppressor protein 101 OS-Drosophila melanogaster OX=7227 GN=TSG101 PE=1 SV=2	13,796	9	2	2	2	4	408	45.2	6.37	6.73	2	0	192.5	73.1	96.6	137.6	85.1	78.9	53.5	89.7
QBWG01	Tyrosine protein phosphatase non-receptor type 61F OS-Drosophila melanogaster OX=7227 GN=Ptp61F PE=1 SV=2	14,366	5	2	4	4	548	62.1	44.8	6.55	15.58	4	4	653.2	312.29	58.2	383.4	263	347	216.3	279.2
MPDQ3	Ubl domain isoform D OS-Drosophila melanogaster OX=7227 GN=Ubl PE=1 SV=1	7,754	2	2	3	2	1175	122.8	6.52	6.06	0	2	872	395.8	483.7	654.7	359.5	35.9	297	427.9	
P43332	U1 small nuclear ribonucleoprotein A OS-Drosophila melanogaster OX=7227 GN=snf PE=1 SV=1	7,207	8	2	3	2	216	24.5	9.64	7.98	2	2	903.8	244.6	425.8	441.2	259.8	242.2	219.1	616.4	
MPBM1	U2 small nuclear ribonucleoprotein auxiliary factor 38, isoform B OS-Drosophila melanogaster OX=7227 GN=U2af38	18,272	7	2	2	2	264	29.9	8.91	9.77	2	2	1264.1	502.4	474.1	484.8	566.5	373.6	260.8	277.8	
QVWV6	Ubiquitin carboxyl-terminal hydrolase COB OS-Drosophila melanogaster OX=7227 GN=	10,122	6	2	2	2	152	17.2	10.1	10.1	2	2	345.9	152.7	165.1	195.7	125.7	105.1	245.7	207.7	
QBMKN0	Ubiquitin nucleiogenesis protein COO9, mitochondrial OS-Drosophila melanogaster OX=7227 GN=Coq9 PE=1 SV=1	11,044	6	2	2	2	326	36.3	7.91	7.75	2	2	184	102.3	491.1	339.2	64	58	194.5	195.6	
QVW462	Ubiquitin carboxyl-terminal hydrolase 30 homolog OS-Drosophila melanogaster OX=7227 GN=Usg30 PE=2 SV=2	28,076	9	4	9	4	558	60.8	7.34	25.09	4	4	139.1	110.2	282.3	222.2	46.8	113.3	129	103	
QVYV08	Ubiquitin carboxyl-terminal hydrolase 30 homolog OS-Drosophila melanogaster OX=7227 GN=Usg30 PE=2 SV=2	28,076	9	4	9	4	558	60.8	7.34	25.09	4	4	139.1	110.2	282.3	222.2	46.8	113.3	129	103	
QVWVNS	Ubiquitin carboxyl-terminal hydrolase MINDY-3 homolog OS-Drosophila melanogaster OX=7227 GN=mindy3 PE=1 SV=1	12,183	4	2	3	2	560	61.7	5.92	10.44	2	2	499.8	220.2	317.3	290.2	184.3	204.5	178.8	146.6	
QVZV27	Ubiquitin carboxyl-terminal hydrolase OS-Drosophila melanogaster OX=7227 GN=Ubp1 PE=1 SV=1	25,332	9	5	6	5	827	92	5.49	19.2	5	5	278.6	171.9	190.8	210.4	142.1	166.8	97.5	177.1	
QVW9W0	Ubiquitin-conjugating enzyme E2M, isoform B OS-Drosophila melanogaster OX=7227 GN=UbcE2M PE=3 SV=2	7,808	6	2	2	2	181	20.7	12.5	12.5	2	2	380.3	152	173.5	152.4	152.4	173.5	128	143.4	
P15357	Ubiquitin-40S ribosomal protein S27a OS-Drosophila melanogaster OX=7227 GN=S27a PE=1 SV=2	47,464	44	7	37	7	156	17.9	97.7	96.27	7	7	10655.2	4347.6	4439.2	6955.4	5210	6857.4	3620.3	6919.9	
PN5128	Ubiquitin-conjugating enzyme E2 N OS-Drosophila melanogaster OX=7227 GN=UbcN PE=1 SV=1	6,923	18	2	2	2	151	17.2	5.6	6.06	2	2	239.3	107.7	184.4	222.4	105	108.3	93.8	117.4	
MNDN19	UDP-galactose 4-epimerase, isoform B OS-Drosophila melanogaster OX=7227 GN=Gale PE=1 SV=1	37,377	8	13	8	13	350	38.7	7.46	35.31	8	8	1849.9	656.4	1171	1700.8	629.6	618.6	573.3	1948.6	
QD2373	UDP-glucose 6-dehydrogenase OS-Drosophila melanogaster OX=7227 GN=Ugd PE=1 SV=1	16,105	14	4	4	4	476	61.8	16.8	11.07	4	4	139.5	74.4	137.3	85	69	65.1	81		
QD9332	UDP-glucose glycoprotein glucosyltransferase OS-Drosophila melanogaster OX=7227 GN=Ugt PE=1 SV=2	48,801	11	13	17	13	1548	174.2	6.15	43.93	13	13	726.4	414.2	1985	2053.3	259.7	277.3	934.7	941	
MPG52	Ultrapsade, isoform B OS-Drosophila melanogaster OX=7227 GN=Usp PE=3 SV=1	4,092	4	3	3	3	308	55.2	8	4.18	3	3	664.3	230	363.6	488.2	251.5	198.9	199.6	393.6	
QVW82	UMP-CMP kinase OS-Drosophila melanogaster OX=7227 GN=Uck1 PE=1 SV=1	46,234	29	8	20	8	253	8.8	8	50.95	8	8	1842.4	691.6	1704.6	1317.1	647.6	617.7	873.2	935.4	
QVWR8	Uncharacterized protein CG2059 OS-Drosophila melanogaster OX=7227 GN=CG2059 PE=1 SV=1	15,214	9	3	5	3	330	35.4	8.27	13.45	3	3	185.8	106.8	414.3	440.1	72.6	68.4	166.8	246.4	
A1Z729	Uncharacterized protein OS-Drosophila melanogaster OX=7227 GN=BcDNA_S07613 PE=1 SV=1	13,258	10	3	5	3	308	36.6	8.66	16.37	3	3	386.2	187.9	697.3	697.4	132.8	164.9	340.6	409.4	
QVW52	Uncharacterized protein OS-Drosophila melanogaster OX=7227 GN=CG12289 PE=1 SV=1	14,813	6	3	5	3	435	47.9	10.04	15.11	3	3	3272.8	713	715.5	699.5	1139.1	1269.3	636.6	621.4	
BZ702	Uncharacterized protein OS-Drosophila melanogaster OX=7227 GN=CG14896 PE=1 SV=1	123,879	9	24	28	24	3441	378.4	4.93	102.94	24	24	4312.4	1691.3	2205.4	2373.1	1651.5	1670.9	1265.9	1481.9	
QBP8P	Uncharacterized protein OS-Drosophila melanogaster OX=7227 GN=CG2907 PE=1 SV=1	38,842	36	6	21	6	256	27.1	8.72	79.79	6	6	936.7	442.3	1621.4	1714.9	346.5	383.6	661.4	2198.5	
QBVV7	Uncharacterized protein OS-Drosophila melanogaster OX=7227 GN=CG3808 PE=1 SV=3	3,437	3	2	2	2	615	68.6	8.23	4.3	2	2	291.3	123.5	222.5	255	130.5	126.7	97.7	290.9	
QBTZ5	Uncharacterized protein OS-Drosophila melanogaster OX=7227 GN=DmelCG1286 PE=1 SV=2	33,129	24	7	14	7	347	38.4	8.27	42.91	7	7	779.3	391.2	1424.5	1262.1	325	372.2	578.6	619.5	
QVNL0	Uncharacterized protein OS-Drosophila melanogaster OX=7227 GN=DmelCG1390 PE=4 SV=1	15,643	13	4	7	4	381	41.4	9.39	20.96	4	4	394.8	253.5	822.5	724.5	117.4	195	355.5	514.5	
A1Z843	Uncharacterized protein OS-Drosophila melanogaster OX=7227 GN=DmelCG1371 PE=1 SV=1	21,35	6	5	8	5	1199	130.8	7.23	22.22	5	5	1166	444.7	1271.6	1240.2	397.1	490.7	655.1	561.9	
QVW9P3	Uncharacterized protein OS-Drosophila melanogaster OX=7227 GN=DmelCG1784 PE=1 SV=1	31,018	6	5	6	5	1200	134.4	6.12	36.61	6	6	814.2	572.2	1280.2	1280.2	474.6	721.4	534	626.6	
A1Z9M5	Uncharacterized protein OS-Drosophila melanogaster OX=7227 GN=CG103089 PE=1 SV=1	6,394	1	2	2	2	4012	460.7	3.85	2.17	2	2	37.4	23.1	54.5	67.1	20.7	22.7	26.5	26.2	
QVFPJ0	Uncharacterized protein OS-Drosophila melanogaster OX=7227 GN=DmelCG1362 PE=4 SV=1	8,908	4	3	3	3	454	49.7	7.31	7.76	3	3	388.9	185.8	673.3	382.5	110.7	149.1	331.1	275	
QBP3D0	Uncharacterized protein OS-Drosophila melanogaster OX=7227 GN=DmelCG1793 PE=4 SV=2	4,247	4	3	4	3	410	97.5	4.37	12.2	4	4	471.3	221.4	518.4	373.4	121	231.8	233	213.8	
QVQL11	Uncharacterized protein OS-Drosophila melanogaster OX=7227 GN=DmelCG4957 PE=4 SV=2	16,589	15	2	3	2	246	27.6	6.04	25.69	2	2	47.2	26.9	91	65.6	56.1	28.4	42.7	41.7	
QVST4	Uncharacterized protein OS-Drosophila melanogaster OX=7227 GN=DmelCG5144 PE=3 SV=1	3,179	4	2	2	2	388	43.6	8.06	1.66	2	2	0	0	0	0	0	0	0	0	
QVBRK3	Uncharacterized protein OS-Drosophila melanogaster OX=7227 GN=DmelCG5913 PE=1 SV=1	12,475	6	3	3	3	454	49.9	9.7	9.12	3	3	431.6	182.4	249.7	270	164.1	200.7	151.9	146	
A1Z9H6	Uncharacterized protein OS-Drosophila melanogaster OX=7227 GN=DmelCG1791 PE=1 SV=1	5,743	6	3	3	3	324	39.9	10.2	17.6	3	3	142.6	104.2	1348.7	1042	1348.7	1042	1348.7	1042	
QVWZM4	Uncharacterized protein OS-Drosophila melanogaster OX=7227 GN=FAM67 PE=1 SV=1	5,743	6	3	3	3	296	31.5	4.77	6.73	2	2	99.3	26.2	72.4	81.5	42.8	30.3	32.3	200.5	
QVW1M9	Uncharacterized protein, isoform A OS-Drosophila melanogaster OX=7227 GN=APJ12 PE=1 SV=1	9,558	5	2	2	2	596	65.4	4.99	6.39	2	2	47.9	20.9	39.1	54.8	16.2	16.4	25.4	45.7	
QVYVY2	Uncharacterized protein, isoform A OS-Drosophila melanogaster OX=7227 GN=an=H0012374.89 PE=1 SV=1	10,212	2	2	2	2	317	35.8	8.27	11.81	2	2	203.2	109.9	274.2	203.2	109.9	274.2	203.2	109.9	
QVVP8	Uncharacterized protein, isoform A OS-Drosophila melanogaster OX=7227 GN=DmelCG10512 PE=1 SV=1	8,844	5	4	6	4	446	47	8.25	13.63	4	4	620.1	289.1	750.8	846.2	211.7	205.5	299.9	429.3	
QVFPF2	Uncharacterized protein, isoform A OS-Drosophila melanogaster OX=7227 GN=DmelCG10576 PE=1 SV=1	18,975	17	6	10	6	391	42.7	7.11	23.49	6	6	2600.1	1063.7	1810.1	1645.9	990.6	1100.2	1209.7	1081.8	
MPV4A1	Uncharacterized protein, isoform A OS-Drosophila melanogaster OX=7227 GN=DmelCG10576 PE=1 SV=1	18,975	17	6	10	6	391	42.7	7.11	23.49	6	6	2600.1	1063.7	1810.1	1645.9	990.6	1100.2	1209.7	1081.8	
A1Z830	Uncharacterized protein, isoform A OS-Drosophila melanogaster OX=7227 GN=DmelCG1218 PE=1 SV=1	8,62	6	3	3	3	485	53.8	7.27	9.05	3	3	415.5	199.9	213.7	280.9	177.2	167.7	148.5	296.4	
QVPRD4	Uncharacterized protein, isoform A OS-Drosophila melanogaster OX=7227 GN=DmelCG1532 PE=1 SV=1	22,943	20	3	4	3	288	31.6	3.99	18.48	3	3	290.2	142.9	297.3	331.4	114.5	126.5	130.4	163	
QVZ60	Uncharacterized protein, isoform A OS-Drosophila melanogaster OX=7227 GN=DmelCG1186 PE=1 SV=1	8,243	2	2	2	2	1128	122.6	9.6	6.42	2	2	130.9	58.6	76.9	84.1	58.5	52.2	47.2	54.3	
QVW51	Uncharacterized protein, isoform A OS-Drosophila melanogaster OX=7227 GN=DmelCG5813 PE=4 SV=1	9,567	8	3	4	3	463	52.7	6.55	9.67	4	4	863.1	409.7	695.3	695.3	449.2	449.2	449.2	449.2	
QVWU2	Uncharacterized protein, isoform A OS-Drosophila melanogaster OX=7227 GN=DmelCG5828 PE=1 SV=1	7,758	8	3	4	3	325	40.4	5.53	6.28	8	8	379.3	353.8	553.5	578.8	158.4	196.4	278.2	347.4	
QKQZ6	Uncharacterized protein, isoform A OS-Drosophila melanogaster OX=7227 GN=DmelCG7834 PE=1 SV=1	93,275	51	11	49	11	253	27.2	8.05	171.19	11	11	4065.8	2237.9	7886.5	5843.2	1286.7	1744.7	3427.2	3467	
QVWV5	Uncharacterized protein, isoform A OS-Drosophila melanogaster OX=7227 GN=DmelCG1565 PE=1 SV=1	13,177	11	3	3	3	375	41.6	13.55	15.52	3	3	131.7	58.6	157.5	157.5	53.2	48.5	49.5	53.2	
QVW39	Uncharacterized protein, isoform A OS-Drosophila melanogaster OX=7227 GN=DmelCG9018 PE=1 SV=1	14,983	11	3	3	3	375	41.6	13.55	15.52	3	3	112.4	41.7	74.5	101.5	47.6	39.8	40.2	192.7	
QVW10	Uncharacterized protein, isoform A OS-Drosophila melanogaster OX=7227 GN=DmelCG9147 PE=1 SV=2	12,015	9	3	6	3	391	43.7	6.1	17.49	3	3	245	111.5	323.4	396.6	99.6	118.2	134.1	300	
QVWMD3	Uncharacterized protein, isoform A OS-Drosophila melanogaster OX=7227 GN=snf PE=4 SV=1	9,386	6	3	3	3	323	36.8	8.61	6.88	3	3	384.7	215	449.4	449.4	324.6	324.6	324.6	324.6	
QVW48	Uncharacterized protein, isoform A OS-Drosophila melanogaster OX=7227 GN=Spq7 PE=1 SV=1	134,474	26	18	42	18	1819	90	8.46	136.17	18	18	2907.2	1401.7	6173.6	4872.5	1195.9	1360.7	2804.2	3587.8	
QVQ19	Uncharacterized protein, isoform B OS-Drosophila melanogaster OX=7227 GN=BEST-LD19244 PE=1 SV=3	28,602	4	7	7	7	2663	292.4	5.27	31.08	7	7	564.2	271.9	443.6	472.8	245.8	247.2	227.6	282.5	
XJ2JF6	Uncharacterized protein, isoform B OS-Drosophila melanogaster OX=7227 GN=COA PE=1 SV=1	30,44	13	5	9	5	335	37.2	9.7	19.48	5	5	3343.3	1168	975.8	1243.9	1298.1	2032.4	980.7	688.5	
QVQ15	Uncharacterized protein, isoform B OS-Drosophila melanogaster OX=7227 GN=CG10092 PE=4 SV=2	4,955	4	2	3	2	510	58.1	6.98	8.38	2	2	109.4	57.6	156.3	137.1	42.9	34.9	144.9	193.6	
AOA84LGA9	Uncharacterized protein, isoform B OS-Drosophila melanogaster OX=7227 GN=CG3884 PE=4 SV=1	6,946	7	3	4	3	450	48.3	6.32	9.78	3	3	627.3	358.8	650.3	719.2	397.3	380.5	391.5		

Q94920	Voltage-dependent anion-selective channel OS=Drosophila melanogaster OX=7227 GN=porn PE=1 SV=3	38.676	34	7	39	7	282	30.5	6.96	50.31	7	0	734.1	885.3	1972.4	1767.6	420.1	659.6	785	1754.2
Q7KM64	Wains, isoform A OS=Drosophila melanogaster OX=7227 GN=wal PE=1 SV=1	74.63	33	8	35	8	330	34.2	8.32	147.3	8	0	1868.1	980.1	3737.2	2716.9	635.6	775.7	1627.2	2293
A8JRE3	Without children, isoform B OS=Drosophila melanogaster OX=7227 GN=woc PE=1 SV=1	51.848	6	12	16	12	1703	188.6	4.75	46.94	12	0	3016.4	1356.2	1625.6	1972.4	1300.2	1301.8	1153.5	1390.9
Q9VJG0	Xaa-Pro aminopeptidase ApepP OS=Drosophila melanogaster OX=7227 GN=ApepP PE=1 SV=1	4.452	3	2	2	2	613	68.5	5.95	5.16	2	0	363.8	166.9	380.1	353.5	147	141.9	171.5	277.6
Q7KVP9	Xeroderma pigmentosum D OS=Drosophila melanogaster OX=7227 GN=Xpd PE=1 SV=1	9.753	2	2	2	2	769	88	6.77	6.07	2	0	387.5	142.6	200.6	235	135.1	156.6	107.2	162.8
A0A0B4KFY4	YME1 like ATPase, isoform D OS=Drosophila melanogaster OX=7227 GN=YME1L PE=1 SV=1	73.93	17	11	16	11	739	80.9	8.67	57.31	11	0	980	519.7	1720.3	1226.4	342.1	489.4	804.6	936.2
X2JEX8	Yolk protein 3, isoform B OS=Drosophila melanogaster OX=7227 GN=Yp3 PE=1 SV=1	7.81	8	2	2	2	420	46.1	8.5	6.59	2	0	206.6	210.8	199.2	425.5	139.8	188.4	115	324.8
Q9VBZ5	YTH domain-containing family protein OS=Drosophila melanogaster OX=7227 GN=Ythd PE=2 SV=1	7.957	3	2	2	2	700	78.9	8.95	6.93	2	0	694.4	125.4	333.3	364.7	133.9	142.7	180.9	271.4
Q7JWR9	Zinc finger CCH domain-containing protein 15 homolog OS=Drosophila melanogaster OX=7227 GN=CQ863	14.376	9	3	5	3	404	45.3	5.55	13.5	3	0	833.2	424.5	1081.6	967.2	359.5	534.7	662.5	572.7
P28166	Zinc finger protein 1 OS=Drosophila melanogaster OX=7227 GN=zfh1 PE=1 SV=2	9.545	2	2	2	2	1054	116.5	7.15	6.24	2	0	63.5	22.4	27	26.7	20.6	25.8	15.7	22
Q9WQY0	Zinc finger protein 593 homolog OS=Drosophila melanogaster OX=7227 GN=CG3224 PE=2 SV=1	12.886	17	2	2	2	162	16.9	9.67	7.75	2	0	436.5	172.1	167.2	227	146.6	161.6	95.1	109.5
Q8IRH5	Zinc finger protein CG2199 OS=Drosophila melanogaster OX=7227 GN=CG2199 PE=1 SV=1	24.181	9	5	9	5	733	81.9	8.56	28.27	5	0	2618.7	553.1	693.4	715.3	776.2	887.9	517.5	637.7
Q9VXG1	Zinc finger protein hangover OS=Drosophila melanogaster OX=7227 GN=hang PE=1 SV=4	24.183	2	4	6	4	1959	213.7	5.38	16.58	4	0	1096.6	490	650.5	882.1	438.3	383.5	338.8	434.9
P41073	Zinc finger protein on ecdyone puffs OS=Drosophila melanogaster OX=7227 GN=Pep PE=1 SV=1	70.698	11	9	23	9	716	78	5.58	82.83	9	0	2507.4	946.3	1213.3	1356.7	924.3	965.1	727.5	1003.1
Q86B13	Zinc finger protein at 72D, isoform B OS=Drosophila melanogaster OX=7227 GN=Zn72D PE=1 SV=1	18.936	6	5	5	5	884	96	8.44	13.39	5	0	850.9	355.8	507.5	531.1	336.5	367.3	277	414.5
A0A0B4JD57	Zipper, isoform F OS=Drosophila melanogaster OX=7227 GN=zip PE=1 SV=1	234.717	20	30	64	30	1979	227.7	5.47	204.67	30	0	2771.2	1429.9	3767.9	3943.3	1137	1636.9	2119.8	2316.6

P2507	RegIb1 protein domain 1, isoform A OS-Drosophila melanogaster OX1272 OlnbP1 PE1 SV1	10.5259874	10.4829487	10.4129266	9.9324705	9.7773005	9.8298481	10.1743426	10.56223	9.9276774	6.0311629	1.5491925	0.050912	0.00347
E2073	Phosphatidylinositol 3-OH kinase OS-Drosophila melanogaster OX1272 OlnbP1 PE1 SV1	9.6444345	9.5293708	9.3949505	9.0591283	8.7264444	8.5261985	8.6712583	9.0792447	8.2024469	6.7343637	1.6077337	0.02368	0.01324
OV192	Phospholipase A2 activator protein, isoform A OS-Drosophila melanogaster OX1272 OlnbP1 PE1 SV1	5.64044837	5.12399706	5.5707122	5.6328284	4.7655471	4.8793518	4.9858015	5.4760138	4.9174375	3.5842505	1.4781767	0.0104	0.01784
OV199	Phospholipase activator protein, isoform A OS-Drosophila melanogaster OX1272 OlnbP1 PE1 SV1	1.7510022	1.7480981	1.7680419	1.8001195	1.5164878	1.5344928	1.5220228	1.6411977	1.7420719	1.3041830	0.8482423	1.7077235	0.01205
PI187	Polysialyltransferase OS-Drosophila melanogaster OX1272 OlnbP1 PE1 SV1	8.65316838	10.018948	8.9668332	10.1251148	8.9504606	8.4325637	9.2648267	8.9084841	9.9528714	8.192519	0.7882552	1.7027042	0.01756
OV238	Polysialyltransferase OS-Drosophila melanogaster OX1272 OlnbP1 PE1 SV1	8.6008387	8.5059876	8.1261245	8.7851195	7.7428187	7.6851407	7.3778237	7.4683137	8.3949832	7.6089122	0.7185861	1.6454813	0.02633
AI238	Protein alpha-1,3-galactosyltransferase OS-Drosophila melanogaster OX1272 OlnbP1 PE1 SV1	9.2079707	9.5541473	8.9187205	8.4651861	8.6413209	8.5092100	8.4624715	7.9816647	8.9224224	8.0745691	0.4656199	1.0781982	0.02076
OV187	Protein alpha-1,3-galactosyltransferase OS-Drosophila melanogaster OX1272 OlnbP1 PE1 SV1	5.98365141	5.5328986	5.6245461	4.9068016	5.449924	5.4018883	4.9217301	5.6445485	5.0262484	4.6172146	1.5330994	0.05878	0.04339
OV191	Protein alpha-1,3-galactosyltransferase OS-Drosophila melanogaster OX1272 OlnbP1 PE1 SV1	8.3126201	7.8449718	7.4458871	7.063714	7.5071003	7.4557721	6.1517034	6.9018902	7.8517331	7.1444675	0.2742706	0.6508387	0.02171
OV192	Protein alpha-1,3-galactosyltransferase OS-Drosophila melanogaster OX1272 OlnbP1 PE1 SV1	10.3933478	10.824183	11.327597	11.171393	8.686005	8.426289	10.288441	10.289142	10.920244	9.8613859	0.8282205	0.01738	0.02331
OV193	Protein alpha-1,3-galactosyltransferase OS-Drosophila melanogaster OX1272 OlnbP1 PE1 SV1	6.1784486	6.8487974	6.2878695	6.9308747	5.9774327	6.0122888	5.1972949	5.2018662	6.6613236	5.6120389	1.0482186	2.0977489	0.012
OV201	Protein alpha-1,3-galactosyltransferase OS-Drosophila melanogaster OX1272 OlnbP1 PE1 SV1	7.8426363	7.8946487	7.8861697	7.8076171	7.5164764	7.2053763	7.0148344	6.7800544	7.9148344	6.7800544	0.4642475	1.0216514	0.01726
OV194	Protein alpha-1,3-galactosyltransferase OS-Drosophila melanogaster OX1272 OlnbP1 PE1 SV1	8.44800347	8.37872638	8.1956577	8.1104234	8.9683706	8.1765380	8.3268317	7.5904812	8.2093474	8.48712239	0.8122124	1.7509189	0.01061
PI193	Protein alpha-1,3-galactosyltransferase OS-Drosophila melanogaster OX1272 OlnbP1 PE1 SV1	8.3387140	8.1214026	7.9841038	8.0448193	7.4151808	7.0142088	7.9052050	7.6388874	8.0293385	7.2041178	0.8088663	1.1813373	0.0148
OV195	Protein alpha-1,3-galactosyltransferase OS-Drosophila melanogaster OX1272 OlnbP1 PE1 SV1	1.0092204	6.0271689	7.4242811	7.491504	6.7114627	6.2840247	6.2840247	6.4479284	1.8734183	6.5004401	0.6173386	1.6545209	0.04815
OV224	Protein alpha-1,3-galactosyltransferase OS-Drosophila melanogaster OX1272 OlnbP1 PE1 SV1	8.6691026	8.2326884	8.1051878	8.9633701	8.6713812	8.6463172	8.3406907	7.7275845	8.3617987	8.5421147	1.0074821	2.0193244	0.01182
PI278	Protein alpha-1,3-galactosyltransferase OS-Drosophila melanogaster OX1272 OlnbP1 PE1 SV1	8.7027971	8.6526279	8.2746655	8.4651861	7.8243844	7.6200574	8.2746655	7.8194544	8.6454433	7.8913023	0.4642475	1.0216514	0.01726
OV234	Protein alpha-1,3-galactosyltransferase OS-Drosophila melanogaster OX1272 OlnbP1 PE1 SV1	8.89078813	8.8246105	8.4651036	8.4171468	8.3137283	7.5201538	7.5996931	7.1751277	8.6480791	7.4480235	0.9987356	1.9843067	0.02005
OV196	Protein alpha-1,3-galactosyltransferase OS-Drosophila melanogaster OX1272 OlnbP1 PE1 SV1	8.3099024	8.3488884	8.9817882	8.4378801	9.0542709	9.0318487	8.6022774	8.141825	8.4251945	8.840832	0.5425115	1.0528232	0.02467
OV197	Protein alpha-1,3-galactosyltransferase OS-Drosophila melanogaster OX1272 OlnbP1 PE1 SV1	7.4883801	7.3116277	7.1178614	7.1580065	7.0581814	6.4181463	6.4222684	6.5118278	7.2754242	6.9613058	0.8722654	1.5984814	0.03864
PI788	Protein alpha-1,3-galactosyltransferase OS-Drosophila melanogaster OX1272 OlnbP1 PE1 SV1	9.39285147	9.42165237	8.1497854	8.9785888	8.4373017	8.3781756	8.1849425	8.1021165	9.021811	8.1824297	0.8377421	1.7883004	0.00952
OV235	Protein alpha-1,3-galactosyltransferase OS-Drosophila melanogaster OX1272 OlnbP1 PE1 SV1	7.4271262	7.0964986	7.0280003	7.0320052	6.9128175	6.9021812	6.9162709	7.4518209	6.9184684	6.4073854	1.0633851	0.43371	0.01267
GI185	Protein alpha-1,3-galactosyltransferase OS-Drosophila melanogaster OX1272 OlnbP1 PE1 SV1	7.0584881	6.17078305	7.4345566	7.2474688	8.35846613	8.2237895	8.6420114	8.368004	7.2378106	6.5465483	0.8012873	1.6170157	0.03103
PI872	Protein alpha-1,3-galactosyltransferase OS-Drosophila melanogaster OX1272 OlnbP1 PE1 SV1	7.2554521	6.8829216	6.8971708	6.8072041	6.350440	6.1548518	6.6488885	6.1519427	8.9701025	6.0714643	0.9842102	1.8613144	0.00905
OV198	Protein alpha-1,3-galactosyltransferase OS-Drosophila melanogaster OX1272 OlnbP1 PE1 SV1	8.6849233	7.4851406	7.9848969	8.0228025	7.0241861	7.2440247	7.5526562	8.0227718	7.3887381	7.0814389	0.8154871	1.5971628	0.03865
OV199	Protein alpha-1,3-galactosyltransferase OS-Drosophila melanogaster OX1272 OlnbP1 PE1 SV1	8.6691026	8.2326884	8.1051878	8.9633701	8.6713812	8.6463172	8.3406907	7.7275845	8.3617987	8.5421147	1.0074821	2.0193244	0.01182
AI238	Protein alpha-1,3-galactosyltransferase OS-Drosophila melanogaster OX1272 OlnbP1 PE1 SV1	9.2079707	9.5541473	8.9187205	8.4651861	8.6413209	8.5092100	8.4624715	7.9816647	8.9224224	8.0745691	0.4656199	1.0781982	0.02076
OV238	Protein alpha-1,3-galactosyltransferase OS-Drosophila melanogaster OX1272 OlnbP1 PE1 SV1	5.98365141	5.5328986	5.6245461	4.9068016	5.449924	5.4018883	4.9217301	5.6445485	5.0262484	4.6172146	1.5330994	0.05878	0.04339
OV191	Protein alpha-1,3-galactosyltransferase OS-Drosophila melanogaster OX1272 OlnbP1 PE1 SV1	8.3126201	7.8449718	7.4458871	7.063714	7.5071003	7.4557721	6.1517034	6.9018902	7.8517331	7.1444675	0.2742706	0.6508387	0.02171
OV192	Protein alpha-1,3-galactosyltransferase OS-Drosophila melanogaster OX1272 OlnbP1 PE1 SV1	10.3933478	10.824183	11.327597	11.171393	8.686005	8.426289	10.288441	10.289142	10.920244	9.8613859	0.8282205	0.01738	0.02331
OV193	Protein alpha-1,3-galactosyltransferase OS-Drosophila melanogaster OX1272 OlnbP1 PE1 SV1	6.1784486	6.8487974	6.2878695	6.9308747	5.9774327	6.0122888	5.1972949	5.2018662	6.6613236	5.6120389	1.0482186	2.0977489	0.012
OV201	Protein alpha-1,3-galactosyltransferase OS-Drosophila melanogaster OX1272 OlnbP1 PE1 SV1	7.8426363	7.8946487	7.8861697	7.8076171	7.5164764	7.2053763	7.0148344	6.7800544	7.9148344	6.7800544	0.4642475	1.0216514	0.01726
OV194	Protein alpha-1,3-galactosyltransferase OS-Drosophila melanogaster OX1272 OlnbP1 PE1 SV1	8.44800347	8.37872638	8.1956577	8.1104234	8.9683706	8.1765380	8.3268317	7.5904812	8.2093474	8.48712239	0.8122124	1.7509189	0.01061
PI193	Protein alpha-1,3-galactosyltransferase OS-Drosophila melanogaster OX1272 OlnbP1 PE1 SV1	8.3387140	8.1214026	7.9841038	8.0448193	7.4151808	7.0142088	7.9052050	7.6388874	8.0293385	7.2041178	0.8088663	1.1813373	0.0148
OV195	Protein alpha-1,3-galactosyltransferase OS-Drosophila melanogaster OX1272 OlnbP1 PE1 SV1	1.0092204	6.0271689	7.4242811	7.491504	6.7114627	6.2840247	6.2840247	6.4479284	1.8734183	6.5004401	0.6173386	1.6545209	0.04815
OV224	Protein alpha-1,3-galactosyltransferase OS-Drosophila melanogaster OX1272 OlnbP1 PE1 SV1	8.6691026	8.2326884	8.1051878	8.9633701	8.6713812	8.6463172	8.3406907	7.7275845	8.3617987	8.5421147	1.0074821	2.0193244	0.01182
PI278	Protein alpha-1,3-galactosyltransferase OS-Drosophila melanogaster OX1272 OlnbP1 PE1 SV1	8.7027971	8.6526279	8.2746655	8.4651861	7.8243844	7.6200574	8.2746655	7.8194544	8.6454433	7.8913023	0.4642475	1.0216514	0.01726
OV234	Protein alpha-1,3-galactosyltransferase OS-Drosophila melanogaster OX1272 OlnbP1 PE1 SV1	8.89078813	8.8246105	8.4651036	8.4171468	8.3137283	7.5201538	7.5996931	7.1751277	8.6480791	7.4480235	0.9987356	1.9843067	0.02005
OV196	Protein alpha-1,3-galactosyltransferase OS-Drosophila melanogaster OX1272 OlnbP1 PE1 SV1	8.3099024	8.3488884	8.9817882	8.4378801	9.0542709	9.0318487	8.6022774	8.141825	8.4251945	8.840832	0.5425115	1.0528232	0.02467
OV197	Protein alpha-1,3-galactosyltransferase OS-Drosophila melanogaster OX1272 OlnbP1 PE1 SV1	7.4883801	7.3116277	7.1178614	7.1580065	7.0581814	6.4181463	6.4222684	6.5118278	7.2754242	6.9613058	0.8722654	1.5984814	0.03864
PI788	Protein alpha-1,3-galactosyltransferase OS-Drosophila melanogaster OX1272 OlnbP1 PE1 SV1	9.39285147	9.42165237	8.1497854	8.9785888	8.4373017	8.3781756	8.1849425	8.1021165	9.021811	8.1824297	0.8377421	1.7883004	0.00952
OV235	Protein alpha-1,3-galactosyltransferase OS-Drosophila melanogaster OX1272 OlnbP1 PE1 SV1	7.4271262	7.0964986	7.0280003	7.0320052	6.9128175	6.9021812	6.9162709	7.4518209	6.9184684	6.4073854	1.0633851	0.43371	0.01267
GI185	Protein alpha-1,3-galactosyltransferase OS-Drosophila melanogaster OX1272 OlnbP1 PE1 SV1	7.0584881	6.17078305	7.4345566	7.2474688	8.35846613	8.2237895	8.6420114	8.368004	7.2378106	6.5465483	0.8012873	1.6170157	0.03103
PI872	Protein alpha-1,3-galactosyltransferase OS-Drosophila melanogaster OX1272 OlnbP1 PE1 SV1	7.2554521	6.8829216	6.8971708	6.8072041	6.350440	6.1548518	6.6488885	6.1519427	8.9701025	6.0714643	0.9842102	1.8613144	0.00905
OV198	Protein alpha-1,3-galactosyltransferase OS-Drosophila melanogaster OX1272 OlnbP1 PE1 SV1	8.6849233	7.4851406	7.9848969	8.0228025	7.0241861	7.2440247	7.5526562	8.0227718	7.3887381	7.0814389	0.8154871	1.5971628	0.03865
OV199	Protein alpha-1,3-galactosyltransferase OS-Drosophila melanogaster OX1272 OlnbP1 PE1 SV1	8.6691026	8.2326884	8.1051878	8.9633701	8.6713812	8.6463172	8.3406907	7.7275845	8.3617987	8.5421147	1.0074821	2.0193244	0.01182
AI238	Protein alpha-1,3-galactosyltransferase OS-Drosophila melanogaster OX1272 OlnbP1 PE1 SV1	9.2079707	9.5541473	8.9187205	8.4651861	8.6413209	8.5092100	8.4624715	7.9816647	8.9224224	8.0745691	0.4656199	1.0781982	0.02076
OV238	Protein alpha-1,3-galactosyltransferase OS-Drosophila melanogaster OX1272 OlnbP1 PE1 SV1	5.98365141	5.5328986	5.6245461	4.9068016	5.449924	5.4018883	4.9217301	5.6445485	5.0262484	4.6172146	1.5330994	0.05878	0.04339
OV191	Protein alpha-1,3-galactosyltransferase OS-Drosophila melanogaster OX1272 OlnbP1 PE1 SV1	8.3126201	7.8449718	7.4458871	7.063714	7.5071003	7.4557721	6.1517034	6.9018902	7.8517331	7.1444675	0.2742706	0.6508387	0.02171

Supplemental Table 3-5: Primers used in iPOND study**dsRNAs Primers:**

GFP-dsRNA-RP	TAATACGACTCACTATAGGGGTGAGTTATAGTTGTATTC
GFP-dsRNA-FP	TAATACGACTCACTATAGGGGGAGAAGAAGAACTTTTCACTGG
BRWD3-dsRNA1-FP	TAATACGACTCACTATAGGGAAACGACTACCCAGGACATT
BRWD3-dsRNA1-RP	TAATACGACTCACTATAGGGCCCACGGAGCTGTTCTTT
BRWD3-dsRNA2-FP	TAA TAC GAC TCA CTA TAG GAT GGA AAC TAG ACAACC CAG TTC
BRWD3-dsRNA2-RP	TAA TAC GAC TCA CTA TAG GAT GTC TGT AAT CTC GGA TGA GG
Hd-dsRNA-FP	TAATACGACTCACTATAGGGGTGCGAGCTCACGCTC
Hd-dsRNA-RP	TAATACGACTCACTATAGGGGGTTCAACCAATGCAATTACTA
CuI4-dsRNA-FP	TAATACGACTCACTATAGGGATCTGTGGTTCCCTTGTTGC
CuI4-dsRNA-RP	TAATACGACTCACTATAGGGGCCGAACACCTAACGTCAAT
RTEL-dsRNA-FP	TAATACGACTCACTATAGGGAGACGCGAAGTAGGGACAGA
RTEL-dsRNA-RP	TAATACGACTCACTATAGGGCAGATTTTTTCGGGTCTTGGA
ELG1-dsRNA-FP	TAATACGACTCACTATAGGGCTTGGCAGCGTTCTACTTC
ELG1-dsRNA-RP	TAATACGACTCACTATAGGGCCTAATCGAGGATGCGGATA
Polybromo-dsRNA-FP	TAATACGACTCACTATAGGGGATTTTCCATTCTGCTCCCA
Polybromo-dsRNA-RP	TAATACGACTCACTATAGGGGGAAAGTGTCAAGAGCAGCC
Pont -dsRNA-FP	TAATACGACTCACTATAGGGTCAGTTTTTCTCGGCTTCA
Pont -dsRNA-RP	TAATACGACTCACTATAGGGGTATTTCAGCAATGAGATCAAGA
Fifi-dsRNA-RP	TAATACGACTCACTATAGGGGTATCTGAAGCAGTTAGCCA
Fifi-dsRNA-FP	TAATACGACTCACTATAGGGGCCGATTGGCCTGGTTG
Hyd -dsRNA-FP	TAATACGACTCACTATAGGGCTTGTGCAGCGTTTGAATA
Hyd -dsRNA-RP	TAATACGACTCACTATAGGGAGGGTTCGCAATGTTAGCAC
Mei41 (ATR)-dsRNA-RP	TAATACGACTCACTATAGGGGTGCGACATGGACACAAAAC
Mei41 (ATR)-dsRNA-FP	TAATACGACTCACTATAGGGTTTGGTAAGCACTTGGACC
DNApol-alpha180-dsRNA-RP	TAATACGACTCACTATAGGGTCTTGGCTGATTTTTGGGC
DNApol-alpha180-dsRNA-FP	TAATACGACTCACTATAGGGGAAACCTTCTCGGTCTGCTG
DEK-dsRNA-FP	TAATACGACTCACTATAGGGGACTCGTCCGGTTCATTAG
DEK-dsRNA-RP	TAATACGACTCACTATAGGGATGGCCTGGACAAGAACAAC

qPCR Primers:

BRWD3-qPCR-FP	CAGTGCGCTATTTGAGTCGC
BRWD3-qPCR-RP	TCGCTCCTTTTTGACTCGCT
DEK-qPCR-FP	ACAAATGTTTAACTGCTGTTCCCA
DEK-qPCR-RP	GCAGGAGTTGGGATGCGATA
Hyd-qPCR-FP	TGTGAGGTATCCGAGGCTCT
Hyd-qPCR-RP	TCGTGAGGTTATCCAGATTCGAC
DNApolalpha180-qPCR-FP	CACAGCAGACCGAGAAGGTT
DNApolalpha180-qPCR-RP	TTTCGGCGACTTTGCTTTGG
Hd-qPCR-FP	CGTTTCTTCTGTCCCACGGA
Hd-qPCR-RP	CGTTGCGTCCGAGATATCCA
CuI4-qPCR-FP	CGCCAGCTAATAGTGTAGCGA
CuI4-qPCR-RP	TTTCAAAGGACTCGGCTTGT
RTEL-qPCR-FP	CCCAGGCGGATATCACCTTC
RTEL-qPCR-RP	ATGTTGTGGCCTCATCTG
ELG1-qPCR-FP	ATGCTCGGAATCGCTCTCTG
ELG1-qPCR-RP	TGCCTCACTGCCGATTTCTT
Polybromo-qPCR-FP	CATGCGCAAGTTCCAACACA
Polybromo-qPCR-RP	GAGCTCAGCGAGGGTGTATC
Pont-qPCR-FP	GCTGTGTTATTCGTGGCACC
Pont-qPCR-RP	GAGCTGGTTCCAATCTCGCT
mei41(ATR)-qPCR-FP	GATCGCATCTTCCGGCAAAC
mei41(ATR)-qPCR-RP	CTGACTCCTGGAAGCCACTG
fifi-qPCR-RP2	CGTGAGGATGTCGATGGAGG
fifi-qPCR-FP2	CGCGACACAGTTCTTCTCCT
alphanub84b qPCR Fwd	CACACCACCTGGAGCATTC
alphanub84b qPCR Rev	CCAATCAGACGGTTCAGGTTG

Chapter IV: R-loop mapping and characterization during *Drosophila* embryogenesis reveals developmental plasticity in R-loop signatures

Abstract

R-loops are involved in transcriptional regulation, DNA and histone post-translational modifications, genome replication and genome stability. To what extent R-loop abundance and genome-wide localization is actively regulated during metazoan embryogenesis is unknown. *Drosophila* embryogenesis provides a powerful system to address these questions due to its well-characterized developmental program, the sudden onset of zygotic transcription and available genome-wide data sets. Here, we measure the overall abundance and genome localization of R-loops in early and late-stage embryos relative to *Drosophila* cultured cells. We demonstrate that absolute R-loop levels change during embryogenesis and that RNaseH1 catalytic activity is critical for embryonic development. R-loop mapping by strand-specific DRIP-seq reveals that R-loop localization is plastic across development, both in the genes which form R-loops and where they localize relative to gene bodies. Importantly, these changes are not driven by changes in the transcriptional program. Negative GC skew and absolute changes in AT skew are associated with R-loop formation in *Drosophila*. Furthermore, we demonstrate that while some chromatin binding proteins and histone modifications such as H3K27me3 are associated with R-loops throughout development, other chromatin factors associated with R-loops in a developmental specific manner. Our findings highlight the importance and developmental plasticity of R-loops during *Drosophila* embryogenesis.

* This chapter is in press as Munden, A., Benton, M. L., Capra, J. A. & Nordman, J. R-loop mapping and characterization during *Drosophila* embryogenesis reveals developmental plasticity in R-loop signatures. *Journal of Molecular Biology*. (2021). doi: 10.1016/j.jmb.2022.167645.

Introduction

R-loops are a three-stranded nucleic acid structure canonically formed when nascent RNA from transcription reanneals to the template DNA strand, resulting in a displaced single strand of DNA (Aguilera and García-Muse 2012). R-loops were initially identified at the highly transcribed 18S and 28S sequences within the rDNA locus of *Drosophila melanogaster* (White and Hogness 1977; Glover and Hogness 1977). More recent studies have demonstrated that R-loops are critical for a diverse set of biological processes (Chédin 2016; Skourtie-Stathaki and Proudfoot 2014). In fact, genome-wide R-loop mapping studies have revealed that R-loops are abundant in eukaryotes and can occupy 10% or more of the genome (Dumelie and Jaffrey 2018; Wahba and Koshland et al. 2016; Fang and Zhang et al. 2019; Xu and Sun et al. 2017; Yan and Liu et al. 2020; Zeller and Gasser et al. 2016; Chen and Fu et al. 2017; Chen and Fazzio et al. 2015; Crossley and Cimprich et al. 2020; Ginno and Chédin et al. 2012; Tan-Wong and Proudfoot et al. 2019; Chan and Hieter et al. 2014; Liu and Han et al. 2021). While R-loops were identified over 40 years ago, their physiological relevance remained elusive for many years.

R-loops are found in all domains of life and their formation is often conserved across cell types and even species (Sanz and Chédin et al. 2016). Deciphering the function of R-loops, however, has been challenging due to their diverse and sometimes contradictory roles in genome function. R-loops are essential for initiation of replication in

plasmids and promote mitochondrial genome stability (Dasgupta and Tomizawa et al. 1987; Silva and Aguilera et al. 2018). In contrast, R-loops can block replication fork progression and promote genome instability in an orientation-specific manner (Hamperl and Cimprich et al. 2017; Lang and Merrih et al. 2017). While potentially causing double-strand breaks at head-on replication-transcription conflicts, R-loops can promote recombination and double strand break repair pair (Stork and Cimprich et al. 2016; Ouyang and Zou et al. 2021). R-loops also have diverse roles in transcription and chromatin function. In mammalian cells, R-loops have been shown to regulate both histone and DNA methylation at promoter regions (Ginno and Chédin et al. 2012; Chen and Fazio et al. 2015). While R-loops are often associated with histone modifications correlated with active transcription, recent work has shown that R-loops can help recruit the Polycomb complex to target loci to promote transcriptional silencing (Skourti-Stathaki and Pombo et al. 2019; Alecki and Francis et al. 2020). Genome-wide R-loop mapping studies in yeast, plants and mammalian cultured cells have identified factors such as DNA sequence, DNA topology and histone modifications associated with R-loop formation (Ginno and Chédin et al. 2012; Stolz and Chédin et al. 2019; Hage and Tollervey et al. 2010). R-loop mapping studies in plants and mammalian cells have further revealed that R-loop formation can be dynamic as a function of development (Fang and Zhang et al. 2019; Xu and Sun et al. 2020; Yan and Liu et al. 2020). The extent of R-loop plasticity in other metazoans has yet to be defined. Studying R-loops in the context of development could provide insight into the functional roles R-loops play in establishing developmental-specific changes in chromatin structure, function and transcriptional programs.

Drosophila provide a well-established developmental system to interrogate R-loop plasticity during development. At the earliest stages of *Drosophila* embryogenesis, rapid cell proliferation is driven by maternally stockpiled proteins and RNA (Tadros and Lipshitz 2009). Approximately two hours after fertilization, zygotic genome activation is triggered and the transcription of over 3000 genes necessary for growth and differentiation are induced in a process known as the maternal-to-zygotic transition (MZT) (Hamm and Harrison 2018; Harrison and Eisen et al. 2011). Prior to the MZT, cells are largely undifferentiated and have abbreviated cell cycles (Foe and Alberts 1983). After the MZT, however, the cell cycle slows and cells become differentiated as morphogenesis proceeds (Farrell and O'Farrell 2014). The changes in cell cycle programs, the onset of zygotic gene activation and cell differentiation during embryogenesis provide a unique system to interrogate whether R-loop formation or resolution impacts embryogenesis and the extent to which, if any, R-loop position and properties change as a function of development.

In this study, we measured R-loop abundance and position in *Drosophila* embryos and cultured cells. We show that absolute R-loop levels change during embryogenesis and resolution of R-loops is essential for embryogenesis. We mapped R-loops at near base-pair resolution in 2-3 hour embryos (immediately after the MZT), late-stage embryos (14-16 hours after fertilization) and cultured S2 cells, which are derived from late-stage embryos. We show that, while some sites of R-loop formation are constant during development, there is extensive R-loop plasticity during *Drosophila* development. Furthermore, we were able to demonstrate changes in the localization of R-loops across gene bodies and the role AT and GC skew play in *Drosophila* R-loop formation. By

leveraging data available through modENCODE and other publicly available datasets, we were able to identify specific histone modifications and chromatin binding proteins associated with R-loop formation in *Drosophila* and the role active transcription has on R-loop formation. Importantly, developmental-specific R-loops are not driven by transcriptional changes, emphasizing the role that chromatin and R-loop binding proteins play in regulating R-loop formation. Our work establishes *Drosophila* as a powerful developmental model system to study R-loop biology.

Results

R-loop abundance is developmentally regulated and R-loop homeostasis is necessary for development

To determine if R-loop abundance and genomic location are regulated throughout development, we turned to the powerful *Drosophila* embryogenesis system. For our analysis, we chose embryos at two distinct time points: 2-3 hours after egg laying (AEL) and 14-16 hours AEL (Figure 4-1A). The 2-3 hour time point corresponds with the onset of the maternal-to-zygotic transition (MZT) occurring during nuclear cleavage cycle 14 (Blythe and Wieschaus 2015). This time point represents the onset of zygotic transcription and allows us to draw upon the wealth of scientific literature that has previously been published, including time-matched modENCODE datasets. The wide-scale activation of zygotic transcription at this time point should provide the first opportunity for R-loop formation during development. To complement this developmental stage, we chose 14-16 hour AEL embryos to understand how R-loop formation might differ in differentiated cells with a more mature chromatin environment and a transcription program

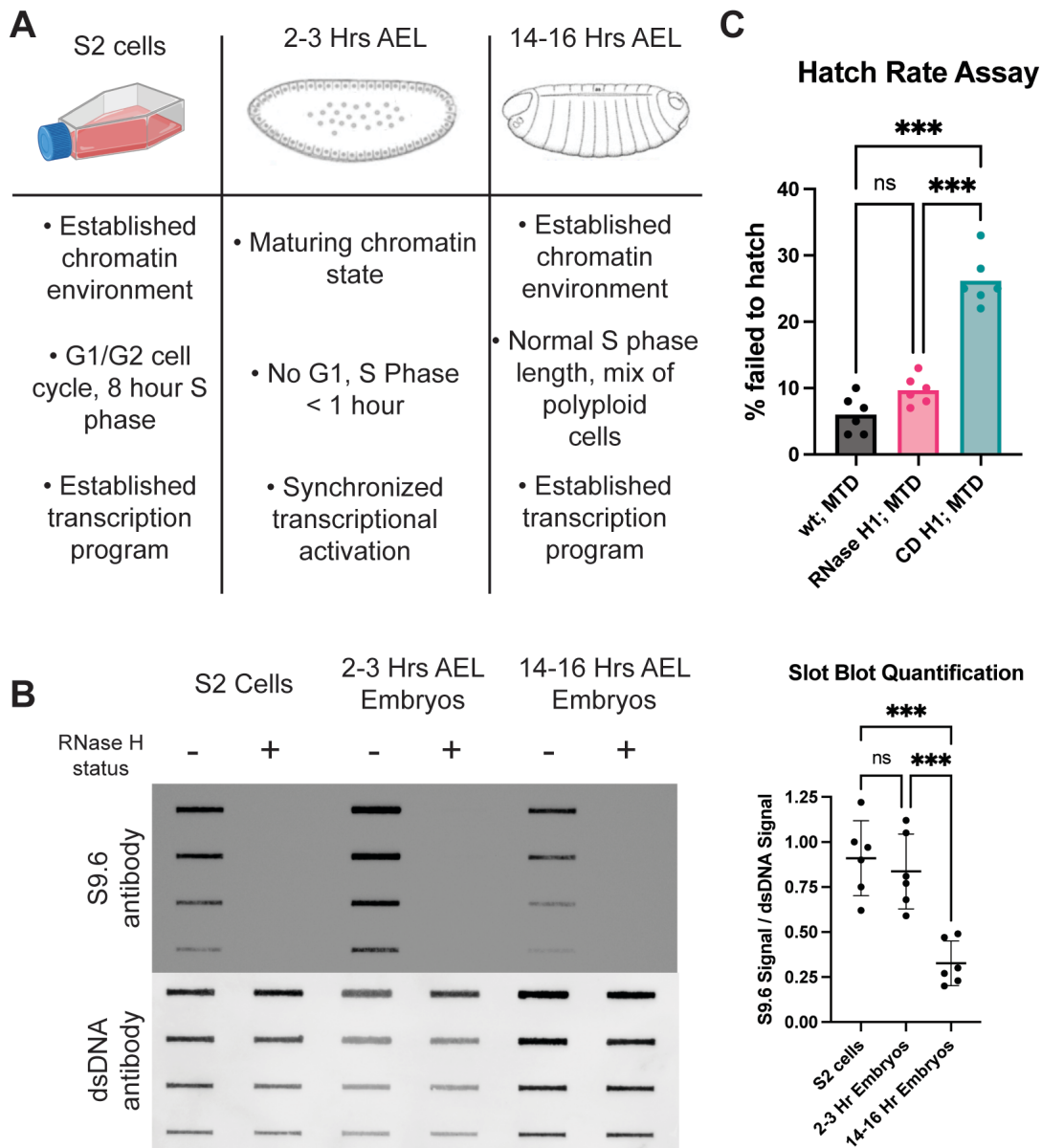


Figure 4-1. **R-loop abundance is developmentally regulated and R-loop homeostasis is necessary for development.** (A) Schematic summarizing how the chromatin environment, developmental stage, and replication program vary among the developmental samples used. (B) Representative slot blot of RNA:DNA hybrid levels, measured by S9.6 antibody intensity, across samples. RNase H treatment verifies specificity of antibody, and antibody specific for double-stranded DNA is used as a loading control. Quantification of signal for six biological replicates is to the right. *** < 0.05, one-way ANOVA with Tukey's multiple comparisons test. (C) Hatch rate among embryos that overexpress RNase H1 (H1) or a catalytic dead RNase H1 (CD). 6 biological replicates from 2 independent crosses, counting 100 embryos in each replicate. *** < 0.05, one-way ANOVA with Tukey's multiple comparisons test. Contributions: Experiment, analysis, visualization.

characterized by cell-type-specific maintenance (Bonnet and Müller et al. 2019; Bowman and Bender 2014; Smith and Orr-Weaver 1991). S2 cells, an established *Drosophila* cell

culture line derived from late-stage embryos (Schneider 1972), were used to determine how R-loops might differ between embryos and cultured cells, where the majority of R-loop research has been conducted.

To begin, we asked whether the absolute levels of R-loops are influenced by development. To this end, genomic DNA was extracted from each sample and spotted onto a nitrocellulose membrane and probed with the S9.6 antibody, which recognizes RNA:DNA hybrids (Boguslawski and Carrico 1986). S2 cells and 2-3h embryos showed similar amounts of S9.6 signal, while DNA from 14-16h embryos showed a significant decrease in S9.6 signal (Figure 4-1B). To ensure that the S9.6 signal stems from R-loops, we pretreated control samples with RNase H, which degrades the RNA moiety of a RNA:DNA hybrid. The S9.6 antibody has some specificity to double-stranded RNA and *Drosophila* embryos are known to contain dsRNA (Hartono and Vanoosthuysen et al. 2018). In fact, in the RNase H treated control samples we initially detected some signal with the S9.6 antibody, which was completely eliminated by pretreatment with RNase III. Therefore, for all R-loop assays we pretreat our samples with RNase III to ensure S9.6 signal isn't due to dsRNA.

Next, we asked whether perturbing R-loop homeostasis affects embryogenesis. *rnh1* mutants survive into larval development, which suggests that *rnh1* and R-loop processing may be dispensable during embryogenesis (Filippov et al 2001). More likely, however, *rnh1* mutant embryos survive from maternal stockpiles of RNase H1. To circumvent this, we generated flies that overexpress a GFP-tagged, nuclear localized version of *Drosophila* RNase H1 or a catalytically dead version of the same protein (RNase H1^{CD}). To ensure that the RNase H1 proteins were maternally deposited and

present at the earliest stages of embryogenesis, we used the pUASz expression system coupled with the maternal triple driver (DeLuca and Spradling 2018; Rørth 1998). After confirming that the GFP was observable by Western blot (Supplemental Figure 4-1A), we performed a hatch rate assay to determine if perturbing RNaseH1 catalytic activity affects embryogenesis. We observed a consistent but statistically insignificant hatching defect in the RNase H1 overexpression embryos (Figure 4-1C). The RNase H1^{CD} expressing embryos, however, had a ~25% failure to hatch rate, which was significantly different from the wild-type and the RNase H1 overexpression controls. To determine the effect overexpression of RNase H1 or RNase H1^{CD} constructs have on absolute R-loop levels, we measured bulk R loop levels from 2-6h embryos expressing these constructs. While there wasn't a significant reduction in R-loop levels upon RNaseH1 overexpression, R-loop levels increased upon overexpression of the RNaseH1^{CD} mutant, suggesting the catalytic dead mutant blocks the processing of R-loops even in the presence of endogenous RNaseH1 (Supplemental Figure 4-1B). Overall, we conclude that the absolute abundance of R-loops changes during development and that RNase H1 catalytic activity is important for R-loop resolution and embryonic development.

R-loop position and properties are influenced during development

While the absolute abundance of R-loops changes during development, we wanted to determine how R-loop position throughout the genome changes during *Drosophila* development. Genome-wide R-loop mapping during *Drosophila* development would allow us to ask if R-loop formation is hardwired into the genome and driven only by cell-type-specific transcription, or, more interestingly, is R-loop formation plastic during

development changing independent of sequence composition and transcription status. To address this question, we performed DNA:RNA immunoprecipitation on sonicated nucleic acids followed by strand-specific sequencing of the DNA strand (ssDRIP-seq) in S2 cells, 2-3h and 14-16h embryos (Figure 4-2A) (Xu and Sun 2017). We initially tried DNA-RNA immunoprecipitation followed by cDNA conversion coupled to high-throughput sequencing (DRIPc-seq) (Sanz and Chédin et al. 2016). When conducted in *Drosophila*, however, we found high levels of RNA contamination in the final sequencing results (data not shown). Even with the ssDRIP-seq method, it was necessary to pre-treat genomic DNA preps with RNase A and RNase III as *Drosophila* embryos are stockpiled with RNA. ssDRIP-seq of embryos and S2 cells revealed strand-specific signal that was sensitive to RNase H pretreatment, and showed cell-type specific R-loop formation (Figure 4-2B and 4-2C). Providing validity to our data sets, biological replicates were highly correlated (Supplemental Figure 4-2A) and our ssDRIP data sets correlated with recently published ssDRIP-seq data sets in *Drosophila* S2 cells and embryos as expected based on the similar but different time points (Supplemental Figure 4-2B) (2-3h and 14-16h vs. 2-6h and 10-14h embryos) and known differences in R-loop mapping between different labs (Alecki et al 2020, Chédin et al 2021). Furthermore, our S2 data sets were highly correlated with two R-loop mapping studies performed in cultured cells, but not correlated with an R-loop data set generated for a spike-in control and not used in mapping studies (Supplemental Figure 4-2C, D) (Crossley et al 2020, Bayona-Feliu et al 2017). We validated several sites using DRIP-qPCR to confirm our sequencing results (Supplemental Figure 4-2F-G). Taken together, these data indicate that our ssDRIP

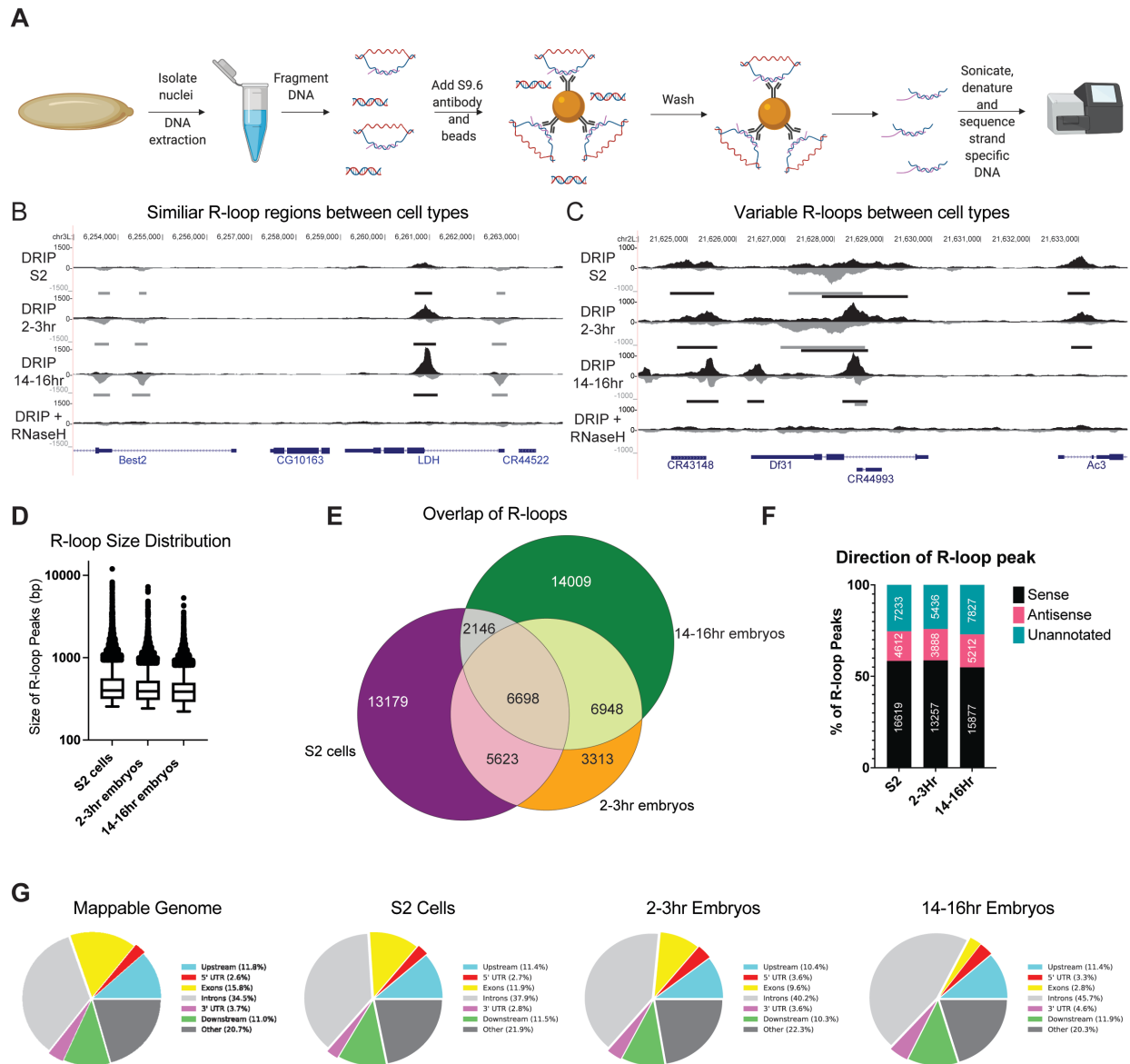


Figure 4-2: The R-loop landscape changes as a function of development. (A) Diagram of the ssDRIP-seq mapping strategy. **(B)** ssDRIP-seq snapshot of a 10kb region on chromosome 3L where R-loop distribution is similar between samples. Black and grey bars below each track represent peak calls for forward and reverse strands, respectively **(C)** ssDRIP-seq snapshot of a 10kb region on chromosome 2L where R-loop distribution varies between samples. Note the reverse strand coming from a lncRNA in the middle of the Df31 gene. **(D)** The distribution of R-loop sizes for each developmental sample. **(E)** Overlap of R-loops between developmental samples. **(F)** Quantification of the percent of R-loops mapping to sense, antisense and untranscribed regions of the genome. Numbers represent absolute R-loop peaks in each category **(G)** R-loop enrichment relative to the expected distribution for common genomic features. Contributions: Experiment, analysis, visualization.

signal reflects high quality and robust RNA:DNA hybrid mapping throughout the genome and that ssDRIP is a robust method to map sites of R-loop formation in *Drosophila*.

To map the precise location of R-loops throughout the genome and allow us to compare both quantitative and qualitative properties of R-loops, we used MACS to define R-loop peaks. Peaks were called separately against the input samples and RNase H treated controls, and only overlapping peaks were kept for analysis. Using this criterion, we identified 27,646, 22,581 and 29,801 peaks in S2 cells, 2-3h and 14-16h, respectively, which occupied between 8.3 and 12.5% of the genome. The overlap of sense and antisense R-loops had similar ratios (Supplemental Figure 4-2E). R-loop peak size was similar between sample types with a median of approximately 500 bp, but R-loops could occupy zones up to 10kb in size (Figure 4-2D). Out of the 51,916 total unique R-loop peaks identified between all samples, 12.9% were common to all sample types, 28.3% were present in at least two samples and 58.8% were specific to an individual sample (Figure 4-2E).

Since ssDRIP allows for strand-specific annotation, we characterized R-loops relative to strand-specific genomic features. Relative to transcription units, 55-60% of R-loops occur in sense to transcription in S2 cells and 2-3h embryos, whereas ~15% of R-loops are antisense (Figure 4-2F). In all samples, 25-30% of the R-loops form in unannotated regions of the genome. Next, we used Pavis to annotate R-loop signal relative to genomic features. In all samples, we found that ~50% of R-loops mapped to introns or exons (Figure 4-2G). This is expected given that a significant fraction of R-loops should be produced from coding regions. GO term analysis of R-loop forming genes revealed that R-loops preferentially form in genes associated with RNA Pol II-dependent transcription and sample-specific R-loops form in genes associated with sample-specific

development (Supplemental Table 4-2). Taken together, these results demonstrate that R-loop signal across *Drosophila* development is dynamic.

R-loop enrichment at transcription units changes during development

In mammals, R-loops are known to preferentially form at transcription start sites (TSS), gene bodies and transcription termination sites (TTS) (Sanz and Chédin et al. 2016; Skourti-Stathaki and Proudfoot et al. 2014). To ask if this pattern of R-loop formation is similar in *Drosophila*, and whether it changes during development, we measured R-loop abundance across gene bodies in our developmental samples. We then generated metaplots using strand-specific data for all time points. S2 cells and 2-3h embryos display a very similar pattern of R-loop formation, with a strong peak at the TSS and continued signal over the gene body (Figure 4-3A), which is similar to R-loop positions in other metazoans (Sanz and Chédin et al. 2016). In 2-3h embryos and S2 cells, there was a greater signal for sense R-loop over the gene body, as would be expected given that the majority of R-loops are generated during transcription. Antisense R-loop signal was prevalent at the TSS and close to the TTS in 2-3h embryos (Figure 4-3A). Interestingly, there is a depletion of R-loops immediately after the TTS in 2-3h embryos and S2 cells (Figure 4-3A). The 14-16h embryos, however, have a significantly different pattern altogether. In 14-16h embryos, we observed the most abundant signal within and around the TSS and TTS regions with a relative reduced signal within the gene body (Figure 4-3A). The enrichment of R-loops at the TTS in 14-16h embryos was not driven by differences in R-loop forming genes between the samples as R-loop forming

genes are similar between 2-3h and 14-16h embryos (Supplemental Figure 4-3B). In the 14-16h

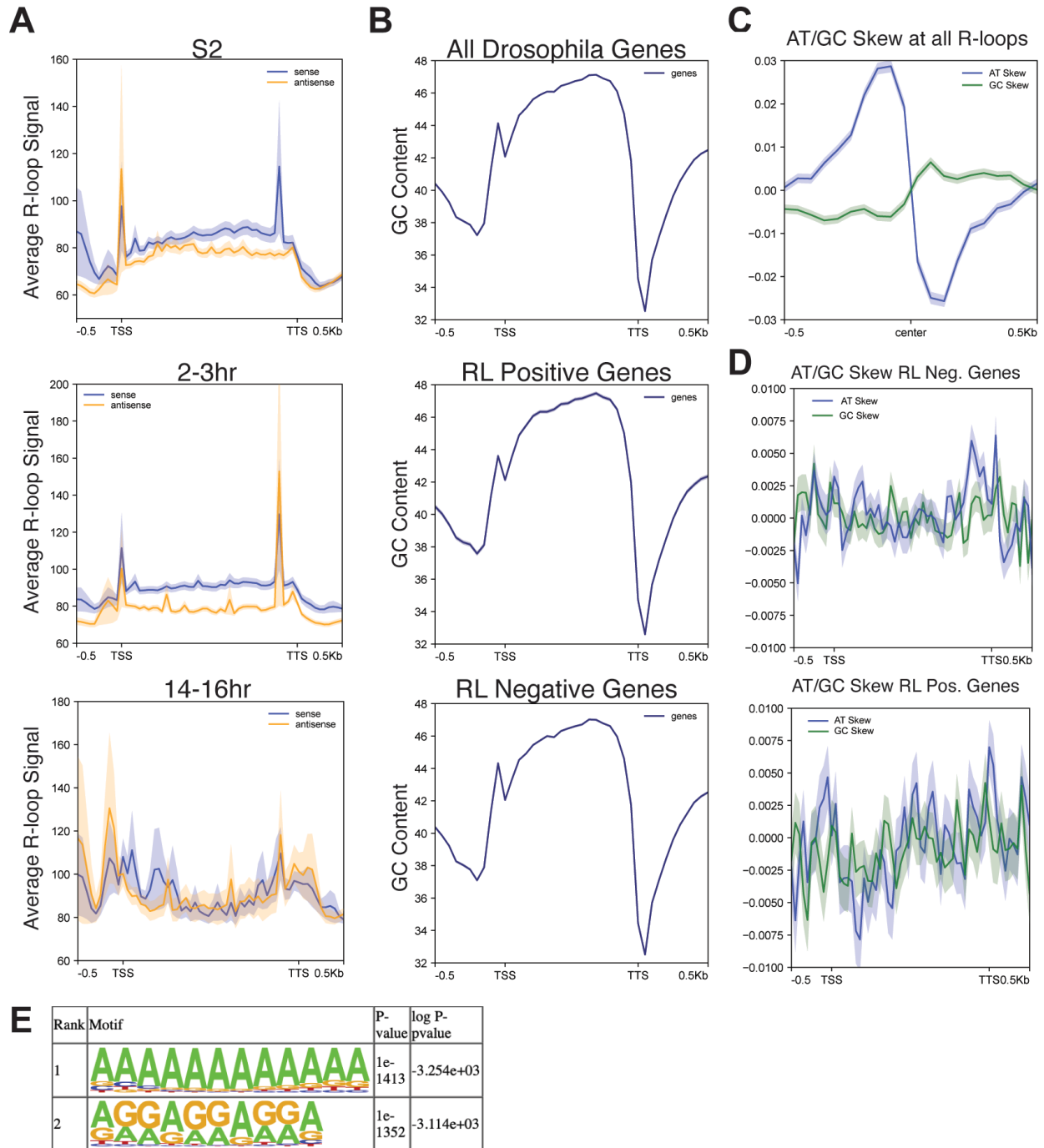


Figure 4-3. **R-loop signal as a function of transcription unit and sequence composition.** (A) Metaplots of ssDRIP-seq signal for all samples relative to the gene body. Each plot represents the signal derived from sense R-loops in blue and antisense R-loops in orange. Shaded region represents the standard error of the mean (SEM). (B) The GC composition of all Drosophila genes, genes that have an R-loop in one of the developmental samples and genes that lack any R-loop signal. Shaded region represents the SEM. (C)

Metaplot of GC and AT skew across all identified R-loops. Shaded region represents the SEM. **(D)** Metaplot of GC and AT skew across the gene body of genes that lack R-loops (top) and genes that form an R-loop. Shaded region represents the SEM. **(E)** DNA sequence motifs in the peaks of all R-loops identified by HOMER. Motif analysis was not strand specific. Contribution: Experiment, partial analysis, and visualization.

embryos, however, both sense and antisense R-loops have similar levels throughout the transcription unit (Figure 4-3A). Taken together, we conclude that R-loop enrichment at transcription units is not hardwired into the genome, but can be dynamic as a function of development.

Given that the absolute levels and relative position of R-loops can change between developmental states in *Drosophila*, we wanted to assess the contribution DNA sequence composition has on R-loop formation in *Drosophila*. Unlike in mouse and human cells, *Drosophila* lack high GC content at the TSS. In fact, GC content decreases relative to the gene body in *Drosophila* (Figure 4-3B). We asked if R-loop forming genes differ in their GC content relative to genes that lack R-loops. We found that genes with and without R-loops have a near-identical GC content along the gene body (Figure 4-3B). While overall GC content is not different in R-loop positive or negative genes, GC and AT skew has been shown to be a contributing factor to R-loop formation (Ginno and Chédin et al. 2012). To test if GC or AT skew is associated with R-loop formation in *Drosophila*, we measured the AT/GC skew directly over all identified R-loops. This analysis revealed a striking transition from positive to negative AT skew at the center of our combined R-loop signal. This is mirrored by a less dramatic transition from negative to positive GC skew centered at the combined R-loop signal (Figure 4-3C). Interestingly, developmental-specific R-loops had AT/GC skew profiles that were distinct from all R-loops combined (Figure 4-3C; Supplemental Figure 4-3A).

We also calculated GC and AT skew for R-loop forming and deficient genes in all samples. Stronger negative GC skew at the TSS was observed in R-loop forming genes relative to genes that fail to form R-loops (Figure 4-3D). Specifically, AT skew at the TSS transitioned from positive skew in R-loop deficient genes to negatively skew in R-loop forming genes. At the TTS, there is a strong positive AT skew around the TTS in both R-loop positive and negative genes (Figure 4-3D). Negative GC skew is stronger at the TSS in R-loop forming genes. This analysis reveals a correlation between altered AT skew and negative GC skew in R-loop forming genes, suggesting that AT/GC skew could contribute to R-loop formation in *Drosophila*. Due to the strong presence of R-loops at promoters and TSS in this and other R-loop mapping studies, we examined whether the AT and GC skew specifically at the promoter or TSS regions to determine if they were driving the overall skew. AT and GC skew was calculated for R-loops at promoter and TSS regions versus every other R-loop peak for each cell type (Supplemental Figure 4-3B). AT and GC skew at promoter and TSS regions was similar to overall skew, though this varied in S2 cells. Together, we conclude that while AT and GC skew could facilitate R-loop formation, developmental-specific R-loop formation is not likely driven by changes in AT or GC skew. This suggests that transcription, chromatin environment or other factors could contribute to cell type specific R-loop formation.

To test whether any specific DNA sequence motifs are associated with R-loop formation, we searched for motifs enriched in the set of all *Drosophila* R-loops. Two motifs stood out as an order of magnitude more significantly enriched than any others: a polyadenine tract and a polypurine tract (Figure 4-3D, Supplemental Figure 4-3B for the entire table). This indicates that polypurine tracts are conducive to R-loop formation,

which is consistent with the known thermodynamic stability of RNA:DNA hybrid formation in purine-rich template sequences (Huppert 2008).

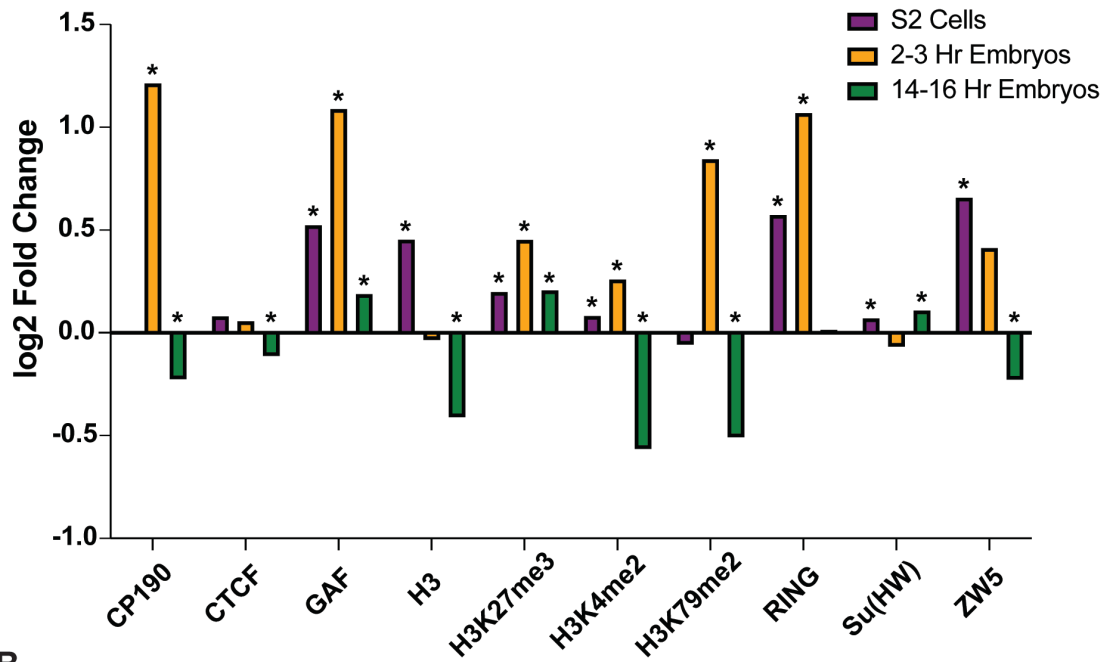
Common and cell-type specific chromatin features associated with R-loops

R-loops are associated with activating chromatin marks such as H3K4me1/2/3 and H3K9ac and, to a lesser extent, with repressive chromatin marks such as H3K27me3 (Sanz and Chédin et al. 2016). Chromatin marks associated with R-loops, however, vary depending on species. One possibility is that there are marks that are universally associated with R-loop formation whereas some chromatin marks could associate with R-loops in a developmental-specific manner. To answer this question, we leveraged time-matched ChIP-seq modENCODE datasets for S2 cells, 2-4h embryos (ChIP-chip and ChIP-seq) and 14-16h embryos.

To quantitatively determine if chromatin marks were positively or negatively associated with R-loops, we evaluated the probability of R-loops overlapping a variety of histone modifications and chromatin-associated proteins by chance using a peak shuffling bootstrap procedure (see Materials and Methods). The available chromatin proteins vary for each sample, but there are 10 chromatin or histone markers common in all three developmental samples (Figure 4-4A). Several factors that are associated with transcriptional activation, and have been previously shown to be associated with R-loops, are enriched at R-loops in S2 cells and 2-3 hour embryos (Figure 4-4A, Supplemental Figure 4-4). Additionally, repressive chromatin marks such as Polycomb complex subunits and H3K27me3 are enriched in all samples, which is consistent with recent work

A

Enrichment for Chromatin Associated Factors Across R-loops



B

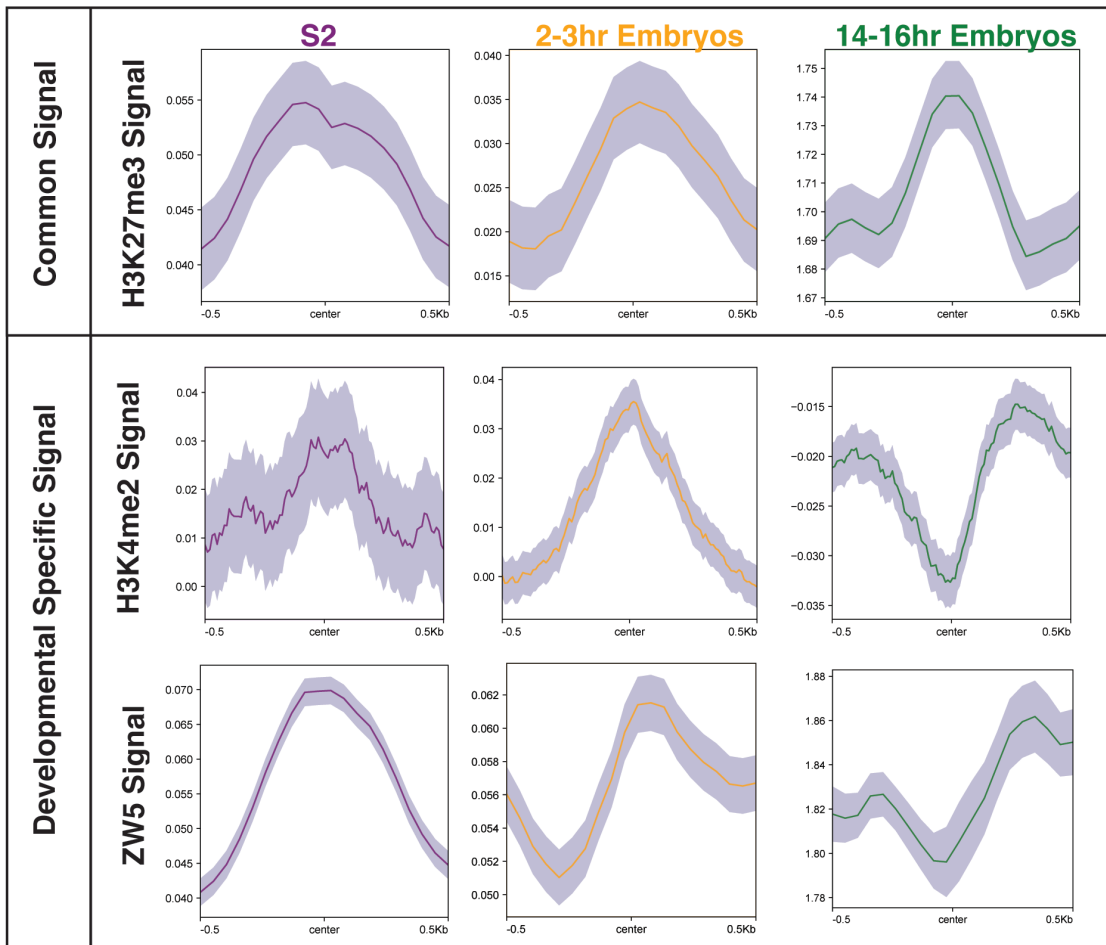


Figure 4-4. **Common chromatin features associated with R-loops.** (A) Log₂ fold enrichments of chromatin-associated factors within R-loop regions in common for S2 cells, 2-3 hour embryos and 14-16 hour embryos. * < 0.05 with Bonferroni correction for multiple testing. (B) Metaplots of H3K27me₃, H3K4me₂, and ZW5 ChIP-chip (S2 and 2-4 hour embryos) and ChIP-seq (14-16 hour embryos) confirming common and developmental-specific enrichment of chromatin factors at R-loops. Shaded region represents the standard error of the mean (SEM). Contribution: Analysis for B, visualization.

linking R-loops to transcriptional repression (Figure 4-4A, Supplemental Figure 4-4) (Skourti-Stathaki and Pombo et al. 2019; Alecki and Francis et al. 2020).

We asked which marks are consistently associated with R-loops (positively or negatively) across development and which factors are developmental specific. We found that the repressive mark H3K27me₃ was positively associated with R-loops in all developmental samples, highlighting the link between R-loops and transcriptional repression (Figure 4-4B). Interestingly, we identified factors (H3K4me₂ and ZW5) that were enriched in one developmental sample but not in others (Figure 4-4B). These results suggest while some factors are associated with R-loops regardless of development state, other factors are associated with R-loops in a developmentally-specific manner.

R-loop formation as a function of transcription

In this study, we have noted distinctive changes in R-loop formation across development. One possibility is that these changes are driven by developmental-specific changes in the transcription program. As embryos are stockpiled with maternally deposited RNA and RNA-seq is an indirect readout of active transcription, we turned to previously published and time-matched GRO-seq datasets in S2 cells and 2-2.5h embryos, respectively (Core and Lis et al. 2012; Saunders and Ashe et al. 2013). Unfortunately, time-matched GRO or PRO-seq datasets do not exist for 14-16h embryos. We converted GRO-seq signal to FPKM for each annotated transcript in the *Drosophila*

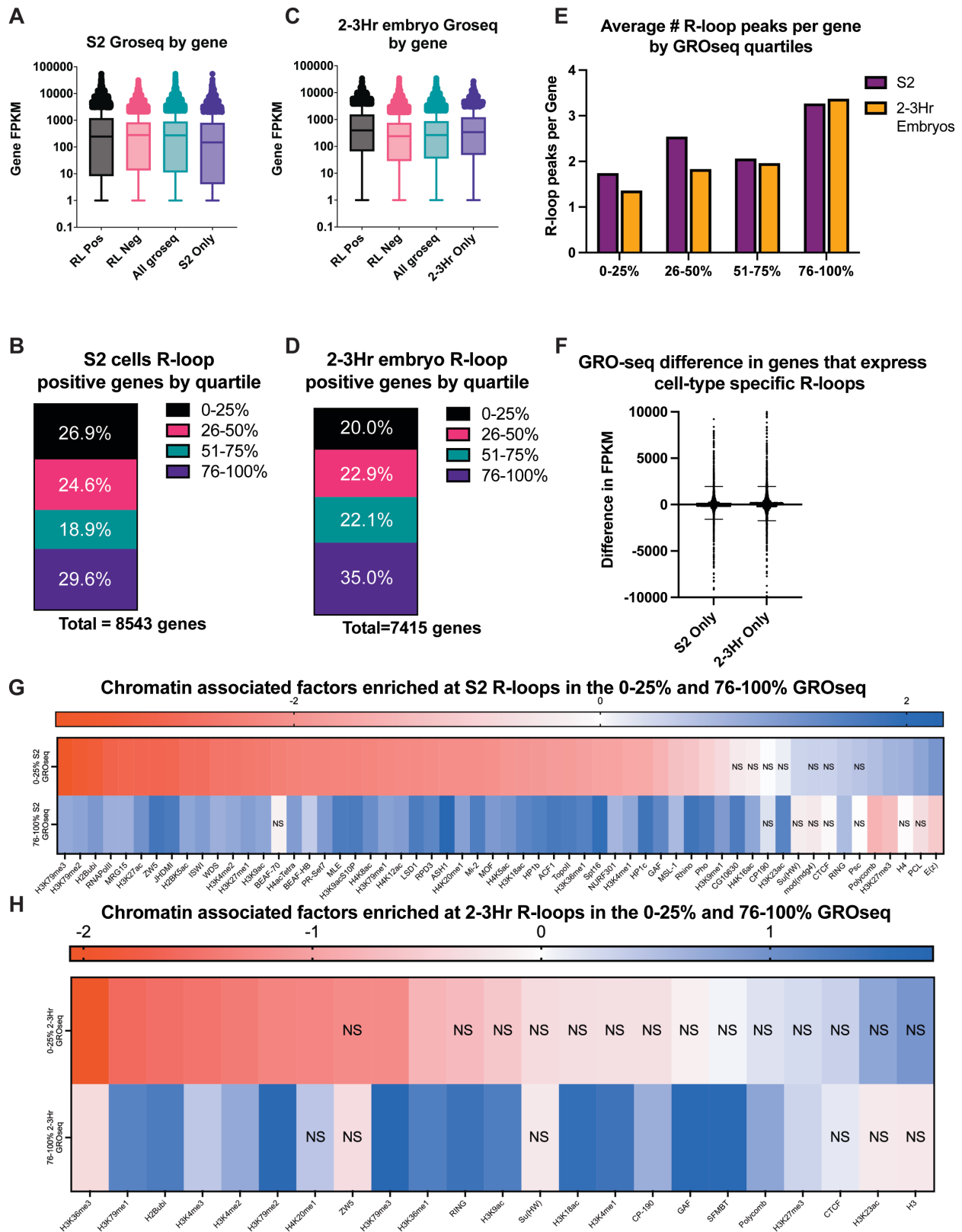


Figure 4-5. R-loop formation as a function of transcription. (A) GRO-seq values for genes that contain strand-specific R-loops (RL Pos), genes that do not contain strand-specific R-loops (RL Neg) in S2 cells,

every transcript in S2 cells, and transcripts that only form R-loops in S2 cells. **(B)** Transcripts were sorted into quartiles based upon GRO-seq expression, and R-loop forming genes were assigned to their respective quartile. **(C)** Same as A, except for 2-3h embryos. **(D)** Same as B, except for 2-3h embryos. **(E)** The average number of R-loops peaks detected for each gene in each of the expression quartiles is graphed for S2 cells and 2-3h embryos. **(F)** The difference in GRO-seq values between S2 cell and 2-3h embryos were queried for genes that showed developmental-specific R-loop formation. **(G)** Log2 fold enrichments of chromatin-associated factors within R-loop regions in the highest or lowest expression quartiles in S2 cells. ns > 0.05 with Bonferroni correction for multiple testing. **(H)** Log2 fold enrichments of chromatin-associated factors within R-loop regions in the highest or lowest expression quartiles in 2-3h embryos. ns > 0.05 with Bonferroni correction for multiple testing. Contributions: Analysis, visualization.

transcriptome. Then, we compared the GRO-seq value of all R-loop-containing genes to genes devoid of R-loops. In S2 cells, R-loop positive and negative genes had a similar median FPKM value by GRO-seq (Figure 4-5A). R-loop-containing genes in 2-3h embryos, however, revealed a different paradigm. R-loop positive genes had a significantly higher expression level than R-loop negative genes (Figure 4-5C).

To ask if R-loop-containing genes were over or underrepresented with genes that have high or low expression levels, we binned GRO-seq FPKM values into quartiles and asked what fraction of R-loop containing genes fell within each expression quartile (Figure 4-5B, D). In S2 cells, R-loop containing genes were slightly overrepresented in the highest expression quartile and, to a lesser extent, in the lowest expression quartile (Figure 4-5B). In 2-3h embryos, however, R-loops were significantly overrepresented in the highest expression quartile and underrepresented from the lowest expression quartile (Figure 4-5D). While analyzing this data, we also found the number of R-loops forming sites per gene was correlated with transcriptional activity (Figure 4-5E). We observe a consistent increase in the average number of R-loops per gene as transcriptional activity increases (Figure 4-5E). The increase in the average number of R-loops per gene could represent multiple R-loops within a given gene or larger R-loop zones allowing R-loops to form over a larger target region.

One explanation for developmental-specific R-loop formation is that specificity is driven by developmental-specific transcription status. To test this, we compared expression level of genes that exhibit R-loops only in S2 cell or only in 2-3h embryos (Figure 4-5F). If active transcription drives the changes in R-loop formation, we would expect R-loop positive genes that are unique to 2-3h embryos would have significantly higher expression level in 2-3h embryos relative to S2 cells, and vice-versa. The median difference of GRO-seq values in developmental-specific R-loop-containing genes, however, is approximately zero with a normal distribution (Figure 4-5F). Therefore, we conclude that active transcription is not a driver of developmental-specific R-loop formation and that factors such as chromatin state or R-loop-specific proteins drive these differences.

We asked if the chromatin signature of R-loops in highly expressed genes differs from the signature of R-loops in transcriptionally repressed genes. To this end, we selected R-loops in the highest expression quartile and lowest expression quartile from S2 cells (Figure 4-5B). Next, we used the random shuffling method to identify chromatin-associated factors enriched at R-loops derived from highly and lowly expressed genes. This analysis revealed that the chromatin signature of R-loops in highly and lowly expressed genes are distinct (Figure 4-5G). For example, R-loops in highly expressed genes are enriched for active chromatin marks (e.g. H3K27ac and H3K36me1; Figure 4-5G). In contrast, repressive chromatin marks such as H3K27me3 are enriched at R-loops derived from lowly expressed genes. We repeated the same analysis with the 2-3h embryo time point and noticed a striking difference; both active chromatin marks and repressive chromatin marks were associated with highly expressed genes (Figure 4-5H).

Given the differentiation state of cells in the early embryo, this would suggest that R-loops can be associated with poised or bivalent genes (Lesch and Page, 2014).

R-loops have the potential to trigger ATR activation at the MZT

The onset of zygotic transcription at the MZT is associated with RPA accumulation at the 5' end of genes and activation of the ATR-mediated DNA damage checkpoint response (Blythe and Wieschaus, 2015). Delaying the onset of zygotic transcription delays the activation of ATR (Mei41 in *Drosophila*), indicating that replication-transcription conflicts drive the activation of the DNA damage response at the MZT (Blythe and Wieschaus, 2015; Sibon and Theurkauf et al. 1999). It is unknown, however, what aspect of the replication-transcription conflict triggers ATR activation at the MZT. If genome instability at the MZT was at least partially due to R-loops, we would predict to see an enrichment of RPA at R-loop forming sequences in 2-3h embryos. Qualitatively, we see overlap between RPA and R-loops in 2-3h embryos (Figure 4-6A). We tested the significance of this overlap by using the random shuffling method previously described. Quantitatively, we observe a significant enrichment of RPA at R-loop forming sequences in the 2-3h embryo. Importantly, there was an even more substantial enrichment of RPA at R-loop peaks that are unique to 2-3h embryos (Figure 4-6B). Further supporting the hypothesis that R-loops could be partially responsible for the transcription-induced genome instability at the MZT, only R-loops from the 2-3h sample were enriched at RPA binding sites (Figure 4-6B). This data suggests that R-loops could contribute to the transcription-induced DNA damage that occurs in the absence of ATR at the MZT. We do note, however, that the RPA ChIP-seq data comes from a time point

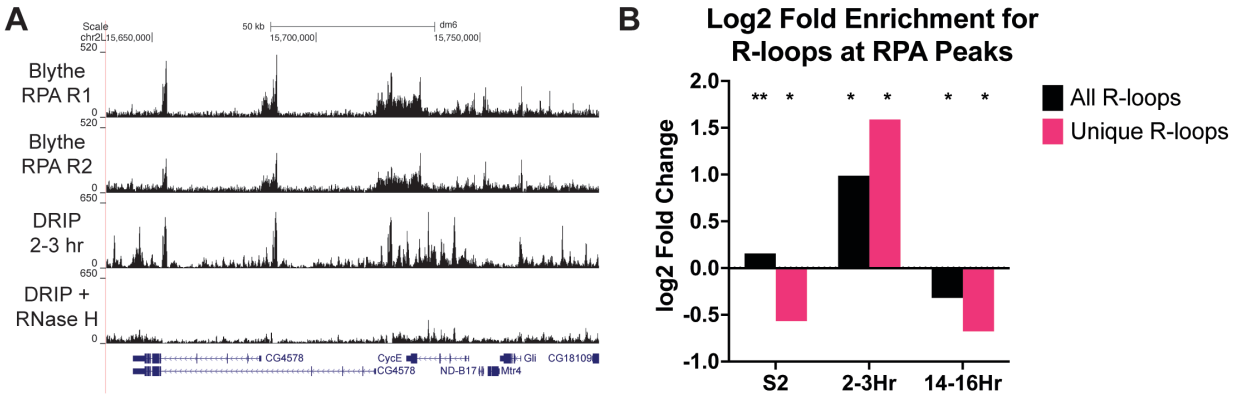


Figure 4-6. **R-loops have the potential to trigger ATR activation at the MZT.** (A) Overlap of RPA ChIP-seq profiles from cycle 13 embryos (Blythe and Wieschaus et al. 2015) and ssDRIP-seq profiles from 2-3h embryos. (B) Log2-fold enrichment of RPA at R-loop peaks for all samples. Each sample was separated into total R-loops or R-loops unique to that sample type. P values were generated with Bonferroni correction for multiple testing. * is P value < 0.01 and ** = P value < 0.001. Contributions: Visualization.

~20 minutes earlier in development than the time point we chose for R-loop mapping (Blythe and Wieschaus, 2015). Given this caveat, we think it is even more notable that significant overlap of RPA and R-loops is observed in this analysis.

Discussion

By mapping R-loops in a developing organism, we have been able to provide new insight into the role that DNA sequence, active transcription and chromatin associated factors has on R-loop formation. While previous R-loop mapping and genome-wide analysis of R-loop metabolism across development has been performed in plants and mammalian cultured cells (Yan and Liu et al. 2020; Xiu and Sun et al. 2020; Shafiq and Sun et al. 2017), we present a functional characterization of R-loops during *Drosophila* embryogenesis. The benefit of a developmental approach to studying R-loop formation is that it allows the distinction between factors that are stably linked to R-loop formation from those that are developmental specific. This has the potential to

identify key molecules and processes that could drive R-loop formation and resolution during development and disease.

One surprising finding is that the absolute level of R-loops changes during embryogenesis. This is unlikely due to changes in transcription during development as the stages of embryogenesis used in this study are similarly active. This suggests that there is an active mechanism which prevents R-loop formation or resolves active R-loops during later stages of *Drosophila* embryogenesis. The importance of R-loop processing during development is further highlighted by the observation that RNase H1 catalytic activity is necessary to prevent hatching defects in *Drosophila* embryos. Interestingly, overexpression of catalytically active and inactive RNaseH1 do not have the same effect. One possible explanation for this is that maternally deposited RNaseH1 is highly active in the embryo. Therefore, additional RNaseH1 has no further effect on R-loop levels. Overexpression of catalytic inactive RNaseH1, however, could bind to RNA:DNA hybrids and block RNaseH1-mediated processing of R-loops.

Consistent with R-loops as a driving force of genome instability during embryogenesis, we have found an enrichment of R-loops at potential sites of replication fork stalling in the early embryo. Given that we see an enrichment of R-loops and RPA specifically in the 2-3h embryo sample, our data suggests that R-loops could contribute to ATR activation at the MZT. It is interesting to note, however, that we do not observe RPA accumulation at all sites of R-loop formation. Therefore, there must be something unique about the R-loops associated with RPA accumulation at this time point. Perhaps these R-loops represent sites of head-on conflicts. Alternatively, hyper stable R-loops could drive chromatin or transcriptional changes that negatively impact embryogenesis

(Lima and Crooke et al. 2016). Further work will be required to distinguish between these and other possibilities.

Specific DNA sequence biases are associated with R-loop formation (Ginno and Chédin et al. 2012; Stolz and Chédin et al. 2019). While we found that overall GC content is the same for R-loop positive and negative genes, AT and GC skew were associated with R-loop forming sequences. Interestingly, this skew varied as a function of the transcription unit (Ginno and Chédin et al. 2012; Lee and Myong et al. 2020). G4 quadruplex forming regions with high GC skew on the non-template strand are associated with R-loop formation (Ginno and Chédin et al. 2012; Lee and Myong et al. 2020). Additionally, R-loops can modulate DNA methylation at CpG islands in promoter regions (Ginno and Chédin et al. 2012). Unlike in plants and mammals, however, *Drosophila* lack wide-scale DNA methylation (Capuano and Ralser et al. 2014). Therefore, *Drosophila* allows the uncoupling between R-loop formation and DNA methylation, which could explain why R-loops are associated with a higher AT skew than GC skew in *Drosophila*. Similar to mammalian cells, we see a transition to positive GC skew at the center of R-loop peaks. What's unique to *Drosophila*, however, is the drastic transition from positive to negative AT skew at the center of R-loop peaks. These biases in AT and GC skew could create a thermodynamically stable environment for R-loop formation and resolution. Similar to other organisms, we have found several polypurine motifs associated with R-loops. Again, this likely reflects the thermodynamic stability associated with RNA:DNA hybrids at purine-rich sequences (Huppert 2008). One interesting observation in *Drosophila* is that the R-loop signal relative to the transcription unit can vary as a function of development. The most significant difference is in 14-16h embryos where R-loops are

broadly enriched at the TSS and the TTS but not the gene body in comparison to 2-3h embryos or S2 cells. This difference does not appear to be driven by AT or GC skew. We propose that a combination of factors such as transcription status, chromatin marks and R-loop binding proteins drive these changes in R-loop formation during development.

We have found that R-loops are positively and negatively associated with specific histone modifications and chromatin associated factors. Many of the factors we analyzed in *Drosophila* have been shown to be enriched or depleted in other systems, including mammalian cells (Sanz and Chédin et al. 2016; Pinter and Rathert et al. 2021; Herrera-Moyano and Aguilera et al. 2014). More importantly, however, factors associated with R-loops can change as a function of development. For example, R-loops in 14-16h embryos lose their association with common activating histone marks such as H3K4me3 and H3K36me2/3. In contrast, H3K27me3 is enriched at R-loops in all developmental states. Therefore, it is critical to assay multiple cell types or developmental states before concluding that a chromatin factor is correlated with R-loop formation.

The link between R-loops, transcription state, histone marks and chromatin associated factors has been seen in other organisms (Sanz and Chédin et al. 2016). In *Drosophila*, we see a consistent relationship between active and repressive chromatin marks, signified by enrichment in both H3K27ac and H3K27me3, and R-loop formation. This is supported by the association of R-loops with both highly active and silent genes in both embryos and cultured cells. Our work, and that of others, identify R-loops associated with transcriptionally active and inactive genes²⁵. This suggests that, at least in *Drosophila*, there may exist at least two classes of R-loops. R-loops that form as a byproduct of active transcription and R-loops that function in a repressive capacity to

prevent transcription within repressive chromatin domains. This would be consistent with recent work demonstrating that R-loops facilitate silencing by the Polycomb complex (Skourti-Stathaki and Pombo et al. 2019). Understanding how different categories of R-loops maintain their identity will be an exciting challenge. For example, how do cells know which R-loops should function in a repressive manner versus those that function as activators? The question of whether R-loops help establish a chromatin state or are a function of it remains an outstanding question in R-loop biology.

Mapping of R-loops has been performed in a variety of organisms ranging from yeast, worms, plants, and mammalian cultured cells. While there are factors and processes that are consistently associated with R-loops across organisms, there are also key differences. For example, in plants there are low levels of R-loops at gene terminators compared to other organisms and high accumulation of antisense R-loops that regulate specific loci (Xu et al. 2020; Sun et al. 2013). In contrast, mammalian cells exhibit R-loops at promoters and TTS and the number of antisense R-loops are much more limited (Sanz and Chédin et al. 2016). The fact that *Drosophila* exhibit changes in antisense R-loop signal across the gene body depending on developmental state highlights the importance of examining R-loops in a developmental context. *Drosophila* provides a powerful model to understand key properties of R-loop biology in the context of unperturbed metazoan development. Here, we demonstrate that R-loop formation within the same genomic sequence can vary as a function of development. Our work suggests that a combination of transcription, chromatin-associated factors and sequence elements drive differential R-loop formation during development. Therefore, *Drosophila* provides a powerful model to

understand, mechanistically, the factors responsible for R-loop formation and resolution to execute specific developmental programs.

Materials and Methods

S9.6 antibody

A hybridoma cell line producing the S9.6 antibody was purchased through ATCC (product #HB-8730). The cell line was grown under recommended conditions. The S9.6 antibody was purified on a protein G column using the GE aKTA system and run over a desalting column for buffer exchange into PBS to obtain a final concentration of 1 mg/mL. The antibody was aliquoted and stored at -80°C. A fresh aliquot was used for every ssDRIP-seq experiment.

RNase H1 overexpression

Drosophila RNase H1 was cloned from RNA derived from Oregon R embryos. RNA was converted into cDNA, PCR amplified, and cloned into the pUASz vector with a C-terminal GFP tag (DeLuca and Spradling 2018). The A isoform was chosen as the isoform B isn't detected in *Drosophila* tissues (Cózar de and Jöers et al. 2019). The mitochondrial localization start site was converted to AAA to ensure RNase H1-GFP would only be present in the nucleus. The catalytically dead version of RNase H1 (D201N) was made by site-directed mutagenesis (Agilent QuickChange Lightning). Plasmids were injected into an *attP2* containing stock (BestGene) for site-specific integration.

Hatch rate assay

For the overexpression experiments, homozygous RNase H1 males were crossed with unmated female homozygous for the maternal triple driver (MTD, Bloomington Stock 31777) to drive expression early in embryogenesis. Male Oregon R flies were crossed with MTD females as a control. Progeny were transferred to bottles with a grape juice agar plate with wet yeast for embryo collection. 100 unhatched embryos were carefully moved to a fresh grape juice plate and incubated overnight at 25°C. After 36 hours, unhatched embryos were counted. This was repeated three times each from two separate crosses.

Cell culture

S2 cells were obtained directly from the Drosophila Genomic Resource Center (DGRC). Cells were confirmed negative for mycoplasma contamination via PCR. Cells were grown at 25°C in Schneider's Drosophila Medium with 10% heat-inactivated FBS (Gemini Bio Products) and 100 U/mL of Penicillin/Streptomycin (Fisher Scientific).

Embryo collection and staging

Oregon R flies were expanded into population cages containing grape juice plates supplemented with wet yeast. Population cages were kept at 25°C in a humidified room and plates were changed daily. Before embryo collections, flies were precleared for at least one hour to minimize the number of late-stage embryos. Embryos were collected and aged at 25°C to obtain embryos that were 2-3 or 14-16 hours old. After aging and collection, embryos were dechorionated in 50% bleach for 2 minutes and thoroughly

rinsed in water. Embryos were flash frozen in liquid nitrogen and kept at -80°C until ready to use. An aliquot of embryos was taken from each batch before freezing to verify staging. For this, embryos were fixed in heptane and 2% paraformaldehyde for 20 minutes with shaking, devitellinized in methanol, washed with methanol and rehydrated in PBS + 0.1% Triton X-100 overnight. Embryos were stained with DAPI and mounted in Vectashield medium (Vector Labs). Images were acquired on a Nikon Ti-E inverted microscope with a Zyla sCMOS digital camera.

Genomic DNA purification and RNase treatment

Genomic DNA purification is based on Alecki et al., 2019. For genomic DNA isolation from S2 cells, cells were collected at 70-80% confluency, washed once in PBS, resuspended in TE with 0.5% SDS and 100 µg/mL proteinase K and incubated at 37C overnight. Embryos were devitellinized in heptane and methanol, rinsed thoroughly in PBS and incubated in 50 mM Tris-HCl pH 8.0, 100 mM EDTA, 100 mM NaCl, 0.5% SDS, and 5 mg/ml proteinase K for 3 hours at 50C. At this point, cells and embryos were processed the same. Extracts were purified with phenol:chloroform, and DNA was precipitated with sodium acetate and ethanol. DNA was spooled using a glass pipette and transferred to 70% ethanol. After several washes in ethanol, the DNA was air dried and resuspended in TE. To degrade free RNA, samples were incubated with 100 µg of RNase A with 500mM NaCl for 1 hour at 37C. RNase A was degraded by spiking in 100 µg/mL proteinase K and incubated for an additional 45 minutes. Samples were cleaned with phenol:chloroform, precipitated with sodium acetate and ethanol, and resuspended in TE. Samples were diluted to 100 ng/µL and sonicated in a Bioruptor Plus for 8 cycles (30"

on/90" off) on low power. 10 µg of nucleic acid was digested with 5 µL RNase H (NEB) at 37C for 16 hours and 10 µg was mock digested without RNase H. Both samples had 1 µL of RNase III added (Thermo Fisher). After phenol:chloroform purification and precipitation, samples were immediately used for DRIP or slot blot experiments.

Slot blot

Hybond Nylon membrane (Amersham) was pre-soaked in TE and a slot blot apparatus was assembled according to manufacturer's instructions (Bio-Rad). Samples with matching RNase H-digested controls were added to the blot in decreasing amounts, and nucleic acids were crosslinked to the membrane with a Strategene UV Stratalinker 1800 using the auto crosslink setting. Blots were blocked in milk, incubated with S9.6 (1:2,000) followed by mouse-HRP and imaged in a Bio-Rad Chemidoc MP. After imaging the R-loops, blots were stripped and re-probed using a dsDNA-specific antibody (Abcam ab27156) at 1:20,000. Intensities were measured with ImageJ (Schneider and Eliceiri et al. 2012), and normalized intensity was obtained by dividing the S9.6 signal by the dsDNA signal (Ramirez and Grunseich et al. 2021). A standard plot was made for each sample and antibody, and samples were chosen for analysis when their intensity was linear.

DRIP-qPCR and ssDRIP-seq

DRIP was carried out as described in Ginno and Chédin et al. 2012. Briefly, 4.4 µg of DNA was resuspended in 500 µL of TE. 10% was taken for the input sample. DRIP binding buffer was added to each sample (10mM sodium phosphate, 140mM NaCl, 0.05% Triton X-100 final concentration) and 20 µL of 1 mg/mL S9.6 was added to each

DRIP reaction. After overnight incubation at 4°C, 50 µL of pre-washed protein G Dynabeads (Life Technologies) were added to the extract. After 2 hours at 4°C, beads with captured nucleic acid were washed in 1x DRIP binding buffer 5 times and eluted in 50mM Tris, 10mM EDTA, 0.5% SDS with proteinase K at 50°C for 45 minutes. Nucleic acid in the eluate was purified with phenol:chloroform, precipitated and resuspended in 10mM Tris. For DRIP-qPCR, 1µL of nucleic acid was diluted 1:10 in water and mixed with 10µL SSoAdvanced Universal Sybr (Bio-Rad). Primers were added to a final concentration of 250 nM each. A list of primers used in this study can be found in Supplemental Table 4-1. qPCR was carried out on a Bio-Rad CFX96 Touch instrument using the following protocol: 98°C heat denaturation for 60" followed by 40 cycles of 98°C for 15" and 60°C for 30". A heat denaturation was included to monitor the purity of the reaction products. For ssDRIP, nucleic acid was sonicated in a Bioruptor Plus for 8 cycles at high power (30" on/30" off) to 250 bp. Libraries were constructed with the Accel-NGS 1S Plus DNA Library Kit according to the manufacturer's instruction (Swift Biosciences 10024). Barcoded libraries were sequenced using an Illumina Novaseq for 150bp PE reads.

Bioinformatics

Alignment and peak calling

Fastq files were initially trimmed of adapters using Trimmomatic v0.3.8 (Bolger and Usadel et al. 2014). Each paired read was trimmed 10 base-pairs at the 3' end to eliminate the additional low complexity from the library preparation kit. Reads for sequencing were mapped to the Drosophila genome (dm6) using bowtie2 version 2.3.4.1 using the `-very-sensitive-local` setting (Li and Durbin et al. 2009). Duplicates were marked using picard

MarkDuplicates v2.17.10, and stranded bam files were created using samtools as described in Xu and Sun et al. 2017. Stranded bam files were used to generate ssDRIP peaks with callpeaks from MAC2 v2.1.2 (Zhang and Liu et al. 2008). The RNase H pretreated DRIP file was used as control, peak calling was done on the 2 replicates in paired-end mode, with `--keep-dup=auto` and effective genome size for *Drosophila dm6*. A small number of peaks mapped to both strands as determined with bedtools. These were discarded for downstream analysis. Bam files were combined and 50 million reads were randomly selected for visualization. Stranded reads were visualized using deeptools `bamCoverage` using `--binSize 50bp`, `--ignoreForNormalization chrY chrM`, and `--normalizeUsing RPKM` (Ramírez and Manke et al. 2014). Pearson correlation plots were created using deeptools `multiBamCoverage` and `plotCorrelation` with default settings, 1kb windows and the mitochondrial genome excluded.

ssDRIP-seq analysis

Peak annotation was performed using Pavis to the dm6 genome with up- and downstream regions set to 5kb (Huang et al. 2013). Overall sense and antisense R-loops were determined via bedtools `intersect` with `strandedness` against the Refseq *Drosophila* transcriptome, downloaded from UCSC genome browser. Metagene plots were made with the Deeptools software package, using `computeMatrix` and `plotProfile`. For `computeMatrix`, `scale-regions` or `reference-point` as appropriate, with a 1kb region size and 500bp up- and down-stream of the start and end site, respectively. For options `-binSize` was 50 and the mean was plotted. For `plotProfile`, 'add standard error' was added

to Plot type. –yMin and –yMax were chosen to be the same for both sense and antisense to aid in visualization.

Gene Ontology enrichment analysis of R-loop containing genes was performed with PANTHER, with Fisher’s exact test and using the Bonferroni correction for multiple testing (Ashburger et al 2000; Consortium et al 2020; Mi et al 2019).

GRO-seq FPKM counts were determined with HOMER analyzeRepeats.pl using S2 datasets from Core and Lis et al. 2012 and GRO-seq data on 2-2.5 embryos from Saunders and Ashe et al. 2013. R-loops peaks were split into 2 files containing their + and – peaks and annotation of R-loop peaks was done with HOMER software package using annotatePeaks.pl against dm6 and requiring the appropriate strandedness. R-loops mapping to transcripts were extracted from the HOMER annotation, and GROseq values for these transcripts was determined using custom R scripts. Plots summarizing these data were created in Prism 9.

Functional genomic data from modENCODE

We downloaded histone modification peaks and transcription factor binding sites identified by ChIP-chip or ChIP-seq in *Drosophila* from ModENCODE (Table 4-1) (Contrino and Hu et al. 2012). We considered samples assayed in S2 cells and at two developmental timepoints (2-4hr, 14-16hr). These were chosen to match the ssDRIP timepoints.

Table 4-1 List of available ChIP-chip and ChIP-seq from modENCODE.

Assay	Time	Mark
-------	------	------

		BEAF-32, CP-190, CTCF, RING, SFMBT, GAF, H2Av, H2Bubi, H3, H3K18ac, H3K23ac H3K27ac, H3K27me3, H3K36me1, H3K36me3, H3K4me1, H3K4me2, H3K4me3, H3K79me1, H3K79me2, H3K79me3, H3K9ac, H3K9me2, H3K9me3, H4, H4K20me1, HP1a, HP1c, HP2, Polycomb, POF, Su(HW), ZW5
ChIP- chip	2-4 hr	ACF1, ASH1, BEAF-70, BEAF-HB, CG10630, Chriz-WR, CP190, CTCF, Mi-2, Topoll, RING, SFMBT, E(z), GAF, H1, H2Av, H2BK5ac, H2Bubi, H3, H3K18ac, H3K23ac, H3K27ac, H3K27me1, H3K27me2, H3K27me3, H3K36me1, H3K36me3, H3K4me1, H3K4me2, H3K4me3, H3K79me1, H3K79me2, H3K79me3, H3K9ac, H3K9acS10P, H3K9me1, H3K9me2, H3K9me3, H4, H4acTetra, H4K12ac, H4K16ac, H4K20me1, H4K5ac, H4K8ac, HP1a, HP1b, HP1c, HP2, HP4, ISWI, JHDMI, JIL-2, JMJD2A, LSD1, MBD-R2, MLE, mod(mdg4), MOF, MRG15, MSL-1, NURF301, ORC2, Polycomb, PCL, Pho, Pof, PR-Set7, Psc, Rhino, RNAPoIII, RPD3, Smc3, Spt16, Su(HW), Su(var)3-7, Su(var)3-9, WDS, ZW5
ChIP- seq	14-16 hr	Beaf-HB, Chriz, CP190, CTCF, Mi-2, RING, GAF, H1, H2Av, H2Bubi, H3, H3K18ac, H3K23ac, H3K27ac, H3K27me2, H3K27me3, H3K36me1, H3K36me2, H3K36me3, H3K4me1, H3K4me3, H3K79me1, H3K79me2, H3K79me3, H3K9acS10P, H3K9me1, H3K9me2, H3K9me3, H4, H4K16ac, H4K20me1, HP1a, HP1b,

HP1c, HP2, HP4, JHDMI, LSD1, MBD-R2, MOF, NURF301, POF,
Psc, RNAPoIII, RPD3, Su(HW), Su(var)3-7, ZW5

Chromatin associated factor enrichment in R-loops

For each ChIP-chip or ChIP-seq marker with a matching DRIP timepoint, we calculated the number of overlapping base-pairs (bp) between the marker and the R-loop peaks. We used permutation-based approach to determine whether the observed amount of overlap was more or less than expected by chance. Briefly, we calculated an empirical p value for the observed amount of overlap by comparing the number of overlapping bp to a null distribution. We obtained the null distribution by randomly shuffling length-matched regions throughout the genome and calculating the amount of overlap in each permutation. The p -values are adjusted for multiple testing using the Bonferroni method.

When permuting, we matched the length distribution of the shuffled peaks to the original set of peaks, and excluded all gap and blacklisted regions from consideration (dm3; version 1) (Amemiya and Boyle et al. 2019). Peaks called from DRIP were lifted over to dm3 for this analysis. For peaks obtained from ChIP-chip data, we required that the shuffled peaks maintained both the overall length distribution and the probe density of the original peak. We reshuffled any peaks that fell more than 2 standard deviations (approx. 0.03) away from the original probe density until at least 99% of the original peaks were appropriately matched. We performed 1000 permutations for each marker and R-loop pair.

For the general analyses, we maintained the location of the R-loop peaks and shuffled the locations of the histone modification or transcription factor binding peaks. For a secondary analysis, we examined a subset of R-loops quantified specifically in the TTS and 3' UTR. For this set of R-loops, we maintained the R-loop location within the TTS/3' UTR and shuffled the chromatin markers.

Calculation of AT- and GC-skew in R-loops

We calculated GC and AT skew over the entire *Drosophila* genome (dm6). GC skew was calculated for 50 bp windows tiled across the annotation regions as $S_i = \frac{(G_i - C_i)}{G_i + C_i}$ (McLean and Devine et al. 1998).

In the equation, G_i represents the frequency of guanine nucleotides and C_i represents the frequency of cytosine nucleotides in the window i . The range of GC skew for a window (S_i) spans from -1 to 1. AT Skew was calculated in the same way. The resulting GC and AT skew was converted to a bigwig file, and the value across each set of genomic regions was calculated using the `computeMatrix` function from `deeptools` and visualized using `plotProfile` (For `computeMatrix`, `scale-regions` or `reference-point` as appropriate, with 500bp up- and down-stream of the start and end site, respectively. For options `-binSize` was 50 and the mean was plotted. For `plotProfile`, 'add standard error' was added to Plot type. `-yMin` and `-yMax` were chosen to be the same for AT and GC skew to aid in visualization).

Accession Numbers

Data sets generated in this study can be found under the GEO accession number: GSE185403.

Acknowledgment

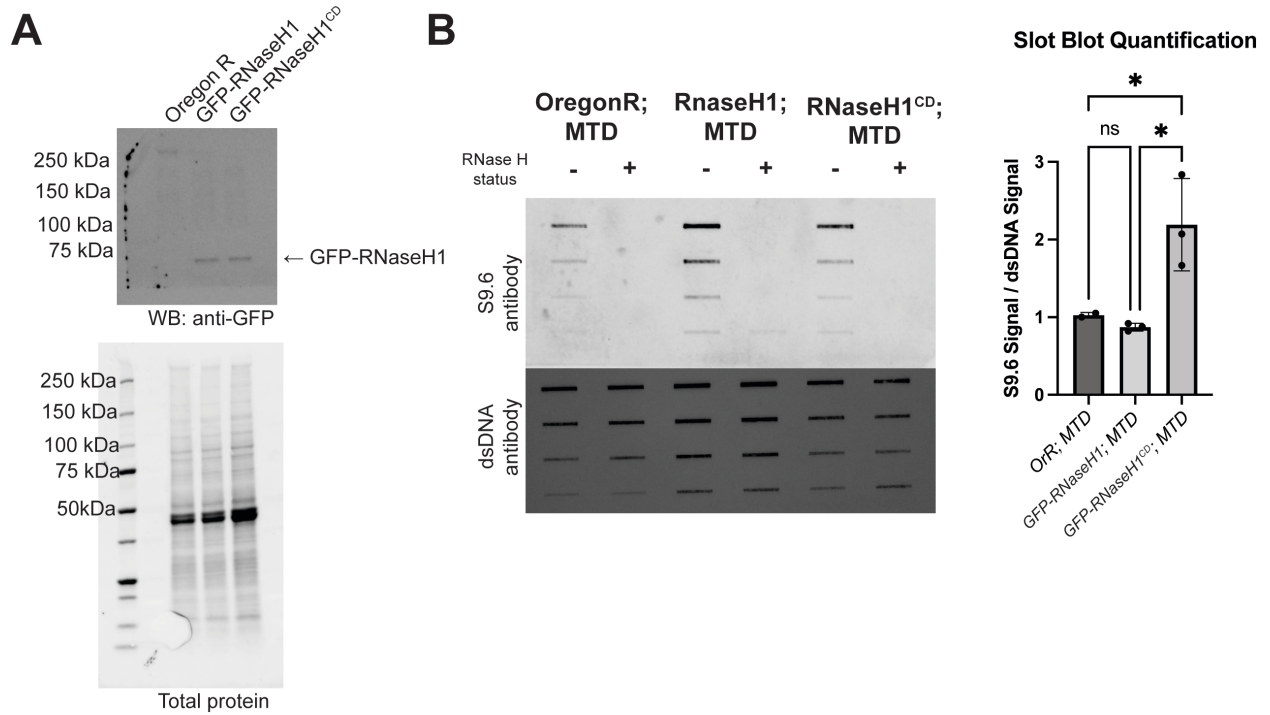
We thank the Vanderbilt VANTAGE core for Illumina sequencing and the Vanderbilt Antibody and Protein Resource core for purifying the S9.6 antibody. The Vanderbilt Antibody and Protein Resource core is supported by the Vanderbilt Institute of Chemical Biology and the Vanderbilt Ingram Cancer Center (P30 CA68485). Figures 4-1 and 4-2 partially created with BioRender.com. We thank Martina Brienza-Ramos for cloning of the RNase H1 plasmids used for fly injections. We thank Emily Hodges, Robin Armstrong and Frederic Chédin for providing critical feedback on the manuscript. We thank Lionel Sanz, Célia Alecki and Nicole Francis for technical advice.

Funding

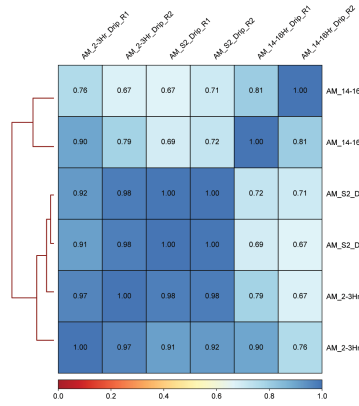
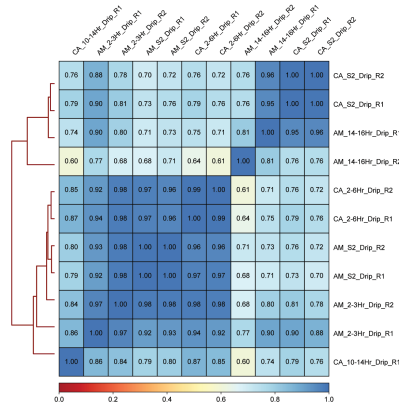
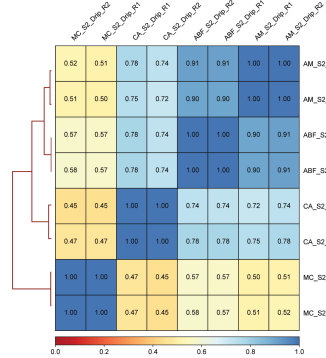
This work was supported by National Institutes of Health (NIH) General Medical Sciences awards [R35GM127087 to JAC] and [R35GM128650 to JTN].

Conflict of Interest

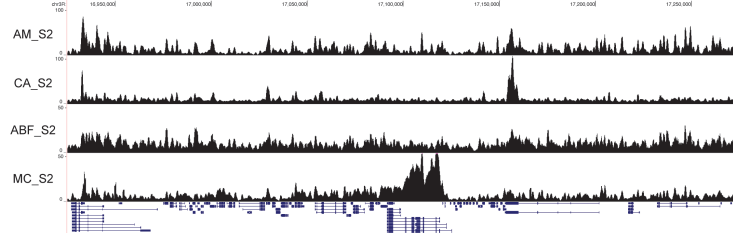
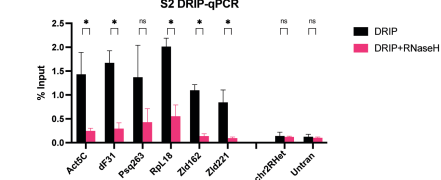
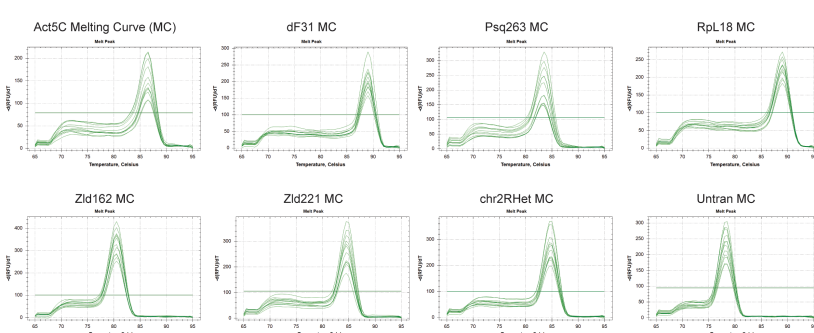
The authors declare no conflicts of interests



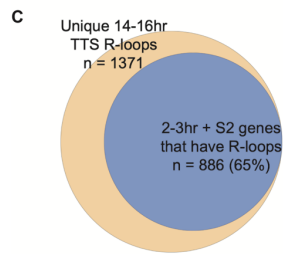
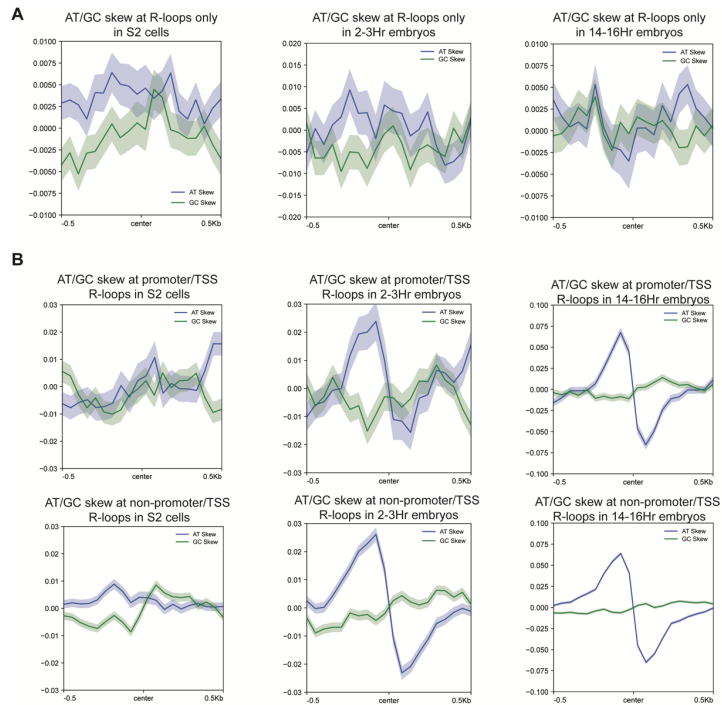
Supplemental Figure 4-1: Expression of RNaseH1 constructs in early embryos. (A) Western blot (anti-GFP) showing maternally deposited GFP-RNaseH1 and GFP-RNaseH1^{CD} in 0-6 hour embryos. Expected size of GFP + RNaseH1 = 65.1 kDa. (B) Representative slot blot of RNA:DNA hybrid levels, measured by S9.6 antibody intensity, from 2-6h embryos upon *RNaseH1* and *RNaseH1^{CD}* overexpression. RNase H treatment verifies specificity of antibody, and antibody specific for double-stranded DNA is used as a loading control. Oregon R is a wildtype control. Quantification of signal for 2 (Oregon R) or 3 (*RNaseH1* and *RNaseH1^{CD}*) biological replicates is to the right. * < 0.05, one-way ANOVA with Tukey's multiple comparisons test. Contributions: Experiment, analysis, and visualization.

A Pearson correlation between samples**B** Pearson correlation between samples**C****E** Overlap of sense R-loops

Overlap of antisense R-loops

**D****F****G**

Supplemental Figure 4-2: **Properties of R-loops in Drosophila** **(A)** Pearson's correlation between ssDRIP-seq replicates at 1kb resolution. AM- Alex Munden, this study. **(B)** Correlation between ssDRIP-seq replicates at 1kb resolution between this study (AM - Alex Munden) or data obtained from Alecki et al. 2020 (CA) **(C)** Correlation at 1kb resolution between ssDRIP-seq replicates specifically from S2 cells. AM – this study; CA – Alecki et al. 2020; ABF – Bayona-Feliu et al., 2017; and MC – Crossley et al., 2020) **(D)** Screen shot of unstranded ssDRIP-seq or DRIP-seq data for the same data sets as in C. **(E)** Venn diagrams of overlap of stranded R-loops between S2 cells, 2-3 hour embryos, and 14-16 hour embryos. Sense R-loops on top, antisense R-loops on bottom. **(F)** DRIP-qPCR validation of several R-loop positive and negative loci in S2 cells. **(G)** Melting curves for the qPCR products from the reactions in F. Contributions: Experiment, analysis, and visualization.

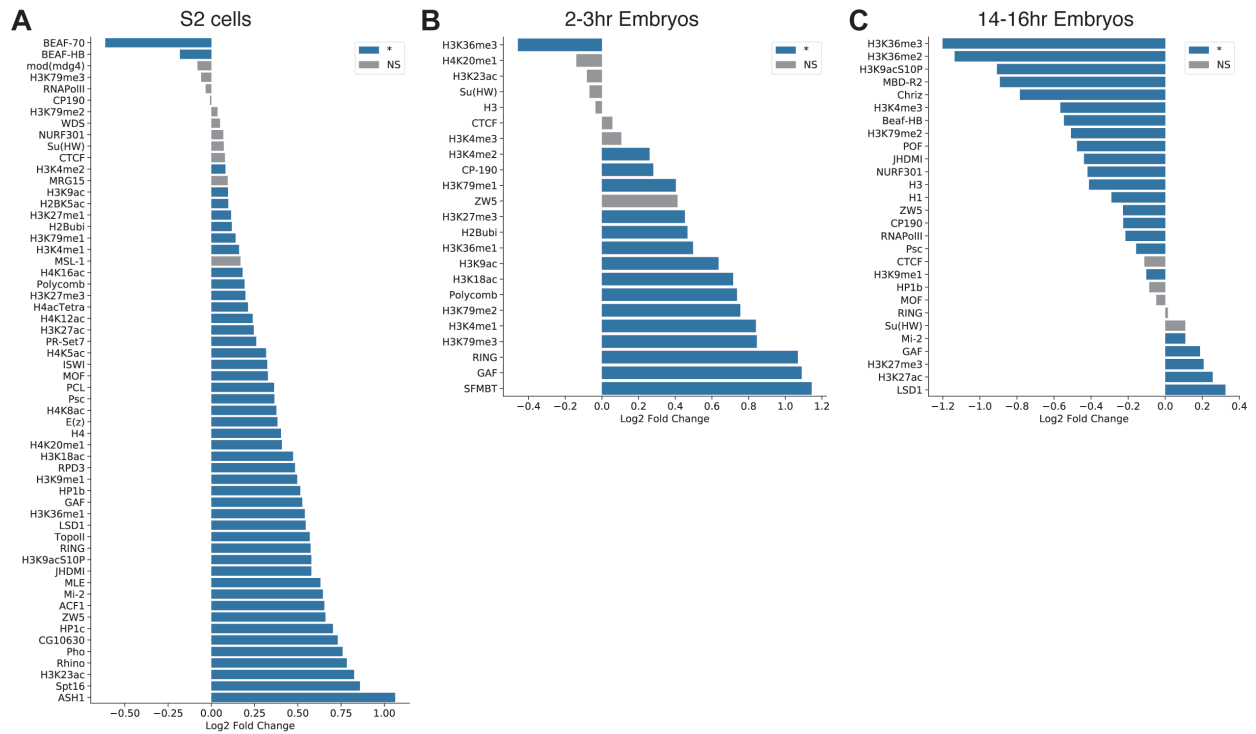


D

Rank	Motif	P-value	log P-value	% of Targets	% of Background	STD/Bg (STD)	Best Match/Details
1	AAAAAAAAAAAAA	1e-1413	-3.254e+03	21.44%	8.73%	48.4bp (78.7bp)	h/dmmpmm(Noyes/fly)(0.794) More Information Similar Motifs Found
2	GGAGGAGGAGGA	1e-1352	-3.114e+03	31.82%	18.65%	51.4bp (70.0bp)	Tr/dmmpmm(Down/fly)(0.559) More Information Similar Motifs Found
3	GAGGAGAG	1e-149	-3.432e+02	42.12%	36.14%	56.1bp (64.8bp)	Tr/Zf/S2-GAGAFactor -ChIP-Seq(GSE40646)/Homer(0.647) More Information Similar Motifs Found
4	CCCCTTCC	1e-127	-2.947e+02	27.92%	23.00%	55.2bp (68.4bp)	Kr/dmmpmm(Noyes/fly)(0.718) More Information Similar Motifs Found
5	AACAACAACA	1e-106	-2.457e+02	14.88%	11.43%	56.1bp (66.6bp)	Tr/MA0205.2/Jaspar(0.781) More Information Similar Motifs Found
6	GAGACAGA	1e-104	-2.398e+02	40.18%	35.22%	56.3bp (67.1bp)	Aef1/dmmpmm(Pollard/fly)(0.864) More Information Similar Motifs Found
7	ATCATCATCA	1e-53	-1.239e+02	7.78%	5.96%	56.7bp (57.1bp)	tk/MA0460.1/Jaspar(0.615) More Information Similar Motifs Found
8	ACCACATAATGA	1e-52	-1.201e+02	0.13%	0.01%	58.2bp (42.2bp)	Btn/dmmpmm(Noyes_hdfly)(0.690) More Information Similar Motifs Found
9	GAITGGAGCTAA	1e-38	-8.804e+01	0.08%	0.00%	53.6bp (31.1bp)	POL013.1_MED-1/Jaspar(0.622) More Information Similar Motifs Found
10	AAGTTTCAGAAAT	1e-37	-8.600e+01	0.12%	0.01%	55.1bp (27.4bp)	ct/MA0218.1/Jaspar(0.627) More Information Similar Motifs Found
11	GTAGTCCCAGGC	1e-36	-8.456e+01	0.07%	0.00%	51.8bp (18.8bp)	sl-8/dmmpmm(Begman/fly)(0.559) More Information Similar Motifs Found
12	AGCATGTTATG	1e-36	-8.456e+01	0.07%	0.00%	53.5bp (38.4bp)	ara/dmmpmm(Noyes_hdfly)(0.712) More Information Similar Motifs Found
13	AAGTTGGGTGCC	1e-34	-7.985e+01	0.09%	0.01%	52.3bp (18.5bp)	Hr46/dmmpmm(Pollard/fly)(0.574) More Information Similar Motifs Found
14	TGTGTCATGT	1e-34	-7.935e+01	2.89%	2.02%	56.0bp (60.3bp)	h/dmmpmm(Noyes/fly)(0.670) More Information Similar Motifs Found
15	CAGTGAACCT	1e-33	-7.768e+01	0.07%	0.00%	56.8bp (15.9bp)	eyg/dmmpmm(Begman/fly)(0.689) More Information Similar Motifs Found
16	AGCGTTGCTCA	1e-30	-7.018e+01	0.09%	0.01%	55.7bp (14.8bp)	POL010.1_DCE_5_III/Jaspar(0.589) More Information Similar Motifs Found

Supplemental Figure 4-3: **Sequence properties of R-loops in Drosophila** **(A)** Metaplots of AT and GC skew at developmental-specific sites of R-loop formation (note the difference in scale for each window). Shaded regions represent the standard error of the mean. **(B)** Metaplots of AT and GC skew at promoter TSS sites and all other R-loops for each cell type. **(C)** Measurement of the R-loops found only at the TTS/3' UTR in the 14-16hr embryos and whether those genes have R-loops elsewhere in the gene in S2 and 2-3hr embryos. **(D)** The top 16 results from the HOMER motif analysis. Only P-values less than $1e-100$ should be considered as potential motifs. Contributions: Analysis for C and D, visualization.

Chromatin associated factors differentially associate with R-loops



Supplemental Figure 4-4: **Expanded chromatin associated factors associated with R-loops for every cell type.** (A) Markers positively and negatively associated with R-loops in S2 cells. * < 0.05 with Bonferroni correction for multiple testing. (B) Same as A, except for 2-3 hour embryos. (C) Same as A, except for 14-16 hour embryos. Contributions: None.

Supplemental Table 4-1: Primers used in R-loop study

Primer Name	Sequence
Act5C_Fwd	CCACGAGACCACCTACAAC
Act5C_Rev	TGATCTTCATGGTCGACGGT
Df31_Fwd	CTCAGACGCCTTTTCACCAT
Df31_Rev	TCGCAGCTGAGGAAGTTGAT
Psq263_Fwd	GTCTGTCCAATTGCTGCGG
Psq263_Rev	TGGCCACCCTCATCTACC
RpL18_Fwd	CTTGCCGAAGTGCTTGCA
RpL18_Rev	TGACCTTCGATCAACTGGCT
Zld162_Fwd	CAACGGAATAGGGTGGGAAT
Zld162_Rev	ACCCCGAATGTGATTAGCCA
Zld221_Fwd	CCACTGGGTTCTGGGTTTTG
Zld221_Rev	CAGTTGCCCGCCGATAATC
chr2RHet_Fwd	TTAAGCGCGGAAAGAAGATCA
chr2RHet_Rev	CAGTTTTGGCGTAGCTAGGGATA
Untranscribed_Fwd	TCAAGCCGAACCCTCTAAAAT
Untranscribed_Rev	AACGCCAACAAACAGAAAATG

Supplemental Table 4-2: GO analysis of R-loop forming genes

S2 cell (total)						
PANTHER GO-Slim Biological Process	#	#	expected	Fold Enrichment	+/-	P value
regulation of transcription by RNA polymerase II	603	243	101.05	2.4	+	1.21E-25
transcription by RNA polymerase II	645	250	108.08	2.31	+	2.25E-24
cell surface receptor signaling pathway	133	56	22.29	2.51	+	0.0000676
negative regulation of cellular process	233	79	39.04	2.02	+	0.000396
chemical synaptic transmission	78	38	13.07	2.91	+	0.000538
actin cytoskeleton organization	88	40	14.75	2.71	+	0.00111
regulation of biological quality	253	81	42.4	1.91	+	0.00156
axogenesis	36	23	6.03	3.81	+	0.00367
cell-cell adhesion	52	28	8.71	3.21	+	0.00397
animal organ development	29	20	4.86	4.12	+	0.00709
cAMP-mediated signaling	43	24	7.21	3.33	+	0.0126
regulation of adenylate cyclase activity	43	24	7.21	3.33	+	0.0126
protein phosphorylation	142	51	23.8	2.14	+	0.0137
adenylate cyclase-modulating G protein-coupled receptor signaling pathway	42	23	7.04	3.27	+	0.0242
regulation of cAMP-mediated signaling	42	23	7.04	3.27	+	0.0242
positive regulation of biological process	296	85	49.6	1.71	+	0.0295
negative regulation of nitrogen compound metabolic process	121	44	20.28	2.17	+	0.0378

2-3h embryo (total)						
PANTHER GO-Slim Biological Process	#	#	expected	Fold Enrichment	+/-	P value
regulation of transcription by RNA polymerase II	603	223	92.89	2.4	+	1.37E-23
transcription by RNA polymerase II	645	228	99.36	2.29	+	3.71E-22
animal organ development	29	22	4.47	4.92	+	0.000215
protein phosphorylation	142	53	21.87	2.42	+	0.000293
G protein-coupled receptor signaling pathway	93	41	14.33	2.86	+	0.000321
axogenesis	36	24	5.55	4.33	+	0.000333
cell-cell adhesion	52	28	8.01	3.5	+	0.000914
regulation of intracellular signal transduction	98	40	15.1	2.65	+	0.00213
chemical synaptic transmission	78	34	12.02	2.83	+	0.00286
regulation of cellular component size	26	17	4.01	4.24	+	0.0223
actin filament organization	60	27	9.24	2.92	+	0.0239
cAMP-mediated signaling	43	22	6.62	3.32	+	0.0257
regulation of adenylate cyclase activity	43	22	6.62	3.32	+	0.0257
negative regulation of RNA metabolic process	61	27	9.4	2.87	+	0.0282
enzyme linked receptor protein signaling pathway	62	27	9.55	2.83	+	0.0338
chemotaxis	31	18	4.78	3.77	+	0.0414
positive regulation of cellular metabolic process	214	62	32.96	1.88	+	0.0435

14-16h embryo (total)						
PANTHER GO-Slim Biological Process	#	#	expected	Fold Enrichment	+/-	P value
regulation of transcription by RNA polymerase II	603	185	82.24	2.25	+	3.59E-17
transcription by RNA polymerase II	645	189	87.97	2.15	+	7.51E-16
chemical synaptic transmission	78	39	10.64	3.67	+	0.0000146
cell-cell adhesion	52	30	7.09	4.23	+	0.000103
positive regulation of cellular process	285	76	38.87	1.96	+	0.000924
protein phosphorylation	142	47	19.37	2.43	+	0.0104
negative regulation of cellular process	233	66	31.78	2.08	+	0.00111
axon guidance	29	19	3.96	4.8	+	0.00141
cAMP-mediated signaling	43	23	5.86	3.92	+	0.00153
regulation of adenylate cyclase activity	43	23	5.86	3.92	+	0.00153
adenylate cyclase-modulating G protein-coupled receptor signaling pathway	42	22	5.73	3.84	+	0.00339
regulation of cAMP-mediated signaling	42	22	5.73	3.84	+	0.00339
positive regulation of catalytic activity	76	30	10.37	2.89	+	0.00751
synapse organization	35	19	4.77	3.98	+	0.011
regulation of membrane potential	43	21	5.86	3.58	+	0.0131
transmembrane receptor protein tyrosine kinase signaling pathway	32	18	4.36	4.12	+	0.0131
animal organ development	29	17	3.96	4.3	+	0.0154
actin filament organization	60	25	8.18	3.06	+	0.0173
ion transport	346	82	47.19	1.74	+	0.0197
regulation of phosphorylation	62	25	8.46	2.96	+	0.027
ncRNA metabolic process	220	8	30.01	0.27	-	0.0106

S2 cell (unique)						
GO biological process complete	#	#	expected	Fold Enrichment	+/-	P value
cellular process	7322	914	764.46	1.2	+	1.64E-10
biological regulation	4402	564	459.6	1.23	+	0.000134
regulation of biological process	3964	513	413.87	1.24	+	0.000299
regulation of cellular process	3661	474	382.23	1.24	+	0.00133
localization	2243	306	234.18	1.31	+	0.00999
transport	1717	241	179.27	1.34	+	0.0267

2-3h embryo (unique)						
GO biological process complete	#	#	expected	Fold Enrichment	+/-	P value
biological regulation	4402	405	290.15	1.4	+	6.31E-11
regulation of biological process	3964	367	261.28	1.4	+	1.55E-09
regulation of cellular process	3661	344	241.31	1.43	+	2.39E-09
cellular process	7322	591	482.62	1.22	+	7.62E-09
multicellular organism development	2280	233	150.28	1.55	+	8.36E-08
system development	1643	178	108.3	1.64	+	6.03E-07
anatomical structure development	2635	253	173.68	1.46	+	0.0000279
developmental process	2765	260	182.25	1.43	+	0.000094
animal organ development	1148	129	75.67	1.7	+	0.000601
multicellular organismal process	3487	305	229.84	1.33	+	0.000271
tube development	689	85	45.41	1.87	+	0.000714
epithelium development	925	105	60.97	1.72	+	0.000966
animal organ morphogenesis	709	86	46.73	1.84	+	0.00105
regulation of macromolecule metabolic process	1989	190	131.1	1.45	+	0.00133
tissue development	1000	110	65.91	1.67	+	0.00182
post-embryonic development	611	76	40.27	1.89	+	0.00207
imaginal disc development	538	69	35.46	1.95	+	0.00256
anatomical structure morphogenesis	1456	146	95.97	1.52	+	0.00325
regulation of metabolic process	2150	199	141.72	1.4	+	0.00487
regulation of nitrogen compound metabolic process	1769	169	116.6	1.45	+	0.00647
regulation of cellular metabolic process	1930	181	127.21	1.42	+	0.00899
regulation of primary metabolic process	1797	170	118.45	1.44	+	0.012
instar larval or pupal development	536	66	35.33	1.87	+	0.0194
post-embryonic animal morphogenesis	444	57	29.27	1.95	+	0.0255
tube morphogenesis	496	61	32.69	1.87	+	0.047
tissue morphogenesis	589	69	38.82	1.78	+	0.0498

14-16h embryo (unique)						
GO biological process complete	#	#	expected	Fold Enrichment	+/-	P value
cellular process	7322	144	98.01	1.47	+	1.9E-08
anatomical structure development	2635	71	35.27	2.01	+	0.0000498
multicellular organismal process	3487	85	46.67	1.82	+	0.0000507
multicellular organism development	2280	63	30.52	2.06	+	0.000255
signaling	1199	42	16.05	2.62	+	0.000316
developmental process	2765	71	37.01	1.92	+	0.000369
cell communication	1269	43	16.99	2.53	+	0.000529
response to stimulus	2513	66	33.64	1.96	+	0.000917
biological regulation	4402	96	58.92	1.63	+	0.000989
signal transduction	994	35	13.31	2.63	+	0.00063
behavior	515	24	6.89	3.48	+	0.000632
system development	1643	47	21.99	2.14	+	0.00188
regulation of cellular process	3661	81	49	1.65	+	0.002
anatomical structure morphogenesis	1456	43	19.49	2.21	+	0.00294
cellular component organization	2598	63	34.78	1.81	+	0.00366
regulation of biological process	3964	84	53.06	1.58	+	0.00607
cellular response to stimulus	1476	42	19.76	2.13	+	0.0123
cell differentiation	1593	44	21.32	2.06	+	0.0151
cellular component organization or biogenesis	2757	64	36.9	1.73	+	0.016
cellular developmental process	1605	44	21.48	2.05	+	0.0164
positive regulation of multicellular organismal process	203	13	2.72	4.78	+	0.0206
positive regulation of biological process	1717	45	22.98	1.96	+	0.0341

Chapter V: Summary and Discussion

DNA is the foundation of genetic information in every eukaryote. Efficiently copying and maintaining DNA is vital for the preservation of the genome. A multitude of studies using yeast, mammalian cell cultures, *in vitro* reconstitution systems, *Xenopus*, *Drosophila*, and other species have laid the groundwork for a greater understanding of the fundamentals of DNA replication. The chromatin environment in which DNA resides is exquisitely regulated in order to safeguard epigenetic information, organize chromatin, and allow for transcription of RNA. However, the confines of development pose a unique obstacle due to the transition from maternal-to-zygotic transcription, establishing the proper cascade of chromatin markers as cells differentiate and divide, constrained cell cycles, and the alternative DNA replication programs needed in certain tissues. By combining next-generation sequencing technologies, mass spectrometry, and other techniques, my work in *Drosophila* has (1) helped define a new role for Rif1 as a regulator of replication fork progression (chapter II); (2) made available new widescale tools to study replication fork composition during development (chapter III); and (3) highlighted the dynamic role of R-loop biology during embryogenesis (chapter IV). However, many questions remain. The rest of this thesis will describe specific experiments that would give new insight to the biology of DNA replication and discuss larger questions that remain in the field.

Rif1 at replication forks

Previous research demonstrated that SuUR acts as a novel regulator of fork progression to control underreplication and gene amplifications programs during

development (Nordman et al. 2014, Kolesnikova et al. 2013). However, due to its likely catalytically dead ATP binding motif and a lack of known functional protein domains, it was unclear how SuUR functioned to control the underreplication and gene amplification program (Yurlova et al. 2009). Our lab's work demonstrated that it controls these programs via an interaction with Rif1. However, SuUR and Rif1 act at only at only a subset of replication forks during gene amplification and underreplication. How both proteins are targeted to specific replication forks remains unknown. Based on how these proteins function to halt replication fork progression and the need for complete replication throughout the remainder of the genome, it is unlikely they are at all replication forks. Previous CHIP-seq and polytene chromosome immunofluorescence demonstrated that they are found only at replication forks in a subset of the genome (Nordman et al. 2014, Kolesnikova et al. 2013). Our own unpublished iPOND mass spectrometry experiments detect SuUR and Rif1 at levels below that of essential proteins present at every replication fork. Therefore, the question remains how SuUR is ultimately targeted to replication forks.

Our immunopurified SuUR mass spectrometry data does not include any obvious candidates for what directs SuUR to replication forks. One possibility is that SuUR is post-translationally modified during S phase to control its localization to the replisome like other dynamic replication fork components are (Sirbu et al. 2011). This could work well during the constrained environment of gene amplification but how it might be targeted to replication forks during a more normal S phase is not clear. Underreplicated regions are normally replicated late in S phase (Belyaeva et al. 2012). Therefore, SuUR might be modified at some point as a byproduct of the replication timing program and is only recruited to replication forks during late S phase. More detailed mass spectrometry

examining changes in posttranslational modifications in early versus late S phase could reveal both the type of modification and where it is modified. These could reveal new insights into what regulates the recruitment of SuUR and Rif1 to replication forks.

Alternatively, recent work has shown that heterochromatin protein 1 (HP1) can exist in a liquid-liquid phase separated compartment (Keenen et al. 2021). SuUR has previously been shown to interact with a variety of chromatin associated factors involved with repressed chromatin including HP1 (Pindyurin et al. 2008). Perhaps SuUR and its interacting partner Rif1 exist in a phase separated environment around potential sites of underreplication, where they can interact with the replication fork machinery only when it enters the compartment and can subsequently be modified (Frattini et al. 2021). This would elegantly allow these complexes to be targeted to the genomic hubs where they are needed. However, some sites of underreplication exist in euchromatin. Specifically testing whether SuUR and Rif1 could form phase separated condensates with other heterochromatin components would be the first step in testing such this hypothesis.

The loss of SuUR or Rif1 lacks obvious phenotypes, such as organismal death or transcriptional derepression of genes within underreplicated regions, therefore it remains unclear why organisms utilize underreplication (Sher et al. 2011). There are several hypotheses as to why underreplication exists. It could be a way to divert developmental resources away from duplicating DNA that is ultimately “useless” as it will no longer be transcriptionally active in a terminally differentiated tissue (Nordman and Orr-Weaver, 2015). The rarity of underreplication in this scenario then is due to the relative rarity of polyploid tissue. Underreplication would normally cause double-strand breaks in a diploid

chromosome, but the polyploid nature of the salivary glands and other tissues that undergo underreplication allow this possibility.

Another hypothesis is that underreplication is involved with or a byproduct of avoiding some cell cycle checkpoints that may need to be suppressed during endoreplication (Hassel et al. 2014). Indeed, loss of function Cdc14 mutants in yeast can result in underreplicated regions (Dulev et al. 2009). Underreplicated regions in these mutants are generally late replicating, which supports the idea that there is some stress response or lack of metabolites available which results in genomic underreplication. Perhaps if Rif1 or SuUR mutant flies were grown under nutrient starved these mutants would be more likely to die. In the trophoblast giant cells of the mammalian placenta where underreplication occurs, a redirection of resources by avoiding cytokinesis and unnecessary DNA replication program in order to better divert resources to the embryo has been hypothesized (Hannibal and Baker, 2016). Experiments with Rif1 and SuUR mutant flies may prove a way to test the theory that the resources saved by underreplication could be significant.

Alternatively, underreplication might occur to resolve probable DNA damage. The dampened DNA damage checkpoints during gene amplification and endoreplication may make it untenable to repair DNA as normal (Mehrotra et al. 2008). Certain cancers with defective DNA damage checkpoints also undergo underreplication (Bertolin et al. 2020). The large size of metazoan genomes increases the probability that, by chance, some replication forks will stall and be unable to replicate some regions of the genome (Bertolin et al. 2020). Therefore, the underreplication program in dispensable regions of the genome may allow the polyploid cell to survive otherwise lethal DNA damage that would

occur without normal DNA damage control. Previous research indicates that underreplicated regions have a mutational signature of DNA damage (Yarosh and Spradling, 2014). Testing SuUR and Rif1 null mutant flies to see if they are more vulnerable to DNA damaging agents could help answer this question.

Replication fork remodeling during embryogenesis

Our work establishing iPOND coupled to quantitative mass spectrometry as a tool to study *Drosophila* embryogenesis likely undercounted the number of proteins at replication forks in embryo. Compared to earlier label-free attempts that we made, significantly fewer proteins at replication forks were found. However, the label-free approach makes it difficult to directly compare proteomics data from multiple different cell types, as absence of a protein does not guarantee it was missing in the alternative sample. It could instead be due to variance in the mass spectrometry run itself. Therefore, we opted for the safer approach of labeling with isobaric reagents that let us definitively ask whether a protein was present or absent in one sample versus the other. The use of stable-isotope labeling by amino acids in cell culture (SILAC) flies in the future could be a valuable improvement upon our method (Beati et al. 2019). This method utilizes flies fed on yeast containing a 'heavy' version of Lysine and Arginine which is incorporated into the fly proteome. The slight mass difference between flies fed on heavy and normal yeast can be detected on modern mass spectrometry machines and obviates the need to label the peptides with a tag. It still retains the simplified and accurate quantitative comparison of isobaric labeling. The post-experiment isobaric labeling has several drawbacks, including loss of sensitivity, which may account for the

decline in identified proteins we observed (Baçhor et al. 2019). This method has other drawbacks, such as the inability to label arginine. This limits the spectrum of peptides that can ultimately be identified.

Nonetheless, this research will be a valuable resource to the community of scientists studying DNA replication during development. It can serve as the jumping off point for a variety of projects examining when precisely during development certain replication fork components are required and demonstrated a novel role of the BRWD3 protein at replication forks in *Drosophila*. Several proteins identified had no known function at the replication fork in *Drosophila*. Comparison of these datasets to those generated in human cells may highlight proteins uniquely required for proper DNA replication in mammalian or *Drosophila* species, respectively (Wessel et al. 2019).

R-loop formation during embryogenesis is dynamic

R-loops have multiple functions such as repair of DNA double strand breaks, promoting transcription termination, preventing DNA methylation, and more (Aguilera and García-Muse, 2012). In contrast, R-loops can be a source of DNA damage. R-loop mapping studies across development have been performed in plants and in induced pluripotent stem cells (Xu et al. 2020, Yan et al. 2020). I showed that bulk R-loop levels vary as a function of development, and that impeding normal R-loop metabolism through overexpression of a catalytically dead RNase H1 causes elevated R-loop levels and embryonic death. This demonstrates the requirement for proper R-loop resolution during development.

I mapped R-loop formation across the *Drosophila* genome at multiple timepoints during embryogenesis and in the S2 cell culture line. Though a core set of sites always form R-loops, many loci vary across development. The overlap of R-loops with many chromatin associated factors changes with development, though a subset of markers associated with both active and repressed chromatin remain consistent. Importantly, I demonstrated that changes in transcription cannot account for the plastic formation of R-loops by examining deposited GRO-seq data. This implies that R-loop formation is actively regulated across cell type and not just a byproduct of changing transcription. By comparing R-loop formation at 2-3 hour embryos with RPA ChIP-seq data from a similar timepoint, I suggest that R-loops may play an important role in activating the ATR checkpoint during the maternal-to-zygotic transition. The groundwork in establishing this system grants us the ability to ask more scintillating questions in the future.

The role of R-loops in establishing the chromatin environment remains a 'chicken or the egg question', and it is unclear whether R-loops modify the chromatin environment around them or if instead their formation is a byproduct of the surrounding genomic landscape (Chédin 2016). There is compelling biochemical evidence that at minimum R-loops play a role in establishing repressive H3K27me3 chromatin domains through its interaction with Polycomb complex members in *Drosophila* and mammals (Alecki et al. 2020, Skourti-Stathaki et al. 2019). In addition, genetic screens in yeast show that R-loops can promote H3S10 phosphorylation (Castellano-Pozo et al. 2013). Proteomics screens for R-loop interacting factors show a wide variety of proteins that can potentially bind R-loops and may play a role in modifying the nearby chromatin either directly or indirectly (Cristini et al. 2018, Mosler et al. 2021).

In early embryogenesis chromatin exists in a naïve state without established histone modification and heterochromatin domains (Eckersley-Maslin et al. 2018). This makes it uniquely suited to interrogate the interplay between R-loops and chromatin and directly ask to what extent R-loops establish the surrounding chromatin environment. By overexpressing RNase H1 using the flies we engineered, R-loops could be degraded prematurely before they have time to modify the surrounding chromatin. My data shows that overexpression does not cause embryonic lethality. Therefore, one could perform ChIP-seq for a variety of different histone markers and chromatin associated proteins in a wild-type and RNase H1 overexpression background and interrogate how disrupting R-loop formation impacts establishment of normal histone modifications and chromatin associated factors. Delay or altered chromatin domain formation, combined with careful RNA-seq controls to ensure that the results aren't due to altered transcription, would conclusively demonstrate the extent to which R-loops determine the chromatin environment.

The RNase H1 overexpression experiment could also be used to address the question to what extent R-loops may play in activating ATR, an essential DNA damage checkpoint regulator, at the maternal-to-zygotic transition (Hamm and Harrison, 2018). Data from previous work combining mutants of ATR and Zelda, a ubiquitous transcription factor necessary for much of the transcription at the maternal-to-zygotic transition, shows that loss of Zelda bypasses the requirement for ATR at the MZT (Blythe and Wieschaus 2015). This demonstrated that the activation of ATR is due to some sort of DNA damage caused by transcription. At cycle 14, the cell cycle is still abbreviated and is concluded within an hour (Farrell and O'Farrell, 2014). One explanation for the activation of ATR is

due to collisions between the replication and transcription machinery occurring within the shortened cell cycle (Hamperl et al. 2017). If the lethality of ATR mutants at this timepoint is bypassed by overexpressing RNase H1 and eliminating R-loops, that would conclusively demonstrate that R-loops drive the requirement for ATR. This would illustrate a new role for R-loops in embryogenesis and DNA damage signaling.

My work and others have shown that R-loops form across the histone locus in *Drosophila* and mice (Wulfridge and Sarma, 2021). The *Drosophila* histone locus body undergoes a precise and well-characterized formation during embryogenesis and has been used as an important model for research in nuclear body formation (Duronio and Marzluff, 2017). Mass spectrometry screens revealed that many putative R-loop interacting factors have intrinsically disordered domains (IDR), which often play a role in formation of nuclear bodies via liquid-liquid phase separation (LLPS) (Protter et al. 2018, Dettori et al. 2021). Formation of the histone locus body occurs through a hierarchal process and is nucleated by the onset of transcription (White et al. 2011, Koreski et al. 2020). It is possible that this process may involve recruitment of IDR-containing proteins via their interaction with R-loops. I performed initial experiments testing whether overexpression of RNase H1 delayed or impacted formation of the histone locus body using immunofluorescence. These preliminary results failed to show a clear delay in histone locus body, though more careful analysis using time-lapse microscopy may yet reveal a role for R-loops in the formation of this nuclear body. Alternatively, initially investigating this question in a tractable cell culture system may be better simpler than the very fast embryonic system.

Finally, R-loops may function in organizing chromatin. Due to the abundance of RNA binding proteins, RNA can make an ideal scaffold for chromatin organization and it is essential for the formation of some nuclear bodies (Chujo and Hirose, 2017). Exciting experiments have been done examining the function of RNA in genome organization by analyzing untreated and RNase A treated with next-generation sequencing approaches. Treatment with RNase A seems to alter genome organization (Barutcu et al. 2019, Thakur et al. 2019). Both facultative and constitutive heterochromatin were impacted in these experiments. However, RNase A is known have off-target R-loop degradation activity in common buffer conditions (Smolka et al. 2021). Indeed, disrupting active transcription where R-loops might form via treatment with actinomycin D had a much greater impact on chromatin organization than treatment with RNase A (Barucu et al. 2019). As R-loops often form as a byproduct of transcription, they may function to regulate chromatin organization and establishment of topologically associating domains. The embryo RNase H1 overexpression system could be utilized to separate the function of active transcription and R-loops in regulating chromatin organization. This line of inquiry is bolstered by recent research demonstrating that R-loop formation at the *HOTTIP* lncRNA loci is required for proper chromatin domain formation in a mouse model of leukemia and disruption of this process promotes tumorigenesis (Luo et al. 2022). The relative infancy of R-loop biology as a field lends itself to reveal key mechanistic insights into a suite of fundamental genome organization and stability. The system I developed mapping and modulating R-loop abundance in *Drosophila* embryogenesis is well-position to answer important questions in R-loop biology in the context of development.

Improvements in R-loop science

The field of R-loop biology is at a crossroads. The last decade has been marked by an explosion of R-loop mapping studies in a multitude of different organisms and an increased appreciation for the variety of roles that R-loops can play in the cell. Due to the newness of the topic and lack of understanding, some research that may be flawed has also come out. For example, several studies have used immunofluorescence with the S9.6 antibody to test whether modulation of a specific protein impacts R-loops levels. In my own hands, this was an ineffective way to measure R-loop levels because there is abundant cytoplasmic S9.6 staining. Recently, other research has demonstrated the shortcomings of the S9.6 antibody and the challenge in properly interpreting R-loop phenotypes. The Chédin lab showed that spike-in fluorescent labeled dsRNA overlaps with the S9.6 antibody and that what S9.6 is binding to is not a bona fide R-loop (Smolka et al. 2021). The Stirling lab examined R-loop dependent genome instability in an RNA processing factor mutant. Instead, they found the supposed R-loop phenotype was driven by changed gene expression of an important cytoskeletal component (Tam et al. 2019). Finally, several studies used the DRIPc method that maps the RNA strand of an R-loop to allow for greater resolution and strand-specificity. A meta-analysis of these studies showed that there was large contamination by RNA not from R-loops (Chédin et al. 2021). Indeed, this is another obstacle I encountered in my own hands mapping R-loops. I mention these studies not to criticize the work done, but to highlight the challenges of developing a new field of biology. What does the field look like going forward? I see several key challenges: (1) develop new mapping strategies and assays for detecting R-

loops; (2) more careful analysis of R-loop phenotypes; and (3) an increased need for precise language to describe R-loops.

Improved R-loop detection. My early attempts at mapping R-loops by sequencing of the RNA strand of the R-loop failed due to contamination of RNA, and this has since been shown to be a wider problem in the field (Chédin et al. 2021). In addition, I was only able to obtain consistent, RNase H1-degradable results through careful reduction of the contaminating RNA in the extract. Many of the studies analyzing R-loops have used the S9.6 antibody. Other alternative approaches relied on expressing tagged, catalytically dead RNase H1 in live cells and purifying the protein:nucleic acid complex (Chen et al. 2017). The dramatic embryonic death I observed when overexpressing catalytically dead RNase H1 demonstrates how this could alter the R-loop environment. If overexpression of this protein perturbs the cell's environment so intensely that embryos die, then it is unlikely to accurately map native R-loop formation.

New methods utilizing *in vitro* purified RNase H1 combined with 'CUT&RUN' purification of R-loops may ultimately be a more consistent and robust method to map R-loop formation genome wide (Yan and Sarma, 2020). RNase H1 recognizes an R-loop over dsRNA with 25-fold greater affinity (Nowotny et al. 2008). In comparison, the S9.6 antibody recognizes R-loops with only 4.5 fold greater affinity than dsRNA (Phillips et al. 2013). The minimum required R-loop size is similar between the RNase H1 and S9.6 antibody (4 basepairs versus 6) (Phillips et al. 2013). The nucleic acid sequence can also have large impacts on the S9.6 antibody's binding affinity to both dsRNA and R-loops, while the sequence preferences for RNase H1 are less clear (Konig et al. 2017).

Therefore, using purified RNase H1 may give more accurate results compared to the S9.6 antibody.

Despite the advantages of RNase H1 over the S9.6 antibody, the affinity of RNase H1 for R-loops is in the order of 10^{-7} M (Nowotny et al. 2008). In comparison, the K_d of commercial antibodies for common epitope tags is in the order of 10^{-9} - 10^{-10} M (Ranawakage et al. 2019). RNase H1 is an essential, well-studied enzyme and is only composed of one subunit. These traits have led it to be the workhorse and first alternative for R-loop mapping. Several proteomic screens have been performed to identify proteins which interact with R-loops (Wu et al. 2021; Mosler et al. 2021; Wang et al. 2018; Cristini et al. 2018). One of these may ultimately prove to be much more robust and reliable way to measure R-loops localization across the genome going forward. Alternatively, directed evolution of RNase H1 may result in a more suitable tool to evaluate R-loop formation (Zeymer and Hilvert 2018).

Proper evaluation of R-loop phenotypes. Due to the excitement in the field around R-loops, there has been a rush to publish and link previously observed mutants and phenotypes to R-loop biology. However, R-loops are involved with double-strand break repair, regulation of chromatin, transcription termination, DNA methylation, modulation of transcription, and mitochondria replication (Santos-Pereira and Aguilera, 2015). These disparate functions and the infancy of the field means that it can be difficult to properly link R-loops to the correct biology. Work by multiple labs emphasized this when they demonstrated that mutants previously thought to cause genome stability in *cis* due to increased R-loops was instead due to altered transcript levels in cohesion proteins (Tam

et al. 2019, Darman et al. 2015). Going forward, careful controls must be done to ensure the veracity of claims made.

The gold standard to specifically test for R-loop driven phenotypes has long been overexpression of RNase H1, used in one of the first papers that showed R-loop driven genome instability (Li and Manley, 2005). This theoretically degrades abundant R-loops. RNase H1 overexpression has been consistently used across the field and despite the potential drawbacks of overexpression mentioned earlier, should still be widely used. Many labs are examining the potential role of RNA processing factors and spliceosome components, as these proteins can impact R-loop formation and resolution. Ensuring that any result is due to impaired R-loop processing and not altered transcription can be done with RNA-seq experiments and should be required in the field.

One of the most exciting research avenues is how R-loops cause DNA damage. While the exposed single-strand of DNA is subject to deamination, this is unlikely to cause damage beyond point mutations. Exceptions can theoretically occur at transcriptionally active loci where high levels of transcription and single strand break from TOP1 cleave complexes can act with nucleases at an R-loop to generate two independent single strand breaks (Cristini et al. 2019, Sollier et al. 2014). The primary source of R-loop driven genome instability occurs during S phase and seems to be driven by collisions with the replication fork machinery (Gan et al. 2011). Careful cell cycle analysis can be used to show that genome instability due to R-loops only occurs during S phase, such as done in some previous work (Stork et al. 2016).

Precise language. While R-loops were originally defined as occurring in *trans*, most R-loops are thought to form in *cis* when nascent RNA reanneals to the template DNA.

There are many exceptions to this rule. The guide RNA of the CRISPR-Cas9 enzyme forms an RNA:DNA hybrid at its target site (Mitchell et al. 2020). Recently it has been shown that R-loops can form at the edges of double-strand breaks, and the prevention of their resolution results in persistent Rad52 foci (Ouyang et al. 2021, Yang et al. 2021). Finally, in plants some lncRNA can invade sites and form R-loops in *trans* (Ariel et al. 2020). It is likely that many more exceptions will be found as R-loop biology progresses. Therefore, it will become increasingly critical to differentiate between those R-loops that arise in *trans* versus those in *cis* as their formation, mode of action, size, and impact may be vastly different.

References

1. Abyzov, A., Urban, A. E., Snyder, M. & Gerstein, M. CNVnator: An approach to discover, genotype, and characterize typical and atypical CNVs from family and population genome sequencing. *Genome Research* **21**, 974-984 (2011).
2. Aggarwal, B. D. & Calvi, B. R. Chromatin regulates origin activity in *Drosophila* follicle cells. *Nature* **430**, 372–376 (2004).
3. Aguilera, A. & García-Muse, T. R Loops: From Transcription Byproducts to Threats to Genome Stability. *Molecular Cell* **46**, 115–124 (2012).
4. Alabert, C. & Groth, A. Chromatin replication and epigenome maintenance. *Nature Reviews Molecular Cell Biology* **13**, 153-167 (2012).
5. Alabert, C., Bukowski-Wills, J.-C., Lee, S.-B., Kustatscher, G., Nakamura, K., Alves, F. de L., Menard, P., Mejlvang, J., Rappsilber, J. & Groth, A. Nascent chromatin capture proteomics determines chromatin dynamics during DNA replication and identifies unknown fork components. *Nature Cell Biology* **16**, 281-291 (2014).
6. Alecki, C., Chiwara, V., Sanz, L. A., Grau, D., Pérez, O. A., Boulier, E. L., Armache, K.-J., Chédin, F. & Francis, N. J. RNA-DNA strand exchange by the *Drosophila* Polycomb complex PRC2. *Nat Commun* **11**, 1781 (2020).
7. Alexander, J. L., Barrasa, M. I. & Orr-Weaver, T. L. Replication Fork Progression during Re-replication Requires the DNA Damage Checkpoint and Double-Strand Break Repair. *Curr Biol* **25**, 1654–1660 (2015).
8. Alver, R. C., Chadha, G. S., Gillespie, P. J. & Blow, J. J. Reversal of DDK-Mediated MCM Phosphorylation by Rif1-PP1 Regulates Replication Initiation and Replisome Stability Independently of ATR/Chk1. *Cell Reports* **18**, 2508–2520 (2017).
9. Amemiya, H. M., Kundaje, A. & Boyle, A. P. The ENCODE Blacklist: Identification of Problematic Regions of the Genome. *Sci Rep* **9**, 9354 (2019).
10. Andreyeva, E. N., Bernardo, T. J., Kolesnikova, T. D., Lu, X., Yarinich, L. A., Bartholdy, B. A., Guo, X., Posukh, O. V., Heaton, S., Willcockson, M. A., Pindyurin, A. V., Zhimulev, I. F., Skoultchi, A. I. & Fyodorov, D. V. Regulatory functions and chromatin loading dynamics of linker histone H1 during endoreplication in *Drosophila*. *Gene Dev* **31**, 603–616 (2017).
11. Andreyeva, E. N., Kolesnikova, T. D., Belyaeva, E. S., Glaser, R. L. & Zhimulev, I. F. Local DNA underreplication correlates with accumulation of phosphorylated H2Av in the *Drosophila melanogaster* polytene chromosomes. *Chromosome Res* **16**, 851–862 (2008).
12. Aranda, S., Rutishauser, D. & Ernfors, P. Identification of a large protein network involved in epigenetic transmission in replicating DNA of embryonic stem cells. *Nucleic Acids Res* **42**, 6972–6986 (2014).
13. Ariel, F., Lucero, L., Christ, A., Mammarella, M. F., Jegu, T., Veluchamy, A., Mariappan, K., Latrasse, D., Blein, T., Liu, C., Benhamed, M. & Crespi, M. R-Loop Mediated trans Action of the APOLO Long Noncoding RNA. *Mol Cell* **77**, 1055-1065 (2020).
14. Ashburner, M., Ball, C. A., Blake, J. A., Botstein, D., Butler, H., Cherry, J. M., Davis, A. P., Dolinski, K., Dwight, S. S., Eppig, J. T., Harris, M. A., Hill, D. P., Issel-Tarver, L., Kasarskis, A., Lewis, S., Matese, J. C., Richardson, J. E., Ringwald, M., Rubin, G. M. & Sherlock, G. Gene Ontology: tool for the unification of biology. *Nat Genet* **25**, 25–29 (2000).

15. Bąchor, R., Waliczek, M., Stefanowicz, P. & Szewczuk, Z. Trends in the Design of New Isobaric Labeling Reagents for Quantitative Proteomics. *Molecules* **24**, 701 (2019).
16. Bailey, E. C., Kobielski, S., Park, J. & Losick, V. P. Polyploidy in Tissue Repair and Regeneration. *Csh Perspect Biol* **13**, a040881 (2021).
17. Bandura, J. L., Beall, E. L., Bell, M., Silver, H. R., Botchan, M. R. & Calvi, B. R. humpty dumpty Is Required for Developmental DNA Amplification and Cell Proliferation in Drosophila. *Curr Biol* **15**, 755–759 (2005).
18. Baris, Y., Taylor, M. R. G., Aria, V. & Yeeles, J. T. P. Fast and efficient DNA replication with purified human proteins. *Nature* **606**, 204–210 (2022).
19. Barolo, S., Carver, L. A. & Posakony, J. W. GFP and -Galactosidase Transformation Vectors for Promoter/Enhancer Analysis in Drosophila. *Biotechniques* **29**, 726–732 (2000).
20. Barutcu, A. R., Blencowe, B. J. & Rinn, J. L. Differential contribution of steady-state RNA and active transcription in chromatin organization. *Embo Rep* **20**, e48068 (2019).
21. Bassett, A. R., Tibbit, C., Ponting, C. P. & Liu, J.-L. Highly Efficient Targeted Mutagenesis of Drosophila with the CRISPR/Cas9 System. *Cell Reports* **4**, 220–228 (2013).
22. Bayona-Feliu, A., Casas-Lamesa, A., Reina, O., Bernués, J. & Azorín, F. Linker histone H1 prevents R-loop accumulation and genome instability in heterochromatin. *Nat Commun* **8**, 283 (2017).
23. Beadle, G. W. & Ephrussi, B. Transplantation in Drosophila. *Proc National Acad Sci* **21**, 642–646 (1935).
24. Beati, H., Langlands, A., Have, S. ten & Müller, H.-A. J. SILAC-based quantitative proteomic analysis of Drosophila gastrula stage embryos mutant for fibroblast growth factor signalling. *Fly* **14**, 1–19 (2019).
25. Belanger, K. G. & Kreuzer, K. N. Bacteriophage T4 Initiates Bidirectional DNA Replication through a Two-Step Process. *Mol Cell* **2**, 693–701 (1998).
26. Beletskii, A. & Bhagwat, A. S. Transcription-induced mutations: Increase in C to T mutations in the nontranscribed strand during transcription in Escherichia coli. *Proc National Acad Sci* **93**, 13919–13924 (1996).
27. Bell, D. W., Sikdar, N., Lee, K., Price, J. C., Chatterjee, R., Park, H.-D., Fox, J., Ishiai, M., Rudd, M. L., Pollock, L. M., Fogoros, S. K., Mohamed, H., Hanigan, C. L., Program, N. C. S., Zhang, S., Cruz, P., Renaud, G., Hansen, N. F., Cherukuri, P. F., Borate, B., McManus, K. J., Stoepel, J., Sipahimalani, P., Godwin, A. K., Sgroi, D. C., Merino, M. J., Elliot, G., Elkahloun, A., Vinson, C., Takata, M., Mullikin, J. C., Wolfsberg, T. G., Hieter, P., Lim, D.-S. & Myung, K. Predisposition to Cancer Caused by Genetic and Functional Defects of Mammalian Atad5. *Plos Genet* **7**, e1002245 (2011).
28. Bell, S. P. & Labib, K. Chromosome Duplication in Saccharomyces cerevisiae. *Genetics* **203**, 1027-1067 (2016).
29. Belotserkovskii, B. P., Liu, R., Tornaletti, S., Krasilnikova, M. M., Mirkin, S. M. & Hanawalt, P. C. Mechanisms and implications of transcription blockage by guanine-rich DNA sequences. *Proc National Acad Sci* **107**, 12816–12821 (2010).

30. Belotserkovskii, B. P., Shin, J. H. S. & Hanawalt, P. C. Strong transcription blockage mediated by R-loop formation within a G-rich homopurine–homopyrimidine sequence localized in the vicinity of the promoter. *Nucleic Acids Res* **45**, 6589–6599 (2017).
31. Belyaeva, E. S., Goncharov, F. P., Demakova, O. V., Kolesnikova, T. D., Boldyreva, L. V., Semeshin, V. F. & Zhimulev, I. F. Late Replication Domains in Polytene and Non-Polytene Cells of *Drosophila melanogaster*. *Plos One* **7**, e30035 (2012).
32. Benna, C., Bonaccorsi, S., Wülbeck, C., Helfrich-Förster, C., Gatti, M., Kyriacou, C. P., Costa, R. & Sandrelli, F. *Drosophila* timeless2 Is Required for Chromosome Stability and Circadian Photoreception. *Curr Biol* **20**, 346–352 (2010).
33. Bertolin, A. P., Hoffmann, J.-S. & Gottifredi, V. Under-Replicated DNA: The Byproduct of Large Genomes? *Cancers* **12**, 2764 (2020).
34. Bhatia, V., Barroso, S. I., García-Rubio, M. L., Tumini, E., Herrera-Moyano, E. & Aguilera, A. BRCA2 prevents R-loop accumulation and associates with TREX-2 mRNA export factor PCID2. *Nature* **511**, 362–365 (2014).
35. Birnstiel, M. L., Sells, B. H. & Purdom, I. F. Kinetic complexity of RNA molecules. *J Mol Biol* **63**, 21–39 (1972).
36. Blasiak, J., Szczepańska, J., Sobczuk, A., Fila, M. & Pawlowska, E. RIF1 Links Replication Timing with Fork Reactivation and DNA Double-Strand Break Repair. *Int J Mol Sci* **22**, 11440 (2021).
37. Blumenthal, A., Kriegstein, H. & Hogness, D. The Units of DNA Replication in *Drosophila melanogaster* Chromosomes. *Cold Spring Harb Sym* **38**, 205–223 (1974).
38. Blythe, S. A. & Wieschaus, E. F. Chapter Four Coordinating Cell Cycle Remodeling with Transcriptional Activation at the *Drosophila* MBT. in *The Maternal to Zygotic Transition*. (ed. Lipshitz, H.D.) 113–148 (Elsevier Inc., 2015).
39. Blythe, S. A. & Wieschaus, E. F. Zygotic Genome Activation Triggers the DNA Replication Checkpoint at the Midblastula Transition. *Cell* **160**, 1169–1181 (2015).
40. Boguslawski, S. J., Smith, D. E., Michalak, M. A., Mickelson, K. E., Yehle, C. O., Patterson, W. L. & Carrico, R. J. Characterization of monoclonal antibody to DNA · RNA and its application to immunodetection of hybrids. *J Immunol Methods* **89**, 123–130 (1986).
41. Bolger, A. M., Lohse, M. & Usadel, B. Trimmomatic: a flexible trimmer for Illumina sequence data. *Bioinformatics* **30**, 2114–2120 (2014).
42. Bonnet, A., Grosso, A. R., Elkaoutari, A., Coleno, E., Presle, A., Sridhara, S. C., Janbon, G., Géli, V., Almeida, S. F. de & Palancade, B. Introns Protect Eukaryotic Genomes from Transcription-Associated Genetic Instability. *Mol Cell* **67**, 608–621 (2017).
43. Bonnet, J., Lindeboom, R. G. H., Pokrovsky, D., Stricker, G., Çelik, M. H., Rupp, R. A. W., Gagneur, J., Vermeulen, M., Imhof, A. & Müller, J. Quantification of Proteins and Histone Marks in *Drosophila* Embryos Reveals Stoichiometric Relationships Impacting Chromatin Regulation. *Dev Cell* **51**, 632–644 (2019).
44. Bowman, S. K., Deaton, A. M., Domingues, H., Wang, P. I., Sadreyev, R. I., Kingston, R. E. & Bender, W. H3K27 modifications define segmental regulatory domains in the *Drosophila* bithorax complex. *Elife* **3**, e02833 (2014).

45. Calvi, B. R., Lilly, M. A. & Spradling, A. C. Cell cycle control of chorion gene amplification. *Gene Dev* **12**, 734–744 (1998).
46. Capuano, F., Mülleder, M., Kok, R., Blom, H. J. & Ralser, M. Cytosine DNA Methylation Is Found in *Drosophila melanogaster* but Absent in *Saccharomyces cerevisiae*, *Schizosaccharomyces pombe*, and Other Yeast Species. *Anal Chem* **86**, 3697–3702 (2014).
47. Carles-Kinch, K. & Kreuzer, K. N. RNA-DNA hybrid formation at a bacteriophage T4 replication origin. *J Mol Biol* **266**, 915–926 (1997).
48. Castellano-Pozo, M., Santos-Pereira, J. M., Rondón, A. G., Barroso, S., Andújar, E., Pérez-Alegre, M., García-Muse, T. & Aguilera, A. R Loops Are Linked to Histone H3 S10 Phosphorylation and Chromatin Condensation. *Molecular Cell* **52**, 583-590 (2013).
49. Cayrou, C., Coulombe, P., Vigneron, A., Stanojic, S., Ganier, O., Peiffer, I., Rivals, E., Puy, A., Laurent-Chabalier, S., Desprat, R. & Méchali, M. Genome-scale analysis of metazoan replication origins reveals their organization in specific but flexible sites defined by conserved features. *Genome Research* **21**, 1438-1449 (2011).
50. Chan, Y. A., Aristizabal, M. J., Lu, P. Y. T., Luo, Z., Hamza, A., Kobor, M. S., Stirling, P. C. & Hieter, P. Genome-Wide Profiling of Yeast DNA:RNA Hybrid Prone Sites with DRIP-Chip. *Plos Genet* **10**, e1004288 (2014).
51. Chang, C.-H., Chavan, A., Palladino, J., Wei, X., Martins, N. M. C., Santinello, B., Chen, C.-C., Erceg, J., Beliveau, B. J., Wu, C.-T., Larracuenta, A. M. & Mellone, B. G. Islands of retroelements are major components of *Drosophila* centromeres. *Plos Biol* **17**, e3000241 (2019).
52. Chapman, J. R., Barral, P., Vannier, J.-B., Borel, V., Steger, M., Tomas-Loba, A., Sartori, A. A., Adams, I. R., Batista, F. D. & Boulton, S. J. RIF1 Is Essential for 53BP1-Dependent Nonhomologous End Joining and Suppression of DNA Double-Strand Break Resection. *Mol Cell* **49**, 858–871 (2013).
53. Chaudhuri, J., Tian, M., Khuong, C., Chua, K., Pinaud, E. & Alt, F. W. Transcription-targeted DNA deamination by the AID antibody diversification enzyme. *Nature* **422**, 726–730 (2003).
54. Chédin, F. Nascent Connections: R-Loops and Chromatin Patterning. *Trends Genet* **32**, 828–838 (2016).
55. Chédin, F., Hartono, S. R., Sanz, L. A. & Vanoosthuyse, V. Best practices for the visualization, mapping, and manipulation of R-loops. *Embo J* e106394 (2021).
56. Chen, L., Chen, J.-Y., Zhang, X., Gu, Y., Xiao, R., Shao, C., Tang, P., Qian, H., Luo, D., Li, H., Zhou, Y., Zhang, D.-E. & Fu, X.-D. R-ChIP Using Inactive RNase H Reveals Dynamic Coupling of R-loops with Transcriptional Pausing at Gene Promoters. *Mol Cell* **68**, 745-757 (2017).
57. Chen, P. B., Chen, H. V., Acharya, D., Rando, O. J. & Fazzio, T. G. R loops regulate promoter-proximal chromatin architecture and cellular differentiation. *Nat Struct Mol Biol* **22**, 999–1007 (2015).
58. Christov, C. P., Dingwell, K. S., Skehel, M., Wilkes, H. S., Sale, J. E., Smith, J. C. & Krude, T. A NuRD Complex from *Xenopus laevis* Eggs Is Essential for DNA Replication during Early Embryogenesis. *Cell Reports* **22**, 2265–2278 (2018).

59. Chujo, T. & Hirose, T. Nuclear Bodies Built on Architectural Long Noncoding RNAs: Unifying Principles of Their Construction and Function. *Mol Cells* **40**, 889–896 (2017).
60. Claycomb, J. M. & Orr-Weaver, T. L. Developmental gene amplification: insights into DNA replication and gene expression. *Trends Genet* **21**, 149–162 (2005).
61. Colak, D., Zaninovic, N., Cohen, M. S., Rosenwaks, Z., Yang, W.-Y., Gerhardt, J., Disney, M. D. & Jaffrey, S. R. Promoter-Bound Trinucleotide Repeat mRNA Drives Epigenetic Silencing in Fragile X Syndrome. *Science* **343**, 1002–1005 (2014).
62. Consortium, T. G. O., Carbon, S., Douglass, E., Good, B. M., Unni, D. R., Harris, N. L., Mungall, C. J., Basu, S., Chisholm, R. L., Dodson, R. J., Hartline, E., Fey, P., Thomas, P. D., Albou, L.-P., Ebert, D., Kesling, M. J., Mi, H., Muruganujan, A., Huang, X., Mushayahama, T., LaBonte, S. A., Siegele, D. A., Antonazzo, G., Attrill, H., Brown, N. H., Garapati, P., Marygold, S. J., Trovisco, V., Santos, G. dos, Falls, K., Tabone, C., Zhou, P., Goodman, J. L., Strelets, V. B., Thurmond, J., Garmiri, P., Ishtiaq, R., Rodríguez-López, M., Acencio, M. L., Kuiper, M., Lægreid, A., Logie, C., Lovering, R. C., Kramarz, B., Saverimuttu, S. C. C., Pinheiro, S. M., Gunn, H., Su, R., Thurlow, K. E., Chibucos, M., Giglio, M., Nadendla, S., Munro, J., Jackson, R., Duesbury, M. J., Del-Toro, N., Meldal, B. H. M., Paneerselvam, K., Perfetto, L., Porras, P., Orchard, S., Shrivastava, A., Chang, H.-Y., Finn, R. D., Mitchell, A. L., Rawlings, N. D., Richardson, L., Sangrador-Vegas, A., Blake, J. A., Christie, K. R., Dolan, M. E., Drabkin, H. J., Hill, D. P., Ni, L., Sitnikov, D. M., Harris, M. A., Oliver, S. G., Rutherford, K., Wood, V., Hayles, J., Bähler, J., Bolton, E. R., Pons, J. L. D., Dwinell, M. R., Hayman, G. T., Kaldunski, M. L., Kwitek, A. E., Laulederkind, S. J. F., Plasterer, C., Tutaj, M. A., VEDI, M., Wang, S.-J., D'Eustachio, P., Matthews, L., Balhoff, J. P., Aleksander, S. A., Alexander, M. J., Cherry, J. M., Engel, S. R., Gondwe, F., Karra, K., Miyasato, S. R., Nash, R. S., Simison, M., Skrzypek, M. S., Weng, S., Wong, E. D., Feuermann, M., Gaudet, P., Morgat, A., Bakker, E., Berardini, T. Z., Reiser, L., Subramaniam, S., Huala, E., Arighi, C. N., Auchincloss, A., Axelsen, K., Argoud-Puy, G., Bateman, A., Blatter, M.-C., Boutet, E., Bowler, E., Breuza, L., Bridge, A., Britto, R., Bye-A-Jee, H., Casas, C. C., Coudert, E., Denny, P., Estreicher, A., Famiglietti, M. L., Georghiou, G., Gos, A., Gruaz-Gumowski, N., Hatton-Ellis, E., Hulo, C., Ignatchenko, A., Jungo, F., Laiho, K., Mercier, P. L., Lieberherr, D., Lock, A., Lussi, Y., MacDougall, A., Magrane, M., Martin, M. J., Masson, P., Natale, D. A., Hyka-Nouspikel, N., Pedruzzi, I., Pourcel, L., Poux, S., Pundir, S., Rivoire, C., Speretta, E., Sundaram, S., Tyagi, N., Warner, K., Zaru, R., Wu, C. H., Diehl, A. D., Chan, J. N., Grove, C., Lee, R. Y. N., Muller, H.-M., Raciti, D., Auken, K. V., Sternberg, P. W., Berriman, M., Paulini, M., Howe, K., Gao, S., Wright, A., Stein, L., Howe, D. G., Toro, S., Westerfield, M., Jaiswal, P., Cooper, L. & Elser, J. The Gene Ontology resource: enriching a GOld mine. *Nucleic Acids Res* **49**, D325–D334 (2020).
63. Conticello, S. G. The AID/APOBEC family of nucleic acid mutators. *Genome Biol* **9**, 229 (2008).
64. Contrino, S., Smith, R. N., Butano, D., Carr, A., Hu, F., Lyne, R., Rutherford, K., Kalderimis, A., Sullivan, J., Carbon, S., Kephart, E. T., Lloyd, P., Stinson, E. O., Washington, N. L., Perry, M. D., Ruzanov, P., Zha, Z., Lewis, S. E., Stein, L. D. &

- Micklem, G. modMine: flexible access to modENCODE data. *Nucleic Acids Res* **40**, D1082–D1088 (2012).
65. Core, L. J., Waterfall, J. J., Gilchrist, D. A., Fargo, D. C., Kwak, H., Adelman, K. & Lis, J. T. Defining the Status of RNA Polymerase at Promoters. *Cell Reports* **2**, 1025–1035 (2012).
66. Cornacchia, D., Dileep, V., Quivy, J., Foti, R., Tili, F., Santarella-Mellwig, R., Antony, C., Almouzni, G., Gilbert, D. M. & Buonomo, S. B. C. Mouse Rif1 is a key regulator of the replication-timing programme in mammalian cells. *Embo J* **31**, 3678–3690 (2012).
67. Cortez, D. Chapter Two: Proteomic Analyses of the Eukaryotic Replication Machinery. in *DNA Repair Enzymes: Cell, Molecular, and Chemical Biology* (ed. Eichman, B.F.) 33-53 (Elsevier Inc., 2017).
68. Costantino, L. & Koshland, D. Genome-wide Map of R-Loop-Induced Damage Reveals How a Subset of R-Loops Contributes to Genomic Instability. *Molecular Cell* **71**, 1-34 (2018).
69. Cózar, J. M. G. de, Gerards, M., Teeri, E., George, J., Dufour, E., Jacobs, H. T. & Jöers, P. RNase H1 promotes replication fork progression through oppositely transcribed regions of *Drosophila* mitochondrial DNA. *J Biol Chem* **294**, 4331-4344 (2019).
70. Cristini, A., Groh, M., Kristiansen, M. S. & Gromak, N. RNA/DNA Hybrid Interactome Identifies DXH9 as a Molecular Player in Transcriptional Termination and R-Loop-Associated DNA Damage. *Cell Reports* **23**, 1891-1905 (2018).
71. Cristini, A., Ricci, G., Britton, S., Salimbeni, S., Huang, S. N., Marinello, J., Calsou, P., Pommier, Y., Favre, G., Capranico, G., Gromak, N. & Sordet, O. Dual Processing of R-Loops and Topoisomerase I Induces Transcription-Dependent DNA Double-Strand Breaks. *Cell Reports* **28**, 3167-3181 (2019).
72. Crossley, M. P., Bocek, M. J., Hamperl, S., Swigut, T. & Cimprich, K. A. qDRIP: a method to quantitatively assess RNA–DNA hybrid formation genome-wide. *Nucleic Acids Res* e84 (2020).
73. D’Alessandro, G., Whelan, D. R., Howard, S. M., Vitelli, V., Renaudin, X., Adamowicz, M., Iannelli, F., Jones-Weinert, C. W., Lee, M., Matti, V., Lee, W. T. C., Morten, M. J., Venkitaraman, A. R., Cejka, P., Rothenberg, E. & Fagagna, F. d’Adda di. BRCA2 controls DNA:RNA hybrid level at DSBs by mediating RNase H2 recruitment. *Nat Commun* **9**, 5376 (2018).
74. Darman, R. B., Seiler, M., Agrawal, A. A., Lim, K. H., Peng, S., Aird, D., Bailey, S. L., Bhavsar, E. B., Chan, B., Colla, S., Corson, L., Feala, J., Fekkes, P., Ichikawa, K., Keaney, G. F., Lee, L., Kumar, P., Kunii, K., MacKenzie, C., Matijevic, M., Mizui, Y., Myint, K., Park, E. S., Puyang, X., Selvaraj, A., Thomas, M. P., Tsai, J., Wang, J. Y., Warmuth, M., Yang, H., Zhu, P., Garcia-Manero, G., Furman, R. R., Yu, L., Smith, P. G. & Buonamici, S. Cancer-Associated SF3B1 Hotspot Mutations Induce Cryptic 3’ Splice Site Selection through Use of a Different Branch Point. *Cell Reports* **13**, 1033–1045 (2015).
75. Dasgupta, S., Masukata, H. & Tomizawa, J. Multiple mechanisms for initiation of ColE1 DNA replication: DNA synthesis in the presence and absence of ribonuclease H. *Cell* **51**, 1113–1122 (1987).

76. Daube, S. S. & Hippel, P. H. von. RNA displacement pathways during transcription from synthetic RNA-DNA bubble duplexes. *Biochemistry* **33**, 340–347 (1994).
77. Davé, A., Cooley, C., Garg, M. & Bianchi, A. Protein Phosphatase 1 Recruitment by Rif1 Regulates DNA Replication Origin Firing by Counteracting DDK Activity. *Cell Reports* **7**, 53–61 (2014).
78. Debatisse, M., Tallec, B. L., Letessier, A., Dutrillaux, B. & Brison, O. Common fragile sites: mechanisms of instability revisited. *Trends Genet* **28**, 22–32 (2012).
79. Debatisse, M., Tallec, B. L., Letessier, A., Dutrillaux, B. & Brison, O. Common fragile sites: mechanisms of instability revisited. *Trends Genet* **28**, 22–32 (2012).
80. DeLuca, S. Z. & Spradling, A. C. Efficient Expression of Genes in the Drosophila Germline Using a UAS-Promoter Free of Interference by Hsp70 piRNAs. *Genetics* **209**, 381–387 (2018).
81. Demakova, O. V., Pokholkova, G. V., Kolesnikova, T. D., Demakov, S. A., Andreyeva, E. N., Belyaeva, E. S. & Zhimulev, I. F. The SU(VAR)3-9/HP1 Complex Differentially Regulates the Compaction State and Degree of Underreplication of X Chromosome Pericentric Heterochromatin in *Drosophila melanogaster*. *Genetics* **175**, 609–620 (2007).
82. DePamphilis, M. L. Cell Cycle Dependent Regulation of the Origin Recognition Complex. *Cell Cycle* **4**, 70–79 (2004).
83. Dettori, L. G., Torrejon, D., Chakraborty, A., Dutta, A., Mohamed, M., Papp, C., Kuznetsov, V. A., Sung, P., Feng, W. & Bah, A. A Tale of Loops and Tails: The Role of Intrinsically Disordered Protein Regions in R-Loop Recognition and Phase Separation. *Frontiers Mol Biosci* **8**, 691694 (2021).
84. Doncheva, N. T., Morris, J. H., Gorodkin, J. & Jensen, L. J. Cytoscape StringApp: Network Analysis and Visualization of Proteomics Data. *J Proteome Res* **18**, 623–632 (2019).
85. Douglas, M. E., Ali, F. A., Costa, A. & Diffley, J. F. X. The mechanism of eukaryotic CMG helicase activation. *Nature* **555**, 265–268 (2018).
86. Dulev, S., Renty, C. de, Mehta, R., Minkov, I., Schwob, E. & Strunnikov, A. Essential global role of CDC14 in DNA synthesis revealed by chromosome underreplication unrecognized by checkpoints in *cdc14* mutants. *Proc National Acad Sci* **106**, 14466–14471 (2009).
87. Dumelie, J. G. & Jaffrey, S. R. Defining the location of promoter-associated R-loops at near-nucleotide resolution using bisDRIP-seq. *Elife* **6**, e28306 (2018).
88. Dungrawala, H. & Cortez, D. Purification of Proteins on Newly Synthesized DNA Using iPOND. in *The Nucleus* (ed. Hancock, R.) 123–131 (Springer New York, 2014).
89. Dungrawala, H., Rose, K. L., Bhat, K. P., Mohni, K. N., Glick, G. G., Couch, F. B. & Cortez, D. The Replication Checkpoint Prevents Two Types of Fork Collapse without Regulating Replisome Stability. *Molecular Cell* **59**, 998–1010 (2015).
90. Durkin, S. G. & Glover, T. W. Chromosome Fragile Sites. *Genetics* **41**, 169–192 (2007).
91. Duronio, R. J. & Marzluff, W. F. Coordinating cell cycle-regulated histone gene expression through assembly and function of the Histone Locus Body. *Rna Biol* **726–738** (2017).

92. Dutta, D., Shatalin, K., Epshtein, V., Gottesman, M. E. & Nudler, E. Linking RNA Polymerase Backtracking to Genome Instability in *E. coli*. *Cell* **146**, 533–543 (2011).
93. Dvinge, H., Kim, E., Abdel-Wahab, O. & Bradley, R. K. RNA splicing factors as oncoproteins and tumour suppressors. *Nat Rev Cancer* **16**, 413–430 (2016).
94. Eaton, M. L., Prinz, J. A., MacAlpine, H. K., Tretyakov, G., Kharchenko, P. V. & MacAlpine, D. M. Chromatin signatures of the *Drosophila* replication program. *Genome Res* **21**, 164–174 (2011).
95. Echeverri, C. J. & Perrimon, N. High-throughput RNAi screening in cultured cells: a user's guide. *Nat Rev Genet* **7**, 373–384 (2006).
96. Eckersley-Maslin, M. A., Alda-Catalinas, C. & Reik, W. Dynamics of the epigenetic landscape during the maternal-to-zygotic transition. *Nature Reviews Molecular Cell Biology* **19**, 1-15 (2018).
97. Edgar, B. A. & Orr-Weaver, T. L. Endoreplication Cell Cycles More for Less. *Cell* **105**, 297–306 (2001).
98. Fang, Y., Chen, L., Lin, K., Feng, Y., Zhang, P., Pan, X., Sanders, J., Wu, Y., Wang, X., Su, Z., Chen, C., Wei, H. & Zhang, W. Characterization of functional relationships of R-loops with gene transcription and epigenetic modifications in rice. *Genome Res* **29**, 1287–1297 (2019).
99. Farrell, J. A. & O'Farrell, P. H. From Egg to Gastrula: How the Cell Cycle Is Remodeled During the *Drosophila* Mid-Blastula Transition. *Annu Rev Genet* **48**, 1–26 (2014).
100. Fillion, G. J., Bommel, J. G. van, Braunschweig, U., Talhout, W., Kind, J., Ward, L. D., Brugman, W., Castro, I. J. de, Kerkhoven, R. M., Bussemaker, H. J. & van Steensel, B. Systematic Protein Location Mapping Reveals Five Principal Chromatin Types in *Drosophila* Cells. *Cell* **143**, 212–224 (2010).
101. Filippov, V., Filippova, M. & Gill, S. *Drosophila* RNase H1 is essential for development but not for proliferation. *Mol Genet Genomics* **265**, 771–777 (2001).
102. Foe, V. E. & Alberts, B. M. Studies of nuclear and cytoplasmic behaviour during the five mitotic cycles that precede gastrulation in *Drosophila* embryogenesis. *J Cell Sci* **61**, 31–70 (1983).
103. Fonslow, B. R., Niessen, S. M., Singh, M., Wong, C. C. L., Xu, T., Carvalho, P. C., Choi, J., Park, S. K. & Yates, J. R. Single-Step Inline Hydroxyapatite Enrichment Facilitates Identification and Quantitation of Phosphopeptides from Mass-Limited Proteomes with MudPIT. *J Proteome Res* **11**, 2697–2709 (2012).
104. Foti, R., Gnan, S., Cornacchia, D., Dileep, V., Bulut-Karslioglu, A., Diehl, S., Buness, A., Klein, F. A., Huber, W., Johnstone, E., Loos, R., Bertone, P., Gilbert, D. M., Manke, T., Jenuwein, T. & Buonomo, S. C. B. Nuclear Architecture Organized by Rif1 Underpins the Replication-Timing Program. *Molecular Cell* **61**, 260-273 (2016).
105. Fox, D. T., Soltis, D. E., Soltis, P. S., Ashman, T.-L. & Peer, Y. V. de. Polyploidy: A Biological Force from Cells to Ecosystems. *Trends Cell Biol* **30**, 688–694 (2020).
106. Francia, S., Michelini, F., Saxena, A., Tang, D., Hoon, M. de, Anelli, V., Mione, M., Carninci, P. & Fagagna, F. d'Adda di. Site-specific DICER and DROSHA RNA products control the DNA-damage response. *Nature* **488**, 231–235 (2012).
107. French, S. Consequences of replication fork movement through transcription units in vivo. *Science* **258**, 1362–1365 (2005).

108. Frigola, J., He, J., Kinkelin, K., Pye, V. E., Renault, L., Douglas, M. E., Remus, D., Cherepanov, P., Costa, A. & Diffley, J. F. X. Cdt1 stabilizes an open MCM ring for helicase loading. *Nat Commun* **8**, 15720 (2017).
109. Gambus, A., Jones, R. C., Sanchez-Diaz, A., Kanemaki, M., Deursen, F. van, Edmondson, R. D. & Labib, K. GINS maintains association of Cdc45 with MCM in replisome progression complexes at eukaryotic DNA replication forks. *Nat Cell Biol* **8**, 358–366 (2006).
110. Gan, W., Guan, Z., Liu, J., Gui, T., Shen, K., Manley, J. L. & Li, X. R-loop-mediated genomic instability is caused by impairment of replication fork progression. *Genes & Development* **25**, 2041-2056 (2011).
111. García-Rubio, M. L., Pérez-Calero, C., Barroso, S. I., Tumini, E., Herrera-Moyano, E., Rosado, I. V. & Aguilera, A. The Fanconi Anemia Pathway Protects Genome Integrity from R-loops. *Plos Genet* **11**, e1005674 (2015).
112. Gilbert, D. M. Replication timing and transcriptional control: beyond cause and effect. *Curr Opin Cell Biol* **14**, 377–383 (2002).
113. Ginno, P. A., Lott, P. L., Christensen, H. C., Korf, I. & Chédin, F. R-Loop Formation Is a Distinctive Characteristic of Unmethylated Human CpG Island Promoters. *Mol Cell* **45**, 814–825 (2012).
114. Glover, D. M. & Hogness, D. S. A novel arrangement of the 18S and 28S sequences in a repeating unit of drosophila melanogaster rDNA. *Cell* **10**, 167–176 (1977).
115. Gotter, A. L., Suppa, C. & Emanuel, B. S. Mammalian TIMELESS and Tipin are Evolutionarily Conserved Replication Fork-associated Factors. *J Mol Biol* **366**, 36–52 (2007).
116. Gratz, S. J., Cummings, A. M., Nguyen, J. N., Hamm, D. C., Donohue, L. K., Harrison, M. M., Wildonger, J. & O'Connor-Giles, K. M. Genome Engineering of Drosophila with the CRISPR RNA-Guided Cas9 Nuclease. *Genetics* **194**, 1029–1035 (2013).
117. Gratz, S. J., Rubinstein, C. D., Harrison, M. M., Wildonger, J. & O'Connor-Giles, K. M. CRISPR-Cas9 Genome Editing in Drosophila. *Curr Protoc Mol Biology* **111**, 31.2.1-31.2.20 (2015).
118. Griffin-Shea, R., Thireos, G. & Kafatos, F. C. Organization of a cluster of four chorion genes in Drosophila and its relationship to developmental expression and amplification. *Dev Biol* **91**, 325–336 (1982).
119. Groh, M., Albulescu, L. O., Cristini, A. & Gromak, N. Senataxin: Genome Guardian at the Interface of Transcription and Neurodegeneration. *J Mol Biol* **429**, 3181–3195 (2017).
120. Groh, M., Lufino, M. M. P., Wade-Martins, R. & Gromak, N. R-loops Associated with Triplet Repeat Expansions Promote Gene Silencing in Friedreich Ataxia and Fragile X Syndrome. *Plos Genet* **10**, e1004318 (2014).
121. Grunseich, C., Wang, I. X., Watts, J. A., Burdick, J. T., Guber, R. D., Zhu, Z., Bruzel, A., Lanman, T., Chen, K., Schindler, A. B., Edwards, N., Ray-Chaudhury, A., Yao, J., Lehky, T., Piszczek, G., Crain, B., Fischbeck, K. H. & Cheung, V. G. Senataxin Mutation Reveals How R-Loops Promote Transcription by Blocking DNA Methylation at Gene Promoters. *Mol Cell* **69**, 426-437 (2018).

122. Gupta, S., Friedman, L. J., Gelles, J. & Bell, S. P. A helicase-tethered ORC flip enables bidirectional helicase loading. *Elife* **10**, e74282 (2021).
123. Guttman, M., Donaghey, J., Carey, B. W., Garber, M., Grenier, J. K., Munson, G., Young, G., Lucas, A. B., Ach, R., Bruhn, L., Yang, X., Amit, I., Meissner, A., Regev, A., Rinn, J. L., Root, D. E. & Lander, E. S. lincRNAs act in the circuitry controlling pluripotency and differentiation. *Nature* **477**, 295–300 (2011).
124. Hage, A. E., French, S. L., Beyer, A. L. & Tollervey, D. Loss of Topoisomerase I leads to R-loop-mediated transcriptional blocks during ribosomal RNA synthesis. *Genes & Development* **24**, 1546-1558 (2010).
125. Hamm, D. C. & Harrison, M. M. Regulatory principles governing the maternal-to-zygotic transition: insights from *Drosophila melanogaster*. *Royal Soc Open Biology* **8**, 180-183 (2018).
126. Hamperl, S., Bocek, M. J., Saldivar, J. C., Swigut, T. & Cimprich, K. A. Transcription-Replication Conflict Orientation Modulates R-Loop Levels and Activates Distinct DNA Damage Responses. *Cell* **170**, 774-786 (2017).
127. Hannibal, R. L. & Baker, J. C. Selective Amplification of the Genome Surrounding Key Placental Genes in Trophoblast Giant Cells. *Curr Biol* **26**, 230–236 (2016).
128. Hannibal, R. L., Chuong, E. B., Rivera-Mulia, J. C., Gilbert, D. M., Valouev, A. & Baker, J. C. Copy Number Variation Is a Fundamental Aspect of the Placental Genome. *Plos Genet* **10**, e1004290 (2014).
129. Hardy, C. F., Sussel, L. & Shore, D. A RAP1-interacting protein involved in transcriptional silencing and telomere length regulation. *Gene Dev* **6**, 801–814 (1992).
130. Harrison, M. M., Li, X.-Y., Kaplan, T., Botchan, M. R. & Eisen, M. B. Zelda Binding in the Early *Drosophila melanogaster* Embryo Marks Regions Subsequently Activated at the Maternal-to-Zygotic Transition. *PLoS Genetics* **7**, e1002266 (2011).
131. Hartono, S. R., Malapert, A., Legros, P., Bernard, P., Chédin, F. & Vanoosthuysse, V. The Affinity of the S9.6 Antibody for Double-Stranded RNAs Impacts the Accurate Mapping of R-Loops in Fission Yeast. *J Mol Biol* **430**, 272–284 (2018).
132. Hassel, C., Zhang, B., Dixon, M. & Calvi, B. R. Induction of endocycles represses apoptosis independently of differentiation and predisposes cells to genome instability. *Development* **141**, 112–123 (2013).
133. Hayano, M., Kanoh, Y., Matsumoto, S., Renard-Guillet, C., Shirahige, K. & Masai, H. Rif1 is a global regulator of timing of replication origin firing in fission yeast. *Gene Dev* **26**, 137–150 (2012).
134. Heinz, S., Benner, C., Spann, N., Bertolino, E., Lin, Y. C., Laslo, P., Cheng, J. X., Murre, C., Singh, H. & Glass, C. K. Simple Combinations of Lineage-Determining Transcription Factors Prime cis-Regulatory Elements Required for Macrophage and B Cell Identities. *Mol Cell* **38**, 576–589 (2010).
135. Heller, R. C., Kang, S., Lam, W. M., Chen, S., Chan, C. S. & Bell, S. P. Eukaryotic Origin-Dependent DNA Replication In Vitro Reveals Sequential Action of DDK and S-CDK Kinases. *Cell* **146**, 80–91 (2011).
136. Helmrich, A., Ballarino, M. & Tora, L. Collisions between Replication and Transcription Complexes Cause Common Fragile Site Instability at the Longest Human Genes. *Mol Cell* **44**, 966–977 (2011).

137. Herrera-Moyano, E., Mergui, X., García-Rubio, M. L., Barroso, S. & Aguilera, A. The yeast and human FACT chromatin-reorganizing complexes solve R-loop-mediated transcription–replication conflicts. *Genes & Development* **28**, 735–748 (2014).
138. Hiraga, S., Alvino, G. M., Chang, F., Lian, H., Sridhar, A., Kubota, T., Brewer, B. J., Weinreich, M., Raghuraman, M. K. & Donaldson, A. D. Rif1 controls DNA replication by directing Protein Phosphatase 1 to reverse Cdc7-mediated phosphorylation of the MCM complex. *Gene Dev* **28**, 372–383 (2014).
139. Hiraga, S., Ly, T., Garzón, J., Hořejší, Z., Ohkubo, Y., Endo, A., Obuse, C., Boulton, S. J., Lamond, A. I. & Donaldson, A. D. Human RIF1 and protein phosphatase 1 stimulate DNA replication origin licensing but suppress origin activation. *Embo Rep* **18**, 403–419 (2017).
140. Hogan, B., Constantini, F. and Lacy, E. (1994) Manipulating the mouse embryo, 2nd edn. New York: Cold Spring Harbor Laboratory Press.
141. Hua, B. L. & Orr-Weaver, T. L. DNA Replication Control During Drosophila Development: Insights into the Onset of S Phase, Replication Initiation, and Fork Progression. *Genetics* **207**, 29–47 (2017).
142. Hua, B. L., Bell, G. W., Kashevsky, H., Stetina, J. R. V. & Orr-Weaver, T. L. Dynamic changes in ORC localization and replication fork progression during tissue differentiation. *Bmc Genomics* **19**, 623 (2018).
143. Huang, W., Loganantharaj, R., Schroeder, B., Fargo, D. & Li, L. PAVIS: a tool for Peak Annotation and Visualization. *Bioinformatics* **29**, 3097–3099 (2013).
144. Huertas, P. & Aguilera, A. Cotranscriptionally Formed DNA:RNA Hybrids Mediate Transcription Elongation Impairment and Transcription-Associated Recombination. *Mol Cell* **12**, 711–721 (2003).
145. Huppert, J. L. Thermodynamic prediction of RNA–DNA duplex-forming regions in the human genome. *Mol Biosyst* **4**, 686–691 (2008).
146. Hutchins, J. R. A., Aze, A., Coulombe, P. & Méchali, M. DNA Replication, Recombination, and Repair, Molecular Mechanisms and Pathology. *Dna Replication Recomb Repair* 23–52 (2016).
147. Itoh, T. & Tomizawa, J. Formation of an RNA primer for initiation of replication of ColE1 DNA by ribonuclease H. *Proc National Acad Sci* **77**, 2450–2454 (1980).
148. Jackson, A. P., Laskey, R. A. & Coleman, N. Replication Proteins and Human Disease. *Cold Spring Harbor Perspectives in Biology* **6**, a013060 (2014).
149. Jackson, S. & Xiong, Y. CRL4s: the CUL4-RING E3 ubiquitin ligases. *Trends Biochem Sci* **34**, 562–570 (2009).
150. Jin, J., Arias, E. E., Chen, J., Harper, J. W. & Walter, J. C. A Family of Diverse Cul4-Ddb1-Interacting Proteins Includes Cdt2, which Is Required for S Phase Destruction of the Replication Factor Cdt1. *Molecular Cell* **23**, 709–721 (2006).
151. Jukam, D., Shariati, S. A. M. & Skotheim, J. M. Zygotic Genome Activation in Vertebrates. *Dev Cell* **42**, 316–332 (2017).
152. Kabeche, L., Nguyen, H. D., Buisson, R. & Zou, L. A mitosis-specific and R loop–driven ATR pathway promotes faithful chromosome segregation. *Science* **359**, eaan6490 (2018).
153. Kappes, F., Waldmann, T., Mathew, V., Yu, J., Zhang, L., Khodadoust, M. S., Chinnaiyan, A. M., Luger, K., Erhardt, S., Schneider, R. & Markovitz, D. M. The DEK

- oncoprotein is a Su(var) that is essential to heterochromatin integrity. *Gene Dev* **25**, 673–678 (2011).
154. Keenen, M. M., Brown, D., Brennan, L. D., Renger, R., Khoo, H., Carlson, C. R., Huang, B., Grill, S. W., Narlikar, G. J. & Redding, S. HP1 proteins compact DNA into mechanically and positionally stable phase separated domains. *Elife* **10**, e64563 (2021).
155. Keskin, H., Shen, Y., Huang, F., Patel, M., Yang, T., Ashley, K., Mazin, A. V. & Storici, F. Transcript-RNA-templated DNA recombination and repair. *Nature* **515**, 436–439 (2014).
156. Kim, N. & Jinks-Robertson, S. Transcription as a source of genome instability. *Nat Rev Genet* **13**, 204–214 (2012).
157. Klymenko, T., Papp, B., Fischle, W., Köcher, T., Schelder, M., Fritsch, C., Wild, B., Wilm, M. & Müller, J. A Polycomb group protein complex with sequence-specific DNA-binding and selective methyl-lysine-binding activities. *Gene Dev* **20**, 1110–1122 (2006).
158. Kolesnikova, T. D., Makunin, I. V., Volkova, E. I., Pirrotta, V., Belyaeva, E. S. & Zhimulev, I. F. Functional dissection of the Suppressor of UnderReplication protein of *Drosophila melanogaster*: identification of domains influencing chromosome binding and DNA replication. *Genetica* **124**, 187–200 (2005).
159. Kolesnikova, T. D., Posukh, O. V., Andreyeva, E. N., Bebyakina, D. S., Ivankin, A. V. & Zhimulev, I. F. *Drosophila* SUUR protein associates with PCNA and binds chromatin in a cell cycle-dependent manner. *Chromosoma* **122**, 55–66 (2013).
160. Kolesnikova, T. D., Posukh, O. V., Andreyeva, E. N., Bebyakina, D. S., Ivankin, A. V. & Zhimulev, I. F. *Drosophila* SUUR protein associates with PCNA and binds chromatin in a cell cycle-dependent manner. *Chromosoma* **122**, 55–66 (2013).
161. König, F., Schubert, T. & Längst, G. The monoclonal S9.6 antibody exhibits highly variable binding affinities towards different R-loop sequences. *Plos One* **12**, e0178875 (2017).
162. Koreski, K. P., Rieder, L. E., McLain, L. M., Chaubal, A., Marzluff, W. F. & Duronio, R. J. *Drosophila* histone locus body assembly and function involves multiple interactions. *Mol Biol Cell* **31**, 1525–1537 (2020).
163. Krajewski, W. A., Nakamura, T., Mazo, A. & Canaani, E. A Motif within SET-Domain Proteins Binds Single-Stranded Nucleic Acids and Transcribed and Supercoiled DNAs and Can Interfere with Assembly of Nucleosomes. *Mol Cell Biol* **25**, 1891–1899 (2005).
164. Lang, K. S. & Merrikh, H. Topological stress is responsible for the detrimental outcomes of head-on replication-transcription conflicts. *Cell Reports* **34**, 108797 (2021).
165. Lang, K. S., Hall, A. N., Merrikh, C. N., Ragheb, M., Tabakh, H., Pollock, A. J., Woodward, J. J., Dreifus, J. E. & Merrikh, H. Replication-Transcription Conflicts Generate R-Loops that Orchestrate Bacterial Stress Survival and Pathogenesis. *Cell* **170**, 787–799 (2017).
166. Langmead, B. & Salzberg, S. L. Fast gapped-read alignment with Bowtie 2. *Nat Methods* **9**, 357–359 (2012).

167. Lee, C.-Y., McNerney, C., Ma, K., Zhao, W., Wang, A. & Myong, S. R-loop induced G-quadruplex in non-template promotes transcription by successive R-loop formation. *Nat Commun* **11**, 3392 (2020).
168. Lee, D. Y. & Clayton, D. A. Initiation of Mitochondrial DNA Replication by Transcription and R-loop Processing. *J Biol Chem* **273**, 30614–30621 (1998).
169. Lee, E.-M., Trinh, T. T. B., Shim, H. J., Park, S.-Y., Nguyen, T. T. T., Kim, M.-J. & Song, Y.-H. Drosophila Claspin is required for the G2 arrest that is induced by DNA replication stress but not by DNA double-strand breaks. *Dna Repair* **11**, 741–752 (2012).
170. Lee, J.-H. & Paull, T. T. Cellular functions of the protein kinase ATM and their relevance to human disease. *Nat Rev Mol Cell Bio* **22**, 796–814 (2021).
171. Lesch, B. J. & Page, D. C. Poised chromatin in the mammalian germ line. *Development* **141**, 3619–3626 (2014).
172. Letessier, A., Millot, G. A., Koundrioukoff, S., Lachagès, A.-M., Vogt, N., Hansen, R. S., Malfoy, B., Brison, O. & Debatisse, M. Cell-type-specific replication initiation programs set fragility of the FRA3B fragile site. *Nature* **470**, 120–123 (2011).
173. Li, H. & Durbin, R. Fast and accurate short read alignment with Burrows–Wheeler transform. *Bioinformatics* **25**, 1754–1760 (2009).
174. Li, H., Handsaker, B., Wysoker, A., Fennell, T., Ruan, J., Homer, N., Marth, G., Abecasis, G., Durbin, R. & Subgroup, 1000 Genome Project Data Processing. The Sequence Alignment/Map format and SAMtools. *Bioinformatics* **25**, 2078–2079 (2009).
175. Li, X. & Manley, J. L. Inactivation of the SR Protein Splicing Factor ASF/SF2 Results in Genomic Instability. *Cell* **122**, 365–378 (2005).
176. Lilly, M. A. & Duronio, R. J. New insights into cell cycle control from the Drosophila endocycle. *Oncogene* **24**, 2765–2775 (2005).
177. Limbourg, B. & Zalokar, M. Permeabilization of Drosophila eggs. *Dev Biol* **35**, 382–387 (1973).
178. Liu, L. F. & Wang, J. C. Supercoiling of the DNA template during transcription. *Proc National Acad Sci* **84**, 7024–7027 (1987).
179. Liu, Y., Liu, Q., Su, H., Liu, K., Xiao, X., Li, W., Sun, Q., Birchler, J. A. & Han, F. Genome-wide mapping reveals R-loops associated with centromeric repeats in maize. *Genome Res* **31**, 1409–1418 (2021).
180. Liu, Y., Su, H., Zhang, J., Liu, Y., Feng, C. & Han, F. Back-spliced RNA from retrotransposon binds to centromere and regulates centromeric chromatin loops in maize. *Plos Biol* **18**, e3000582 (2020).
181. Loppin, B. & Berger, F. Histone Variants: The Nexus of Developmental Decisions and Epigenetic Memory. *Annu Rev Genet* **54**, 1–29 (2020).
182. Losick, V. P., Fox, D. T. & Spradling, A. C. Polyploidization and Cell Fusion Contribute to Wound Healing in the Adult Drosophila Epithelium. *Current Biology* **23**, 2224–2232 (2013).
183. Luo, H., Zhu, G., Eshelman, M. A., Fung, T. K., Lai, Q., Wang, F., Zeisig, B. B., Lesperance, J., Ma, X., Chen, S., Cesari, N., Cogle, C., Chen, B., Xu, B., Yang, F.-C., So, C. W. E., Qiu, Y., Xu, M. & Huang, S. HOTTIP-dependent R-loop formation regulates CTCF boundary activity and TAD integrity in leukemia. *Mol Cell* **82**, 833–851 (2022).

184. Mac Auley, A., Werb, Z. & Mirkes, P. E. Characterization of the unusually rapid cell cycles during rat gastrulation. *Dev Camb Engl* **117**, 873–83 (1993).
185. MacAlpine, H. K., Gordân, R., Powell, S. K., Hartemink, A. J. & MacAlpine, D. M. Drosophila ORC localizes to open chromatin and marks sites of cohesin complex loading. *Genome Res* **20**, 201–211 (2010).
186. Madigan, J. P., Chotkowski, H. L. & Glaser, R. L. DNA double-strand break-induced phosphorylation of Drosophila histone variant H2Av helps prevent radiation-induced apoptosis. *Nucleic Acids Res* **30**, 3698–3705 (2002).
187. Magis, A. D., Manzo, S. G., Russo, M., Marinello, J., Morigi, R., Sordet, O. & Capranico, G. DNA damage and genome instability by G-quadruplex ligands are mediated by R loops in human cancer cells. *Proc National Acad Sci* **116**, 816–825 (2019).
188. Mah, L.-J., El-Osta, A. & Karagiannis, T. C. γ H2AX: a sensitive molecular marker of DNA damage and repair. *Leukemia* **24**, 679–686 (2010).
189. Makunin, I. V., Volkova, E. I., Belyaeva, E. S., Nabirochkina, E. N., Pirrotta, V. & Zhimulev, I. F. The Drosophila Suppressor of Underreplication Protein Binds to Late-Replicating Regions of Polytene Chromosomes. *Genetics* **160**, 1023–1034 (2002).
190. Mansfield, E., Hersperger, E., Biggs, J. & Shearn, A. Genetic and Molecular Analysis of hyperplastic discs, a Gene Whose Product Is Required for Regulation of Cell Proliferation in Drosophila melanogaster Imaginal Discs and Germ Cells. *Dev Biol* **165**, 507–526 (1994).
191. Manzo, S. G., Hartono, S. R., Sanz, L. A., Marinello, J., Biasi, S. D., Cossarizza, A., Capranico, G. & Chedin, F. DNA Topoisomerase I differentially modulates R-loops across the human genome. *Genome Biology* **19**, 1-18 (2018).
192. Marco, M.-F., Michele, G., Marco, F. & Paolo, P. The DNA Polymerase alpha-Primase Complex: Multiple Functions and Interactions. *Sci World J* **3**, 21–33 (2003).
193. Masukata, H. & Tomizawa, J. A mechanism of formation of a persistent hybrid between elongating RNA and template DNA. *Cell* **62**, 331–338 (1990).
194. Masukata, H., Dasgupta, S. & Tomizawa, J. Transcriptional activation of ColE1 DNA synthesis by displacement of the nontranscribed strand. *Cell* **51**, 1123–1130 (1987).
195. Matson, J. P., Dumitru, R., Coryell, P., Baxley, R. M., Chen, W., Twaroski, K., Webber, B. R., Tolar, J., Bielinsky, A.-K., Purvis, J. E. & Cook, J. G. Rapid DNA replication origin licensing protects stem cell pluripotency. *Elife* **6**, e30473 (2017).
196. Mattarocci, S., Shyian, M., Lemmens, L., Damay, P., Altintas, D. M., Shi, T., Bartholomew, C. R., Thomä, N. H., Hardy, C. F. J. & Shore, D. Rif1 Controls DNA Replication Timing in Yeast through the PP1 Phosphatase Glc7. *Cell Reports* **7**, 62–69 (2014).
197. McAlister, G. C., Huttlin, E. L., Haas, W., Ting, L., Jedrychowski, M. P., Rogers, J. C., Kuhn, K., Pike, I., Grothe, R. A., Blethrow, J. D. & Gygi, S. P. Increasing the Multiplexing Capacity of TMTs Using Reporter Ion Isotopologues with Isobaric Masses. *Anal Chem* **84**, 7469–7478 (2012).
198. McLean, M. J., Wolfe, K. H. & Devine, K. M. Base Composition Skews, Replication Orientation, and Gene Orientation in 12 Prokaryote Genomes. *J Mol Evol* **47**, 691–696 (1998).

199. Mehrotra, S., Maqbool, S. B., Kolpakas, A., Murnen, K. & Calvi, B. R. Endocycling cells do not apoptose in response to DNA rereplication genotoxic stress. *Gene Dev* **22**, 3158–3171 (2008).
200. Mendez-Bermudez, A., Lototska, L., Bauwens, S., Giraud-Panis, M.-J., Croce, O., Jamet, K., Irizar, A., Mowinckel, M., Koundrioukoff, S., Nottet, N., Almouzni, G., Teulade-Fichou, M.-P., Schertzer, M., Perderiset, M., Londoño-Vallejo, A., Debatisse, M., Gilson, E. & Ye, J. Genome-wide Control of Heterochromatin Replication by the Telomere Capping Protein TRF2. *Molecular Cell* **70**, 449–461 (2018).
201. Merrih, C. N. & Merrih, H. Gene inversion potentiates bacterial evolvability and virulence. *Nat Commun* **9**, 4662 (2018).
202. Merrih, H. Spatial and Temporal Control of Evolution through Replication–Transcription Conflicts. *Trends Microbiol* **25**, 515–521 (2017).
203. Meselson, M. & Stahl, F. W. The replication of DNA in Escherichia coli. *Proc National Acad Sci* **44**, 671–682 (1958).
204. Mesner, L. D., Valsakumar, V., Karnani, N., Dutta, A., Hamlin, J. L. & Bekiranov, S. Bubble-chip analysis of human origin distributions demonstrates on a genomic scale significant clustering into zones and significant association with transcription. *Genome Res* **21**, 377–389 (2011).
205. Mi, H., Muruganujan, A., Ebert, D., Huang, X. & Thomas, P. D. PANTHER version 14: more genomes, a new PANTHER GO-slim and improvements in enrichment analysis tools. *Nucleic Acids Res* **47**, D419–D426 (2019).
206. Miller, T. C., Locke, J., Greiwe, J. F., Diffley, J. F. & Costa, A. Mechanism of head-to-head MCM double-hexamer formation revealed by cryo-EM. *Nature* **575**, 704–710 (2019).
207. Mimura, S., Seki, T., Tanaka, S. & Diffley, J. F. X. Phosphorylation-dependent binding of mitotic cyclins to Cdc6 contributes to DNA replication control. *Nature* **431**, 1118–1123 (2004).
208. Miotto, B., Ji, Z. & Struhl, K. Selectivity of ORC binding sites and the relation to replication timing, fragile sites, and deletions in cancers. *Proc National Acad Sci* **113**, E4810–E4819 (2016).
209. Mitchell, B. P., Hsu, R. V., Medrano, M. A., Zewde, N. T., Narkhede, Y. B. & Palermo, G. Spontaneous Embedding of DNA Mismatches Within the RNA:DNA Hybrid of CRISPR-Cas9. *Frontiers Mol Biosci* **7**, 39 (2020).
210. Moore, D. P. & Orr-Weaver, T. L. 8 Chromosome Segregation during Meiosis: Building an Unambivalent Bivalent. *Curr Top Dev Biol* **37**, 263–299 (1997).
211. Morgan, M. A. J., Rickels, R. A., Collings, C. K., He, X., Cao, K., Herz, H.-M., Cozzolino, K. A., Abshiru, N. A., Marshall, S. A., Rendleman, E. J., Sze, C. C., Piunti, A., Kelleher, N. L., Savas, J. N. & Shilatifard, A. A cryptic Tudor domain links BRWD2/PHIP to COMPASS-mediated histone H3K4 methylation. *Gene Dev* **31**, 2003–2014 (2017).
212. Morgan, T. H. Sex Limited Inheritance in Drosophila. *Science* **32**, 120–122 (1910).
213. Mosler, T., Conte, F., Longo, G. M. C., Mikicic, I., Kreim, N., Möckel, M. M., Petrosino, G., Flach, J., Barau, J., Luke, B., Roukos, V. & Beli, P. R-loop proximity proteomics identifies a role of DDX41 in transcription-associated genomic instability. *Nat Commun* **12**, 7314 (2021).

214. Munden, A., Rong, Z., Sun, A., Gangula, R., Mallal, S. & Nordman, J. T. Rif1 inhibits replication fork progression and controls DNA copy number in *Drosophila*. *Elife* **7**, e39140 (2018).
215. Nadel, J., Athanasiadou, R., Lemetre, C., Wijetunga, N. A., Broin, P. Ó., Sato, H., Zhang, Z., Jeddeloh, J., Montagna, C., Golden, A., Seoighe, C. & Grealley, J. M. RNA:DNA hybrids in the human genome have distinctive nucleotide characteristics, chromatin composition, and transcriptional relationships. *Epigenet Chromatin* **8**, 46 (2015).
216. Nakatani, T., Lin, J., Ji, F., Ettinger, A., Pontabry, J., Tokoro, M., Altamirano-Pacheco, L., Fiorentino, J., Mahammadov, E., Hatano, Y., Rechem, C. V., Chakraborty, D., Ruiz-Morales, E. R., Pascualli, P. Y. A., Scialdone, A., Yamagata, K., Whetstine, J. R., Sadreyev, R. I. & Torres-Padilla, M.-E. DNA replication fork speed underlies cell fate changes and promotes reprogramming. *Nat Genet* **54**, 318–327 (2022).
217. Nambu, Y., Sugai, M., Gonda, H., Lee, C.-G., Katakai, T., Agata, Y., Yokota, Y. & Shimizu, A. Transcription-Coupled Events Associating with Immunoglobulin Switch Region Chromatin. *Science* **302**, 2137–2140 (2003).
218. Nandakumar, S., Grushko, O. & Buttitta, L. A. Polyploidy in the adult *Drosophila* brain. *Elife* **9**, e54385 (2020).
219. Newman, T. J., Mamun, M. A., Nieduszynski, C. A. & Blow, J. J. Replisome stall events have shaped the distribution of replication origins in the genomes of yeasts. *Nucleic Acids Res* **41**, 9705–9718 (2013).
220. Nguyen, H. D., Yadav, T., Giri, S., Saez, B., Graubert, T. A. & Zou, L. Functions of Replication Protein A as a Sensor of R Loops and a Regulator of RNaseH1. *Mol Cell* **65**, 832-847 (2017).
221. Nordman, J. & Orr-Weaver, T. L. Regulation of DNA replication during development. *Development* **139**, 455-464 (2012).
222. Nordman, J. T. & Orr-Weaver, T. L. Understanding replication fork progression, stability, and chromosome fragility by exploiting the Suppressor of Underreplication protein. *BioEssays* **37**, 856-861 (2015).
223. Nordman, J. T., Kozhevnikova, E. N., Verrijzer, C. P., Pindyurin, A. V., Andreyeva, E. N., Shloma, V. V., Zhimulev, I. F. & Orr-Weaver, T. L. DNA Copy-Number Control through Inhibition of Replication Fork Progression. *Cell Reports* **9**, 841-849 (2014).
224. Nordman, J., Li, S., Eng, T., MacAlpine, D. & Orr-Weaver, T. L. Developmental control of the DNA replication and transcription programs. *Genome Res* **21**, 175–181 (2011).
225. Norio, P., Kosiyatrakul, S., Yang, Q., Guan, Z., Brown, N. M., Thomas, S., Riblet, R. & Schildkraut, C. L. Progressive Activation of DNA Replication Initiation in Large Domains of the Immunoglobulin Heavy Chain Locus during B Cell Development. *Mol Cell* **20**, 575–587 (2005).
226. Nowotny, M., Cerritelli, S. M., Ghirlando, R., Gaidamakov, S. A., Crouch, R. J. & Yang, W. Specific recognition of RNA/DNA hybrid and enhancement of human RNase H1 activity by HBD. *Embo J* **27**, 1172–1181 (2008).

227. Nudler, E., Mustaev, A., Goldfarb, A. & Lukhtanov, E. The RNA–DNA Hybrid Maintains the Register of Transcription by Preventing Backtracking of RNA Polymerase. *Cell* **89**, 33–41 (1997).
228. Ohle, C., Tesorero, R., Schermann, G., Dobrev, N., Sinning, I. & Fischer, T. Transient RNA-DNA Hybrids Are Required for Efficient Double-Strand Break Repair. *Cell* **167**, 1001-1010 (2016).
229. Orr-Weaver, T. & Spradling, A. Chromosome Structure and Function, Impact of New Concepts. *Stadler Gen* 243–261 (1988).
230. Orr-Weaver, T. L. When bigger is better: the role of polyploidy in organogenesis. *Trends Genet* **31**, 307–315 (2015).
231. Ouyang, J., Yadav, T., Zhang, J.-M., Yang, H., Rheinbay, E., Guo, H., Haber, D. A., Lan, L. & Zou, L. RNA transcripts stimulate homologous recombination by forming DR-loops. *Nature* **594**, 283-288 (2021).
232. Ouyang, J., Yadav, T., Zhang, J.-M., Yang, H., Rheinbay, E., Guo, H., Haber, D. A., Lan, L. & Zou, L. RNA transcripts stimulate homologous recombination by forming DR-loops. *Nature* 1–6 (2021).
233. Peace, J. M., Ter-Zakarian, A. & Aparicio, O. M. Rif1 Regulates Initiation Timing of Late Replication Origins throughout the *S. cerevisiae* Genome. *Plos One* **9**, e98501 (2014).
234. Peer, Y. V. de, Ashman, T.-L., Soltis, P. S. & Soltis, D. E. Polyploidy: an evolutionary and ecological force in stressful times. *Plant Cell* **33**, koaa015 (2020).
235. Phillips, D. D., Garboczi, D. N., Singh, K., Hu, Z., Leppla, S. H. & Leysath, C. E. The sub-nanomolar binding of DNA–RNA hybrids by the single-chain Fv fragment of antibody S9.6. *J Mol Recognit* **26**, 376–381 (2013).
236. Pindyurin, A. V., Boldyreva, L. V., Shloma, V. V., Kolesnikova, T. D., Pokholkova, G. V., Andreyeva, E. N., Kozhevnikova, E. N., Ivanoschuk, I. G., Zarutskaya, E. A., Demakov, S. A., Gorchakov, A. A., Belyaeva, E. S. & Zhimulev, I. F. Interaction between the *Drosophila* heterochromatin proteins SUUR and HP1. *J Cell Sci* **121**, 1693–1703 (2008).
237. Pindyurin, A. V., Boldyreva, L. V., Shloma, V. V., Kolesnikova, T. D., Pokholkova, G. V., Andreyeva, E. N., Kozhevnikova, E. N., Ivanoschuk, I. G., Zarutskaya, E. A., Demakov, S. A., Gorchakov, A. A., Belyaeva, E. S. & Zhimulev, I. F. Interaction between the *Drosophila* heterochromatin proteins SUUR and HP1. *J Cell Sci* **121**, 1693–1703 (2008).
238. Pindyurin, A. V., Moorman, C., Wit, E. de, Belyakin, S. N., Belyaeva, E. S., Christophides, G. K., Kafatos, F. C., Steensel, B. van & Zhimulev, I. F. SUUR joins separate subsets of PcG, HP1 and B-type lamin targets in *Drosophila*. *J Cell Sci* **120**, 2344–2351 (2007).
239. Pinter, S., Knodel, F., Choudalakis, M., Schnee, P., Kroll, C., Fuchs, M., Broehm, A., Weirich, S., Roth, M., Eisler, S. A., Zuber, J., Jeltsch, A. & Rathert, P. A functional LSD1 coregulator screen reveals a novel transcriptional regulatory cascade connecting R-loop homeostasis with epigenetic regulation. *Nucleic Acids Res* **49**, 4350-4370 (2021).
240. Pozo, P. N. & Cook, J. G. Regulation and Function of Cdt1; A Key Factor in Cell Proliferation and Genome Stability. *Genes-basel* **8**, 2 (2016).

241. Prado, F. & Aguilera, A. Impairment of replication fork progression mediates RNA polII transcription-associated recombination. *Embo J* **24**, 1267–1276 (2005).
242. Promonet, A., Padioleau, I., Liu, Y., Sanz, L., Biernacka, A., Schmitz, A.-L., Skrzypczak, M., Sarrazin, A., Mettling, C., Rowicka, M., Ginalski, K., Chedin, F., Chen, C.-L., Lin, Y.-L. & Pasero, P. Topoisomerase 1 prevents replication stress at R-loop-enriched transcription termination sites. *Nat Commun* **11**, 3940 (2020).
243. Protter, D. S. W., Rao, B. S., Treeck, B. V., Lin, Y., Mizoue, L., Rosen, M. K. & Parker, R. Intrinsically Disordered Regions Can Contribute Promiscuous Interactions to RNP Granule Assembly. *Cell Reports* **22**, 1401–1412 (2018).
244. Proudfoot, N. J. Transcriptional termination in mammals: Stopping the RNA polymerase II juggernaut. *Science* **352**, aad9926 (2016).
245. Quinlan, A. R. & Hall, I. M. BEDTools: a flexible suite of utilities for comparing genomic features. *Bioinformatics* **26**, 841–842 (2010).
246. Racca, C., Britton, S., Hédouin, S., Francastel, C., Calsou, P. & Larminat, F. BRCA1 prevents R-loop-associated centromeric instability. *Cell Death Dis* **12**, 896 (2021).
247. Ramírez, F., Dündar, F., Diehl, S., Grüning, B. A. & Manke, T. deepTools: a flexible platform for exploring deep-sequencing data. *Nucleic Acids Res* **42**, W187–W191 (2014).
248. Ramírez, F., Ryan, D. P., Grüning, B., Bhardwaj, V., Kilpert, F., Richter, A. S., Heyne, S., Dündar, F. & Manke, T. deepTools2: a next generation web server for deep-sequencing data analysis. *Nucleic Acids Res* **44**, W160–W165 (2016).
249. Ramirez, P., Crouch, R. J., Cheung, V. G. & Grunseich, C. R-Loop Analysis by Dot-Blot. *J Vis Exp* **167**, e62069 (2021).
250. Ranawakage, D. C., Takada, T. & Kamachi, Y. HiBiT-qIP, HiBiT-based quantitative immunoprecipitation, facilitates the determination of antibody affinity under immunoprecipitation conditions. *Sci Rep* **9**, 6895 (2019).
251. Randell, J. C. W., Fan, A., Chan, C., Francis, L. I., Heller, R. C., Galani, K. & Bell, S. P. Mec1 Is One of Multiple Kinases that Prime the Mcm2-7 Helicase for Phosphorylation by Cdc7. *Mol Cell* **40**, 353–363 (2010).
252. Remus, D., Beall, E. L. & Botchan, M. R. DNA topology, not DNA sequence, is a critical determinant for Drosophila ORC–DNA binding. *Embo J* **23**, 897–907 (2004).
253. Remus, D., Beuron, F., Tolun, G., Griffith, J. D., Morris, E. P. & Diffley, J. F. X. Concerted Loading of Mcm2–7 Double Hexamers around DNA during DNA Replication Origin Licensing. *Cell* **139**, 719–730 (2009).
254. Reyes, A., Kazak, L., Wood, S. R., Yasukawa, T., Jacobs, H. T. & Holt, I. J. Mitochondrial DNA replication proceeds via a ‘bootlace’ mechanism involving the incorporation of processed transcripts. *Nucleic Acids Res* **41**, 5837–5850 (2013).
255. Rhind, N. & Gilbert, D. M. DNA Replication Timing. *Cold Spring Harbor Perspectives in Biology* **5**, a010132 (2013).
256. Rocha, E. P. Evolutionary patterns in prokaryotic genomes. *Curr Opin Microbiol* **11**, 454–460 (2008).
257. Rogers, S. L. & Rogers, G. C. Culture of Drosophila S2 cells and their use for RNAi-mediated loss-of-function studies and immunofluorescence microscopy. *Nat Protoc* **3**, 606–611 (2008).

258. Rørth, P. Gal4 in the Drosophila female germline. *Mech Develop* **78**, 113–118 (1998).
259. Ross, J. P., Suetake, I., Tajima, S. & Molloy, P. L. Recombinant mammalian DNA methyltransferase activity on model transcriptional gene silencing short RNA–DNA heteroduplex substrates. *Biochem J* **432**, 323–332 (2010).
260. Roy, D. & Lieber, M. R. G Clustering Is Important for the Initiation of Transcription-Induced R-Loops In Vitro, whereas High G Density without Clustering Is Sufficient Thereafter. *Mol Cell Biol* **29**, 3124–3133 (2009).
261. Roy, S., Luzwick, J. W. & Schlacher, K. SIRF: Quantitative in situ analysis of protein interactions at DNA replication forks. *J Cell Biol* **217**, 1521–1536 (2018).
262. Rudkin, G.T. Non replicating DNA in Drosophila. *Genetics* **61**, 227–238 (1969).
263. Sabino, J. C., Almeida, M. R. de, Abreu, P. L., Ferreira, A. M., Caldas, P., Domingues, M. M., Santos, N. C., Azzalin, C. M., Grosso, A. R. & Almeida, S. F. de. Epigenetic reprogramming by TET enzymes impacts co-transcriptional R-loops. *Elife* **11**, e69476 (2022).
264. Saldivar, J. C., Cortez, D. & Cimprich, K. A. The essential kinase ATR: ensuring faithful duplication of a challenging genome. *Nature Reviews Molecular Cell Biology* **18**, 622–636 (2017).
265. Sanz, L. A., Hartono, S. R., Lim, Y. W., Steyaert, S., Rajpurkar, A., Ginno, P. A., Xu, X. & Chédin, F. Prevalent, Dynamic, and Conserved R-Loop Structures Associate with Specific Epigenomic Signatures in Mammals. *Mol Cell* **63**, 167–178 (2016).
266. Saunders, A., Core, L. J., Sutcliffe, C., Lis, J. T. & Ashe, H. L. Extensive polymerase pausing during Drosophila axis patterning enables high-level and pliable transcription. *Gene Dev* **27**, 1146–1158 (2013).
267. Schilling, B., Rardin, M. J., MacLean, B. X., Zawadzka, A. M., Frewen, B. E., Cusack, M. P., Sorensen, D. J., Bereman, M. S., Jing, E., Wu, C. C., Verdin, E., Kahn, C. R., MacCoss, M. J. & Gibson, B. W. Platform-independent and Label-free Quantitation of Proteomic Data Using MS1 Extracted Ion Chromatograms in Skyline: Application to Protein Acetylation and Phosphorylation. *Mol Cell Proteomics* **11**, 202–214 (2012).
268. Schneider, C. A., Rasband, W. S. & Eliceiri, K. W. NIH Image to ImageJ: 25 years of image analysis. *Nat Methods* **9**, 671–675 (2012).
269. Schneider, I. Cell lines derived from late embryonic stages of Drosophila melanogaster. *J Embryol Exp Morph* **27**, 353–65 (1972).
270. Seller, C. A. & O'Farrell, P. H. Rif1 prolongs the embryonic S phase at the Drosophila mid-blastula transition. *Plos Biol* **16**, e2005687 (2018).
271. Shafiq, S., Chen, C., Yang, J., Cheng, L., Ma, F., Widemann, E. & Sun, Q. DNA Topoisomerase 1 Prevents R-loop Accumulation to Modulate Auxin-Regulated Root Development in Rice. *Mol Plant* **10**, 821–833 (2017).
272. Shannon, P., Markiel, A., Ozier, O., Baliga, N. S., Wang, J. T., Ramage, D., Amin, N., Schwikowski, B. & Ideker, T. Cytoscape: A Software Environment for Integrated Models of Biomolecular Interaction Networks. *Genome Res* **13**, 2498–2504 (2003).
273. Shao, Z., Raible, F., Mollaaghababa, R., Guyon, J. R., Wu, C., Bender, W. & Kingston, R. E. Stabilization of Chromatin Structure by PRC1, a Polycomb Complex. *Cell* **98**, 37–46 (1999).

274. Sharan, S. K., Thomason, L. C., Kuznetsov, S. G. & Court, D. L. Recombineering: a homologous recombination-based method of genetic engineering. *Nat Protoc* **4**, 206–223 (2009).
275. Sher, N., Bell, G. W., Li, S., Nordman, J., Eng, T., Eaton, M. L., MacAlpine, D. M. & Orr-Weaver, T. L. Developmental control of gene copy number by repression of replication initiation and fork progression. *Genome Research* **22**, 64-75 (2012).
276. Sher, N., Bell, G. W., Li, S., Nordman, J., Eng, T., Eaton, M. L., MacAlpine, D. M. & Orr-Weaver, T. L. Developmental control of gene copy number by repression of replication initiation and fork progression. *Genome Research* **22**, 64-75 (2012).
277. Sibon, O. C. M., Laurençon, A., Hawley, R. S. & Theurkauf, W. E. The Drosophila ATM homologue Mei-41 has an essential checkpoint function at the midblastula transition. *Curr Biol* **9**, 302–312 (1999).
278. Siddiqui, K., On, K. F. & Diffley, J. F. X. Regulating DNA Replication in Eukarya. *Csh Perspect Biol* **5**, a012930 (2013).
279. Silva, S., Camino, L. P. & Aguilera, A. Human mitochondrial degradosome prevents harmful mitochondrial R loops and mitochondrial genome instability. *Proc National Acad Sci* **115**, 11024-11029 (2018).
280. Sirbu, B. M., Couch, F. B., Feigerle, J. T., Bhaskara, S., Hiebert, S. W. & Cortez, D. Analysis of protein dynamics at active, stalled, and collapsed replication forks. *Gene Dev* **25**, 1320–1327 (2011).
281. Sirbu, B. M., McDonald, W. H., Dungrawala, H., Badu-Nkansah, A., Kavanaugh, G. M., Chen, Y., Tabb, D. L. & Cortez, D. Identification of Proteins at Active, Stalled, and Collapsed Replication Forks Using Isolation of Proteins on Nascent DNA (iPOND) Coupled with Mass Spectrometry. *J Biol Chem* **288**, 31458–31467 (2013).
282. Skourti-Stathaki, K. & Proudfoot, N. J. A double-edged sword: R loops as threats to genome integrity and powerful regulators of gene expression. *Genes & Development* **28**, 1384-1396 (2014).
283. Skourti-Stathaki, K., Kamieniarz-Gdula, K. & Proudfoot, N. J. R-loops induce repressive chromatin marks over mammalian gene terminators. *Nature* **516**, 436-439 (2014).
284. Skourti-Stathaki, K., Triglia, E. T., Warburton, M., Voigt, P., Bird, A. & Pombo, A. R-Loops Enhance Polycomb Repression at a Subset of Developmental Regulator Genes. *Mol Cell* **73**, 930-945 (2019).
285. Smith, A. V. & Orr-Weaver, T. L. The regulation of the cell cycle during Drosophila embryogenesis: the transition to polyteny. *Dev Camb Engl* **112**, 997–1008 (1991).
286. Smolka, J. A., Sanz, L. A., Hartono, S. R. & Chédin, F. Recognition of RNA by the S9.6 antibody creates pervasive artifacts when imaging RNA:DNA hybrids. *J Cell Biology* **220**, e202004079 (2021).
287. Sollier, J. & Cimprich, K. A. Breaking bad: R-loops and genome integrity. *Trends in Cell Biology* **25**, 514-522 (2015).
288. Sollier, J., Stork, C. T., García-Rubio, M. L., Paulsen, R. D., Aguilera, A. & Cimprich, K. A. Transcription-Coupled Nucleotide Excision Repair Factors Promote R-Loop-Induced Genome Instability. *Molecular Cell* **56**, 777-785 (2014).

289. Sousa-Nunes, R., Chia, W. & Somers, W. G. Protein Phosphatase 4 mediates localization of the Miranda complex during *Drosophila* neuroblast asymmetric divisions. *Gene Dev* **23**, 359–372 (2009).
290. Spradling, A. & Orr-Weaver, T. Regulation of DNA Replication During *Drosophila* Development. *Annual Review of Genetics* **21**, 373–403 (2002).
291. Spradling, A. C. & Mahowald, A. P. Amplification of genes for chorion proteins during oogenesis in *Drosophila melanogaster*. *Proc National Acad Sci* **77**, 1096–1100 (1980).
292. Sreesankar, E., Bharathi, V., Mishra, R. K. & Mishra, K. *Drosophila* Rif1 is an essential gene and controls late developmental events by direct interaction with PP1-87B. *Sci Rep* **5**, 10679 (2015).
293. Sreesankar, E., Senthilkumar, R., Bharathi, V., Mishra, R. K. & Mishra, K. Functional diversification of yeast telomere associated protein, Rif1, in higher eukaryotes. *Bmc Genomics* **13**, 255–255 (2012).
294. Stolz, R., Sulthana, S., Hartono, S. R., Malig, M., Benham, C. J. & Chedin, F. Interplay between DNA sequence and negative superhelicity drives R-loop structures. *Proc National Acad Sci* **116**, 6260–6269 (2019).
295. Stork, C. T., Bocek, M., Crossley, M. P., Sollier, J., Sanz, L. A., Chédin, F., Swigut, T. & Cimprich, K. A. Co-transcriptional R-loops are the main cause of estrogen-induced DNA damage. *eLife* **5**, e17548 (2016).
296. Sukackaite, R., Cornacchia, D., Jensen, M. R., Mas, P. J., Blackledge, M., Enervald, E., Duan, G., Auchynnikava, T., Köhn, M., Hart, D. J. & Buonomo, S. B. C. Mouse Rif1 is a regulatory subunit of protein phosphatase 1 (PP1). *Sci Rep* **7**, 2119 (2017).
297. Sun, J. & Kong, D. DNA replication origins, ORC/DNA interaction, and assembly of pre-replication complex in eukaryotes. *Acta Bioch Bioph Sin* **42**, 433–439 (2010).
298. Sun, Q., Csorba, T., Skourti-Stathaki, K., Proudfoot, N. J. & Dean, C. R-Loop Stabilization Represses Antisense Transcription at the *Arabidopsis FLC* Locus. *Science* **340**, 619–621 (2013).
299. Sun, Q., Csorba, T., Skourti-Stathaki, K., Proudfoot, N. J. & Dean, C. R-Loop Stabilization Represses Antisense Transcription at the *Arabidopsis FLC* Locus. *Science* **340**, 619–21 (2013).
300. Swenson, J. M., Colmenares, S. U., Strom, A. R., Costes, S. V. & Karpen, G. H. The composition and organization of *Drosophila* heterochromatin are heterogeneous and dynamic. *Elife* **5**, e16096 (2016).
301. Szklarczyk, D., Gable, A. L., Nastou, K. C., Lyon, D., Kirsch, R., Pyysalo, S., Doncheva, N. T., Legeay, M., Fang, T., Bork, P., Jensen, L. J. & Mering, C. von. The STRING database in 2021: customizable protein–protein networks, and functional characterization of user-uploaded gene/measurement sets. *Nucleic Acids Res* **49**, D605–D612 (2020).
302. Tadros, W. & Lipshitz, H. D. The maternal-to-zygotic transition: a play in two acts. *Development* **136**, 3033–3042 (2009).
303. Taglialatela, A., Alvarez, S., Leuzzi, G., Sannino, V., Ranjha, L., Huang, J.-W., Madubata, C., Anand, R., Levy, B., Rabadan, R., Cejka, P., Costanzo, V. & Ciccia, A. Restoration of Replication Fork Stability in BRCA1- and BRCA2-Deficient Cells by Inactivation of SNF2-Family Fork Remodelers. *Mol Cell* **68**, 414–430 (2017).

304. Tam, A. S., Sihota, T. S., Milbury, K. L., Zhang, A., Mathew, V. & Stirling, P. C. Selective defects in gene expression control genome instability in yeast splicing mutants. *Mol Biol Cell* **30**, 191–200 (2019).
305. Tan-Wong, S. M., Dhir, S. & Proudfoot, N. J. R-Loops Promote Antisense Transcription across the Mammalian Genome. *Mol Cell* **76**, 600-616 (2019).
306. Thakur, J., Fang, H., Llagas, T., Disteche, C. M. & Henikoff, S. Architectural RNA is required for heterochromatin organization. *Biorxiv* 784835 (2019). doi:10.1101/784835
307. Thompson, M. Polybromo-1: The chromatin targeting subunit of the PBAF complex. *Biochimie* **91**, 309–319 (2009).
308. Ticau, S., Friedman, L. J., Ivica, N. A., Gelles, J. & Bell, S. P. Single-Molecule Studies of Origin Licensing Reveal Mechanisms Ensuring Bidirectional Helicase Loading. *Cell* **161**, 513–525 (2015).
309. Tomasetti, C., Li, L. & Vogelstein, B. Stem cell divisions, somatic mutations, cancer etiology, and cancer prevention. *Science* **355**, 1330–1334 (2017).
310. Toriumi, K., Tsukahara, T. & Hanai, R. R-Loop Formation In Trans at an AGGAG Repeat. *J Nucleic Acids* **2013**, 629218 (2013).
311. Townsend, A., Lora, G., Engel, J., Tirado-Class, N. & Dungrawala, H. DCAF14 promotes stalled fork stability to maintain genome integrity. *Cell Reports* **34**, 108669 (2021).
312. Tresini, M., Marteiijn, J. A. & Vermeulen, W. Bidirectional coupling of splicing and ATM signaling in response to transcription-blocking DNA damage. *Rna Biol* **13**, 272–278 (2016).
313. Unhavaithaya, Y. & Orr-Weaver, T. L. Polyploidization of glia in neural development links tissue growth to blood–brain barrier integrity. *Gene Dev* **26**, 31–36 (2012).
314. Vannier, J.-B., Sandhu, S., Petalcorin, M. IR., Wu, X., Nabi, Z., Ding, H. & Boulton, S. J. RTEL1 Is a Replisome-Associated Helicase That Promotes Telomere and Genome-Wide Replication. *Science* **342**, 239–242 (2013).
315. Virgilio, M. D., Callen, E., Yamane, A., Zhang, W., Jankovic, M., Gitlin, A. D., Feldhahn, N., Resch, W., Oliveira, T. Y., Chait, B. T., Nussenzweig, A., Casellas, R., Robbiani, D. F. & Nussenzweig, M. C. Rif1 Prevents Resection of DNA Breaks and Promotes Immunoglobulin Class Switching. *Science* **339**, 711–715 (2013).
316. Vos, S. M., Tretter, E. M., Schmidt, B. H. & Berger, J. M. All tangled up: how cells direct, manage and exploit topoisomerase function. *Nat Rev Mol Cell Bio* **12**, 827 (2011).
317. Wahba, L., Costantino, L., Tan, F. J., Zimmer, A. & Koshland, D. S1-DRIP-seq identifies high expression and polyA tracts as major contributors to R-loop formation. *Gene Dev* **30**, 1327–1338 (2016).
318. Wang, I. X., Grunseich, C., Fox, J., Burdick, J., Zhu, Z., Ravazian, N., Hafner, M. & Cheung, V. G. Human proteins that interact with RNA/DNA hybrids. *Genome Res* **28**, 1405–1414 (2018).
319. Wessel, S. R., Mohni, K. N., Luzwick, J. W., Dungrawala, H. & Cortez, D. Functional Analysis of the Replication Fork Proteome Identifies BET Proteins as PCNA Regulators. *Cell Reports* **28**, 3497-3509 (2019).

320. White, A. E., Burch, B. D., Yang, X., Gasdaska, P. Y., Dominski, Z., Marzluff, W. F. & Duronio, R. J. Drosophila histone locus bodies form by hierarchical recruitment of components. *J Cell Biology* **193**, 677–694 (2011).
321. White, R. L. & Hogness, D. S. R loop mapping of the 18S and 28S sequences in the long and short repeating units of drosophila melanogaster rDNA. *Cell* **10**, 177–192 (1977).
322. Wu, H.-Y., Shyy, S., Wang, J. C. & Liu, L. F. Transcription generates positively and negatively supercoiled domains in the template. *Cell* **53**, 433–440 (1988).
323. Wu, T., Nance, J., Chu, F. & Fazio, T. G. Characterization of R-Loop-Interacting Proteins in Embryonic Stem Cells Reveals Roles in rRNA Processing and Gene Expression. *Mol Cell Proteom Mcp* **20**, 100142 (2021).
324. Wulfridge, P. & Sarma, K. A nuclease- and bisulfite-based strategy captures strand-specific R-loops genome-wide. *Elife* **10**, e65146 (2021).
325. Xu, L. & Blackburn, E. H. Human Rif1 protein binds aberrant telomeres and aligns along anaphase midzone microtubules. *J Cell Biology* **167**, 819–830 (2004).
326. Xu, W., Li, K., Li, S., Hou, Q., Zhang, Y., Liu, K. & Sun, Q. The R-loop Atlas of Arabidopsis Development and Responses to Environmental Stimuli. *Plant Cell* 888–903 (2020).
327. Xu, W., Xu, H., Li, K., Fan, Y., Liu, Y., Yang, X. & Sun, Q. The R-loop is a common chromatin feature of the Arabidopsis genome. *Nat Plants* **3**, 704–714 (2017).
328. Yamazaki, S., Ishii, A., Kanoh, Y., Oda, M., Nishito, Y. & Masai, H. Rif1 regulates the replication timing domains on the human genome. *Embo J* **31**, 3667–3677 (2012).
329. Yan, P., Liu, Z., Song, M., Wu, Z., Xu, W., Li, K., Ji, Q., Wang, S., Liu, X., Yan, K., Esteban, C. R., Ci, W., Belmonte, J. C. I., Xie, W., Ren, J., Zhang, W., Sun, Q., Qu, J. & Liu, G.-H. Genome-wide R-loop Landscapes during Cell Differentiation and Reprogramming. *Cell Reports* **32**, 107870 (2020).
330. Yan, Q. & Sarma, K. MapR: A Method for Identifying Native R-Loops Genome Wide. *Curr Protoc Mol Biology* **130**, e113 (2020).
331. Yan, Q. & Sarma, K. MapR: A Method for Identifying Native R-Loops Genome Wide. *Curr Protoc Mol Biology* **130**, e113 (2020).
332. Yang, X., Zhai, B., Wang, S., Kong, X., Tan, Y., Liu, L., Yang, X., Tan, T., Zhang, S. & Zhang, L. RNA-DNA hybrids regulate meiotic recombination. *Cell Reports* **37**, 110097 (2021).
333. Yarosh, W. & Spradling, A. C. Incomplete replication generates somatic DNA alterations within Drosophila polytene salivary gland cells. *Genes & Development* **28**, 1840–1855 (2014).
334. Yu, K., Chedin, F., Hsieh, C.-L., Wilson, T. E. & Lieber, M. R. R-loops at immunoglobulin class switch regions in the chromosomes of stimulated B cells. *Nature Immunology* **4**, 442–451 (2003).
335. Yuan, K., Sellar, C. A., Shermoen, A. W. & O'Farrell, P. H. Timing the Drosophila Mid-Blastula Transition: A Cell Cycle-Centered View. *Trends in Genetics* **32**, 496–507 (2016).
336. Yurlova, A. A., Makunin, I. V., Kolesnikova, T. D., Posukh, O. V., Belyaeva, E. S. & Zhimulev, I. F. Conservation of Domain Structure in a Fast-Evolving Heterochromatic SUUR Protein in Drosophilids. *Genetics* **183**, 119–129 (2009).

337. Zeman, M. K. & Cimprich, K. A. Causes and consequences of replication stress. *Nature Cell Biology* **16**, 2–9 (2013).
338. Zeng, C., Onoguchi, M. & Hamada, M. Association analysis of repetitive elements and R-loop formation across species. *Mobile Dna-uk* **12**, 3 (2021).
339. Zeymer, C. & Hilvert, D. Directed Evolution of Protein Catalysts. *Annu Rev Biochem* **87**, 1–27 (2018).
340. Zhang, L., Geng, X., Wang, F., Tang, J., Ichida, Y., Sharma, A., Jin, S., Chen, M., Tang, M., Pozo, F. M., Wang, W., Wang, J., Wozniak, M., Guo, X., Miyagi, M., Jin, F., Xu, Y., Yao, X. & Zhang, Y. 53BP1 regulates heterochromatin through liquid phase separation. *Nat Commun* **13**, 360 (2022).
341. Zhang, W., Feng, J. & Li, Q. The replisome guides nucleosome assembly during DNA replication. *Cell Biosci* **10**, 37 (2020).
342. Zhang, Y., Liu, T., Meyer, C. A., Eeckhoute, J., Johnson, D. S., Bernstein, B. E., Nusbaum, C., Myers, R. M., Brown, M., Li, W. & Liu, X. S. Model-based Analysis of ChIP-Seq (MACS). *Genome Biol* **9**, R137–R137 (2008).
343. Zhao, B., Zhang, W., Cun, Y., Li, J., Liu, Y., Gao, J., Zhu, H., Zhou, H., Zhang, R. & Zheng, P. Mouse embryonic stem cells have increased capacity for replication fork restart driven by the specific Fliia-Floped protein complex. *Cell Res* **28**, 69–89 (2018).
344. Zielke, N., Edgar, B. A. & DePamphilis, M. L. Endoreplication. *Csh Perspect Biol* **5**, a012948 (2013).
345. Zimmermann, M., Lotterberger, F., Buonomo, S. B., Sfeir, A. & Lange, T. de. 53BP1 Regulates DSB Repair Using Rif1 to Control 5' End Resection. *Science* **339**, 700–704 (2013).